antioxidants

Special Issue Reprint

Cellular Responses of Antioxidants Related to Degenerative Eye Disease Research

Edited by
Wonkyu Ju and Niina Harju

mdpi.com/journal/antioxidants

MDPI

Cellular Responses of Antioxidants Related to Degenerative Eye Disease Research

Cellular Responses of Antioxidants Related to Degenerative Eye Disease Research

Guest Editors

Wonkyu Ju
Niina Harju

MDPI

Basel • Beijing • Wuhan • Barcelona • Belgrade • Novi Sad • Cluj • Manchester

Guest Editors

Wonkyu Ju
Viterbi Family Department
of Ophthalmology
University of California
San Diego
La Jolla
USA

Niina Harju
School of Pharmacy
Faculty of Health Sciences
University of Eastern Finland
Kuopio
Finland

Editorial Office
MDPI AG
Grosspeteranlage 5
4052 Basel, Switzerland

This is a reprint of the Special Issue, published open access by the journal *Antioxidants* (ISSN 2076-3921), freely accessible at: https://www.mdpi.com/journal/antioxidants/special_issues/Cellular_Antioxidants_Degenerative_Eye_Disease_Research.

For citation purposes, cite each article independently as indicated on the article page online and as indicated below:

Lastname, A.A.; Lastname, B.B. Article Title. *Journal Name* **Year**, *Volume Number*, Page Range.

ISBN 978-3-7258-4527-9 (Hbk)
ISBN 978-3-7258-4528-6 (PDF)
https://doi.org/10.3390/books978-3-7258-4528-6

Contents

Cheol Park, Hee-Jae Cha, Hyun Hwangbo, EunJin Bang, Su Hyun Hong, Kyoung Seob Song, et al.
β-Asarone Alleviates High-Glucose-Induced Oxidative Damage via Inhibition of ROS Generation and Inactivation of the NF-κB/NLRP3 Inflammasome Pathway in Human Retinal Pigment Epithelial Cells
Reprinted from: *Antioxidants* **2023**, *12*, 1410, https://doi.org/10.3390/antiox12071410 . . . . . **1**

Xiao-Na Hao, Na Zhao, Jie-Min Huang, Si-Yu Li, Dong Wei, Ning Pu, et al.
Intravitreal Injection of ZYAN1 Restored Autophagy and Alleviated Oxidative Stress in Degenerating Retina via the HIF-1α/BNIP3 Pathway
Reprinted from: *Antioxidants* **2023**, *12*, 1914, https://doi.org/10.3390/antiox12111914 . . . . . **15**

Manas R. Biswal, Ryan J. Paulson, Riddhi Vichare and Alfred S. Lewin
Buspirone Enhances Cell Survival and Preserves Structural Integrity during Oxidative Injury to the Retinal Pigment Epithelium
Reprinted from: *Antioxidants* **2023**, *12*, 2129, https://doi.org/10.3390/antiox12122129 . . . . . **39**

Shang-Chun Tsou, Chen-Ju Chuang, Inga Wang, Tzu-Chun Chen, Jui-Hsuan Yeh, Chin-Lin Hsu, et al.
Lemon Peel Water Extract: A Novel Material for Retinal Health, Protecting Retinal Pigment Epithelial Cells against Dynamin-Related Protein 1-Mediated Mitochondrial Fission by Blocking ROS-Stimulated Mitogen-Activated Protein Kinase/Extracellular Signal-Regulated Kinase Pathway
Reprinted from: *Antioxidants* **2023**, *13*, 538, https://doi.org/10.3390/antiox13050538 . . . . . **53**

Salvador Mérida, Amparo Návea, Carmen Desco, Bernardo Celda, Mercedes Pardo-Tendero, José Manuel Morales-Tatay and Francisco Bosch-Morell
Glutathione and a Pool of Metabolites Partly Related to Oxidative Stress Are Associated with Low and High Myopia in an Altered Bioenergetic Environment
Reprinted from: *Antioxidants* **2023**, *13*, 539, https://doi.org/10.3390/antiox13050539 . . . . . **73**

Deepak Basyal, Sooyeun Lee and Hye Jin Kim
Antioxidants and Mechanistic Insights for Managing Dry Age-Related Macular Degeneration
Reprinted from: *Antioxidants* **2023**, *13*, 568, https://doi.org/10.3390/antiox13050568 . . . . . **90**

Christina Ortiz, Houda Tahiri, Chun Yang, Claudia Gilbert, Carl Fortin and Pierre Hardy
The microRNA Let-7f Induces Senescence and Exacerbates Oxidative Stress in Retinal Pigment Epithelial Cells
Reprinted from: *Antioxidants* **2023**, *13*, 646, https://doi.org/10.3390/antiox13060646 . . . . . **133**

Seung-Yub Song, Dae-Hun Park, Sung-Ho Lee, Han-Kyu Lim, Jin-Woo Park, Jeong-Woo Seo and Seung-Sik Cho
Protective Effects of 7S,15R-Dihydroxy-16S,17S-Epoxy- Docosapentaenoic Acid (diHEP-DPA) against Blue Light-Induced Retinal Damages in A2E-Laden ARPE-19 Cells
Reprinted from: *Antioxidants* **2023**, *13*, 982, https://doi.org/10.3390/antiox13080982 . . . . . **150**

Seunghwan Choi, Soo-Ho Choi, Tonking Bastola, Keun-Young Kim, Sungsik Park, Robert N. Weinreb, et al.
AIBP Protects Müller Glial Cells Against Oxidative Stress-Induced Mitochondrial Dysfunction and Reduces Retinal Neuroinflammation
Reprinted from: *Antioxidants* **2023**, *13*, 1252, https://doi.org/10.3390/antiox13101252 . . . . . **167**

antioxidants

MDPI

Article

β-Asarone Alleviates High-Glucose-Induced Oxidative Damage via Inhibition of ROS Generation and Inactivation of the NF-κB/NLRP3 Inflammasome Pathway in Human Retinal Pigment Epithelial Cells

Cheol Park [1,†], Hee-Jae Cha [2,†], Hyun Hwangbo [3], EunJin Bang [3], Su Hyun Hong [4], Kyoung Seob Song [5], Jeong Sook Noh [6], Do-Hyung Kim [7], Gi-Young Kim [8] and Yung Hyun Choi [3,4,*]

1 Department Division of Basic Sciences, College of Liberal Studies, Dong-eui University, Busan 47340, Republic of Korea
2 Department of Parasitology and Genetics, College of Medicine, Kosin University, Busan 49104, Republic of Korea
3 Anti-Aging Research Center, Dong-eui University, Busan 47340, Republic of Korea
4 Department of Biochemistry, College of Korean Medicine, Dong-eui University, Busan 47340, Republic of Korea
5 Department of Medical Life Science, College of Medicine, Kosin University, Busan 49104, Republic of Korea
6 Department of Food Science & Nutrition, Tongmyong University, Busan 48520, Republic of Korea
7 Department of Aquatic Life Medicine, College of Fisheries Sciences, Pukyong National University, Busan 48513, Republic of Korea
8 Department of Marine Life Science, Jeju National University, Jeju 63243, Republic of Korea
* Correspondence: choiyh@deu.ac.kr; Tel.: +82-51-890-3319
† These authors contributed equally to this work.

Abstract: Diabetic retinopathy (DR) is the leading cause of vision loss and a major complication of diabetes. Hyperglycemia-induced accumulation of reactive oxygen species (ROS) is an important risk factor for DR. β-asarone, a major component of volatile oil extracted from *Acori graminei* Rhizoma, exerts antioxidant effects; however, its efficacy in DR remains unknown. In this study, we investigated whether β-asarone inhibits high-glucose (HG)-induced oxidative damage in human retinal pigment epithelial (RPE) ARPE-19 cells. We found that β-asarone significantly alleviated cytotoxicity, apoptosis, and DNA damage in HG-treated ARPE-19 cells via scavenging of ROS generation. β-Asarone also significantly attenuated the excessive accumulation of lactate dehydrogenase and mitochondrial ROS by increasing the manganese superoxide dismutase and glutathione activities. HG conditions markedly increased the release of interleukin (IL)-1β and IL-18 and upregulated their protein expression and activation of the nuclear factor-kappa B (NF-κB) signaling pathway, whereas β-asarone reversed these effects. Moreover, expression levels of the NOD-like receptor family pyrin domain-containing 3 (NLRP3) inflammasome multiprotein complex molecules, including thioredoxin-interacting protein, NLRP3, apoptosis-associated speck-like protein containing a caspase-recruitment domain, and cysteinyl aspartate-specific proteinase-1, were increased in ARPE-19 cells under HG conditions. However, their expression levels remained similar to those in the control group in the presence of β-asarone. Therefore, β-asarone protects RPE cells from HG-induced injury by blocking ROS generation and NF-κB/NLRP3 inflammasome activation, indicating its potential as a therapeutic agent for DR treatment.

Keywords: β-asarone; high glucose; ROS; NF-κB; NLRP3 inflammasome

1. Introduction

Diabetic retinopathy (DR), the most common and severe complication of diabetes, is the major cause of visual impairment and vision loss. Hyperglycemia plays a crucial role in DR pathogenesis [1,2]. Oxidative and inflammatory stress induced by hyperglycemia

are involved in the initiation and progression of DR. Accumulation of ROS promote increased oxidative stress due to hyperglycemia, is a key factor in DR-associated retinal pigment epithelial (RPE) cell damage [3–5]. Elevated intracellular ROS levels trigger inflammation and lead to the occurrence and progression of chronic diseases, such as DR. Mitochondria are the major site of ROS generation, which directly stimulate pro-inflammatory cytokine secretion and promote pathological conditions [6]. Hyperglycemia increases the mitochondrial ROS levels, resulting in a chronic inflammatory state [7,8]. Therefore, alleviation of oxidative stress and inflammation may be a promising strategy for the treatment of DR.

Recent studies have suggested the involvement of the NLR family pyrin domain-containing-3 (NLRP3) inflammasome signaling pathway in DR pathogenesis [9–11]. Abnormal activation of this signaling pathway is closely related to aging-related diseases, such as diabetes. Expression levels of the NLRP3 inflammasome multiprotein complex molecules, apoptosis-associated speck-like protein containing a caspase-recruitment domain (ASC) and caspase-1, are markedly increased in patients with DR [12–14]. Activation of the NLRP3 inflammasome pathway is initiated by various stimuli, such as pathogenic molecules, mitochondrial damage, and excessive ROS accumulation. This pathway is divided into canonical and non-canonical pathways depending on the activation of cysteine aspartase during inflammasome formation [15,16]. In canonical signaling, NLRP3 inflammasome priming leads to the nuclear translocation of nuclear factor-kappa B (NF-κB), promoting the expression of precursor proteins, including NLRP3, ASC, pro-caspase-1, pro-interleukin (IL)-1β, and pro-IL-18, which are essential mediators of inflammation. However, in non-canonical signaling pathways, NLRP3 becomes activated through cleaved caspase-11 [17]. Therefore, inflammasome inactivation may be a novel therapeutic strategy to ameliorate the symptoms of various inflammatory diseases, including DR [12,18].

β-Asarone (*cis*-2,4,5-trimethoxy-1-allyl phenyl) is a volatile oil present in various herbal medicines, including *Acorus tatarinowii* Schott. It exerts various biological effects, including antioxidant, anti-inflammatory, and anti-cancer effects [19,20]. For example, β-asarone suppresses the production of pro-inflammatory mediators and cytokines by blocking the NF-κB signaling pathway and preventing the development of neuroinflammatory diseases [21]. In addition, β-asarone directly scavenges hydrogen peroxide and hydroxyl radicals and exerts protective effects against DNA oxidation [22]. Recently, Cai et al. [23] reported that a decrease in amyloid-β-induced neuronal apoptosis and improvement in learning and memory by β-asarone were closely related to the reduction in oxidative stress. Xiao et al. [24] revealed that β-asarone mitigates myocardial ischemia/reperfusion (I/R) injury via the inhibition of NLRP3 inflammasome-mediated lytic cell death. However, the protective effects of β-asarone against oxidative stress and inflammation in hyperglycemic RPE cells and its action mechanism remain unknown. To the best of our knowledge, this study is the first to examine the effects of β-asarone on ROS-mediated NF-κB/NLRP3 inflammasome activation in high-glucose (HG)-induced hyperglycemic RPE cells.

2. Materials and Methods

2.1. Cell Culture and Treatment

ARPE-19 cells (CRL-2302; American Type Culture Collection, Manassas, VA, USA) were cultured as previously described [25]. β-Asarone was obtained from Sigma-Aldrich Co. (St. Louis, MO, USA), and the materials necessary for cell culture were provided by WelGENE Inc. (Gyungsan, Korea). Cells were grown for 48 h in a medium with various doses of β-asarone (0, 10, 25, 50, and 100 μM) and glucose (0, 5, 10, 20, and 40 mM) or pre-treated with optimal concentration of β-asarone (50 μM) or N-acetyl-cysteine (NAC; 10 mM; Thermo Fisher Scientific, Waltham, MA, USA) for 1 h and cultured for an additional 48 h under HG (20 mM) conditions in presence of β-asarone and NAC. The optimal treatment concentrations for β-asarone (50 μM) were selected, as was the highest treatment concentration that showed no decreased cell viability in ARPE-19 cells. The optimal

concentration for glucose (20 mM) was selected, as was the lowest treatment concentration that showed sublethal levels of cell viability.

2.2. Cell Viability and Lactate Dehydrogenase (LDH) Assays

After treatment, cell viability was examined using the 3-(4,5-dimethyl-2-thiazolyl)-2,5-diphenyltetrazolium bromide (MTT) assay (Sigma-Aldrich Co., St. Louis, MO, USA), as previously described [26]. The level of LDH released from the cells into the culture medium was determined using an LDH Cytotoxicity Assay Kit (Thermo Fisher Scientific, Waltham, MA, USA), according to the manufacturer's instructions. To measure LDH activity, the absorbance was measured at 490 nm and 680 nm, in which an absorbance value of 680 nm, a background signal, was subtracted from an absorbance value of 490 nm. The results are presented as values normalized to the control value.

2.3. Determination of the Cell and Nuclear Morphology

Morphological changes in cells treated with HG for 48 h with or without β-asarone (50 μM) were observed under an inverted microscope (Carl Zeiss, Oberkochen, Germany). The morphological changes due to cellular apoptosis in ARPE-19 cells are majorly characterized by disruption of cell monolayer and reduced cell volume, which could be observed under an inverted microscope. To assess the morphological changes in the nucleus, cells were stained with 4′,6-diamidino-2-phenylindole (DAPI; Thermo Fisher Scientific, Waltham, MA, USA) and examined under a fluorescence microscope (Carl Zeiss, Oberkochen, Germany) at the Core-Facility Center for Tissue Regeneration, Dong-eui University (Busan, Korea). The DAPI is a blue fluorescence dye, which could more easily enters the apoptotic cell and stains a stronger blue color. The changes in the nucleus morphology of apoptotic cells include chromosome condensation and fragmentation allows identification of apoptotic cells [27].

2.4. Apoptosis Assay

After culturing the cells under HG conditions in the presence or absence of β-asarone, apoptosis was detected via flow cytometry (Becton Dickinson, San Jose, CA, USA) using the fluorescein isothiocyanate (FITC) Annexin V Apoptosis Detection Kit (BD Biosciences, San Jose, CA, USA). To interpret the results, the percentages of early and late apoptotic cells (Annexin-V^+/propidium iodide $(PI)^-$ and Annexin-V^+/PI^+) were used to determine the total number of apoptotic cells [27].

2.5. Western Blot Analysis

Cells seeded at 2×10^5 cells per well in 6-well plate were lysed using the radioimmunoprecipitation assay lysis buffer (Sigma-Aldrich Co., St. Louis, MO, USA) or NE-PER Nuclear and Cytoplasmic Extraction Reagent (Thermo Fisher Scientific, Waltham, MA, USA), according to the manufacturers' protocols. The experiment was performed at least three times. Briefly, Cytoplasmic Extraction Reagent (CER) I reagent (100–200 μL) was added to cell pellet, followed by CER II reagent (5.5–11 μL). After short ice incubation, cells were centrifuged at 13,000× *g*, 4 °C for 10 min, which then collected supernatant or cytoplasmic protein extract was obtained. Pellet was suspended in ice-cold Nuclear Extraction Reagent. After ice incubation, the resuspended pellet was centrifuged at 13,000× *g*, 4 °C for 10 min. The collected supernatant fraction was obtained nuclear protein extract. The protein quantification was measured by using bicinchoninic acid (BCA) assay, in which proteins induce the reduction of alkaline Cu(II) to Cu(I) with increasing concentration, which BCA specifically forms complex with Cu(I), in which the complex exhibits purple color that can be detected by measuring absorbance at 562 nm. After protein quantification using the BCA Protein Assay Kit (Sigma-Aldrich Co., St. Louis, MO, USA), Western blot analysis was performed as previously described [28]. Antibodies were obtained from Santa Cruz Biotechnology, Inc. (Dallas, TX, USA), Cell Signaling Technology, Inc. (Beverly, MA, USA), Thermo Fisher Scientific, and Abcam (Cambridge, UK). Protein bands were detected

using enhanced chemiluminescence reagents (Thermo Fisher Scientific, Waltham, MA, USA), following the manufacturer's instructions.

2.6. Assessment of DNA Damage

To evaluate the effect of β-asarone on HG-induced oxidative DNA damage, the levels of 8-hydroxy-2′-deoxyguanosine (8-OHdG) in cells were determined using the 8-OHdG enzyme-linked immunosorbent assay (ELISA) kit (Abcam, Cambridge, UK), according to the manufacturer's protocol. The concentrations of 8-OHdG obtained from the standard curve were expressed in ng/mL. In addition, single-stranded DNA breaks were detected to visualize the DNA damage using the Comet Assay kit (Trevigen, Gaithersburg, MD, USA), according to the manufacturer's instructions. Comet images were examined using fluorescence microscopy.

2.7. ROS Assay

Cytosolic ROS levels were assessed using the 5,6-carboxy-2′,7′-dichlorodihydrofluorescein diacetate (DCF-DA) fluorescent probe (Thermo Fisher Scientific, Waltham, MA, USA). Briefly, cells treated with HG for 1 h with or without pre-treatment with β-asarone (50 μM) were collected and reacted with DCF-DA (20 μM), as per the manufacturer's recommendation. After washing the cells with phosphate-buffered saline (PBS), the fluorescence intensity was measured using flow cytometry, and fluorescence images were acquired via fluorescence microscopy [29]. Similarly, mitochondrial ROS production was measured using the MitoSox red dye (Thermo Fisher Scientific, Waltham, MA, USA), which detects the level of superoxide anions in the mitochondria. At the end of treatment, the cells were stained with MitoSox (10 μM), and the fluorescence intensity was analyzed via flow cytometry and fluorescence microscopy [30].

2.8. Evaluation of the Antioxidant Defense System

At the end of treatment, the reduced glutathione (GSH)/oxidized glutathione (GSSG) ratio (GSH/GSSG Ratio Detection Assay Kit, Abcam, Cambridge, UK) and the activity of manganese superoxide dismutase (MnSOD; MnSOD Assay Kit, Cayman Chemical, Ann Arbor, MI, USA) in cells were measured using spectrophotometric and enzymatic methods with commercially available kits, according to the manufacturers' instructions.

2.9. Measurement of IL-1β and IL-18 Levels

Following different treatments, cell supernatants were collected and the concentrations of IL-1β and IL-18 were quantified using specific ELISA kits (R&D Systems Inc., Minneapolis, MN, USA), following the manufacturer's protocol. The absorbance of the final product was measured at 450 nm using a microplate reader (Beckman Coulter Inc., Brea, CA, USA), according to the method described by Hwangbo et al. [31].

2.10. Immunofluorescence Assay for NF-κB, NLRP3, and ASC

To determine the expression level of phosphorylated (p)-NF-κB via immunofluorescence staining, the cells were cultured for 1 h under HG conditions with or without β-asarone, and the expression levels of NLRP3 and ASC were determined after 48 h of culture. Briefly, cells were fixed with formaldehyde after treatment, permeabilized with Triton X-100, reacted with primary antibodies against p-NF-κB (Cell Signaling Technology Inc., Beverly, MA, USA), NLRP3 (Abcam, Cambridge, UK), and ASC (AdipoGen Life Sciences, San Diego, CA, USA), and incubated with FITC-tagged secondary antibody IgG and Alexa Fluor 594-tagged secondary antibody IgG (Thermo Fisher Scientific, Waltham, MA, USA). Subsequently, the nuclei were counterstained with DAPI, and fluorescence images were captured [32].

2.11. Assay of Caspase-1 Activity

Caspase-1 activity in HG-stimulated cells with or without β-asarone was detected using a colorimetric assay kit (R&D Systems Inc., Brea, CA, USA). After the cell pellets were lysed with the lysis buffer provided with the kit, the lysates were reacted with *p*-nitroanilide (pNA)-labeled substrates in the reaction buffer. The enzymatic activity of caspase-1 was calculated from a standard curve prepared using pNA, according to the manufacturer's instructions.

2.12. Statistical Analysis

Data were analyzed via one-way analysis of variance with Tukey's post hoc test using the GraphPad Prism software (GraphPad Software Inc., La Jolla, CA, USA). Statistical significance was set at $p < 0.05$.

3. Results

3.1. β-Asarone Ameliorates HG-Induced Cell Viability Reduction and Cytotoxicity in ARPE-19 Cells

MTT assay was performed to examine the effect of β-asarone on the proliferation of ARPE-19 cells cultured under HG conditions. Compared to the control group, β-asarone did not show a notable difference in cell viability at concentrations <50 μM, but was slightly decreased in cells treated with 100 μM (Figure 1A). In cells treated with glucose, cell viability was significantly inhibited in a concentration-dependent manner. Notably, in cells treated with 20 mM glucose, viability decreased to approximately 60% (Figure 1B). Based on this result, the 20 mM glucose-treated group was set as the HG group, and the pre-treatment concentration of β-asarone was set as 50 μM. As shown in Figure 1C results, pre-treatment with 50 μM β-asarone significantly suppressed the inhibitory effect of HG on ARPE-19 cell viability, and the HG-induced decrease in cell viability was also reversed in NAC pre-treated cells. LDH assay revealed that β-asarone and NAC significantly ameliorated lytic cell death measured by LDH release HG-induced cytotoxicity in cells (Figure 1D).

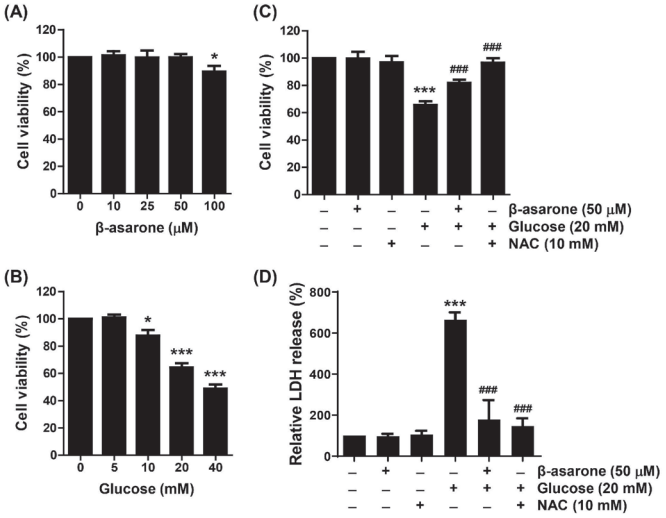

Figure 1. Inhibitory effects of β-asarone on high-glucose (HG)-induced cell viability reduction and cytotoxicity in ARPE-19 cells. Cells were grown for 48 h in a medium with various doses of β-asarone (0, 10, 25, 50, and 100 μM) (**A**) and glucose (0, 5, 10, 20, and 40 μM) (**B**) or pre-treated with β-asarone (50 μM) or *N*-acetyl-cysteine (NAC; 10 mM) for 1 h and cultured for an additional 48 h under HG (20 mM glucose) conditions in presence of β-asarone or NAC (**C**,**D**). Cell viability and cytotoxicity were determined using the 3-(4,5-dimethyl-2-thiazolyl)-2,5-diphenyltetrazolium bromide (MTT) (**A**–**C**) and lactate dehydrogenase (LDH) (**D**) assays, respectively. Numerical values are represented as the mean ± standard deviation of three independent experiments (SD; * $p < 0.05$ and *** $p < 0.001$ vs. control group; ### $p < 0.001$ vs. HG-treated group).

3.2. β-Asarone Reduces Apoptosis and DNA Damage in HG-Treated ARPE-19 Cells

As indicated in Figure 2A, treatment of cells with HG induced changes in their cell morphology, such as rounding of cells and loss of cell anchorage to the culture plate, but these effects were not observed in β-asarone-pre-treated cells. Therefore, we evaluated whether the HG-induced inhibition of cell viability and morphological changes are associated with the induction of apoptosis and whether β-asarone suppresses apoptosis. DAPI staining and flow cytometry revealed that cells cultured under HG conditions showed a significant increase in apoptosis. However, the upward trend in the HG-mediated apoptosis rate was notably attenuated in the presence of β-asarone (Figure 2B–E). In addition, the cleavage of poly(ADP ribose) polymerase, a marker of apoptosis [27], in HG-treated cells was attenuated by pre-treatment with β-asarone (Figure 2F,G). Furthermore, the level of 8-OHdG, a marker of oxidative DNA damage [33], was significantly higher in HG-stimulated cells than in the control cells (Figure 2H). Furthermore, increased comet tail formation, which indicates broken DNA strands [34], was clearly observed in HG-treated cells (Figure 2I). Interestingly, β-asarone ameliorated the HG-induced DNA damage as indicated by reversed 8-OhdG levels and comet tail formation. These results indicate that β-asarone inhibits HG-induced apoptosis and DNA damage in ARPE-19 cells.

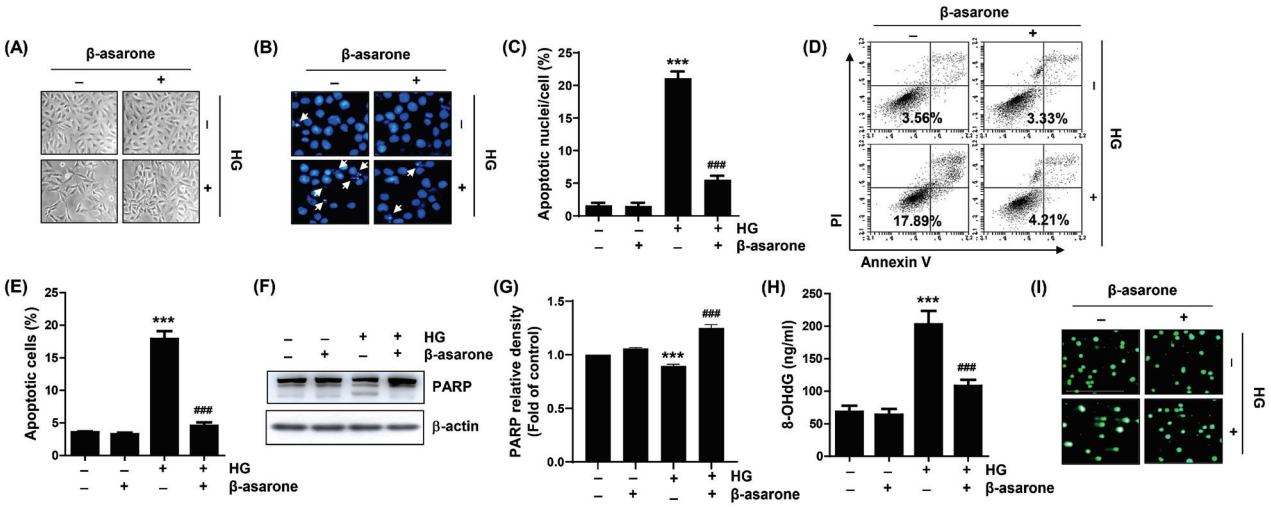

Figure 2. Inhibition of HG-induced apoptosis and DNA damage by β-asarone in ARPE-19 cells. Cells were treated with β-asarone (50 μM) for 1 h and cultured for an additional 48 h under HG (20 mM glucose) conditions. (**A**) Representative images of cell morphology changes as observed by using inverted microscope. (**B**,**C**) 4′,6-diamidino-2-phenylindole (DAPI) staining was performed to observe morphological changes in the nuclei by using fluorescence microscopy. Representative images of DAPI-stained nuclei (**B**) and quantification results of apoptotic nuclei (**C**). (**D**,**E**) Apoptosis was measured using flow cytometry after Annexin V-fluorescein isothiocyanate (FITC)/propidium iodide (PI) staining. Representative images of flow cytometry (**D**) and quantification results (**E**). (**F**,**G**) After the lysis of collected cells, equal amounts of protein from each cell lysate were loaded and blotted with poly(ADP ribose) polymerase (PARP) and β-actin antibodies. (**H**,**I**) DNA damage was assessed using the 8-hydro'y-2′-deoxyguanosine (8-OHdG) (**H**) and comet (**I**) assays. (**C**,**E**,**G**) Numerical values are represented as the mean ± SD of three independent experiments (*** $p < 0.001$ vs. control group; ### $p < 0.001$ vs. HG-treated group).

3.3. β-Asarone Decreases ROS Generation in HG-Treated ARPE-19 Cells

As decreased cell viability and the induction of cytotoxicity by HG stimulation were blocked not only by β-asarone but also by the ROS scavenger NAC, we investigated whether the beneficial effects of β-asarone on HG were related to the mitigation of oxidative stress in ARPE-19 cells. In both flow cytometry and fluorescence microscopy results using DCF-DA staining, which reflects the amount of cytosolic ROS generation, increased ROS levels were detected in cells cultured under HG conditions; however, pre-treatment with

β-asarone reduced the ROS levels by >90% compared to HG conditions (Figure 3A–D). In addition, as shown in Figure 3E, the GSH/GSSG ratio was significantly reduced when cells were challenged with HG, but not when cells were treated with β-asarone alone. However, β-asarone prevented GSH depletion, indicating that β-asarone alleviates oxidative stress in ARPE-19 cells exposed to HG.

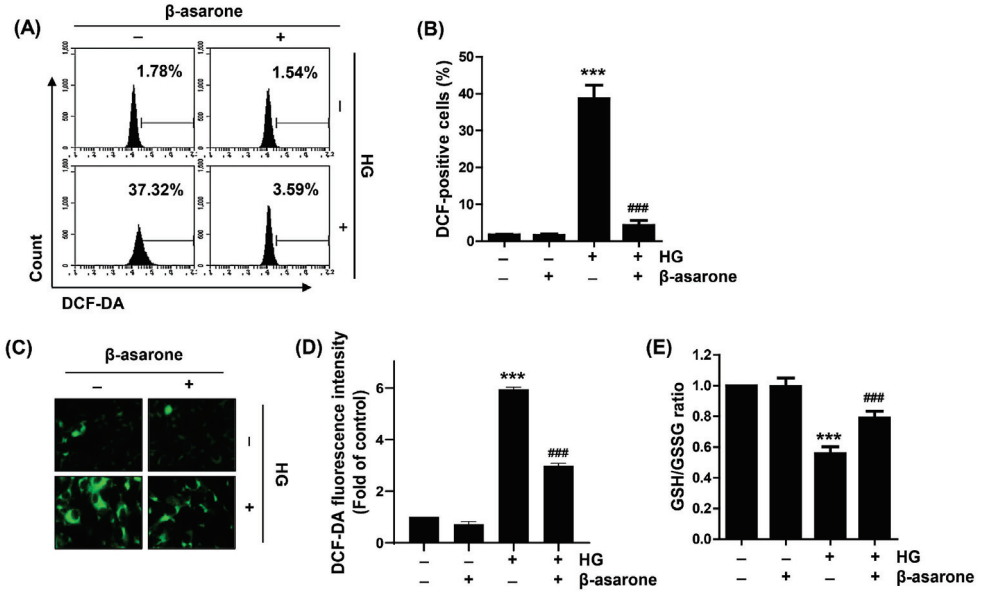

Figure 3. Suppression of HG-induced cytosolic reactive oxygen species (ROS) accumulation by β-asarone in ARPE-19 cells. (**A**–**D**) Cells pre-treated with β-asarone for 1 h were cultured in an HG medium for 1 h and stained with 5,6-carboxy-2′,7′-dichlorodihydrofluorescein diacetate (DCF-DA). (**A**,**B**) Representative images of flow cytometry (**A**) and quantification results (**B**). (**C**) Representative images (green) of cytosolic ROS levels visualized using fluorescence microscopy (200×). (**E**) Reduced glutathione/oxidized glutathione (GSH/GSSG) ratio was measured using a commercially available kit. (**B**,**D**,**E**) Numerical values are represented as the mean ± SD of three independent experiments (*** $p < 0.001$ vs. control group; ### $p < 0.001$ vs. HG-treated group).

3.4. β-Asarone Attenuates HG-induced Production of Mitochondrial Superoxide Radicals and Inactivation of MnSOD in ARPE-19 Cells

To investigate that mitochondria are the main source of ROS production in HG-treated ARPE-19 cells, mitochondrial superoxide levels were quantified using MitoSOX staining. Similar to the DCF-DA results, the levels of mitochondrial superoxide greatly increased in cells cultured under HG conditions, which was further confirmed by the increased MitoSOX fluorescence intensity observed using fluorescence microscopy (Figure 4A–D). However, β-asarone dramatically abrogated the HG-induced superoxide production. In addition, the expression and activity of MnSOD, a scavenger of mitochondrial superoxide radicals [35,36], were decreased by HG stimulation but were significantly restored in the presence of β-asarone (Figure 4E–G). These results suggest that β-asarone relieved oxidative stress by blocking the production of superoxide, a major ROS produced in the mitochondria, under HG conditions.

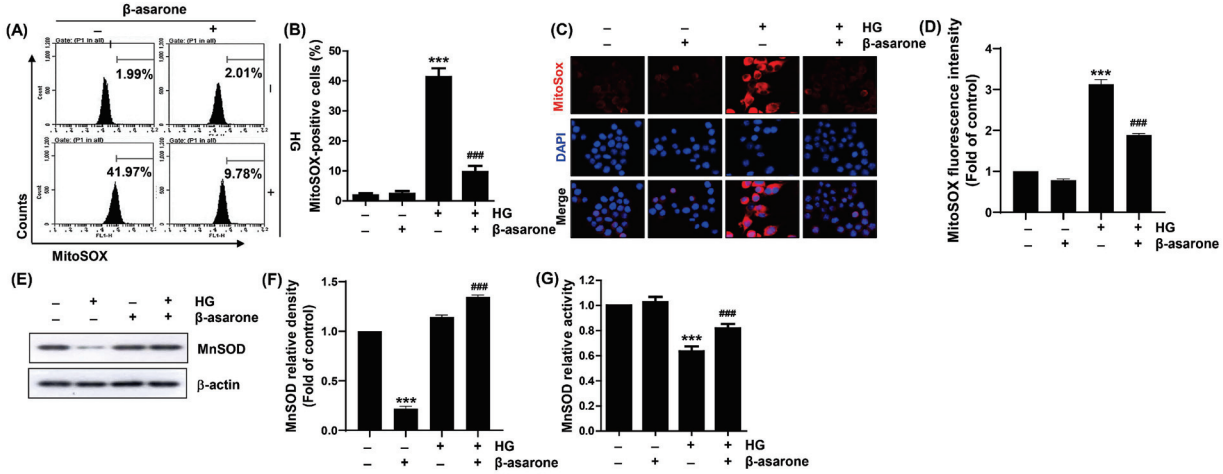

Figure 4. Blockade of HG-induced mitochondrial ROS accumulation by β-asarone in ARPE-19 cells. Cells pre-treated with β-asarone for 1 h were cultured in an HG medium for 1 h and stained with MitoSOX. (**A**,**B**) Representative images of flow cytometry (**A**) and quantification results (**B**). (**C**,**D**) Representative images of mitochondrial ROS levels (red) visualized using fluorescence microscopy (400×). Nuclei (blue) were stained with DAPI. (**E**,**F**) After the lysis of collected cells, equal amounts of protein from each cell lysate were loaded and blotted with manganese superoxide dismutase (MnSOD) and β-actin antibodies. (**G**) Activity of Mn-SOD was measured using a commercially available kit. (**B**,**D**,**F**,**G**) Numerical values are represented as the mean ± SD of three independent experiments (*** $p < 0.001$ vs. control group; ### $p < 0.001$ vs. HG-treated group).

3.5. β-Asarone Alleviates HG-Induced Inflammatory Response in ARPE-19 Cells

Next, we investigated the secretion of pro-inflammatory cytokines, such as IL-1β and IL-18, in the supernatants of ARPE-19 cells cultured under HG conditions in the presence or absence of β-asarone to explore the blocking effect of β-asarone on HG-induced inflammatory response. ELISA revealed that HG stimulation increased the inflammatory response as indicated by the enhanced levels of IL-1β and IL-18 in the cell supernatants (Figure 5A,B). Additionally, the protein expression levels of IL-1β and IL-18 were elevated under HG conditions (Figure 5C,D). However, after β-asarone intervention, the levels and protein expression of these inflammatory factors were significantly decreased compared to those in the HG group (Figure 5A–D), indicating that β-asarone counteracts HG-induced inflammation in ARPE-19 cells.

3.6. β-Asarone Mitigates NF-κB Signaling Activation in HG-Treated ARPE-19 Cells

As NF-κB plays a critical role in the transcription of inflammation-related factors [37,38], we verified whether the blockade of HG-induced inflammation by β-asarone is dependent on the NF-κB signaling pathway. According to the results of immunoblotting and immunofluorescence assays presented in Figure 5E–G, NF-κB protein levels were significantly increased in the nuclear fraction rather than in the cytoplasmic fraction of cells cultured under HG conditions. Moreover, p-NF-κB was preferentially expressed in the nuclei of HG-treated cells but not in cells treated with β-asarone alone. Additionally, the expression levels of IκB-α were downregulated in the cytoplasm. However, in the presence of β-asarone, the nuclear localization of HG-induced NF-κB as well as the expression levels of p-IκB-α and IκB-α were reduced to the control levels. These results indicate that β-asarone alleviates HG-induced NF-κB activation, thereby reducing the associated inflammatory response.

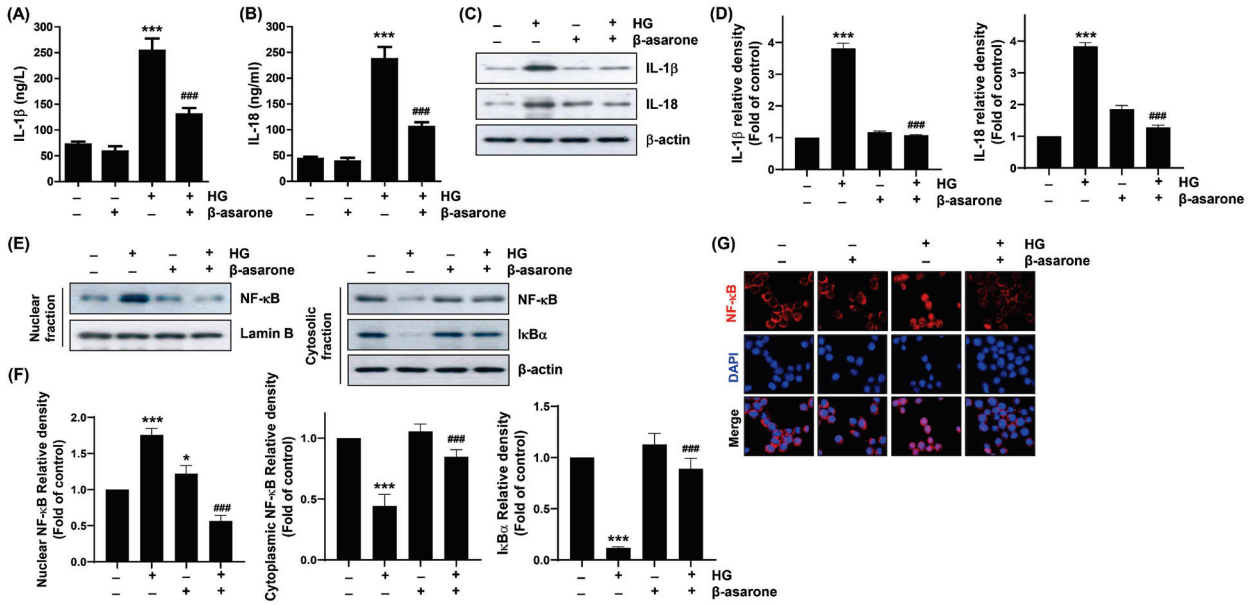

Figure 5. Attenuation of HG-induced cytokine production and nuclear factor-kappa B (NF-κB) activation by β-asarone in ARPE-19 cells. (**A**,**B**) Concentrations of interleukin (IL)-1β (**A**) and IL-18 (**B**) released in the supernatant of cells exposed to HG for 48 h in the presence or absence of β-asarone were measured using enzyme-linked immunosorbent assay (ELISA) kits. (**C**,**D**) Expression levels of IL-1β and IL-18 proteins were determined via Western blot analysis using cells cultured under the same conditions. (**E**–**G**) Cells pre-treated with β-asarone for 1 h were further cultured in an HG medium for another 1 h. (**E**,**F**) Nuclear and cytosolic fractions were used to detect the indicated proteins. (**G**) Cellular localization of p-NF-κB p65 (red) in cells cultured under the same experimental setting was observed using the immunofluorescence assay. Nuclei (blue) were counterstained with DAPI. (**A**,**B**,**D**,**F**) Numerical values are represented as the mean ± SD of three independent experiments (* $p < 0.05$, *** $p < 0.001$ vs. control group; ### $p < 0.001$ vs. HG-treated group).

3.7. β-Asarone Attenuates HG-Induced NLRP3 Inflammasome Activation in ARPE-19 Cells

NF-κB-induced NLRP3 inflammasome activation plays critical roles in the onset and progression of DR. NLRP3 inflammasome is a multiprotein complex that mediates the secretion of pro-inflammatory cytokines, including IL-1β and IL-18 [15,17]. As β-asarone attenuated HG-induced secretion of IL-1β and IL-18 and NF-κB activation, we further investigated whether these inhibitory effects contributed to the blocking of the NLRP3 inflammasome pathway. Immunoblotting revealed that the expression levels of thioredoxin (Trx)-interacting protein (TXNIP), an NLRP3 interacting molecule [9,11], and the NLRP3 inflammasome multiprotein complex molecules, ASC and caspase-1, were upregulated under HG conditions, whereas β-asarone reduced these levels similar to those in the control group (Figure 6A,B). To confirm these results, fluorescence and immunofluorescence assays were conducted to measure the intracellular caspase-1 activity and levels of NLRP3 and ASC. We found that caspase-1 activity and NLRP3 and ASC expression levels were notably enhanced under HG conditions but reduced by β-asarone to levels similar to those in the control (Figure 6C–G). These results suggest that β-asarone counteracts the activation of NLRP3 inflammasome under HG conditions in ARPE-19 cells.

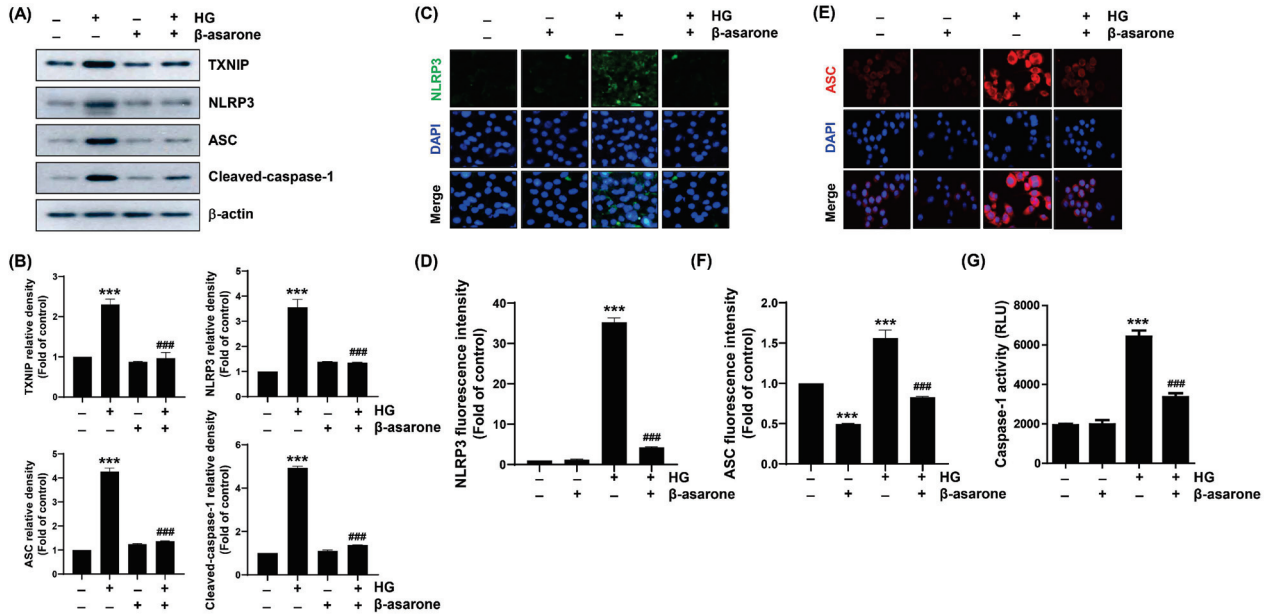

Figure 6. Suppression of HG-induced NOD-like receptor family pyrin domain-containing 3 (NLRP3) inflammasome activation by β-asarone in ARPE-19 cells. Cells pre-treated with β-asarone for 1 h were further cultured in an HG medium for 48 h, and Western blot analysis was conducted to determine the expression levels of the indicated proteins (**A**,**B**). (**C**–**F**) Cellular localization of NLRP3 (green) and apoptosis-associated speck-like protein containing a caspase-recruitment domain (ASC) (red) in cells cultured under same experimental setting was observed using the immunofluorescence assay. Nuclei (blue) were counterstained with DAPI. (**G**) Activity of caspase-1 was measured using a fluorescence assay kit. (**B**,**D**,**F**,**G**) Numerical values are represented as the mean ± SD of three independent experiments (*** $p < 0.001$ vs. control group; ### $p < 0.001$ vs. HG-treated group).

4. Discussion

Elevated glucose levels are a potent pathogenic feature of DR [39,40]. Excess ROS production due to hyperglycemia initiates oxidative stress and inflammatory responses, which are mechanisms involved in the pathogenesis of DR [3,7]. Antioxidants with anti-inflammatory effects exert inhibitory effects on the onset and progression of DR [41–43]. β-asarone, a type of volatile oil, exerts multiple pharmacological effects, including antioxidant and anti-inflammatory effects [19,20,44]. In addition to these pharmacological effects, β-asarone is also known for toxicological effects in hepatoma, mutagenic, and genotoxic action [20]. Even with toxicological effects of β-asarone, it demonstrates therapeutic properties by targeting various pharmacological molecular targets such as apoptotic pathway modulator [20]. In particular, the antioxidant activity of β-asarone is related to the quenching of ROS generation in various experimental systems, including Alzheimer's disease and diabetic encephalopathy models [23,45,46]. Chang and Teng [47] reported that β-asarone inhibits the production of inflammatory cytokines, including tumor necrosis factor-α (TNF-α), IL-1β, and IL-6, and induction of autophagy, while reducing apoptosis. The results of this study provide the first evidence that β-asarone suppresses NLRP3 inflammasome activation and consequent DNA damage and lytic cell death by reducing ROS production in RPE ARPE-19 cells under HG conditions.

In this study, ARPE-19 cells were treated with HG (20 mM) to mimic hyperglycemia and the ROS levels were measured. Both cytosolic and mitochondrial ROS levels were markedly increased in ARPE-19 cells, confirming that the hyperglycemic state was characterized by high oxidative stress. Similar to previous studies, the present results showed that culturing ARPE-19 cells with HG leads to apoptosis and DNA damage via ROS generation [48–51]. However, in the presence of β-asarone, the production of ROS and induction of apoptosis and DNA damage were significantly abolished in HG-treated ARPE-19 cells.

In particular, the expression and activity of MnSOD, which is an NF-κB-dependent antioxidant that plays a key role in scavenging mitochondrial superoxide [34,35], were decreased under HG conditions but recovered by β-asarone. This result implies that mitochondria are sources of ROS under HG conditions and potentially MnSOD may partially contribute to reduction in oxidative stress by β-asarone. In addition, β-asarone blocked the activation of NF-κB by HG and decreased the production and expression of IL-1β and IL-18, which are pro-inflammatory cytokines associated with NLRP3 inflammasome activation [15,16]. β-asarone inhibits HG-induced NLRP3 inflammasome activation in a myocardial I/R model [23]. These results imply that β-asarone protects ARPE-19 cells from HG-mediated oxidative stress, inflammation, and apoptosis via the regulation of NF-κB-related pathways.

NLRP3 inflammasome plays an important role in the pathogenesis of diabetes and its representative complication, DR [10,11,52]. Singh et al. [53] showed that the blockade of TXNIP activity, which is strongly induced by diabetes and inhibits the antioxidant function of Trx, prevents or slows down the progression of DR by normalizing mitophagic flux and NLRP3 inflammasome activation. This suggests the involvement of the TXNIP–Trx redox pathway in the dysfunction of RPE cells in retinal neurodegenerative diseases, such as DR [54]. Unlike apoptosis, lytic cell death is a programmed inflammatory cell death induced by the activation of caspase-1, which plays a key role in the release of IL-1β and IL-18 [12,52]. NF-κB priming signals for the transcriptional activation of NLRP3, pro-IL-1β, and pro-IL-18 are required for the activation of the NLRP3 inflammasome. Caspase-1 activation following the assembly of the NLRP3 inflammasome complex leads to the cleavage of pro-IL-1β and pro-IL-18 to IL-1β and IL-18, respectively, and the induction of lytic cell death [15,17]. Gan et al. [55] reported that retinal pericytes exposed to hyperglycemic conditions are lost via NLRP3–caspase-1-mediated lytic cell death and that lytic cell death by NLRP3 inflammasome activation is a key process in triggering DR pathogenesis [10,11,52]. The results of this study indicate that β-asarone attenuates HG-stimulated NLRP3 inflammasome-mediated lytic cell death and inactivates NF-κB in ARPE-19 cells, indicating its potential to treat hyperglycemia-induced DR.

Taken together, our results revealed that β-asarone inhibits the inflammatory response and oxidative stress, the two major steps in the vicious cycle of DR. Moreover, the attenuation of lytic cell death by β-asarone in HG-treated RPE ARPE-19 cells may be due to the inactivation of NF-κB and NLRP3 inflammasomes following oxidative stress relaxation (Figure 7). These results indicate that β-asarone exhibits therapeutic potential for hyperglycemia-induced DR. However, the possible involvement of other pathways in the inhibition of NF-κB and NLRP3 inflammasome requires further evaluation via animal experiments.

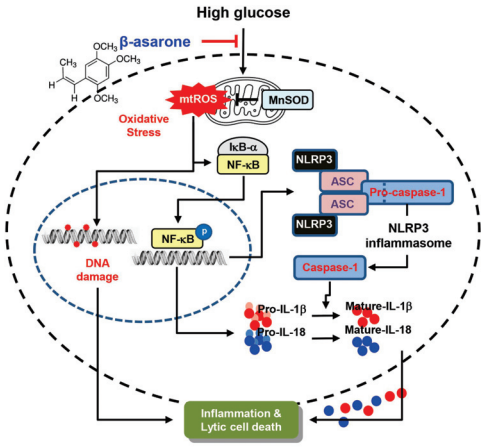

Figure 7. Schematic diagram of the inhibitory effects of β-asarone on mitochondrial ROS-mediated activation of NF-κB/NLRP3 signaling, resulting in the alleviation of inflammation in hyperglycemic RPE cells.

5. Conclusions

In conclusion, this study demonstrated that β-asarone counteracts HG-induced lytic cell death and DNA damage by reducing the oxidative stress and inflammatory responses in RPE cells. These protective effects may be attributed to its ability to suppress NLRP3 inflammasome-mediated lytic cell death. Our findings suggest β-asarone as a promising preventive and therapeutic agent for hyperglycemia-induced DR.

Author Contributions: Conceptualization, C.P. and Y.H.C.; methodology, C.P., H.-J.C. and H.H.; software, E.B. and D.-H.K.; validation, H.H., H.-J.C., S.H.H. and J.S.N.; formal analysis, E.B. and K.S.S.; investigation, C.P., H.H. and H.-J.C.; resources, S.H.H., K.S.S., J.S.N. and D.-H.K.; data curation, C.P., H.-J.C. and D.-H.K.; writing—original draft preparation, C.P.; writing—review and editing, Y.H.C.; visualization, C.P., G.-Y.K. and E.B.; supervision, Y.H.C.; project administration, Y.H.C.; funding acquisition, Y.H.C. All authors have read and agreed to the published version of the manuscript.

Funding: This research was funded by Basic Science Research Program through the National Research Foundation of Korea (NRF) grant funded by the Korea government (2021R1A2C2009549).

Institutional Review Board Statement: Not applicable.

Data Availability Statement: All of the data is contained within the article.

Conflicts of Interest: The authors declare no conflict of interest. Each author of this study further declares no relationships with the companies or manufacturers who will benefit from the results of the present study.

References

1. Cheng, Y.; Ren, T.; Wang, N. Biomechanical homeostasis in ocular diseases: A mini-review. *Front. Public Health* **2023**, *11*, 1106728. [CrossRef] [PubMed]
2. Zhou, Z.; Xu, S.; Jiang, L.; Tan, Z.; Wang, J. A systematic pan-cancer analysis of CASP3 as a potential target for immunotherapy. *Front. Mol. Biosci.* **2022**, *9*, 776808. [CrossRef] [PubMed]
3. Wang, J.; Li, M.; Geng, Z.; Khattak, S.; Ji, X.; Wu, D.; Dang, Y. Role of oxidative stress in retinal disease and the early intervention strategies: A review. *Oxid. Med. Cell. Longev.* **2022**, *2022*, 7836828. [CrossRef] [PubMed]
4. Dammak, A.; Huete-Toral, F.; Carpena-Torres, C.; Martin-Gil, A.; Pastrana, C.; Carracedo, G. From oxidative stress to inflammation in the posterior ocular diseases: Diagnosis and treatment. *Pharmaceutics* **2021**, *13*, 1376. [CrossRef] [PubMed]
5. Kang, Q.; Yang, C. Oxidative stress and diabetic retinopathy: Molecular mechanisms, pathogenetic role and therapeutic implications. *Redox Biol.* **2020**, *37*, 101799. [CrossRef] [PubMed]
6. Li, X.; Fang, P.; Mai, J.; Choi, E.T.; Wang, H.; Yang, X.F. Targeting mitochondrial reactive oxygen species as novel therapy for inflammatory diseases and cancers. *J. Hematol. Oncol.* **2013**, *6*, 19. [CrossRef]
7. Patergnani, S.; Bouhamida, E.; Leo, S.; Pinton, P.; Rimessi, A. Mitochondrial oxidative stress and "Mito-Inflammation": Actors in the diseases. *Biomedicines* **2021**, *9*, 216. [CrossRef]
8. Naik, E.; Dixit, V.M. Mitochondrial reactive oxygen species drive proinflammatory cytokine production. *J. Exp. Med.* **2011**, *208*, 417–420. [CrossRef]
9. Kuo, C.Y.; Maran, J.J.; Jamieson, E.G.; Rupenthal, I.D.; Murphy, R.; Mugisho, O.O. Characterization of NLRP3 inflammasome activation in the onset of diabetic retinopathy. *Int. J. Mol. Sci.* **2022**, *23*, 14471. [CrossRef]
10. Zhao, M.; Li, S.; Matsubara, J.A. Targeting pyroptotic cell death pathways in retinal disease. *Front. Med.* **2022**, *8*, 802063. [CrossRef]
11. Al Mamun, A.; Mimi, A.A.; Zaeem, M.; Wu, Y.; Monalisa, I.; Akter, A.; Munir, F.; Xiao, J. Role of pyroptosis in diabetic retinopathy and its therapeutic implications. *Eur. J. Pharmacol.* **2021**, *904*, 174166. [CrossRef]
12. Xiaodong, L.; Xuejun, X. GSDMD-mediated pyroptosis in retinal vascular inflammatory diseases: A review. *Int. Ophthalmol.* **2023**, *43*, 1405–1411. [CrossRef] [PubMed]
13. Lim, R.R.; Wieser, M.E.; Ganga, R.R.; Barathi, V.A.; Lakshminarayanan, R.; Mohan, R.R.; Hainsworth, D.P.; Chaurasia, S.S. NOD-like receptors in the eye: Uncovering its role in diabetic retinopathy. *Int. J. Mol. Sci.* **2020**, *21*, 899. [CrossRef]
14. Chen, H.; Zhang, X.; Liao, N.; Mi, L.; Peng, Y.; Liu, B.; Zhang, S.; Wen, F. Enhanced expression of NLRP3 inflammasome-related inflammation in diabetic retinopathy. *Invest. Ophthalmol. Vis. Sci.* **2018**, *59*, 978–985. [CrossRef]
15. Paerewijck, O.; Lamkanfi, M. The human inflammasomes. *Mol. Asp. Med.* **2022**, *88*, 101100. [CrossRef] [PubMed]
16. Duez, H.; Pourcet, B. Nuclear receptors in the control of the NLRP3 inflammasome pathway. *Front. Endocrinol.* **2021**, *12*, 630536. [CrossRef] [PubMed]
17. Mathur, A.; Hayward, J.A.; Man, S.M. Molecular mechanisms of inflammasome signaling. *J. Leukoc. Biol.* **2018**, *103*, 233–257. [CrossRef]
18. Mandell, J.T.; de Rivero Vaccari, J.P.; Sabater, A.L.; Galor, A. The inflammasome pathway: A key player in ocular surface and anterior segment diseases. *Surv. Ophthalmol.* **2023**, *68*, 280–289. [CrossRef]

19. Wen, J.; Yang, Y.; Hao, J. *Acori tatarinowii* Rhizoma: A comprehensive review of its chemical composition, pharmacology, pharmacokinetics and toxicity. *Front. Pharmacol.* **2023**, *14*, 1090526. [CrossRef]
20. Chellian, R.; Pandy, V.; Mohamed, Z. Pharmacology and toxicology of α- and β-asarone: A review of preclinical evidence. *Phytomedicine* **2017**, *32*, 41–58. [CrossRef]
21. Lim, H.W.; Kumar, H.; Kim, B.W.; More, S.V.; Kim, I.W.; Park, J.I.; Park, S.Y.; Kim, S.K.; Choi, D.K. β-asarone (cis-2,4,5-trimethoxy-1-allyl phenyl), attenuates pro-inflammatory mediators by inhibiting NF-κB signaling and the JNK pathway in LPS activated BV-2 microglia cells. *Food Chem. Toxicol.* **2014**, *72*, 265–272. [CrossRef] [PubMed]
22. Hermes, L.; Haupenthal, S.; Uebel, T.; Esselen, M. DNA double strand break repair as cellular response to genotoxic asarone isomers considering phase I metabolism. *Food Chem. Toxicol.* **2020**, *142*, 111484. [CrossRef] [PubMed]
23. Cai, J.; Cai, M.; Xia, W.; Jiang, L.; Song, H.; Chen, X. Explore the mechanism of β-asarone on improving cognitive dysfunction in rats with diabetic encephalopathy. *J. Alzheimers Dis. Rep.* **2022**, *6*, 195–206. [CrossRef]
24. Xiao, B.; Huang, X.; Wang, Q.; Wu, Y. β-asarone alleviates myocardial ischemia-reperfusion injury by inhibiting inflammatory response and NLRP3 inflammasome mediated pyroptosis. *Biol. Pharm. Bull.* **2020**, *43*, 1046–1051. [CrossRef]
25. Hong, S.H.; Park, C.; Hwangbo, B.; Bang, E.J.; Kim, S.O.; Shim, J.H.; Park, S.H.; Lee, H.; Leem, S.H.; Kim, G.Y.; et al. Activation of heme oxygenase-1 is involved in the preventive effect of honokiol against oxidative damage in human retinal pigment epithelial cells. *Biotechnol. Bioprocess Eng.* **2022**, *27*, 975–986. [CrossRef]
26. Kim, C.; Ryu, S.H.; Choi, H.; Park, D.H.; Bae, J.S. The inhibitory functions of sparstolonin B against ambient fine particulate matter induced lung injury. *Biotechnol. Bioprocess Eng.* **2022**, *27*, 949–960. [CrossRef]
27. Choi, Y.H. Tacrolimus induces apoptosis in leukemia Jurkat cells through inactivation of the reactive oxygen species-dependent phosphoinositide-3-kinase/Akt signaling pathway. *Biotechnol. Bioprocess Eng.* **2022**, *27*, 183–192. [CrossRef]
28. di Vito, R.; Levorato, S.; Fatigoni, C.; Acito, M.; Sancineto, L.; Traina, G.; Villarini, M.; Santi, C.; Moretti, M. *In vitro* toxicological assessment of PhSeZnCl in human liver cells. *Toxicol. Res.* **2023**, *39*, 105–114. [CrossRef]
29. Park, C.; Lee, H.; Kim, S.O.; Lee, E.W.; Lee, H.T.; Kwon, H.J.; Kim, B.W.; Kim, G.Y.; Kim, M.R.; Choi, Y.H. The preventive effect of Mori Ramulus on oxidative stress-induced cellular damage in skeletal L6 myoblasts through Nrf2-mediated activation of HO-1. *Toxicol. Res.* **2022**, *39*, 25–36. [CrossRef]
30. Kim, M.Y.; Bang, E.; Hwangbo, H.; Ji, S.Y.; Kim, D.H.; Lee, H.; Park, C.; Hong, S.H.; Kim, G.Y.; Choi, Y.H. Diallyl trisulfide inhibits monosodium urate-induced NLRP3 inflammasome activation via NOX3/4-dependent mitochondrial oxidative stress in RAW 264.7 and bone marrow-derived macrophages. *Phytomedicine* **2023**, *112*, 154705. [CrossRef]
31. Hwangbo, H.; Kim, M.Y.; Ji, S.Y.; Kim, S.Y.; Lee, H.; Kim, G.Y.; Park, C.; Keum, Y.S.; Hong, S.H.; Cheong, J.; et al. Auranofin attenuates non-alcoholic fatty liver disease by suppressing lipid accumulation and NLRP3 inflammasome-mediated hepatic inflammation in vivo and in vitro. *Antioxidants* **2020**, *9*, 1040. [CrossRef] [PubMed]
32. Mukherjee, S.; Choi, M.; Yun, J.W. Trans-anethole induces thermogenesis *via* activating SERCA/SLN axis in C2C12 muscle cells. *Biotechnol. Bioprocess Eng.* **2022**, *27*, 938–948. [CrossRef]
33. AbuArrah, M.; Yuli Setianto, B.; Faisal, A.; Hamim Sadewa, A. 8-Hydroxy-2-deoxyguanosine as oxidative DNA damage biomarker of medical ionizing radiation: A scoping review. *J. Biomed. Phys. Eng.* **2021**, *11*, 389–402. [CrossRef] [PubMed]
34. Møller, P.; Stopper, H.; Collins, A.R. Measurement of DNA damage with the comet assay in high-prevalence diseases: Current status and future directions. *Mutagenesis* **2020**, *35*, 5–18. [CrossRef] [PubMed]
35. Liu, M.; Sun, X.; Chen, B.; Dai, R.; Xi, Z.; Xu, H. Insights into manganese superoxide dismutase and human diseases. *Int. J. Mol. Sci.* **2022**, *23*, 15893. [CrossRef]
36. Indo, H.P.; Hawkins, C.L.; Nakanishi, I.; Matsumoto, K.I.; Matsui, H.; Suenaga, S.; Davies, M.J.; St Clair, D.K.; Ozawa, T.; Majima, H.J. Role of mitochondrial reactive oxygen species in the activation of cellular signals, molecules, and function. *Handb. Exp. Pharmacol.* **2017**, *240*, 439–456.
37. Mussbacher, M.; Derler, M.; Basílio, J.; Schmid, J.A. NF-κB in monocytes and macrophages—An inflammatory master regulator in multitalented immune cells. *Front. Immunol.* **2023**, *14*, 1134661. [CrossRef]
38. Capece, D.; Verzella, D.; Flati, I.; Arboretto, P.; Cornice, J.; Franzoso, G. NF-κB: Blending metabolism, immunity, and inflammation. *Trends Immunol.* **2022**, *43*, 757–775. [CrossRef]
39. Kaur, G.; Harris, N.R. Endothelial glycocalyx in retina, hyperglycemia, and diabetic retinopathy. *Am. J. Physiol. Cell. Physiol.* **2023**, *324*, C1061–C1077. [CrossRef]
40. Rodríguez, M.L.; Millán, I.; Ortega, Á.L. Cellular targets in diabetic retinopathy therapy. *World J. Diabetes* **2021**, *12*, 1442–1462. [CrossRef]
41. Jin, Y.; Arroo, R. The protective effects of flavonoids and carotenoids against diabetic complications-A review of in vivo evidence. *Front. Nutr.* **2023**, *10*, 1020950. [CrossRef] [PubMed]
42. Khazeei Tabari, M.A.; Mirjalili, R.; Khoshhal, H.; Shokouh, E.; Khandan, M.; Hasheminasabgorji, E.; Hafezi-Moghadam, A.; Bagheri, A. Nature against diabetic retinopathy: A review on antiangiogenic, antioxidant, and anti-Inflammatory phytochemicals. *Evid. Based Complement. Alternat. Med.* **2022**, *2022*, 4708527. [CrossRef] [PubMed]
43. Matos, A.L.; Bruno, D.F.; Ambrósio, A.F.; Santos, P.F. Benefits of flavonoids in diabetic retinopathy. *Nutrients* **2020**, *12*, 3169. [CrossRef]

44. Du, X.Y.; Cao, Y.S.; Yang, J.; Guo, L.C.; Zhang, T.; Yuan, Q.; Chen, X.; Hu, L.M. Preclinical evidence and possible mechanisms of β-asarone for rats and mice with Alzheimer's disease: A systematic review and meta-analysis. *Front. Pharmacol.* **2022**, *13*, 956746. [CrossRef] [PubMed]
45. Meng, M.; Zhang, L.; Ai, D.; Wu, H.; Peng, W. β-asarone ameliorates β-amyloid-induced neurotoxicity in PC12 cells by activating P13K/Akt/Nrf2 signaling pathway. *Front. Pharmacol.* **2021**, *12*, 659955. [CrossRef]
46. Hei, X.; Xie, M.; Xu, J.; Li, J.; Liu, T. β-asarone exerts antioxidative effects on H_2O_2-stimulated PC12 cells by activating Nrf2/HO-1 pathway. *Neurochem. Res.* **2020**, *45*, 1953–1961. [CrossRef]
47. Chang, W.; Teng, J. b-asarone prevents Aβ25-35-induced inflammatory responses and autophagy in SH-SY5Y cells: Down expression Beclin-1, LC3B and up expression Bcl-2. *Int. J. Clin. Exp. Med.* **2015**, *8*, 20658–20663.
48. Daldal, H.; Nazıroğlu, M. Carvacrol protects the ARPE19 retinal pigment epithelial cells against high glucose-induced oxidative stress, apoptosis, and inflammation by suppressing the TRPM2 channel signaling pathways. *Graefes. Arch. Clin. Exp. Ophthalmol.* **2022**, *260*, 2567–2583. [CrossRef]
49. Li, M.; Tian, M.; Jiang, X.; Liu, Y.; Wang, Y.; Li, Y. Inhibition of galectin-3 ameliorates high-glucose-induced oxidative stress and inflammation in ARPE-19 cells. *Cutan. Ocul. Toxicol.* **2022**, *41*, 179–186. [CrossRef]
50. Chiang, Y.F.; Chen, H.Y.; Chang, Y.J.; Shih, Y.H.; Shieh, T.M.; Wang, K.L.; Hsia, S.M. Protective effects of fucoxanthin on high glucose- and 4-hydroxynonenal (4-HNE)-induced injury in human retinal pigment epithelial cells. *Antioxidants* **2020**, *9*, 1176. [CrossRef]
51. Tokarz, P.; Kaarniranta, K.; Blasiak, J. Inhibition of DNA methyltransferase or histone deacetylase protects retinal pigment epithelial cells from DNA damage induced by oxidative stress by the stimulation of antioxidant enzymes. *Eur. J. Pharmacol.* **2016**, *776*, 167–175. [CrossRef] [PubMed]
52. Zhang, Y.; Jiao, Y.; Li, X.; Gao, S.; Zhou, N.; Duan, J.; Zhang, M. Pyroptosis: A new insight into eye disease therapy. *Front. Pharmacol.* **2021**, *12*, 797110. [CrossRef] [PubMed]
53. Singh, L.P.; Devi, T.S.; Yumnamcha, T. The role of Txnip in mitophagy dysregulation and inflammasome activation in diabetic retinopathy: A new perspective. *JOJ Ophthalmol.* **2017**, *4*, 555643. [CrossRef] [PubMed]
54. Yumnamcha, T.; Devi, T.S.; Singh, L.P. Auranofin mediates mitochondrial dysregulation and inflammatory cell death in human retinal pigment epithelial cells: Implications of retinal neurodegenerative diseases. *Front. Neurosci.* **2019**, *13*, 1065. [CrossRef]
55. Gan, J.; Huang, M.; Lan, G.; Liu, L.; Xu, F. High glucose induces the loss of retinal pericytes partly via NLRP3-caspase-1-GSDMD-mediated pyroptosis. *Biomed. Res. Int.* **2020**, *2020*, 4510628. [CrossRef]

antioxidants

MDPI

Article

Intravitreal Injection of ZYAN1 Restored Autophagy and Alleviated Oxidative Stress in Degenerating Retina via the HIF-1α/BNIP3 Pathway

Xiao-Na Hao †, Na Zhao †, Jie-Min Huang, Si-Yu Li, Dong Wei, Ning Pu, Guang-Hua Peng * and Ye Tao *

Department of Physiology and Neurobiology, Laboratory of Visual Cell Differentiation and Regulation, School of Basic Medical Sciences, Zhengzhou University, 100 Science Avenue, Zhengzhou 450001, China; haoxn0126@163.com (X.-N.H.); zn0114@gs.zzu.edu.cn (N.Z.); huangjm1217@163.com (J.-M.H.); lsiyu@gs.zzu.edu.cn (S.-Y.L.); 202047000423@stu.zzu.edu.cn (D.W.); 202051081418@stu.zzu.edu.cn (N.P.)
* Correspondence: ghp@zzu.edu.cn (G.-H.P.); panghtoyezz@zzu.edu.cn (Y.T.)
† These authors contributed equally to this work.

Abstract: Mitochondrial autophagy plays a contributary role in the pathogenesis of retina degeneration (RD). ZYAN1 is a novel proline hydroxylase domain (PHD) inhibitor that can enhance the expression of hypoxia-inducible factor 1-alpha (HIF-1α). This study investigated whether ZYAN1 could alleviate progressive photoreceptor loss and oxidative damage in a pharmacologically induced RD model via the modulation of mitophagy. ZYAN1 was injected into the vitreous body of the RD model, and the retinal autophagy level was analyzed. The therapeutic effects of ZYAN1 were evaluated via a function examination, a morphological assay, in situ reactive oxygen species (ROS) detection, and an immunofluorescence assay. It was shown that the thickness of the outer nuclear layer (ONL) increased significantly, and visual function was efficiently preserved via ZYAN1 treatment. The mitochondria structure of photoreceptors was more complete in the ZYAN1-treated mice, and the number of autophagosomes also increased significantly. Membrane disc shedding and ROS overproduction were alleviated after ZYAN1 treatment, and the axonal cilia were more structurally intact. A Western blot analysis showed that the expression levels of the autophagy-related proteins LC3-B, Beclin-1, and ATG5 increased significantly after ZYAN1 treatment, while the expression of P62 was down-regulated. Moreover, the expression levels of HIF-1α and BNIP3 were up-regulated after ZYAN1 treatment. Therefore, an intravitreal injection of ZYAN1 can act as part of the pharmacologic strategy to modulate mitophagy and alleviate oxidative stress in RD. These findings enrich our knowledge of RD pathology and provide insights for the discovery of a therapeutic molecule.

Keywords: retina; oxidative damage; neurodegeneration; mitophagy; visual function

1. Introduction

Retinal degeneration (RD) is a group of blinding eye diseases caused by heredity, phototoxicity, aging, and other environmental factors. These diseases are characterized by the progressive loss of photoreceptors and visual impairments [1]. The entire retinal ecosystem consists of rod and cone photoreceptors, neuroglia cells, and the retinal pigment epithelium (RPE), which are extremely sensitive to genetic or metabolic changes [2]. RD imposes a significant health burden, as more than 18 million individuals are affected [3]. Thus far, several etiological factors have been shown to be implicated in the pathophysiological mechanism of RD, including oxidative stress, inflammation, and aging-related impairments [4,5]. Due to the disease's complex pathogenic background, the current existing therapeutic methods cannot completely arrest the photoreceptor death in RD. Autophagy plays a critical role in maintaining the homeostasis of photoreceptors. A reduced autophagy level can lead to the accumulation of damaged organelles; nonfunctional molecules; and toxic proteins, including lysosomal lipofuscin [6,7]. Autophagy acts as

an important cellular clearance system in which cells utilize complex lysosome clearance processes to degrade and eliminate intracellular components [8,9]. During this process, damaged metabolites and organelles are removed from the cytoplasm. In the retina, RPE cells have the typical autophagy ability to continuously engulf the detached membrane disk of the photoreceptors [10]. Mitochondria are key organelles responsible for modulating energy metabolism and aerobic respiration. They significantly participate in the overproduction of reactive oxygen species (ROS) when their own redox balance is impaired [11]. However, mitochondria can be attacked by deleterious ROS, as their membrane proteins and DNAs are easily accessible [12]. Upon damage, mitochondria release pro-apoptotic proteins, such as cytochrome c (Cytc), apoptosis-inducing factor (AIF), and endonuclease G [13,14]. Therefore, it is well accepted that mitochondrial damage marks the so-called "point of no return", meaning that cells with impaired mitochondria cannot survive for a long period of time [15].

Mitochondrial autophagy (mitophagy) acts as a selective degradation activity that can control the quality and quantity of mitochondria [16]. It has been shown that mitochondrial dysfunction, mitochondrial DNA (mt DNA) damage, and abnormal mitochondrial autophagy collectively contribute to RD pathology [17,18]. Therefore, modulating mitochondrial autophagy might be an effective strategy to maintain energy metabolism and inhibit ROS overproduction, thereby alleviating photoreceptor death [19–22].

Hypoxia-inducible factor (HIF) acts as a key transcription factor in the adaptive response to hypoxic environments [15]. HIF can reduce oxygen consumption in mitochondria by inhibiting the conversion of pyruvate to acetyl-CoA. It can also suppress mitochondrial biogenesis and activate mitochondrial autophagy [23]. Proline hydroxylase domain (PHD) is the most important protease that degrades HIF. HIF levels increase significantly when PHD activity is suppressed [24,25]. Therefore, PHD inhibitors may act as promising candidates for preventing metabolic stress [26]. Several lines of evidence lend support to the safety and therapeutic benefits of PHD inhibition in neurological disease [27–30]. ZYAN1 is a novel PHD inhibitor with strong permeability and tissue specificity. Pioneering reports have demonstrated that ZYAN1 analogs can enhance HIF-1α expression and consequently protect brain neurons from ischemic stroke [28,29]. However, whether ZYAN1 can modulate the HIF-1α expression in degenerating retinas remains an enigma.

Systemically administered sodium iodate ($NaIO_3$) rapidly moves to the retina and selectively destroys RPE cells, leading to geographic atrophy, lipofuscin deposition, and progressive photoreceptor death [31–33]. Thus far, the $NaIO_3$-induced RD model has been extensively used to study the pathology of and develop therapies for RD [34,35]. In this paper, we study the ZYAN1-induced effects on the photoreceptor survival and visual function in the RD model. We show that an intravitreal injection of ZYAN1 can enhance autophagy levels, reduce ROS production, and protect photoreceptors via the HIF-1α/BNIP3 signaling pathway. These findings may shed light on the discovery of a therapeutic molecule for RD.

2. Materials and Methods

2.1. Animals and Pharmacological Agents

C57BL/6J mice (aged 6–8 weeks) were fed a normal diet at a temperature ranging from 21 to 25 °C, humidity ranging between 40 and 60%, and a light cycle of 24 h (8:00–20:00 light). The protocol of animal use was in accordance with the ARVO guidelines for ophthalmic and visual research. All animal experimental processes were approved by the Animal Ethics Review Committee of Zhengzhou University. $NaIO_3$ (Sigma, 7681-55-2, Saint Louis, MO, USA) was stored at −20 °C and dissolved in phosphate-buffered saline (PBS) immediately before use. The mice were given a single intraperitoneal injection of $NaIO_3$ solution at a dose of 60 mg/kg to induce RD. ZYAN1 (ChemeGen, C104783, Los Angeles, CA, USA) was firstly dissolved in DMSO and then injected into the vitreous using a 30 G microliter syringe (Hamilton Company, Model 701, Reno, NV, USA). All the experimental animals were randomly divided into 5 groups: (1) a normal control group; (2) an RD

group: C57BL/6J mice were intraperitoneally injected with 60 mg/kg $NaIO_3$ to establish the RD model; (3) an RD + ZYAN1 group: RD model received an intravitreal injection of 3 µL ZYAN1 (3.57 ng/µL); (4) an RD + vehicle group: RD model received an intravitreal injection of the same volume of DMSO; and (5) an RD + ZYAN1 + 3MA group: RD model received the ZYAN1 treatment and an intraperitoneal injection of 3-Methyladenine (3MA, at a dose of 30 mg/kg). The mice were sacrificed at different time points to harvest eye tissue for further analysis. Figure 1 is a schematic illustration of the experimental protocols.

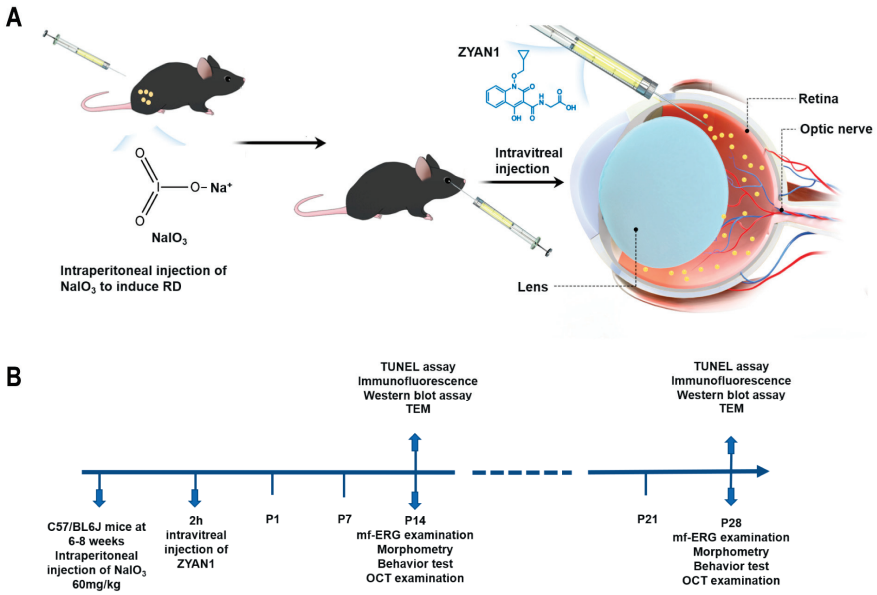

Figure 1. A schematic illustration of experimental protocols. (**A**) Intraperitoneal injection of $NaIO_3$ to induce RD model, and injection of ZYAN1 was intravitreally delivered in the eyes of the RD model. (**B**) ZYAN1-administered mice were then subjected to a series of morphologic, functional, and mechanism analyses.

2.2. Light/Dark Transition Behavior Test

Light/dark boxes (TopScan, CleverSys, Inc., Reston, VA, USA) were separated by a partition with a small hole underneath for the mouse to move through. A researcher adjusted the program settings of the computer's topscan version 3.0 software. The monitoring device recorded the number of times that the mouse shuttled between the dark/light box and the time that they stayed in the dark box. After each test, the box was disinfected with the 75% alcohol.

2.3. Open-Field Behavior Test

The bottom surface of the open-field device (TopScan, CleverSys, Inc., Reston, VA, USA) was a square with the size of 40 cm × 40 cm. The surrounding environment was kept quiet to reduce possible influences on the mice. The mouse was placed in the middle of an open-field setup with a video detection system connected to a computer analysis system. The system synchronized and automatically recorded the autonomous activity of the mouse in the central and peripheral regions within a period of 10 min. GraphPad Prism Version 7.0 software (Graph Pad software, San Diego, CA, USA) was used to statistically analyze the total distance of mouse activity and the time spent in the central or periphery area.

2.4. Multifocal Electroretinography (mf-ERG) Examination

The mice were anesthetized via an intraperitoneal injection of 5% chloral hydrate (0.08 mL/10 g). Their eyes were dilated with compound tropicamide eye drops. Carbomer ophthalmic gel was used to prevent corneal dryness. Regional retinal function was measured using an image-guided mf-ERG system [36] (RETIscan, Roland Consult, Wiesbaden,

Germany). RETIscan uses a confocal scanning laser ophthalmoscope (cSLO) to track the retinal region of interest when a stimulus is projected from a digital light processor (DLP). The mouse was positioned 1 to 2 mm in front of the cSLO device with a built-in light source for stimulus projection. A 3 mm gold ring was placed on the cornea to serve as a recording electrode. Meanwhile, a pair of subcutaneous silver needle electrodes served as reference and ground electrodes. The data obtained through the electrode were processed via the instrument's supporting system to obtain digital signals and generate Excel tables. A total of 19 hexagonal stimuli were used to analyze the mean amplitude densities of the N-1 and P-1 waves corresponding to each ring [37].

2.5. Optical Coherence Tomography (OCT) and Fundus Photography

OCT (Heidelberg Engineering, Carlsbad, CA, USA) and fundus photography were used for in vivo retinal imaging. The mice were anaesthetized via an intraperitoneal injection of 5% chloral hydrate (0.08 mL/10 g). Tropicamide eye drops were used to dilate the eyes, and carbomer gel was used to prevent corneal dryness and cataracts. The mice were placed on a special small animal testing table in front of a corneal contact probe. The pupil of the mouse was aligned with the OCT probe, and the light angle was adjusted to obtain a clear retinal image. A circular scan was performed with the focus centered on the optic nerve papilla. The fundus photographs and OCT images were simultaneously captured on the exact retinal locus in a 30° circle surrounding the optic nerve head. After examination, the mouse was placed on a 37 °C thermal insulation blanket and resuscitated.

2.6. Hematoxylin and Eosin (H&E) Staining

Eyeballs were immediately removed and immersed in a fixation fluid. The cornea, lens, and iris tissues were removed under a stereo-microscope (Olympus, SZ61, Manila, Philippines). The retained optic cup was embedded in paraffin wax (SAKURA, TEC 5 EM JC-2, Tokyo, Japan) after conventional gradient alcohol dehydration, xylene clarity, and wax immersion (SAKURA, VIP-5-J R-JC2, Tokyo, Japan). Paraffin-embedded tissue was cut into 4 μm thick sections using a microtome (YAMATO, RX-860, Tokyo, Japan). Retinal sections were baked at 65 °C for 60 min, dewaxed with xylene, hydrated with gradient alcohol, soaked in pure water for 5 min, stained with hematoxylin for 20 s, and sealed with neutral resin. A fluorescence microscope (Olympus, BX53, Tokyo, Japan) was used to capture the retina images with a 4× or 20× objective lens. The outer nuclear layer (ONL) thickness in each image was measured with ImageJ Version 1.8.0 software (National Institutes of Health, Bethesda, MD, USA).

2.7. In Situ ROS Detection

Eyecups were harvested and embedded in an optimal cutting temperature compound (Tissue-Tek, Sakura, Torrance, CA, USA). Frozen sections were cut vertically into 6 μm thick sections using a Leica CM1900 cryostat (Leica, Wetzlar, Germany). ROS production was evaluated via dihydroethidium (DHE) (DHE, BBoxiProbe, BB-470516, China) staining. Briefly, a DHE activated oxygen fluorescence probe was diluted with pure water according to the number of samples, and a dye probe working solution was prepared. Each retinal section was incubated with DHE for 30 min at 37 °C and then rinsed three times with PBS for 5 min. Then, the retinal sections were photographed with a fluorescence microscope at 40× magnification and quantified via ImageJ Version 1.8.0 software.

2.8. Transmission Electron Microscope (TEM) Examination

Retinal tissue was peeled off under the stereo-microscope (Olympus, SZ61, Tokyo, Japan) and then quickly cut into small patches at a size of 1 mm^3. The retinal patches were fixed in an electron microscope fixation solution (2.5% glutaraldehyde). Subsequently, the retinal tissue was washed with 0.1 M phosphate buffer PB (PH7.4) three time, and then fixed with 1% OsO4 at room temperature for 2 h. The retinal tissue was put in ethanol with a density gradient for upward dehydration. After being dehydrated with 100% acetone

twice (15 min each time), the embedded tissue was polymerized in a 60 °C oven for 48 h, and a resin block was used for slicing. After being stained with citric acid, the sections were sent for TEM photography (Hitach, HT7800/HT7700, Tokyo, Japan).

2.9. Immunohistochemistry Assay

Experimental animals were sacrificed via cervical dislocation. Their eyeballs were enucleated, and the anterior segments were removed. The specimen was fixed in 4% paraformaldehyde for 2 h. Then, the specimen was dehydrated in a 30% sucrose solution overnight at 4 °C. Eyecups were embedded in optimal cutting temperature compounds (Tissue-Tek, Sakura, Torrance, CA, USA), and they were cut vertically into 6 μm thick sections using a Leica CM1900 cryothermostat (Leica, Wetzlar, Germany). Twenty slices were collected from each eyeball, and six were randomly selected for staining. Retinal sections were washed with PBS at room temperature. After immunohistochemical circles were drawn, sections were penetrated with 0.1% Triton X-100 for 20 min and then incubated with a blocking solution (3% BSA in PBS containing 0.1% Triton X-100) for 30 min at 37 °C. Then, they were incubated with primary antibodies, such as the autophagy markers rabbit anti-LC3B (Cell Signaling Technology, Danvers, MA, USA, 83506, 1:100), GFAP (Sigma, G3893, 1:200), and IBA1 (Abcam, Cambridge, UK, AB178847, 1:100), overnight at 4 °C. Retinal sections were rinsed three times with PBS and incubated with a secondary antibody (Alexa Fluor 488: Abcam, ab6785, ab150077) at room temperature for 1 h. The secondary antibodies were then washed with PBS, and the sections were sealed with an anti-fluorescence quencher containing DAPI (Invitrogen, P36971, Carlsbad, CA, USA). A clear visual field photo was taken on both sides of the optic nerve using a 40-fold mirror., The morphological indicators were analyzed via ImageJ software or GraphPad Prism version 7.0 software.

2.10. Terminal Deoxynucleotidyl Transferase Biotin-dUTP Nick End Labeling (TUNEL) Assay

Cell apoptosis was evaluated via an in situ cell death detection TUNEL kit (Roche, 11684817910, Mannheim, Germany). Frozen sections were washed three times with PBS for 5 min and then incubated with the TUNEL reaction mixture (TDT enzyme: fluorescent labeling solution = 1:9) for 1 h at 37 °C. Then, the retinal sections were incubated with 10 μL DAPI for 3 min at room temperature, sealed with anti-fluorescence quenching solution, and were photographed using the fluorescence microscope.

2.11. Western Blot Assay

Retinal tissue was placed in a solution containing RIPA lysate, a phosphatase inhibitor. After being centrifuged at 1800 r for 60 s, the specimens were left on ice for 10 min. The concentration of the extracted protein was determined using a BCA protein concentration assay kit (Beyotime, P0010, China). Then, the samples were adjusted to the same protein concentration (1 μg/μL) and denatured. Next, 10 μL of each sample containing an equal amount of protein was used for electrophoresis. The protein was transferred to a polyvinylidene difluoride (PVDF) membrane (Millipore, Billerica, MA, USA) in a transfer buffer. After blocking with 5% non-fat dry milk at room temperature for 2 h, the PVDF membranes were washed with Tris-buffered saline containing 0.1% Tween-20 (TBST) three times and incubated overnight at 4 °C with different primary antibodies, namely, HIF-1α (Cell signaling technology, 36169, 1:1000, USA), BNIP3 (Cell signaling technology, 3769, 1:1000, USA), LC3-B (Cell signaling technology, 83506, 1:1000, USA), ATG5 (Cell signaling technology, 12994T, 1:1000, USA), P62 (Abcam, ab109012, 1:10,000, UK), Beclin-1 (Cell signaling technology, 3738, 1:1000, USA), and GAPDH (glyceraldehyde 3-phosphate dehydrogenase) (Abcam, ab181602, 1:10,000, UK), overnight at 4 °C. After washing, the PVDF membrane was incubated with a goat anti-mouse IgG secondary antibody (Abcam, ab6789, 1:10,000, UK) or goat anti-rabbit IgG secondary antibody (Abcam, ab6721, 1:20,000, UK) at room temperature for 2 h. After three washes with TBST, ECL droplets were added

to the PVDF membrane to evenly distribute its entire surface, and then it was transferred into a gel imaging system for photographing.

2.12. Statistical Analysis

All data are expressed as mean ± standard deviation (SD). They were statistically analyzed via a one-way ANOVA test using GraphPad Prism version 7.0 (Graph Pad software, San Diego, CA, USA). A p-value < 0.05 was considered statistically significant.

3. Results

3.1. Altered Autophagy Status in RD Model

In the RD model, the retinal morphology was damaged profoundly over time (Figure 2A). Initially, at P1, the retinal architecture was intact with clear boundaries, and the retinal cells were densely arranged. Subsequently, the boundary of ONL became blurred, and the cell density prominently reduced. The thickness of ONL reduced significantly in a time-dependent manner ($p < 0.0001$, $n = 6$, Figure 2A). The TUNEL assay showed that the number of apoptotic cells in the retina of the RD model increased over time. The apoptosis index increased significantly and peaked at P14 ($p < 0.001$, $n = 6$, Figure 2B). Similarly, the fluorescence intensity of DHE staining peaked at P14 and then decreased until P28 ($p < 0.001$, $n = 6$), indicating that ROS accumulated in the retina of the RD model (Figure 2C).

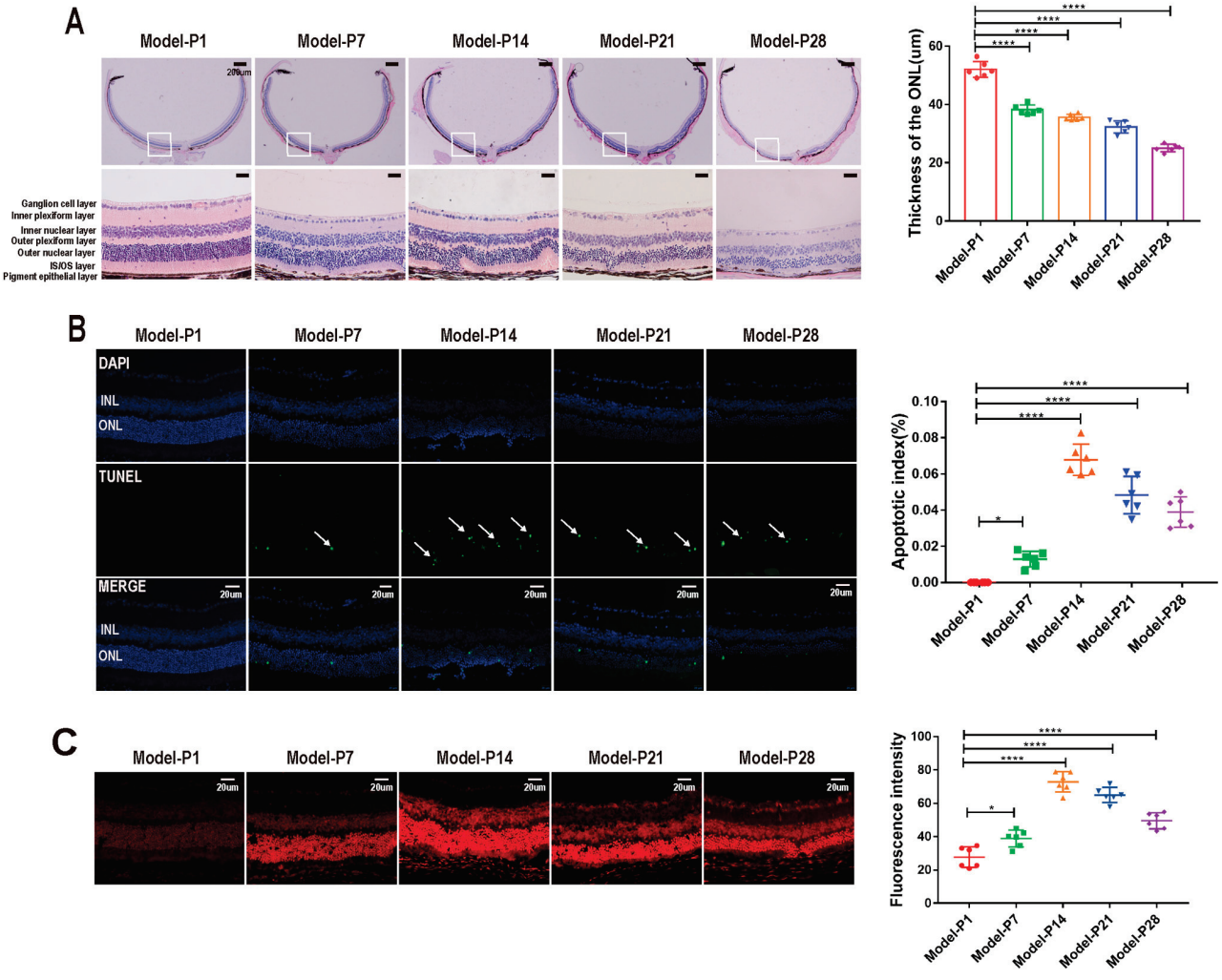

Figure 2. Morphological damage in the RD model. (**A**) The retinal morphology was damaged profoundly over time in the RD model. (**B**) The number of apoptotic cells in the RD model increased

significantly. The apoptosis index peaked at P14. The white arrows represent TUNEL-positive cells. (**C**) The DHE staining showed that ROS accumulated in the retina of the RD model (one-way ANOVA multiple comparisons were analyzed; ns, * $p < 0.05$, **** $p < 0.0001$ for differences compared with P1; $n = 6$).

Microtubule-associated protein 1 light chain 3 (LC3) is the main biochemical marker of autophagy activation [38]. The LC3-B (green) staining was extremely faint in the retinal sections at P1. However, LC3-B immunoreactivity increased after P7, as evidenced by the clusters of strongly stained small particles. Subsequently, at P14, the LC3-B immunostaining decreased over time (Figure 3A). When autophagy was activated, cytoplasmic LC3 (LC3-I) hydrolyzed a small polypeptide and transformed it into an autophagy membrane type (LC3-II). The ratio of LC3-II/LC3I was used as a typical indicator to quantify the autophagy level. The Western blot assay showed that LC3II/LC3I expression increased significantly at P7 ($p < 0.05$, $n = 6$). Subsequently, at P14, LC3II/LC3I expression underwent a sharp reduction and then displayed a downward trend until P28 (Figure 4A). Lysosomal-associated membrane protein 1 (LAMP1) is a typical lysosomal marker. At P1, small spots of the LAMP1 immunostaining were distributed dispersedly in the retinal sections. Subsequently, the LAMP1-positive organelles in the RD models were enlarged and looped at P7, indicating that the cell debris degradation efficiency and the membrane recovery efficiency in lysozyme were extremely low. The intensity of the LAMP1-positive immunostaining peaked at P14 and then decreased progressively until P28 (Figure 3B).

The Bcl-2-interactin protein (Beclin-1) is a key regulator of autophagosome formation. The expression levels of Beclin-1 and autophagy-related 5 (ATG5) increased significantly between P7 and P14 ($p < 0.001$, $n = 6$, Figure 4A) and then reduced significantly until P28. Sequestosome1 (SQSTM1, also named P62) is a critical indicator of autophagy flux, which can be combined with a lysosome to form an autophagolysosome [39,40]. Its expression level is up-regulated when autophagy is inhibited. In the RD model, P62 expression peaked at P1 and decreased progressively until P14 ($p < 0.0001$, $n = 6$). Thereafter, P62 expression increased gradually until P28, indicating that dysfunctional autophagy may lead to lower autophagic flux and the accumulation of cytoplasmic debris (Figure 4B). As an important target of HIF-1α, BNIP3 can mediate autophagy activation. After modeling, the HIF-1α and BNIP3 expressions showed a transient increase and then reduced prominently at the later stages (Figure 4C,D).

3.2. Neuroglia Activation and Gliosis Reaction in the Retinas of RD Model

The immunostaining intensity of ionized calcium binding adapter molecule 1 (IBA1), a microglia-specific marker, increased at the onset of RD ($p < 0.0001$, $n = 6$). IBA1-positive cells were distributed in the inner nuclear layer (INL), with a multi-branched shape. However, the activated microglia migrated into ONL at P14 and showed an "amoeba" shape with hypertrophy and a reduced number of branches (Figure 5A). The glial fibrillary acidic protein (GFAP) is a specific marker of activated Müller cells. In RD models, the GFAP expression was distributed exclusively at the feet of the ganglion cell layer (GCL) to form the inner limiting membrane (ILM) at P1. Subsequently, at P7, the distribution of GFAP immunostaining expanded to ONL. The number of GFAP-positive cells increased significantly over time, peaked at P14, and then decreased gradually until P28 ($p < 0.0001$, $n = 6$, Figure 5B). Glutamine synthetase (GS) is a Müller cell-specific enzyme involved in neurotransmitter cycling and ammonia detoxification. Initially, at P1, the positive signal of GS was uniformly expressed and neatly arranged. However, GS immunostaining decreased gradually after P7, and its distribution was disordered and sparsely arranged ($p < 0.0001$, $n = 6$, Figure 6). These results indicate that the retinal neuroglia in the retina of the RD model were activated and resulted in glia hyperplasia.

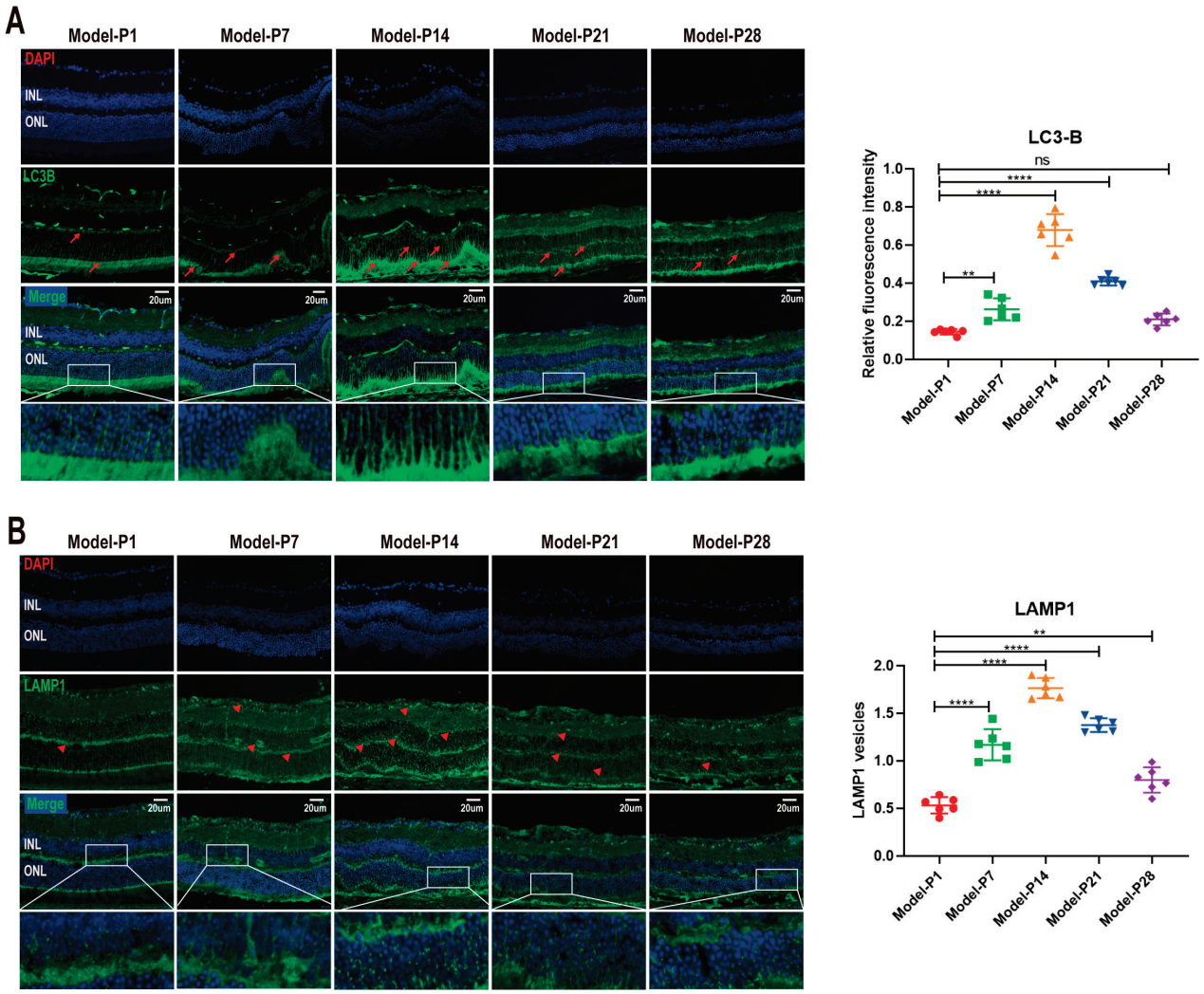

Figure 3. (**A**) LC3-B immunoreactivity in the retina sections of RD model. The LC3-B (green) staining was extremely faint at P1. However, LC3-B immunoreactivity increased at P7, as evidenced by the clusters of strongly stained small particles. Subsequently, at P14, the LC3-B immunostaining decreased over time. (**B**) The red arrows represent positive cells. The LAMP1-positive organelles in RD models were enlarged and looped at P7. The intensity of LAMP1-positive immunostaining peaked at P14 and then decreased progressively until P28. The red triangles represent positive cells (one-way ANOVA multiple comparisons were analyzed; ns, ** $p < 0.01$, **** $p < 0.0001$ for differences compared with P1; $n = 6$).

3.3. ZYAN1 Alleviated Retinal Photoreceptor Damage in RD Model

The retinal structure in the RD + ZYAN1 group was intact with a consolidated cell density. The ONL in the RD + ZYAN1 group was thicker than in the RD group ($p < 0.0001$, $n = 6$, Figures 7A and S1A). The immunofluorescence staining of rhodopsin showed that the rod photoreceptors in the RD + ZYAN1 group were effectively preserved (Figures 7C and S1C). As shown in the fundus photography, numerous yellow-light verruca-like lesions were detected in the RD model. The scale of the retinal lesions reduced prominently after ZYAN1 treatment (Figures 7B and S1B). The OCT examination also showed the pigment disturbance, increased reflectivity, and decreased retinal thickness in the RD model. However, the boundary between the retinal layers was clear in the RD + ZYAN1 group, and the retinal thickness was significantly larger than in the RD group ($p < 0.0001$, $n = 6$, Figures 7B and S1B). In particular, the ZYAN1-induced beneficial effects on retinal morphology were disrupted by 3MA, a specific autophagy inhibitor.

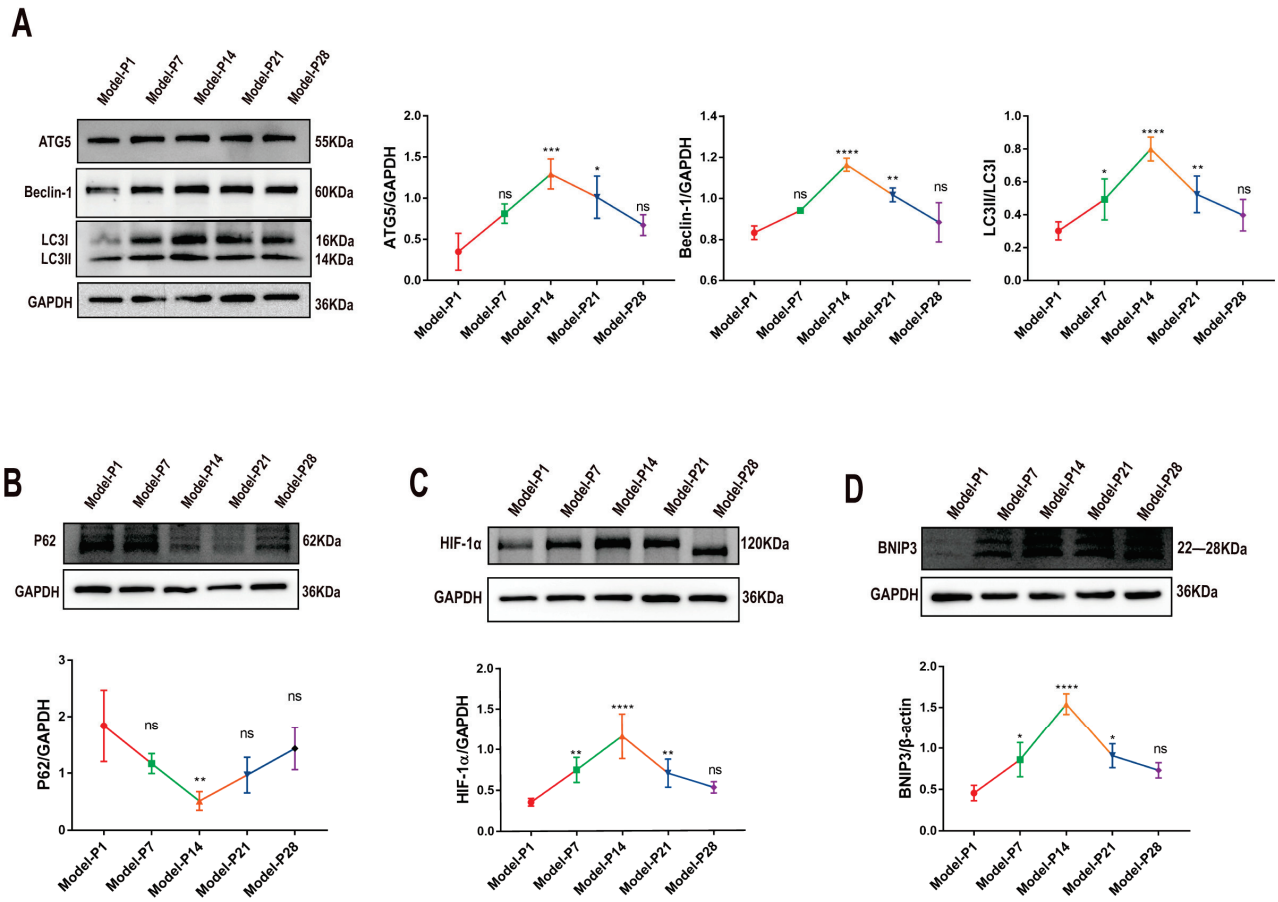

Figure 4. Expression levels of autophagy-related proteins in RD model. (**A**) Representative Western blot images of ATG5, Beclin-1, and LC3-B, and statistical line chart of gray value. (**B**) Representative Western blot images of P62 and statistical line chart of gray value. (**C**,**D**) Representative Western blot images of HIF-1α and BNIP3, and statistical line chart of gray value (one-way ANOVA multiple comparisons were analyzed; ns, * $p < 0.05$, ** $p < 0.01$, *** $p < 0.001$, **** $p < 0.0001$ for differences compared with P1; $n = 6$).

The photoreceptor cilium is essential for light sensation and phototransduction. The TEM observation showed that the membrane disc and axonal cilia in the RD model were abnormal. A large number of shaded membrane discs were found at the end of the outer segment. After ZYAN1 treatment, the membrane disc shedding was ameliorated, and the structure of the axonal cilia was relatively intact. The ZYAN1-induced protective effects on the microstructure of the photoreceptors were abolished by 3MA (Figures 8A,B and S2A,B). These results suggest that ZYAN1 could enhance photoreceptor survival and alleviate the morphological damage in RD mice.

3.4. ZYAN1 Improved Visual Function and Behavioral Activity in RD Model

The behavioral examination showed that ZYAN1 improved the visual function and behavior of the RD model. The behavioral parameters, including the residence time in the dark box, the movement speed in the light box, and the shuttle times between the two boxes, increased significantly in the RD + ZYAN1 group compared with the RD group ($p < 0.05$, $n = 8$, Figures 9A,B and S3A,B). However, the movement distance in the light box reduced significantly in the RD + ZYAN1 group compared with in the RD group. In the open-field test, the duration in the central area, the number of times entering the central area, the total moving speed, and the total distance in the open area increased significantly in the RD + ZYAN1 group compared with in the RD group ($p < 0.05$, $n = 8$, Figures 9C,D and

S3C,D). In the mf-ERG examination, the amplitude of the RD + ZYAN1 group increased significantly compared with that of the RD group (n = 6, Figures 10A,D and S4A,D). In particular, the mf-ERG amplitude increased comprehensively in all the ST, SN, IT, and IN quadrants after ZYAN1 treatment (Figures 10B and S4B). In the RD + ZYAN1 group, the retinal amplitudes were significantly larger than those in the RD group in ring1, ring2, and ring3 (Figures 10C and S4C). In particular, these improvements in behavioral activity and mf-ERG function could be blocked by 3MA.

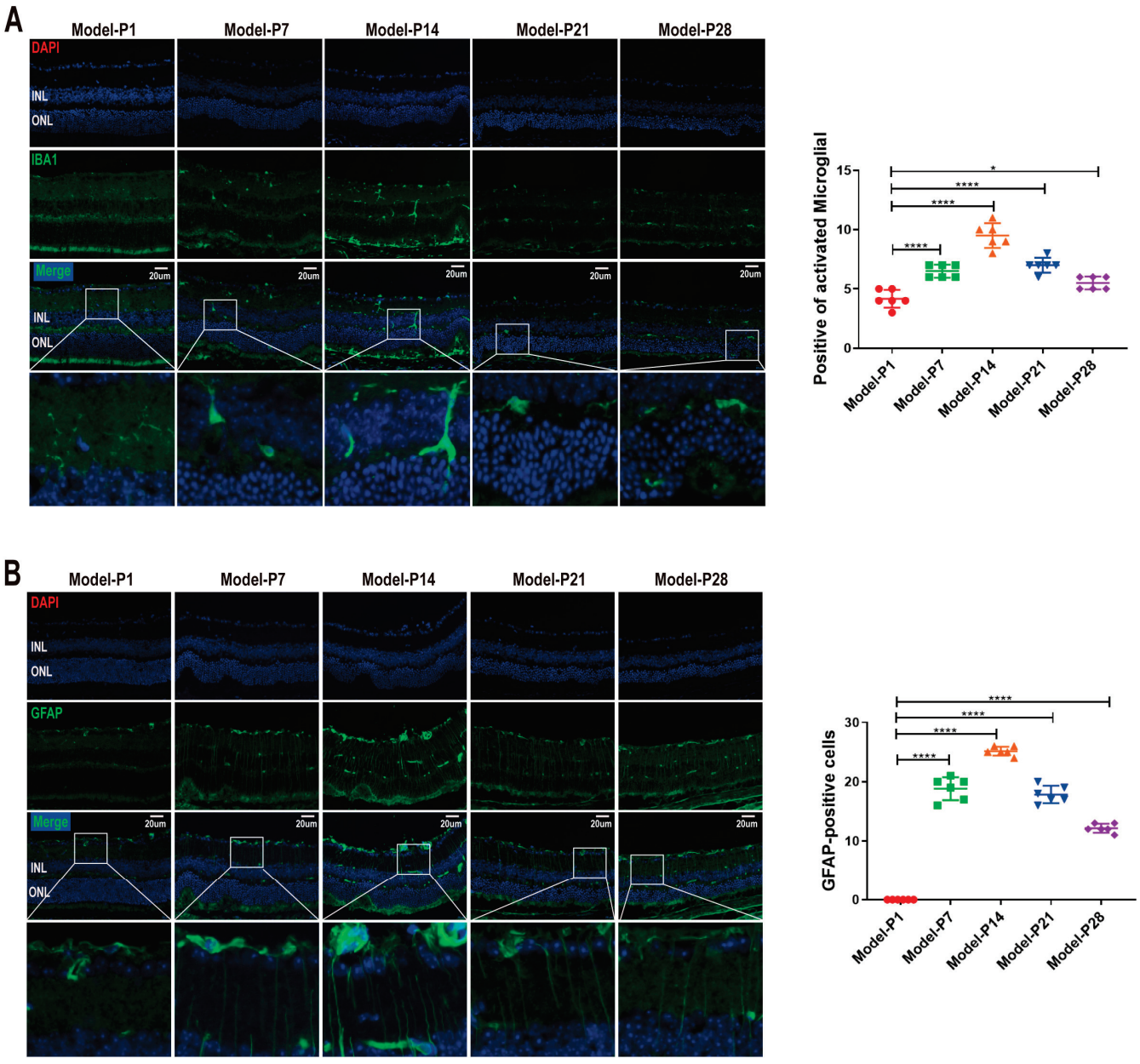

Figure 5. Activation of microglia and Müller cells in RD model. (**A**) The immunostaining intensity of IBA1 increased at the onset of RD. IBA1-positive cells were distributed in the inner nuclear layer with multi-branched shape. The activated microglia migrated into ONL at P14. (**B**) The GFAP expression was located exclusively at the feet of the ganglion cell layer (GCL) to form the inner limiting membrane (ILM) at P1. At P7, the distribution of GFAP immunostaining expanded to ONL. The number of GFAP-positive cells then decreased gradually until P28 (one-way ANOVA multiple comparisons were analyzed; * $p < 0.05$, **** $p < 0.0001$ for differences compared with P1; n = 6).

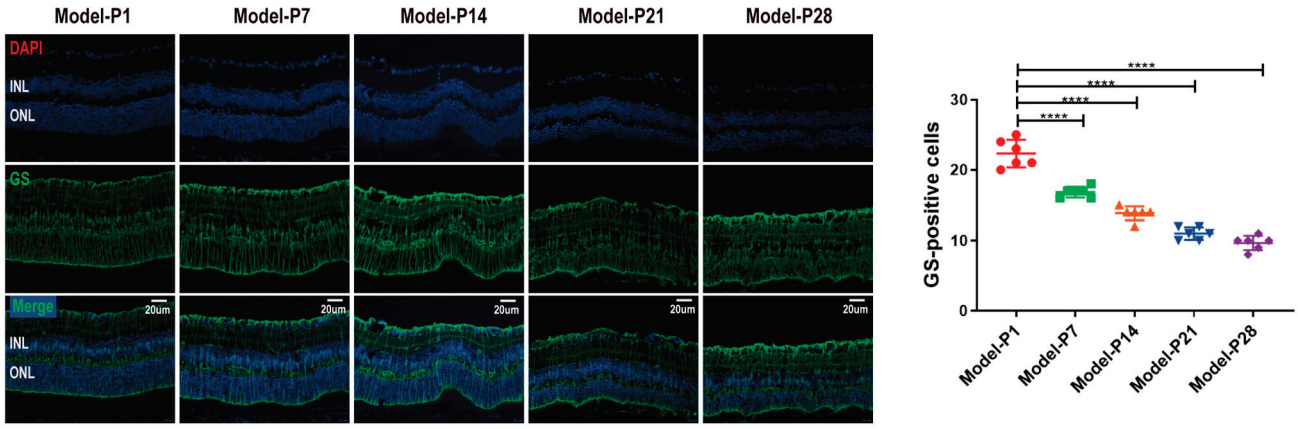

Figure 6. Activation of Müller cells in RD model. The positive signal of GS was uniformly expressed and neatly arranged at P1. The immunostaining intensity decreased gradually after P7, and its distribution was disordered and sparsely arranged. These results indicate that the Müller cells were activated in the retina of RD model (one-way ANOVA multiple comparisons were analyzed; **** $p < 0.0001$ for differences compared with P1; $n = 6$).

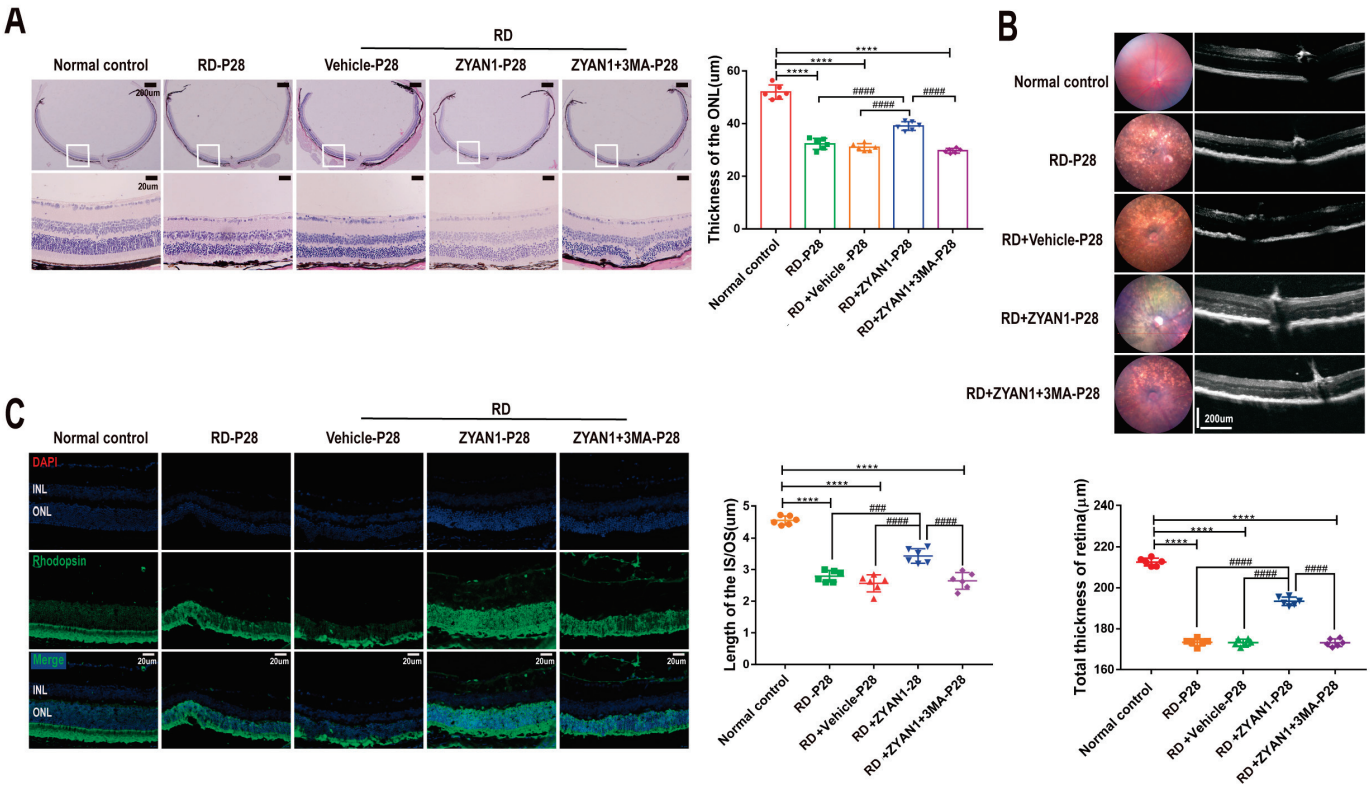

Figure 7. ZYAN1 alleviates the morphology damage in RD model at P28. (**A**) Retinal structure in the RD + ZYAN1 group was intact. The ONL in RD + ZYAN1 group was thicker than in RD group. (**B**) In OCT examination, the boundary between retinal layers was clear in the RD + ZYAN1 group, and the retinal thickness was significantly larger than in RD group. The scale of retinal lesions reduced prominently after ZYAN1 treatment. (**C**) Immunofluorescence staining of rhodopsin showed that the rod photoreceptors in the RD + ZYAN1 group were effectively preserved. The IS/OS length was significantly larger than in RD group (**** $p < 0.0001$ for differences compared with normal control group; ### $p < 0.001$, #### $p < 0.0001$ for differences compared with RD + ZYAN1 group, $n = 6$).

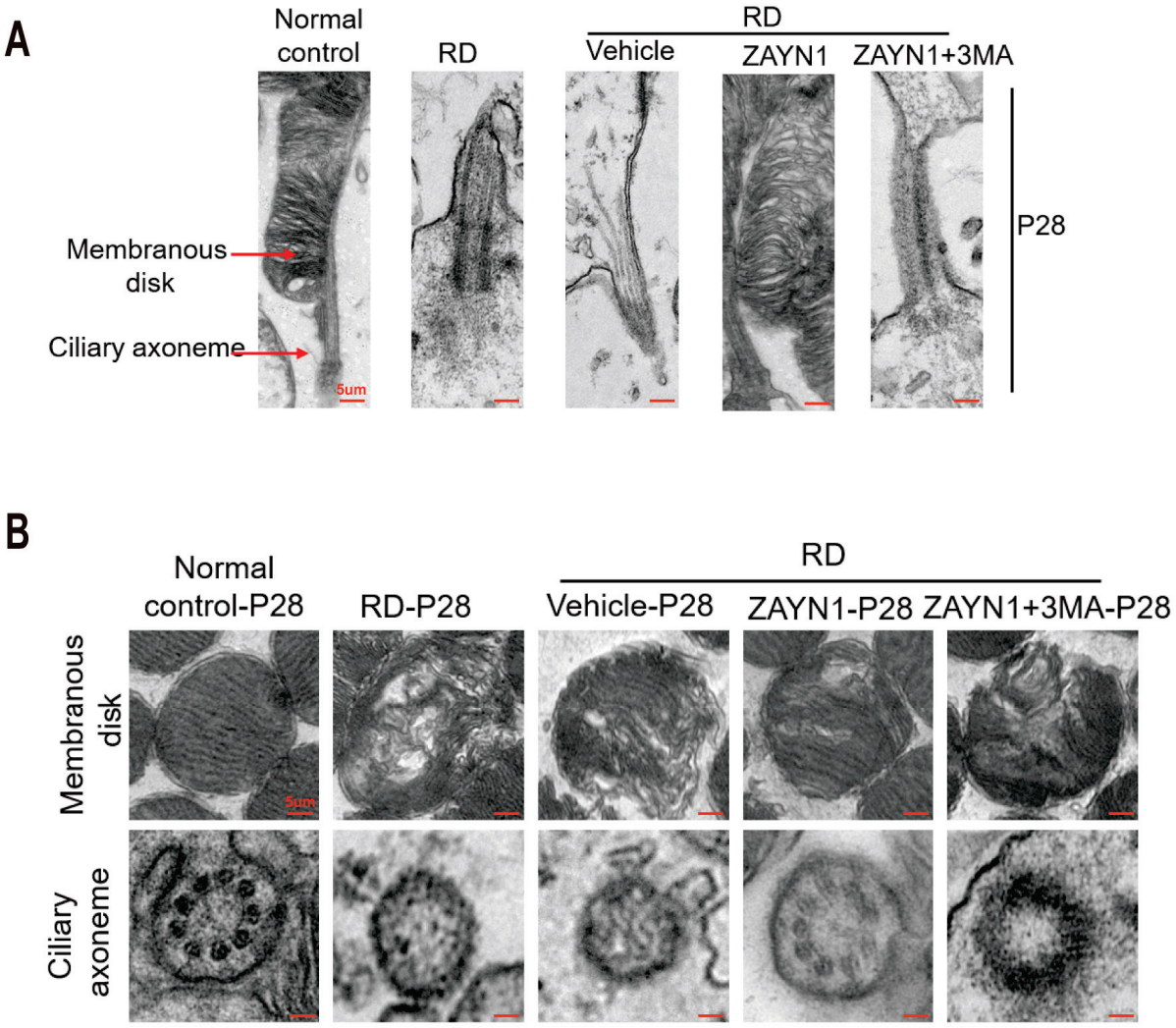

Figure 8. ZYAN1 mitigated the injury of ciliary axonemes and membranous disks in RD model mice at P28. (**A**) Transmission electron microscopy images of the longitudinal sections of photoreceptors. (**B**) Transmission electron microscopy images of the cross-sections of ciliary axonemes and membranous disks. After ZYAN1 treatment, the membrane disc shedding was ameliorated, and the structure of axonal cilia was relatively intact.

3.5. ZYAN1 Restored Retinal Autophagy in RD Model

The immunofluorescence staining showed that the density of LC3-B immunoreactivity increased in the RD + ZYAN1 group. Strong LC3-B spots were found in INL and ONL, indicating that autophagy polymerization occurred in the retinas of the RD + ZYAN1 group (n = 6, Figures 11A and S5A). Compared with the RD model, more LAMP1-positive cells were detected in the retinas of the RD + ZYAN1 group (n = 6, Figures 11B and S5B). The Western blot assay showed that the expression levels of LC3-B, Beclin-1, and ATG5 were significantly higher in the RD + ZYAN1 group than in the RD model (Figures 12B and S6B). However, the expression level of the P62 protein in the RD + ZYAN1 group was significantly lower than that in the RD model (Figures 12C and S6C). In addition, the expressions levels of HIF-1α and BNIP3 increased significantly after ZYAN1 treatment (Figures 12D,E and S6D,E). 3MA could disrupt the ZYAN1-induced effects on autophagy markers. The TEM examination showed that the number of autophagosomes in the retina of the RD group increased at P14 and then decreased sharply (Figures 12A and S6A). In greater detail, the mitochondrial structure in the normal controls was intact, while the mitochondria in the RD group were swollen, with diffused crista and cytoplasmic vacuolation. However,

the mitochondrial damage was ameliorated by ZYAN1 treatment, as evidenced by the increased number of autophagosomes ($p < 0.01$ and $p < 0.05$, respectively, $n = 6$) and the reduced number of autophagy vacuoles. These results suggest that ZYAN1 can enhance mitochondrial autophagy via the HIF-1α/BNIP3 pathway.

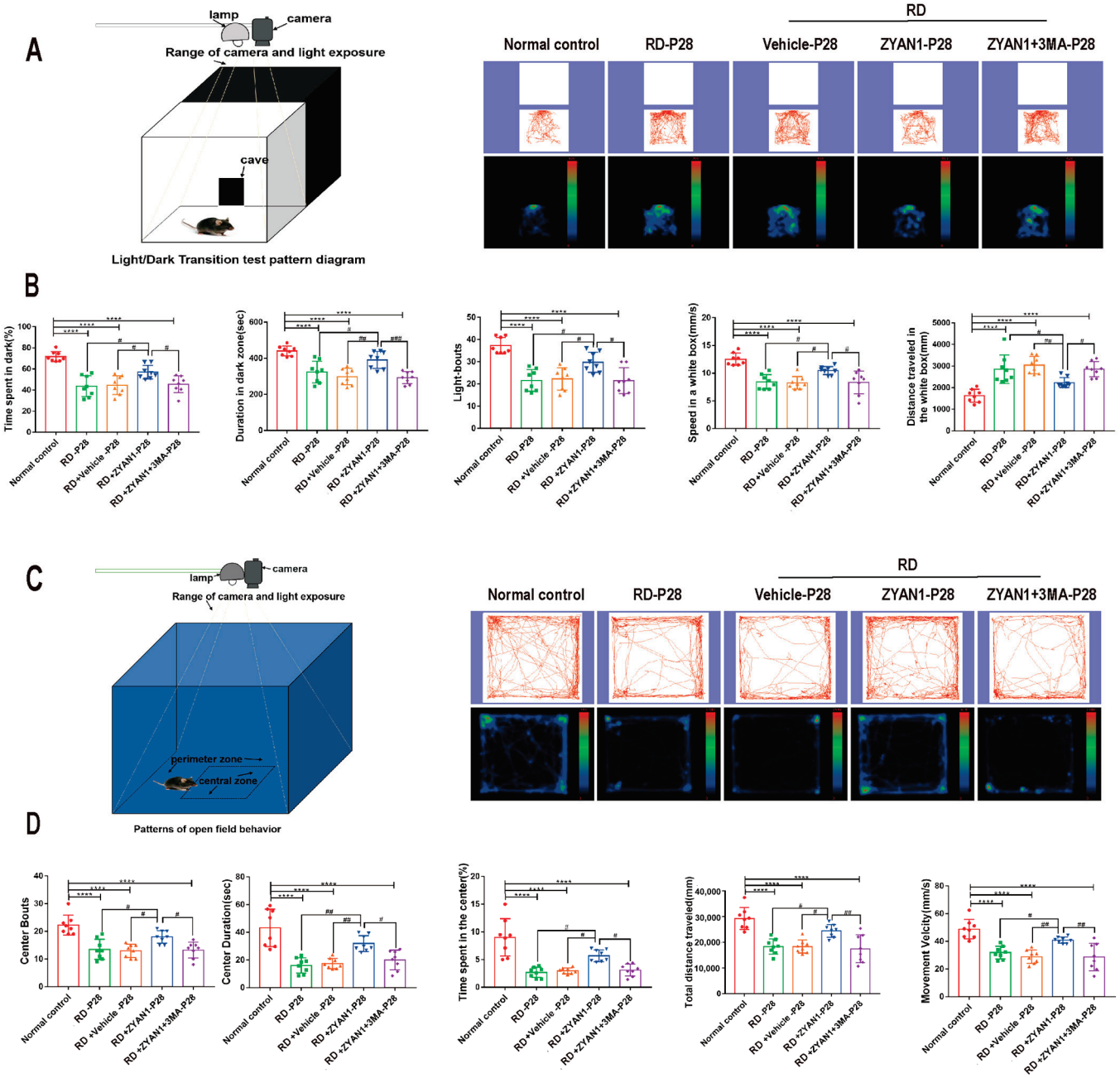

Figure 9. Effect of ZYAN1 on the behavioral activity of RD model. (**A**) Tracks and density maps of light/dark transition test. (**B**) The residence time in the dark box, the movement speed in the light box, and the shuttle times between two boxes in the RD + ZYAN1 group increased significantly compared with in RD group. (**C**) Track and density map of open-field test. (**D**) In the open-field experiment, the duration in the central area, the number of times entering the central area, the total moving speed, and the total distance in the open area increased significantly in the RD + ZYAN1 group compared with in RD group (**** $p < 0.0001$ for differences compared with normal control group; $^{\#}$ $p < 0.05$, $^{\#\#}$ $p < 0.01$, $^{\#\#\#}$ $p < 0.001$ for differences compared with RD + ZYAN1 group, $n = 8$).

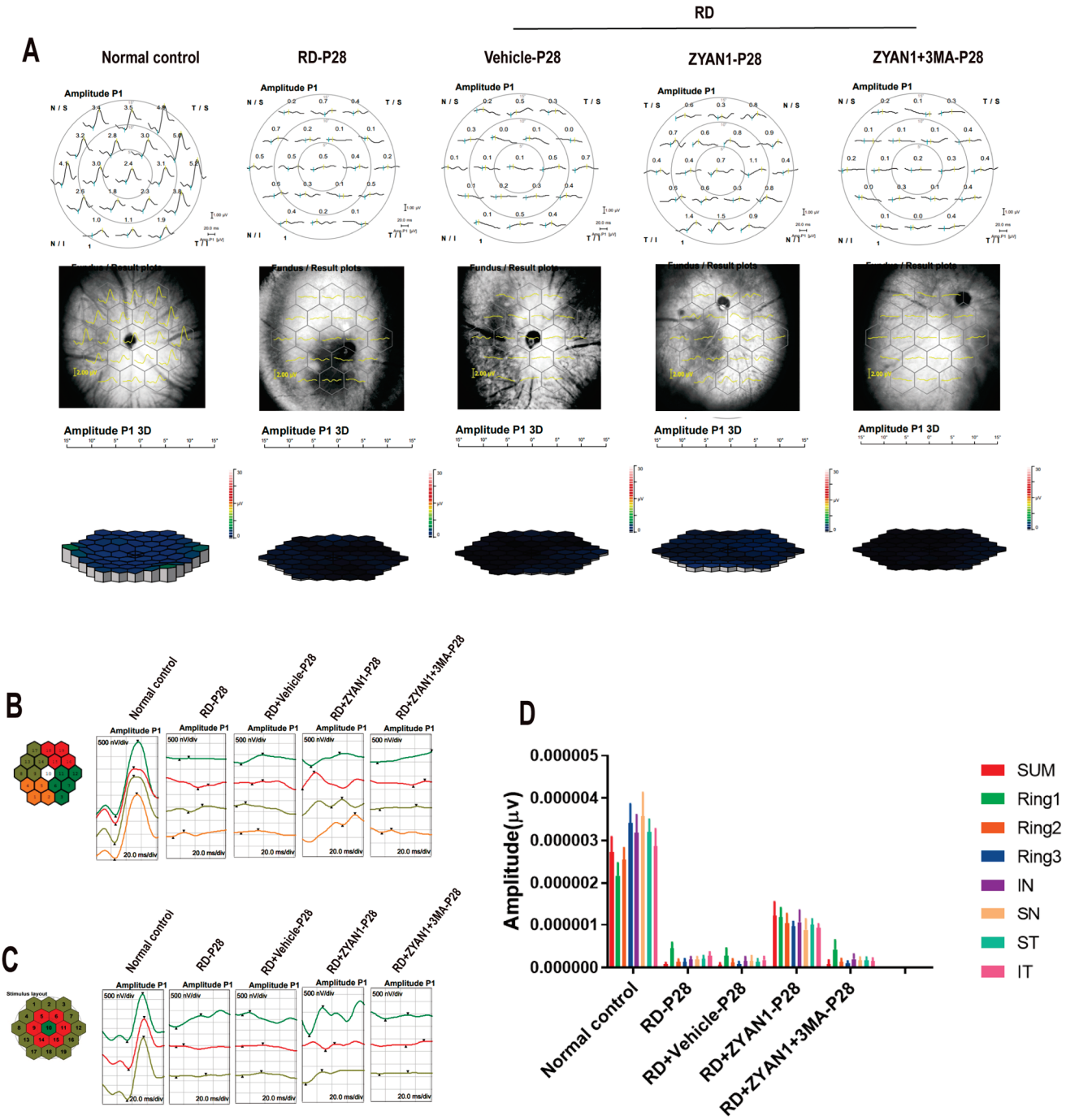

Figure 10. ZYAN1 can protect retinal function of RD mice at P28. (**A**) In mf-ERG examination, the amplitude of RD + ZYAN1 group increased significantly compared with that of RD group. (**B**) The mf-ERG amplitude increased comprehensively in all the ST, SN, IT, and IN quadrants after ZYAN1 treatment. (**C**) In the RD + ZYAN1 group, retinal amplitudes were significantly larger than in the RD group in ring1, ring2, and ring3. (**D**) mf-ERG amplitude histogram of different quadrants and rings.

3.6. ZYAN1 Inhibited Neuroglia Activation and Alleviated Oxidative Stress

The immunofluorescence staining showed that the number of IBA1-positive cells in the RD + ZYA1N group reduced significantly compared with that in the RD group. The IBA1 immunostaining in the RD + ZYAN1 group was limited to the interior retina. The IBA1-positive cells in the RD + ZYAN1 group had multiple-branch protrusion, indicating that they were maintained at a static state ($p < 0.01$ and $p < 0.001$, respectively, $n = 6$,

Figures 13A and S7A). The intensity of the GFAP immunostaining in the RD + ZYAN1 group decreased compared with that in the RD group ($p < 0.0001$, $n = 6$, Figures 13B and S7B). However, the intensity of the GS immunostaining in the RD + ZYAN1 group increased significantly compared with that in the RD group ($n = 6$, Figures 14A and S8A). The number of TUNEL-positive apoptotic cells in the RD + ZYAN1 group was significantly smaller than in the RD group ($p < 0.001$, $n = 6$, Figures 14B and S8B). Moreover, the fluorescence intensity of DHE in the RD + ZYAN1 group reduced significantly compared with that in the RD group (Figures 14C and S8C). These results indicate that ZYAN1 could inhibit microglia activation and alleviate the oxidative stress in RD mice.

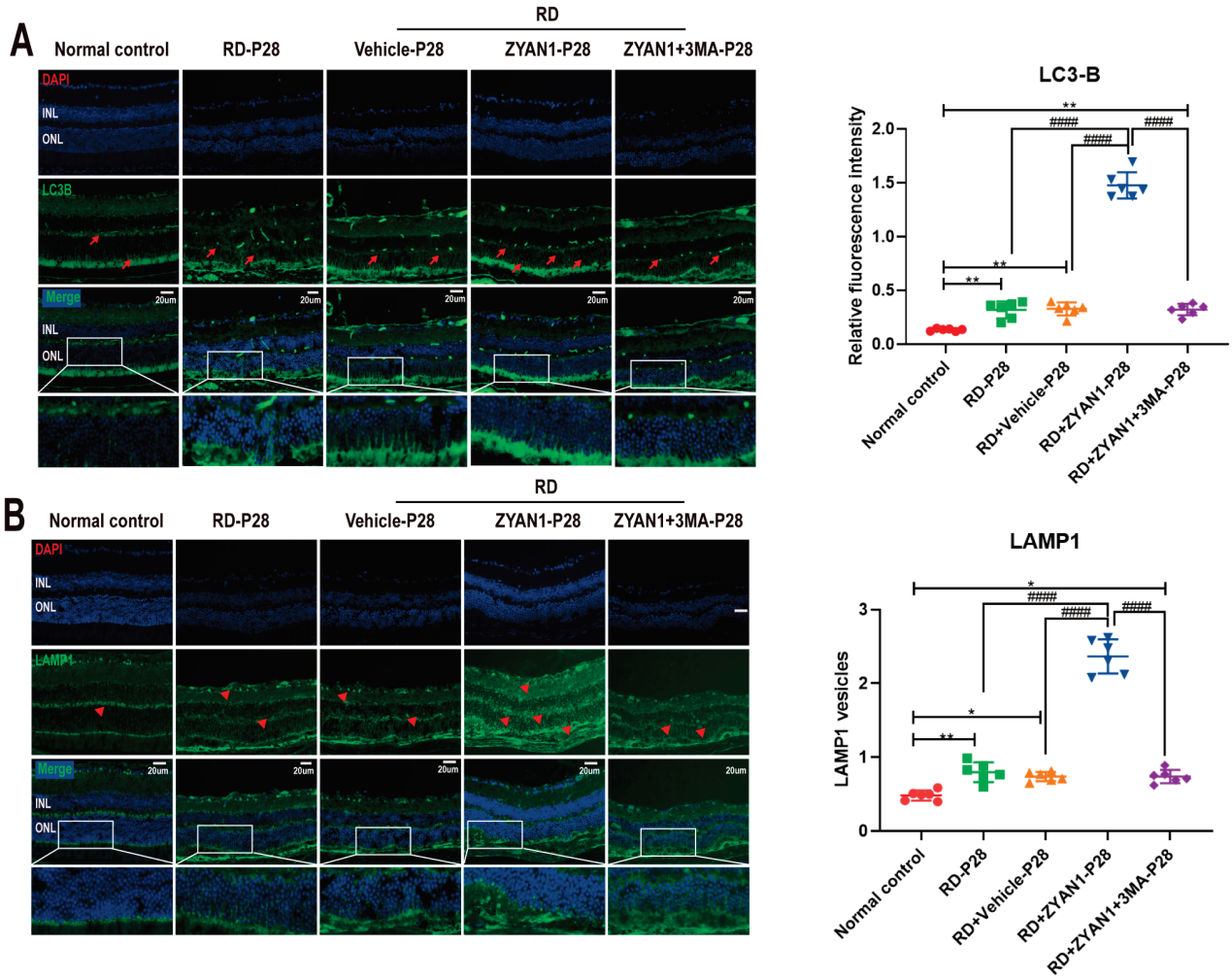

Figure 11. ZYAN1 enhanced the positive signal of LC3B and LAMP1 in RD models at P28. (**A**) Strong LC3-B spots were found in INL and ONL. Red arrows indicate positive cells. (**B**) Compared with RD model, more LAMP1-positive cells were detected in the retinas of RD + ZYAN1 group. Red triangle indicates positive cells (* $p < 0.05$, ** $p < 0.01$ for differences compared with normal control group; #### $p < 0.0001$ for differences compared with RD + ZYAN1 group, $n = 6$).

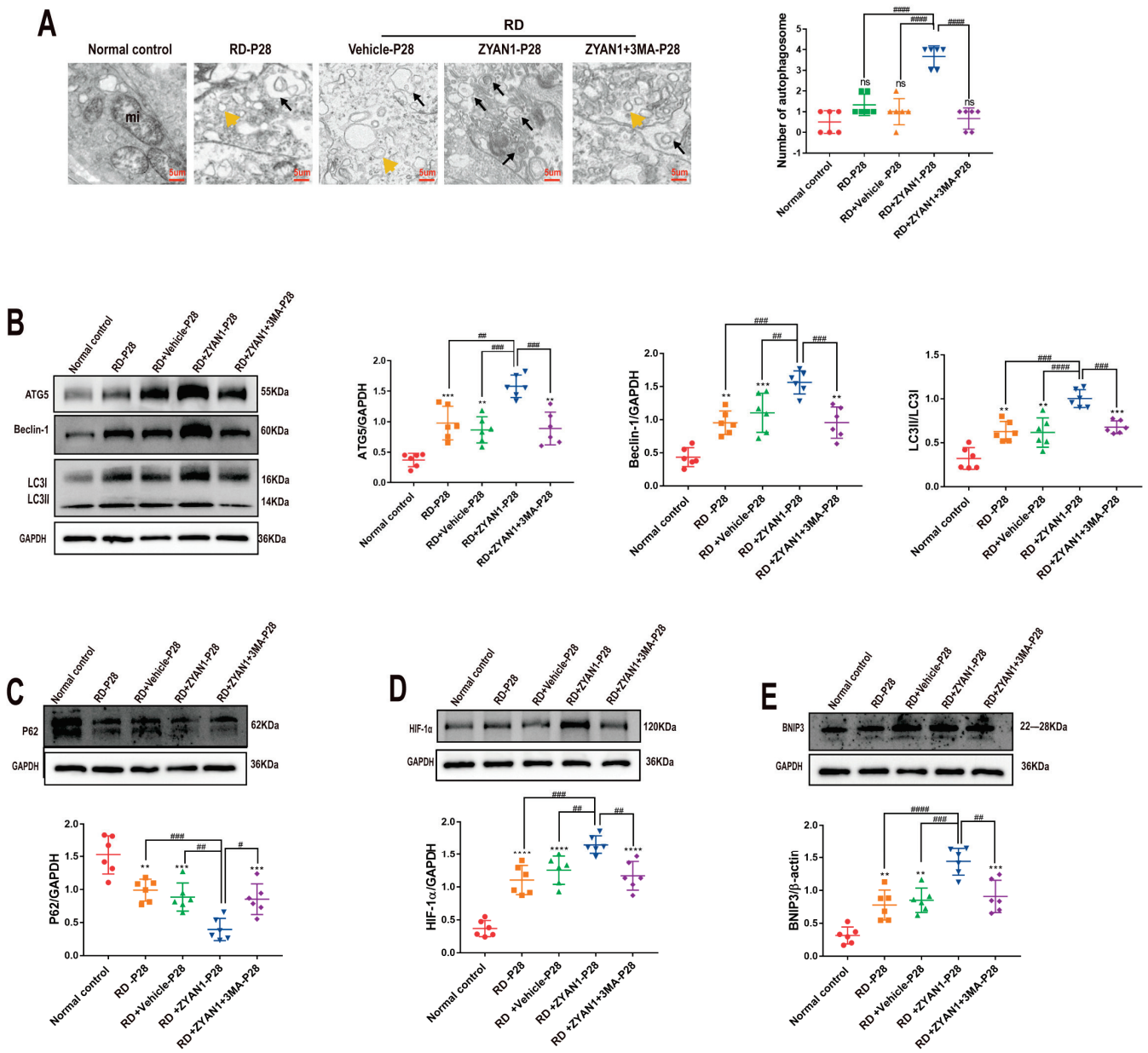

Figure 12. ZYAN1 enhances expressions of autophagy-related proteins and promotes the formation of autophagosome at P28. (**A**) TEM examination showed that the mitochondrial damage was ameliorated by ZYAN1 treatment, as evidenced by increased number of autophagosomes and reduced number of autophagy vacuoles. The black arrows represent autophagosomes; the yellow triangle represents autophagy vacuoles. (**B**) Western blot showed that the expression levels of ATG5, Beclin-1, and LC3-B in the retina of RD + ZYAN1 group increased at P28. (**C**) The expression level of P62 in RD + ZYAN1 group was significantly lower than that in RD model (**D**,**E**) Western blot showed that the expression levels of HIF-1α and BNIP3 protein in the retina of RD + ZYAN1 group increased compared with those in the RD group (ns, ** $p < 0.01$, *** $p < 0.001$, **** $p < 0.0001$ for differences compared with normal control group; $^{\#}$ $p < 0.05$, $^{\#\#}$ $p < 0.01$, $^{\#\#\#}$ $p < 0.001$, $^{\#\#\#\#}$ $p < 0.0001$ for differences compared with RD + ZYAN1 group, $n = 6$).

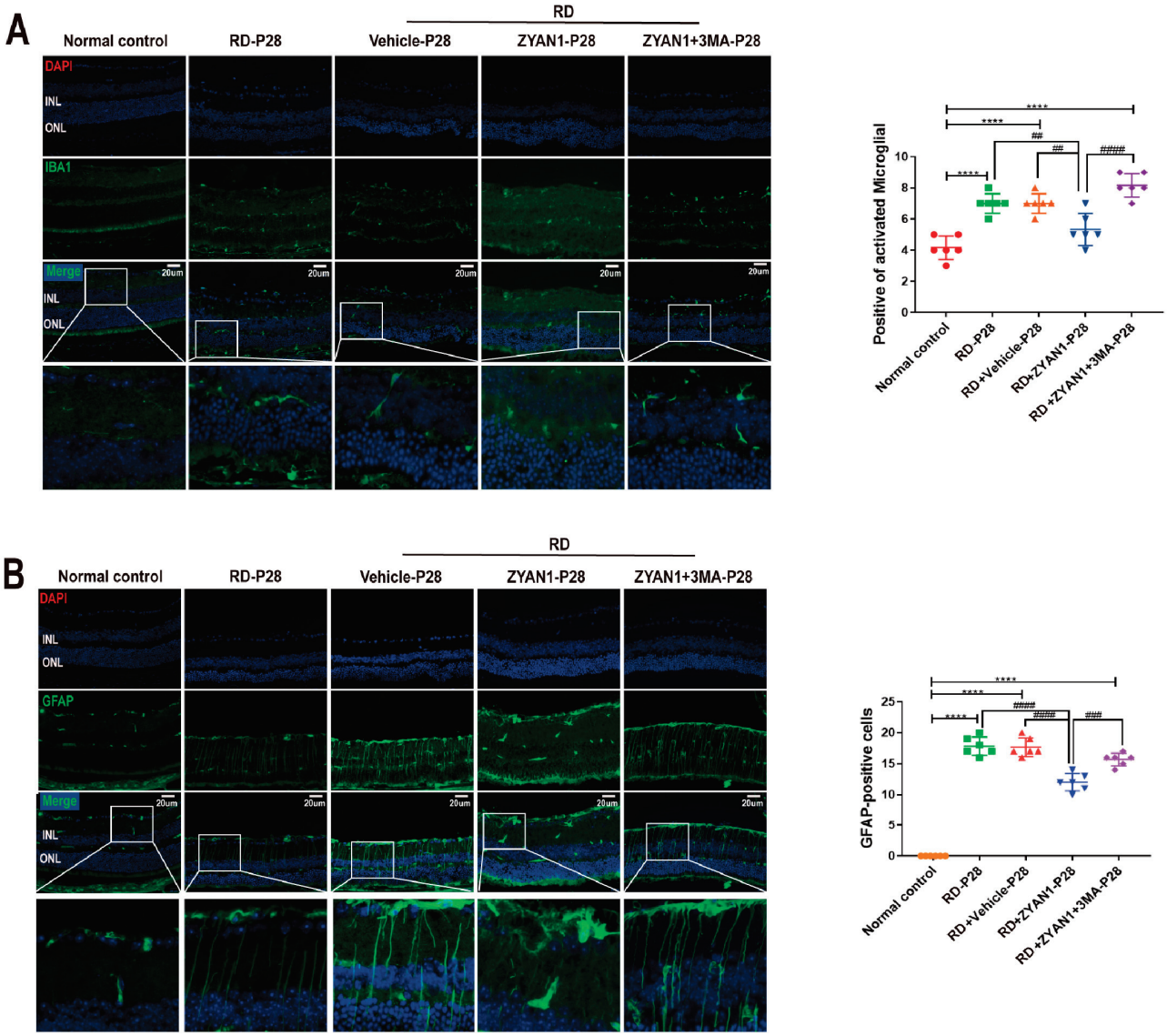

Figure 13. ZYAN1 inhibited the Müller and microglia activation in RD model at P28. (**A**) The number of IBA1-positive cells in RD+ZYA1N group reduced significantly compared with that in RD group. (**B**) The intensity of GFAP immunostaining in the RD + ZYAN1 group decreased compared with that in the RD group (**** $p < 0.0001$ for differences compared with normal control group; $^{\#\#}$ $p < 0.01$, $^{\#\#\#}$ $p < 0.001$, $^{\#\#\#\#}$ $p < 0.0001$ for differences compared with RD + ZYAN1 group, $n = 6$).

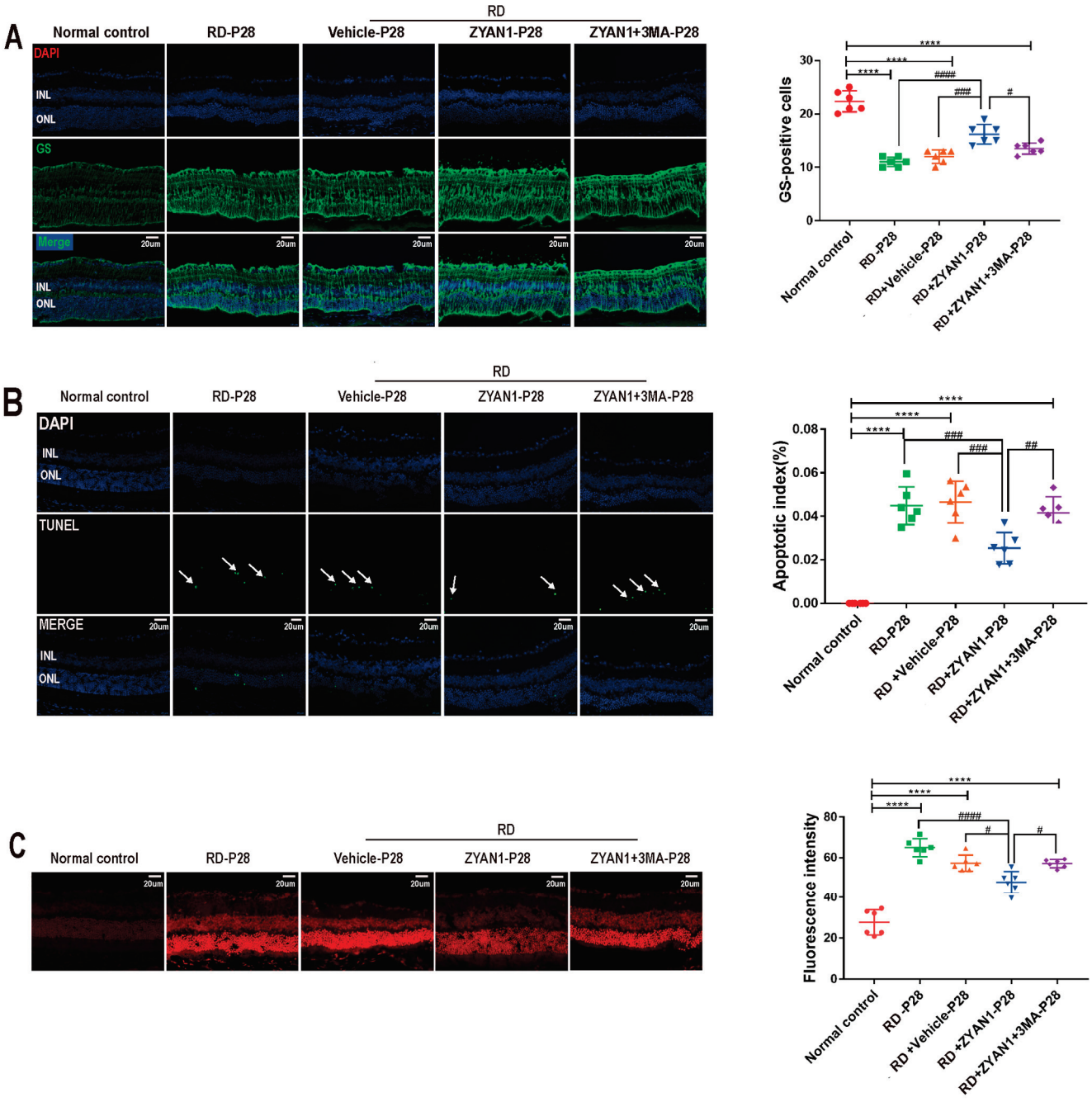

Figure 14. ZYAN1 mitigated photoreceptor cell death and ROS production in RD model at P28. (**A**) The density of GS immunostaining in RD + ZYAN1 group increased significantly compared with that in RD group. (**B**) The number of TUNEL-positive apoptotic cells in RD + ZYAN1 group reduced significantly compared with that in RD group. The white arrows represent TUNEL-positive cells. (**C**) The fluorescence intensity of DHE in RD + ZYAN1 group reduced significantly compared with that in RD group (**** $p < 0.0001$ for differences compared with normal control group; $^{\#}p < 0.05$, $^{\#\#}p < 0.01$, $^{\#\#\#}p < 0.001$, $^{\#\#\#\#}p < 0.0001$ for differences compared with RD + ZYAN1 group, $n = 6$).

4. Discussion

Multiple genetic and environmental factors are involved in RD pathogenesis, including excessive oxidative stress, an impaired capacity of autophagy clearance, and chronic retinal inflammation [41–43]. Currently, there is no effective treatment for RD in clinical practice. There is an urgent need to deepen our understanding of RD pathophysiology and to develop integrated therapeutic strategies. At the initial stage of RD, the autophagy level

increases to compensate for the oxidative stress and to scavenge the damaged organelles. During this time, the expression levels of autophagic factors, such as LC3, ATG9, and ATG7, increase significantly in retinal tissue [44]. However, at the advanced stages of RD, the expression levels of autophagic factors reduce markedly, leading to the accelerated progression of RD [45]. HIF-1 is a key heterodimer transcription factor in the oxygen homeostasis signaling system. It consists of an oxygen-regulated α subunit and a constitutionally expressed β subunit. The β subunit is expressed stably, and its expression is not affected by fluctuations in the oxygen concentration. Conversely, the expression of the α subunit is unstable, and it is regulated by PHD [46]. BNIP3 is a HIF-1-dependent gene that is responsible for promoting autophagic activity, thereby maintaining cellular homeostasis and facilitating the adaptation to stressful conditions [47]. In this study, we found that the autophagy level experiences a transitional increase and then declines sharply in the retina of the RD model. Autophagy can maintain cell survival by recycling abnormal proteins and removing abnormal cellular components through lysosomal-dependent degradation [48]. The decreased autophagy activity of the retinal cell leads to the accumulation of lipofuscins, the overproduction of ROS, protein aggregation, and inflammatory reactions [49]. In this context, ZYAN1, a novel prolyl hydroxylase inhibitor, is injected into the vitreous cavity to enhance mitochondrial autophagy. Dysautophagy is implicated in the occurrence and progression of RD [7,50,51]. Calpain activation can inhibit the autophagy of photoreceptors, thereby exacerbating the visual impairments in RD models. When calpain activation is blocked by SNJ-1945, autophagy levels are restored, and the photoreceptors survive [52]. Another in vitro study shows that cone cells with ATG5 gene defects are more susceptible to phototoxicity [53]. Rapamycin, an autophagy activator, alleviates the visible light-induced photoreceptor damage by alleviating endoplasmic reticulum stress [54]. Collectively, these findings suggest that autophagy should be modulated appropriately to maintain the survival of photoreceptors. Several pathways are involved in modulating the balance of mitochondrial autophagy. PINK1 can directly promote non-Parkin-dependent mitochondrial autophagy by collecting nuclear dot protein 52 and optineurin [55]. Another mitochondrial membrane protein, FUNDC1, can also enhance autophagy and mitigate photoreceptor damage [56,57]. In particular, the autophagy mediated by the HIF-1α/BNIP3 signaling pathway is implicated in the pathogenesis of RD. Studies have shown that the overexpression of BNIP3 can induce autophagy, while the knockout of BNIP3 aggravates anoxic injury in RPE cells [58]. Agreeing well with aforementioned reports, we showed that ZYAN1 can enhance the mitochondrial autophagy in retinal cells via the HIF-1α/BNIP3 pathway. ZYAN1 can act as an agonist with HIF-1α, which acts as an indispensable component of proteolytic mechanisms [59]. As the downstream target gene of HIF-1α, BNIP3 is specifically localized to mitochondria and participates in the autophagic clearance of damaged mitochondria [60]. HIF-1α silencing mitigates the expressions of BNIP3 and LC3-II in rat retina, resulting in exacerbated photoreceptor death [61]. However, the application of a PHD inhibitor in retinal detachment models significantly activates the HIF-1α/BNIP3 pathway, enhances mitochondrial autophagy, and thus alleviates histopathologic lesions [62]. As expected, the expression levels of the autophagy-related proteins LC3-B, ATG5, and Beclin-1 increase after ZYAN1 treatment, indicating that autophagy is activated in the retinas. Autophagy activation confers tremendous benefits on degenerating retinas, such as increased ONL thickness and tighter retinal structures with clear boundaries. The ZYAN1-treated mice also maintained a substantial proportion of visual function, as evidenced by the mf-ERG examination and behavioral test. These findings highlight the possibility that ZYAN1 may act as a therapeutic molecule to slow down the pathologic process of RD.

Oxidative stress causes a pigment disorder, the accumulation of intracellular lipofuscin, and the activation of apoptotic cascades [63]. As an important source of ROS, mitochondria are vulnerable to oxidative insults [64]. Abnormalities in the respiratory chain and mitochondrial membrane potential lead to the overproduction of ROS, which, in turn, attack mitochondria [65,66]. Mitochondrial autophagy is a form of selective autophagy highly sensitive to fluctuations in oxidative stress. Studies have shown that mitophagy can protect

mitochondria from environmental insults [62,67]. In diabetic retinopathy, mitochondrial autophagy is down-regulated, and these damaged organelles cannot be cleared in a timely manner, resulting in the depletion of energy sources [68]. However, PINK1 can accumulate on the surface of the mitochondrial membrane to initiate mitochondrial autophagy and prevent the deterioration of retinopathy [69]. Accordingly, enhancing mitochondrial autophagy may act as a promising therapeutic strategy for RD. In this study, ZYAN1 treatment restored mitochondrial autophagy and inhibited ROS production. As shown in the TEM examination, ZYAN1 also restored the mitochondria structure and promoted the formation of autophagosomes. These anti-oxidative mechanisms may contribute to the ZYAN- mediated protection of degenerating retinas.

Microglia and Müller cells interact with each other to maintain the homeostasis of the retina. Under physiological conditions, microglia cells are mainly distributed in the inner plexiform layer (IPL) and outer plexiform layer (OPL), with a multiple-branched shape. When the retina is exposed to pathologic insults, microglia undergo morphological changes from branching to an "amoeba" shape, with an accompanying tendency to migrate to ONL [70]. These activated microglia impair the RPE's ability to phagocytize the oxidized photoreceptor lipoproteins [71]. Moreover, activated microglia can produce a burst of cytotoxic molecules, including proteases, ROS, and nitric oxide, which can subsequently lead to an inflammatory microenvironment in the retina [72,73]. In particular, activated microglia can mitigate basal autophagy activity [74]. Therapeutically, ZYAN1 suppresses the microglia activation and the downstream inflammatory response in RD mice. This may be an important mechanism underlying the restored autophagy activity in the ZYAN1-treated mice. Additionally, ZYAN1 can ameliorate the retinal gliosis in RD mice. A retinal gliosis scar is formed by Müller cell hypertrophy and proliferation [75]. During the gliosis process, GFAP immunostaining is up-regulated, especially in a radial direction from the foot of Müller cells [71]. Müller cells further communicate with the activated microglia and promote the formation of drusen [76]. In this context, the reactive gliosis may impose a thorny challenge for any therapy. Encouragingly, ZYAN1 can inhibit the Müller cell activation and ameliorate the gliosis response in the RD model. This should be considered an advantage of ZYAN1 treatment.

Although we demonstrated that ZYAN1 could activate mitochondrial autophagy via the HIF-1α-BNIP3 pathway, the causal relationship among mitophagy, HIF-1α/BNIP3 signaling, and degenerating retinas has not been well established. In this context, further studies are necessary to elucidate the underlying mechanism with the assistance of some protein antagonists.

5. Conclusions

ZYAN1 can protect the photoreceptors in the RD model via the HIF-1α/BNIP3 pathway. Mitochondrial autophagy in retinal cells is recovered by ZYAN1, while the oxidative stress and glia hyperplasia are inhibited. These beneficial effects can be translated into prominent improvements in visual function and behavioral activity. Further refinements of these findings would enrich our knowledge of RD and contribute to the development of pharmacological therapy.

Supplementary Materials: The following supporting information can be downloaded at: https://www.mdpi.com/article/10.3390/antiox12111914/s1, Figure S1: ZYAN1 alleviates the morphology damage in RD model at P14; Figure S2: ZYAN1 mitigated the injury of ciliary axonemes and membranous disks in RD model mice at P14; Figure S3: Effect of ZYAN1 on the behavior of RD model in light/dark transition test and open-field transition at P14; Figure S4: ZYAN1 can mitigate the impairments of retinal function in RD mice at P14; Figure S5: ZYAN1 enhanced the positive signal of LC3B and LAMP1 in RD models at P14; Figure S6: ZYAN1 enhanced retinal autophagy in RD model at P14; Figure S7: ZYAN1 inhibited the Müller and microglia activation in RD model at P14; Figure S8: ZYAN1 reduces reactive gliosis, mitigated photoreceptor cell death, and ROS production in RD model at P14.

Author Contributions: X.-N.H.: Conceptualization, Investigation, Methodology, Writing—Original Draft. J.-M.H. and N.Z.: Methodology, Formal Analysis. J.-M.H.: Writing—Original Draft, Formal Analysis. S.-Y.L., D.W. and N.P.: Methodology, Resources. Y.T. and G.-H.P.: Conceptualization, Funding Acquisition, Project Administration, Supervision, Writing—Review and Editing, Validation. All authors have read and agreed to the published version of the manuscript.

Funding: This research was supported by the National Key Research and Development Program (2018YFA0107303) and the Natural Science Foundation of China (No. 82070990).

Institutional Review Board Statement: The ethical approval number for animal experiments: SCXK (YU) 2020-016713.

Informed Consent Statement: Not applicable.

Data Availability Statement: All of the data are contained within the article.

Conflicts of Interest: The authors declare no conflict of interest. Each author of this study further declares no relationships with the companies or manufacturers who will benefit from the results of the present study.

References

1. Wu, X.; Yan, N.; Zhang, M. Retinal Degeneration: Molecular Mechanisms and Therapeutic Strategies. *Curr. Med. Chem.* **2022**, *29*, 6125–6140. [CrossRef] [PubMed]
2. Masek, M.; Zang, J.; Mateos, J.M.; Garbelli, M.; Ziegler, U.; Neuhauss, S.C.F.; Bachmann-Gagescu, R. Studying the morphology, composition and function of the photoreceptor primary cilium in zebrafish. *Methods Cell Biol.* **2023**, *175*, 97–128. [PubMed]
3. Santiago, C.P.; Keuthan, C.J.; Boye, S.L.; Boye, S.E.; Imam, A.A.; Ash, J.D. A Drug-Tunable Gene Therapy for Broad-Spectrum Protection against Retinal Degeneration. *Mol. Ther.* **2018**, *26*, 2407–2417. [CrossRef] [PubMed]
4. Keenan, T.D.; Chew, E.Y. Association Between C-Reactive Protein and Age-Related Macular Degeneration: Les Liaisons Dangereuses. *JAMA Ophthalmol.* **2017**, *135*, 916–917. [CrossRef] [PubMed]
5. Rullo, J.; Bae, S.; Far, P.M.; Hazimi, A.A.; Gupta, V.; Bal, M.; Hopman, W.M.; Irrcher, I.; Urton, T.; Bona, M.; et al. Measuring intraocular antibodies in eyes treated with anti-vascular endothelial growth factor. *Can. J. Ophthalmol.* **2020**, *55*, 263–271. [CrossRef] [PubMed]
6. Lemasters, J.J. Selective mitochondrial autophagy, or mitophagy, as a targeted defense against oxidative stress, mitochondrial dysfunction, and aging. *Rejuvenation Res.* **2005**, *8*, 3–5. [CrossRef] [PubMed]
7. Ferrington, D.A.; Sinha, D.; Kaarniranta, K. Defects in retinal pigment epithelial cell proteolysis and the pathology associated with age-related macular degeneration. *Prog. Retin. Eye Res.* **2016**, *51*, 69–89. [CrossRef] [PubMed]
8. Lee, J.; Giordano, S.; Zhang, J. Autophagy, mitochondria and oxidative stress: Cross-talk and redox signalling. *Biochem. J.* **2012**, *441*, 523–540. [CrossRef]
9. Rodríguez-Muela, N.; Koga, H.; García-Ledo, L.; de la Villa, P.; de la Rosa, E.J.; Cuervo, A.M.; Boya, P. Balance between autophagic pathways preserves retinal homeostasis. *Aging Cell* **2013**, *12*, 478–488. [CrossRef]
10. Sun, T. Long noncoding RNAs act as regulators of autophagy in cancer. *Pharmacol. Res.* **2018**, *129*, 151–155. [CrossRef]
11. Fleury, C.; Mignotte, B.; Vayssière, J.L. Mitochondrial reactive oxygen species in cell death signaling. *Biochimie* **2002**, *84*, 131–141. [CrossRef] [PubMed]
12. Orrenius, S.; Nicotera, P.; Zhivotovsky, B. Cell death mechanisms and their implications in toxicology. *Toxicol. Sci. Off. J. Soc. Toxicol.* **2011**, *119*, 3–19. [CrossRef] [PubMed]
13. Landshamer, S.; Hoehn, M.; Barth, N.; Duvezin-Caubet, S.; Schwake, G.; Tobaben, S.; Kazhdan, I.; Becattini, B.; Zahler, S.; Vollmar, A.; et al. Bid-induced release of AIF from mitochondria causes immediate neuronal cell death. *Cell Death Differ.* **2008**, *15*, 1553–1563. [CrossRef] [PubMed]
14. Galluzzi, L.; Blomgren, K.; Kroemer, G. Mitochondrial membrane permeabilization in neuronal injury. *Nat. Rev. Neurosci.* **2009**, *10*, 481–494. [CrossRef] [PubMed]
15. Neitemeier, S.; Dolga, A.M.; Honrath, B.; Karuppagounder, S.S.; Alim, I.; Ratan, R.R.; Culmsee, C. Inhibition of HIF-prolyl-4-hydroxylases prevents mitochondrial impairment and cell death in a model of neuronal oxytosis. *Cell Death Dis.* **2016**, *7*, e2214. [CrossRef] [PubMed]
16. Chen, M.; Chen, Z.; Wang, Y.; Tan, Z.; Zhu, C.; Li, Y.; Han, Z.; Chen, L.; Gao, R.; Liu, L.; et al. Mitophagy receptor FUNDC1 regulates mitochondrial dynamics and mitophagy. *Autophagy* **2016**, *12*, 689–702. [CrossRef] [PubMed]
17. Keeling, E.; Lotery, A.J.; Tumbarello, D.A.; Ratnayaka, J.A. Impaired Cargo Clearance in the Retinal Pigment Epithelium (RPE) Underlies Irreversible Blinding Diseases. *Cells* **2018**, *7*, 16. [CrossRef]
18. Blasiak, J.; Pawlowska, E.; Szczepanska, J.; Kaarniranta, K. Interplay between Autophagy and the Ubiquitin-Proteasome System and Its Role in the Pathogenesis of Age-Related Macular Degeneration. *Int. J. Mol. Sci.* **2019**, *20*, 210. [CrossRef]
19. Fletcher, E.L.; Jobling, A.I.; Vessey, K.A.; Luu, C.; Guymer, R.H.; Baird, P.N. Animal models of retinal disease. *Prog. Mol. Biol. Transl. Sci.* **2011**, *100*, 211–286.

20. Markovets, A.M.; Saprunova, V.B.; Zhdankina, A.A.; Fursova, A.; Bakeeva, L.E.; Kolosova, N.G. Alterations of retinal pigment epithelium cause AMD-like retinopathy in senescence-accelerated OXYS rats. *Aging* **2011**, *3*, 44–54. [CrossRef]
21. Zhao, C.; Yasumura, D.; Li, X.; Matthes, M.; Lloyd, M.; Nielsen, G.; Ahern, K.; Snyder, M.; Bok, D.; Dunaief, J.L.; et al. mTOR-mediated dedifferentiation of the retinal pigment epithelium initiates photoreceptor degeneration in mice. *J. Clin. Investig.* **2011**, *121*, 369–383. [CrossRef] [PubMed]
22. Kolosova, N.G.; Muraleva, N.A.; Zhdankina, A.A.; Stefanova, N.A.; Fursova, A.Z.; Blagosklonny, M.V. Prevention of age-related macular degeneration-like retinopathy by rapamycin in rats. *Am. J. Pathol.* **2012**, *181*, 472–477. [CrossRef] [PubMed]
23. Goda, N.; Kanai, M. Hypoxia-inducible factors and their roles in energy metabolism. *Int. J. Hematol.* **2012**, *95*, 457–463. [CrossRef] [PubMed]
24. Ivan, M.; Haberberger, T.; Gervasi, D.C.; Michelson, K.S.; Günzler, V.; Kondo, K.; Yang, H.; Sorokina, I.; Conaway, R.C.; Conaway, J.W.; et al. Biochemical purification and pharmacological inhibition of a mammalian prolyl hydroxylase acting on hypoxia-inducible factor. *Proc. Natl. Acad. Sci. USA* **2002**, *99*, 13459–13464. [CrossRef] [PubMed]
25. Majmundar, A.J.; Wong, W.J.; Simon, M.C. Hypoxia-inducible factors and the response to hypoxic stress. *Mol. Cell* **2010**, *40*, 294–309. [CrossRef] [PubMed]
26. Niatsetskaya, Z.; Basso, M.; Speer, R.E.; McConoughey, S.J.; Coppola, G.; Ma, T.C.; Ratan, R.R. HIF prolyl hydroxylase inhibitors prevent neuronal death induced by mitochondrial toxins: Therapeutic implications for Huntington's disease and Alzheimer's disease. *Antioxid. Redox Signal.* **2010**, *12*, 435–443. [CrossRef] [PubMed]
27. Schneider, C.; Krischke, G.; Keller, S.; Walkinshaw, G.; Arend, M.; Rascher, W.; Gassmann, M.; Trollmann, R. Short-term effects of pharmacologic HIF stabilization on vasoactive and cytotrophic factors in developing mouse brain. *Brain Res.* **2009**, *1280*, 43–51. [CrossRef]
28. Reischl, S.; Li, L.; Walkinshaw, G.; Flippin, L.A.; Marti, H.H.; Kunze, R. Inhibition of HIF prolyl-4-hydroxylases by FG-4497 reduces brain tissue injury and edema formation during ischemic stroke. *PLoS ONE* **2014**, *9*, e84767. [CrossRef]
29. Trollmann, R.; Richter, M.; Jung, S.; Walkinshaw, G.; Brackmann, F. Pharmacologic stabilization of hypoxia-inducible transcription factors protects developing mouse brain from hypoxia-induced apoptotic cell death. *Neuroscience* **2014**, *278*, 327–342. [CrossRef]
30. Gong, H.; Rehman, J.; Tang, H.; Wary, K.; Mittal, M.; Chaturvedi, P.; Zhao, Y.Y.; Komarova, Y.A.; Vogel, S.M.; Malik, A.B. HIF2α signaling inhibits adherens junctional disruption in acute lung injury. *J. Clin. Investig.* **2015**, *125*, 652–664. [CrossRef]
31. Baich, A.; Ziegler, M. The effect of sodium iodate and melanin on the formation of glyoxylate. *Pigment. Cell Res.* **1992**, *5*, 394–395. [CrossRef] [PubMed]
32. Kiuchi, K.; Yoshizawa, K.; Shikata, N.; Moriguchi, K.; Tsubura, A. Morphologic characteristics of retinal degeneration induced by sodium iodate in mice. *Curr. Eye Res.* **2002**, *25*, 373–379. [CrossRef] [PubMed]
33. Moriguchi, M.; Nakamura, S.; Inoue, Y.; Nishinaka, A.; Nakamura, M.; Shimazawa, M.; Hara, H. Irreversible Photoreceptors and RPE Cells Damage by Intravenous Sodium Iodate in Mice Is Related to Macrophage Accumulation. *Invest. Ophthalmol. Vis. Sci.* **2018**, *59*, 3476–3487. [CrossRef] [PubMed]
34. Franco, L.M.; Zulliger, R.; Wolf-Schnurrbusch, U.E.; Katagiri, Y.; Kaplan, H.J.; Wolf, S.; Enzmann, V. Decreased visual function after patchy loss of retinal pigment epithelium induced by low-dose sodium iodate. *Investig. Ophthalmol. Vis. Sci.* **2009**, *50*, 4004–4010. [CrossRef] [PubMed]
35. Redfern, W.S.; Storey, S.; Tse, K.; Hussain, Q.; Maung, K.P.; Valentin, J.P.; Ahmed, G.; Bigley, A.; Heathcote, D.; McKay, J.S. Evaluation of a convenient method of assessing rodent visual function in safety pharmacology studies: Effects of sodium iodate on visual acuity and retinal morphology in albino and pigmented rats and mice. *J. Pharmacol. Toxicol. Methods* **2011**, *63*, 102–114. [CrossRef] [PubMed]
36. Schroeder, M.; Kjellström, U.; Lövestam-Adrian, M. Electrophysiological evaluation and 18-month follow-up of two regimens with aflibercept for neovascular age-related macular degeneration. *Doc. Ophthalmol.* **2022**, *144*, 99–115. [CrossRef] [PubMed]
37. Holm, K.; Schroeder, M.; Lövestam Adrian, M. Peripheral retinal function assessed with 30-Hz flicker seems to improve after treatment with Lucentis in patients with diabetic macular oedema. *Doc. Ophthalmol.* **2015**, *131*, 43–51. [CrossRef]
38. Schaaf, M.B.; Keulers, T.G.; Vooijs, M.A.; Rouschop, K.M. LC3/GABARAP family proteins: Autophagy-(un)related functions. *FASEB J. Off. Publ. Fed. Am. Soc. Exp. Biol.* **2016**, *30*, 3961–3978. [CrossRef]
39. Bjørkøy, G.; Lamark, T.; Brech, A.; Outzen, H.; Perander, M.; Overvatn, A.; Stenmark, H.; Johansen, T. p62/SQSTM1 forms protein aggregates degraded by autophagy and has a protective effect on huntingtin-induced cell death. *J. Cell Biol.* **2005**, *171*, 603–614. [CrossRef]
40. Wirawan, E.; Lippens, S.; Vanden Berghe, T.; Romagnoli, A.; Fimia, G.M.; Piacentini, M.; Vandenabeele, P. Beclin1: A role in membrane dynamics and beyond. *Autophagy* **2012**, *8*, 6–17. [CrossRef]
41. Beatty, S.; Koh, H.; Phil, M.; Henson, D.; Boulton, M. The role of oxidative stress in the pathogenesis of age-related macular degeneration. *Surv. Ophthalmol.* **2000**, *45*, 115–134. [CrossRef] [PubMed]
42. Mitter, S.K.; Rao, H.V.; Qi, X.; Cai, J.; Sugrue, A.; Dunn, W.A., Jr.; Grant, M.B.; Boulton, M.E. Autophagy in the retina: A potential role in age-related macular degeneration. *Adv. Exp. Med. Biol.* **2012**, *723*, 83–90. [PubMed]
43. Rullo, J.; Far, P.M.; Quinn, M.; Sharma, N.; Bae, S.; Irrcher, I.; Sharma, S. Local oral and nasal microbiome diversity in age-related macular degeneration. *Sci. Rep.* **2020**, *10*, 3862. [CrossRef] [PubMed]

44. Bellot, G.; Garcia-Medina, R.; Gounon, P.; Chiche, J.; Roux, D.; Pouysségur, J.; Mazure, N.M. Hypoxia-induced autophagy is mediated through hypoxia-inducible factor induction of BNIP3 and BNIP3L via their BH3 domains. *Mol. Cell. Biol.* **2009**, *29*, 2570–2581. [CrossRef] [PubMed]
45. Wang, A.L.; Lukas, T.J.; Yuan, M.; Du, N.; Tso, M.O.; Neufeld, A.H. Autophagy and exosomes in the aged retinal pigment epithelium: Possible relevance to drusen formation and age-related macular degeneration. *PLoS ONE* **2009**, *4*, e4160. [CrossRef] [PubMed]
46. Semenza, G.L. Hypoxia-inducible factor 1: Regulator of mitochondrial metabolism and mediator of ischemic preconditioning. *Biochim. Biophys. Acta* **2011**, *1813*, 1263–1268. [CrossRef] [PubMed]
47. Novak, I.; Kirkin, V.; McEwan, D.G.; Zhang, J.; Wild, P.; Rozenknop, A.; Rogov, V.; Löhr, F.; Popovic, D.; Occhipinti, A.; et al. Nix is a selective autophagy receptor for mitochondrial clearance. *EMBO Rep.* **2010**, *11*, 45–51. [CrossRef]
48. Nazim, U.M.; Moon, J.H.; Lee, J.H.; Lee, Y.J.; Seol, J.W.; Eo, S.K.; Lee, J.H.; Park, S.Y. Activation of autophagy flux by metformin downregulates cellular FLICE-like inhibitory protein and enhances TRAIL- induced apoptosis. *Oncotarget* **2016**, *7*, 23468–23481. [CrossRef]
49. Kaarniranta, K.; Sinha, D.; Blasiak, J.; Kauppinen, A.; Veréb, Z.; Salminen, A.; Boulton, M.E.; Petrovski, G. Autophagy and heterophagy dysregulation leads to retinal pigment epithelium dysfunction and development of age-related macular degeneration. *Autophagy* **2013**, *9*, 973–984. [CrossRef]
50. Wang, J.; Ohno-Matsui, K.; Yoshida, T.; Shimada, N.; Ichinose, S.; Sato, T.; Mochizuki, M.; Morita, I. Amyloid-beta up-regulates complement factor B in retinal pigment epithelial cells through cytokines released from recruited macrophages/microglia: Another mechanism of complement activation in age-related macular degeneration. *J. Cell Physiol.* **2009**, *220*, 119–128. [CrossRef]
51. Yao, J.; Jia, L.; Khan, N.; Lin, C.; Mitter, S.K.; Boulton, M.E.; Dunaief, J.L.; Klionsky, D.J.; Guan, J.L.; Thompson, D.A.; et al. Deletion of autophagy inducer RB1CC1 results in degeneration of the retinal pigment epithelium. *Autophagy* **2015**, *11*, 939–953. [CrossRef]
52. Kuro, M.; Yoshizawa, K.; Uehara, N.; Miki, H.; Takahashi, K.; Tsubura, A. Calpain inhibition restores basal autophagy and suppresses MNU-induced photoreceptor cell death in mice. *In Vivo* **2011**, *25*, 617–623. [PubMed]
53. Zhou, Z.; Vinberg, F.; Schottler, F.; Doggett, T.A.; Kefalov, V.J.; Ferguson, T.A. Autophagy supports color vision. *Autophagy* **2015**, *11*, 1821–1832. [CrossRef] [PubMed]
54. Li, G.Y.; Fan, B.; Jiao, Y.Y. Rapamycin attenuates visible light-induced injury in retinal photoreceptor cells via inhibiting endoplasmic reticulum stress. *Brain Res.* **2014**, *1563*, 1–12. [CrossRef] [PubMed]
55. Lazarou, M.; Sliter, D.A.; Kane, L.A.; Sarraf, S.A.; Wang, C.; Burman, J.L.; Sideris, D.P.; Fogel, A.I.; Youle, R.J. The ubiquitin kinase PINK1 recruits autophagy receptors to induce mitophagy. *Nature* **2015**, *524*, 309–314. [CrossRef] [PubMed]
56. Wu, W.; Tian, W.; Hu, Z.; Chen, G.; Huang, L.; Li, W.; Zhang, X.; Xue, P.; Zhou, C.; Liu, L.; et al. ULK1 translocates to mitochondria and phosphorylates FUNDC1 to regulate mitophagy. *EMBO Rep.* **2014**, *15*, 566–575. [CrossRef] [PubMed]
57. Hui, L.; Wu, H.; Wang, T.W.; Yang, N.; Guo, X.; Jang, X.J. Hydrogen peroxide-induced mitophagy contributes to laryngeal cancer cells survival via the upregulation of FUNDC1. *Clin. Transl. Oncol.* **2019**, *21*, 596–606. [CrossRef]
58. Feng, J.; Tan, W.; Li, T.; Yan, Q.; Zhu, H.; Sun, X. Human retinal pigment epithelial cells are protected against hypoxia by BNIP3. *Ann. Transl. Med.* **2020**, *8*, 1502. [CrossRef]
59. Zhang, Y.; Liu, D.; Hu, H.; Zhang, P.; Xie, R.; Cui, W. HIF-1α/BNIP3 signaling pathway-induced-autophagy plays protective role during myocardial ischemia-reperfusion injury. *Biomed. Pharmacother.* **2019**, *120*, 109464. [CrossRef]
60. Wei, H.; Liu, L.; Chen, Q. Selective removal of mitochondria via mitophagy: Distinct pathways for different mitochondrial stresses. *Biochim. Biophys. Acta* **2015**, *1853*, 2784–2790. [CrossRef]
61. Shelby, S.J.; Angadi, P.S.; Zheng, Q.D.; Yao, J.; Jia, L.; Zacks, D.N. Hypoxia inducible factor 1α contributes to regulation of autophagy in retinal detachment. *Exp. Eye Res.* **2015**, *137*, 84–93. [CrossRef] [PubMed]
62. Liu, H.; Zhu, H.; Li, T.; Zhang, P.; Wang, N.; Sun, X. Prolyl-4-Hydroxylases Inhibitor Stabilizes HIF-1α and Increases Mitophagy to Reduce Cell Death After Experimental Retinal Detachment. *Investig. Ophthalmol. Vis. Sci.* **2016**, *57*, 1807–1815. [CrossRef] [PubMed]
63. Zhu, D.; Xie, M.; Gademann, F.; Cao, J.; Wang, P.; Guo, Y.; Zhang, L.; Su, T.; Zhang, J.; Chen, J. Protective effects of human iPS-derived retinal pigmented epithelial cells on retinal degenerative disease. *Stem Cell Res. Ther.* **2020**, *11*, 98. [CrossRef] [PubMed]
64. Ott, M.; Gogvadze, V.; Orrenius, S.; Zhivotovsky, B. Mitochondria, oxidative stress and cell death. *Apoptosis Int. J. Program. Cell Death* **2007**, *12*, 913–922. [CrossRef] [PubMed]
65. Liu, L.; Feng, D.; Chen, G.; Chen, M.; Zheng, Q.; Song, P.; Ma, Q.; Zhu, C.; Wang, R.; Qi, W.; et al. Mitochondrial outer-membrane protein FUNDC1 mediates hypoxia-induced mitophagy in mammalian cells. *Nat. Cell Biol.* **2012**, *14*, 177–185. [CrossRef]
66. Panieri, E.; Gogvadze, V.; Norberg, E.; Venkatesh, R.; Orrenius, S.; Zhivotovsky, B. Reactive oxygen species generated in different compartments induce cell death, survival, or senescence. *Free Radic. Biol. Med.* **2013**, *57*, 176–187. [CrossRef] [PubMed]
67. Datta, S.; Cano, M.; Ebrahimi, K.; Wang, L.; Handa, J.T. The impact of oxidative stress and inflammation on RPE degeneration in non-neovascular AMD. *Prog. Retin. Eye Res.* **2017**, *60*, 201–218. [CrossRef] [PubMed]
68. Hernández, C.; Bogdanov, P.; Corraliza, L.; García-Ramírez, M.; Solà-Adell, C.; Arranz, J.A.; Arroba, A.I.; Valverde, A.M.; Simó, R. Topical Administration of GLP-1 Receptor Agonists Prevents Retinal Neurodegeneration in Experimental Diabetes. *Diabetes* **2016**, *65*, 172–187. [CrossRef]

69. Lee, S.Y.; Oh, J.S.; Rho, J.H.; Jeong, N.Y.; Kwon, Y.H.; Jeong, W.J.; Ryu, W.Y.; Ahn, H.B.; Park, W.C.; Rho, S.H.; et al. Retinal pigment epithelial cells undergoing mitotic catastrophe are vulnerable to autophagy inhibition. *Cell Death Dis.* **2014**, *5*, e1303. [CrossRef]
70. Jiang, D.; Ryals, R.C.; Huang, S.J.; Weller, K.K.; Titus, H.E.; Robb, B.M.; Saad, F.W.; Salam, R.A.; Hammad, H.; Yang, P.; et al. Monomethyl Fumarate Protects the Retina From Light-Induced Retinopathy. *Investig. Ophthalmol. Vis. Sci.* **2019**, *60*, 1275–1285. [CrossRef]
71. Reichenbach, A.; Bringmann, A. Glia of the human retina. *Glia* **2020**, *68*, 768–796. [CrossRef]
72. Kingwell, K. Neurodegenerative disease: Microglia in early disease stages. *Nat. Rev. Neurol.* **2012**, *8*, 475. [CrossRef]
73. Rullo, J.; Pennimpede, T.; Mehraban Far, P.; Strube, Y.N.; Irrcher, I.; Urton, T.; Bona, M.; Gonder, T.; Campbell, R.J.; Ten Hove, M.; et al. Intraocular calcidiol: Uncovering a role for vitamin D in the eye. *J. Steroid Biochem. Mol. Biol.* **2020**, *197*, 105536. [CrossRef]
74. Mora, R.; Régnier-Vigouroux, A. Autophagy-driven cell fate decision maker: Activated microglia induce specific death of glioma cells by a blockade of basal autophagic flux and secondary apoptosis/necrosis. *Autophagy* **2009**, *5*, 419–421. [CrossRef]
75. Bringmann, A.; Pannicke, T.; Grosche, J.; Francke, M.; Wiedemann, P.; Skatchkov, S.N.; Osborne, N.N.; Reichenbach, A. Müller cells in the healthy and diseased retina. *Prog. Retin. Eye Res.* **2006**, *25*, 397–424. [CrossRef]
76. Kugler, E.; Bravo, I.; Durmishi, X.; Marcotti, S.; Beqiri, S.; Carrington, A.; Stramer, B.; Mattar, P.; MacDonald, R.B. GliaMorph: A modular image analysis toolkit to quantify Müller glial cell morphology. *Development* **2023**, *150*, dev201008. [CrossRef] [PubMed]

antioxidants

Article

Buspirone Enhances Cell Survival and Preserves Structural Integrity during Oxidative Injury to the Retinal Pigment Epithelium

Manas R. Biswal [1,*], Ryan J. Paulson [1], Riddhi Vichare [1] and Alfred S. Lewin [2]

[1] Department of Pharmaceutical Sciences, USF Taneja College of Pharmacy, Tampa, FL 33612, USA; vicharer@usf.edu (R.V.)
[2] Department of Molecular Genetics & Microbiology, College of Medicine, University of Florida, Gainesville, FL 32603, USA; lewin@ufl.edu
* Correspondence: biswal@usf.edu

Abstract: Chronic oxidative stress impairs the normal functioning of the retinal pigment epithelium (RPE), leading to atrophy of this cell layer in cases of advance age-related macular degeneration (AMD). The purpose of our study was to determine if buspirone, a partial serotonin 1A (5-HT1A) receptor agonist, protected against oxidative stress-induced changes in the RPE. We exposed differentiated human ARPE-19 cells to paraquat to induce oxidative damage in culture, and utilized a mouse model with sodium iodate ($NaIO_3$)-induced oxidative injury to evaluate the effect of buspirone. To investigate buspirone's effect on protective gene expression, we performed RT–PCR. Cellular toxicities and junctional abnormalities due to paraquat induction in ARPE-19 cells and buspirone's impact were assessed via WST-1 assays and ZO-1 immunostaining. We used spectral-domain optical coherence tomography (SD-OCT) and ZO-1 immunostaining of RPE/choroid for structural analysis. WST-1 assays showed dose-dependent protection of viability in buspirone-treated ARPE-19 cells in culture and preservation of RPE junctional integrity under oxidative stress conditions. In the $NaIO_3$ model, daily intraperitoneal injection (i.p.) of buspirone (30 mg/kg) for 12 days improved the survival of photoreceptors compared to those of vehicle-treated eyes. ZO-1-stained RPE flat-mounts revealed the structural preservation of RPE from oxidative damage in buspirone-treated mice, as well as in buspirone-induced *Nqo1*, *Cat*, *Sqstm1*, *Gstm1*, and *Sod2* genes in the RPE/choroid compared to untreated eyes. Since oxidative stress is implicated in the pathogenesis AMD, repurposing buspirone, which is currently approved for the treatment of anxiety, might be useful in treating or preventing dry AMD.

Keywords: retina; buspirone; oxidative stress; retinal pigment epithelium; antioxidants; ZO-1; ARPE-19; $NaIO_3$

1. Introduction

Age-related macular degeneration (AMD) is a prevalent and debilitating ocular disease that affects millions of individuals worldwide, leading to progressive central vision loss and a substantial burden on healthcare systems. The hallmark of AMD is the degeneration of the retinal pigment epithelium (RPE), a critical cell monolayer essential for maintaining retinal health. While the pathogenesis of AMD is multifactorial, oxidative stress and chronic inflammation are pivotal contributors [1,2], making them compelling targets for therapeutic intervention.

Buspirone, a widely recognized anxiolytic agent [3–5], has recently garnered significant attention in the realm of ophthalmology due to its potential to address a critical unmet need in the treatment of age-related macular degeneration (AMD) [6]. This innovation lies in buspirone's distinctive pharmacological profile, which includes serotonin 1A (5-HT1A) receptor agonism alongside antioxidant and neuroprotective properties. This

combination positions buspirone as a multifaceted candidate for retinal therapy. Studies have shown that 5-HT1A receptor activation can exert neuroprotective effects in various neuronal systems [7–9], and emerging evidence suggests it has relevance to the retina, particularly in contexts involving oxidative stress and neuroinflammation. Moreover, buspirone has exhibited robust antioxidant capabilities in preclinical models [10,11] aiding in the attenuation of oxidative damage, a pivotal hallmark of AMD pathogenesis [12,13].

The retinal pigment epithelium (RPE) serves as a vital cellular barrier and orchestrates critical functions essential for the maintenance of retinal homeostasis and visual function. In the face of oxidative stress and the constant challenge posed by environmental factors, the RPE relies on a sophisticated network of protective genes to safeguard its integrity and ensure optimal functionality. Among these, the genes NAD(P)H dehydrogenase quinone 1 (*Nqo1*), catalase (*Cat*), Sequestosome 1 (*Sqstm1*), glutathione S-transferase M1 (*Gstm1*), and superoxide dismutase 2 (*Sod2*) have emerged as pivotal guardians, actively participating in the defense against various insults. This introduction seeks to elucidate why the expression and functionality of these genes are crucial to the protective milieu within the RPE.

Nqo1, a multifunctional enzyme and a targeted gene of transcription factor nuclear factor erythroid-2-related factor 2 Nfe2l2 (also known as Nrf2), plays a central role in the detoxification of reactive quinones and the maintenance of cellular redox balance [14]. Its ability to neutralize electrophilic compounds and mitigate oxidative stress positions *Nqo1* as a crucial guardian against cellular damage in the RPE [15]. By preventing the accumulation of harmful species, *Nqo1* acts as an indispensable component of the RPE's defense mechanism [16]. Catalase, an enzymatic cornerstone in the breakdown of hydrogen peroxide, assumes a paramount role in mitigating oxidative damage within the RPE. As a primary defender against reactive oxygen species (ROS), catalase serves to preserve the delicate equilibrium of the cellular microenvironment, preventing oxidative stress-induced harm and bolstering the resilience of the RPE. Sqstm1, a regulator of autophagy and cellular quality control, emerges as a key player in maintaining RPE homeostasis. Its involvement in the clearance of damaged cellular components and misfolded proteins positions *Sqstm1* as a safeguard against the deleterious consequences of cellular stress. Via the orchestration of autophagic processes, Sqstm1 contributes to the overall protection and longevity of RPE cells.

Gstm1, an integral member of the glutathione S-transferase family, plays a pivotal role in detoxification processes within the RPE. By catalyzing the conjugation of electrophilic compounds with glutathione, *Gstm1* enhances cellular defense against oxidative stress and maintains the integrity of critical cellular components [17]. Its presence in the RPE improves efficient detoxification mechanisms with oxidative damage and enhances RPE protection. *Sod2*, a mitochondrial antioxidant enzyme, serves as a frontline defender against superoxide radicals within the RPE [18]. By catalyzing the dismutation of superoxide into oxygen and hydrogen peroxide, *Sod2* acts as a critical component of the RPE's antioxidant arsenal. Its capacity to neutralize one of the primary reactive oxygen species reinforces the importance of *Sod2* in preserving redox balance and cellular viability in the RPE [19]. These protective genes weave a complex yet interdependent web of defense mechanisms crucial for the RPE's ability to withstand oxidative stress and maintain its pivotal role in retinal health.

Previous research has demonstrated the efficacy of 5-HTA1 receptor agonists in mitigating oxidative stress in diverse cellular and animal models [20–23], offering a solid foundation for the application of buspirone in retinal protection. Additionally, its favorable safety profile and established clinical use in psychiatry underscore its potential to be repurposed in ophthalmology, offering an expedited pathway for clinical translation. The convergence of these factors presents an opportunity to explore buspirone's therapeutic potential in preserving retinal function and combating AMD, with implications for patients worldwide.

Paraquat and sodium iodate ($NaIO_3$) are both chemical agents used to induce oxidative stress in cell culture and animal models, respectively, for studying retinal degenera-

tion [22,24]. However, it is important to note that they are distinct agents with different mechanisms of action and applications. While paraquat-induced cell models and $NaIO_3$-induced mouse models are distinct, they can be used in complementary ways. Paraquat-induced cell models can provide insights into the cellular and molecular responses of retinal cells to oxidative stress, which is a component of the broader retinal degeneration process. Understanding how oxidative stress affects cellular responses in vitro (paraquat model) in response to a therapeutic agent can inform the interpretation of the in vivo effects observed in $NaIO_3$-induced mouse models. The paraquat model may be useful for studying early responses to oxidative stress at the cellular level, while the $NaIO_3$-induced mouse model allows for the investigation of downstream consequences in the context of the intact retina and interactions between different retinal cell types [25]. The relationship lies in their shared focus on oxidative stress and their potential synergy in providing a more comprehensive view of retinal pathology and potential interventions.

In this study, we tested an well-known anxiolytic drug in mitigating RPE atrophy using a two-tiered approach. First, we investigated the effects of buspirone in ARPE-19 cells, an established in vitro model for RPE function, to understand its impact on cell viability and protective mechanisms against oxidative stress. ARPE-19 cells, derived from the human RPE, offer valuable insights into the cellular aspects of AMD pathology, and serve as a practical platform for drug testing [26,27]. Subsequently, we translated our findings to an in vivo setting by employing a mouse model of RPE atrophy induced using sodium iodate ($NaIO_3$). The $NaIO_3$ model is characterized by oxidative stress-mediated damage to the RPE, closely mimicking certain features of AMD [28–31]. Buspirone was administered to assess its potential in ameliorating retinal degeneration, evaluating its suitability as a therapeutic agent.

By adopting this dual approach, we aim to provide a comprehensive evaluation of buspirone's efficacy in preserving RPE function and retinal health. Our findings hold promise for the development of novel therapies to combat AMD, potentially offering renewed hope for individuals afflicted by this devastating ocular disease.

2. Materials and Methods

2.1. Cell Culture

ARPE-19 cells (Cat no: CRL-2302™), derived from the human retinal pigment epithelium, were purchased from ATCC (Manassas, VA, USA) and maintained in our laboratory according to established protocols [32,33]. Cells were cultured in T75 flasks using Dulbecco's Modified Eagle Medium (DMEM)/F-12 supplemented with 10% fetal bovine serum (FBS) and 1% penicillin–streptomycin solution (ATCC, Manassas, VA, USA). The culture medium was changed every 2–3 days, and cells were maintained in a humidified incubator at 37 °C with 5% CO_2. Subculturing was performed when cells reached 80–90% confluency, using a trypsin-EDTA solution to detach the cells from the flask. For experimental assays, ARPE-19 cells were seeded at an appropriate density in 6-well plates or culture dishes, depending on the specific requirements of the assay. All experiments were conducted using cells between passages 4 and 10 to ensure consistency and minimize potential phenotypic drift. To obtain RPE monolayers with cobblestone appearance and tight junctions, ARPE-19 cells sere cultured in Minimum Essential Medium including nicotinamide, as described by Hazim et al. [26].

2.2. Cellular Apoptosis Assay

Cell viability was assessed using the cell proliferation reagent (WST-1, Cat no: 05015944001, Germany) [34,35] to evaluate the impact of buspirone on ARPE-19 cells. The WST-1 assay protocol is based on the cleavage of the tetrazolium salt WST-1 to formazan using cellular mitochondrial dehydrogenases. Briefly, ARPE-19 cells were seeded in 96-well plates at a density of 6000 cells per well and allowed to adhere overnight. Following adherence, cells were treated with varying concentrations of buspirone and paraquat for a specified duration. Control wells received equivalent volumes of the vehicle solution. After treatment, 10 µL of

WST-1 reagent was added to each well, and the plates were incubated for an additional two hours at 37 °C. Absorbance was measured at 450 nm using a microplate reader. Data were analyzed using GraphPad-Prism (version 9), and viability percentages were calculated relative to vehicle-treated controls. All experiments were conducted in triplicate and repeated at least three times to ensure statistical significance.

2.3. Animals

Male C57BL/6J mice, aged 6–8 weeks, were utilized in accordance with University of South Florida (USF) Institutional Animal Care and Use Committees (IACUCs) for animal care and use. To induce retinal degeneration, a sodium iodate ($NaIO_3$) model was employed. Mice were randomly assigned to experimental groups: the $NaIO_3$-treated group and the $NaIO_3$ + buspirone-treated group. $NaIO_3$ was administered via a single intraperitoneal injection at a dosage of 20 mg/kg body weight. Buspirone treatment commenced three days before $NaIO_3$ injection, with daily intraperitoneal administrations at a dosage of 30 mg/kg body weight for next 12 days post $NaIO_3$ injection. Control animals received equivalent volumes of the vehicle solution. SD-OCT and RPE/Choroid flat mount assessments were conducted one day after the last buspirone treatment to evaluate the efficacy of buspirone in ameliorating retinal degeneration induced by $NaIO_3$.

2.4. Real Time PCR

Our investigation was designed to assess gene expression changes within the retinal pigment epithelium (RPE) and choroidal tissues. To investigate the potential therapeutic effects of buspirone, RPE and choroid tissues were carefully dissected, and total RNA was extracted using the RNeasy Mini Kit (Qiagen, MD, USA). The resulting RNA samples were then reverse-transcribed into complementary DNA (cDNA), quantitative real-time PCR was performed using CFX Opus 96 Real-Time PCR System (Bio-Rad, CA, USA) [36], and its program was used to analyze the expression levels of key genes implicated in retinal degeneration. The PCR primers used for this analysis are listed in Table 1.

Table 1. Essential details for the genes analyzed, including their respective gene names, RefSeq IDs, forward primer sequences, and reverse primer sequences. These primer sequences are crucial for the accurate amplification of the target genes in real time PCR experiments.

Genes	Ref. Seq	Forward Primer	Reverse Primer
Beta-Actin	NM_007393.3	CGAGCACAGCTTCTTTGCAG	TTCCCACCATCACACCCTGG
Nqo1	NM_008706.5	CGACAACGGTCCTTTCCAGA	CCAGACGGTTTCCAGACGTT
Cat	NM_009804.2	CGCAATCCTACACCATGTCG	AGTATCCAAAAGCACCTGCTCC
Sqstm1	NM_011018.2	GGAAGCTGCCCTATACCCAC	GCTTGGCCACAGCACTATCA
Gstm1	NM_010358.5	GGGATACTGGAACGTCCGC	GCTCTGGGTGATCTTGTGTGA
Sod2	NM_013671.3	CAGGATGCCGCTCCGTTAT	TGAGGTTTACACGACCGCTG

2.5. SD-OCT Imaging and Measurement of Total Retinal Thickness

Spectral-domain optical coherence tomography (SD-OCT) imaging with the Phoenix Micron IV system was used to assess retinal morphology in our study [37]. Both male and female C57BL/6 mice, aged 8–10 weeks, were selected for this investigation. After appropriate anesthesia and pupil dilation, mice were gently positioned, and SD-OCT scans were obtained with high resolution and precision. Specifically, we focused on measuring total retinal thickness, which encompasses the entire retinal structure, from the inner limiting membrane to the retinal pigment epithelium. Multiple scans were acquired per eye to ensure data accuracy and consistency. The acquired images were subsequently processed and analyzed using the intelligent eye segmentation software "InSight" (version -2) to visualize retinal layers automatically or interactively to obtain precise measurements of total retinal

thickness. This approach provided a detailed assessment of retinal structural alterations, offering valuable insights into the effects of drugs or oxidants on retinal integrity.

2.6. Immunohistochemistry

For the assessment of tight junction integrity, differentiated ARPE-19 cells [26] were grown on coverslips and fixed with 4% paraformaldehyde [38]. After permeabilization with 0.3% Triton X-100, cells were incubated with a primary antibody against ZO-1 (Invitrogen, Waltham, MA, USA) (Cat. No-40-2200, 1:200 ratio) overnight at 4 °C, followed by Alexa Fluor 488 goat anti-rabbit (Molecular Probes; Invitrogen, Waltham, MA, USA) (Cat no: A11008) secondary antibody incubation (1:1000) for an 1 h. Imaging was performed using a Keyence fluorescence microscope imaging system. For the examination of ZO-1 expression in retinal pigment epithelium (RPE) and choroidal tissues, enucleated mouse eyes were dissected to obtain RPE/choroid flat mounts. These were fixed, blocked, and incubated with the same primary antibody against ZO-1 (1:200) overnight at 4 °C [39]. Subsequently, tissues were treated with DyLight 650 conjugated goat anti-rabbit secondary antibody (Invitrogen, Waltham, MA, USA) (Cat no: SA5-10041, 1:1000). Flat mounts were mounted on glass slides and visualized using a Keyence fluorescence microscope imaging system. This dual approach allowed for a comprehensive evaluation of ZO-1 expression patterns both at the cellular level in ARPE-19 cells and within intact RPE/choroid tissues from mice [40].

2.7. Statistical Analysis

For experiments involving ARPE-19 cell cultures, results were expressed as mean ± standard deviation (SD) of three independent experiments. Statistical significance was determined using Student's *t*-test (two-tailed) using GraphPad Prism software (version 9). For assessments involving C57BL/6J mice and RPE/choroid flat mounts, data were analyzed using GraphPad Prism. Differences between the two groups were evaluated using Student's *t*-test (two-tailed). Results were considered statistically significant when $p < 0.05$. All statistical analyses were performed by an investigator blinded to the experimental conditions to minimize bias.

3. Results

3.1. Buspirone Prevented Oxidative Stress Induced Cell Death

In our investigation, the potential of buspirone in mitigating oxidative stress-induced cell death was evaluated utilizing ARPE-19 cells, an established in vitro model for retinal pigment epithelium (RPE) function. Following exposure to paraquat (at 400 μM), which induces mitochondrial oxidative stress, cells treated with buspirone exhibited a pronounced increase in viability. Treatment with buspirone, at concentrations ranging from 0.1 μM to 10 μM, conferred a significant protective effect against oxidative stress-induced cell death compared to untreated controls (Figure 1). The results, assessed via WST-1 assay, revealed a robust preservation of cell viability, indicative of buspirone's potent cytoprotective properties in the face of oxidative insult.

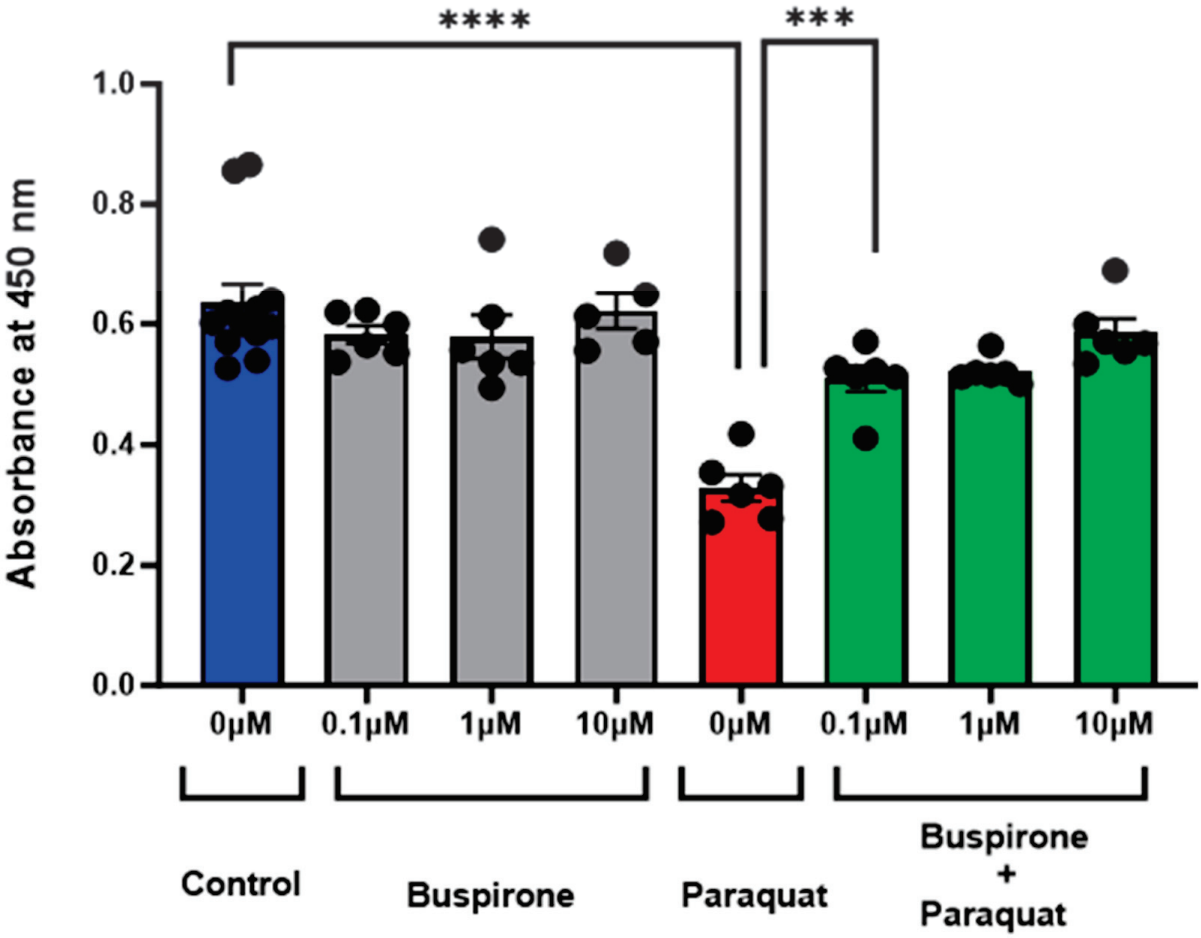

Figure 1. Effect of Buspirone Pretreatment on Paraquat-Induced Cell Death in ARPE-19 Cells as Assessed via WST-1 Assay. The graph depicts the absorbance values obtained via WST-1 assay, reflecting cell viability, in ARPE-19 cells subjected to various treatments. The x-axis represents different treatment groups: (1) control, (2) buspirone-treated, (3) induced cell death, and (4) buspirone pre-treatment + paraquat. The y-axis denotes the absorbance measured at 450 nm. Data points represent the mean ± standard error of mean of n = 6, with 3 independent experiments. Statistical significance was determined using Student's *t*-test between two groups, with $p < 0.05$ considered as statistically significant. *** $p < 0.001$, **** $p < 0.0001$.

3.2. Buspirone Prevented RPE Structural Disintegration from Oxidative Damage

To assess the protective effects of buspirone on differentiated ARPE-19 cells, we employed ZO-1 immunocytochemistry on cells cultured in 8-well chamber slides. Following differentiation [26], ARPE-19 cells were subjected to oxidative stress induced using paraquat (1000 μM) treatment. Strikingly, cells pre-treated with buspirone demonstrated a substantial preservation of structural integrity compared to untreated counterparts (Figure 2). ZO-1, a critical tight junction protein, exhibited a robust and organized distribution pattern along the cell–cell boundaries, indicative of maintained cellular architecture. Conversely, in the absence of buspirone, paraquat-induced oxidative stress led to a noticeable disruption of ZO-1 staining, reflecting compromised cell–cell interactions and structural disintegration. These findings underscore the potent protective effect of buspirone in shielding differentiated ARPE-19 cells against oxidative damage, highlighting its potential as a therapeutic candidate for retinal degenerative conditions characterized by heightened oxidative stress.

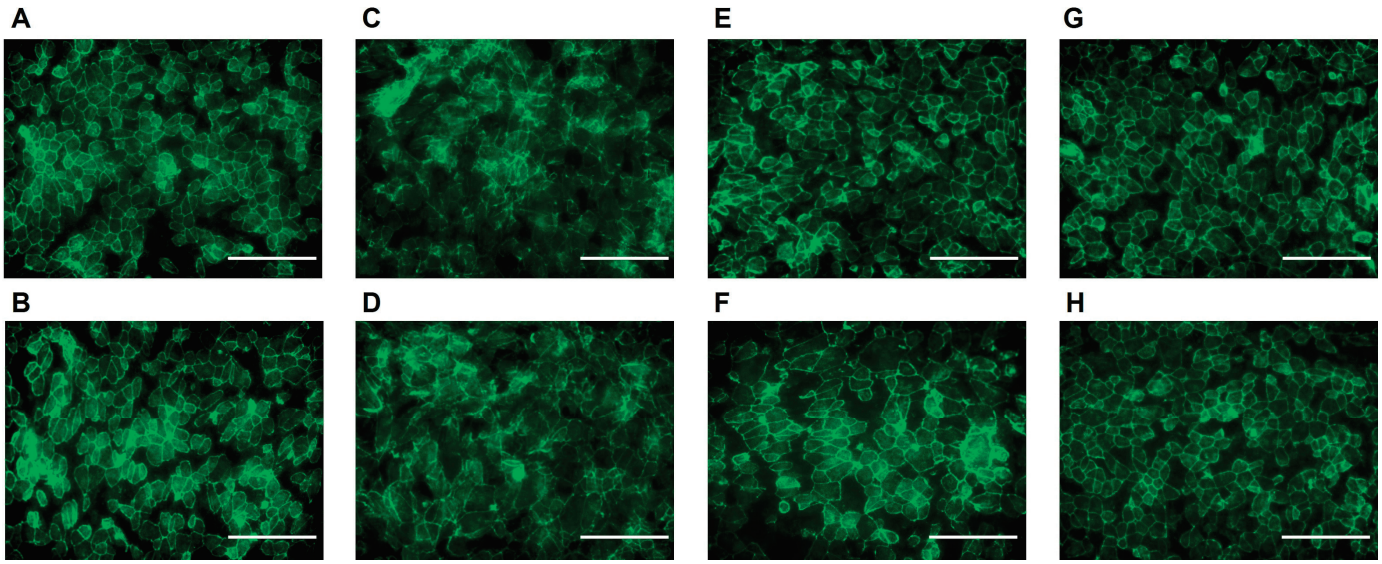

Figure 2. Immunocytochemical Staining of Differentiated ARPE-19 Cells Treated with Paraquat and Buspirone. The images display the immunocytochemistry of differentiated ARPE-19 cells subjected to different treatments. ZO-1, a marker for tight junctions, is labeled in green. (**A**,**B**) Control group, (**C**,**D**) paraquat (1000 μM)-induced cell stress, (**E**,**F**) buspirone (1 μM)-pre-treated cells followed by paraquat (1000 μM) exposure, and (**G**,**H**) buspirone (10 μM) pre-treated cells followed by paraquat (1000 μM) exposure. (40× magnification, scale bar 100 micron).

3.3. Presence of Buspirone-Preserved Retinal Structure in an Acute Model of RPE Oxidative Damge

Utilizing spectral-domain optical coherence tomography (SD-OCT), we assessed the impact of buspirone on the preservation of retinal structure in an acute model of retinal pigment epithelium (RPE) oxidative damage (Figures 3 and S1). The measurements of total retinal thickness and outer nuclear layer (ONL) thickness provided insights into the integrity of the retinal architecture. Strikingly, the presence of buspirone conferred a preservation of both total retinal thickness and ONL thickness. Notably, the photoreceptor layer, a critical component of retinal function, exhibited a significant conservation, emphasizing buspirone's protective effect. These findings underscore the potency of buspirone in mitigating acute RPE oxidative damage, leading to the preservation of retinal layers and, particularly, the photoreceptor layer, which holds significance for vision maintenance.

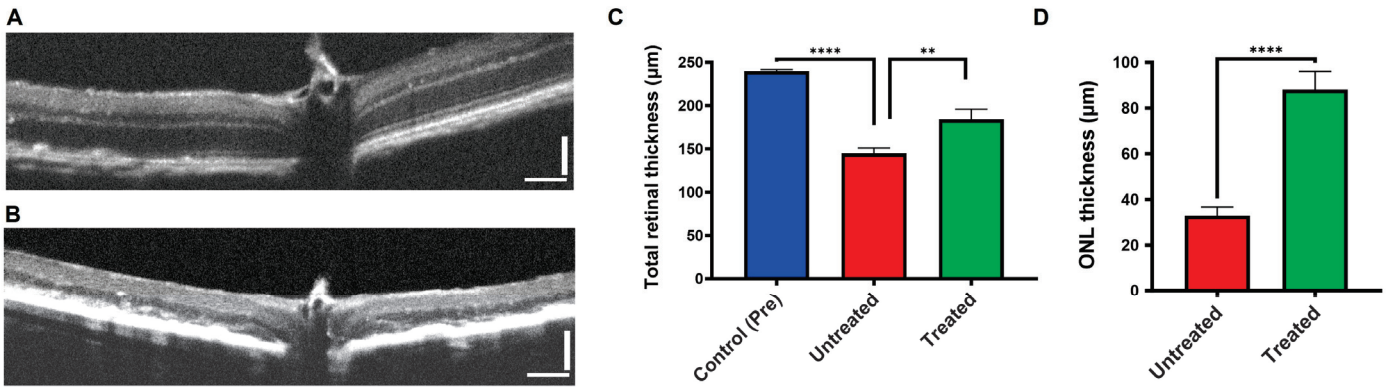

Figure 3. Retinal Thickness Analysis in Response to Buspirone Treatment. The figure illustrates the impact of buspirone treatment on retinal structure in a $NaIO_3$-induced RPE injury model at the 12-day time point. Representative SD-OCT images depict the structural changes in the retinal layers

in response to buspirone treatment (**A**). An image from a $NaIO_3$ injected mouse without buspirone treatment (**B**) is shown for comparison. (**C**) Total retinal thickness was measured, indicating the effects of buspirone treatment on overall retinal architecture. (**D**) Measurement of the outer nuclear layer quantifies the impact of buspirone on photoreceptor survival. Data represent the mean ± s.e.m. (Control pre-treatment, n= 20; untreated, n = 9; treated, n = 11). ** $p < 0.01$, **** $p < 0.0001$. (Scale bar 75 micron).

3.4. Buspirone Preserved RPE Structural Integrity In Vivo from Oxidative Damage

The potential of buspirone in preserving retinal structure was evaluated in an acute model of retinal pigment epithelium (RPE) oxidative damage, using RPE/choroidal flat mount assessments coupled with ZO-1 staining. Following exposure to $NaIO_3$, a striking contrast in retinal structural integrity became evident. In the presence of buspirone, the retinal flat mounts displayed a well-preserved and -organized arrangement of hexagonal cells, characteristic of healthy RPE tissue, as observed via fluorescent imaging (Figure 4). The ZO-1 staining patterns further emphasized the intact cellular architecture, with the critical tight junction protein maintaining its well-defined distribution. Conversely, in the absence of buspirone, oxidative damage induced using the acute model led to a distinct disarray of hexagonal cells, indicative of structural damage. ZO-1 staining corroborated these findings by highlighting disrupted cell–cell interactions. These results underscore the robust retinal-preserving potential of buspirone, offering promising prospects for its application in retinal degenerative conditions characterized by oxidative stress.

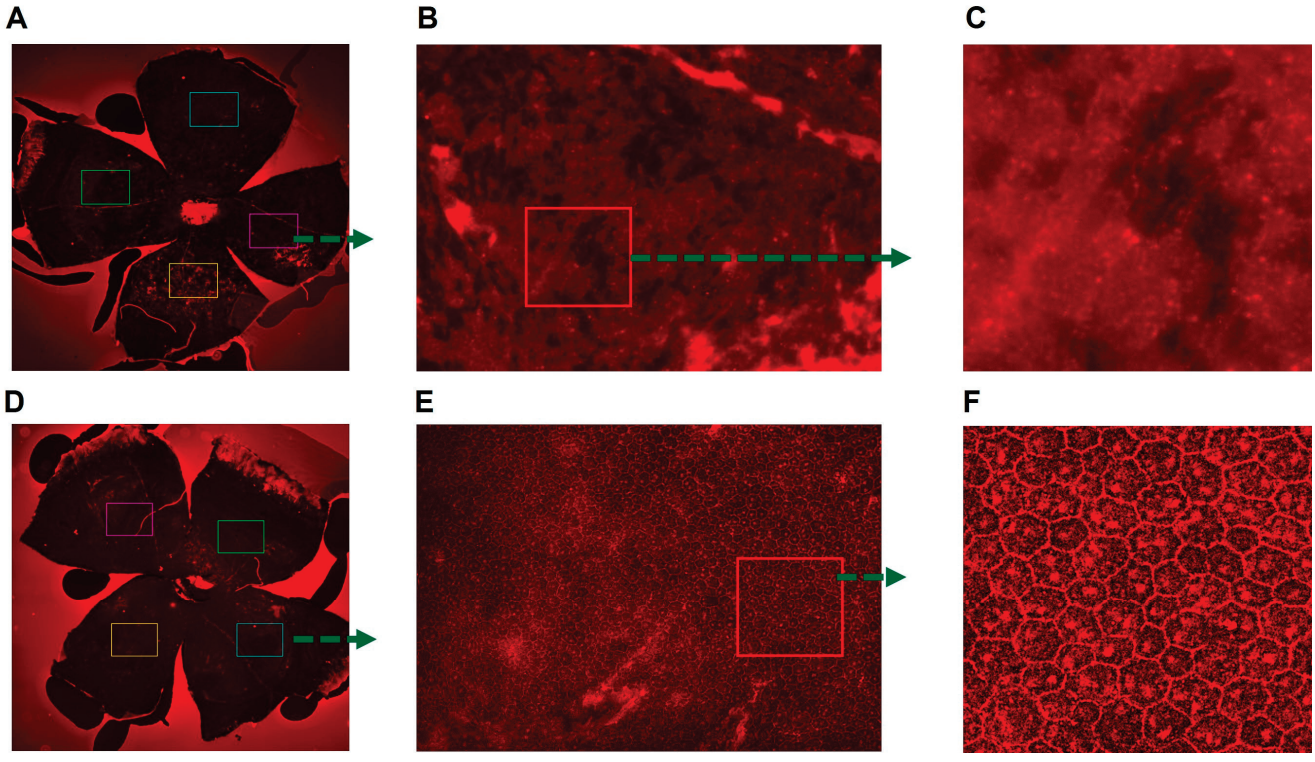

Figure 4. Buspirone Preserves RPE Structural Integrity In Vivo: RPE Flat Mount Immunostaining for ZO-1. The images demonstrate the effects of buspirone treatment on RPE (Retinal Pigment Epithelium) structural integrity in vivo. (**A**) Mice injected with NaOI3 but untreated with buspirone served as a comparison (4× magnification). (**B**) 20× magnification, (**C**) 100× magnification, (**D**) The buspirone treated mouse showed preserved RPE morphology in response to buspirone administration (4× magnification). (**E**) 20× magnification. (**F**) 100× magnificationThe RPE choroid tissues were processed for immunostaining for ZO-1 (Zonula Occludens-1) and red fluorescence is visualized using fluorescence microscopy, highlighting tight junctions within the RPE.

3.5. Increased Expression of Antioxidant Genes in the RPE/Choroid in Response to Buspirone Treatment

To explore the impact of buspirone treatment on the expression of key antioxidant genes within the retinal pigment epithelium (RPE) and choroidal tissues, we used reverse transcription–polymerase chain reaction (RT-PCR) to analyze the expression profiles of the antioxidant enzymes *Nqo1*, *Sod2*, *Gstm1*, and *Cat* [21] (Figure 5). Remarkably, buspirone treatment led to a significant and robust upregulation of these antioxidant genes compared to control groups. *Nqo1*, a critical player in cellular defense against oxidative stress, exhibited a substantial increase in expression. Similarly, the expression of *Sod2* and *Gstm1*, crucial components of the antioxidant defense network, displayed marked elevations. In a separate experiment, we also observed a dose-dependent and elevated trend of expression of key antioxidant genes in ARPE-19 cells under normal conditions (Figure S2).

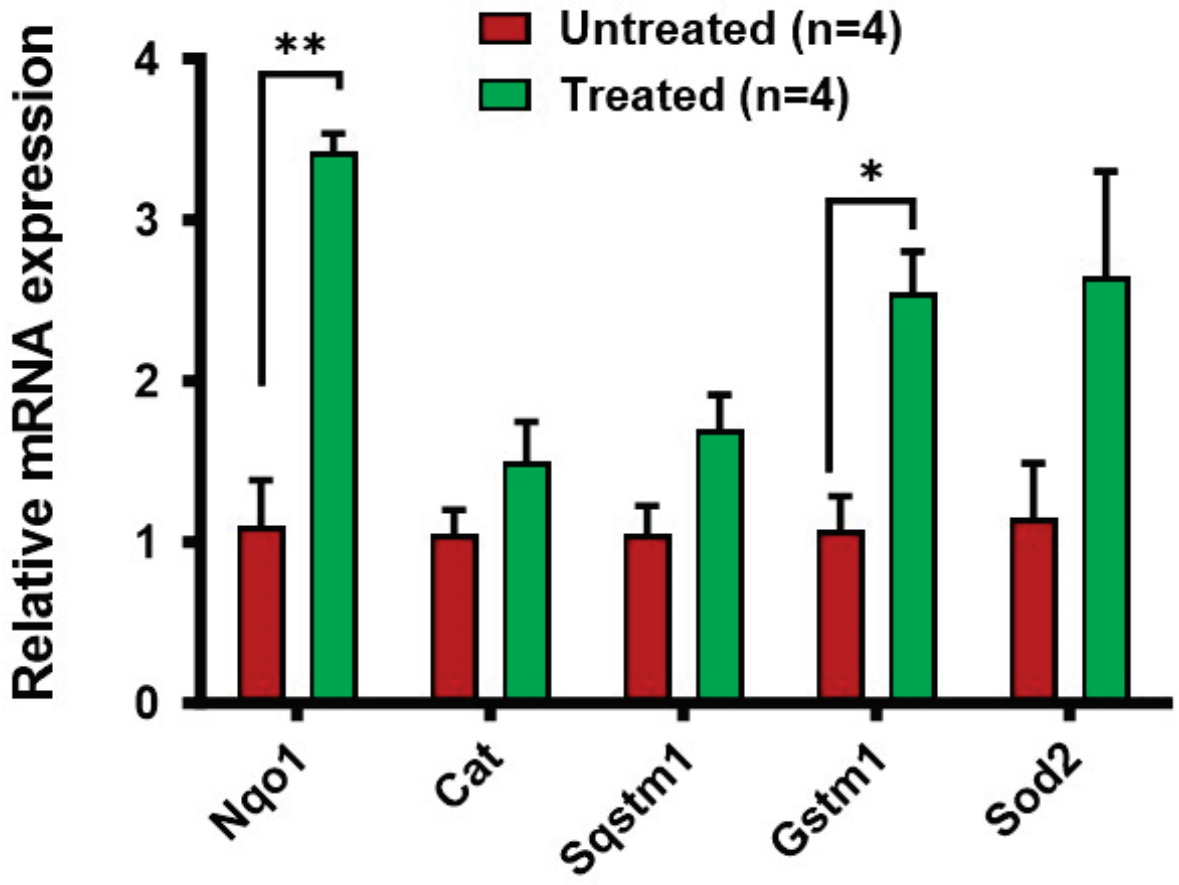

Figure 5. Relative mRNA Expression of Antioxidant Genes in RPE/Choroid: Buspirone-Treated Eyes vs Untreated Control Eyes. The graph illustrates the comparative mRNA expression levels of key antioxidant genes in the RPE/choroid complex. Buspirone-treated eyes are represented in green, while untreated control eyes are indicated in red. Data are normalized to *beta-actin* and presented as fold change relative to control. Antioxidant genes analyzed include *Nqo1*, *Cat*, *Sqstm1*, *Gstm1*, and *Sod2*, known for their pivotal role in oxidative stress response. Data represents the mean ± standard error of the mean (SEM) of n = 4. Statistical significance was determined using Student's *t*-test between two groups, with $p < 0.05$ considered as statistically significant. * $p < 0.05$, ** $p < 0.01$.

4. Discussion

4.1. Buspirone's Multifaceted Protective Effects in Retinal Health

The results of our study reveal a multifaceted potential for buspirone in preserving retinal health under conditions of oxidative stress. Our findings in differentiated ARPE-19 cells demonstrate a substantial protective effect against oxidative damage, evident in the

preservation of structural integrity as assessed via ZO-1 immunocytochemistry. This effect extended to an acute model of retinal pigment epithelium (RPE) oxidative damage, where buspirone treatment led to a pronounced conservation of total retinal thickness and outer nuclear layer (ONL) thickness, crucial indicators of retinal structural integrity. Notably, the heightened preservation of the photoreceptor layer highlights the therapeutic promise of buspirone in conditions characterized by retinal degeneration. The observed increase in expression of antioxidant genes, including *Nqo1*, *Sod2*, and Gstm1, within the RPE/choroid further underscores buspirone's capacity to bolster cellular defense mechanisms against oxidative stress. Collectively, these findings paint a compelling picture of buspirone as a potent candidate for therapeutic intervention in retinal degenerative conditions, offering a multi-pronged approach to combat oxidative stress-induced damage.

4.2. Potential Mechanisms Underlying Buspirone's Protective Effects

The mechanisms underlying buspirone's protective effects in the retina merit further exploration. Buspirone's 5-HT1A receptor agonism has been implicated in neuroprotection in various neuronal systems, suggesting a potential neuroprotective role in the retina. Additionally, the observed increase in expression of antioxidant genes may contribute to the heightened cellular defense against oxidative stress. *Nqo1* is a key player in the cellular response to oxidative damage [41], and its upregulation may signify a critical aspect of buspirone's mechanism of action. These results underscore the potency of buspirone in inducing the upregulation of antioxidant genes in the RPE/choroid, indicative of its capacity to bolster the cellular defense mechanisms against oxidative stress. It is important to note that the exact mechanisms by which buspirone influences antioxidative gene expression in RPE cells may involve multiple pathways and factors. The molecular details of buspirone's actions in the context of retinal protection are an active area of research and may involve intricate interactions within the cellular environment. Further studies, including molecular analyses and gene expression profiling, are needed to elucidate the specific pathways and genes influenced by buspirone in the RPE and to establish a more comprehensive understanding of its antioxidative effects. Furthermore, the potential interplay between buspirone's 5-HT1A receptor agonism and its antioxidant properties warrants investigation in other models of retinal or RPE atrophy, as it may shed light on the synergistic mechanisms underlying its protective effects.

4.3. Clinical Implications and Future Directions

The promising outcomes of our study hold significant clinical implications for the treatment of age-related macular degeneration (AMD) and other retinal degenerative conditions characterized by oxidative stress [42,43]. Buspirone's primary pharmacological use has been as an anxiolytic agent, and its potential therapeutic effects in the field of ophthalmology are an emerging area of research. Buspirone's demonstrated capacity to preserve retinal structure and enhance antioxidant defense mechanisms positions it as a potential game-changer in the field of retinal therapeutics. Furthermore, its well-established safety profile in psychiatric applications provides a solid foundation for expedited clinical translation. Future studies may delve deeper into the specific molecular pathways activated via buspirone in the retina and explore potential synergistic effects with other therapeutic agents. Urbina and colleagues have reported that a 5HT1a agonist (5OH-DPAT) produces a dose dependent increase in cAMP in the goldfish retina, and they suggest that the impact of 5HT1a agonists is mediated via cAMP-regulated pathways [44]. Additionally, investigations into the long-term effects of buspirone treatment on retinal health and function will be crucial for a comprehensive understanding of its therapeutic potential in retinal degenerative diseases. There has been no widespread exploration of buspirone specifically in recent studies or clinical trials evaluating buspirone in the context of other eye diseases, including glaucoma. Given buspirone's potential antioxidative and neuroprotective effects, it could be of interest to study conditions involving retinal degeneration or optic nerve damage, and our future studies will investigate it.

4.4. Limitations of the Study

While our study provides compelling evidence for buspirone's therapeutic potential, certain limitations must be acknowledged and will be explored in our future studies. Firstly, our experiments were primarily conducted in cell culture and in acute in vivo models, and as such, the long-term effects of buspirone treatment in chronic conditions require further investigation. Our study did not provide enough information related to retention of buspirone following i.p. delivery of buspirone and RNA changes of *Nqo1*, *Cat*, *Sqstm1*, *Gstm1*, and *Sod2* genes in RPE without $NaIO_3$ treatment. We are aiming for future studies where we will investigate RNA and proteome changes in response to buspirone treatment in retinal cells in presence or absence of oxidants. Additionally, the specific dose–response relationships and optimal treatment durations necessitate refinement in future studies. Moreover, while our focus was primarily on the antioxidant properties of buspirone, other potential mechanisms of action may contribute to its observed effects, warranting comprehensive exploration. Lastly, clinical translation will require rigorous evaluation of safety and efficacy in human subjects, mandating further preclinical and clinical investigations.

5. Conclusions

In conclusion, our study illuminates a groundbreaking avenue in the pursuit of effective treatments for retinal degenerative disorders. Via a comprehensive assessment of buspirone's multifaceted effects, we have uncovered its remarkable potential in preserving retinal structure and fortifying cellular defenses against oxidative stress. This innovative approach, harnessing the synergistic power of buspirone's 5-HT1A receptor agonism and potent antioxidant properties, represents a promising breakthrough in retinal therapeutics. By targeting not only the structural integrity of the retina but also its underlying cellular resilience, buspirone holds the promise of transformative interventions for conditions like age-related macular degeneration. The safety and established clinical usage of buspirone further expedites its potential translation to clinical settings, opening a new chapter in the treatment of retinal degenerative disorders. As we stand at the precipice of a new era in ophthalmology, the potential of buspirone offers renewed hope for those affected by these devastating conditions, paving the way for a brighter future in retinal health.

Supplementary Materials: The following supporting information can be downloaded at: https://www.mdpi.com/article/10.3390/antiox12122129/s1, Figure S1: The SD-OCT images provide detailed cross-sectional views of the retina, allowing visualization of retinal layers and structural changes from untreated and treated mice (4 different mice) from both eyes (Scale bar 75 micron); Figure S2: Effect of buspirone on Antioxidant mRNA Expression in normal ARPE-19 Cells without and oxidative damage. The figure depicts the relative fold change in mRNA expression levels of antioxidant genes in ARPE-19 cells following 24 h of treatment with buspirone. Cells were treated with three different concentrations: Control (untreated), 1 μM (micromolar), and 10 μM (micromolar). Quantitative real-time polymerase chain reaction (qPCR) was employed to assess the mRNA expression of key antioxidant genes in each treatment group. This result highlighted the dose-dependent effects and observed elevated trends in the mRNA expression levels. Notable antioxidants gene examined include; (A) GSTM1: Glutathione S-Transferase Mu 1, (B) CAT: Catalase, (C) HO1: Heme Oxygenase 1, (D) SOD2: Superoxide Dismutase 2, (E) MT1: Metallothionein 1, (F) NRF2: Nuclear Factor (Erythroid-Derived 2)-Like 2. The expression levels were normalized to Glyceraldehyde 3-Phosphate Dehydrogenas (GAPDH) for internal control. Statistical significance was determined using unpaired Student *t*-test (n = 4–6), with $p < 0.05$ considered as statistically significant. Significant differences indicated by asterisks.

Author Contributions: Conceptualization, M.R.B. and A.S.L.; methodology, M.R.B.; Animal experiment Data acquisition, R.J.P.; Cell culture data acquisition, R.V.; Data extraction and analysis, M.R.B., R.J.P. and R.V. Supervision, project administration, funding acquisition, M.R.B. Original draft preparation, M.R.B. Review and editing, A.S.L. and M.R.B. All authors have read and agreed to the published version of the manuscript.

Funding: This research was supported by grants from the National Eye Institute (NEI) (R00EY027013, R01EY033415) [M.R.B.], and USF TCOP start up [M.R.B.].

Institutional Review Board Statement: The study was conducted in accordance with the the Association for Research in Vision and Ophthalmology (ARVO) guidelines for the responsible use of animals in biological and biomedical research and approved by the IACUC Committee of University of South Florida (protocol code IS00005958 and date of approval 5/20/2019)." for studies involving animals.

Informed Consent Statement: Not applicable.

Data Availability Statement: All the data are available via this manuscript.

Acknowledgments: We acknowledge Anshuman Khadanga for his timely help in data acquisition and analysis. We also acknowledge Harshita Chitturi and Priyanka Lakhimsetti for data acquisition and analysis of experiments supporting results shown in Figure S2.

Conflicts of Interest: The authors declare no conflict of interest. The funders had no role in the design of the study; in the collection, analyses, or interpretation of data; in the writing of the manuscript; or in the decision to publish the results.

References

1. Abokyi, S.; To, C.-H.; Lam, T.T.; Tse, D.Y. Central Role of Oxidative Stress in Age-Related Macular Degeneration: Evidence from a Review of the Molecular Mechanisms and Animal Models. *Oxidative Med. Cell. Longev.* **2020**, *2020*, e7901270. [CrossRef] [PubMed]
2. Piippo, N.; Korhonen, E.; Hytti, M.; Kinnunen, K.; Kaarniranta, K.; Kauppinen, A. Oxidative Stress Is the Principal Contributor to Inflammasome Activation in Retinal Pigment Epithelium Cells with Defunct Proteasomes and Autophagy. *CPB* **2018**, *49*, 359–367. [CrossRef] [PubMed]
3. Taylor, D.P. Buspirone, a New Approach to the Treatment of Anxiety. *FASEB J.* **1988**, *2*, 2445–2452. [CrossRef] [PubMed]
4. Jann, M.W. Buspirone: An Update on a Unique Anxiolytic Agent. *Pharmacotherapy* **1988**, *8*, 100–116. [CrossRef] [PubMed]
5. Gupta, N.; Gupta, M.; Gandhi, R. Buspirone in Autism Spectrum Disorder: A Systematic Review. *Cureus* **2023**, *15*, e39304. [CrossRef]
6. Fernández-Robredo, P.; Sancho, A.; Johnen, S.; Recalde, S.; Gama, N.; Thumann, G.; Groll, J.; García-Layana, A. Current Treatment Limitations in Age-Related Macular Degeneration and Future Approaches Based on Cell Therapy and Tissue Engineering. *J. Ophthalmol.* **2014**, *2014*, 510285. [CrossRef]
7. Gibbs, W.S.; Collier, J.B.; Morris, M.; Beeson, C.C.; Megyesi, J.; Schnellmann, R.G. 5-HT_{1F} Receptor Regulates Mitochondrial Homeostasis and Its Loss Potentiates Acute Kidney Injury and Impairs Renal Recovery. *Am. J. Physiol.-Ren. Physiol.* **2018**, *315*, F1119–F1128. [CrossRef]
8. Eriksen, J.L.; Druse, M.J. Astrocyte-Mediated Trophic Support of Developing Serotonin Neurons: Effects of Ethanol, Buspirone, and S100B. *Brain Res. Dev. Brain Res.* **2001**, *131*, 9–15. [CrossRef]
9. Marazziti, D.; Palego, L.; Giromella, A.; Mazzoni, M.R.; Borsini, F.; Mayer, N.; Naccarato, A.G.; Lucacchini, A.; Cassano, G.B. Region-Dependent Effects of Flibanserin and Buspirone on Adenylyl Cyclase Activity in the Human Brain. *Int. J. Neuropsychopharmacol.* **2002**, *5*, 131–140. [CrossRef]
10. Thomas Broome, S.; Castorina, A. The Anxiolytic Drug Buspirone Prevents Rotenone-Induced Toxicity in a Mouse Model of Parkinson's Disease. *Int. J. Mol. Sci.* **2022**, *23*, 1845. [CrossRef]
11. Kumar, A.; Kaur, G.; Rinwa, P. Buspirone along with Melatonin Attenuates Oxidative Damage and Anxiety-like Behavior in a Mouse Model of Immobilization Stress. *Chin. J. Nat. Med.* **2014**, *12*, 582–589. [CrossRef]
12. Kushwah, N.; Bora, K.; Maurya, M.; Pavlovich, M.C.; Chen, J. Oxidative Stress and Antioxidants in Age-Related Macular Degeneration. *Antioxidants* **2023**, *12*, 1379. [CrossRef] [PubMed]
13. Beatty, S.; Koh, H.; Phil, M.; Henson, D.; Boulton, M. The Role of Oxidative Stress in the Pathogenesis of Age-Related Macular Degeneration. *Surv. Ophthalmol.* **2000**, *45*, 115–134. [CrossRef] [PubMed]
14. Ross, D.; Siegel, D. Functions of NQO1 in Cellular Protection and CoQ10 Metabolism and Its Potential Role as a Redox Sensitive Molecular Switch. *Front. Physiol.* **2017**, *8*, 595. [CrossRef] [PubMed]
15. Yuan, Z.; Du, W.; He, X.; Zhang, D.; He, W. Tribulus Terrestris Ameliorates Oxidative Stress-Induced ARPE-19 Cell Injury through the PI3K/Akt-Nrf2 Signaling Pathway. *Oxidative Med. Cell. Longev.* **2020**, *2020*, 7962393. [CrossRef] [PubMed]
16. Suárez-Barrio, C.; Del Olmo-Aguado, S.; García-Pérez, E.; de la Fuente, M.; Muruzabal, F.; Anitua, E.; Baamonde-Arbaiza, B.; Fernández-Vega-Cueto, L.; Fernández-Vega, L.; Merayo-Lloves, J. Antioxidant Role of PRGF on RPE Cells after Blue Light Insult as a Therapy for Neurodegenerative Diseases. *Int. J. Mol. Sci.* **2020**, *21*, 1021. [CrossRef] [PubMed]
17. Yang, Y.; Parsons, K.K.; Chi, L.; Malakauskas, S.M.; Le, T.H. Glutathione S-Transferase-M1 Regulates Vascular Smooth Muscle Cell Proliferation, Migration, and Oxidative Stress. *Hypertension* **2009**, *54*, 1360–1368. [CrossRef]

18. Sandbach, J.M.; Coscun, P.E.; Grossniklaus, H.E.; Kokoszka, J.E.; Newman, N.J.; Wallace, D.C. Ocular Pathology in Mitochondrial Superoxide Dismutase (Sod2)-Deficient Mice. *Investig. Ophthalmol. Vis. Sci.* **2001**, *42*, 2173–2178.
19. Kasahara, E.; Lin, L.-R.; Ho, Y.-S.; Reddy, V.N. SOD2 Protects against Oxidation-Induced Apoptosis in Mouse Retinal Pigment Epithelium: Implications for Age-Related Macular Degeneration. *Investig. Ophthalmol. Vis. Sci.* **2005**, *46*, 3426–3434. [CrossRef]
20. Collier, R.J.; Patel, Y.; Martin, E.A.; Dembinska, O.; Hellberg, M.; Krueger, D.S.; Kapin, M.A.; Romano, C. Agonists at the Serotonin Receptor (5-HT(1A)) Protect the Retina from Severe Photo-Oxidative Stress. *Investig. Ophthalmol. Vis. Sci.* **2011**, *52*, 2118–2126. [CrossRef]
21. Biswal, M.R.; Ahmed, C.M.; Ildefonso, C.J.; Han, P.; Li, H.; Jivanji, H.; Mao, H.; Lewin, A.S. Systemic Treatment with a 5HT1a Agonist Induces Anti-Oxidant Protection and Preserves the Retina from Mitochondrial Oxidative Stress. *Exp. Eye Res.* **2015**, *140*, 94–105. [CrossRef] [PubMed]
22. Ahmed, C.M.; Biswal, M.R.; Li, H.; Han, P.; Ildefonso, C.J.; Lewin, A.S. Repurposing an Orally Available Drug for the Treatment of Geographic Atrophy. *Mol. Vis.* **2016**, *22*, 294–310. [PubMed]
23. Coyner, A.S.; Ryals, R.C.; Ku, C.A.; Fischer, C.M.; Patel, R.C.; Datta, S.; Yang, P.; Wen, Y.; Hen, R.; Pennesi, M.E. Retinal Neuroprotective Effects of Flibanserin, an FDA-Approved Dual Serotonin Receptor Agonist-Antagonist. *PLoS ONE* **2016**, *11*, e0159776. [CrossRef] [PubMed]
24. Liu, Y.; Li, Y.; Wang, C.; Zhang, Y.; Su, G. Morphologic and Histopathologic Change of Sodium Iodate-Induced Retinal Degeneration in Adult Rats. *Int. J. Clin. Exp. Pathol.* **2019**, *12*, 443–454. [PubMed]
25. Upadhyay, M.; Bonilha, V.L. Regulated Cell Death Pathways in the Sodium Iodate Model: Insights and Implications for AMD. *Exp. Eye Res.* **2023**, *238*, 109728. [CrossRef] [PubMed]
26. Hazim, R.A.; Volland, S.; Yen, A.; Burgess, B.L.; Williams, D.S. Rapid Differentiation of the Human RPE Cell Line, ARPE-19, Induced by Nicotinamide. *Exp. Eye Res.* **2019**, *179*, 18–24. [CrossRef] [PubMed]
27. Dunn, K.C.; Aotaki-Keen, A.E.; Putkey, F.R.; Hjelmeland, L.M. ARPE-19, a Human Retinal Pigment Epithelial Cell Line with Differentiated Properties. *Exp. Eye Res.* **1996**, *62*, 155–169. [CrossRef]
28. Chen, W.; Lin, B.; Xie, S.; Yang, W.; Lin, J.; Li, Z.; Zhan, Y.; Gui, S.; Lin, B. Naringenin Protects RPE Cells from $NaIO_3$-Induced Oxidative Damage in Vivo and in Vitro through up-Regulation of SIRT1. *Phytomedicine* **2021**, *80*, 153375. [CrossRef]
29. Juel, H.B.; Faber, C.; Svendsen, S.G.; Vallejo, A.N.; Nissen, M.H. Inflammatory Cytokines Protect Retinal Pigment Epithelial Cells from Oxidative Stress-Induced Death. *PLoS ONE* **2013**, *8*, e64619. [CrossRef]
30. Xie, R.; Wang, B.; Zuo, S.; Du, M.; Wang, X.; Yu, Y.; Yan, H. Protective Effects of CRTH2 Suppression in Dry Age-Related Macular Degeneration. *Biochem. Biophys. Res. Commun.* **2022**, *624*, 8–15. [CrossRef]
31. Ma, H.; Yang, F.; Ding, X.-Q. Inhibition of Thyroid Hormone Signaling Protects Retinal Pigment Epithelium and Photoreceptors from Cell Death in a Mouse Model of Age-Related Macular Degeneration. *Cell Death Dis.* **2020**, *11*, 24. [CrossRef] [PubMed]
32. Bardak, H.; Uğuz, A.C.; Bardak, Y.; Rocha-Pimienta, J.; Delgado-Adámez, J.; Espino, J. Selenium Protects ARPE-19 and ACBRI 181 Cells against High Glucose-Induced Oxidative Stress. *Molecules* **2023**, *28*, 5961. [CrossRef] [PubMed]
33. Hanneken, A.; Lin, F.-F.; Johnson, J.; Maher, P. Flavonoids Protect Human Retinal Pigment Epithelial Cells from Oxidative-Stress–Induced Death. *Investig. Ophthalmol. Vis. Sci.* **2006**, *47*, 3164–3177. [CrossRef] [PubMed]
34. He, H.; Kuriyan, A.E.; Su, C.-W.; Mahabole, M.; Zhang, Y.; Zhu, Y.-T.; Flynn, H.W.; Parel, J.-M.; Tseng, S.C.G. Inhibition of Proliferation and Epithelial Mesenchymal Transition in Retinal Pigment Epithelial Cells by Heavy Chain-Hyaluronan/Pentraxin 3. *Sci. Rep.* **2017**, *7*, srep43736. [CrossRef] [PubMed]
35. Haranahalli Shivarudrappa, A.; Gopal, S.S.; Ponesakki, G. An in Vitro Protocol to Study the Effect of Hyperglycemia on Intracellular Redox Signaling in Human Retinal Pigment Epithelial (ARPE-19) Cells. *Mol. Biol. Rep.* **2019**, *46*, 1263–1274. [CrossRef] [PubMed]
36. Biswal, M.R.; Justis, B.D.; Han, P.; Li, H.; Gierhart, D.; Dorey, C.K.; Lewin, A.S. Daily Zeaxanthin Supplementation Prevents Atrophy of the Retinal Pigment Epithelium (RPE) in a Mouse Model of Mitochondrial Oxidative Stress. *PLoS ONE* **2018**, *13*, e0203816. [CrossRef]
37. Wenzel, A.A.; O'Hare, M.N.; Shadmand, M.; Corson, T.W. Optical Coherence Tomography Enables Imaging of Tumor Initiation in the TAg-RB Mouse Model of Retinoblastoma. *Mol. Vis.* **2015**, *21*, 515–522.
38. Zou, X.-L.; Wang, G.-F.; Li, D.-D.; Chen, J.-X.; Zhang, C.-L.; Yu, Y.-Z.; Zhou, W.-J.; Zou, Y.-P.; Rao, B.-Q. Protection of Tight Junction between RPE Cells with Tissue Factor Targeting Peptide. *Int. J. Ophthalmol.* **2018**, *11*, 1594–1599. [CrossRef]
39. Obert, E.; Strauss, R.; Brandon, C.; Grek, C.; Ghatnekar, G.; Gourdie, R.; Rohrer, B. Targeting The Tight Junction Protein, Zonula Occludens-1, With The Connexin 43 Mimetic Peptide, αCT1, Reduces VEGF-Dependent RPE Pathophysiology. *J. Mol. Med.* **2017**, *95*, 535–552. [CrossRef]
40. Trakkides, T.-O.; Schäfer, N.; Reichenthaler, M.; Kühn, K.; Brandwijk, R.J.M.G.E.; Toonen, E.J.M.; Urban, F.; Wegener, J.; Enzmann, V.; Pauly, D. Oxidative Stress Increases Endogenous Complement-Dependent Inflammatory and Angiogenic Responses in Retinal Pigment Epithelial Cells Independently of Exogenous Complement Sources. *Antioxidants* **2019**, *8*, 548. [CrossRef]
41. Frede, K.; Ebert, F.; Kipp, A.P.; Schwerdtle, T.; Baldermann, S. Lutein Activates the Transcription Factor Nrf2 in Human Retinal Pigment Epithelial Cells. *J. Agric. Food Chem.* **2017**, *65*, 5944–5952. [CrossRef] [PubMed]
42. Ku, C.A.; Ryals, R.C.; Jiang, D.; Coyner, A.S.; Weller, K.K.; Sinha, W.; Robb, B.M.; Yang, P.; Pennesi, M.E. The Role of ERK1/2 Activation in Sarpogrelate-Mediated Neuroprotection. *Investig. Ophthalmol. Vis. Sci.* **2018**, *59*, 462–471. [CrossRef] [PubMed]

43. Tullis, B.E.; Ryals, R.C.; Coyner, A.S.; Gale, M.J.; Nicholson, A.; Ku, C.; Regis, D.; Sinha, W.; Datta, S.; Wen, Y.; et al. Sarpogrelate, a 5-HT2A Receptor Antagonist, Protects the Retina From Light-Induced Retinopathy. *Investig. Ophthalmol. Vis. Sci.* **2015**, *56*, 4560–4569. [CrossRef] [PubMed]
44. Urbina, M.; Schmeer, C.; Lima, L. 5HT1A Receptor Agonist Differentially Increases Cyclic AMP Concentration in Intact and Lesioned Goldfish Retina. In Vitro Inhibition of Outgrowth by Forskolin. *Neurochem. Int.* **1996**, *29*, 453–460. [CrossRef]

antioxidants

MDPI

Article

Lemon Peel Water Extract: A Novel Material for Retinal Health, Protecting Retinal Pigment Epithelial Cells against Dynamin-Related Protein 1-Mediated Mitochondrial Fission by Blocking ROS-Stimulated Mitogen-Activated Protein Kinase/Extracellular Signal-Regulated Kinase Pathway

Shang-Chun Tsou [1,†], Chen-Ju Chuang [2,†], Inga Wang [3], Tzu-Chun Chen [4], Jui-Hsuan Yeh [4], Chin-Lin Hsu [1], Yu-Chien Hung [5], Ming-Chung Lee [6], Yuan-Yen Chang [7,8,*] and Hui-Wen Lin [9,*]

[1] Department of Nutrition, Chung Shan Medical University, Taichung 40201, Taiwan; 0946003@live.csmu.edu.tw (S.-C.T.); clhsu@csmu.edu.tw (C.-L.H.)
[2] Emergency Department, St. Martin De Porres Hospital, Chiayi 60069, Taiwan; ilovespurs168@gmail.com
[3] Rehabilitation Sciences & Technology, University of Wisconsin-Milwaukee, Milwaukee, WI 53211, USA; wang52@uwm.edu
[4] Institute of Medicine, Chung Shan Medical University, Taichung 40201, Taiwan; 1103012@live.csmu.edu.tw (T.-C.C.); 1003023@live.csmu.edu.tw (J.-H.Y.)
[5] Department of Ophthalmology, Chung Shan Medical University Hospital, Taichung 40201, Taiwan; b92401086@ntu.edu.tw
[6] Brion Research Institute of Taiwan, New Taipei City 23143, Taiwan; i1es@herbbiotek.com
[7] Department of Microbiology and Immunology, School of Medicine, Chung Shan Medical University, Taichung 40201, Taiwan
[8] Clinical Laboratory, Chung Shan Medical University Hospital, Taichung 40201, Taiwan
[9] Department of Optometry, Asia University, Taichung 413305, Taiwan
* Correspondence: cyy0709@csmu.edu.tw (Y.-Y.C.); d9138001@asia.edu.tw (H.-W.L.)
† These authors have contributed equally to this work and share the first authorship.

Abstract: Previous studies showed that $NaIO_3$ can induce oxidative stress-mediated retinal pigment epithelium (RPE) damage to simulate age-related macular degeneration (AMD). Lemon peel is rich in antioxidants and components that can penetrate the blood–retinal barrier, but their role in retinal oxidative damage remains unexplored. Here, we explore the protection of lemon peel ultrasonic-assisted water extract (LUWE), containing large amounts of flavonoids and polyphenols, against $NaIO_3$-induced retinal degeneration. We initially demonstrated that LUWE, orally administered, prevented retinal distortion and thinning on the inner and outer nuclei layers, downregulating cleaved caspase-3 protein expression in RPE cells in $NaIO_3$-induced mice. The effect of LUWE was achieved through the suppression of apoptosis and the associated proteins, such as cleaved PARP and cleaved caspase-3, as suggested by $NaIO_3$-induced ARPE-19 cell models. This is because LUWE reduced reactive oxygen species-mediated mitochondrial fission via regulating p-Drp-1 and Fis1 expression. We further confirmed that LUWE suppresses the expression of p-MEK-1/2 and p-ERK-1/2 in $NaIO_3$-induced ARPE-19 cells, thereby providing the protection described above, which was confirmed using PD98059 and U0126. These results indicated that LUWE prevents mitochondrial oxidative stress-mediated RPE damage via the MEK/ERK pathway. Elucidation of the molecular mechanism may provide a new protective strategy against retinal degeneration.

Keywords: sodium iodate ($NaIO_3$); lemon peel ultrasonic-assisted water extract (LUWE); retinal degeneration; reactive oxygen species (ROS); apoptosis

1. Introduction

Age-related macular degeneration (AMD), the third leading cause of blindness [1], is characterized by the atrophy of photoreceptors, caused by dysfunction of the retinal

pigment epithelium (RPE), which is responsible for retinal physiology and toxicology [2]. Reactive oxygen species (ROS) accumulation with age is the primary cause of RPE cell senescence and apoptosis [3], triggering lysosomal acidification, DNA fragmentation, and mitochondrial fission [4,5]. Sodium iodate ($NaIO_3$), a natural oxidizing agent, has become an effective model for simulating AMD disease due to its specificity to induce the symptoms described above [6]; however, its complexity in mitochondrial homeostasis requires further clarification [7,8]. The mitochondrial fission regulators, dynamin-related protein 1 (Drp1) and mitochondrial fission protein 1 (Fis1), stabilize mitochondrial function by regulating mitochondrial dynamics. However, they can also promote intrinsic apoptosis by accelerating cytochrome c into the cytoplasm through Bcl2-associated X protein (Bax) [9,10].

MEK/ERK (mitogen-activated protein kinase/extracellular signal-regulated kinase) signaling may be a risk factor for RPE mitochondrial dysfunction [11]. ERK is traditionally recognized for cell proliferation and survival; however, it can stimulate pro-apoptotic signals, initiate Ca^{2+}-dependent endoplasmic reticulum stress, and induce retinal pigment epithelial–mesenchymal transition (EMT) under ROS stimulation [12]. Furthermore, it was revealed that $NaIO_3$ triggers Drp-1-mediated mitochondrial fission to initiate cell death through the MAPK pathway [4]. Accumulating evidence, in conjunction with the above concepts, suggests that mitochondrial dynamics play a crucial role in $NaIO_3$-induced cell death.

While anti-vascular endothelial growth factor (VEGF) agents and laser therapy have been employed in treating choroidal neovascularization, the FDA (U.S. Food and Drug Administration) has not approved any treatment strategies for retinal atrophy [13]. The bioavailability of most antioxidant formulas is limited by the blood–retinal barrier (BRB) [14]. Therefore, research into new materials may offer a promising avenue for AMD.

Lemon (*Citrus limon*) is widely popular and consumed for its unique flavor. However, as it is primarily used for juicing, over 50% of the total fruit weight (mainly consisting of peels and seeds) often goes underutilized, leading to environmental pollution or soil acidification [15]. The peel of lemon is a rich source of polyphenols and flavonoids [16,17], such as hesperidin and naringin, possessing strong antioxidant properties and blood–brain barrier permeability [18,19]. Quercetin, a citrus flavonone, can also protect RPE cells against oxidative damage [20]. In addition, recent research has emphasized the synergistic potential of natural formulations in terms of bioavailability [21,22], while the high content of vitamin C in lemon has been reported to enhance the bioavailability of lutein in rats [23]. These findings engender our expectations of the potential benefits of lemon by-products in addressing AMD.

Here, we evaluated the protection of lemon peel water extract against retinal degeneration using $NaIO_3$-induced ARPE-19 cells (a human RPE cell line) and a mouse model. We further investigated its mechanism for reducing p-Drp-1-mediated mitochondrial fission and RPE cell apoptosis, by inhibiting the MEK/ERK pathway. This study first reports the protective effect of lemon peel extract against retinal oxidative damage and provides a novel protective strategy.

2. Material and Methods

2.1. Chemicals

The 2,2′-azino-bis (3-ethylbenzothiazoline-6-sulfonic acid) (ABTS, CAS 30931-67-0), hydrogen peroxide (H_2O_2, CAS 7722-84-1), peroxidase (CAS 9003-99-0), 2,2-diphenyl-1-picrylhydrazyl (DPPH, CAS 1898-66-4), sodium nitrite ($NaNO_2$, CAS 7632-00-0), aluminum chloride ($AlCl_3$, CAS 7446-70-0), sodium hydroxide (NaOH, CAS 1310-73-2), Folin–Ciocalteu's phenol reagent (CAS F9252), and sodium carbonate (Na_2CO_3, CAS 56169) were all purchased from Merck (Rahway, NJ, USA). U0126 (Cat. HY-12031A) and PD98059 (Cat. HY-12028) were purchased from MedChemExpress (Monmouth Junction, NJ, USA).

2.2. Preparation of LUWE

This study utilized Eureka lemon (*Citrus limon*) sourced from Pingtung, Taiwan. The by-products of lemon peel, including the endocarp residual membranes and exocarp, are the residues generated after juicing. The samples were washed, seeds removed, and diced to 0.5–1 cm^3. Then, the samples were soaked in 95 °C distilled water at a ratio of 1:10 (g/mL) for 1 min for sterilization, referring to the methodology of Karbuz and Tugrul [24]. After that, the lemon peel was cooled down in an ice-cold water bath, followed by the extraction.

The ultrasonic-assisted water extraction (UWE) procedure was conducted with reference to previous literature, incorporating some modifications [25,26]. Extraction solutions were prepared at a peel/solvent ratio of 1:10 (g/mL) as described above. Extraction was performed using a 2 L ultrasonic bath with a frequency of 43 ± 2 kHz and a power of 80 W (Homelike Electronic CO., LTD., Kaohsiung, Taiwan) for 1 h at 50 °C. The extracts were filtered through double-layer gauze (Cat. 161363, Good Verita Enterprise CO., LTD., Taipei, Taiwan), and concentrated by freeze-drying (BTP-9ES, Benchtop Pro, Wolflabs, Pocklington, UK) for experimental use.

2.3. Trolox Equivalent Antioxidant Capacity Assay (TEAC)

The rapid $ABTS^+$ peroxidase assay protocol was adapted from Konan et al. [27]. In brief, the $ABTS^+$ working solution was prepared by mixing equal volumes of 100 μM ABTS, 4.4 units/mL peroxidase, and 50 μM H_2O_2. Subsequently, 30 μL of the sample was added to 970 μL of the $ABTS^+$ working solution, in the dark at room temperature for 1 min. A 200 μL aliquot of the mixture was transferred to a 96-well plate, and the absorbance was measured at 410 nm using an ELISA reader to establish a standard curve and calculate the half maximal inhibitory concentration (IC50). Trolox was used as a standard, and the interpolation method was employed to calculate the sample's Trolox equivalent antioxidant activity.

2.4. DPPH Radical Scavenging Activity

The DPPH free radical scavenging activity experiment, as described by Anggraini et al., was conducted [28]. A 1 mM DPPH working solution was prepared by dissolving DPPH in methanol and mixing it thoroughly. Then, 200 μL of the sample and 50 μL of the DPPH working solution were added to a 96-well plate and allowed to react in the dark at room temperature for 30 min. The absorbance was measured at 517 nm using an ELISA reader to establish a standard curve and calculate the half maximal inhibitory concentration (IC50). Finally, the catechin equivalent antioxidant activity was calculated using interpolation compared to the standard curve of catechin.

2.5. Analysis of Flavonoid Content

The total flavonoid content of the samples was determined using the aluminum chloride method as reported by Shraim et al. [29]. Firstly, 250 μL of the sample was mixed with 75 μL of 5% $NaNO_2$ and reacted for 6 min. Then, 150 μL of 10% $AlCl_3$ was added and reacted for 5 min. Finally, 0.5 mL of 1M NaOH was added, and the absorbance was measured at 510 nm using an ELISA reader. A standard curve was established, and the content of flavonoids in terms of their catechin equivalent was calculated using the interpolation method and compared with the catechin standard curve.

2.6. Analysis of Polyphenol Content

The total polyphenol content of the samples was determined following the method described by Carmona-Hernandez et al. [30]. The amount of 50 μL of the sample was mixed with 0.5 mL of 1N Folin–Ciocalteu's phenol reagent and 2.5 mL of 10% (*w*/*w*) Na_2CO_3. The mixture was allowed to react in the dark at room temperature for 20 min. Next, 200 μL of the mixture was transferred to a 96-well plate, and the absorbance was measured at 700 nm using an ELISA reader. A standard curve was constructed and compared with the gallic

acid standard curve using the interpolation method to calculate the gallic acid equivalent polyphenol content.

2.7. Analysis of LUWE Components

The components of LUWE were analyzed using 3D high-performance liquid chromatography (3D-HPLC) with a photodiode array detector (Burdick & Jackson, Seongnam, Republic of Korea) to generate 3D graphs, and identification was carried out through liquid chromatography/mass spectrometry (LC/MS).

The HPLC column dimensions are 4.6 mm × 250 mm × 5 μm, with the mobile phase consisting of solvent A (0.1% TFA aqueous solution) and solvent B (0.1% TFA acetonitrile solution). HPLC parameters include a column temperature of 35 °C, a flow rate of 1.0 mL/min, and an analysis time of 65 min.

The LC/MS system comprises the Shimadzu LC-20AD UFLC and LCMS-8040 mass spectrometer. The mobile phase consisted of solvent A (0.1% formic acid and 1 g/L ammonium acetate in distilled water) and solvent B (0.1% formic acid and 1 g/L ammonium acetate in distilled water), with methanol used for gradient elution. The gradient curve was as follows: 0–40 min, A decreases from 100% to 70%, and B increases from 0% to 30%; 40–70 min, A decreases from 70% to 0%, and B increases from 30% to 100%. At 70–70.1 min, A is held at 0%, and B becomes 100%. From 70.1 to 80 min, A is maintained at 100%, and B at 0%. The flow rate is 0.4 mL/min, the column temperature is 40 °C, the injection volume is 30 μL, and a Shim-pack XR-ODS II column is used.

MS was conducted using electrospray ionization (ESI) in dual ionization modes ([ESI][+] and [−]), with a full scan range of 400–800 amu. The interface voltage for ESI (+) was set at 4.5 kV, and for ESI (−), it was −3.5 kV. Nitrogen was used for nebulization and drying, with flow rates of 3.0 and 10 L/min, respectively. Collision-induced dissociation gas was argon, maintained at 230 kPa. The desolvation line temperature was set to 150 °C, and the heat block temperature was maintained at 400 °C.

2.8. Animal Model

Eight-week-old Balb/c mice from the National Laboratory Animal Center of Taiwan (Taipei, Taiwan) were housed in compliant cages with a 12/12 h light/dark cycle and free access to food and water. Under the guidance of the Institutional Animal Care and Use Committee of Chung Shan Medical University (IACUC number: 2595), mice were randomly divided into three groups (n = 6) for the following treatments:

$NaIO_3$ + LUWE: Mice received a daily oral feed of 200 μL LUWE (100 mg/ mL in PBS) for 7 days, followed by an intravenous (IV) injection of $NaIO_3$ (40 mg/ kg in PBS).

$NaIO_3$: Mice received a daily oral feed of 200 μL PBS for 7 days, followed by an intravenous injection of $NaIO_3$ (40 mg/ kg).

Mock: Mice received a daily oral feed of 200 μL PBS) for 7 days, followed by an intravenous injection of 100 μL PBS.

All mice were continuously fed as described after receiving intravenous injections (only once) until sacrifice.

2.9. Tissue Sections and Thickness Measurement

All mice were sacrificed on the 7th day following the intravenous injection of $NaIO_3$. Their right eyes were collected and fixed with 10% formalin. The fixed eye tissues were sectioned and stained with hematoxylin/eosin. As described in previous studies [20,31], the thickness of the ONL (outer nuclear layer) and INL (inner nuclear layer) of the retina was measured at 50 μm intervals within 600 μm to 900 μm outward from the center of the retina or optic nerve, and the average was calculated. The immunohistochemical staining of cleaved caspase-3 (31A106, Santa Cruz) was performed using the BondMax automated staining system (Vision BioSystems Ltd., Newcastle Upon Tyne, UK).

2.10. Human RPE Cell Model

The ARPE-19 cell line (adult male RPE cells) was purchased from the American Type Culture Collection (Manassas, VA, USA). Cells were cultured in DMEM (Dulbecco's Modified Eagle's Medium, Hyclone, Grand Island, NY, USA) containing 10% FBS (Gibco, Grand Island, NY, USA) with 100 U/mL penicillin and streptomycin (Gibco, Grand Island, NY, USA) at 37 °C and 5% CO_2. The ARPE-19 cells were seeded into a 12-well plate at a density of 2.0×10^5 cells per well and incubated for 12 h to ensure cell recovery and adhesion before conducting the experiments.

2.11. Cell Viability Assay

After processing according to the design, ARPE-19 cells were treated with 2% CCK-8 (Dojindo Molecular Technologies, Tokyo, Japan) and incubated at 37 °C for 1 h. The absorbance of each group was quantified by an ELISA reader at a wavelength of 450–595 nm and adjusted according to the color caused by the acidity of the sample.

2.12. Cell Morphology and Apoptosis Analysis

Following the designated treatments, morphological changes in ARPE-19 cells from each group were recorded, and subsequently, cell separation was performed using 0.25% Trypsin–EDTA (Gibco, Grand Island, NY, USA). The separated ARPE-19 cells were stained with annexin V-FITC (0.25 μg/mL) and propidium iodide (1 μg/mL) for 1 h, and the fluorescence was detected by flow cytometry (BD Biosciences, San Jose, CA, USA). FITC is detected at 515 nm, and PI is detected at 590 nm.

2.13. Mitochondrial ROS Level Analysis

The ARPE-19 cells in each group were replaced with DMEM containing 4 μM MitoSOX Red (M36008, Thermo Fisher Scientific, Waltham, MA, USA) for 30 min. The cells were washed twice with 1X PBS and then detached with 0.25% Trypsin–EDTA from a 12-well plate. The fluorescence content was detected using a flow cytometer (Accuri C6 Plus, BD Bioscience, San Jose, CA, USA) with an excitation wavelength of 590 nm.

2.14. Western Blotting

ARPE-19 cells in each group were removed from the supernatant and lysed with cell lysis buffer (containing 10 mM Tris, 0.1% Triton X-100, and 1 mM EDTA) to collect protein samples. To analyze the expression levels of specific proteins, all samples were separated by 10% SDS-PAGE gel electrophoresis and transferred to PVDF membranes for binding with corresponding antibodies. After adding ECL substrate, all proteins were visualized using MultiGel-21 (GIS-21-C2-6M, TOPBIO) for imaging (Taipei, Taiwan). The antibodies, including cleaved caspase-3 (31A106), p-MEK-1/2 (7E10), p-ERK (12D4), p-p38 (D8), p-JNK (G7), and Fis1 (B5) were all purchased from Santa Cruz Biotechnology (Santa Cruz, CA, USA). Cleaved caspase-9 (9505T), cleaved PARP (Asp214, D64E10), and p-Drp-1 (3455S) were purchased from Cell Signaling Technology (Beverly, MA, USA).

2.15. Mitochondrial Dimension Measurements

We inoculated 1×10^6 cells into a 12-well plate. Following experimental treatments as per the design, we washed the cells twice with 1 X PBS, then separated them using 0.25% Trypsin–EDTA. Subsequently, mitochondria were isolated using a Mitochondria Isolation Kit (Catalog number 89874, Thermo Fisher Scientific, Waltham, MA, USA) following the manufacturer's instructions. The size of mitochondrial particles was measured using forward scatter light (FSC-A) on a flow cytometer (NovoCyte, Agilent Technologies, Santa Clara, CA, USA), following the methods reported by Tzur et al. and Stern et al. [32,33].

2.16. Statistical Analysis

All data were analyzed using SAS version 9.4 (SAS Institute Inc., Cary, NC, USA), and all values were expressed as mean ± standard deviation (SD). One-way analysis of

variance (ANOVA) was used to determine differences in all data from in vitro and in vivo experiments, and Tukey's HSD test was used to further analyze significant differences between groups. The significance level was set at 0.05.

3. Results

3.1. Analysis of Antioxidant Activity in LUWE

We prepared a lemon ultrasonic-assisted water extract (LUWE), referring to the previous literature. This method has been proven effective in separating antioxidant components and maintaining their activity [25,26]. LUWE samples were analyzed for antioxidant activity within 6 h after extraction and were stored at 4 °C during this period. In Table 1, the LUWE exhibited an antioxidant capacity in $ABTS^+$ (5.65 ± 0.06 mmole Trolox/g LUWE) and DPPH (2.51 ± 0.03 mmole catechin/g LUWE).

Table 1. Antioxidant activity of LUWE.

	Content
ABTS+ scavenging activity (mmole TE/g sample)	5.65 ± 0.06
DPPH scavenging activity (mmole CE/g sample)	2.51 ± 0.03
Polyphenol content (mmole GAE/g sample)	10.24 ± 0.09
Flavonoids content (μmole CE/g sample)	964 ± 46.61

The data are given as the mean ± SEM (n = 3). TE, Trolox equivalent; CE, catechin equivalent; GAE, gallic acid equivalent.

We determined the content of polyphenols and flavonoids in these samples using the Folin–Ciocalteu reagent and aluminum chloride, as these are typically the sources of antioxidant activity in natural extracts [34]. LUWE contains a 10.24 ± 0.09 mmole gallic acid/g LUWE polyphenol content and a 964 ± 46.61 μmoles catechin/g LUWE flavonoid content. Based on the previous literature, we established a chromatogram using 3D-HPLC (Figure 1) and identified polyphenols and flavonoids in LUWE through LC/MS analysis (Table 2). The chromatogram illustrates 24 polyphenols and flavonoids present in LUWE. Specifically, LUWE exhibited high concentrations of isocitric acid, citric acid, limocitrin-Glu-HMG-Glu, neoeriocitrin, p-coumatric acid, luteolin, and limocitrin.

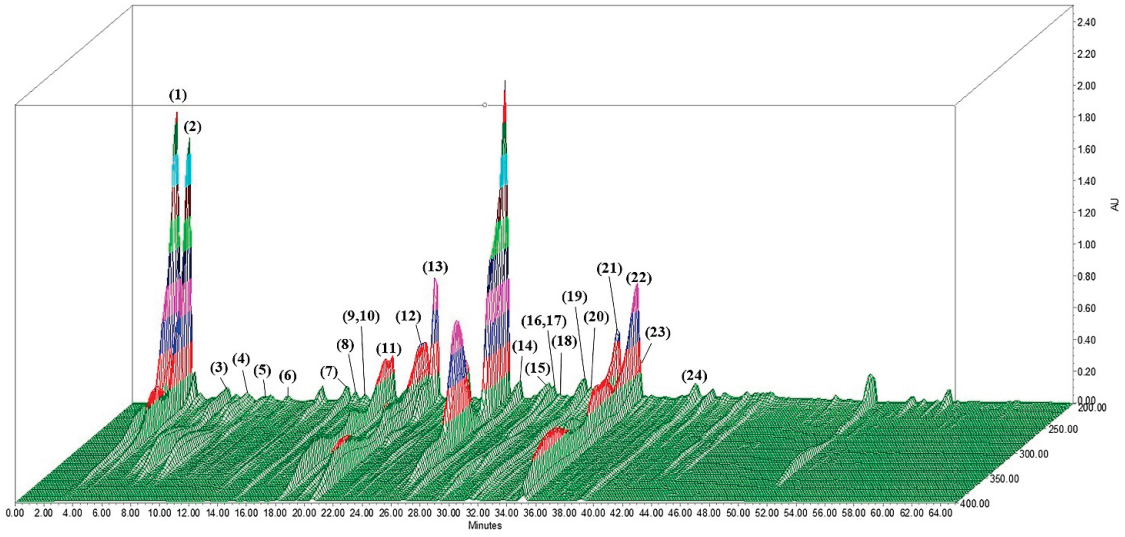

Figure 1. The 3D-HPLC chromatographic fingerprint analysis of LUWE. The chemical compositions of the LUWE samples were analyzed using high-performance liquid chromatography (HPLC) with a photodiode array detector (PDA). Twenty-four polyphenolic or flavonoid compounds were detected and are displayed in Table 2 according to their corresponding peak numbers. AU = arbitrary perfusion units.

Table 2. Identification parameters for the 24 flavonoids tentatively identified include the flavonoid name, neutral mass, retention time (R.T.), adduct formed, and main product ions (*m*/*z*).

No.	Compound	Neutral Mass	R.T. (min)	Adduct	Main *m*/*z* Fragments	References
1	Isocitric acid	192.12	2.95	$[M+H]^-$	111.00, 390.90	[35,36]
2	Citric acid	192.12	3.83	$[M+H]^-$	111.00, 390.90	[36–38]
3	Gentiopicroside	356.10	6.53	$[M+H]^-$	91.00, 191.00, 719.05	[37]
4	Ferulic acid hexoside	356.32	7.57	$[M+H]^-$	91.00, 191.00, 615.15	[38]
5	Quercetin-3-O-rutinoside-7-O-glucoside	772.66	10.12	$[M+H]^-$	365.05	[39]
6	Quinic acid	192.06	10.55	$[M+H]^+$	83.05, 354.95, 523.05	[35]
7	Limocitrol-O-Glu	538.46	14.72	$[M+H]^+$	83.05	[38]
8	Chrysoeriol-6,8-di-C-Glu/stellarin-2	624.50	15.20	$[M+H]^-$	91.00, 757.10	[38,40–42]
9	p-Coumaroyl quinic acid	338.10	15.73	$[M+H]^-$	391.05, 577.05, 755.10	[36]
10	Apigenin-7-O-Neo/rhoifolin	578.16	15.73	$[M+H]^-$	336.95, 391.05, 755.10	[38,40,42]
11	Limocitrin-Glu-HMG-Glu	816.22	18.10	$[M+H]^-$	391.05	[35,38,43]
12	Sinapoyl-O-glucoside	386.35	20.23	$[M+H]^-$	91.00, 336.90	[36,38]
13	Eriodictyol-7-O-Rut/neoeriocitrin	596.17	21.67	$[M+H]^-$	659.15	[35,43]
14	Naringenin-7-O-Neo/naringin	580.18	26.30	$[M+H]^-$	91.00, 501.00	[35,39,41,43]
15	Hesperetin	302.08	29.17	$[M+H]^-$	471.05, 681.15	[35,36,39,43]
16	Hesperetin-7-O-Rut/hesperidin	610.19	29.32	$[M+H]^-$	300.95, 471.05	[35,39,41,43,44]
17	Hesperetin-7-O-Neo/neohesperidin	610.19	29.32	$[M+H]^-$	301.10, 471.05	[35,36,43]
18	Limonexic acid/limonexin	502.52	30.98	$[M+H]^+$	83.05, 687.10	[36]
19	Limocitrol-O-Glu-HMG	682.17	31.38	$[M+H]^-$	579.05	[35,36,43]
20	Naringenin-7-O-Neo/naringin	580.18	32.10	$[M+H]^-$	91.05, 409.10, 543.10	[35,39,41,43]
21	p-Coumatric acid	164.05	32.95	$[M+H]^-$	119.05, 350.95	[36]
22	Luteolin	286.24	34.52	$[M+H]^+$	83.05	[36,39]
23	Limocitrin	346.29	34.92	$[M+H]^+$	83.05, 797.10	[36]
24	Limocitrol	376.31	39.40	$[M+H]^-$	91.05, 435.05, 841.15,	[36]

Glu, glucoside; Neo, neohesperidoside; Rut, rutinoside; HMG, 3-hydroxy-3-methyl-glutaryl.

3.2. LUWE Mitigates Retinal Degeneration in Morphology and Thickness Induced by $NaIO_3$

To confirm retinal protection, mice were orally administered 100 mg/mL LUWE for 7 days, followed by a tail vein injection of 40 mg/kg $NaIO_3$ [20,31]. Our results showed that intravenous injection of $NaIO_3$ resulted in numerous obvious elevations on the 7th day, originating from the basal layer of the retina (indicated by red arrows). Additionally, $NaIO_3$ disrupted the boundaries between the inner nuclear layer (INL) and outer nuclear layer (ONL) and led to unidentified nuclei migration (indicated by yellow arrows), observed in the inner segments (ISs) and outer segments (OSs) (Figure 2A). These nuclei may originate from RPE cells, photoreceptor cells, or choroidal endothelial cells [45,46]. However, LUWE significantly relieved the retinal morphological changes induced by $NaIO_3$, resulting in clearer boundaries between each layer (Figure 2A). These results demonstrate that LUWE can protect the structural integrity of the retina against the pathological features induced by $NaIO_3$.

We further measured the average thickness of the INL and ONL based on H&E staining results. The total retinal thickness of the mock group was 199.57 ± 6.1 μm (Figure 2B), with an average thickness of 44.65 ± 3.29 μm for the ONL (Figure 2C) and 37.22 ± 1.99 μm for the INL (Figure 2D). $NaIO_3$ significantly reduced the average thickness of both the ONL (35.60 ± 2.16 μm) and INL (30.72 ± 1.78 μm), consequently decreasing the total retinal thickness (83.74 ± 13.59 μm). In contrast, LUWE maintained the thickness of the ONL (43.24 ± 4.99 μm) and INL (35.60 ± 2.16 μm), thereby protecting the total retinal thickness (43.24 ± 4.99 μm).

The apoptosis regulated by the caspase cascade following $NaIO_3$ exposure has been previously confirmed as a major cause of retinal oxidative damage [7]. Our immunohistochemical staining showed that $NaIO_3$ only promoted the expression of cleaved caspase-3 protein in RPE cells (marked by red arrows), while other cells did not express it. In LUWE-

pretreated retina, the above-mentioned protein expression was significantly diminished (Figure 2E). Past reports indicate that the INL and ONL rely on intact RPE cells to maintain their physiological metabolism and assist in the removal of RPE toxicity [8], suggesting that LUWE may prevent $NaIO_3$-induced retinal degeneration by inhibiting RPE cell apoptosis. Therefore, the molecular mechanisms underlying this protection were further investigated.

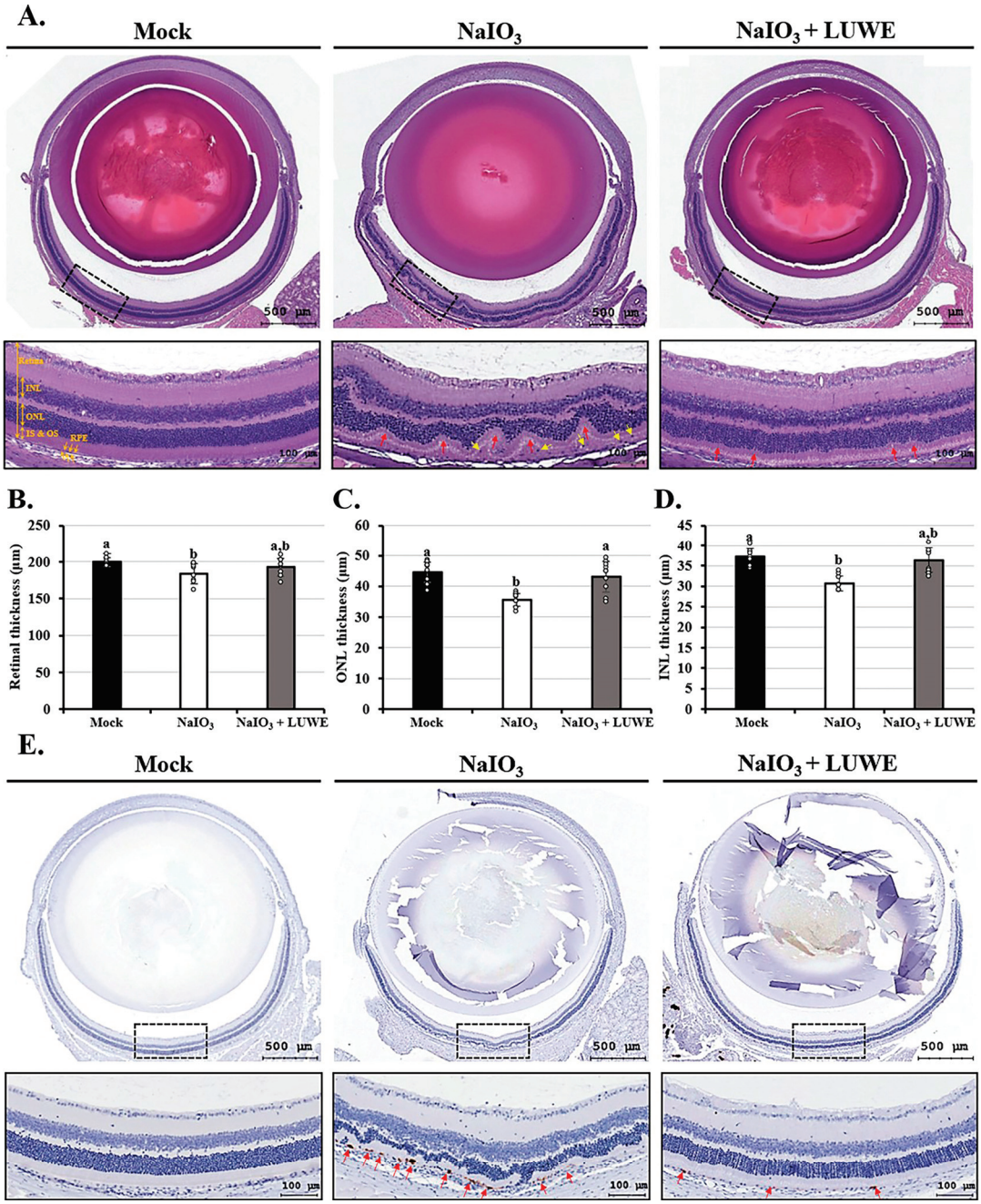

Figure 2. Effects of LUWE on retinal histological changes in Balb/c mice induced by $NaIO_3$. All mice were sacrificed after 7 days of intravenous injection. Mouse eyeballs were (**A**) stained with hematoxylin and eosin to quantify the thickness of the (**B**) retina, (**C**) ONL, (**D**) INL, or (**E**) immunohistochemically stained with cleaved caspase-3 antibody. Scale bar = 100 μm. The red arrows marked irregular deformations at the base of the retina, while the yellow arrows indicated migrated cell nucleus. All data on thickness were expressed as mean ± standard deviation (n = 6). Different letters (a,b) superscripted in the statistical chart indicate that there is statistical significance between groups ($p < 0.05$); on the contrary, being marked with the same letter indicates that there is no statistical significance.

3.3. LUWE Attenuates Cell Death in $NaIO_3$-Treated ARPE-19 Cells

To confirm the effect of LUWE on RPE cells, we pretreated ARPE-19 cells (an adult RPE cell line) with different concentrations of LUWE for 1.5 h, followed by co-incubation with 6 mM $NaIO_3$ for 24 h, which induced approximately 50% cell death, as previously reported by our group [20,31]. The results showed that 10 mg/mL LUWE slightly increased the viability of ARPE-19 cells (Figure 3A), and a concentration as low as 2.5 mg/mL effectively prevented $NaIO_3$-induced cell death (Figure 3B).

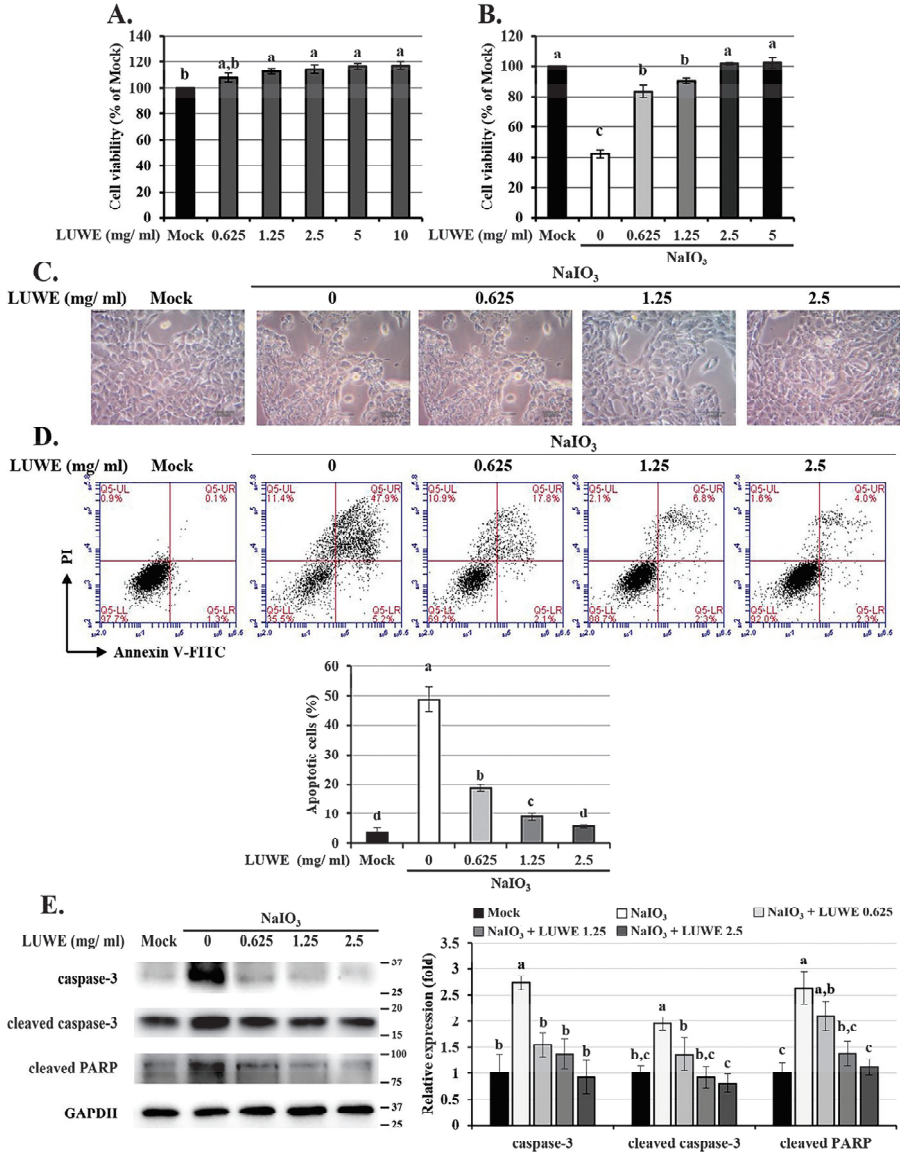

Figure 3. Protection of LUWE in $NaIO_3$-induced ARPE-19 cell apoptosis. ARPE-19 cells were (**A**) treated with different doses of LUWE, or (**B**) pretreated with LUWE as designed for 1.5 h, and then co-cultured with 6 mM $NaIO_3$ for 24 h to detect cell viability. (**C**) The cell morphology was recorded (bar = 10 μm), and (**D**) annexin V/PI staining was performed. The percentage of apoptotic cells is the sum of early apoptotic cells (Q5-LR: annexin V+/PI−) and late apoptotic cells (Q5-UR: annexin V+/PI+). (**E**) Cell lysates were collected for analysis of caspase-3, cleaved caspase-3, and cleaved PARP protein expression by Western blotting. Protein expression is represented by the fold of the mock group. All data are expressed as the mean ± SD (n = 3). Different letters (a–d) superscripted in the statistical chart indicate that there is statistical significance between groups ($p < 0.05$); on the contrary, being marked with the same letter indicates that there is no statistical significance.

We observed that $NaIO_3$ stimulated morphological changes in ARPE-19 cells characterized by cell swelling and vacuolation, reminiscent of the apoptotic cells described by Godwin et al. [47] (Figure 3C). Therefore, annexin V/PI staining was performed to determine the pathway of cell death according to the method described by Balmer et al. [7]. The results showed that $NaIO_3$ induced 48.9 ± 4.2% apoptotic cells, while 0.625, 1.25, and 2.5 mg/mL of LUWE reduced the apoptotic cells to 18.75 ± 1.15%, 7.9 ± 1.2%, and 5.65 ± 0.65%, respectively (Figure 3D).

We also collected cell lysates from each group for further analysis of the expression of the pro-apoptotic proteins caspase-3 and PARP [7]. As shown in Figure 3E, LUWE not only inhibited the activated forms of caspase-3 and PARP but also reduced the full-length expression of these proteins. These results confirm that LUWE can protect ARPE-19 cell viability by suppressing the apoptotic pathway induced by $NaIO_3$.

3.4. LUWE Attenuates the Mitochondrial ROS-Stimulated MEK/ERK Signaling Pathway in $NaIO_3$-Treated ARPE-19 Cells

Mitochondrial oxidative stress is one of the major factors accelerating the progression of AMD by driving RPE cell autophagy, DNA damage, or cell cycle arrest, resulting in cellular senescence and apoptosis [48]. Our MitoSOX Red staining demonstrated that LUWE could dose-dependently inhibit mitochondrial ROS production in $NaIO_3$-treated ARPE-19 cells (Figure 4A). Therefore, we further collected the cell lysates from each group to analyze the expression of mitogen-activated protein kinases (MAPKs), including p-ERK, p-p38, and p-JNK. As crucial secondary messengers in cells, this pathway directly mediates RPE cell mesenchymal transition, autophagy, and apoptosis under oxidative stress or hypoxic conditions [12,49]. In $NaIO_3$-induced ARPE-19 cells, LUWE inhibited the expression of the above-mentioned proteins, with the most significant difference observed in p-ERK (Figure 4B). Therefore, we also analyzed the expression of its core upstream factor, p-MEK-1/2 [50], and confirmed its consistent trend with p-ERK across all cell groups (Figure 4C). These results suggest that LUWE may primarily target ROS-regulated MEK/ERK signaling, thereby protecting against $NaIO_3$-induced cell death in ARPE-19 cells.

3.5. LUWE Inhibits the Intrinsic Apoptosis Induced by $NaIO_3$ through the MEK/ERK Signaling Pathway

To confirm the role of MEK/ERK signaling in $NaIO_3$-induced cytotoxicity, we pretreated ARPE-19 cells with 20 μM MEK inhibitor PD98059 or 10 μM ERK inhibitor U0126 before co-culturing them with $NaIO_3$ [51]. In Figure 5A, it can be seen that U0126 and PD98059 can significantly restore the cell viability induced by $NaIO_3$. Meanwhile, the results of annexin V/PI staining showed that U0126 and PD98059 effectively reduced apoptotic ARPE-19 cells (Figure 5B). The above effects were further enhanced upon cotreatment with LUWE.

Therefore, we also examined the expression of pro-apoptotic proteins using Western blotting. We first confirmed that U0126 and PD98059 inhibited the expression of p-MEK-1/2 and p-ERK-1/2 induced by $NaIO_3$, which showed a positive correlation with cytotoxicity (Figure 5C). Furthermore, we observed that U0126, PD98059, and LUWE could inhibit $NaIO_3$-induced cleaved PARP protein expression, consistent with the trend of cleaved caspase-9 (Figure 5D), which is the initiator of intrinsic apoptotic bodies triggered by mitochondrial damage [52]. Based on the above results, we understand that LUWE protects against intrinsic apoptosis in RPE cells by reducing mitochondrial oxidative stress-stimulated MEK/ERK pathways.

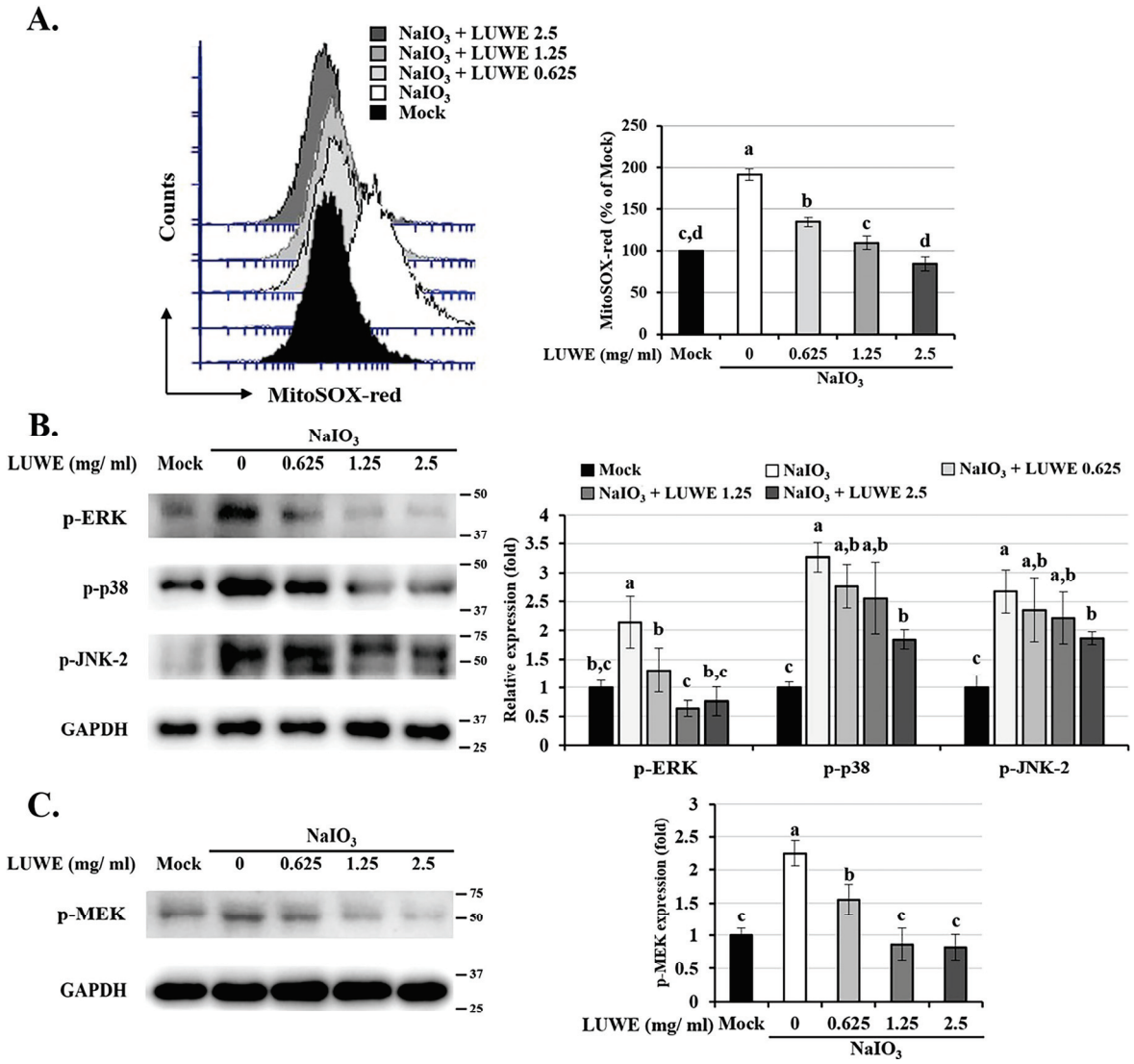

Figure 4. Effects of LUWE on the mitochondrial ROS level and MAPK proteins induced by $NaIO_3$. After treatment according to the experimental design, ARPE-19 cells in each group (**A**) were analyzed for mitochondrial ROS levels using MitoSOX Red staining or were collected for analyzing (**B**) the p-ERK, p-p38, p-JNK2, and (**C**) p-MEK protein expression by Western blotting. MitoSOX Red in each group was quantified as a percentage compared with the fluorescent values of the mock group. Protein expression was represented by the fold of the mock group. All data are expressed as the mean ± SD (n = 3). Different letters (a–d) superscripted in the statistical chart indicate that there is statistical significance between groups ($p < 0.05$); on the contrary, being marked with the same letter indicates that there is no statistical significance.

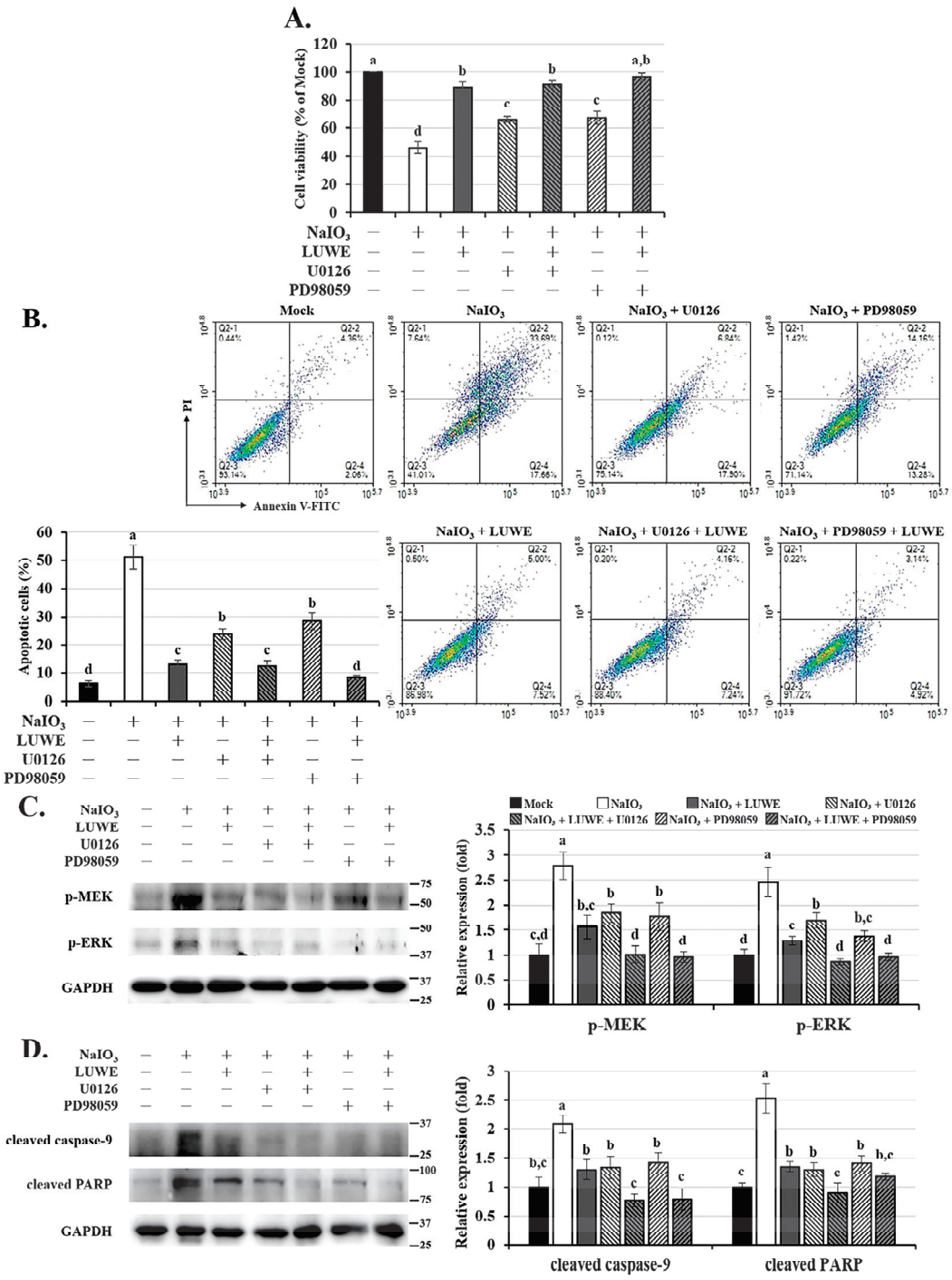

Figure 5. Effects of LUWE, U0126, and PD98059 on $NaIO_3$-induced ARPE-19 cell apoptosis. ARPE-19 cells were pretreated with 10 μM U0126 or 20 μM PD98059 mixed with 2.5 mg/ mL LUWE or not for 1.5 h, and then cotreated with $NaIO_3$ for 24 h. (**A**) The cell viability was analyzed using the CCK-8 reagent, and (**B**) the ratio of apoptotic cells was determined by annexin V/PI staining. Cell lysates were collected for analysis of (**C**) p-MEK-1/2, p-ERK-1/2, (**D**) cleaved caspase-9 PARP, and cleaved PARP protein expression by Western blotting. Protein expression was represented by the fold of the mock group. All data are expressed as the mean ± SD (n = 3). Different letters (a–d) superscripted in the statistical chart indicate that there is statistical significance between groups ($p < 0.05$); on the contrary, being marked with the same letter indicates that there is no statistical significance.

3.6. LUWE Reduces Mitochondrial Fission Regulated by the MEK/ERK Signaling Pathway in $NaIO_3$-Treated ARPE-19 Cells

Reportedly, $NaIO_3$ can regulate mitochondrial dynamics through ERK and AMPK signaling pathways, involving mitochondrial fission and fusion [12,49]. This process may disrupt mitochondrial membrane potential and promote the release of cytochrome c, triggering a caspase-mediated intrinsic apoptosis cascade [53,54]. Therefore, we conducted protein analysis to determine the expression of factors regulating mitochondrial dynamics. As shown in Figure 6A, $NaIO_3$ increased the expression of the mitochondrial division proteins p-Drp-1 and Fis1 in ARPE-19 cells, as well as the expression of cytochrome c; however, LUWE, U0126, or PD98059 can suppress the expression of the aforementioned proteins.

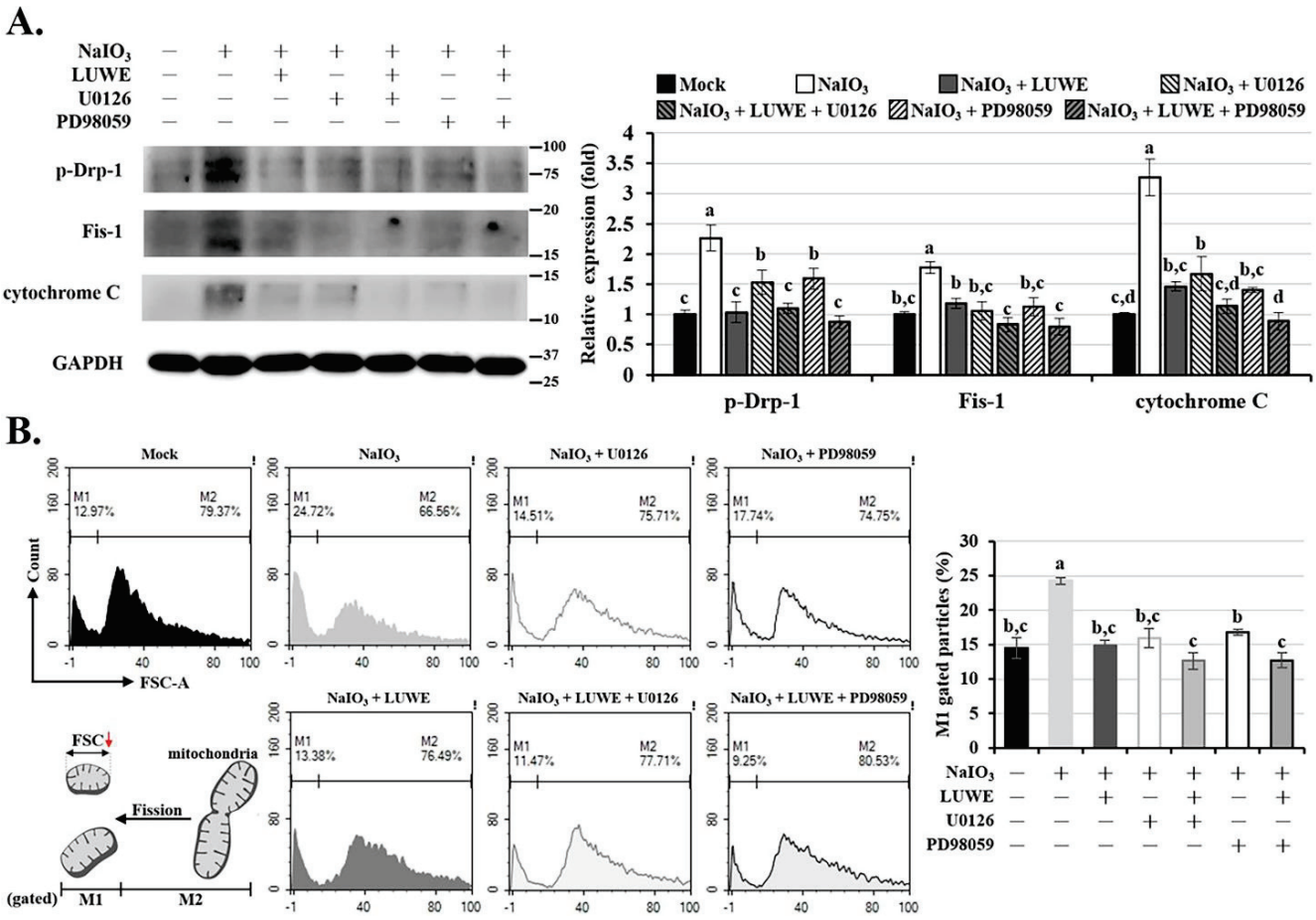

Figure 6. Effects of LUWE, U0126, and PD98059 on $NaIO_3$-induced mitochondrial homeostasis. ARPE-19 cells were pretreated with 10 μM U0126 or 20 μM PD98059 mixed with 2.5 mg/mL LUWE or not for 1.5 h, and then cotreated with sodium iodate for 24 h. (**A**) Cell lysates were collected for analysis of p-Drp-1, Fis1, and cytochrome c protein expression by Western blotting. Protein expression was represented by the fold of the mock group. (**B**) The isolated mitochondria from cells in each group were analyzed for particle size using forward scatter (FSC-A) with flow cytometry. All data are expressed as the mean ± SD (n = 3). Different letters (a–d) superscripted in the statistical chart indicate that there is statistical significance between groups ($p < 0.05$); on the contrary, being marked with the same letter indicates that there is no statistical significance.

To further determine the influence of LUWE on mitochondrial homeostasis, we isolated mitochondria from cells in each group and measured their size using forward scatter (FSC) in flow cytometry. The results indicate that $NaIO_3$ increased the small-sized mitochondrial content (M1-gated particles) in ARPE-19 cells. Meanwhile, LUWE, U0126, or PD98059 can significantly reduce the number of small-sized mitochondria.

Based on the above results, we conclude that LUWE can suppress the mitochondrial oxidative stress-mediated MEK/ERK signaling pathway, thus protecting ARPE-19 cells against mitochondrial fission-stimulated intrinsic apoptosis induced by $NaIO_3$.

4. Discussion

RPE cell dysfunction is considered a major factor in the onset of AMD. Oxidative stress mediates various physiological mechanisms of RPE cells, including aging, cellular autophagy, and apoptosis [20,31], making antioxidant strategies play a crucial role in slowing the progression of AMD [48].

Citrus fruits are among the most popular fruits globally. Unripe lemons are favored for their acidic juice, but they also generate acidic agricultural waste that cannot be easily disposed of, resulting in additional costs for both the economy and the environment [55]. Reportedly, the polyphenol content in citrus fruits reaches its peak before reaching maturity. This suggests that these by-products of lemons are suitable for extracting antioxidant compounds [56]. In this study, we selected the Eureka variety of lemons referred to in the work of Perez-Perez et al., which is known to have higher contents of flavonoids and polyphenols, commonly found in Southeast Asian regions [57]. Considering the most direct method for handling agricultural waste, we employed water extraction with fresh by-products from lemons, and ultrasound application was applied to shorten the extraction time and enhance the release of antioxidant compounds [26].

It was reported that lemon peel contains 16.71 ± 0.40 mg GAE of polyphenol content and 21.38 ± 1.53 mg TE of ABTS clearance activity per gram (dry weight), extracted using a solvent composed of 50% alcohol and 50% water [58]. Our samples exhibited a polyphenol content of 10.24 ± 0.09 mmole GAE and an ABTS clearance activity of 5.65 ± 0.06 mmole TE (Table 1). Considering that the fresh by-products of lemon contain over 80% water and that most flavonoids and polyphenolic compounds are hydrophobic [59], the above results align with our expectations. In addition, we identified the main components of LUWE as citric acid, limocitrin derivative, neoeriocitrin, p-coumaric acid, and luteolin (Figure 1 and Table 2), which roughly align with those reported by Ledesma-Escobar [43]. Among these, p-coumaric acid has been previously shown to protect lens epithelial cells from MAPK-mediated apoptosis [60], while luteolin can mitigate the inflammatory response regulated by the MAPK pathway in RPE cells [61]. These findings supported our discoveries and suggested the potential of LUWE as a natural compound for retinal injury.

The exact way $NaIO_3$ damages RPE cells is not fully known yet. $NaIO_3$ triggers oxidative stress and boosts genes linked to dealing with oxidative stress. Mouse models induced by $NaIO_3$ mimic some aspects of dry AMD, showing partial loss of RPE cells in patches and the subsequent death of photoreceptor cells and choriocapillaris. Targeting oxidative stress could help ease RPE cell issues and prevent cell death. As shown in Figure 2A, we found that $NaIO_3$ caused the destruction and loss of photoreceptor cells in the mouse retina, accompanied by cellular infiltration in the photoreceptor outer segment (OS) and inner segment (IS) regions, a result similar to that of Chowers et al. [62]. At the same time, we also observed that LUWE effectively restricted the development of retinal folds and maintained the structural integrity of each layer. Furthermore, LUWE protected the retina against thickness reduction and cell loss induced by $NaIO_3$, primarily occurring in the ONL and INL (Figure 2B–D). These two layers consist of the nuclei of photoreceptor cells and neuronal cells. Their distortion and cell loss directly lead to decreased photosensitivity and visual signal transmission efficiency, making them important indicators for evaluating visual function [63,64]. Thus, the above results indicate that LUWE can mitigate $NaIO_3$-induced retinal degeneration.

A previous study indicates that $NaIO_3$, by targeting RPE apoptosis, leads to retinal degeneration [12,20,56,65]. In our study, we observed through immunofluorescence staining that LUWE can significantly suppress the expression of cleaved caspase-3 induced by $NaIO_3$. This protein was specifically expressed in the RPE cells at the base of the retina, while there was no expression in other locations (Figure 2E). This phenomenon may be due

to severe RPE damage induced by NIO_3 in mice, followed by visual impairment, functional impairment, and photoreceptor loss. The above results suggest that LUWE may protect the retina against $NaIO_3$-induced degeneration by preventing RPE cell apoptosis.

To understand the protective mechanisms, we observed the protection of LUWE using $NaIO_3$-induced ARPE-19 cells based on previous studies [20,31,66]. We observed that 2.5 mg/mL LUWE can effectively suppress $NaIO_3$-induced ARPE-19 cell death (Figure 3B). Therefore, we used annexin V/PI staining to determine the protective pathway of LUWE against cell death, which method has been widely used to distinguish between necrotic and apoptotic cells [67]. The results demonstrate that LUWE effectively reduces the number of apoptotic cells induced by $NaIO_3$ (Figure 3D), characterized by a swollen and vacuolated morphology (Figure 3C). Based on the above, we further analyzed the protein expression of apoptotic proteins. The results showed that LUWE effectively suppressed the protein expression of both full-length and activated forms of caspase-3 and PARP induced by $NaIO_3$. These findings confirm the protective effect of LUWE against $NaIO_3$-induced apoptosis in RPE cells, supporting our observations in the mouse retina.

The MAPK signaling pathway is well known as a central regulator, mediating the cellular response of RPE cells to oxidative stress [12,49]. We used MitoSOX Red staining to confirm that LUWE effectively reduces the mitochondrial ROS levels induced by $NaIO_3$ (Figure 4A), thereby inhibiting MAPK signals, especially the MEK/ERK pathway (Figure 4B). The sequential relationship between them has been established in previous literature [4,68]. To observe the importance of the MEK/ERK pathway in the protection of RPE cell damage by LUWE, we pretreated ARPE-19 cells with PD98059 and U0126 before $NaIO_3$ treatment, which have been previously confirmed to inhibit ERK signaling through different pathways [51]. Through the CCK-8 assay and annexin V/PI staining, we observed that U0126 and PD98059 can significantly reduce the number of apoptotic cells induced by $NaIO_3$ (Figure 5A,B). Furthermore, we observed a significant decrease in the protein expression of cleaved caspase-9 and cleaved PARP induced by $NaIO_3$ in the pretreatment groups with LUWE, U0126, and PD98059 (Figure 5C). Therefore, our data reveal that LUWE can suppress the $NaIO_3$-induced MEK/ERK pathway, thereby blocking an intrinsic apoptotic pathway.

Past studies have confirmed that $NaIO_3$ can disrupt mitochondrial dynamics and activity through the ERK signaling pathway [49,69]. However, further exploration is needed to determine whether targeting ERK-mediated mitochondrial homeostasis can be a viable strategy for formulating AMD treatment approaches. Here, we observed that LUWE can suppress the expression of pro-fission proteins p-Drp-1 and Fis1 induced by $NaIO_3$, thereby stabilizing the mitochondrial dynamics and reducing the expression of cytochrome c in ARPE-19 cells (Figure 6A). It is worth noting that the aforementioned mitochondrial damage was also decreased to varying degrees with the pretreatment of U0126 and PD98059. These results demonstrate that LUWE can inhibit mitochondrial ROS-mediated fission, thereby alleviating the intrinsic apoptosis of RPE cells and protecting against retinal degeneration. As reported by Chan et al., our data also indicate that the mitochondrial damage induced by $NaIO_3$ is regulated through the MEK/ERK pathway [49].

5. Conclusions

This study establishes the effectiveness of isolating antioxidant components from lemon by-products. Using in vitro and in vivo models of $NaIO_3$-induced retinal degeneration, we demonstrated that lemon by-product extracts can inhibit ROS-mediated MEK/ERK signaling, thereby preventing mitochondrial fission-triggered RPE cell apoptosis and subsequent neuroretina and photoreceptor loss (Figure 7). Our study not only highlights the innovation of using lemon by-product water extracts for maintaining ocular health but also provides insights and development strategies for functional materials targeting physiological barrier organs like the brain or eyes.

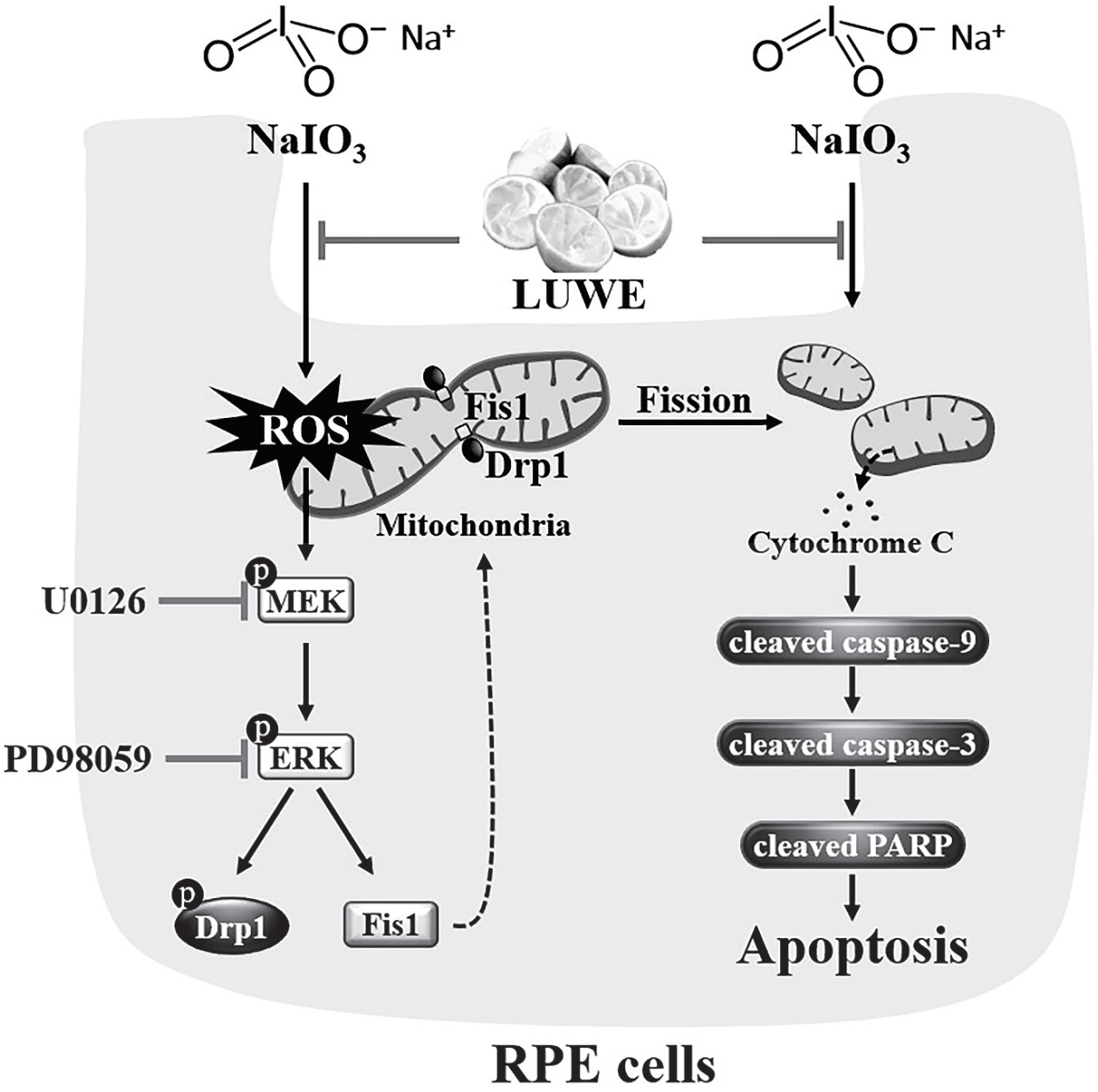

Figure 7. Protection of LUWE against sodium iodate-induced apoptosis in RPE cells. LUWE mitigates mitochondrial ROS-mediated MEK/ERK signaling, consequently reducing mitochondrial fission regulated by Drp-1 and Fis1. As a result, LUWE suppresses the expression of cytochrome c protein, leading to a reduction in RPE cell apoptosis regulated through the caspase-9/caspase-3/PARP cascade. LUWE protected against sodium iodate-induced RPE cell death, thereby reducing retinal thinning and distortion.

Author Contributions: S.-C.T.: Writing—review and editing, Writing—original draft, Validation, Software, Resources, Project administration, Data curation. C.-J.C.: Writing—review and editing, Writing—original draft, Validation, Software, Resources, Project administration, Data curation. I.W.: Writing—review and editing, Validation, Data curation. T.-C.C.: Validation, Data curation. J.-H.Y.: Methodology, Investigation. C.-L.H.: Validation, Data curation. Y.-C.H.: Validation, Investigation. M.-C.L.: Validation, Data curation. Y.-Y.C.: Writing—review and editing, Supervision, Project administration, Conceptualization. H.-W.L.: Writing—review and editing, Supervision, Project administration, Conceptualization. All authors have read and agreed to the published version of the manuscript.

Funding: The authors would like to thank the Ministry of Science and Technology, Taiwan (project numbers: MOST 111-2320-B-040-006-MY3 and MOST-112-2320-B-468-002-MY3) for financially supporting this research.

Institutional Review Board Statement: Ethics approval and consent to participate. All animal use protocols in this study were approved by the Institutional Animal Care and Use Committee at the Chung Shan Medical University (IACUC approval number: 2595), and all investigations were carried out following the "Guide to the Care and Use of Experimental Animals".

Informed Consent Statement: Not applicable.

Data Availability Statement: Data is contained within the article.

Acknowledgments: We also thank the Instrument Resource Centre of Chung Shan Medical University for its technical support. The authors are grateful to Wallace Academic Editing, Taiwan, for proofreading the manuscript. The authors express their gratitude to Herbiotek (Taipei, Taiwan) for its analysis of the extract components.

Conflicts of Interest: There are no conflicts to declare.

References

1. Guymer, R.H.; Campbell, T.G. Age-related macular degeneration. *Lancet* **2023**, *10386*, 1459–1472. [CrossRef]
2. Khachigian, L.M.; Liew, G.; Teo, K.Y.; Wong, T.Y.; Mitchell, P. Emerging therapeutic strategies for unmet need in neovascular age-related macular degeneration. *J. Transl. Med.* **2023**, *21*, 133. [CrossRef]
3. Eshaq, R.S.; Wright, W.S.; Harris, N.R. Oxygen delivery, consumption, and conversion to reactive oxygen species in experimental models of diabetic retinopathy. *Redox Biol.* **2014**, *2*, 661–666. [CrossRef]
4. Chan, C.-M.; Huang, D.-Y.; Sekar, P.; Hsu, S.-H.; Lin, W.-W. Reactive oxygen species-dependent mitochondrial dynamics and autophagy confer protective effects in retinal pigment epithelial cells against sodium iodate-induced cell death. *J. Biomed. Sci.* **2019**, *26*, 40. [CrossRef]
5. Park, C.; Cha, H.-J.; Kim, M.Y.; Bang, E.; Moon, S.-K.; Yun, S.J.; Kim, W.-J.; Noh, J.S.; Kim, G.-Y.; Cho, S.; et al. Phloroglucinol Attenuates DNA Damage and Apoptosis Induced by Oxidative Stress in Human Retinal Pigment Epithelium ARPE-19 Cells by Blocking the Production of Mitochondrial ROS. *Antioxidants* **2022**, *11*, 2353. [CrossRef] [PubMed]
6. Kim, S.-Y.; Zhao, Y.; Kim, H.-L.; Oh, Y.; Xu, Q. Sodium iodate-induced retina degeneration observed in non-separate sclerochoroid/retina pigment epithelium/retina whole mounts. *Ann. Eye Sci.* **2022**, *3*, 21–27. [CrossRef] [PubMed]
7. Balmer, J.; Zulliger, R.; Roberti, S.; Enzmann, V. Retinal cell death caused by sodium iodate involves multiple caspase-dependent and caspase-independent cell-death pathways. *Int. J. Mol. Sci.* **2015**, *7*, 15086–15103. [CrossRef]
8. Enzbrenner, A.; Zulliger, R.; Biber, J.; Pousa, A.M.Q.; Schäfer, N.; Stucki, C.; Giroud, N.; Berrera, M.; Kortvely, E.; Schmucki, R.; et al. Sodium iodate-induced degeneration results in local complement changes and inflammatory processes in murine retina. *Int. J. Mol. Sci.* **2021**, *22*, 9218. [CrossRef] [PubMed]
9. Zhang, K.; Wang, T.; Sun, G.-F.; Xiao, J.-X.; Jiang, L.-P.; Tou, F.-F.; Qu, X.-H.; Han, X.-J. Metformin protects against retinal ischemia/reperfusion injury through AMPK-mediated mitochondrial fusion. *Free Radic. Biol. Med.* **2023**, *205*, 47–61. [CrossRef]
10. Zhang, S.-M.; Fan, B.; Li, Y.-L.; Zuo, Z.-Y.; Li, G.-Y. Oxidative Stress-Involved Mitophagy of Retinal Pigment Epithelium and Retinal Degenerative Diseases. *Cell. Mol. Neurobiol.* **2023**, *43*, 3265–3276. [CrossRef]
11. McCubrey, J.A.; LaHair, M.M.; Franklin, R.A. Reactive oxygen species-induced activation of the MAP kinase signaling pathways. *Antioxid. Redox Signal.* **2006**, *8*, 1775–1789. [CrossRef] [PubMed]
12. Yang, Y.-C.; Chien, Y.; Yarmishyn, A.A.; Lim, L.-Y.; Tsai, H.-Y.; Kuo, W.-C.; Tsai, P.-H.; Yang, S.-H.; Hong, S.-I.; Chen, S.-J.; et al. Inhibition of oxidative stress-induced epithelial-mesenchymal transition in retinal pigment epithelial cells of age-related macular degeneration model by suppressing ERK activation. *J. Adv. Res.* **2023**, *23*, 00167-4. [CrossRef] [PubMed]
13. Flaxel, C.J.; Adelman, R.A.; Bailey, S.T.; Fawzi, A.; Lim, J.I.; Vemulakonda, G.A.; Ying, G.-s. Age-related macular degeneration preferred practice pattern®. *Ophthalmology* **2020**, *127*, P1–P65. [CrossRef] [PubMed]
14. Gardner, T.W.; Antonetti, D.A.; Barber, A.J.; Lieth, E.; Tarbell, J.A.; The Penn State Retina Research Group. The molecular structure and function of the inner blood-retinal barrier. *Doc. Ophthalmol.* **1999**, *97*, 229–237. [CrossRef] [PubMed]
15. Zema, D.; Calabrò, P.; Folino, A.; Tamburino, V.; Zappia, G.; Zimbone, S. Valorisation of citrus processing waste: A review. *Waste Manag.* **2018**, *80*, 252–273. [CrossRef] [PubMed]
16. Park, Y.-S.; Kim, I.-d.; Dhungana, S.K.; Park, E.-J.; Park, J.-J.; Kim, J.-H.; Shin, D.-H. Quality Characteristics and Antioxidant Potential of Lemon (*Citrus limon* Burm. f.) seed oil extracted by different methods. *Front. Nutr.* **2021**, *8*, 644406. [CrossRef]
17. Saini, R.K.; Ranjit, A.; Sharma, K.; Prasad, P.; Shang, X.; Gowda, K.G.M.; Keum, Y.-S. Bioactive compounds of citrus fruits: A review of composition and health benefits of carotenoids, flavonoids, limonoids, and terpenes. *Antioxidants* **2022**, *11*, 239. [CrossRef]
18. Youdim, K.A.; Qaiser, M.Z.; Begley, D.J.; Rice-Evans, C.A.; Abbott, N.J. Flavonoid permeability across an in situ model of the blood–brain barrier. *Free Radic. Biol. Med.* **2004**, *36*, 592–604. [CrossRef]

19. Muhammad, T.; Ikram, M.; Ullah, R.; Rehman, S.U.; Kim, M.O. Hesperetin, a citrus flavonoid, attenuates LPS-induced neuroinflammation, apoptosis and memory impairments by modulating TLR4/NF-κB signaling. *Nutrients* **2019**, *11*, 648. [CrossRef]
20. Chang, Y.-Y.; Lee, Y.-J.; Hsu, M.-Y.; Wang, M.; Tsou, S.-C.; Chen, C.-C.; Lin, J.-A.; Hsiao, Y.-P.; Lin, H.-W. Protective effect of quercetin on sodium iodate-induced retinal apoptosis through the reactive oxygen species-mediated mitochondrion-dependent pathway. *Int. J. Mol. Sci.* **2021**, *22*, 4056. [CrossRef]
21. Tungmunnithum, D.; Thongboonyou, A.; Pholboon, A.; Yangsabai, A. Flavonoids and other phenolic compounds from medicinal plants for pharmaceutical and medical aspects: An overview. *Medicines* **2018**, *5*, 93. [CrossRef]
22. Costa, R.; Costa Lima, S.A.; Gameiro, P.; Reis, S. On the development of a cutaneous flavonoid delivery system: Advances and limitations. *Antioxidants* **2021**, *10*, 1376. [CrossRef] [PubMed]
23. Song, M.-H.; Shin, E.-C.; Hwang, D.-Y.; Jang, I.-S. Effects of lutein or lutein in combination with vitamin C on mRNA expression and activity of antioxidant enzymes and status of the antioxidant system in SD rats. *Lab. Anim. Res.* **2015**, *31*, 117–124. [CrossRef] [PubMed]
24. Karbuz, P.; Tugrul, N. Microwave and ultrasound assisted extraction of pectin from various fruits peel. *J. Food Sci. Technol.* **2021**, *58*, 641–650. [CrossRef] [PubMed]
25. Papoutsis, K.; Pristijono, P.; Golding, J.B.; Stathopoulos, C.E.; Bowyer, M.C.; Scarlett, C.J.; Vuong, Q.V. Optimizing a sustainable ultrasound-assisted extraction method for the recovery of polyphenols from lemon by-products: Comparison with hot water and organic solvent extractions. *Eur. Food Res. Technol.* **2018**, *244*, 1353–1365. [CrossRef]
26. Jagannath, A.; Biradar, R. Comparative evaluation of soxhlet and ultrasonics on the structural morphology and extraction of bioactive compounds of lemon (*Citrus limon* L.) peel. *J. Food Chem. Nanotechnol.* **2019**, *5*, 56–64. [CrossRef]
27. Konan, K.; Le Tien, C.; Mateescu, M. Electrolysis-induced fast activation of the ABTS reagent for an antioxidant capacity assay. *Anal. Methods.* **2016**, *8*, 5638–5644. [CrossRef]
28. Anggraini, T.; Nanda, R.F.; Syukri, D. Effect of processing on green and black tea DPPH radical scavenging activity, IC50 value, total polyphenols, catechin and epigallocatechin gallate content. In Proceedings of the 7th International Conference on Sustainable Agriculture, Food and Energy, Phuket, Thailand, 18–21 October 2019; IOP Conference Series: Earth and Environmental Science. IOP Publishing: Bristol, UK, 2021; p. 012017.
29. Shraim, A.M.; Ahmed, T.A.; Rahman, M.M.; Hijji, Y.M. Determination of total flavonoid content by aluminum chloride assay: A critical evaluation. *LWT-Food Sci. Technol.* **2021**, *150*, 111932. [CrossRef]
30. Carmona-Hernandez, J.C.; Taborda-Ocampo, G.; González-Correa, C.H. Folin-Ciocalteu reaction alternatives for higher polyphenol quantitation in Colombian passion fruits. *Int. J. Food Sci.* **2021**, *2021*, 8871301. [CrossRef]
31. Hsu, M.-Y.; Hsiao, Y.-P.; Lin, Y.-T.; Chen, C.; Lee, C.-M.; Liao, W.-C.; Tsou, S.-C.; Lin, H.-W.; Chang, Y.-Y. Quercetin alleviates the accumulation of superoxide in sodium iodate-induced retinal autophagy by regulating mitochondrial reactive oxygen species homeostasis through enhanced deacetyl-SOD2 via the Nrf2-PGC-1α-Sirt1 pathway. *Antioxidants* **2021**, *10*, 1125. [CrossRef]
32. Tzur, A.; Moore, J.K.; Jorgensen, P.; Shapiro, H.M.; Kirschner, M.W. Optimizing optical flow cytometry for cell volume-based sorting and analysis. *PLoS ONE* **2011**, *1*, e16053. [CrossRef] [PubMed]
33. Stern, A.D.; Rahman, A.H.; Birtwistle, M.R. Cell size assays for mass cytometry. *Cytom. Part A* **2017**, *91*, 14–24. [CrossRef] [PubMed]
34. Kushwah, N.; Bora, K.; Maurya, M.; Pavlovich, M.C.; Chen, J. Oxidative stress and antioxidants in age-related macular degeneration. *Antioxidants* **2023**, *7*, 1379. [CrossRef] [PubMed]
35. Ledesma-Escobar, C.; Priego-Capote, F.; Luque de Castro, M. Characterization of lemon (*Citrus limon*) polar extract by liquid chromatography–tandem mass spectrometry in high resolution mode. *J. Mass Spectrom.* **2015**, *50*, 1196–1205. [CrossRef] [PubMed]
36. El-Sayed, M.A.; Al-Gendy, A.A.; Hamdan, D.I.; El-Shazly, A.M. Phytoconstituents, LC-ESI-MS profile, antioxidant and antimicrobial activities of Citrus x limon L. Burm. f. Cultivar Variegated Pink Lemon. *Int. J. Pharm. Sci.* **2017**, *9*, 375.
37. Wang, Z.; Jablonski, J.E. Targeted and non-targeted detection of lemon juice adulteration by LC-MS and chemometrics. *Food Addit. Contam. Part A* **2016**, *33*, 560–573. [CrossRef] [PubMed]
38. Gargouri, B.; Ammar, S.; Verardo, V.; Besbes, S.; Segura-Carretero, A.; Bouaziz, M. RP-HPLC–DAD-ESI-TOF–MS based strategy for new insights into the qualitative and quantitative phenolic profile in Tunisian industrial Citrus Limon by-product and their antioxidant activity. *Eur. Food Res. Technol.* **2017**, *243*, 2011–2024. [CrossRef]
39. Brito, A.; Ramirez, J.E.; Areche, C.; Sepúlveda, B.; Simirgiotis, M.J. HPLC-UV-MS profiles of phenolic compounds and antioxidant activity of fruits from three citrus species consumed in Northern Chile. *Molecules* **2014**, *19*, 17400–17421. [CrossRef] [PubMed]
40. García-Salas, P.; Gómez-Caravaca, A.M.; Arráez-Román, D.; Segura-Carretero, A.; Guerra-Hernández, E.; García-Villanova, B.; Fernández-Gutiérrez, A. Influence of technological processes on phenolic compounds, organic acids, furanic derivatives, and antioxidant activity of whole-lemon powder. *Food Chem.* **2013**, *141*, 869–878. [CrossRef]
41. Guccione, C.; Bergonzi, M.C.; Piazzini, V.; Bilia, A.R. A simple and rapid HPLC-PDA MS method for the profiling of citrus peels and traditional Italian liquors. *Planta Med.* **2016**, *82*, 1039–1045. [CrossRef]
42. Sanches, V.L.; Cunha, T.A.; Viganó, J.; de Souza Mesquita, L.M.; Faccioli, L.H.; Breitkreitz, M.C.; Rostagno, M.A. Comprehensive analysis of phenolics compounds in citrus fruits peels by UPLC-PDA and UPLC-Q/TOF MS using a fused-core column. *Food Chem. X* **2022**, *14*, 100262. [CrossRef]

43. Ledesma-Escobar, C.A.; Priego-Capote, F.; Luque de Castro, M.D. Comparative study of the effect of sample pretreatment and extraction on the determination of flavonoids from lemon (*Citrus limon*). *PLoS ONE* **2016**, *11*, e0148056. [CrossRef]
44. Castro-Vázquez, L.; Lozano, M.V.; Rodríguez-Robledo, V.; González-Fuentes, J.; Marcos, P.; Villaseca, N.; Arroyo-Jiménez, M.M.; Santander-Ortega, M.J. Pressurized Extraction as an Opportunity to Recover Antioxidants from Orange Peels: Heat treatment and Nanoemulsion Design for Modulating Oxidative Stress. *Molecules* **2021**, *26*, 5928. [CrossRef]
45. Miura, M.; Makita, S.; Sugiyama, S.; Hong, Y.-J.; Yasuno, Y.; Elsner, A.E.; Tamiya, S.; Tsukahara, R.; Iwasaki, T.; Goto, H. Evaluation of intraretinal migration of retinal pigment epithelial cells in age-related macular degeneration using polarimetric imaging. *Sci. Rep.* **2017**, *7*, 3150. [CrossRef] [PubMed]
46. Alizadeh, E.; Mammadzada, P.; André, H. The different facades of retinal and choroidal endothelial cells in response to hypoxia. *Int. J. Mol. Sci.* **2018**, *19*, 3846. [CrossRef] [PubMed]
47. Godwin, W.C.; Hoffmann, G.F.; Gray, T.J.; Hughes, R.M. Imaging of morphological and biochemical hallmarks of apoptosis with optimized optogenetic tools. *J. Biol. Chem.* **2019**, *294*, 16918–16929. [CrossRef] [PubMed]
48. Evans, J.R.; Lawrenson, J.G. Antioxidant vitamin and mineral supplements for slowing the progression of age-related macular degeneration. *Cochrane Database Syst. Rev.* **2017**, *7*, CD000254. [CrossRef]
49. Chan, C.-M.; Sekar, P.; Huang, D.-Y.; Hsu, S.-H.; Lin, W.-W. Different effects of metformin and A769662 on sodium iodate-induced cytotoxicity in retinal pigment epithelial cells: Distinct actions on mitochondrial fission and respiration. *Antioxidants* **2020**, *9*, 1057. [CrossRef]
50. McCubrey, J.A.; Steelman, L.S.; Chappell, W.H.; Abrams, S.L.; Wong, E.W.; Chang, F.; Lehmann, B.; Terrian, D.M.; Milella, M.; Tafuri, A.; et al. Roles of the Raf/MEK/ERK pathway in cell growth, malignant transformation and drug resistance. *Biochim. Biophys. Acta Mol. Cell Res.* **2007**, *1773*, 1263–1284. [CrossRef]
51. Wang, J.-Z.; Long, C.; Li, K.-Y.; Xu, H.-T.; Yuan, L.-L.; Wu, G.-Y. Potent block of potassium channels by MEK inhibitor U0126 in primary cultures and brain slices. *Sci. Rep.* **2018**, *8*, 8808. [CrossRef]
52. Wu, Y.; Zhao, D.; Zhuang, J.; Zhang, F.; Xu, C. Caspase-8 and caspase-9 functioned differently at different stages of the cyclic stretch-induced apoptosis in human periodontal ligament cells. *PLoS ONE* **2016**, *11*, e0168268. [CrossRef]
53. Sivandzade, F.; Bhalerao, A.; Cucullo, L. Analysis of the mitochondrial membrane potential using the cationic JC-1 dye as a sensitive fluorescent probe. *Bio-Protocol* **2019**, *9*, e3128. [CrossRef]
54. Yako, T.; Nakamura, M.; Nakamura, S.; Hara, H.; Shimazawa, M. Pharmacological inhibition of mitochondrial fission attenuates oxidative stress-induced damage of retinal pigmented epithelial cells. *J. Pharmacol. Sci.* **2021**, *146*, 149–159. [CrossRef]
55. Suri, S.; Singh, A.; Nema, P.K. Current applications of citrus fruit processing waste: A scientific outlook. *Appl. Food Res.* **2022**, *2*, 100050. [CrossRef]
56. Rekha, C.; Poornima, G.; Manasa, M.; Abhipsa, V.; Devi, J.P.; Kumar, H.T.V.; Kekuda, T.R.P. Ascorbic acid, total phenol content and antioxidant activity of fresh juices of four ripe and unripe citrus fruits. *Chem. Sci. Trans.* **2012**, *1*, 303–310. [CrossRef]
57. Perez-Perez, J.; Castillo, I.P.; Garcia-Lidon, A.; Botia, P.; Garcia-Sanchez, F. Fino lemon clones compared with the lemon varieties Eureka and Lisbon on two rootstocks in Murcia (Spain). *Sci. Hortic.* **2005**, *106*, 530–538. [CrossRef]
58. Durmus, N.; Kilic-Akyilmaz, M. Bioactivity of non-extractable phenolics from lemon peel obtained by enzyme and ultrasound assisted extractions. *Food Biosci.* **2023**, *53*, 102571. [CrossRef]
59. M'hiri, N.; Ghali, R.; Nasr, I.B.; Boudhrioua, N. Effect of different drying processes on functional properties of industrial lemon byproduct. *Process Saf. Environ. Prot.* **2018**, *116*, 450–460. [CrossRef]
60. Peng, J.; Zheng, T.-t.; Liang, Y.; Duan, L.-f.; Zhang, Y.-d.; Wang, L.-J.; He, G.-m.; Xiao, H.-t. *p*-Coumaric acid protects human lens epithelial cells against oxidative stress-induced apoptosis by MAPK signaling. *Oxid. Med. Cell. Longev.* **2018**, *2018*, 8549052. [CrossRef]
61. Huang, W.-C.; Liou, C.-J.; Shen, S.-C.; Hu, S.; Hsiao, C.-Y.; Wu, S.-J. Luteolin attenuates IL-1β-induced THP-1 adhesion to ARPE-19 cells via suppression of NF-κB and MAPK pathways. *Mediators Inflamm.* **2020**, *2020*, e9421340. [CrossRef]
62. Chowers, G.; Cohen, M.; Marks-Ohana, D.; Stika, S.; Eijzenberg, A.; Banin, E.; Obolensky, A. Course of sodium iodate–induced retinal degeneration in albino and pigmented mice. *Investig. Ophthalmol. Vis. Sci.* **2017**, *58*, 2239–2249. [CrossRef]
63. Wang, J.; Iacovelli, J.; Spencer, C.; Saint-Geniez, M. Direct effect of sodium iodate on neurosensory retina. *Investig. Ophthalmol. Vis. Sci.* **2014**, *55*, 1941–1953. [CrossRef]
64. Zhou, P.; Kannan, R.; Spee, C.; Sreekumar, P.G.; Dou, G.; Hinton, D.R. Protection of retina by αB crystallin in sodium iodate induced retinal degeneration. *PLoS ONE* **2014**, *9*, e98275. [CrossRef]
65. Kim, J.; Lee, Y.J.; Won, J.Y. Molecular mechanisms of retinal pigment epithelium dysfunction in age-related macular degeneration. *Int. J. Mol. Sci.* **2021**, *22*, 12298. [CrossRef]
66. Chang, Y.-Y.; Wang, M.; Yeh, J.-H.; Tsou, S.-C.; Chen, T.-C.; Hsu, M.-Y.; Lee, Y.-J.; Wang, I.; Lin, H.-W.J.F. The protective effects of beta-mangostin against sodium iodate-induced retinal ROS-mediated apoptosis through MEK/ERK and p53 signaling pathways. *Food Funct.* **2023**, *14*, 10896–10909. [CrossRef]
67. Crowley, L.C.; Marfell, B.J.; Scott, A.P.; Waterhouse, N.J. Quantitation of apoptosis and necrosis by annexin V binding, propidium iodide uptake, and flow cytometry. *Cold Spring Harb. Protoc.* **2016**, *2016*, 953–957. [CrossRef]

68. Luo, X.; Gu, S.; Zhang, Y.; Zhang, J. Kinsenoside ameliorates oxidative stress-induced RPE cell apoptosis and inhibits angiogenesis via Erk/p38/NF-κB/VEGF signaling. *Front. Pharmacol.* **2018**, *9*, 240. [CrossRef]
69. Tsai, H.-Y.; Lai, H.I.A.M.; Chen, Z.-Y.; Lin, T.-C.; Khor, W.; Kuo, W.-C.; Syu, J.-P.; Tsai, P.-H.; Yang, Y.-P.; Chien, Y.; et al. Inhibition of DUSP6 activates autophagy and rescues the retinal pigment epithelium in sodium iodate-induced retinal degeneration models in vivo and in vitro. *Biomedicines* **2022**, *10*, 159. [CrossRef]

antioxidants

MDPI

Article

Glutathione and a Pool of Metabolites Partly Related to Oxidative Stress Are Associated with Low and High Myopia in an Altered Bioenergetic Environment

Salvador Mérida [1], Amparo Návea [2], Carmen Desco [1,2,3], Bernardo Celda [4], Mercedes Pardo-Tendero [5,6], José Manuel Morales-Tatay [5,6,*] and Francisco Bosch-Morell [1,*]

[1] Department of Biomedical Sciences, Faculty of Health Sciences, Universidad Cardenal Herrera-CEU, CEU Universities, Alfara del Patriarca, 46115 Valencia, Spain; salvador.merida@uchceu.es (S.M.); carmen.desco@uchceu.es (C.D.)
[2] Instituto de la Retina y Enfermedades Oculares, 46005 Valencia, Spain; doctoranavea@retinavalencia.com
[3] FOM, Fundación de Oftalmología Médica de la Comunidad Valenciana, 46015 Valencia, Spain
[4] Physical Chemistry Department, University of Valencia, 46100 Valencia, Spain; bernardo.celda@uv.es
[5] Department of Pathology, Medicine and Odontology Faculty, University of Valencia, 46010 Valencia, Spain; m.mercedes.pardo@uv.es
[6] INCLIVA Biomedical Research Institute, 46010 Valencia, Spain
* Correspondence: j.manuel.morales@uv.es (J.M.M.-T.); fbosch@uchceu.es (F.B.-M.)

Abstract: Oxidative stress forms part of the molecular basis contributing to the development and manifestation of myopia, a refractive error with associated pathology that is increasingly prevalent worldwide and that subsequently leads to an upsurge in degenerative visual impairment due to conditions that are especially associated with high myopia. The purpose of our study was to examine the interrelation of potential oxidative-stress-related metabolites found in the aqueous humor of high-myopic, low-myopic, and non-myopic patients within a clinical study. We conducted a cross-sectional study, selecting two sets of patients undergoing cataract surgery. The first set, which was used to analyze metabolites through an NMR assay, comprised 116 patients. A total of 59 metabolites were assigned and quantified. The PLS-DA score plot clearly showed a separation with minimal overlap between the HM and control samples. The PLS-DA model allowed us to determine 31 major metabolite differences in the aqueous humor of the study groups. Complementary statistical analysis of the data allowed us to determine six metabolites that presented significant differences among the experimental groups ($p < 005$). A significant number of these metabolites were discovered to have a direct or indirect connection to oxidative stress linked with conditions of myopic eyes. Notably, we identified metabolites associated with bioenergetic pathways and metabolites that have undergone methylation, along with choline and its derivatives. The second set consisted of 73 patients who underwent a glutathione assay. Here, we showed significant variations in both reduced and oxidized glutathione in aqueous humor among all patient groups ($p < 0.01$) for the first time. Axial length, refractive status, and complete ophthalmologic examination were also recorded, and interrelations among metabolic and clinical parameters were evaluated.

Keywords: myopia; oxidative stress; metabolomics; glutathione; 2-aminobutyrate; choline; acetate; lactate; glycine; sn-glycero-3-phosphocholine; 2-hydroxybutyrate

1. Introduction

Myopia, also known as short-sightedness or near-sightedness, affects one-quarter of the world's population, significantly impacting visual function. This condition is becoming increasingly prevalent worldwide, particularly in East Asia [1]. Based on current trends, it is estimated that myopia will affect 49.8% of the population by 2050 [2,3]. In patients with myopia, images are focused in front of the retina due to excessive curvature of the

cornea or lens and elongation of the eye [4]. As such, myopia is one of the most common forms of refractive error. In some types of myopia, excessive axial elongation of the eyeball leads to thinning of the choroid, retinal pigment epithelium, and scleral layer, particularly at the posterior pole [4,5]. Myopia can be caused by both genetic and environmental factors [1,6,7].

High myopia (HM) is usually considered a refractive error with a cutoff in the range of ≥ -5.0 D to -10.0 D (spherical equivalent) concomitant with an excessive elongation of axial length longer than 26.0 mm [8–10]. HM is also frequently called pathologic myopia. This condition can lead to degenerative changes in the posterior segment of the eye. These changes can include posterior staphyloma, retina choroidal atrophy, myopic maculopathy, or retinal detachment, leading to blindness in several cases [11].

In a healthy eye, the ciliary processes secrete aqueous humor (AH) into the posterior chamber; AH is a clear fluid found in both the anterior and posterior chambers of the eye. It then flows into the anterior chamber and drains out through the trabecular meshwork and Schlemm's canal. Neurotransmitters are key mediators for regulating the AH dynamics. AH provides nutrition, removes metabolic waste products, and generally supports the avascular ocular structures [12]. Previously, our research team applied metabolomics for the first time in characterizing human AH [13], finding significant metabolic differences in patients with high and low myopia (CE–MS and LC–MS platform methods). Similarly, a member of our team has been a pioneer in the metabolomic characterization of rat AH using NMR for glaucoma research [14].

Metabolomics, which represent the global profiling of metabolites in biological fluids, cells, and tissues, have the potential to discover new biomarkers for diseases [15]. Hence, through the integration of metabolomics with advanced statistical methodologies, one can discern comprehensive alterations in networks and modified biochemical pathways resulting from a pathological process, even during the initial stages of the disease.

Nuclear magnetic resonance (NMR) spectroscopy is one of the technological options for analyzing metabolic profiles and providing a representation of the phenotype at the molecular level [16]. This technique holds significant advantages over other analytical methods, including reproducibility and simplicity in sample preparation. Conversely, its constraints include low sensitivity and a relatively large volume of the sample (~500 μL). However, the present study illustrates that these limitations can be overcome through the utilization of microprobes (~20 μL).

Oxidative stress forms part of the molecular bases that participate in the growth and appearance of diseases associated with myopia [17]. In previous studies, we found that oxidative stress parameters, total antioxidant capacity, and total nitrite/nitrates are significantly altered in the AH of HM patients [18]. Therefore, in this study, we aimed to build on our previous metabolomic research focusing specifically on the study of oxidative stress in myopia by interrelating potential oxidative-stress-related metabolites found in AH and conducting a clinical study of myopic and non-myopic patients.

2. Materials and Methods

2.1. Experimental Groups and Patient Selection

We conducted a cross-sectional study, selecting two sets of patients undergoing cataract surgery at the FISABIO Medical Ophthalmological Clinic in Valencia, Spain. All participants provided written informed consent to participate in the study, which was conducted according to the principles of the Declaration of Helsinki. The study received ethical approval from the FISABIO Medical Ophthalmological Clinic Ethics Committee (3001/14).

The first set, comprising 116 eyes from different patients, was used to analyze metabolites in the AH of both myopic and control eyes. Similarly, the second set, consisting of 73 eyes from different patients, was used to measure the concentrations of glutathione (GSH) and the oxidized disulfide glutathione form (GSSG) in the AH of both myopic and control patients. The inclusion criteria were patients with cataracts ready to be operated on, refractive myopia, and hypermetropic defects and astigmatism below +0.75 D and

−1.75 D, respectively. The exclusion criteria were concomitant eye disease that could interfere with the results (ongoing maculopathy other than myopic maculopathy, uncontrolled glaucoma with two topical drugs, any stage of uveitis, venous or retinal arterial occlusions, diabetic retinopathy, hypermetropia over +2 D, and astigmatism over −2 D). Patients with uncontrolled high blood pressure despite treatment, diabetes, and a high cholesterol index despite treatment were also excluded. All participants in this study were identified as Caucasian. They presented nuclear and/or cortical cataracts, as well as posterior subcapsular cataracts 2–3, according to the Lens Opacities Classification System III.

Experimental groups were formed based on the axial length of the eyeball. Eyes with an axial length exceeding 26 mm were classified as HM. Those with axial lengths between 23.5 and 25.9 mm and presenting physiological myopia results from failure of correlation between the refractive components of the eye were classified as low myopia (LM). Eyes with axial lengths below 23.4 mm were used as the control group [18–20]. As all the patients had cataracts, refractive status was not used to classify our patients in order to avoid any bias caused by index myopia [21]. Previous works have shown that axial length is not associated with nuclear cataracts in myopic patients [22].

2.2. Clinical Exploration

This study received approval from the FISABIO Ethics and Clinical Research Committee and was conducted in full compliance with the Declaration of Helsinki. All patients provided informed consent and underwent a comprehensive ophthalmological examination, including ETDRS best-corrected visual acuity (BCVA), exploration of the anterior segment with a slit-lamp, binocular ophthalmoscopy and wide-field retinography using Optos® Optomap® P200Tx (Optos PLC, Dunfermline, UK) to study fundus oculi, detection of the presence of staphyloma or lack thereof, and classification of maculopathy according to the IMI's classification [23]. The axial length measurements were taken via interferometry (Zeiss IOLMaster 700®, Carl Zeiss Meditec AG, Jena, Germany), and optical coherence tomography (swept-source optic coherence tomography SSOCT TOPCON, Tokyo, Japan) was used to obtain the subfoveal choroidal thickness measurement. This measurement was manually taken with a measuring instrument (caliper) facilitated by the software (9.30.003.02) that came with the apparatus. Measurements were performed by two different observers (C.D.E. and R.A.M.) and were masked for the axial length of the patient. Sections where foveal depression was well observed were selected; a measurement was made for each patient and observer (two measurements per eye in total) at the point corresponding to the center of the fovea. The concordance rate between them was 95%.

2.3. Aqueous Humor Sample Recollection

AH samples were collected during cataract surgery. All procedures were performed according to standard protocols. All patients received preoperative therapy, which included antibiotic prophylaxis (Oftalmowell, UCB Pharma, an eyedrop solution containing a combination of gramicidin, neomycin, and polymyxin B) and local anesthesia (Colircusí, Alcon Healthcare, an eyedrop solution containing tetracaine and oxybuprocaine). The eyelids and eyelashes were sterilized, and 5% iodine povidone was instilled on the conjunctival sac. A sterile adhesive dressing was then applied to separate the lashes. The eye surface was rinsed with saline solution, and paracentesis was performed at the site of the planned surgical incision using a sterile, single-use 30 G needle. This allowed for the aspiration of a 120 µL AH sample into a 1 cc sterile single-use syringe. Following this, the surgery proceeded using the standard technique. The collected sample was placed inside an Eppendorf tube, frozen in liquid nitrogen, and stored at −80 °C until it was needed.

2.4. NMR Assay

For NMR measurements, 20 µL of AH was mixed with 2.5 µL of sodium-30-trimethylsilylpropionate-2,2,3,3-d4 (TSP; 0.5 mM) dissolved in deuterium oxide (D2O), and that entire mixture was placed in a 1 mm high-quality NMR tube. The NMR spectra

were obtained with a Bruker Avance III DRX 600 (Bruker Biospin GmbH, Rheinstetten, Germany) spectrometer operating at 600.13 MHz equipped with a 1 mm 1H/13C/31P TXI probe. A single pulse with water presaturation was acquired in all samples. The number of transients was 256, and they were collected into 64 k data points with a spectral width of 14 ppm and a recycle delay of 1 s. The nominal temperature of the sample was kept at 310 K. In addition, 2D 1H-1H TOCSY and 2D 1H-13C-HSQC NMR experiments were recorded on some selected samples for the assignment of relevant metabolites. Spectra were manually phase corrected, the baseline was adjusted, and the chemical shift was referenced to the TSP signal using MestReNova 6.2 (Mestrelab Research S.L., Santiago de Compostela, Spain). The metabolite spin systems and resonances were identified and quantified using data obtained from previously reported data [14] and the commercial resonance database Chenomx NMR Suite Profiler (Chenomx NMR Suite 8.1, Chenomx Inc., Edmonton, AB, Canada). The final metabolite levels were calculated in arbitrary units as the area under the peak normalized to the total metabolic concentration.

2.5. Glutathione Assay

The second set consisting of 73 eyes from different patients was used to analyze oxidative-stress-related markers, specifically, reduced glutathione (GSH) and its ratio with oxidized glutathione (GSSG). The use of a second set was justified because the technique used required the immediate acidification of the samples. Consequently, the procedure was based on the initial formation of S-carboxymethyl derivatives of free thiols with iodoacetic acid followed by the conversion of free amino groups to 2,4-dinitrophenyl derivatives through a reaction with 1-fluoro-2,4-dinitrobenzene. Glutathione was measured in AH via HPLC (Gilson International B.V., Middleton, WI, USA) in accordance with a widely referenced method [24]. A 3-Spherisorb NH2 5 μm, 250 mm × 4.6 mm column (Waters Cromatography, Milford, MA, USA) was used at a 1 mL/min flow rate. Values are expressed as nmol/mg of protein.

2.6. Statistical Analysis

Chemometric analyses were performed with PLS ToolBox 8.0 (Eigenvector Inc., Wenatchee, WA, USA) and using in-house scripts developed by the Metabolomic Laboratory for data analysis in MATLAB (The MathWorks Inc., Natick, MA, USA). The NMR spectra were statistically analyzed by using principal component analysis (PCA) to check the homogeneity of the dataset and to identify and exclude possible outliers. Outliers were defined as samples that were situated outside the 95% confidence interval of the Hoteling T-squared distribution. Partial Least Squares Discriminant Analysis (PLS-DA) is a supervised extension of PCA that is used to distinguish two or more classes by searching for variables that maximize the separation between the groups of samples. The datasets used in this analysis were autoscaled prior to multivariate analysis. The determination of statistical significance between the means of different groups was performed using one-way analysis of variance (ANOVA). The spectral regions responsible for the classification of the models were identified using the variable importance in projections (VIP) coefficients obtained during the PLS-DA. The threshold used for VIP selection was ≥ 1. Spectral regions with high VIP coefficients were more important in terms of providing class separation during the analysis, while those with very small VIP coefficients provided only a small contribution to the classification.

Complementary statistical analyses were conducted using the IBM SPSS software (Version 29.0, IBM Corp., Armonk, NY, USA). The Kolmogorov–Smirnov test was used to verify data normality ($p > 0.05$). If the homogeneity of variances was indicated ($p < 0.05$) by Levene's test, an ANOVA was performed with Tukey's test as a post hoc analysis. For variables that did not present homogeneity of variances, the Kruskal–Wallis test was used for non-parametric analysis. Pearson's or Spearman's correlations were employed to examine the association between two variables. Statistical significance was set to $p < 0.05$. Values are expressed as the mean ± standard deviation (SD).

3. Results

3.1. The Clinical Data Recorded Were Very Consistent

In the first set of 116 patients, 40 were controls, 48 had LM, and 28 had HM. Their respective mean ages were 74.7 ± 7.1, 72.8 ± 11.9, and 68.1 ± 13.5 years, with 56% women and 44% men. Key clinical features such as axial length, spherical equivalent, macular thickness, and choroidal thickness are documented in Table 1. The choroidal thickness, as measured via optical coherence tomography, was notably reduced in the HM group (125.5 ± 106.7 µm) compared to the control (237.1 ± 64.5 µm) and LM (196.2 ± 77.3 µm) groups, with a significance of 0.01 (Table 1). Since there were no significant differences between the sexes, the patients were considered as a single group.

Table 1. Relevant clinical characteristics of the studied patients. Groups were distributed as the HM, LM, and control groups for emmetropia according to their axial length. Each value is shown as the mean ± SE.

	N	Axial Length (mm)	Spherical Equivalent	Macular Thickness (µm)	Choroidal Thickness (µm)
C	40	22.6 ± 0.4	−1.1 ± 1.5	259.2 ± 33.0	237.1 ± 64.5
LM	48	24.2 ± 0.7 *	−3.4 ± 3.0 *	249.7 ± 26.3	196.2 ± 77.3
HM	28	28.4 ± 1.9 *#	−9.7 ± 7.6 *#	269.7 ± 42.4	125.5 ± 106.7 *#

* $p \leq 0.01$ vs. the control group, and # $p \leq 0.01$ vs. the low-myopia group.

To analyze the pathologies developed in our study patients, we followed the IMI's classification, which includes five degrees of macular degeneration (Table 2). In 93.7% of the control patients, the eyes appeared normal, with tessellation being observed in 6.3% of the cases. Macular degeneration was more predominant in the HM group, along with diffuse chorioretinal atrophy, lacquer cracks, and macular atrophy, which were observed in 85.2% of the cases (Table 2).

Table 2. Distribution of maculopathies in the eyes of the studied patients following the IMI's classification expressed as the percentage of the entire study population.

Degrees of Maculopathy	C	LM	HM
No myopic degenerative retinal lesion	29.5	32.8	0.8
Tessellated fundus	1.6	5.7	3.3
Diffuse chorioretinal atrophy	0	0	5.7
Patchy chorioretinal atrophy	0.2	0.5	1.3
Macular atrophy	0	0	5.7
PLUS: NEOVASCULARIZATION/FUCHS	0	0	4.1
PLUS: LACQUER CRACKS	0	0	4.9

Ocular biometric parameters were also characterized through post-operative best-corrected visual acuity (BCVA post) and corneal parameters—keratometry, flat keratometry (K1), and steep keratometry (K2)—all of which are shown in Figure 1.

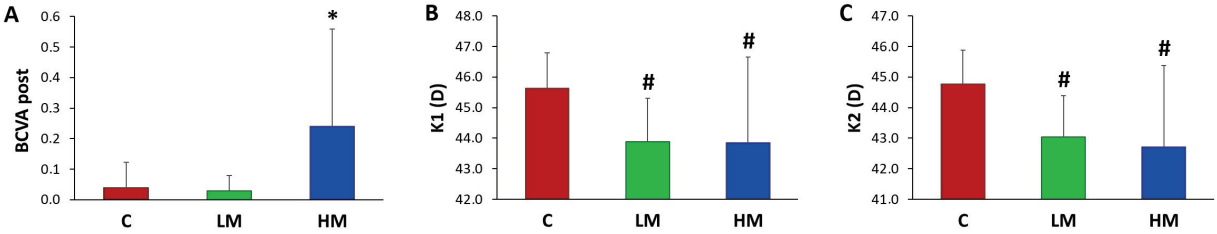

Figure 1. Post-operative best-corrected visual acuity (**A**) and corneal parameters K1 (**B**) and K2 (**C**). Each value is shown as the mean ± SE. * $p \leq 0.01$ vs. the control and LM groups. # $p \leq 0.01$ vs. the control group. D: diopters.

Spearman's rank correlation coefficient of the strength of a linear relationship between paired clinical data (Figure 2, * $p < 0.05$) showed the consistency in axial length, reciprocal length (diopters), and choroidal thickness as relevant parameters in the development of myopia. In this way, many of these correlations between clinical variables reached a significance level of $p < 0.01$, including those between the axial length and reciprocal length ($\rho = 0.745$, $p < 0.01$), reciprocal length and choroidal thickness ($\rho = -0.351$, $p < 0.01$), and axial length and choroidal thickness ($\rho = -0.427$, $p < 0.01$).

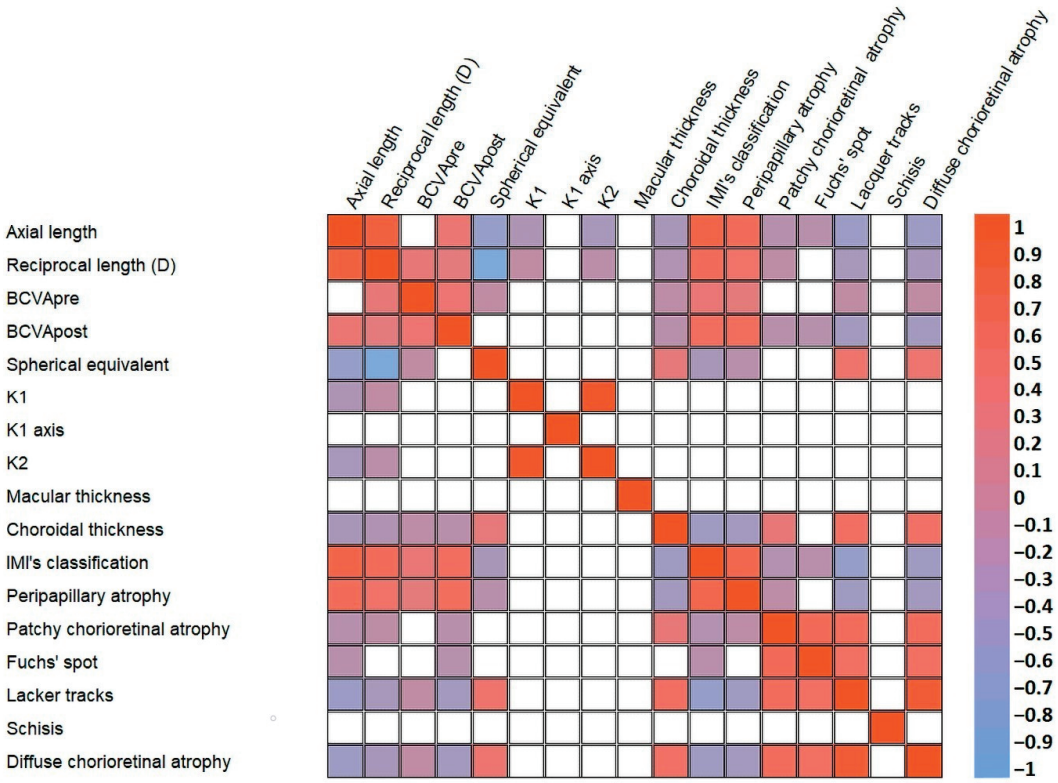

Figure 2. Spearman's rank correlation coefficient of the strength of the linear relationships between pairs of clinical data. Tabular data are presented as heatmaps ($p < 0.05$): blue (negative correlation) and red (positive correlation). D: diopters.

3.2. PLS-DA Confirmed the Significant Differences between the Control and High-Myopia Groups

A total of 59 metabolites were assigned and quantified in 40 AH samples from the control subjects, 48 samples for the low-myopia patients, and 28 samples for the HM patients. The list of chemical shifts that were used for metabolite assignment is presented in Table S1 (see the Supplementary Data). The metabolic profiles of the three groups were compared by means of PCA, which is an unsupervised test for the homogeneity of the set of samples. Based on the PCA, two samples were identified as outliers and excluded from further statistical analyses. Outliers were defined as samples located far outside the 95% confidence interval on the score scatter plot. The exploratory analysis did not show a spontaneous grouping of the samples according to the classification into control and myopia patients, so PLS-DA was used to maximize the separation of the three groups and to reveal specific metabolic changes between the defined ones. Three independent discriminative models were created.

In a first approach, we constructed a model aimed at separating the samples into the three previously defined groups. The outcome is shown in Figure 3A, where we observe an initial division of the samples into three groups. However, the overlap among them is so significant that it lacks discriminatory potential as evidenced by the ROC curves constructed for each of the three groups (cross-validated ROC curve close to the diagonal line), along with the correspondingly low values of the area under the curve obtained

(Figure S2). In the second stage, we constructed a new supervised classification model with the aim of separating the LM samples from the control samples (Figure S1A). Unlike in the previous model, in this case, the overlap zone between the two groups was more substantial, implying that the LM patients exhibited a metabolomic profile more similar to that of the controls. The ROC curve (Figure S1B) confirmed that the model exhibited a very limited classification capacity. Finally, we constructed a new discriminative model designed to maximize the separation between the two most extreme groups—high myopes versus controls (Figure 3B). The PLS-DA score plot clearly showed a separation with minimum overlap between the HM and control samples, confirming the existence of significant differences in the metabolic profiles between the two groups. The area under the ROC curve of the final model (Figure 3C) was 0.74. This model had a Q2 value of 0.77 (a Q2 value superior to 0.5 is generally considered to be a good predictor) and an R2 value of 0.65 (error of calibration). The final cross-validated sensitivity and specificity of the model were 82.5% and 71.4%, respectively. The positive and negative predictive values were 93% and 96%, respectively.

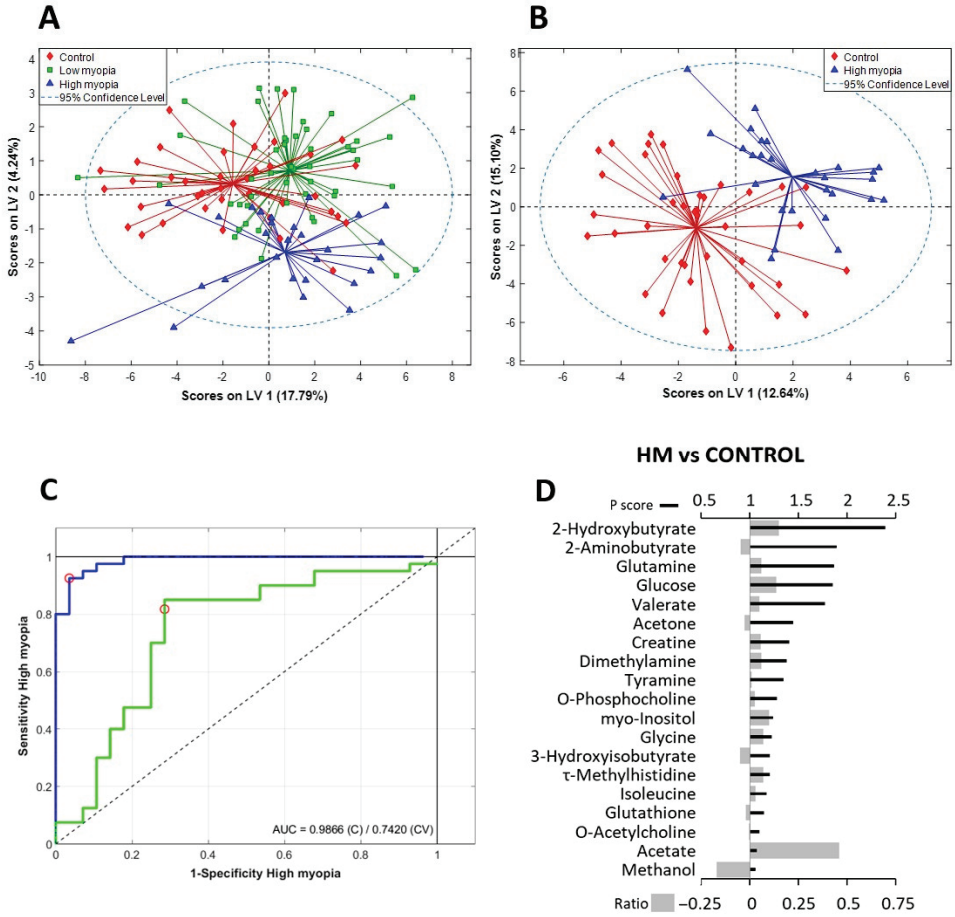

Figure 3. (**A**) Scores plot of the PLS-DA of the metabolome for the discrimination between the control group (red diamonds), LM group (green squares), and HM group (blue triangles). (**B**) Score plot of the PLS-DA for the discrimination between the control group (red diamonds) and HM group (blue triangles). All models were built using the first two latent variables (LVs). (**C**) Receiver-operating curve (ROC) analysis for discrimination between the HM group and control samples showing the prediction capacity of the model. (**D**) VIP score and relative fold change bar plot of the HM/control discriminative model (blue line: estimated ROC curve; green line: cross-validated ROC curve; red circle: model threshold). VIP scores are represented as thick black lines (scale on the top), and the relative fold change was calculated as follows: (Metabolite mean concentration of HM—metabolite mean concentration control)/Metabolite mean concentration of control. These are represented by gray bars (scale on the bottom).

3.3. Main Metabolite Differences in the Aqueous Humor of the Study Groups

The spectral regions and peaks with the highest contribution in the HM vs. CTRL PLS-DA model (VIP scores of > 1) allowed us to determine the major metabolic differences in the AH of the study groups (Figures 3D and S3).

These included metabolites involved in bioenergetic pathways, such as glucose and lactate, as well as ketone bodies, such as 2-Hydroxybutyrate and 3-Hydroxybutyrate. We also found direct oxidative-stress-related metabolites, including 2-aminobutyrate and glutathione. Additionally, choline and its derivatives (o-acetylcholine, o-phosphocholine, and sn-Glycero-3-phosphocholine) and methylated metabolites were found, among other contributing metabolites.

A complementary statistical analysis of the data (IBM SPSS software, version 29.0) allowed us to determine six metabolites that presented significant differences among the experimental groups ($p < 0.05$). These compounds are listed in Table 3.

Table 3. A list of compounds showing significant differences among the experimental groups.

ID	Formula	LM %change	HM %change
2-Aminobutyrate	$C_4H_9NO_2$	−12.54	+18.64 #
Acetate	$C_2H_4O_2$	+40.87 *	+12.72
Choline	$C_5H_{14}NO$	+119.66 *	+9.39 *#
Glycine	$C_2H_5NO_2$	+5.13	−21.45 #
Lactate	$C_3H_6O_3$	+2.22	−8.40 #
sn-Glycero-3-phosphocholine	$C_8H_{21}NO_6P$	−19.19 *	−15.47

The percentage change value was calculated with respect to the control group. * $p < 0.05$ vs. the control group. # $p < 0.05$ vs. the LM group.

Additionally, Spearman's rank correlation coefficient was used to determine the strength of the linear relationships between all paired AH metabolites (Figure S4, Supplementary Data, * $p < 0.05$) and between the clinical data and AH metabolites (Figure S5, Supplementary Data, * $p < 0.05$). Figure 4 highlights the linear relationships ($p < 0.01$) between metabolites that were found to have statistically significant differences, as listed in Table 3, as well as metabolites that contributed to the discrimination between the HM and control groups in our PLS-DA model (Figure 3D, VIP scores > 1.0).

3.4. All Derivate Glutathione Biomarkers Showed Significant Differences among All Patient Groups

The 73 patients in the second set were distributed as follows: 33 were the controls, 20 were in the LM group, and 20 were in the HM group. The clinical characteristics of the studied patients in this set showed similar values to those of the first set of patients. The GSH level in the LM group (Figure 5A) was significantly lower than that in the control group ($p \leq 0.01$). Similarly, we observed a significant decrease in the reduced glutathione (GSH) concentration in the HM group versus the control and LM groups. Concomitantly, the level of oxidized glutathione was significantly higher in the study groups than in the control group (Figure 5B, $p < 0.01$). Therefore, a significant increase in the GSSG concentration in the HM group versus both the control and LM groups was also observed. Figure 5C shows the GSH/GSSG ratio to highlight these results.

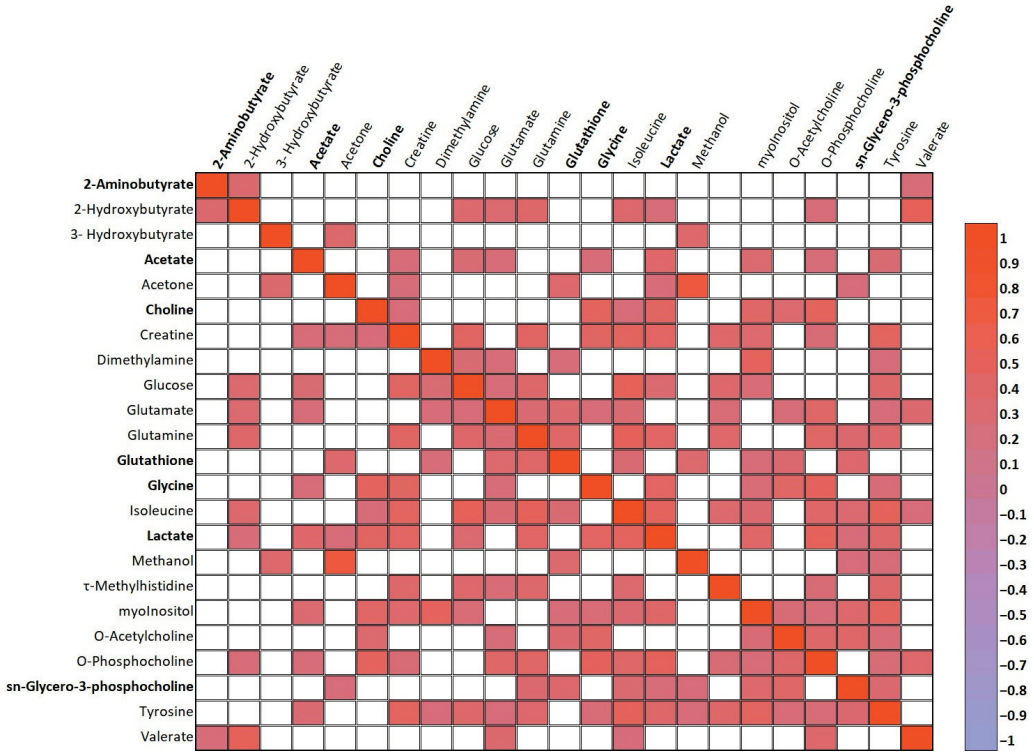

Figure 4. Spearman's rank correlation coefficient of the strength of the linear relationships between the metabolites present in AH and found to be statistically significant according to the differences among experimental groups and the metabolites that contributed to the discrimination between the HM and control groups in our PLS-DA model. Tabular data are presented as a heatmap ($p < 0.01$): blue (negative correlation) and red (positive correlation). All the metabolites that showed significant differences among groups are highlighted in bold.

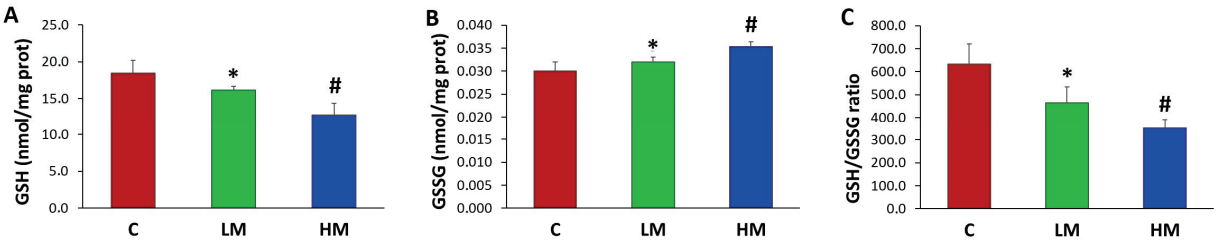

Figure 5. (**A**) Reduced glutathione (GSH), (**B**) oxidized glutathione (GSSG), and (**C**) the GSH/GSSG ratio. Each value is shown as the mean ± SE. * $p \leq 0.01$ vs. the control group. # $p \leq 0.01$ vs. the control and LM groups.

4. Discussion

4.1. NMR Metabolomic and Chemometric Approaches

Metabolites are the endpoints of many biological and physiological processes, and metabolomics may, thereby, provide snapshots of different physiological states. The use of 1H NMR spectroscopy allowed us to identify and quantify sets of metabolites in human AH using a simple sample preparation method. The use of a 1 mm microprobe provided us with the additional advantage of being able to use the smallest amount of sample to run all high-resolution NMR experiments with outstanding sensitivity, without sacrificing the quality of the spectroscopic signal. Additionally, the metabolite profile could be acquired relatively rapidly (10 min with a short routine), with a sufficient ability to evaluate subtle differences even in the early stages of the disease. By employing the combination of NMR metabolomic and chemometric approaches, we were able to establish a metabolic snapshot of the different physiological states associated with myopic and control subjects.

We analyzed the mean differences, multivariate PCA and PLS-DA models, VIP scores, and relative fold changes between metabolically healthy individuals and those with high and low myopia to gain a better understanding of possible altered metabolic pathways. Furthermore, NMR metabolomics is an effective approach for identifying potential disease biomarkers in human AH.

4.2. Direct Oxidative-Stress-Related Metabolites

Recently, in the serum of myopic children and adolescents, Du et al. (2020) found selected pathways where metabolic features showed regulations with oxidative stress, including lysine degradation, arginine and proline metabolism, arachidonic acid metabolism, linoleic acid metabolism, and sphingolipid metabolism [25]. In our study, L-2-aminobutyric acid, a conjugate acid of an L-2-aminobutyrate metabolite, showed significantly higher levels in the HM group. 2-aminobutyric acid is a non-protein amino acid with relevant physiological skills linked to oxidative stress in different systems [26,27], including the human corneal endothelium [28]. This metabolite is a key intermediate in the biosynthesis of ophthalmic acid (γ-glutamyl-L-2-aminobutyryl-glycine), and it is significantly elevated in oxidative stress conditions [27,29]. Since ophthalmic acid, which was originally isolated from a calf eye lens, is a tripeptide analog of glutathione, it has been proposed that 2-aminobutyric acid regulates glutathione homeostasis [25]. Moreover, in a recent rat model study of neuroprotection in glaucoma [30] against mitochondrial and metabolic dysfunction, some low-weight metabolites, such as 2-aminobutyric acid, creatine, and glycerophosphocholine, seemed to be relevant in the retina. Our results seem to confirm that similar methods are active in high-myopia patients.

Both metabolites (2-aminobutyric acid and glutathione) were relevant in our PLS-DA model. Similarly, concomitant with the increased levels of 2-aminobutyric acid, we found a depletion of GSH levels in the patients of the second set. In fact, ophthalmic acid is formed by the same enzymes as glutathione, with the incorporation of 2-aminobutyric acid instead of Z-cysteine in the first biosynthetic step in such a way that the dismissal of GSH by the oxidative stress environment induced increased 2-aminobutyric acid levels and ophthalmate synthesis [26]. Interestingly, 2-aminobutyric acid was one of the two metabolites that presented the most significant correlations with the clinical parameters of pathological myopia, such as macular thickness, peripapillary atrophy, lacquer tracks, and diffuse chorioretinal atrophy (Figure S5, $p < 0.05$).

Oxidative stress participates in the growth and appearance of diseases associated with myopia [17,18]. In this study, we implemented a new set of patients (second set) to measure reduced glutathione (gamma-glutamyl-cysteinyl-glycine, GSH) and glutathione disulfide (GSSG) levels in samples of AH from myopic patients for first time. In animal cells, GSH is the most abundant low-molecular-weight antioxidant thiol and co-substrate for detoxification enzymes such as glutathione peroxidase. The redox state of the GSH/GSSG couple serves as a leading indicator of a redox environment. Both GSH and GSSG are exported from cells through multidrug resistance protein; extracellular GSH is metabolized by membrane-bound γ-glutamyl transpeptidase into cysteinylglycine and γ-glutamyl products, and dipeptidase hydrolyzes cysteinylglycine to cysteine and glycine [31]. We observed markedly diminished GSH levels in the LM and HM groups in the second set of patients. Simultaneously, the levels of oxidized glutathione (GSSG) were also increased in the LM and HM groups. In the same way, the GSH/GSSG ratio showed marked differences among the groups. All of these results reaffirm the role of oxidative stress in the evolution of myopia as a disease and are in concordance with some of the altered metabolites related to oxidative stress found in the first set, such as 2-aminobutyrate, glycine, and lactate. Interestingly, recent works have postulated the redox communication network as a regulator of metabolism [32].

4.3. Scleral Remodeling and Metabolites Involved in Bioenergetic Pathways

There are different pathways connecting the retina to scleral remodeling [33]. It is known that chemical signals from photoreceptors may be transferred to the choroid via the retinal pigment epithelium and, finally, modify the scleral remodeling [33]. On the one hand, the retinal pigment epithelium presents receptors for key signaling molecules, such as cholinergic, glycine, and dopamine receptors. On the other hand, scleral fibroblasts express growth factors, including insulin [34] and glucagon [35], which also participate in scleral remodeling. We found altered levels of several metabolites related to these pathways (Table 3 and Figure 3D), including neurotransmitters responsible for mediating interactions in retinal cells, such as glycine and choline/acetylcholine derivates, as well as glucagon and insulin receptors expressed in scleral fibroblasts.

Glycine plays significant roles in human metabolism and nutrition. Therefore, glycine is present in macromolecules such as collagen, provides flexibility of active sites on enzymes, and plays crucial roles as a neurotransmitter. In our study, the glycine levels significantly decreased in patients with HM. There are several ways in which glycine might participate in the pathology of the myopic eye, presenting a certain protective effect. Firstly, glycine modulates the production of superoxides and the synthesis of cytokines by modifying the intracellular Ca^{2+} levels [36]. Glycine is also released by AII amacrine cells to inhibit OFF-cone bipolar cell neurotransmission [37]. Interestingly, AII amacrine cells show increased phosphorylation of Cx36, which could indicate increased functional gap junction coupling in the myopic retina [38]. Glycine is likewise one of the three amino acids that constitute ophthalmic acid, the tripeptide analog of GSH [26]. Moreover, recent studies showed that genetic variations in glycine receptor alpha 2 expression may be considered HM-causing genes by harming photoperception and visual transmission [39].

Glucose and lactate play known crucial roles in our body's metabolic processes. We found a positive correlation of glucose with the axial length of the studied patients (Figure S5, $\rho = 0.226$, $p < 0.05$) and a lightly negative correlation for lactate. Glucose levels contributed to the discrimination between groups in our PLS-DA model (Figure 3D, VIP scores > 1.0, HM vs. control group; Figure S3, VIP scores > 1.0, LM vs. control). Li et al. [40] recently evaluated multiple glycemic traits related to the risk of myopia, finding that low adiponectin levels and high hemoglobin A1c were linked to an increased risk of myopia. In our study, we also found that methanol levels contributed to the discrimination between groups in our PLS-DA model (Figure 3D, VIP scores > 1.0, HM vs. control group; Figure S3, VIP scores > 1.0, LM vs. control). Zhu [41] proposed that an increase in cellular glucose levels would lead to increased metabolic formation of endogenous methanol, which may be further metabolically converted into formic acid or formate, a cytotoxic metabolite that we also found in the AH of patients (Table S1). In this way, the methanol/formic acid biotransformation might cause cytotoxicity by directly inhibiting the cytochrome oxidase complex of the mitochondrial respiratory chain, thereby reducing the cellular ATP production, increasing ROS production, and reducing NAD to NADH.

Lactate is a three-carbon molecule generated through glycolytic metabolism that acts as a relevant carbohydrate fuel and is especially relevant in a fasted state [42]. In our study, the LM group showed a little and non-significant increase in lactate levels. However, we found that the HM group displayed significantly diminished levels of lactate. Arising evidence connects the pyruvate dehydrogenase kinase–lactic acid axis and the pathophysiology of neurological disorders [43]. Traditionally, hypoxia linked to ischemic injury directly leads to lactate accumulation. Therefore, Lin et al. [44] recently proposed that, in an animal model, scleral glycolysis contributed to myopia by promoting fibroblast-to-myofibroblast transdifferentiation via lactate-induced histone lactylation. Our results agree in the LM group but not in the HM group. This paradoxical result may be related to the fact that lactate is also admitted as a signaling molecule involved in cell survival, as a potential energy substrate, and as a redox buffer molecule that equilibrates the NADH/NAD ratio [45]. Recent evidence suggested that lactate treatment lessened brain damage and improved behavior in neonatal rat models of hypoxic ischemia [46], indicating that lactate may

play a neuroprotective role in ischemic conditions. Thus, elevated levels of lactate may be related to the development of myopia, and diminishing levels of lactate might be linked to advanced damage in the highly myopic eye in different ways. On the one hand, lactate diminishes oxidative-stress-induced cell death and promotes oxidative stress resistance via the UPR and p38MAPK pathways [45], and on the other hand, lactate triggers an immunomodulatory response via G-protein-coupled receptor 81 and reduces the production of pro-inflammatory cytokines [47]. Likewise, lactate interferes in classical microglial polarization, decreasing neuroinflammatory parameters [48].

Ketone bodies, 2-hydroxybutyrate, and 3-hydroxybutyrate metabolites highly contributed to the PLS-DA model for discriminating among groups, reaching VIP scores above 2.0 (Figures 3D and S3). These two metabolites are derived from fatty acid oxidation and serve as a fuel source for peripheral tissues, including the brain and eye [49,50]. In the retina, 3-hydroxybutyrate, acetoacetate, and acetone serve as energy sources during nutritional deprivation [50]. In addition, 2-hydroxybutyrate works as an energy substrate for maintaining metabolic homeostasis and organ integrity in response to ischemia and reperfusion by suppressing lipolysis, mitochondrial dysfunction, and oxidative stress [51,52].

Creatine phosphate was the other metabolite that presented the most significant correlations with the clinical parameters of pathological myopia, correlating significantly with choroidal thickness, peripapillary atrophy, lacquer tracks, and diffuse chorioretinal atrophy (Figure S5, $p < 0.05$). Creatine phosphate is a phosphorylated form of creatine that serves as a rapidly mobilizable reserve of high-energy phosphates. Both creatine and phosphocreatine are required to preserve ATP, which is needed for normal retinal function and development [53]. In our study, creatine was one of the relevant metabolites in our PLS-DA model. It has been proposed that phosphocreatine may reduce the ADP-induced stimulation of mitochondrial metabolism, and it would be related to the inability of the neuroprotective role of creatine to protect retinal neurons in vivo [54]. In any case, these correlations reaffirm the great relevance of oxidative stress in pathological myopia.

In a previous metabolomic study using serum samples from myopic patients, Ke et al. (2021) discovered intermediates in energy metabolism, such as citric acid and oxaloacetic acid [55]. It has been proposed that a surge in energy metabolism could lead to a rise in extracellular adenosine levels [56]. This, in turn, stimulates the activation of adenosine receptors, which contribute to the control of eye growth [57]. Interestingly, adenosine has been suggested to exert a consistent inhibitory impact on the release of acetylcholine in the retina by interacting with adenosine 1 receptors, as in other cholinergic synapses [58].

4.4. Choline and Choline Derivates

Choline and choline derivates, such as o-acetylcholine, o-phosphocholine, and sn-glycero-3-phosphocholine, showed relevant variations in their levels in the AH of the study groups (Figure 3D, VIP scores > 1, PLS-DA model; Figure S3, VIP scores > 1, PLS-DA model). We found elevated levels of choline in the AH samples from both low- and high-myopic eyes. Choline has been suggested to have key roles in neurotransmission, the structural integrity of membranes, and methyl group metabolism, and it is a precursor for the synthesis of acetylcholine, a relevant neurotransmitter not only in muscle contraction signaling but also in the brain and retina [59,60]. In fact, acetylcholine plays an important role in the developing retina and regulates the growth of the eye [61]. We also found higher levels of acetate in myopic samples (Figure 3D, VIP scores > 1, PLS-DA model; Figure S3, VIP scores > 1, PLS-DA model)—specifically, high acetate levels were significant in the LM group. As is known, acetylcholinesterase immediately hydrolyzes acetylcholine into acetate and choline, terminating neuronal transmission and signaling between synapses. Interestingly, choline and acetate levels also showed a significant and positive correlation (Figure S4, $\rho = 0.183$, $p < 0.05$).

We did not find significant differences in acetylcholine levels between groups. However, acetylcholine played a role in distinguishing between the HM and control groups in our PLS-DA model. It showed significant correlations with several pertinent clini-

cal variables, such as axial length (Figure S5, $\rho = -0.194$, $p < 0.05$), diopters (Figure S5, $\rho = -0.276$, $p < 0.01$), and the spherical equivalent (Figure S5, $\rho = 0.214$, $p < 0.05$). At the same time, it demonstrated a significant and positive correlation with choline, phosphocholine, and sn-glycero-3-phosphocholine. In the eye, the five subtypes of muscarinic acetylcholine receptors are broadly distributed and exert many functions, such as neurotransmission, modulation of the intraocular pressure, tear secretion, regulation of vascular diameter in the retina, and contraction of the pupillary constrictor muscle, together with the ciliary muscle, which regulates accommodation [59]. The M1 receptor could be essential for the survival of retinal ganglion cells and helps to increase nitric oxide production from neuronal nitric oxide synthase [62]. The M2 receptor is relevant in the development of myopia by delaying scleral fibroblast cell proliferation and additionally reducing scleral remodeling [63], and the M3 receptors intervene in the cholinergic response in the retinal arterioles and the ophthalmic artery [64]. Conversely, nicotinic acetylcholine receptors (nAChR) have been shown to be present in both the retina and choroid [65]. Endogenous activation of nAChR contributes to the increased incidence of choroidal neovascularization. Moreover, nicotinic acetylcholine receptors (α3, α4, α6, α7, β2, and β4 subunits) in amacrine and ganglion cells have been observed in the retinas of Rhesus monkeys and rabbits [59]. These retinal nicotinic acetylcholine receptors are involved in the processing of visual information and could also influence the progression of retina pathologies, as well as the formation of new blood vessels in the eye [59].

Another choline derivative, sn-glycero-3-phosphocholine, showed diminished levels in myopic samples, and this decrease was significant in the LM group. sn-Glycero-3-phosphocholine plays a role as an osmoprotectant by stabilizing intracellular macromolecules and by protecting inner medullary cells [66]. Interestingly, in recent research, Wu et al. (2023) discovered that the degree of myopia was significantly influenced by the corneal levels of various metabolites, including derivatives of sn-glycero-3-phosphocholine [67]. We did not find further similarities to this previous study in our work. Traditionally, a thinner choroid has been related to the presence of osmotically active molecules [68]. The blood-ocular barriers, including the blood-aqueous barrier and the blood-retinal barrier, are essential for normal visual function and maintaining the eye as a privileged site. While these barriers can be affected by various conditions that affect the eye or have a marked effect on the blood composition [69], the specific alteration of these barriers in axial myopia is not well-established. Therefore, sn-glycero-3-phosphocholine is a precursor of choline mediated by glycerophosphodiester phosphodiesterases, which seems to be in concordance with the high levels of choline found. In fact, the lipid composition of the retina is mostly represented by glycerophospholipids—remarkably, sn-glycero-3-phosphocholine and glycerophosphoethanolamine [70]. Thus, diminished levels of sn-glycero-3-phosphocholine may indicate membrane cell damage, osmodysregulation, and alterations in the biosynthesis of choline in the retina.

4.5. Methylated Metabolites

Methylated metabolites, such as τ-methylhistidine, π-methylhistidine, dimethylamine, 1,7-dimethylxanthine, trimethylamine, and N-nitrosodimethylamine (Figures 3D and S3, VIP scores > 1, PLS-DA model), contributed to the discrimination between groups in our PLS-DA model. In a previous work [13], our research team found various metabolites related to methylation processes. This finding has been confirmed by other researchers in retinal eye diseases related to oxidative stress, such as glaucoma, dry eye syndrome, and diabetic retinopathy [71].

The formation of these methyl metabolites relies on methyltransferases, which transfer methyl groups from S-adenosylmethionine (SAM). Wang et al. [72] proposed that the consumption of methyl groups to generate these methylated metabolites might limit the availability of SAM for DNA methylation in the aging eye. DNA methylation is generally thought to be a gene-repressing modification. Moreover, many of these enzymes responsible for preserving the methylated status of DNA are redox-sensitive [71]. Therefore,

the regulation of oxidative stress increased DNA methyltransferase 1 binding in retinal endothelial cells [72]. In a recent study focused on DNA methylation in age-related macular degeneration, Advani et al. [73] revealed significant epigenetic regulation of the immune response and metabolism, including the glutathione pathway and glycolysis.

All of these findings suggest that both DNA methylation and oxidative stress play significant roles in myopia. However, the exact mechanisms and their interplay are complex and require further research.

4.6. Study Limitations

The age of the patients was high, since the samples were taken from patients undergoing cataract processes. Nevertheless, the groups had similar average ages, and there were no significant differences between them. In fact, the group with HM had the lowest non-significant average age.

The hypothesis that there is a trend of increasing axial myopia with age-related cataracts is still under discussion. Pan et al. (2013) demonstrated that myopia—but not axial length—may be associated with nuclear cataracts [22]. Regardless, the clinical data recorded in our study are very consistent, reaching a significance level of $p < 0.01$ between the main clinical parameters according to the Spearman correlation.

5. Conclusions

In the first set of patients, we identified and quantified a total of 59 metabolites. The PLS-DA score plot clearly demonstrated a separation with minimal overlap between HM and control samples. This model enabled us to identify 31 major metabolite differences in the AH of the study groups. Many of these metabolites have been found to be directly or indirectly related to the oxidative stress associated with myopic eye conditions. Interestingly, we found metabolites involved in bioenergetic pathways, methylated metabolites, and choline and choline derivatives. A complementary statistical analysis of the data allowed us to identify six metabolites that showed significant differences among the experimental groups. Additionally, in a second set of patients, we were able to demonstrate significant variations in both reduced and oxidized glutathione in the AH across all patient groups for the first time.

Supplementary Materials: The following supporting information can be downloaded at: https://www.mdpi.com/article/10.3390/antiox13050539/s1, Table S1: List of the chemical shifts used to make metabolite assignments in AH—1H NMR spectra; Figure S1: (A) Score plot of the PLS-DA of the metabolome for the discrimination between the control group (red diamonds) and LM group (green squares). (B) Receiver-operating curve (ROC) analysis for discrimination between the control group and HM samples based on our PLS-DA model; Figure S2: Receiver-operating curve (ROC) analysis for the classification of each individual group: (A) control group, (B) LM group, and (C) HM group based on our PLS-DA model. Figure S3: VIP score and relative fold change bar plot of the model for discriminating between the LM and control groups. Figure S4: Spearman's rank correlation coefficient of the strength of linear relationships between AH metabolites (* $p < 0.05$). Figure S5: Spearman's rank correlation coefficient of the strength of linear relationships between paired clinical data and AH metabolites (* $p < 0.05$).

Author Contributions: Conceptualization, F.B.-M., S.M. and A.N.; methodology, S.M., C.D., J.M.M.-T. and M.P.-T.; formal analysis, S.M. and J.M.M.-T.; investigation, F.B.-M., S.M., C.D. and A.N., resources, F.B.-M. and B.C.; data curation, F.B.-M. and B.C.; writing—original draft preparation, S.M. and J.M.M.-T.; writing—review and editing, S.M. and F.B.-M.; funding acquisition, F.B.-M. and S.M. All authors have read and agreed to the published version of the manuscript.

Funding: This work was supported by funds from Generalitat Valenciana (GV/2020/138) and from Fundación San Pablo (CEU FUSP-PPC-22-063 and GIR23/07).

Institutional Review Board Statement: This study was conducted in accordance with the Declaration of Helsinki and was approved by the Institutional Review Board of FISABIO Medical Ophthalmological Clinic in Valencia (Spain) (protocol code: 3001/14).

Informed Consent Statement: Informed consent was obtained from all subjects involved in the study.

Data Availability Statement: The data presented in this study are available in this article.

Conflicts of Interest: The authors declare no conflicts of interest.

References

1. Baird, P.N.; Saw, S.M.; Lanca, C.; Guggenheim, J.A.; Smith, E.L., III; Zhou, X.; Matsui, K.H.; Wu, P.C.; Sankaridurg, P.; Chia, A.; et al. Myopia. *Nat. Rev. Dis. Primers* **2020**, *6*, 99. [CrossRef]
2. Holden, B.A.; Fricke, T.R.; Wilson, D.A.; Jong, M.; Naidoo, K.S.; Sankaridurg, P.; Wong, T.Y.; Naduvilath, T.J.; Resnikoff, S. Global prevalence of myopia and high myopia and temporal trends from 2000 through 2050. *Ophthalmology* **2016**, *123*, 1036–1042. [CrossRef]
3. Han, X.; Liu, C.; Chen, Y.; He, M. Myopia prediction: A systematic review. *Eye* **2022**, *36*, 921–929. [CrossRef] [PubMed]
4. Yu, Q.; Zhou, J.B. Scleral remodeling in myopia development. *Int. J. Ophthalmol.* **2022**, *15*, 510–514. [CrossRef] [PubMed]
5. Ostrin, L.A.; Harb, E.; Nickla, D.L.; Read, S.A.; Alonso-Caneiro, D.; Schroedl, F.; Kaser-Eichberger, A.; Zhou, X.; Wildsoet, C.F. IMI-The Dynamic Choroid: New Insights, Challenges, and Potential Significance for Human Myopia. *Investig. Ophthalmol. Vis. Sci.* **2023**, *64*, 6. [CrossRef]
6. Cai, X.B.; Shen, S.R.; Chen, D.F.; Zhang, Q.; Jin, Z.B. An overview of myopia genetics. *Exp. Eye Res.* **2019**, *188*, 107778. [CrossRef]
7. Jiang, Y.; Xiao, X.; Sun, W.; Wang, Y.; Li, S.; Jia, X.; Wang, P.; Hejtmancik, J.F.; Zhang, Q. Clinical and genetic risk factors underlying severe consequence identified in 75 families with unilateral high myopia. *J. Transl. Med.* **2024**, *22*, 75. [CrossRef] [PubMed]
8. Morgan, I.G.; Ohno-Matsui, K.; Saw, S.M. Myopia. *Lancet* **2012**, *379*, 1739–1748. [CrossRef]
9. Haarman, A.E.; Enthoven, C.A.; Tideman, J.W.L.; Tedja, M.S.; Verhoeven, V.J.; Klaver, C.C. The complications of myopia: A review and meta-analysis. *Investig. Ophthalmol. Vis. Sci.* **2020**, *61*, 49. [CrossRef] [PubMed]
10. Kim, H.K.; Kim, S.S. Factors associated with axial length elongation in high myopia in adults. *Int. J. Opthalmol.* **2021**, *14*, 1231–1236. [CrossRef]
11. Ohno-Matsui, K.; Wu, P.C.; Yamashiro, K.; Vutipongsatorn, K.; Fang, Y.; Cheung, C.M.G.; Lai, T.Y.Y.; Ikuno, Y.; Cohen, S.Y.; Gaudric, A.; et al. IMI pathologic myopia. *Investig. Ophthalmol. Vis. Sci.* **2021**, *62*, 5. [CrossRef] [PubMed]
12. Freddo, T.F. A contemporary concept of the blood-aqueous barrier. *Prog. Retin. Eye Res.* **2013**, *32*, 181–195. [CrossRef] [PubMed]
13. Barbas-Bernardos, C.; Armitage, E.G.; García, A.; Mérida, S.; Navea, A.; Bosch-Morell, F.; Barbas, C. Looking into aqueous humor through metabolomics spectacles− exploring its metabolic characteristics in relation to myopia. *J. Pharm. Biomed. Anal.* **2016**, *127*, 18–25. [CrossRef]
14. Mayordomo-Febrer, A.; López-Murcia, M.; Morales-Tatay, J.M.; Monleón-Salvado, D.; Pinazo-Durán, M.D. Metabolomics of the aqueous humor in the rat glaucoma model induced by a series of intracamerular sodium hyaluronate injection. *Exp. Eye Res.* **2015**, *131*, 84–92. [CrossRef] [PubMed]
15. Johnson, C.H.; Ivanisevic, J.; Siuzdak, G. Metabolomics: Beyond Biomarkers and towards Mechanisms. *Nat. Rev. Mol. Cell Biol.* **2016**, *17*, 451–459. [CrossRef]
16. Sengupta, A.; Narad, P. Metabolomics. In *Metabolomics, Omics Approaches, Technologies and Applications: Integrative Approaches for Understanding OMICS Data*; Arivaradarajan, P., Misra, G., Eds.; Springer: Singapore, 2018; pp. 75–97. ISBN 978-981-13-2924-1.
17. Francisco, B.M.; Salvador, M.; Amparo, N. Oxidative stress in myopia. *Oxid. Med. Cell. Longev.* **2015**, *2015*, 750637. [CrossRef]
18. Mérida, S.; Villar, V.M.; Navea, A.; Desco, C.; Sancho-Tello, M.; Peris, C.; Bosch-Morell, F. Imbalance between oxidative stress and growth factors in human high myopia. *Front. Physiol.* **2020**, *11*, 463. [CrossRef]
19. Flores-Moreno, I.; Lugo, F.; Duker, J.S.; Ruiz-Moreno, J.M. The relationship between axial length and choroidal thickness in eyes with high myopia. *Am. J. Ophthalmol.* **2013**, *155*, 314–319.e1. [CrossRef]
20. Hosoda, Y.; Yoshikawa, M.; Miyake, M.; Tabara, Y.; Shimada, N.; Zhao, W.; Oishi, A.; Nakanishi, H.; Masayuki, H.; Akagi, T.; et al. CCDC102B confers risk of low vision and blindness in high myopia. *Nat. Commun.* **2018**, *9*, 1782. [CrossRef]
21. Ajenjo, M.A.D.; Domene, M.C.G.; Martínez, C.P. Refractive changes in nuclear, cortical and posterior subcapsular cataracts. Effect of the type and grade. *J. Optom.* **2015**, *8*, 86–92. [CrossRef]
22. Pan, C.W.; Boey, P.Y.; Cheng, C.Y.; Saw, S.M.; Tay, W.T.; Wang, J.J.; Tan, A.G.; Mitchell, P.; Wong, T.Y. Myopia, axial length, and age-related cataract: The Singapore Malay eye study. *Investig. Ophthalmol. Vis. Sci.* **2013**, *54*, 4498–4502. [CrossRef] [PubMed]
23. Flitcroft, D.I.; He, M.; Jonas, J.B.; Jong, M.; Naidoo, K.; Ohno-Matsui, K.; Rahi, J.; Resnikoff, S.; Vitale, S.; Yannuzzi, L. IMI—Defining and Classifying Myopia: A Proposed Set of Standards for Clinical and Epidemiologic Studies. *Investig. Ophthalmol. Vis. Sci.* **2019**, *60*, M20–M30. [CrossRef] [PubMed]
24. Reed, D.J.; Babson, J.R.; Beatty, P.W.; Brodie, A.E.; Ellis, W.W.; Potter, D.W. High-performance liquid chromatography analysis of nanomole levels of glutathione, glutathione disulfide, and related thiols and disulfides. *Anal. Biochem.* **1980**, *106*, 55–62. [CrossRef] [PubMed]
25. Du, B.; Jin, N.; Zhu, X.; Lu, D.; Jin, C.; Li, Z.; Han, C.; Zhang, Y.; Lai, D.; Liu, K.; et al. A prospective study of serum metabolomic and lipidomic changes in myopic children and adolescents. *Exp. Eye Res.* **2020**, *199*, 108182. [CrossRef] [PubMed]

26. Soga, T.; Baran, R.; Suematsu, M.; Ueno, Y.; Ikeda, S.; Sakurakawa, T.; Kakazu, Y.; Ishikawa, T.; Robert, M.; Nishioka, T.; et al. Differential metabolomics reveals ophthalmic acid as an oxidative stress biomarker indicating hepatic glutathione consumption. *J. Biol. Chem.* **2006**, *281*, 16768–16776. [CrossRef] [PubMed]
27. Irino, Y.; Toh, R.; Nagao, M.; Mori, T.; Honjo, T.; Shinohara, M.; Tsuda, S.; Nakajima, S.; Satomi-Kobayashi, S.; Shinke, T.; et al. 2-Aminobutyric acid modulates glutathione homeostasis in the myocardium. *Sci. Rep.* **2016**, *6*, 36749. [CrossRef] [PubMed]
28. Ueno, M.; Yoshii, K.; Yamashita, T.; Sonomura, K.; Asada, K.; Ito, E.; Fujita, T.; Sotozono, C.; Kinoshita, S.; Hamuro, J. The interplay between metabolites and microRNAs in aqueous humor to coordinate corneal endothelium integrity. *Ophthalmol. Sci.* **2023**, *3*, 100299. [CrossRef] [PubMed]
29. Servillo, L.; Castaldo, D.; Giovane, A.; Casale, R.; D'Onofrio, N.; Cautela, D.; Balestrieri, M.L. Ophthalmic acid is a marker of oxidative stress in plants as in animals. *Biochim. Biophys. Acta Gen. Subj.* **2018**, *1862*, 991–998. [CrossRef] [PubMed]
30. Tribble, J.R.; Otmani, A.; Sun, S.; Ellis, S.A.; Cimaglia, G.; Vohra, R.; Jöe, M.; Lardner, E.; Venkataraman, A.P.; Domínguez-Vicent, A.; et al. Nicotinamide provides neuroprotection in glaucoma by protecting against mitochondrial and metabolic dysfunction. *Redox. Biol.* **2021**, *43*, 101988. [CrossRef]
31. Tuell, D.; Ford, G.; Los, E.; Stone, W. The Role of Glutathione and Its Precursors in Type 2 Diabetes. *Antioxidants* **2024**, *13*, 184. [CrossRef]
32. Corkey, B.E.; Deeney, J.T. The redox communication network as a regulator of metabolism. *Front. Physiol.* **2020**, *11*, 567796. [CrossRef] [PubMed]
33. Wang, W.Y.; Chen, C.; Chang, J.; Chien, L.; Shih, Y.F.; Lin, L.L.; Pang, C.P.; Wang, I.J. Pharmacotherapeutic candidates for myopia: A review. *Biomed. Pharmacother.* **2021**, *133*, 111092. [CrossRef] [PubMed]
34. Penha, A.M.; Schaeffel, F.; Feldkaemper, M. Insulin, insulin-like growth factor–1, insulin receptor, and insulin-like growth factor–1 receptor expression in the chick eye and their regulation with imposed myopic or hyperopic defocus. *Mol. Vis.* **2011**, *17*, 1436–1448. [PubMed]
35. Vessey, K.A.; Rushforth, D.A.; Stell, W.K. Glucagon-and secretin-related peptides differentially alter ocular growth and the development of form-deprivation myopia in chicks. *Investig. Ophthalmol. Vis. Sci.* **2005**, *46*, 3932–3942. [CrossRef] [PubMed]
36. Razak, M.A.; Begum, P.S.; Viswanath, B.; Rajagopal, S. Multifarious beneficial effect of nonessential amino acid, glycine: A review. *Oxid. Med. Cell. Longev.* **2017**, *2017*, 1716701. [CrossRef] [PubMed]
37. Ivanova, E.; Müller, U.; Wässle, H. Characterization of the glycinergic input to bipolar cells of the mouse retina. *Eur. J. Neurosci.* **2006**, *23*, 350–364. [CrossRef] [PubMed]
38. Banerjee, S.; Wang, Q.; Zhao, F.; Tang, G.; So, C.; Tse, D.; To, C.H.; Feng, Y.; Zhou, X.; Pan, F. Increased Connexin36 phosphorylation in AII amacrine cell coupling of the mouse myopic retina. *Front. Cell. Neurosci.* **2020**, *14*, 124. [CrossRef] [PubMed]
39. Tian, Q.; Tong, P.; Chen, G.; Deng, M.; Cai, T.; Tian, R.; Zhang, Z.; Zhang, Z.; Xia, K.; Hu, Z. GLRA2 gene mutations cause high myopia in humans and mice. *J. Med. Genet.* **2023**, *60*, 193–203. [CrossRef] [PubMed]
40. Li, F.F.; Zhu, M.C.; Shao, Y.L.; Lu, F.; Yi, Q.Y.; Huang, X.F. Causal relationships between glycemic traits and myopia. *Investig. Ophthalmol. Vis. Sci.* **2023**, *64*, 7. [CrossRef]
41. Zhu, B.T. Biochemical mechanism underlying the pathogenesis of diabetic retinopathy and other diabetic complications in humans: The methanol-formaldehyde-formic acid hypothesis. *Acta Biochim. Biophys. Sin.* **2022**, *54*, 415–451. [CrossRef]
42. Rabinowitz, J.D.; Enerbäck, S. Lactate: The ugly duckling of energy metabolism. *Nat. Metab.* **2020**, *2*, 566–571. [CrossRef] [PubMed]
43. Jha, M.K.; Lee, I.K.; Suk, K. Metabolic reprogramming by the pyruvate dehydrogenase kinase–lactic acid axis: Linking metabolism and diverse neuropathophysiologies. *Neurosci. Biobehav. Rev.* **2016**, *68*, 1–19. [CrossRef] [PubMed]
44. Lin, X.; Lei, Y.; Pan, M.; Hu, C.; Xie, B.; Wu, W.; Su, J.; Li, Y.; Tan, Y.; Wei, X.; et al. Augmentation of scleral glycolysis promotes myopia through histone lactylation. *Cell Metab.* **2024**, *36*, 511–525. [CrossRef] [PubMed]
45. Tauffenberger, A.; Fiumelli, H.; Almustafa, S.; Magistretti, P.J. Lactate and pyruvate promote oxidative stress resistance through hormetic ROS signaling. *Cell Death Dis.* **2019**, *10*, 653. [CrossRef] [PubMed]
46. Tassinari, I.D.; Andrade, M.K.G.; da Rosa, L.A.; Hoff, M.L.M.; Nunes, R.R.; Vogt, E.L.; Fabres, R.B.; Sanches, E.F.; Netto, C.A.; Paz, A.H.; et al. Lactate administration reduces brain injury and ameliorates behavioral outcomes following neonatal hypoxia-ischemia. *Neuroscience* **2020**, *448*, 191–205. [CrossRef] [PubMed]
47. Hu, J.; Cai, M.; Liu, Y.; Liu, B.; Xue, X.; Ji, R.; Bian, X.; Lou, S. The roles of GRP81 as a metabolic sensor and inflammatory mediator. *J. Cell. Physiol.* **2020**, *235*, 8938–8950. [CrossRef] [PubMed]
48. Kong, L.; Wang, Z.; Liang, X.; Wang, Y.; Gao, L.; Ma, C. Monocarboxylate transporter 1 promotes classical microglial activation and pro-inflammatory effect via 6-phosphofructo-2-kinase/fructose-2, 6-biphosphatase 3. *J. Neuroinflamm.* **2019**, *16*, 1–12. [CrossRef] [PubMed]
49. Jensen, N.J.; Wodschow, H.Z.; Nilsson, M.; Rungby, J. Effects of ketone bodies on brain metabolism and function in neurodegenerative diseases. *Int. J. Mol. Sci.* **2020**, *21*, 8767. [CrossRef] [PubMed]
50. Izuta, Y.; Imada, T.; Hisamura, R.; Oonishi, E.; Nakamura, S.; Inagaki, E.; Ito, M.; Soga, T.; Tsubota, K. Ketone body 3-hydroxybutyrate mimics calorie restriction via the Nrf2 activator, fumarate, in the retina. *Aging Cell* **2018**, *17*, e12699. [CrossRef]
51. Nelson, A.B.; Queathem, E.D.; Puchalska, P.; Crawford, P.A. Metabolic Messengers: Ketone bodies. *Nat. Metab.* **2023**, *5*, 2062–2074. [CrossRef]

52. Rojas-Morales, P.; Pedraza-Chaverri, J.; Tapia, E. Ketone bodies, stress response, and redox homeostasis. *Redox Biol.* **2020**, *29*, 101395. [CrossRef]
53. Acosta, M.L.; Kalloniatis, M.; Christie, D.L. Creatine transporter localization in developing and adult retina: Importance of creatine to retinal function. *Am. J. Physiol. Cell Physiol.* **2005**, *289*, C1015–C1023. [CrossRef] [PubMed]
54. Sia, P.I.; Wood, J.P.; Chidlow, G.; Casson, R. Creatine is neuroprotective to retinal neurons in vitro but not in vivo. *Investig. Ophthalmol. Vis. Sci.* **2019**, *60*, 4360–4377. [CrossRef]
55. Ke, C.; Xu, H.; Chen, Q.; Zhong, H.; Pan, C.W. Serum metabolic signatures of high myopia among older Chinese adults. *Eye* **2021**, *35*, 817–824. [CrossRef]
56. Cui, D.; Trier, K.; Ribel-Madsen, S.M. Effect of day length on eye growth, myopia progression, and change of corneal power in myopic children. *Ophthalmology* **2013**, *120*, 1074–1079. [CrossRef]
57. Cui, D.; Trier, K.; Zeng, J.; Wu, K.; Yu, M.; Ge, J. Adenosine receptor protein changes in guinea pigs with form deprivation myopia. *Acta Ophthalmol.* **2010**, *88*, 759–765. [CrossRef]
58. Santiago, A.R.; Madeira, M.H.; Boia, R.; Aires, I.D.; Rodrigues-Neves, A.C.; Santos, P.F.; Ambrosio, A.F. Keep an eye on adenosine: Its role in retinal inflammation. *Pharmacol. Ther.* **2020**, *210*, 107513. [CrossRef] [PubMed]
59. Ruan, Y.; Patzak, A.; Pfeiffer, N.; Gericke, A. Muscarinic acetylcholine receptors in the retina—Therapeutic implications. *Int. J. Mol. Sci.* **2021**, *22*, 4989. [CrossRef] [PubMed]
60. Yang, J.; Ouyang, X.; Fu, H.; Hou, X.; Liu, Y.; Xie, Y.; Yu, H.; Wang, G. Advances in biomedical study of the myopia-related signaling pathways and mechanisms. *Biomed. Pharmacother.* **2022**, *145*, 112472. [CrossRef]
61. Ford, K.J.; Feller, M.B. Assembly and disassembly of a retinal cholinergic network. *Vis. Neurosci.* **2012**, *29*, 61–71. [CrossRef]
62. Laspas, P.; Zhutdieva, M.B.; Brochhausen, C.; Musayeva, A.; Zadeh, J.K.; Pfeiffer, N.; Xia, N.; Li, H.; Wess, J.; Gericke, A. The M1 muscarinic acetylcholine receptor subtype is important for retinal neuron survival in aging mice. *Sci. Rep.* **2019**, *9*, 5222. [CrossRef]
63. Barathi, V.A.; Kwan, J.L.; Tan, Q.S.; Weon, S.R.; Seet, L.F.; Goh, L.K.; Vithana, E.N.; Beuerman, R.W. Muscarinic cholinergic receptor (M2) plays a crucial role in the development of myopia in mice. *Dis Model Mech* **2013**, *6*, 1146–1158. [CrossRef]
64. Gericke, A.; Steege, A.; Manicam, C.; Böhmer, T.; Wess, J.; Pfeiffer, N. Role of the M3 muscarinic acetylcholine receptor subtype in murine ophthalmic arteries after endothelial removal. *Investig. Ophthalmol. Vis. Sci.* **2014**, *55*, 625–631. [CrossRef]
65. Kiuchi, K.; Matsuoka, M.; Wu, J.C.; Silva, R.L.; Kengatharan, M.; Verghese, M.; Ueno, S.; Yokoi, K.; Khu, N.H.; Cooke, J.P.; et al. Mecamylamine suppresses basal and nicotine-stimulated choroidal neovascularization. *Investig. Ophthalmol. Vis. Sci.* **2008**, *49*, 1705–1711. [CrossRef] [PubMed]
66. Gallazzini, M.; Ferraris, J.D.; Burg, M.B. GDPD5 is a glycerophosphocholine phosphodiesterase that osmotically regulates the osmoprotective organic osmolyte GPC. *Proc. Natl. Acad. Sci. USA* **2008**, *105*, 11026–11031. [CrossRef]
67. Wu, W.; Song, Y.; Sun, M.; Li, Y.; Xu, Y.; Xu, M.; Yang, Y.; Li, S.; Zhang, F. Corneal metabolic biomarkers for moderate and high myopia in human. *Exp. Eye Res.* **2023**, *237*, 109689. [CrossRef]
68. Liu, Y.; Wang, L.; Xu, Y.; Pang, Z.; Mu, G. The influence of the choroid on the onset and development of myopia: From perspectives of choroidal thickness and blood flow. *Acta Ophthalmol.* **2021**, *99*, 730–738. [CrossRef] [PubMed]
69. Cunha-Vaz, J.G. The blood-ocular barriers: Past, present, and future. *Doc. Ophthalmol.* **1997**, *93*, 149–157. [CrossRef]
70. Marshall, D.L.; Criscuolo, A.; Young, R.S.; Poad, B.L.; Zeller, M.; Reid, G.E.; Mitchell, T.W.; Blanksby, S.J. Mapping unsaturation in human plasma lipids by data-independent ozone-induced dissociation. *J. Am. Soc. Mass Spectrom.* **2019**, *30*, 1621–1630. [CrossRef]
71. Wu, J.; Liu, L.L.; Cao, M.; Hu, A.; Hu, D.; Luo, Y.; Wang, H.; Zhong, J.N. DNA Methylation plays important roles in retinal development and diseases. *Exp. Eye Res.* **2021**, *211*, 108733. [CrossRef] [PubMed]
72. Wang, Y.; Grenell, A.; Zhong, F.; Yam, M.; Hauer, A.; Gregor, E.; Zhu, S.; Lohner, D.; Zhu, J.; Du, J. Metabolic signature of the aging eye in mice. *Neurobiol. Aging* **2018**, *71*, 223–233. [CrossRef] [PubMed]
73. Advani, J.; Mehta, P.A.; Hamel, A.R.; Mehrotra, S.; Kiel, C.; Strunz, T.; Corso-Díaz, X.; Kwicklis, M.; van Asten, F.; Ratnapriya, R.; et al. QTL mapping of human retina DNA methylation identifies 87 gene-epigenome interactions in age-related macular degeneration. *Nat. Commun.* **2024**, *15*, 1972. [CrossRef] [PubMed]

antioxidants

MDPI

Review

Antioxidants and Mechanistic Insights for Managing Dry Age-Related Macular Degeneration

Deepak Basyal, Sooyeun Lee and Hye Jin Kim *

College of Pharmacy, Keimyung University, Dauge 42601, Republic of Korea
* Correspondence: hjk0901@kmu.ac.kr

Abstract: Age-related macular degeneration (AMD) severely affects central vision due to progressive macular degeneration and its staggering prevalence is rising globally, especially in the elderly population above 55 years. Increased oxidative stress with aging is considered an important contributor to AMD pathogenesis despite multifaceted risk factors including genetic predisposition and environmental agents. Wet AMD can be managed with routine intra-vitreal injection of angiogenesis inhibitors, but no satisfactory medicine has been approved for the successful management of the dry form. The toxic carbonyls due to photo-oxidative degradation of accumulated bisretinoids within lysosomes initiate a series of events including protein adduct formation, impaired autophagy flux, complement activation, and chronic inflammation, which is implicated in dry AMD. Therapy based on antioxidants has been extensively studied for its promising effect in reducing the impact of oxidative stress. This paper reviews the dry AMD pathogenesis, delineates the effectiveness of dietary and nutrition supplements in clinical studies, and explores pre-clinical studies of antioxidant molecules, extracts, and formulations with their mechanistic insights.

Keywords: AMD; oxidative stress; antioxidants; dietary supplements; extract; formulation

1. Introduction

Oxidative stress occurs due to redox modulation of the oxidant–antioxidant balance in cells and tissues shifting towards a more oxidative environment [1]. It is the precursor to degenerative diseases including age-related macular degeneration (AMD) in the eye [2]. Distortion in the retinal homeostasis, including increased oxidative stress levels and neuroinflammation, can progress to degeneration and blindness [3,4]. Vision impairment can compromise an individual's independence and quality of life, significantly impacting overall well-being [5]. The pathophysiology of AMD is complicated due to the retina's incredible structural and cellular complexity [6]. Still, this disease is implicated in progressive atrophy of the retinal pigment epithelium (RPE) and macular degeneration due to the accumulation of oxidative stress with increasing age [7]. Moreover, the link between oxidative-stress-led inflammation impacts the multifaceted etiology of AMD [8].

A plethora of studies show dietary antioxidants can attenuate oxidative stress and chronic inflammation [9,10]. A considerable amount of the literature suggests long-term high-antioxidant nutrients display preventive and restorative roles in eye diseases related to oxidative damage and aging [11,12]. There is renewed interest in formulating new dietary supplements or functional foods with antioxidant and cytoprotective ingredients to repress injuries due to oxidative stress. Protection against oxidative injury is a critical avenue for the early management of dry AMD and halting its progression to the devastating neovascular stage. Currently, there is no effective remedy to rectify the oxidative stress-induced pathogenesis in dry AMD and the search for a remedy continues. Meanwhile, most of the available measures are based on delaying vision loss and partly limiting further progression in AMD patients. Moreover, many clinical and preclinical studies report cmixed results regarding antioxidants for alleviating degenerative disease [13–15].

Therefore, understanding the interplay between antioxidants and retinal degeneration is crucial to building novel and tailored therapeutic strategies. In this review, the systematic search approach was employed to identify all the articles assessing the therapeutic benefits of antioxidants in the context of dry AMD. The following eligibility criteria were set for the inclusion of the articles in the study: (i) preclinical and clinical studies, (ii) dry AMD as a disease model, and (iii) articles published in English. Conference abstracts, proceedings, and in silico studies were excluded. This review aims to delineate the underlying mechanisms of the cytoprotective activities of antioxidant dietary supplements, herbal extracts, herbal formulations, endogenous substances, and natural and synthetic compounds for addressing dry AMD and its progression.

2. Age-Related Macular Degeneration (AMD)

2.1. AMD Affects Central Photopic Vision Due to Progressive Macular Degeneration

AMD is a global health burden affecting 8.7% of people worldwide, especially the elderly population above 50 years, and is estimated to increase to 288 million (95% Crl, 205–399) in 2040 from 196 million (95% Crl, 140–261) in 2020 [16]. The macula is the central part of the retina, amidst the major retinal vascular arcades [17]. Lutein and zeaxanthin contents (0.1–1 mM) are 5-fold greater in the macula compared to in the peripheral retina [18]. The fovea centralis (1.5–2 mm diameter) with a high concentration of cone cells is responsible for high-resolution central vision and lies in the middle of the macula [19]. The darker appearance of the fovea is due to taller RPE cells and dense xanthophyll pigment deposition [20]. Moreover, the fovea is encircled by the parafovea belt and the perifovea outer region [21]. Reduced contrast sensitivity, metamorphopsia, and blurry vision are the preliminary symptoms of AMD, which subsequently progresses to the damage of the photoreceptor, the RPE, Bruch's membrane (BrM), and the choroid vascular network [22]. It has been shown that AMD primarily affects the RPE and photoreceptor cells and its progression is elicited by oxidative stress [23].

2.2. Classification of AMD

There are two clinical phenotypes of AMD, dry (atrophic or non-exudative) and wet (neovascular or exudative) AMD. Dry AMD, with progressive atrophy of the RPE and overlying photoreceptors, accounts for 80–90% of all AMD cases. Abnormal pathological fenestration of choroidal capillaries causing choroidal neovascularization (CNV) into the sub-RPE and subretinal space is seen in exudative AMD, resulting in the detachment of the retina/RPE, lipid exudates, subretinal hemorrhage, inflammation, and fibrotic scar formation in the retina. Although less common than non-exudative AMD, wet AMD is more vicious and can cause sudden and irreversible vision loss [24]. With aging, the thickening and loss of elasticity of BrM occurs resulting in hypoxia, increasing vascular endothelial growth factor (VEGF) secretion, and the neovascularization of the choriocapillaris due to the disintegration of the blood–retinal barrier causing blood and serum leakage into the neural retina [25]. Almost 90% of the vision loss in AMD occurs due to anomalistic choroidal circulation [26]. Intravitreally injected VEGF inhibitors and laser photocoagulation therapy have provided effective therapeutic management for wet AMD [27], but no potential restorative treatment is available for dry AMD, particularly early and intermediate AMD, despite the recent advent of several treatment options [28]. Understanding and halting the mechanism of AMD progression can help clinicians intervene early to prevent the devastating consequences, preserve vision, and improve quality of life. Recently, Pegcetacoplan intravitreal injection (complement C3-cleavage inhibitor) was approved by the FDA in 2023 for a reduction in the further progression of advanced-stage non-exudative AMD, which is the only treatment available to date. Monthly intravitreal injections of 15 mg Pegcetacoplan for 12 months significantly reduced the growth of lesions in geographic atrophy, with no improvement in visual function [29,30].

2.3. Drusen Are the Hallmark for AMD

The word drusen is derived from "druse" meaning a mass of small crystals. Drusen can be seen as tiny yellowish dots detected ophthalmoscopically and are insoluble aggregates of oxidized proteins and lipids [31]. They accumulate amidst the RPE basal labyrinth and BrM. The primary factor responsible for this aggregation is still elusive [32]. Heterogeneous debris of several components including lipofuscin (LF), advanced glycation end products, apolipoprotein E, cholesterol, peroxidized lipids, carboxyethyl pyrrole adducts, vitronectin, amyloid P component, C-reactive protein, and complement factors (C3, C5, C9) have been reported in drusen and AMD lesions. About 40% of the composition consists of lipid components, so drusen are also known as an "oil leak on the BrM" [33–37]. Many of the molecules in drusen arise from inflammatory cascades; hence, inflammation is implicated in the progression of AMD [38]. Based on size, drusen can be categorized into small (less than 64 μm), intermediate (between 64 and 124 μm), and large (more than 124 μm). Moreover, drusen can also be categorized into two main phenotypes as hard and soft drusen, based on their composition, morphology, and the level of risk conferred [33]. Hard drusen are small, round, or oval-shaped yellowish-white dots with distinct margins, whereas soft drusen are an irregular large-sized confluence of drusen with poorly demarcated boundaries. They exhibit pale-yellow to grayish-white, dome-shaped elevations resembling localized serous RPE detachment [39]. Soft drusen, found exclusively in the macula, display homogenous content (more than 75% of the cross-sectional area contains a single material) and a lack of internal structures, alongside abundant basal laminar deposits (BlamDs). In contrast, hard drusen exhibit a more complex substructure and less homogeneity (43.3%) in the macula compared to those found in the periphery (80.5%) [40]. Soft drusen maculopathy is associated with higher risk and generally precedes the advanced stage of AMD [41]. It has been reported that Ccl2 knockout in aging mice exhibits a drusen-like phenotype similar to that of AMD due to enhanced subretinal microglia/macrophage trafficking in the subretinal space [42]. Furthermore, senescent $Ccl2^{-/-}/Cx3cr^{-/-}$ mice develop broad-spectrum AMD lesions including drusen formation and retinal degeneration [43]. Besides drusen, reticular pseudodrusen (PEDs) or vitelliform lesions are also seen amidst the retina and RPE, which can lead to the formation of geographic atrophy (GA). PEDs exhibit different composition compared to that of typical drusen and the underlying etiology is still a matter of debate [44]. The term "geographic" in GA refers to patchy, map-like areas of lesions that are seen in the macula. It resembles continents on a map with demarcated borders and irregular shapes, similar to the outlines of geographic regions. The concept of "geographic areas of atrophy" was introduced in ophthalmology to describe "senile macular degeneration" before the term AMD was coined in the medical literature [45]. GA is the advanced stage of dry or non-exudative AMD, resulting in the most damaging endpoint of the drusen cycle causing progressive degeneration of photoreceptors, RPE cells, and the choriocapillaris in the macula [46].

2.4. Etiology of AMD

The main etiology of AMD development is still elusive, but oxidative stress leading to RPE and accompanying cell dysfunction is considered to be involved in the pathogenesis [47]. Several studies suggest a complex coaction of genetic factors, environmental factors, and advanced aging (>50 years). Smoking is linked with an increased risk (OR 1.8–3) of AMD [48]. Blue light irradiation to the macula is another risk factor for AMD pathogenesis [49]. Dietary intake enriched with vitamins, minerals, docosahexaenoic acid, omega-3 fatty acids, and carotenoids can decrease the risk of AMD progression [50]. Hypertension, dyslipidemia, high mass index, obesity, and diabetes are associated with increased risk/progression to AMD [51]. Moreover, Caucasians, females, and individuals with a family history of AMD are at greater risk [52]. The pathogenesis of AMD also involves crosstalk between oxidative stress and genetic polymorphism [53]. The clear genetic marker for AMD is elusive, but 103 genetic loci have been identified as susceptible to AMD development. Polymorphism in genes regulating complement activation and lipid

metabolism show an increased risk of developing AMD. CFH and ARMS2/HTRA1 genes, which regulate complement pathways, are the two most notable risk loci for AMD. The CFH gene polymorphism (Y402H) is associated with up to 43% of all AMD cases [54], which results in reduced transport of oxidized phospholipids out of the RPE membrane leading to the over-activation of the alternative complement system triggering RPE cell apoptosis [55]. Similarly, single nucleotide polymorphisms in the ARMS2/HTRA1 gene on the chromosome 10q26 region are responsible for BrM extracellular matrix turnover, RPE senescence, drusen deposits, chronic inflammation, and wet AMD progression [53]. Additionally, polymorphism in lipid metabolism and related transport-related genes, for instance, lipase c (LIPC), cholesteryl ester transfer protein (CETP), ATP-binding cassette subfamily A member 1 (ABCA1), and apolipoprotein E (APOE), also impart higher risk for AMD pathogenesis due to the accumulation of lipids and thickening of BrM [56].

2.5. Disruption of Retinal Integrity in AMD

The macula in primates is adapted for high visual acuity. It is continuously exposed to high-intensity light and hyperbaric oxygen (70–90 mm Hg) [57]. The dynamic photoreceptor outer segment (POS) is amassed with polyunsaturated fatty acids (PUFAs) and phospholipids, for providing the high malleability necessary for the regulation of signaling within the disc membrane [58]. The large area of PUFA-enriched membranes makes the POS extremely sensitive to elevated ROS and lipid peroxidation [59]. The lower concentration of PUFAs in the macula compared to in the peripheral retina might be due to increased lipid peroxidation in the macular area [60]. Docosahexaenoic acid (DHA) (22:6 omega 3) is the most abundant (30–40%) and oxidizable PUFA in the POS. The singlet oxygen abstracts hydrogen atoms from DHA to generate lipid hydroperoxides [61]. The decomposition of lipid hydroperoxides produces lipid peroxyl radicals, which further degrade into a plethora of peroxidation products including electrophilic reactive aldehydes like malondialdehyde (MDA) and 4-hydroxy-2-nonenal (4-HNE) in the retina due to chain reactions [62,63]. 4-HNE forms adducts with cysteine, histidine, and lysine residues of enzymes and protein, whereas MDA forms a stable covalent bond with the nitrogen atom of guanine residues of DNA (MDA–guanine adduct) resulting in DNA modification [64].

Recently, biomarker analysis of donor eyes derived from AMD patients showed elevated degraded DNA, protein, and lipid biomarkers due to oxidative stress [65]. Additionally, a protein adduct by carboxyethyl pyrrole (CEP), a result of the oxidative cleavage of DHA, is also abundantly present in the outer retina of AMD patients [66]. A previous study also reports elevated levels of 4-HNE and CEP-modified protein adducts in AMD donor eyes. Moreover, the protein adducts are resistant to proteolysis resulting in autophagy dysfunction [67]. Our innate immune system recognizes the various protein adducts as damage-associated molecular patterns (DAMPs) causing the activation of pattern recognition receptors and increased expression of pro-inflammatory cytokines and chemokines. Considering this, MDA, 4-HNE, and CEP have been used to induce AMD phenotype in in vitro and animal models [68–70].

2.6. Retinal Pigment Epithelium: The Primary Site of AMD Pathology

RPE cells consist of a monolayer of cuboidal, melanin-pigmented, and polarized cells [71]. Being post-mitotic, these cells maintain photoreceptor integrity and retinal homeostasis without undergoing cell growth and division for the overall lifespan of an individual. Due to a non-dividing system or dormancy, there are structural and functional changes in the RPE cells with aging, including the loss of melanin granules, the progressive accumulation of aging pigment, a weakened antioxidant system, and the gradual development of drusen deposits within BrM. RPE cells originate embryologically from the neuroectoderm [72], more specifically the optic cup outer layer in the forebrain, and has a sandwiched arrangement, with the apical microvilli surface being intimately connected with the distal tip of the light-sensitive POS of the neuroretina while its highly convoluted basolateral side is adherent to BrM and the choriocapillaris [73]. Similar to the retina, the

RPE cells are also extremely prone to oxidative stress owing to their metabolic activity along with continuous exposure to intense irradiation, hyperbaric oxygen, and intracellular iron [74].

The human blood–retinal barrier consists of the monolayer of the RPE, BrM, and the choriocapillaris. The 2–4 μm pentalaminar matrix of BrM, with alternating layers of collagen and elastin, separates the RPE with the choriocapillaris and forms an outer blood–retinal barrier (BRB), which governs the permeation of ions and other substances between the choroid and retina. The choriocapillaris removes the metabolic byproducts produced in the outer retina and sustain homeostasis in the BRB [75]. The RPE has a crucial role in the nursing of retinal cells and imparts important functions including the revival of 11-*cis*-retinal in the retinoid cycle, epithelial transport of nutrients and waste, potassium ion spatial buffering, heat exchange, maintenance of the choriocapillaris, immune modulation, and phagocytosis (heterophagy) of the POS. Moreover, the polarized secretion of neurotrophic or antiangiogenic pigment-epithelium-derived factor (PEDF) and angiogenic VEGF by the RPE is critical for regulating neuroprotection and angiogenesis in the retina. Daily phagocytosis of spent outer segments is critical for optimizing visual function. Each RPE cell phagocytoses around 300 million POS discs during its lifetime and is regulated by circadian rhythms [76]. The recognition and binding of the shed photoreceptors are regulated by two key receptor–ligand phagocytic machineries: the integrin receptor $\alpha v\beta 5$ with its ligand MFG-E8 and the receptor tyrosine kinase MerTK with its ligand protein S and Gas6. The lack of MerTK or its ligands triggers swift and total retinal degeneration in both RCS rats and mutant mice, whereas age-related accumulations of POS remnants and oxidized proteins are seen in integrin receptor $\alpha v\beta 5$ deficiency. Moreover, the cytoplasmic proteins annexin A2, myosin VIIa, and protein melanoregulin (MREG) also play a crucial role in phagocytosis owing to the delayed phagosome trafficking in the mutant mice lacking these proteins [77]. In addition to VEGF, the RPE cells also produce other angiogenic markers, including MCP-10, IL 6, and IL 8, to regulate vascular alterations in the choroidal endothelium [78]. They also release matrix metalloproteases (MMP2 and MMP9) and their inhibitors (TIMP1 and TIMP3) to control BrM permeability to water and other substances. Elevated oxidative-stress-impaired autophagy and aging lead to the increased accumulation of drusen within the sub-RPE space, impeding the normal physiological function of the RPE. The innate immune system pathways including complement system activation, the migration of microglia cells, and inflammasome assembly in the RPE cells also act to restore homeostasis [79]. However, the interminable oxidative stress and hyperactive inflammatory response cause the consistent remodeling and destruction of retinal tissue, leading to irreversible retinal pathologies. Taken together, the functioning and survival of photoreceptors rely solely on RPE cells, so any distortion in their functioning leads to photoreceptor degeneration and AMD pathogenesis.

3. Mechanistic Insights of Pathogenesis in AMD

3.1. Oxidative Stress Induced by Free Radicals Is the Principal Factor for Pathogenesis in AMD

Free radicals consist of chemically reactive, highly unstable, and excited atoms, molecules, or ions containing unpaired valence electrons and unstable bounds [80]. Based on the elements they are derived from, free radicals can be reactive oxygen species (ROS), reactive nitrogen species (RNS), or reactive sulfur species (RSS) (Figure 1) [81]. ROS can be further distinguished into radicals or non-radicals. The superoxide anion ($O_2^{\bullet -}$), singlet oxygen ($^1O_2$), hydrogen peroxide (H_2O_2), hydroxyl radical ($HO^{\bullet}$), nitric oxide ($NO^{\bullet}$), and peroxy radical ($ROO^{\bullet}$) are extensively studied intracellular ROS [82]. Intriguingly, ROS also act as a crucial inter- and intracellular signaling molecule in signal transduction cascades regulating gene expression, apoptosis, and ion transportation. However, augmented ROS levels have detrimental effects on the cellular system. Factors including the half-life, concentration, and diffusibility of the generated ROS can differentiate its beneficial and negative effects [83].

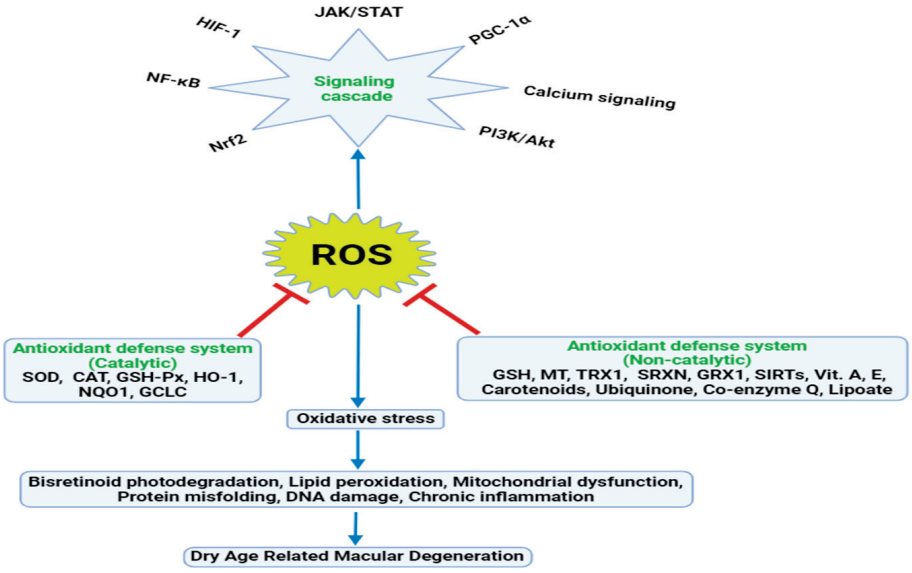

Figure 1. Schematic representation of the implication of oxidative stress and the endogenous antioxidant defense system combating oxidative stress. Antioxidant defense network is classified into enzymatic and non-enzymatic systems with a diverse array of antioxidant defense mechanisms [84]. Dysregulation of the balance of prooxidant and antioxidant defense systems has various implications ranging from lipid peroxidation to declined mitochondrial function and ultimately apoptosis of cells [85]. Oxidative stress has the potential to trigger various cascading events, including bisretinoid photodegradation, lipid peroxidation, mitochondrial dysfunction, development of ER stress, DNA damage, and chronic inflammation, which ultimately converge to initiate macular degeneration [86,87]. Moreover, free radicals can instigate several signaling pathways culminating in a variety of specific biological responses. For instance, NFE2L2 signaling plays a vital role in the expression of antioxidant and detoxification enzymes [88]. PI3K/Akt signaling regulates cell survival, proliferation, and migration [89]. NF-κB signaling regulates the expression of genes for immune response and inflammation [90]. PGC-1α signaling regulates energy metabolism and mitochondrial biogenesis [91]. HIF-1 signaling regulates cellular adaptation during hypoxia [92]. JAK/STAT regulates cell growth and differentiation [93]. Calcium signaling regulates cell cycle, cell communication, immune response, and apoptosis [94]. NFE2L2, nuclear factor erythroid 2-related factor 2; PI3K/Akt, phosphatidylinositol 3 kinase; NF-κB, nuclear factor-kappa B; PGC-1α, peroxisome proliferator-activated receptor γ coactivator 1α; HIF-1, hypoxia-inducible factor 1; JAK/STAT, janus kinase/signal transducer and activator of transcription; SOD, superoxide dismutase; CAT, catalase; GSH-Px, glutathione peroxidase; HO-1, heme oxygenase-1; NQO1, NAD(P)H quinone dehydrogenase 1; GCLC, glutamate-cysteine ligase; GSH, glutathione; MT, metallothionein; TRX1, thioredoxin; SRXN1, sulfiredoxin 1; GRX1, glutaredoxin-1; SIRTs, sirtuins.

It is evident from several studies that elevated ROS levels have a prominent role in aging and neurodegenerative diseases [95,96]. The retinal tissue is highly susceptible to ROS generation. First, RPE and photoreceptors are routinely encountered with high-intensity light energy. Second, oxygen utilization in the body tissue is highest in the retina. Third, the photoreceptor membrane discs contain abundant PUFAs, which are highly prone to oxidation. Finally, the daily phagocytosis function of RPE cells to remove and digest the spent outer segment occurs with a respiratory burst and rapid increase in ROS levels [4]. The generation and neutralization of ROS (oxidants) are not detrimental under normal physiological conditions provided the cellular antioxidant system effectively stabilizes the free radicals [97,98].

3.2. Implications of Compromised Cellular Antioxidant System on Pathogenesis of AMD

Antioxidants are essential for maintaining cellular defense against oxidative stress, which is vital for preventing disease progression and preserving vision in various age-

related eye disorders, notably AMD. Endogenous antioxidants can be classified into enzymatic and non-enzymatic systems and work synergistically (Figure 1). SOD catalyzes superoxide radical dismutation to convert into oxygen and hydrogen peroxide (H_2O_2), which is further converted to water and oxygen by CAT. Similarly, GSH-Px reduces H_2O_2 to water and lipid peroxides to corresponding alcohol at the expense of GSH. GST catalyzes the detoxification of endogenous substances by conjugation with glutathione. NQO1 reduces superoxide radical formation by catalyzing the reduction of quinones to hydroquinone. HO-1 catalyzes heme degradation to convert into biliverdin and then to bilirubin, carbon monoxide, and iron. Additionally, the yellow pigment bilirubin traps free radicals to exhibit cytoprotective action. The free iron produced during the reaction is sequestered by ferritin to prevent iron-catalyzed oxidative stress. TRX1 donates electrons to the ROS-oxidized cellular protein for the reduction of the disulfide bond to thiol form. SIRTs are an important regulator of cellular longevity by combating oxidative stress. SRXN1 catalyzes the regeneration of overoxidized peroxiredoxin (Prx) by the reduction of sulfinic acid (SO_2H) to thiol (SH) in the cysteine residue. Activated Prx is an important antioxidant enzyme for neutralizing ROS and reducing peroxides [84,99]. SOD, HO-1, CAT, GSH, GSH-Px, and ferritin are common downstream molecules of the endogenous antioxidant defense system to scavenge ROS [100]. Additionally, other non-enzymatic antioxidants like metallothionein, peroxiredoxin, thioredoxin, vitamins A, C, E, polyphenols, and carotenoids have significant contributions in mopping up ROS (Figure 1) [101]. SOD, CAT, and GPx constitute the primary defense against oxidative RPE damage. The synergistic action of these three enzymes creates a single metabolic pathway that defends oxidative assault [102]. SOD exists in three isoforms: cytosolic Cu/Zn-SOD (SOD1, encoded by Sod1 gene and localized on chromosome 21q22), mitochondrial Mn-SOD (SOD2, encoded by Sod2 gene and localized on chromosome 6q25.3), and extracellular Cu/Zn-SOD (SOD3, encoded by Sod3 gene and localized on chromosome 4) [103]. SOD1 and SOD2 show increased expression in the retina, and manipulation of SODs in mice displays AMD phenotypes [104]. Their levels were found to be upregulated in immunoblots of early- and intermediate-stage AMD donor eyes, reflecting a compensatory response for pro-survival signaling during oxidative stress [105]. Oxidative stress induced due to high ROS levels poses a critical threat to cellular organelles such as mitochondria, lysosomes, and the ER. The mitochondrial damage results in the decreased expression of SOD2 leading to RPE and photoreceptor degeneration. *Sod2*$^{-/-}$ albino BALB/cJ mice exhibited RPE dysfunction with age and increased oxidative stress when compared to the wild type [106]. Similarly, *Sod1*$^{-/-}$ mice can also be considered as mouse models of AMD since they exhibited the retinal degeneration phenotype including the thickening of BrM, microglia/macrophage accumulation, positive staining for oxidative stress markers, the thinning of the RPE and retina layer, and the presence of basal laminar and linear deposits [107]. A study carried out on a North Indian population with AMD also reported significantly higher levels of SOD1 compared to those of the controls [108]. Another study carried out on Chinese patients with AMD also reported increased serum SOD activity compared to that of controls supporting compensatory mechanisms against oxidative stress [109]. The adenovirus-mediated in vitro and in vivo gene therapy carrying the catalase gene protected RPE cells and photoreceptors from photo-oxidative stress, indicating that the overexpression of CAT in the RPE protects photoreceptor degeneration [110]. Implementing a therapeutic approach focused on the re-establishment of the antioxidant–enzyme balance may offer a promising avenue for addressing AMD. Moreover, the upregulation of genes encoding antioxidant enzymes may be much more effective than supplementation with antioxidant enzymes [111].

3.3. Oxidative Stress and Mitochondrial Dysfunction Are Implicated in the Progression of Aging and Neurodegeneration

The retina with the highest metabolic rates has increased adenosine triphosphate (ATP) demand to support visual phototransduction, neurotransmission, POS renewal, and retinal homeostasis [112]. Mitochondria are the dynamic organelles regulating many

critical functions including energy production, redox balance, cellular signaling, calcium buffering, cell growth, differentiation, and apoptosis [113]. Mitochondria generate ATP through oxidative phosphorylation, β-oxidation, and Krebs cycle to meet the energy demand of cells [114]. Circular double-stranded 16kb mitochondrial DNA (mtDNA) without introns encodes 13 essential proteins for executing several bioenergetics processes including the Krebs cycle and complex I–V of the electron transport chain (ETC) [115]. Mitochondria are the principal intracellular source (90%) of ROS generation. During oxidative phosphorylation, mitochondria consume 0.4–4% of the oxygen, which is reduced due to leakage of electron-generating superoxide radicals (primary ROS) [116]. Superoxide radicals are relatively short-lived and undergo dismutation to secondary ROS (H_2O_2), which diffuses through the membrane and gets transformed to the hydroxyl radical ($HO^{\bullet}$) and iron of higher oxidation states through the Fenton reaction [117].

Mitochondrial quality control (MQC) mechanisms like mitogenesis, fission, fusion, and mitophagy are required for homeostasis. Peroxisome proliferator-activated receptor γ coactivator 1α (PGC-1α) is a master transcriptional cofactor for the regulation of nuclear respiratory factor (NRF1/2) and mitochondrial transcription factor A (TFAM). The upregulated NRF1/2 and TFAM increase the gene expression for modulating MQC. It promotes mitochondrial biogenesis for tissue adaptation to increased energy demands. Furthermore, it activates mitophagy to remove dysfunctional mitochondria. Additionally, it mediates the balance between the fusion (increased expression of Mfn1/2 and Opa1) and fission (decreased expression of Drp1 and Fis1) process in the mitochondria [91]. The protein carbonylation due to the lipid peroxidation of the mitochondrial membrane critically affects the mitochondrial respiratory chain function as a result of the impairment of protein complexes, particularly I and II [118]. The decreased ATP production due to the impaired protein complex can damage nucleic acids, lipids, and the mitochondrial protein leading to the mutation of mtDNA and the further generation of ROS due to a vicious cycle [119]. It is also evident that the site of mtDNA is in close vicinity to the ROS creation site, and it is not preserved by the histone protein and is highly vulnerable and predisposed to mutation owing to a compromised restoring system compared to that of nuclear DNA. Moreover, with consistent oxidative stress due to high metabolic activity, high oxygen tension, and the continuous production of ROS, the DNA repair mechanism is reduced in the macular region as compared to in the peripheral retina, presenting significant implications for progressive degeneration [120]. Oxidative stress also affects the integrity of the permeability transition pore (PTP), the transmembrane channel formed by the interaction of voltage-dependent anion channel (VDAC) and adenine nucleotide translocator (ANT) in the mitochondria. The aberrant opening of the PTP results in depolarization of mitochondrial membrane potential (ΔΨm) due to membrane permeabilization. Thus, the electrochemical gradients for ATP production and calcium homeostasis are distorted due to the loss of ΔΨm [121]. Additionally, PTEN-induced putative kinase 1 (PINK1)–parkin mediates mitophagy targeting dysfunctional mitochondria for quality control. During dissipated ΔΨm, the translocation of PINK1 into the inner membrane for protease (mitochondrial processing peptidase) degradation is inhibited, which results in the accumulation and autophosphorylation of PINK1 in the outer membrane. The E3 ubiquitin ligase, parkin, is then recruited to the damaged mitochondria for ubiquitination of the outer membrane protein [122]. The adapter protein Nucleoporin 62/sequestosome 1 (p62/SQSTM1), which binds the ubiquitinated cargo, is a crucial platform for autophagosome formation. The interaction between SQSTM1 and microtubule-associated protein 1A/1B-light chain 3 (LC3) through the LC3-interacting region (LIR) motif initiates the formation of a double membrane around SQSTM1-tagged cargo resulting in the autophagosome. The autophagosome after maturation fuses with the lysosome for degradation of mitochondrial cargo. In Parkin-independent mitophagy, Bcl2/adenovirus E1B 19 kDa-interacting protein 3 (BNIP3) senses the damaged mitochondria and directly interacts with LC3 of the autophagosome membrane. On the contrary, oxidative stress impairs both parkin-dependent and -independent mitophagy signaling, resulting in the accumulation of dysfunctional mitochondria [123,124].

Aging mitochondria generate more ROS than young cells, rendering aging RPE cells vulnerable to elevated ROS generation. Although RPE cells harbor multiple cytoprotective antioxidant mechanisms, chronic oxidative stress due to the accumulation of ROS and mitochondrial dysfunction with aging leads to a reduction in antioxidative capacity [125,126]. Excessive mitochondrial ROS can also cause the shortening of the telomere region inducing cell senescence [127,128]. The glucose from the choriocapillaris is transported to photoreceptors by RPE cells, which utilize this glucose and produce lactate to be used by the mitochondria of RPE cells for ATP generation through oxidative phosphorylation. The lactate acts as a signal to restrain the glucose utilization by RPE. However, during mitochondrial dysfunction, RPE relies more on glycolysis than oxidative phosphorylation for ATP requirements, leading to photoreceptor and RPE cell death due to disruption of the metabolic ecosystem [46]. Taken together, mitochondrial dysfunction has been a prominent factor to be considered in age-related neurodegeneration, and boosting mitophagy and mitochondrial biogenesis may prevent mitochondrial dysfunction and the vicious cycle of oxidative stress. Exploiting the regulatory mechanism and factors involved in dynamics for maintaining mitochondrial homeostasis is a crucial avenue for developing potential interventions for age-related vision pathogenesis.

3.4. Oxidative Stress Triggers Endoplasmic Reticulum Stress Leading to Apoptosis

The intricated tubular network of the endoplasmic reticulum (ER) has contact sites with endosomes, lysosomes, the golgi network, mitochondria, and nuclei for regulating protein processing, lipid biogenesis, calcium homeostasis, and apoptosis [129]. The production, folding, quality control, and post-translational modification of secretory and transmembrane proteins occur in ER and its function is critically affected by changes in extracellular–intracellular environment like hypoxia, pH change, nutrient deprivation, aberrant disulfide bond formation, protein overexpression, asparagine (N)-linked glycosylation inhibition, calcium ion depletion, and changes in redox status resulting in ER stress [130–132]. Chaperones like calnexin, binding immunoglobulin protein (BiP), and protein disulfide isomerase (PDI) present in the ER recognize the misfolded proteins and maintain protein folding for proteostasis. BiP, also known as glucose-regulated protein 78 kDa (GRP78), is the best-characterized molecular chaperone with a high binding affinity for misfolded membrane and secretory proteins. Upon folding, the matured proteins are released from the ER to the golgi apparatus for further processing, sorting, and packaging in transport vesicles. If refolding fails, the misfolded proteins are translocated to the cytosol for ER-associated degradation (ERAD) using ubiquitin–proteasome and lysosome–autophagy machinery [133].

Unfolded protein response (UPR) is a dynamic and complex surveillance network that restores homeostasis during ER stress by decreasing protein synthesis, removing misfolded protein through ERAD, and increasing the protein folding capacity of ER. RNA-dependent protein kinase (PEKR), Activating transcription factor 6 (ATF6), and inositol-requiring enzyme 1 (IRE1) are the three important stress sensors and transducers under UPR signaling. The activation of these transmembrane proteins is inhibited under normal conditions by BiP binding. These proteins become dissociated with the accumulation of misfolded or unfolded proteins in the ER and transduce the abnormal signal from the ER lumen to the cytosol for the activation of transcription factors like X-box binding protein 1 (XBP1), C/EBP homologous protein (CHOP), Activating transcription factor 4 (ATF4), and nuclear factor-erythroid 2 (NFE2L2) for regulating gene expression for adaptive response to restore ER homeostasis. ROS are produced as a byproduct of protein oxidation in ER machinery during protein folding, suggesting UPR signaling as an adaptive process to balance ER-induced oxidative stress. However, during severe and prolonged ER stress, UPR signaling fails to restore normal ER function and gets switched from pro-survival mode to pro-apoptotic mode. To sum up, UPR signaling is a conserved host defense system acting as a two-edged sword because it can be cytoprotective to maintain cellular homeostasis or apoptotic during acute or chronic ER stress, respectively [134,135].

The generation of ROS during ER stress is mediated by redox signaling systems such as NADPH oxidase 4, protein disulfide isomerase (PDI), glutathione (GSH)/glutathione disulfide, Ca^{2+}, NADPH-P450 reductase, and ER oxidoreductin 1 (ERO1) [136]. Interestingly, disulfide bond formation mediates the generation of around 25% ROS during oxidative protein folding in the ER [137]. Mitochondria–ER communication is considered a crucial signaling hub for regulating vital cellular function. Mitochondria-associated membrane (MAM) is a 10–25 nm dynamic interface, which mediates the crosstalk between ER and outer mitochondrial membrane through structural and functional networks. MAM consists of many proteins and transporters and plays a crucial role in Ca^{2+} homeostasis, lipid transport, mitochondrial bioenergetics, and apoptosis [138]. During oxidative stress in ER, Ca^{2+} is released and taken up through VDAC of mitochondria. The increase in Ca^{2+} ions increases the metabolic activity and ROS generation in mitochondria. This causes a vicious cycle of further Ca^{2+} ions release due to the feedback mechanism, amplifying ROS generation. The stress-triggered mitochondrial PTP causes depolarization of mitochondrial membrane potential ($\Delta\Psi m$) which, ultimately, results in cytochrome c release due to a swollen mitochondrial matrix. The cytochrome c forms apoptosome with procaspase 9 and apoptotic releasing factor 1 (Apaf1) in the cytosol leading to the activation of caspase 3, an executioner caspase of apoptosis. Ultimately, unresolved and chronic ER stress leads to the global collapse of homeostasis and triggers apoptotic pathways [139]. Taken together, comprehensive mechanistic insights of how oxidative stress affects protein folding or misfolding causing ER stress and disruption of UPR signaling is crucial for targeted therapeutic intervention to ER/oxidative stress pathogenesis.

Oxidative stress, inflammation, proteostasis stress, and hypoxia, which are commonly encountered during the progression of AMD, are also potent inducers of ER stress. Moreover, the expression of crucial enzymes and transcription factors for adaptive ER stress balance declines with aging causing impairment of proteasomal activity and aggregation of oxidized proteins such as LF. A polycyclic aromatic compound, benzopyrene, present in cigarette smoke elicited disruption in the lysosomal homeostasis to provoke ER stress via the PEKR pathway. It also activated caspase cascades including caspase 3, 9, and 12 in ARPE-19 cells [140]. In another study, methylglyoxal, the toxic carbonyl compound produced due to the oxidative degradation of bisretinoid-induced caspase-independent apoptosis through ER stress was linked with ROS generation and mitochondrial dysfunction [141]. It is also evident that persistent upregulation of UPR signaling may induce pro-inflammatory cytokine IL-1β to promote retinal degeneration [142]. Taken together, ER stress can be taken as a potential pathogenic mediator of AMD due to its involvement in oxidative injury and RPE degeneration.

3.5. Bisretinoids Are the Primary Constituents of RPE Lipofuscin

3.5.1. Biogenesis of Bisretinoids Initiates within POS

Bisretinoids are the predominant constituents of LF in the RPE that accumulate with age, and they are implicated in the development of certain retinal diseases. LF is a generic name for the heterogeneous mixture of deposits and can be easily detected owing to its autofluorescence. Bisretinoid biosynthesis initiates within the POS through non-enzymatic reactions involving two molecules of vitamin A aldehyde with phosphatidylethanolamine (PE) (Figure 2) leading to the formation of A2PE, the precursor of bisretinoid biogenesis [143]. Bisretinoids consist of a polar pyridinium head and two non-polar retinoid tails. It has been reported that various unsaturated fatty acids are attached to glycerophosphoethanolamine of the A2PE species [144]. A2PE is detectable only in the POS whereas other bisretinoids are detected mainly in the RPE cells [145]. POS shedding containing bisretinoids is continuously transferred to the RPE during phagocytosis and deposited secondarily within the lysosomes of the RPE as LF [146]. A2PE undergoes phosphate hydrolysis and removes phosphatic acid moiety by phospholipase D within lysosomes to generate A2E. Various bisretinoids in LF of the RPE, including A2-glycerol phospho-

ethanolamine (A2GPE), A2E, all-*trans*-retinal dimer (atRALdi), and isoA2E have been successfully isolated and structurally characterized [147].

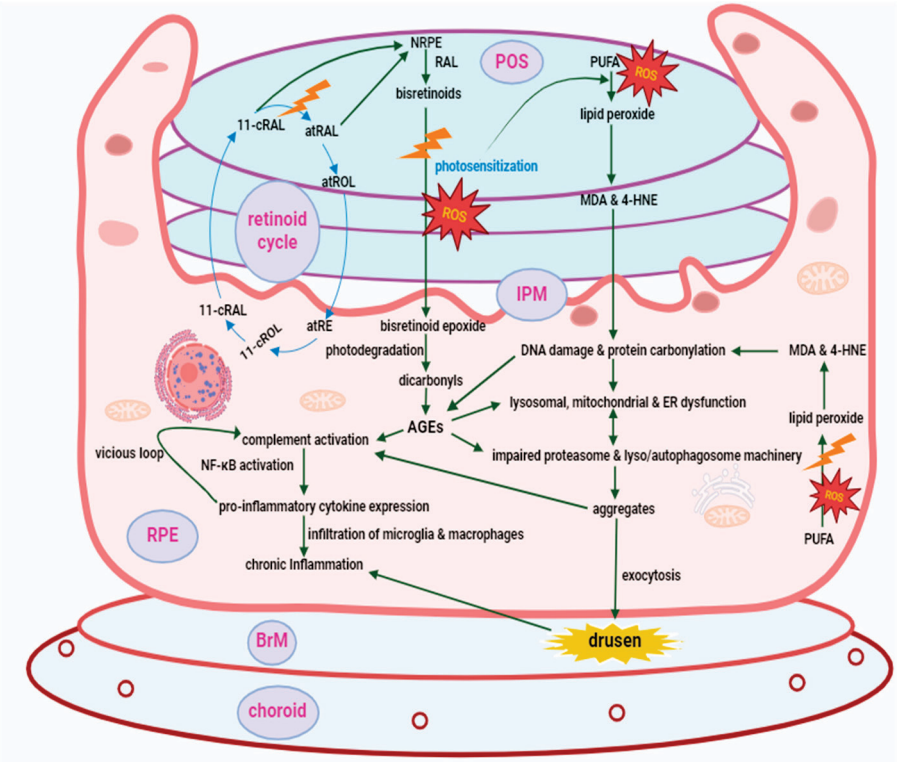

Figure 2. Schematic representation of retinoid visual cycle, bisretinoid biogenesis, implication of bisretinoid oxidation, and photodegradation in macular degeneration. During the visual cycle, the chromophore rhodopsin absorbs light and gets isomerized to atRAL and transported to RPE as atROL after reduction. The transconfiguration is then isomerized to 11-cRAL, which binds with opsin to regenerate rhodopsin [148]. atRAL binds with PE to form a Schiff base adduct, NRPE, which sequesters the toxic aldehyde. Non-catalytic condensation of another molecule of atRAL with NRPE initiates the biogenesis of bisretinoids [149]. Moreover, non-enzymatic lipid peroxidation of PUFAs (mostly DHA) generates lipid peroxides and ultimately toxic carbonyl compounds, i.e., MDA, and 4-HNE [150]. Singlet oxygen, generated due to bisretinoid excitation reacts with the bisretinoid polyene chain producing epoxides [151], which generates toxic electrophilic dicarbonyls, i.e., glyoxal and methyl glyoxal causing accumulation of AGEs. Complement activation triggers NF-κB activation and the expression of pro-inflammatory cytokines. The dysfunction in the integrity of lysosome, mitochondria, and ER is followed by impairment in autophagy [152]. The vicious cycle of oxidative damage results in chronic inflammation, a key contributor to RPE atrophy and macular degeneration [153,154]. atRAL, all-*trans*-retinal; atROL, all-trans-retinol; 11-cRAL, 11-*cis*-retinal; PE, phosphatidylethanolamine; NRPE, N-retinylidine phosphatidylethanolamine; PUFAs, polyunsaturated fatty acids; MDA, malondialdehyde; 4-HNE, 4-hydroxynonenal; AGEs, advanced glycation end products; POS, photoreceptor outer segment; IPM, interphotoreceptor matrix; RPE, retinal pigment epithelium; BrM, Bruch's membrane; ER, endoplasmic reticulum.

3.5.2. Bisretinoid Accumulation in RPE Lysosome Is Implicated in AMD

The fundus autofluorescence of RPE cells overlying the macula exhibits a significant accumulation of bisretinoids within the lysosome, particularly in elderly AMD patients [155]. Several studies reveal that bisretinoids disrupt normal RPE functions through various mechanisms [156,157]. Bisretinoid A2E destabilizes cell membranes [158] and induces RPE cell death when exposed to blue light by altering the levels of caspase-3 and antiapoptotic (Bcl-2) protein within mitochondria [159]. Progressive bisretinoid accumulation induces aberrant cholesterol metabolism and trafficking resulting in progressive cholesterol and

lipid deposits in the sub-RPE space. Additionally, ceramide deposits on the apical RPE surface lead to abnormally swollen early endosomes and the generation of complement C3a fragments from internalized complement C3. The uncontrolled activation of the complement system causes aberrant activation of the mechanistic target of rapamycin (mTOR), a regulator of autophagy. The dysregulated autophagy is manifested in dry AMD pathogenesis [160]. To sum up, intervention against A2E accumulation can provide a potential avenue in AMD therapy.

3.6. Bisretinoid-Derived Protein Adduct and Dysregulated Autophagy Induce Retinal Degeneration in AMD

3.6.1. Lysosomes Are the Site of Enzymatic Degradation of RPE Phagocytosis Cargo

A lysosome is a single membrane-bound spherical vesicle located in the cytosol of eukaryotic cells (except erythrocytes) [161]. It exhibits a multitude of functions including waste and organelle degradation, nutrient sensing, cellular stress response, and antigen presentation, which declines with aging [162]. The acidic interior (pH 4–5) of the lysosome is regulated by a vacuolar-type ATPase proton (V-ATPase H^+) pump, which controls the activity of more than 50 intralysosomal enzymes, including phosphatases, proteases, nucleases, lipases, sulfatases, and glycosidases. These enzymes are produced and matured in the ER and the golgi apparatus, respectively, and finally transported in secretory vesicles which ultimately release their contents to endosomes to form a lysosome [163]. The intracellular and extracellular trafficking of waste or damaged organelles into lysosomes occurs by autophagy and endocytic pathways, respectively. The phagocytic pathway in RPE cells starts with the formation of a phagophore in the phagophore assembly site of the ER, which engulfs the phagocytosed cargo forming a double-layered vesicle, the autophagosome. The conjugation of autophagy-associated proteins (ATGs) and LC3 is required for the maturation of autophagosomes. Moreover, the endo–lysosomal pathway can also operate simultaneously within RPE cells, which begins with the formation of early endosomes after engulfing extracellular materials through clathrin-mediated endocytosis. These endosomes gradually mature into late endosomes or multivesicular bodies with a decrease in luminal pH facilitated by proton ATPase. Ultimately, the lysosome coalesces with autophagosomes or late endosomes to form autolysosomes, where phagocytosis materials are degraded [164]. Consequently, the amino acids, polyunsaturated fatty acids, retinoids, and other degradation products are transported into the cytosol for utilization [165].

Progressive accumulation of LF occurs within lysosomes with a decrease in phagocytic activity of post-mitotic RPE cells with age. The gradual amassing of LF occurs within RPE cells from a 1% and 19% of cytoplasmic volume during the first decade and 80 years, respectively, indicating it is a prominent marker of cellular senescence [166]. The lysosome tolerates LF well up to a certain concentration, but an exceeded accumulation can impair lysosomal function due to the binding of LF with the L0 domain of the V-ATPase H^+ pump and distorting acidification. The detergent action of LF can also impair the membrane integrity of the lysosomal membrane. Consequently, the accumulated LF suppresses the cellular proteolytic system (i.e., lysosome, proteasome), attenuating the digestion of oxidized proteins triggering more LF formation and generating a vicious cycle (Figure 2). Consequently, it leads to ROS generation and cytotoxicity in RPE cells [167]. Additionally, the lysosome harbors higher iron levels owing to the digestion of metalloproteins and iron-rich mitochondria [168]. The ferrous ion triggers the formation generation of $HO^{\bullet}$ through the Fenton reaction [145,169]. $HO^{\bullet}$ is the most reactive ROS and has a very short half-life (10^{-9} s). Several in vitro studies have reported that iron chelator supplementation decreased oxidative stress during H_2O_2 exposure [170–172]. Taken together, targeting oxidative stress-induced V-ATPase H^+ pump inhibition and iron accumulation need to be explored as a potential therapeutic strategy to mitigate the occurrence of and pathological progressions in AMD.

3.6.2. Dysregulated Autophagy and Perturbed Proteasome Machinery Is Involved in AMD Pathogenesis

Autophagy is a cytoprotective catabolic process to get rid of aberrant proteins and organelles under stressful conditions by sequestrating and transferring them to the lysosome for intracellular quality control [173], which is regulated by the Mammalian target of rapamycin (mTOR) and the AMP-activated protein kinase (AMPK) [174]. The various steps of autophagy, induction, nucleation, elongation, fusion, and degradation are controlled by more than 30 autophagy-related genes [175]. The accumulation of SQSTM1/p62, which is regarded as a marker for dysfunctional autophagy, has been reported in the macula of AMD donors [176]. The decreased number of autophagic vesicles in the RPE of AMD donors compared to that of controls has also been reported [177]. Furthermore, the accumulation of damaged mtDNA has been shown in the RPE of AMD donors indicating dysfunction in mitophagy [178]. The exact involvement of autophagy in AMD is elusive, but there is a correlation between the lysosomal accumulation of LF and drusen deposits in the sub-RPE space. It is known that the upregulation of autophagic and lysosomal activity is essential to preserve the RPE cell from detrimental cargo accumulation [179]. Intracellular RPE stress is overwhelmed if the phagocytized POS is not effectively degraded with hydrolytic enzymes initiating the process of lipofuscinogenesis and the aggregation of lysosomal LF might restrain autophagic flux regulation [46]. To sum up, autophagy increases with oxidative stress in early AMD to ameliorate oxidative injury on the post-mitotic RPE but cannot cope with the upsurge in organelle dysfunction during later stages, leading to its impairment.

The ubiquitin–proteasome pathway (UPP) is a non-lysosomal proteolytic cargo clearance system within the cell. About 80–90% of short-lived or aberrant proteins in the cells are degraded by proteasome pathways for regulating transcription, signal transduction, cell cycle progression, immune response, apoptosis, and proteostasis. A recent study has reported the crosstalk between autophagy and proteasome degradation due to SQSTM1/p62 bridging. Impaired proteostasis in aging RPE cells due to oxidative stress has mechanistic links with AMD [180]. During the UPP, the targeted protein is first conjugated with E3-ubiquitin ligase chains and subsequently degraded by proteasome in coordination with heat-shock proteins. Several studies support the notion that the UPP system is disrupted during the AMD pathogenesis due to oxidative stress leading to the accumulation of misfolded or aggregated proteins, which are extracellularly deposited in the sub-RPE as drusen (Figure 2) [126,180,181]. Taken together, preventing oxidative stress-induced proteasome inactivation can be a valid interventional strategy against AMD pathogenesis.

3.6.3. Protein Adducts with Bisretinoid Degradation Products Precipitate AMD Pathogenesis

RPE cells are especially susceptible to damage from blue light due to the presence of unique photosensitizers. A2E is the most widely studied and well-characterized bisretinoid fluorophore in LF contributing to the etiology of AMD. During photo-oxidation, almost nine oxygen atoms can be incorporated into the polyene side arm of A2E releasing a multitude of oxygen-rich moieties including peroxy A2E, furano A2E, and epoxy A2E. Moreover, these oxides alter the UV spectral properties of A2E due to an interruption in the electron delocalization of the polyene chain. This is the reason why A2E oxiranes need LC-MS for identification [182]. Additionally, oxiranes are highly reactive and susceptible to nucleophilic attack. The subsequent degradation of these oxides results in highly reactive dicarbonyls bearing fragments like methylglyoxal and glyoxal [183]. These dicarbonyls are relatively long-lived and highly reactive owing to their electrophilic character. These species can easily permeate from their origin site to attack intracellular or extracellular biomolecules and targets. They can alter the structural conformation and function of proteins by forming glycated covalent adducts (Schiff base) due to spontaneous reaction with nucleophilic thiol groups on arginine, cysteine, and lysine residue of proteins [184]. This complex mixture elicits alternative complement pathway activation as these adducts are recognized as foreign. Moreover, complement activation fragments C3a and C5a are

mediators of pro-inflammatory cytokine generation indicating complement dysregulation can precede chronic inflammation and underlying AMD pathology [185]. One study reported that incubation of A2E with ARPE-19 cells followed by irradiative photo-oxidation resulted in increased levels of complement 3 split products C3b and C3a. Similar results were obtained when peroxy A2E and Furano A2E were incubated with serum [37]. In proteomic analysis of LF, minimal protein content and no identifiable proteins were found in purified LF granules; however, the granules exhibited oxidative protein modifications. Furthermore, the modified proteins are also the mediators for the formation of stable cross-linked protein aggregates and advanced glycation end products (AGEs) [155]. Glycative stress is also accelerated with aging due to diminished autophagy and proteasome clearance and increases the risk of diabetes, as well as cardiovascular, ocular, and neurodegenerative diseases [186]. Moreover, the ubiquitin–proteolysis system in the RPE is critically affected by AGE accumulation in RPE cells, which further triggers the vicious cycle of LF accumulation and elevated glyoxal and methyl glyoxal generation contributing to drusen formation (Figure 2). Autophagy and proteasome degradation machinery, individually or collectively, can get rid of these aggregated AGEs, but the exact molecular processes or factors involved during degradation are still elusive. Downstream aberrant AGE accumulation consequently activates the receptor for advanced glycation end product (RAGE) signaling, a pattern recognition receptor that binds with a multitude of ligands including AGEs, amyloid beta protein, S-100 calcium-binding protein, and high-mobility group box-1 [187]. It has been reported that RAGE knock-out mice are resistant to the detrimental consequences of AGE accumulation. Ultimately, transmembrane protein RAGE activation provokes oxidative stress and inflammation by activation of different intracellular signaling cascades like PI3K/Akt, NF-κB, JAK/STAT, p38MAPK, and ERK1/2. To sum up, intervention against the glycated burden of AGE accumulation, RAGE activation, and modulating the proteasome and autophagy degradation pathway for AGE remediation with potential antioxidants can be a promising direction.

3.7. Crosstalk between ROS Generation and Expression of Pro-Inflammatory Markers

Though inflammation is a vital biological response against acute stimuli and infections, prolonged and self-perpetuating inflammation has detrimental consequences. Accumulating evidence indicates that oxidative stress led to inflammation as the foremost mediator of several neurodegenerative diseases [188]. Oxidative stress, lipid peroxidation, and photo-oxidized species found in drusen and LF may act as stress or DAMPs to trigger the activation of pattern recognition receptors (PPRs) leading to the activation of transcription factors (NF-κB) in the RPE and the expression of pro-inflammatory cytokines and chemokines (Figure 2). NOD-like receptors (NLRs) and Toll-like receptors (TLRs) are the prominent PPRs in RPE cells. NOD-like receptor protein P3 (NLRP3), Adaptor protein (ASC), and procaspase-1 form a multiprotein intracellular complex (NLRP3 inflammasome). This assembly generates cleaved caspase-1 due to autocatalytic cleavage, which elicits the production and expression of functional interleukins IL-1β and IL-18. [189]. Also, H_2O_2, paraquat, or A2E-induced photo-oxidation of human RPE cells elevated the expression of IL-8 and inactivated the proteasome system indicating a mechanistic link between oxidative stress and inflammation [190]. Consequently, these inflammatory mediators recruit and activate immune cells (macrophage, microglia) in the retina–choroid microenvironment leading to a downstream inflammatory cascade [191]. Cleaved caspase-1 also causes cleavage of Gasdermin D leading to the pyroptosis of cells due to membrane rupture [192]. The abnormal opening of connexin 43 hemichannels induced by oxidative stress is another mechanism for exacerbating NLRP3 by releasing ATP [193]. A study has also reported the increased expression of NLRP3, ASC, and caspase-1 in patients with geographic atrophy [194]. Consequently, pharmacological intervention against the activation of NLRP3 and downstream inflammatory mediators can prevent inflammation. Taken together, understanding the mutual relationship and interplay between oxidative stress and the expression

of pro-inflammatory markers is indispensable for the profound elucidation of mechanistic insights into AMD pathogenesis to limit its progression to a chronic state.

4. Antioxidants in Management of Dry AMD: Fortifying the Fortress for Protection from Macular Degeneration

4.1. Classification of Antioxidants

Antioxidants are substances that may protect against the detrimental effects of free radicals (Figure 1) and neutralize the adverse effects of oxidative stress at low concentrations [100]. They can be classified into natural and synthetic antioxidants. Carotenoids, polyphenols, and vitamins are the common natural antioxidants obtained from plant sources. Natural antioxidants can be obtained from medicinal herbs, legumes, spices, nuts, fruits, vegetables, cereals, animals, minerals, and microorganisms. Common synthetic antioxidants include propyl gallate, butylated hydroxytoluene (BHT), butylated hydroxyanisole (BHA), citric acid, ethylene diamine tetra acetic acid (EDTA), ascorbyl palmitate, and tert-butyl hydroquinone (TBHQ). Synthetic antioxidants are commonly used in the food and cosmetic industry to combat lipid peroxidation and sustain product quality. They can be further categorized into primary and secondary antioxidants. Primary antioxidants are the chain terminators and transform free radicals into non-radical forms by resonance stabilization while secondary antioxidants are the inhibitors of chain initiation and act as metal chelators and turn hydroperoxides into inactive forms [195]. Additionally, there is a de novo or tertiary antioxidant system for the repairing of damaged biomolecules due to oxidation. Replenishing with exogenous antioxidants is indispensable to combat a compromised antioxidant defense system during oxidative stress for homeostatic balance [196].

4.2. Mechanism of Action of Antioxidants against Free Radicals

There are two main antioxidant mechanisms to counteract free radicals directly: electron donation and hydrogen (H) atom transfer. During H atom transfer, the antioxidant molecule generates hydrogen radicals and antioxidant radicals due to homolytic fission. The hydrogen radical then binds and neutralizes free radicals whereas the antioxidant radical binds with another antioxidant radical to form a less reactive dimer. Similarly, antioxidant compounds with conjugated double bonds donate electrons to free radicals and neutralize them. The conjugated compound also stabilizes itself by electron delocalization. The antioxidant molecule can also indirectly avert free radicals by activating endogenous antioxidant transcription factors and enzymes [197]. The global trend of using natural antioxidants is escalating owing to the strict regulation of synthetic antioxidants due to health detriments and increasing consumer preferences. Several evidence-based studies support the effectiveness of antioxidants in preventing and delaying the progression of dry AMD. The experimental studies using antioxidants also report the significant protection of RPE and retinal degeneration [198,199].

4.3. Cellular Defense Mechanism against Oxidative Stress: NFE2L2 and REV-ERBα Signaling

There has been a notable surge in antioxidant research since the 1990s driven by perceived benefits in disease prevention and overall health promotion [197]. The antioxidant system in the human body is a complex web of enzymes, molecules, and transcription factors. Nuclear factor-erythroid 2 (NFE2L2) is an emerging and highly conserved transcription factor for resistance to oxidative and electrophilic stress during redox perturbation to maintain redox homeostasis in vertebrates. NFE2L2 is bound to Kelch-like ECH-associated protein 1 (Keap1), a redox-sensitive substrate in the cytoplasm. Polyubiquitination by CUL3-based E3 ubiquitin ligase and subsequent 26S proteasomal degradation of NFE2L2 is facilitated by Keap1. During oxidative stress, there is modification in the critical cysteine residue (Cys151, Cys273, and Cys288) of Keap1 by electrophilic species leading to disruption in the NFE2L2-Keap1 network. The phosphorylated NFE2L2 then translocates to the nucleus and forms a heterodimer complex with a musculoaponeurotic fibrosarcoma (Maf)

protein in DNA to bind the antioxidant response element (ARE) in the promotor region of the cognate target gene for the expression of an array of phase II antioxidant enzymes and proteins including SOD, CAT, HO-1, NQO1, GST, and GCLC [88]. Importantly, NFE2L2 is the vital antioxidant hierarchical axis that senses redox stress. Moreover, dry AMD-like cardinal features including inflammation, retinal dysfunction, photoreceptor degeneration, and ROS accumulation are exhibited in *Nfe2l2*$^{-/-}$ mice, highlighting their critical role in pathogenesis [200]. REV-ERBα (aka NR1D1), a dithiol-disulfide redox-sensing nuclear transcription factor, which regulates metabolism and circadian rhythm is also the transcriptional regulator of NFE2L2. Moreover, REV-ERBα-deficient aging mice show AMD-like pathologies, including RPE and photoreceptor degeneration, fundus lesions, BrM thickening, and pseudo-drusen deposits. Additionally, REV-ERBα-deficient mice are also more prone to RPE oxidative damage when exposed to oxidative stress [201]. In summary, targeting NFE2L2 and REV-ERBα signaling can be ideal therapeutic approaches against oxidative stress-induced macular degeneration [202–204].

4.4. Harmful or Unintended Consequences of Antioxidant Supplementation

The allure of antioxidant therapy for combating disease and health promotion by alleviating oxidative stress is undeniable, but its supplementation may also be associated with harmful effects. Antioxidants can surprisingly act as prooxidants under different conditions, e.g., vitamin C has an antioxidant action at low doses (30–100 mg/kg) and a prooxidant effect at high doses (100 mg/kg). The case with α-tocopherol is similar. Flavonoids under transition metal environment and phenolics in the presence of redox-active metals behave as prooxidants [205]. High serum levels of β-carotene in smokers have been linked to an increased risk of lung cancer [206] and cardiovascular disease [207]. Controversy still exists about whether dietary antioxidant supplementation interferes with chemo and radiation therapy promoting tumorigenesis [208]. Taken together, antioxidant supplementation should be limited to evidence-based and well-documented cases of oxidative stress.

5. Exploring the Therapeutic Potential of Antioxidants: Insights from Preclinical and Clinical Studies

5.1. Clinical Studies of Dietary Supplements, Nutrients, and Antioxidants

Several reports (Table 1) depict the potential efficacy of dietary supplements, functional food, and antioxidants for diminishing oxidative stress. In 2001, age-related eye disease studies (AREDSs) tested the efficacy of antioxidant supplementation incorporating β-carotene, vitamin C, E, Cu, and Zn in early, intermediate, late, and wet AMD patients. The formula does not prevent or control the early and intermediate stages but reduces the progression to wet AMD by 25% in 5 years [209]. In 2006, a second clinical study (AREDS2) was conducted by the National Eye Institute (NEI) supplementing 10 mg lutein and 2 mg zeaxanthin and omitting β-carotene in the original AREDS formula with incremental benefits. Lutein, zeaxanthin, and its stereoisomer meso-zeaxanthin are important carotenoids that accumulate within the macula. Furthermore, an epidemiological follow-up study on AREDS2 by Chew et al. concluded a decreased risk of late AMD progression with no sign of toxicity [210]. Macular pigment optical density positively (MPOD) correlates the macular pigmentation and decreased MPOD with age and is considered another determinant of AMD pathogenesis. Daily supplementation of lutein with antioxidant vitamins and minerals improved visual acuity and increased MPOD. Furthermore, the incorporation of ω-3 fatty acids into the carotenoids showed significant improvement in plasma antioxidant capacity [211]. The blue mountain eye study carried out on 3654 Australian cohorts reported a decreased risk of early AMD incidence with the intake of dietary ω-3 fatty acids. The study also reported a 40% reduction in early AMD incidence on at least weekly fish consumption. Moreover, fish consumption thrice weekly even reduced the incidence of late AMD [212]. Furthermore, the US twin study [213], the Rotterdam study [214], and the Women's health study [215] reported that the dietary intake of ω-3 fatty acids is inversely related to AMD

incidence. Also, adding DHA and/or eggs to lutein and zeaxanthin supplementation significantly increased MPOD [216,217]. In another study, daily supplementation with acetyl L-carnitine, ω-3 fatty acids, and coenzyme Q10 showed remarkable improvement in visual function [218]. Pre-clinical studies report that saffron can protect photoreceptor degeneration and retinal morphology owing to its neuroprotective action [219]. In a clinical study, saffron improved macular function in AMD patients [220]. Copper and zinc are important cofactors of ocular antioxidant metalloenzymes and their concentration is notably high in the neural retina, RPE, and choroid complex and accumulative evidence suggests their deficiency results in AMD [221]. Supplementing with 25 mg zinc monocysteine twice daily for 6 months in 80 participants (40 per group, 37 in each group completed all visits) with macular drusen enhanced macular function compared to that of the placebo group [222]. These above findings elucidate the potential applications of carotenoids, unsaturated fatty acids, vitamins, and minerals for improving visual acuity and reducing progression in dry AMD patients by counteracting oxidative damage to the retina and underlying tissues. A noteworthy point to contemplate about antioxidants is their emerging potential to mitigate the degeneration of the RPE and photoreceptors intricated with oxidative stress. To sum up, specifically, tailored antioxidant dietary formulation with prospective interventional studies is needed for a paradigm shift. Table 1 also includes various antioxidant molecules currently under different phases of clinical trials for the management of AMD.

Table 1. Clinical Studies of Dietary Supplements, Nutrients, and Antioxidants for Management of Dry AMD.

Antioxidant	Population	Study Design	Study Duration	Intervention	Outcome (s)	Citation
AREDS formulation	Early, intermediate, late, and wet AMD patients (Four different groups)	Multicenter, double-blind, placebo-controlled RCT	6.3 years (Average)	Vitamin C, E, β-carotene, and/or Zn	Decreased 25% risk of wet AMD progression	[209]
	3549 patients (different stages of AMD)	Epidemiological follow-up study of AREDS RCT	10 years	AREDS supplement with Vitamin C, E, β-Carotene, Cu, and Zn.	Significant reduction in risk of progression to exudative AMD	[223]
Dietary nutrients	4504 AREDS and 3738 (AREDS2) participants	Post hoc analysis of AREDS and AREDS2	-	AREDS and AREDS2	Nutrients rich in carotenoids, vitamins, and minerals decrease the risk of late AMD progression	[50]
Lutein and Zeaxanthin	Uni- or bilateral intermediate AMD	Epidemiological follow-up study of AREDS2 RCT	6 years	AREDS2 supplement with Lutein, zeaxanthin, Vitamin C, E, Cu, and Zn.	Lutein and zeaxanthin showed improved association in preventing AMD progression with no sign of toxicity as compared to beta-carotene	[210]
	108 patients (early AMD)	Double-blind, placebo-controlled RCT	48 weeks	Daily supplementation with 10 mg lutein or 20 mg lutein 10 mg + 10 mg zeaxanthin or placebo	The lutein and zeaxanthin group showed a significant increase in MPOD	[224]
Lutein	25 AMD patients	Double-blind, placebo-controlled RCT	9 months	Supplement of 6 mg lutein with vitamins and minerals	The supplement has no significant difference in contrast sensitivity in people with AMD	[225]
	90 dry AMD patients	Double-blind, placebo-controlled RCT	12 months	Daily intake of 10 mg lutein or 10 mg lutein + antioxidants, vitamins and minerals	Improved visual acuity in both groups	[226]

Table 1. *Cont.*

Antioxidant	Population	Study Design	Study Duration	Intervention	Outcome (s)	Citation
Lutein	126 AMD patients (Stages 2, 3 and 4)	Double-blind, placebo-controlled RCT	6 months	Daily intake of 20 mg lutein for 3 months then 10 mg for another 3 months	Lutein supplementation increased MPOD	[227]
PUFAs	Early AMD in one eye and wet AMD in another (263 patients)	Double-blind, placebo-controlled RCT	3 years	Daily supplementation with fish oil capsule (DHA 840 mg and EPA 270 mg)	No significant difference in the incidence of CNV in the study eye compared to the placebo	[228]
Lutein, zeaxanthin, and ω-3 fatty acids	172 patients (dry AMD)	Double-blind, RCT	12 months	Daily supplementation with 1 capsule	Significant improvement in plasma antioxidant capacity	[211]
Lutein and DHA	100 healthy participants	Multicenter, double-blind study	3 months	Daily supplementation with lutein or lutein + DHA	MPOD is significantly higher in the lutein + DHA group	[217]
Eggs	24 healthy females	RCT	12 weeks	6 eggs per week (Egg 1 and Egg 2 with different concentrations of Lutein and Zeaxanthin per yolk)	Significantly increased MPOD in both groups	[229]
Eggs+ lutein and DHA	99 healthy participants	Double-blind RCT	4 months	Daily 2 standard eggs or enriched eggs with lutein, zeaxanthin, and DHA	Significantly increased MPOD in both groups	[216]
Eggs+ lutein or zeaxanthin	100 healthy participants	RCT	90 days	Daily supplementation with lutein/zeaxanthin-enriched egg or lutein-rich egg yolk	No changes in MPOD but an increase in dutein and zeaxanthin serum concentration	[230]
Lutein+ zeaxanthin and ω-3 fatty acids	120 participants with a family history of wet AMD	Double-blind, placebo-controlled RCT	1 year	Daily supplementation	Significant association with macular pigment optical density (MPOD)	[231]
ω-3 fatty acids and Vit D	25,871 healthy participants	Nationwide, double-blind, placebo-controlled RCT	25 Months	Vitamin D (2000 IU/day) ω-3 fatty acids (1g/day)	No impact on AMD incidence	[232]
Caroteninoids+ ω-3 fatty acids and vitamins	80 patients with intermediate AMD	Double-blind, placebo-controlled RCT	2 year	Daily supplementation with 1 Tablet	Clinically prevented intermediate AMD progression	[233]
Acetyl L-Carnitine, ω-3 fatty acids, and coenzyme Q10	106 early AMD patients	Double-blind, placebo-controlled RCT	12 months	Daily supplementation with 2 capsules	Significant improvement in visual functions in treated groups	[218]
Zinc-monocysteine (ZMC)	74 participants with macular drusen (37 per group)	Double-blind, placebo-controlled RCT	6 months	25 mg ZMC twice daily supplementation	ZMC is well tolerated and improves the macular function in AMD compared to placebo	[222]
Saffron	100 patients with mild/moderate AMD	Double-blind, placebo-controlled, crossover RCT	6 months	Daily supplementation with 20 mg saffron for 3 months	Improved visual function in AMD patients	[220]

Table 1. *Cont.*

Antioxidant	Population	Study Design	Study Duration	Intervention	Outcome (s)	Citation
Vitamin E	1193 participants	Placebo-controlled RCT	4 years	Daily supplementation with Vitamin E 400 IU	No effect on the incidence of early AMD and its progression	[234]
ARMD antioxidant capsule	71 dry AMD patients	Double-blind, placebo-controlled RCT	18 months	Twice daily supplementation	No improvement in the fundus appearance	[235]
Elamipretide	Adults $\geq$ 55 years with dry AMD	Phase III, double-blind, placebo RCT	96 weeks	Daily 40 mg subcutaneous injection	Evaluate safety and efficacy	[236]
CT1812	246 patients with GA	Phase II, double-blind, placebo-controlled RCT	104 weeks	200 mg oral daily	Evaluate safety and efficacy	[237]
Iptacopan (LNP023)	146 patients with early/intermediate AMD in one eye and CNV in the other	Phase II, double-blind, placebo-controlled RCT	-	Oral capsules	Evaluate safety and efficacy	[238]
Avacincaptad pegol (Zimura)	286 participants with GA	Phase II/III, double-blind, placebo-controlled RCT	18 months	Monthly 1–4 mg IV injection	Evaluate safety and efficacy	[239]
Luminate (ALG-1001)	40 participants with dry AMD with BVCA of 20/40–20/200	Phase II, single-blind, placebo-controlled RCT	16 weeks	1 mg intravitreal injection	Evaluate safety and efficacy	[240]
Antiplatelets with or without antioxidant	174 dry AMD patients with at least 1 large drusen	Phase III, single-blind, placebo-controlled RCT	-	Aspirin 81 mg, clopidogrel 75 mg, and N-aceytl cysteine 600 mg per day	Evaluate safety and efficacy	[241]
EG-301	90 intermediate AMD patients	Phase II, open-label, placebo-controlled RCT	-	150 mg daily	Evaluate safety and efficacy	[242]
Tandonspirone (AL-8309B	48 patients with GA	Phase III, double-blind, placebo-controlled RCT	36 months	1% and 1.75% eye drops	No difference in the GA lesion growth between treatment and control	[243]
Danicopan (ALXN2040)	365 patients with GA	Phase II, double-blind, placebo-controlled RCT	104 weeks	100 mg bid 200 mg bid 400 mg qid	Dose finding study	[244]
Alpha Lipoic acid	68 patients with GA	Phase II, double-blind, placebo-controlled RCT	18 months	1200 mg oral daily	No beneficial effect on GA lesions	[245]

5.2. Antioxidant Compounds from Natural Sources

Table 2 shows the in vitro and in vivo antioxidant and cytoprotective activity of several compounds obtained from natural sources under different oxidative stress conditions

mimicking dry AMD pathogenesis. Diverse classes of phytochemicals including flavonoids, phenylpropanoids, carotenoids, alkaloids, and terpenoids have exhibited potential antioxidant activity to resist oxidative stress in several experimental studies. Plants secrete these secondary metabolites for resistance against predators, pathogens, and environmental stress [246]. Phenolic compounds consist of at least one aromatic ring and one or more hydroxy groups. They are electron donors owing to the presence of polarized hydroxyl groups. More than 8000 polyphenols are reported and broadly categorized as flavonoids and non-flavonoids. Flavonoids consist of a phenyl benzopyran ring (C_6-C_3-C_6 skeleton) with hydroxyl groups usually at 4′, 5, and 7 and also at 3′ and 5′ positions. They are further classified into different subclasses based on hydroxylation patterns and linkage between phenol rings [247]. Multiple studies exhibited the protective role of a flavonoid, quercetin, against oxidative stress. It preserved the mitochondrial function, reduced sub-RPE deposits in mice, and suppressed the generation of ROS and pro-inflammatory mediators [248–254]. It also prevented A2E photo-oxidation and the formation of protein adducts [255]. Another flavonoid, apigenin, in solid dispersion reduced ROS levels and showed a protective effect by upregulating antioxidant signaling [256]. Cynaroside, a flavone also called luteoside, induced autophagy and ameliorated retinal morphology by suppressing inflammation and apoptosis [257]. Carotenoids are highly conjugated compounds capable of donating electrons and stabilizing free radicals to protect against oxidative damage. Retinal thickness is considered a hallmark of retinal structural integrity. Macular carotenoids, lutein, and zeaxanthin prevented the thinning of the photoreceptor layer due to apoptosis, decreased oxidative stress markers, and protected photo-oxidation in RPE cells by quenching singlet oxygen [258–264]. Other carotenoids like astaxanthin, fucoxanthin, and crocin also displayed cytoprotective effects by suppressing ROS generation and inflammation [265–267]. Turmeric (*Curcuma longa* Linn.) has a long history of use in Indian and Chinese traditional medicine. Curcumin derived from turmeric has poor in vivo bioavailability and undergoes rapid metabolism. Hexahydrocurcumin, a major metabolite of curcumin, promoted the autophagy and autophagic flux in RPE cells [268]. Epicatechin and its ester reduced AGE accumulation and preserved the photoreceptor morphology [269–271]. Another polyphenol, resveratrol (RSV), preserved the cytoskeleton architecture of the RPE by ameliorating the redox balance and mitochondrial integrity [272]. Piceid octanoate (PIC-OCT), a synthetic acylated prodrug of RSV with a better ADME profile, exhibited amelioration of retinal integrity and photoreceptor protection in the rd10 mice model of retinal degeneration by modulating the SIRT1/PARP1 axis [273]. Cia et al. [274] showed that phloroglucinol reduces A2E levels in rat primary RPE cells by forming a chromene adduct during atRAL-induced oxidative stress. A terpene glycoside, paeoniflorin is reported to suppress mitochondrial dysfunction and ER stress during oxidative damage in RPE cells [275]. Oleuropein, a secoiridoid, attenuated the generation of inflammatory mediators by repressing the NF-κB and MAPKs activation in IL-1β-treated RPE cells [276]. An isoquinoline alkaloid, berberine, upregulated Rho, Rpe65, and mct3 mRNA expression and preserved the photoreceptor degeneration in a light-treated mice model [277]. Furthermore, puerarin, an isoflavone glycoside, suppressed the apoptosis induced by AGE-BSA in rats and retinal pericyte bovine retina by blocking Rac1, p47phox, and NF-κB [278]. This converging accumulative scientific evidence of antioxidant molecules reverting oxidative stress illuminates a ray of hope to impede the onset and progression of AMD pathogenesis.

Table 2. Preclinical studies of compounds derived from natural products for combating oxidative stress.

Antioxidant Compound	Experimental Model	Dose	Observation	Citation
Quercetin (solid dispersion)	NFE2L2 knock-out mice (dry AMD model)	200 mg/kg	↓ RPE deposits and thickness of BrM ↑ levels of HO-1, HQO-1, and GCL in NFE2L2 knockout mice	[248]
Quercetin	Cybrid ARPE-19 cells	20 μM	↓ ROS levels and increased cellular metabolism	[249]
	Ccl2/Cx3cr1 DKO mice	50 μM	↓ oxidative damage in RPE cells by suppressing pro-inflammatory mediators and intrinsic apoptotic pathway	[250]

Table 2. *Cont.*

Antioxidant Compound	Experimental Model	Dose	Observation	Citation
Quercetin	Oxidative injury in ARPE-19 cells by H_2O_2	50 μM	↓ oxidative damage, senescence, and apoptosis in RPE cells	[251]
	4-HNE-induced cytotoxicity in ARPE-19 cells	50 μM	preserved mitochondrial function and cell membrane integrity, ↓ expression of pro-inflammatory molecules by regulating ERK, p38 MAPK, and CREB signaling	[252]
	IL-1β caused the generation of inflammatory mediators in ARPE-19 cells	2.5–20 μM	↓ secretion of IL-6, IL-8, sICAM-1, ICAM-1, and MCP-1 by inhibiting NF-κB and MAPK pathway	[253]
Quercetin-3-O-α-L-arabinopyranoside	Light-induced oxidative injury in A2E-laden ARPE-19 and mice primary RPE cells	12.5–200 μM 25–100 mg/kg	↓ inflammation and apoptosis by inhibition of AP1, NF-κB, C3, and PARP activity	[254]
Quercetin and Cyanidin 3-glucoside	Oxidative stress in A2E-loaded ARPE-19 cells induced by light	10–50 μM 200–500 μM (acellular assay)	↓ ROS production, A2E photo-oxidation, methylglyoxal adduct formation, and RAGE mRNA expression ↓ release of 4-HNE when incubated with bovine rod outer segment and all-trans-retinal followed by irradiation	[255]
Apigenin (solid dispersion)	Dry AMD mice model	20–60 mg/kg	↓ ROS and MDA levels due to upregulation of the NFE2L2 pathway and its downstream genes HO-1, NQO-1, and antioxidant enzymes SOD, GSH-Px	[256]
Cynaroside	Phototoxicity in A2E-loaded ARPE-19 cells and rat retina induced by light	10–20 μM 2–4 μg/eye	↑ cell viability, ↓ ROS generation ↓ apoptosis by increasing Bcl2/Bax levels and decreasing caspase 3 and 9 expression induced autophagy and ↓ levels of IL-1β, IL-8, and TNFα by ↓ NLRP3 signaling ameliorated retinal morphology and thickness and ↓ retinal degeneration	[257]
Lutein	Retinal injury in mice induced by light	170 mg/kg	ameliorated visual impairment, a and b wave changes in ERG, and thinning of photoreceptor layer ↓ upregulation of γH2AX preventing apoptosis in the photoreceptor layer Promoted DNA repair and survival by activating eyes absent (EYA)	[259]
	Oxidative damage and retinal injury in rats induced by light	25–100 mg/kg	↓ oxidative stress and suppressed pro-inflammatory cytokine levels ameliorated a and b waves of electroretinogram and thinning of photoreceptor layer due to apoptosis	[260]
Lutein and zeaxanthin	A2-PE/A2E induced photo-oxidation in *BALB/cByJ* and *C57BL/6J* mice primary RPE cells	100–200 μM	↓ photo-oxidation in RPE cells by quenching singlet oxygen	[258]
	Oxidative stress in *Abca4/Bco2* double knock-out mice induced by light	2.5 mg	↓ levels of A2E and isoA2E in RPE/choroid and increased carotenoid accumulation in the retina	[261]

Table 2. *Cont.*

Antioxidant Compound	Experimental Model	Dose	Observation	Citation
Lutein and zeaxanthin	A2E- and blue light-induced photo-oxidation in ARPE-19 cells	10 μM	↓ proteasomal inactivation and changes in MCP-1, CFH, and IL-8	[262]
	Oxidative damage in rat retina induced by light	100 mg/kg	↑ antioxidant capacity, Gnat, retinal rho, Rod-arrestin, NCAM, BDNF, NFE2L2, HO-1, GAP43, IGIF, and NGF gene expression levels ↓ levels of pro-inflammatory markers NF-κB and GFAP	[263]
(3R, 3′R)-zeaxanthin	Oxidative damage in rat retina induced by light	100 mg/kg	alleviated oxidative damage by activating antioxidant enzymes ↑ gene expression of Gnat, retinal rho, Rod-arrestin, NCAM, GAP43, NFE2L2, HO-1, and downregulated gene expression of GFAP, NF-κB. ↓ MDA levels, morphological alterations, and edema in the retinal layer	[264]
Astaxanthin	Oxidative damage in 661W photoreceptor cells induced by light	5–50 μM	↑ expression of phase II antioxidant enzymes and suppressed ROS production and apoptotic markers by activating PI3K/Akt and NFE2L2 signaling pathway	[265]
Fucoxanthin	Phagocytosis disruption in ARPE-19 cells mediated by light and lipid peroxidation	5–20 μg/mL	↓ ROS, MDA, TNF-α, IL-1β, and IL-6 levels recovered phagocytic index via NFE2L2 pathway	[266]
Crocin	Photoreceptor degeneration in bovine and primate primary retinal cells mediated by light	80–160 μM	↓ photoreceptor cell death (EC_{50} 30 μM) ↓ number of TUNEL-positive cells	[267]
Hexahydrocurcumin	Oxidative injury in ARPE-19 and primary mice RPE cells induced by light	1–15 μM	↓ oxidative and ER stress-induced damage by promoting autophagic flux	[268]
Epicatechin	AGE-induced retinal apoptosis in diabetic rats	50–100 mg/kg 0.01–1 μM	↓ AGE accumulation in the retina and enhanced in vitro glycated human serum albumin breaking activity (cross-link breaking activity) ↓ number of TUNEL-positive cells	[269]
Epigallocatechin gallate	TNF-α elicited oxidative stress in ARPE-19 cells	10–100 μM	↓ ROS generation, monocyte RPE adhesion, IkB degradation, ICAM-1, and phosphorylated NF-κB expression via NF-κB signaling	[270]
	Photoreceptor damage in mice retina induced by light	50 mg/kg	Preserved photoreceptor morphology, increased amplitude of ERG waves ↑ mRNA expression of SOD2	[271]
Resveratrol	Phototoxicity in A2E-laden ARPE-19 cells induced by light	25 μM	↓ apoptosis by preserving transepithelial resistance, cytoskeleton architecture, Preserved intracellular redox balance, and mitochondrial integrity	[272]

Table 2. *Cont.*

Antioxidant Compound	Experimental Model	Dose	Observation	Citation
Phloroglucinol	atRAL induced oxidative stress in rat primary RPE cells	0.5–50 μg/mL	↑ cell viability ameliorated retinal morphology ↓ A2E formation and producing chromene adduct	[274]
Paeoniflorin	atRAL induced oxidative injury in ARPE-19 cells	50–200 μM	↓ ROS levels, mitochondrial dysfunction, and ER stress due to Ca^{2+}/CaMKII-mediated AMPK activation	[275]
Oleuropein	Inflammatory injury in ARPE-19 cells stimulated by IL-1β	3–100 μM	↓ secretion of IL-6, sICAM-1, and MCP-1 by blocking p38 MAPK and JNK1/2 pathways	[276]
Berberine	Light-mediated photoreceptor damage in mice retina	200 mg/kg	ameliorated distortion in the photoreceptor layer, ERG activity, and number of TUNEL-positive photoreceptor cells ↑ Rho, Rpe65, and mct3 mRNA expression ↓ oxidative stress by repression of oxidative stress mRNA expression, MDA, and expression of microglia/macrophages	[277]
Puerarin	Apoptosis induced by AGE-BSA in rats and bovine retinal pericytes	10 μM 1–10 μM	Ameliorated retinal microvasculature by ↓ ROS levels, NADPH oxidase activity, and pericyte apoptosis via suppression of Rac1, p47phox, and NF-κB.	[278]
Nepetin	Inflammation in ARPE-19 cells mediated by IL-1β	2.5–10 μM	↓ secretion of IL-8, IL-6, and MCP-1 by repressing the NF-κB and MAPKs activation	[279]

5.3. Plant Extracts

Table 3 shows the antioxidant activity of several plant extracts under oxidative stress conditions in the retina, a cultured RPE, and photoreceptor cells mimicking dry AMD pathogenesis. A considerable amount of studies have been published reporting the potential effect of plant extracts for the protection of a highly susceptible RPE and retina against oxidative stress. The phenolic compounds in the self-heal (*Prunella vulgaris* L.) extract decreased A2E accumulation and apoptosis in A2E-laden RPE cells by upregulating antioxidant NFE2L2/HO-1 signaling and suppressing pro-inflammatory gene expression [280]. In another study, wolfberry water extract prevented apoptosis by preserving the mitochondrial membrane potential against elevated oxidative stress markers [281]. Indian english gurjun tree (*Dipterocarpus tuberculatus* Roxb.) and sweet corn extract attenuated the generation of inflammatory mediators in cultured RPE cells [282,283]. *Ginkgo biloba* L. extract protects light-induced damage in rat retinas by increasing levels of antioxidant enzymes [284]. The amelioration of retinal architecture and the inhibition of apoptosis by ginseng berry extract was reported by Cho et al. [285] in A2E-loaded ARPE-19 cells. The decreased accumulation of A2E and increased cell viability was reported for *Arctium lappa* L., *Vaccinium uliginosum* L., *Solanum melongena* L., *Ribes nigrum* L., and *Chrysanthemum boreale* M. extract in RPE cells under oxidative stress [286–290]. *Curcuma longa* L. extract and its fractions inhibited apoptosis by the downregulation of c-Abl and p53 mRNA expression [291]. Maccarone et al. [292] reported the cytoprotective action of saffron (*Crocus sativus* L.) extract on the photoreceptor and ONL layer. In another study, phenolic acids, β-carotene, and tocopherols present in microalgae (*Spirulina maxima*) extract suppressed inflammatory gene expression and apoptosis preventing macular degeneration [293]. Rosemary (*Rosmarinus officinalis* L.) extract decreased the formation of a CEP protein adduct and suppressed the loss of opsin and arrestin from cone cells in rat retina induced by light [294]. The phenol-rich fractions of blueberry reduced intracellular ROS generation

and improved the phagocytic index in ARPE-19 cells under light–lipid elicitation [295]. In another study, blueberry anthocyanin extract suppressed premature senescence in ARPE-19 cells by preventing ROS generation and apoptosis [296]. Flaxseed (*Linum usitatissimum* L.) oil protected light-induced oxidative damage in rat retina by decreasing MDA and protein carbonyls and increasing levels of SOD, GSH, and GSH-Px. The exhibited activity can be linked to high unsaturated fatty acid content [297]. Cranberry (*V. macrocarpon* Ait.) juice fractions also contributed to increased cell viability by displaying greater free radical scavenging activity [298]. Similar activity was also reported in photoreceptor (661W) cells by purple rice extract [299]. In another study, coconut (*Cocos nucifera* L.) oil prevented light-induced oxidative damage in rat retina by suppressing the MDA generation and caspase-3 activity [300]. Furthermore, bilberry (*V. myrtillus* L.) and lingonberry (*V. vitis-idea* L.) extract protected photoreceptor (661W) cells damage during oxidative stress by suppression of NF-κB, p38 MAPK activation and LC3-I to LC3-II conversion [301]. Grape skin extract suppressed ER stress-mediated apoptosis in A2E-loaded ARPE-19 cells [302]. *Cistanche tubulosa* (Schrenk) Hook is an important Chinese traditional medicinal plant, which imparts a wide spectrum of biological activity including antioxidant, neuroprotection, anti-aging, and anti-inflammation primarily due to phenylethanoid glycosides. *C. tubulosa* extract suppressed apoptosis in blue light-induced retinal degeneration by decreasing the expression of caspase 3 and inhibiting the phosphorylation of c-JNK, p38, and ERK1/2 [303]. It has been conclusively shown that different plant extracts have shown increased promise to combat oxidative stress and its implications to revert AMD pathogenesis, which needs to be validated with further clinical studies.

Table 3. Preclinical studies of extracts for combating oxidative stress.

Antioxidant Extract	Experimental Model	Dose	Observation	Citation
Prunella vulgaris L. extract	Retinal damage in A2E-laden ARPE-19 cells and mice retina mediated by blue light	100 μg/mL 100–200 mg/kg	ameliorated cell viability, A2E accumulation, ROS/MDA generation, GSH, and SOD activity due to upregulation of NFE2L2/HO-1 signaling ↓ apoptosis by inhibiting the expression of c-caspase-3 and c-PARP ↓ translocation of NF-κB and upregulation of pro-inflammatory genes IL-1β, IL-6, MCP-1, VEGFA	[280]
Wolfberry water extract	Oxidative injury in A2E-treated ARPE-19 cells and mice retina induced by light	0.1–1 mg/mL 470 mg/kg	↓ ROS accumulation and apoptosis by maintaining mitochondrial membrane potential due to NFE2L2 signaling ↑ antioxidant enzyme genes and decreased MDA levels Increased amplitudes of a and b ERG waves and ONL thickness	[281]
Dipterocarpus tuberculatus Roxb. extract	Macular degeneration induced by A2E and blue light in ARPE-19 cells and retina of mice	50–200 μg/mL 100–200 mg/kg	↑ cytoprotective actions by activating SOD and NFE2L2 and ↓ COX-2, iNOS, NLRP3 inflammasome, and pro-inflammatory cytokine expression depicted increase in thickness of the retina, POS, ONL, and INL in Balb/c mice	[282]
Sweet corn extract	Inflammation in ARPE-19 cells induced by IL-1β	1–100 μg/mL	↓ inflammation by reducing levels of MCP-1, IL-6, IL-8, ICAM-1, and iNOS by inhibiting p65 NF-κB and MAPK signaling pathways	[283]
Ginkgo biloba L. extract	Light-induced oxidative stress and retinal damage in Rats	100 mg/kg	↓ oxidative stress by increasing CAT, T-SOD, GSH-Px, and decreasing MDA levels ↓ apoptosis in photoreceptors within ONL and ameliorated ONL thickness	[284]

Table 3. *Cont.*

Antioxidant Extract	Experimental Model	Dose	Observation	Citation
Ginseng berry extract	Retinal injury in A2E-loaded ARPE-19 cells and mice mediated by light	80 μM 50–200 mg/kg	↓ apoptosis by decreasing the expression of ROS, caspase-3, c-PARP, and apoptotic-related factors ameliorated retinal architecture by restoring thickness of retinal layer repressing inflammation and apoptosis mediated by NF-κB, SIRT1/PGC-1α signaling	[285]
Arctium lappa L. extract	Phototoxicity in A2E-loaded ARPE-19 cells and mice retina induced by light	10–25 μM 100–200 mg/kg	↓ A2E accumulation and suppressed apoptosis signaling in RPE cells. ↓ retinal damage by mitigating histological disturbances in POS, ONL, INL, and GCL.	[286]
Vaccinium uliginosum L. extract and fractions	Phototoxicity in A2E-laden ARPE-19 cells induced by light	12.5–100 μg/mL	↓ intracellular A2E accumulation, photo-oxidation, and apoptosis in RPE cells	[287]
	Retinal damage in A2E-loaded ARPE-19 cells and mice retina induced by light	100–500 μg/mL 25–100 mg/kg	↓ intracellular A2E accumulation and photo-oxidation in RPE cells rescued ONL thickness and nuclei count of the retina in a murine model	[287]
Solanum melongena L. extract	Light-mediated phototoxicity in A2E-laden ARPE-19 cells and mice retina	10–100 μg/mL 100–200 mg/kg	↓ ROS level, A2E accumulation, and downregulated NF-κB genes (IL-1β and CXCL8) ↓ fundus damage and retinal layer degeneration in BALB/c mice	[288]
Ribes nigrum L. extract	Macular degeneration in A2E-loaded ARPE-19 cells and mice retina mediated by light	10–50 μg/mL 25–100 mg/kg	↓ the accumulation of LF and ROS levels ↓ ocular lesions in mice retina and rescued the whole retina, POS, ONL, and INL thickness	[289]
Chrysanthemum boreale M. flower extract	Oxidative injury in ARPE-19 cells laden with A2E	5–30 μg/mL (different fractions)	↓ intracellular A2E accumulation and increased cell viability	[290]
Curcuma longa L. extract and fractions	Cytotoxicity in A2E-laden ARPE-19 cells induced by light	10 μg/mL 15 μM	↓ apoptosis by downregulation of c-Abl and p53 mRNA expression	[291]
Crocus sativus L. extract	Retinal stress in rats induced by light	1 mg/kg	ameliorated photoreceptor and ONL layer by preventing apoptosis	[292]
Spirulina maxima extract	Macular degeneration mediated by A2E and light in ARPE-19 cells and mice	100 μg/mL 50–200 mg/kg	↓ ROS production and downregulated inflammatory gene expression and apoptosis restored ONL thickness of the whole retina, POS, ONL, and INL	[293]
Rosemary Extract	Oxidative injury and retinal damage in rats induced by light	1.3 mg/kg 17 mg/kg	ameliorated oxidative stress protein markers, cell viability, photoreceptor morphology, and DNA degradation ↓ formation of CEP protein adduct and suppressed loss of opsin and arrestin from cone cells	[294]
Blueberry phenol-rich fraction	Light–lipid elicited oxidative injury in ARPE-19 cells	10 μg/mL	↓ intracellular ROS generation and ↑ phagocytic index ↓ SA -β-gal and VEGF expression	[295]

Table 3. *Cont.*

Antioxidant Extract	Experimental Model	Dose	Observation	Citation
Blueberry anthocyanin extract	Premature senescence in ARPE-19 cells induced by light	0.1–10 μg/mL	↓ oxidative damage by ↓ ROS levels, VEGF expression, and apoptosis ↓ percentage of senescent cells as depicted by β-galactosidase positive staining	[296]
Linum usitatissimum L. oil	Oxidative injury and apoptosis in rat retina induced by light	4 mL/kg	↓ photoreactive retinal damage by ↓ protein carbonyl and MDA levels and increasing SOD, GSH, and GSH-Px activity	[297]
Cranberry juice fractions	Oxidative injury in ARPE-19 cells due to light	5–50 μg/mL	↑ free radical scavenging activity and cell viability	[298]
Purple rice extract	Oxidative injury in murine photoreceptor 661W cells and retina induced by light	3–30 μg/mL 10 μg/eye	↑ cell viability and ↓ ROS generation ↑ free radical scavenging activity	[299]
Cocos nucifera L. oil	Oxidative stress and retinal injury in rats induced by light	5 mL/kg	↓ MDA levels and caspase-3 activity	[300]
Bilberry and lingonberry extract	Oxidative injury in murine photoreceptor 661W cells induced by light	10 μg/mL	Protected photoreceptor cell damage by ↓ ROS generation and ↓ NF-κB, p38 MAPK activation, and LC3-I to LC3-II conversion. ↓ apoptosis by ↓ caspase-3/7 activity	[301]
Grape skin extracts	Oxidative injury in A2E-treated ARPE-19 cells	5–25 μM	↓ ROS and suppressed ER stress-mediated apoptosis in a dose-dependent manner	[302]
Cistanche tubulosa (Schrenk) Hook. F. extract	Light-induced degenerative neuropathy in ARPE-19 and rat RPE cells	50–100 μg/mL 100 mg/kg	↓ expression of caspase-3 and number of TUNEL-positive cells ↓ phosphorylation of c-JNK, ERK 1/2, and p38 ameliorated retinal thickness	[303]

5.4. Endogenous Substances

Table 4 shows the antioxidant activity of several endogenous substances in rat/mice retina, primary RPE cells, and cultured ARPE-19 cells under oxidative stress conditions mimicking dry AMD pathogenesis. The clinical practice of using endogenous substances as a therapeutic approach against oxidative injuries and inflammation is called resolution pharmacology. Exploring endogenous substances for disease management can be the ideal biomimetic approach to modulate the targeted signaling pathways [304]. Taurine (2-amino sulfonic acid) is a cytoprotective non-proteinogenic amino acid, which regulates diverse functions including osmoregulation, antioxidant response, bile acid conjugation, calcium ion regulation, and lipid metabolism. It preserved the retinal morphology, increased SOD, and GSH-Px expression, and prevented photoreceptor apoptosis in rat retina via AP1/NF-κB/caspase-1 signaling [305]. Tanito et al. [306] reported decreased expression of tyrosine phosphorylated and oxidized proteins in the retina of mice treated with thioredoxin, a crucial ubiquitous redox-active protein. Lipoxin A4 is a bioactive lipid molecule derived from arachidonic acid and regulates tissue homeostasis by resolution of inflammation. This anti-inflammatory mediator modulated the Keap1/NFE2L2/ARE/HO-1 pathway to decrease ROS generation in ARPE-19 cells and ONL degeneration in the retina of mice under A2E- and light-mediated oxidative injury [307]. In another study, phosphatidylglycerol, a key component of the mitochondrial membrane prevented the detachment of cytochrome c from mitochondria and suppressed apoptosis in A2E-loaded human primary RPE cells [308]. These promising findings corroborate the existing knowledge of the use of endogenous substances against oxidative stress-induced RPE and retinal injury.

Table 4. Preclinical studies of endogenous substances for combating oxidative stress.

Antioxidant Endogenous Substances	Experimental Model	Dose	Observation	Citation
Taurine	Oxidative injury in rat retina induced by light	4 g/100 g diet (4% Taurine)	ameliorated retinal morphology, ONL thickening, and amplitude of a and b ERG waves ↓ MDA level, ↑ SOD, GSH-Px expression, and prevented photoreceptor apoptosis via AP1/NF-κB/caspase-1 mechanism	[305]
Thioredoxin	Oxidative injury in mice retina induced by light	5 μg	↓ the number of TUNEL-positive nuclei and degeneration of photoreceptor cells ↑ thioredoxin expression in retinal and RPE ↓ expression of tyrosine phosphorylated and oxidized proteins in the retina	[306]
Lipoxin A4	A2E- and light-mediated oxidative injury in ARPE-19 cells and mice retina	50–100 nM	↓ ROS production and maintained the tight junctions of RPE by modulating the Keap1/NFE2L2/ARE/HO-1 pathway ↓ ONL degeneration in the retina of mice	[307]
Phosphatidylglycerol	A2E-mediated apoptosis in human primary RPE cells	2–50 μg/mL	↓ apoptosis by preventing detachment of cytochrome c in mitochondria	[308]

5.5. Formulations

Table 5 shows the antioxidant activity of different formulations in rat/mice retina, under oxidative stress conditions mimicking dry AMD pathogenesis. β-cryptoxanthin (BCX) is a pro-vitamin A carotenoid richly found in papaya, peaches, oranges, tangerines, and maize. Dietary oral supplementation of BCX (2–4 mg/kg dose) to rats for 4 weeks suppressed retinal oxidative damage induced by light. It reduced the oxidative and mitochondrial stress markers and ameliorated retinal thickness. Furthermore, it also alleviated inflammatory and apoptotic markers to prevent retinal degeneration [309]. KIOM-79, an 80% ethanolic extract prepared from Glycyrrhiza root, pueraria root, Euphorbia root, and Magnolia bark. It alleviates DNA damage and methylglyoxal accumulation in the primary retinal pericytes of rats [310]. In another novel approach for managing dry AMD and Stargardt's disease, Vincent et al. [311] reported photoreceptor protection by phloroglucinol-isopropyl-DHA (IP-DHA), a lipophenol drug incorporated in a self-nanoemulsifying drug delivery system (SNEDDS) under acute and chronic light stress. It is irrefutably pivotal to highlight the rationale for the development of antioxidant formulations incorporating evidence-based antioxidants to effectively counteract the detrimental effect of oxidative damage. Antioxidants might possess a risk of being metabolized by the enzymes in the body reducing their bioavailability and efficacy. So, improving metabolic stability and bioavailability by designing formulation strategies are the two important milestones that antioxidant formulations must overcome for better health outcomes. Furthermore, it is imperative to develop targeted drug delivery to the specific retinal layer or pathological site by overcoming the formidable blood–retinal barrier for effective treatment.

Table 5. Preclinical studies of formulations for combating oxidative stress.

Antioxidant Formulation	Experimental Model	Dose	Observation	Citation
BCX oral formulation	Oxidative injury in rat retina due to light	2–4 mg/kg	↓ MDA levels rescued antioxidant enzyme level and retinal and ONL thickening ameliorated mitochondrial stress markers (Grp78, Grp94, ATF4, ATF6), growth factors (VEGF, GAP43), neuronal protein (GFAP, NCAM), inflammatory mediators (IL-1β, IL-6, NF-κB), apoptotic proteins (caspase-3, Bax, Bcl-2), and antioxidant HO-1 levels	[309]

Table 5. *Cont.*

Antioxidant Formulation	Experimental Model	Dose	Observation	Citation
KIOM-79	Methylglyoxal-induced apoptosis in primary retinal pericytes of rats	10 μg/mL	ameliorated retinal microvasculature and ↓ ROS generation, oxidative DNA damage, and methylglyoxal accumulation	[310]
	AGE-induced apoptosis in rat retinal pericyte	50 mg/kg	ameliorated retinal vasculature, suppressed NF-κB activation, and inhibited pericyte apoptosis	[312]
SNEDDS loaded lipophenol	Retinal degeneration in Abca4 knock-out mice induced by light	50–100 mg/kg	↓ photoreceptor degeneration ↑ amplitudes of a and b ERG waves ↑ INL and ONL thickness in the retina	[311]

5.6. Synthetic Compounds

Table 6 shows the antioxidant activity of several synthetic compounds in rat/mice retina, primary RPE cells, and cultured ARPE-19 cells under oxidative stress conditions mimicking dry AMD pathogenesis. Naloxone is an antagonist of opioid receptors and is used for the reversal of opioid toxicity. It reduced OX42-positive microglia and TUNEL-positive ONL in light-induced rat retina [313]. Zhang et al. reported the protection of light-induced retinal degeneration in mice by a tetracycline antibiotic: minocycline [314]. It also exhibits antioxidant, anti-inflammatory, and anti-apoptotic activities [315]. In another study, fenofibrate, a peroxisome proliferator-activated receptor type α (PPAR-α) agonist, reversed the iron-induced upregulation of Wnt/β-catenin signaling in ARPE-19 cells and mouse model under iron-induced oxidative stress [316]. OT-674, the reduction product (Tempol-H) of the nitroxide tempol, exhibited increased cell viability and singlet oxygen quenching in A2E-loaded and light-irradiated ARPE-19 cells. This can be attributed to its antioxidant activity [317]. Extrapolating these findings, we can conclude that exploration for the repurposing of synthetic compounds effective against oxidative stress can be a potential game changer for preserving vision in dry AMD research.

Table 6. Preclinical studies of synthetic compounds for combating oxidative stress.

Synthetic Compound	Experimental Model	Dose	Observation	Citation
Naloxone	Photoreceptor degeneration in rats induced by light	1 mg/mL	↓ number of OX42-positive microglia and TUNEL-positive ONL in the retina ↓ expression of IL-1β and preserved amplitude of a and b ERG waves	[313]
Minocycline	Retinal degeneration in mice induced by light	45 mg/kg	ameliorated loss of photoreceptor cells and depicted marked preservation of outer retina preserved amplitudes of a and b ERG waves	[314]
Fenofibrate	Iron-induced oxidative stress in ARPE-19 cells and mouse model	50–100 μM	reversed iron-induced upregulation of Wnt/β-catenin signaling owing to chelation of iron	[316]
OT-674	Oxidative stress in A2E-loaded and light-irradiated ARPE-19 cells	0.01–10 mM	↑ cell viability and ↓ photo-oxidation by quenching singlet oxygen	[317]

6. Gene Therapy for Regulation of Antioxidant Gene Expression

Apart from antioxidant-based therapies, gene therapy for mitigating oxidative stress by modulating gene expression presents an emerging avenue. Manipulating specific antioxidant genes or genes regulating cellular pathways involved in oxidative stress and inflammation can alleviate the pathogenesis of AMD [318]. Gene therapy aims to deliver therapeutic genes using viral vectors. Adeno-associated virus (AAV) and lentivirus (LV) vectors

are widely used delivery vehicles for ocular gene therapy [319]. In 2017, the FDA approved Luxturna, the first intraocular AAV-based gene therapy for treating RPE-65-mediated retinal disease. Other gene therapies, including AAVCAGsCD59 (NCT03144999, Phase I), RGX-314 (NCT048322724, Phase II), ADVM-022 (NCT05536973, Phase II), GT-005 (NCT04437368, Phase II), NG101 AAV (NCT05984927, Phase II), KH631 (NCT05672121, Phase I/II), FT-003 (NCT05611424, Phase I), LX102 (NCT06196840, Phase II), SKG0106 (NCT05986864, Phase I/II), RRG001 (NCT06141460, Phase I/II), and 4D-150 (NCT055197270, Phase I/II), are ongoing in clinical trials. Gene therapy aims to achieve sustained improvement in vision through single subretinal or intravitreal injection for both dry and wet AMD, leading to a decrease in the need for frequent administration [320] For detailed insights into gene therapy for AMD, we recommend consulting the following references for a comprehensive understanding [321].

7. Conclusions and Future Prospects

AMD is a multifactorial neurodegenerative disease affecting central vision and is responsible for severe vision loss. The major etiology for AMD includes age, smoking, diet, genetics, and oxidative stress, which are mainly the generators of ROS. Chronic oxidative stress-induced activation of inflammatory signaling cascade and a compromised autophagy and proteasome system play a central role in AMD pathogenesis. Growing shreds of evidence have also highlighted mitochondrial dysfunction and ER stress in an aging RPE as important determinants in AMD. Supplementation with dietary antioxidants can effectively halt the progression of AMD for better functional outcomes, so there is an urgent need to translate scientific knowledge of evidence-based antioxidants into practical solutions. Furthermore, interventions targeting the upregulation of endogenous antioxidant defenses against oxidative stress can be potential therapeutic avenues for preventing or slowing down the progression of retinal degeneration by promoting cytoprotective signaling pathways. The synergistic combination of multiple antioxidants can also be a robust therapeutic approach for improving vision functionality and durability by targeting the lesions in AMD. Meanwhile, most of the suggested compounds, formulations, and extracts have not been endorsed by the USFDA for clinical use; thus, caution is advised for ophthalmologists when recommending these products. Also, the potential harms of high-dose antioxidant supplementation warrant thorough investigation. Critical pharmacokinetic parameters including bioavailability and metabolism as well as toxicokinetics of antioxidants need to be wisely considered for better clinical outcomes. Furthermore, large-scale clinical studies are required to warrant their risk–benefit ratio.

Therapeutic strategies for halting A2E accumulation and oxidation, drusen formation, and the upregulation of autophagy and proteasome machinery in the senescent retina can be another attractive avenue. Moreover, prospective studies are required to unfold the crosstalk between oxidative stress and AMD pathology to explore novel targets, biomarkers, and signaling pathways involved in disease progression. Aging is a significant contributor to AMD, and its interconnection with chronic and progressive macular degeneration needs to be thoroughly explored. The identification of specific and reliable biomarkers for early detection and prognosis is critical for successful preventive and therapeutic strategies. Additionally, identifying specific molecular targets taking account of personalized genetic information is also crucial by employing therapeutic genes encoding antioxidant enzymes. Finally, AMD is a multifactorial disease, and considering multifaceted interventions to cope with multiple pathological mechanisms can be a critical avenue.

Author Contributions: Writing—original draft preparation, D.B.; writing—review and editing, D.B., S.L. and H.J.K.; funding acquisition, S.L. All authors have read and agreed to the published version of the manuscript.

Funding: This research was supported by the Basic Science Research Program through the National Research Foundation of Korea (NRF) funded by the Ministry of Education (NRF-2016R1A6A1A03011325) and the Bisa Research Grant of Keimyung University in 2022.

Acknowledgments: Figures were created with www.biorender.com (accessed on 22 February 2024).

Conflicts of Interest: The authors declare no conflicts of interest.

References

1. Rahal, A.; Kumar, A.; Singh, V.; Yadav, B.; Tiwari, R.; Chakraborty, S.; Dhama, K. Oxidative stress, prooxidants, and antioxidants: The interplay. *Biomed Res. Int.* **2014**, *2014*, 761264. [CrossRef]
2. Chen, X.; Guo, C.; Kong, J. Oxidative stress in neurodegenerative diseases. *Neural Regen. Res.* **2012**, *7*, 376. [PubMed]
3. Tezel, G. Multifactorial pathogenic processes of retinal ganglion cell degeneration in glaucoma towards multi-target strategies for broader treatment effects. *Cells* **2021**, *10*, 1372. [CrossRef] [PubMed]
4. Nita, M.; Grzybowski, A. The role of the reactive oxygen species and oxidative stress in the pathomechanism of the age-related ocular diseases and other pathologies of the anterior and posterior eye segments in adults. *Oxid. Med. Cell. Longev.* **2016**, *2016*, 3164734. [CrossRef]
5. Khorrami-Nejad, M.; Sarabandi, A.; Akbari, M.-R.; Askarizadeh, F. The impact of visual impairment on quality of life. *Med. Hypothesis Discov. Innov. Ophthalmol.* **2016**, *5*, 96. [PubMed]
6. Nowak, J.Z. Age-related macular degeneration (AMD): Pathogenesis and therapy. *Pharmacol. Rep.* **2006**, *58*, 353. [PubMed]
7. Liguori, I.; Russo, G.; Curcio, F.; Bulli, G.; Aran, L.; Della-Morte, D.; Gargiulo, G.; Testa, G.; Cacciatore, F.; Bonaduce, D. Oxidative stress, aging, and diseases. *Clin. Interv. Aging* **2018**, *13*, 757–772. [CrossRef]
8. Jadeja, R.N.; Martin, P.M. Oxidative stress and inflammation in retinal degeneration. *Antioxidants* **2021**, *10*, 790. [CrossRef]
9. Andre, C.M.; Larondelle, Y.; Evers, D. Dietary antioxidants and oxidative stress from a human and plant perspective: A review. *Curr. Nutr. Food Sci.* **2010**, *6*, 2–12. [CrossRef]
10. Tan, B.L.; Norhaizan, M.E.; Liew, W.-P.-P.; Sulaiman Rahman, H. Antioxidant and oxidative stress: A mutual interplay in age-related diseases. *Front. Pharmacol.* **2018**, *9*, 1162. [CrossRef]
11. Kunwar, A.; Priyadarsini, K. Free radicals, oxidative stress and importance of antioxidants in human health. *J. Med. Allied Sci.* **2011**, *1*, 53–60.
12. Van Leeuwen, R.; Boekhoorn, S.; Vingerling, J.R.; Witteman, J.C.; Klaver, C.C.; Hofman, A.; de Jong, P.T. Dietary intake of antioxidants and risk of age-related macular degeneration. *JAMA* **2005**, *294*, 3101–3107. [CrossRef]
13. Dziedziak, J.; Kasarełło, K.; Cudnoch-Jędrzejewska, A. Dietary antioxidants in age-related macular degeneration and glaucoma. *Antioxidants* **2021**, *10*, 1743. [CrossRef]
14. Arslan, S.; Kadayifçilar, S.; Samur, G. The potential role of dietary antioxidant capacity in preventing age-related macular degeneration. *J. Am. Coll. Nutr.* **2019**, *38*, 424–432. [CrossRef] [PubMed]
15. Wang, P.; Chin, E.K.; Almeida, D. Antioxidants for the treatment of retinal disease: Summary of recent evidence. *Clin. Ophthalmol.* **2021**, *15*, 1621–1628. [CrossRef]
16. Commissioning Guidance: Age-related Macular Degeneration Services. The Royal College of Ophthalmologists. 2021. Available online: https://www.rcophth.ac.uk/wp-content/uploads/2021/08/AD-Commissioning-Guidance-Full-June-2021.pdf (accessed on 22 April 2024).
17. Jonas, J.B.; Weber, P.; Nagaoka, N.; Ohno-Matsui, K. Temporal vascular arcade width and angle in high axial myopia. *Retina* **2018**, *38*, 1839–1847. [CrossRef] [PubMed]
18. Mozaffarieh, M.; Sacu, S.; Wedrich, A. The role of the carotenoids, lutein and zeaxanthin, in protecting against age-related macular degeneration: A review based on controversial evidence. *Nutr. J.* **2003**, *2*, 20. [CrossRef] [PubMed]
19. Bodis-Wollner, I. Foveal vision is impaired in Parkinson's disease. *Park. Relat. Disord.* **2013**, *19*, 1–14. [CrossRef]
20. Khandhadia, S.; Lotery, A. Oxidation and age-related macular degeneration: Insights from molecular biology. *Exp. Rev. Mol. Med.* **2010**, *12*, e34. [CrossRef] [PubMed]
21. Tran, H.T.; Nguyen, D.V.; Ngoc, N.P.; Hoang, T.H.; Huong, T.T.; Thang, T.C. Impacts of retina-related zones on quality perception of omnidirectional image. *IEEE Access* **2019**, *7*, 166997–167009. [CrossRef]
22. Hogg, R.; Chakravarthy, U. Visual function and dysfunction in early and late age-related maculopathy. *Prog. Retin. Eye Res.* **2006**, *25*, 249–276. [CrossRef] [PubMed]
23. Datta, S.; Cano, M.; Ebrahimi, K.; Wang, L.; Handa, J.T. The impact of oxidative stress and inflammation on RPE degeneration in non-neovascular AMD. *Prog. Retin. Eye Res.* **2017**, *60*, 201–218. [CrossRef] [PubMed]
24. Stahl, A. The diagnosis and treatment of age-related macular degeneration. *Dtsch. Arztebl. Int.* **2020**, *117*, 513. [CrossRef]
25. Bhutto, I.; Lutty, G. Understanding age-related macular degeneration (AMD): Relationships between the photoreceptor/retinal pigment epithelium/Bruch's membrane/choriocapillaris complex. *Mol. Asp. Med.* **2012**, *33*, 295–317. [CrossRef] [PubMed]
26. Metelitsina, T.I.; Grunwald, J.E.; DuPont, J.C.; Ying, G.-S.; Brucker, A.J.; Dunaief, J.L. Foveolar choroidal circulation and choroidal neovascularization in age-related macular degeneration. *Investig. Ophthalmol. Vis. Sci.* **2008**, *49*, 358–363. [CrossRef] [PubMed]
27. Papadopoulos, Z. Recent developments in the treatment of wet age-related macular degeneration. *Curr. Med. Sci.* **2020**, *40*, 851–857. [CrossRef] [PubMed]
28. Buschini, E.; Fea, A.M.; Lavia, C.A.; Nassisi, M.; Pignata, G.; Zola, M.; Grignolo, F.M. Recent developments in the management of dry age-related macular degeneration. *Clin. Ophthalmol.* **2015**, *9*, 563–574. [CrossRef] [PubMed]

29. Heier, J.S.; Lad, E.M.; Holz, F.G.; Rosenfeld, P.J.; Guymer, R.H.; Boyer, D.; Grossi, F.; Baumal, C.R.; Korobelnik, J.-F.; Slakter, J.S. Pegcetacoplan for the treatment of geographic atrophy secondary to age-related macular degeneration (OAKS and DERBY): Two multicentre, randomised, double-masked, sham-controlled, phase 3 trials. *Lancet* **2023**, *402*, 1434–1448. [CrossRef]
30. Liao, D.S.; Grossi, F.V.; El Mehdi, D.; Gerber, M.R.; Brown, D.M.; Heier, J.S.; Wykoff, C.C.; Singerman, L.J.; Abraham, P.; Grassmann, F.; et al. Complement C3 inhibitor pegcetacoplan for geographic atrophy secondary to age-related macular degeneration: A randomized phase 2 trial. *Ophthalmology* **2020**, *127*, 186–195. [CrossRef] [PubMed]
31. Crabb, J.W. The proteomics of drusen. *Cold Spring Harb. Perspect. Biol.* **2014**, *4*, a017194. [CrossRef]
32. Curcio, C.A.; Johnson, M. Structure, function, and pathology of Bruch's membrane. *Retina* **2013**, *1*, 466–481.
33. Zhang, X.; Sivaprasad, S. Drusen and pachydrusen: The definition, pathogenesis, and clinical significance. *Eye* **2021**, *35*, 121–133. [CrossRef] [PubMed]
34. Johnson, L.V.; Leitner, W.P.; Staples, M.K.; Anderson, D.H. Complement activation and inflammatory processes in Drusen formation and age related macular degeneration. *Exp. Eye Res.* **2001**, *73*, 887–896. [CrossRef]
35. Anderson, D.H.; Mullins, R.F.; Hageman, G.S.; Johnson, L.V. A role for local inflammation in the formation of drusen in the aging eye. *Am. J. Opthalmol.* **2002**, *134*, 411–431. [CrossRef] [PubMed]
36. Hageman, G.S.; Mullins, R.F. Molecular composition of drusen as related to substructural phenotype. *Mol. Vis.* **1999**, *5*, 10562652.
37. Zhou, J.; Jang, Y.P.; Kim, S.R.; Sparrow, J.R. Complement activation by photooxidation products of A2E, a lipofuscin constituent of the retinal pigment epithelium. *Proc. Natl. Acad. Sci. USA* **2006**, *103*, 16182–16187. [CrossRef]
38. Knickelbein, J.E.; Chan, C.-C.; Sen, H.N.; Ferris, F.L.; Nussenblatt, R.B. Inflammatory mechanisms of age-related macular degeneration. *Int. Ophthalmol. Clin.* **2015**, *55*, 63. [CrossRef]
39. Abdelsalam, A.; Del Priore, L.; Zarbin, M.A. Drusen in age-related macular degeneration: Pathogenesis, natural course, and laser photocoagulation-induced regression. *Surv. Ophthalmol.* **1999**, *44*, 1–29. [CrossRef]
40. Rudolf, M.; Clark, M.E.; Chimento, M.F.; Li, C.M.; Medeiros, N.E.; Curcio, C.A. Prevalence and morphology of druse types in the macula and periphery of eyes with age-related maculopathy. *Investig. Ophthalmol. Vis. Sci.* **2008**, *49*, 1200–1209. [CrossRef]
41. Roquet, W.; Roudot-Thoraval, F.; Coscas, G.; Soubrane, G. Clinical features of drusenoid pigment epithelial detachment in age related macular degeneration. *Br. J. Ophthalmol.* **2004**, *88*, 638–642. [CrossRef]
42. Luhmann, U.F.; Robbie, S.; Munro, P.M.; Barker, S.E.; Duran, Y.; Luong, V.; Fitzke, F.W.; Bainbridge, J.W.; Ali, R.R.; MacLaren, R.E. The drusenlike phenotype in aging Ccl2-knockout mice is caused by an accelerated accumulation of swollen autofluorescent subretinal macrophages. *Investig. Ophthalmol. Vis. Sci.* **2009**, *50*, 5934–5943. [CrossRef]
43. Tuo, J.; Bojanowski, C.M.; Zhou, M.; Shen, D.; Ross, R.J.; Rosenberg, K.I.; Cameron, D.J.; Yin, C.; Kowalak, J.A.; Zhuang, Z.; et al. Murine ccl2/cx3cr1 deficiency results in retinal lesions mimicking human age-related macular degeneration. *Investig. Ophthalmol. Vis. Sci.* **2007**, *48*, 3827–3836. [CrossRef]
44. Spaide, R.F.; Ooto, S.; Curcio, C.A. Subretinal drusenoid deposits AKA pseudodrusen. *Surv. Ophthalmol.* **2018**, *63*, 782–815. [CrossRef]
45. Schmitz-Valckenberg, S. The Journey of "Geographic Atrophy" through Past, Present, and Future. *Ophthalmologica* **2017**, *237*, 11–20. [CrossRef]
46. Somasundaran, S.; Constable, I.J.; Mellough, C.B.; Carvalho, L.S. Retinal pigment epithelium and age-related macular degeneration: A review of major disease mechanisms. *J. Clin. Exp. Ophthalmol.* **2020**, *48*, 1043–1056. [CrossRef]
47. Plafker, S.M.; O'Mealey, G.B.; Szweda, L.I. Mechanisms for countering oxidative stress and damage in retinal pigment epithelium. *Int. Rev. Cell Mol. Biol.* **2012**, *298*, 135–177.
48. Chen, Y.; Bedell, M.; Zhang, K. Age-related macular degeneration: Genetic and environmental factors of disease. *Mol. Interv.* **2010**, *10*, 271–281. [CrossRef]
49. Age-Related Macular Degeneration Guidelines for Management. The Royal College of Ophthalmologists. 2009. Available online: https://www.amedeolucente.it/pdf/age-related_macular_degeneration.pdf (accessed on 22 April 2024).
50. Agrón, E.; Mares, J.; Clemons, T.E.; Swaroop, A.; Chew, E.Y.; Keenan, T.D.L. Dietary nutrient intake and progression to late age-related macular degeneration in the age-related eye disease studies 1 and 2. *Ophthalmology* **2021**, *128*, 425–442. [CrossRef] [PubMed]
51. 2019 Clinical Practice Guide for the Diagnosis, Treatment and Management of Age-Related Macular Degeneration. Optometry Australia. Available online: https://www.optometry.org.au/wp-content/uploads/Professional_support/Practice_notes/AMD-Clinical-Practice-Guide-2019_final_designed_v5.pdf (accessed on 22 April 2024).
52. Flaxel, C.J.; Adelman, R.A.; Bailey, S.T.; Fawzi, A.; Lim, J.I.; Vemulakonda, G.A.; Ying, G.S. Age-Related Macular Degeneration Preferred Practice Pattern. *Ophthalmology* **2019**, *127*, 1–65. [CrossRef] [PubMed]
53. Lu, Z.G.; May, A.; Dinh, B.; Lin, V.; Su, F.; Tran, C.; Adivikolanu, H.; Ehlen, R.; Che, B.; Wang, Z.H.; et al. The interplay of oxidative stress and ARMS2-HTRA1 genetic risk in neovascular AMD. *Vessel Plus* **2021**, *5*, 4. [CrossRef]
54. Sawitzke, J.; Im, K.M.; Kostiha, B.; Dean, M.; Gold, B. Association assessment of copy number polymorphism and risk of age-related macular degeneration. *Ophthalmology* **2011**, *118*, 2442–2446. [CrossRef] [PubMed]
55. Borras, C.; Canonica, J.; Jorieux, S.; Abache, T.; El Sanharawi, M.; Klein, C.; Delaunay, K.; Jonet, L.; Salvodelli, M.; Naud, M.C.; et al. CFH exerts anti-oxidant effects on retinal pigment epithelial cells independently from protecting against membrane attack complex. *Sci. Rep.* **2019**, *9*, 13873. [CrossRef]

56. Fletcher, E.L.; Jobling, A.I.; Greferath, U.; Mills, S.A.; Waugh, M.; Ho, T.; de Iongh, R.U.; Phipps, J.A.; Vessey, K.A. Studying age-related macular degeneration using animal models. *Optom. Vis. Sci.* **2014**, *91*, 878–886. [CrossRef] [PubMed]
57. Ruan, Y.; Jiang, S.; Gericke, A. Age-related macular degeneration: Role of oxidative stress and blood vessels. *Int. J. Mol. Sci.* **2021**, *22*, 1296. [CrossRef] [PubMed]
58. Lewandowski, D.; Sander, C.L.; Tworak, A.; Gao, F.; Xu, Q.; Skowronska-Krawczyk, D. Dynamic lipid turnover in photoreceptors and retinal pigment epithelium throughout life. *Prog. Retin. Eye Res.* **2022**, *89*, 101037. [CrossRef] [PubMed]
59. Saccà, S.C.; Cutolo, C.A.; Ferrari, D.; Corazza, P.; Traverso, C.E. The eye, oxidative damage and polyunsaturated fatty acids. *Nutrients* **2018**, *10*, 668. [CrossRef] [PubMed]
60. Rapp, L.M.; Maple, S.S.; Choi, J.H. Lutein and zeaxanthin concentrations in rod outer segment membranes from perifoveal and peripheral human retina. *Investig. Ophthalmol. Vis. Sci.* **2000**, *41*, 1200–1209.
61. Shahidi, F.; Zhong, Y. Lipid oxidation and improving the oxidative stability. *Chem. Soc. Rev.* **2010**, *39*, 4067–4079. [CrossRef] [PubMed]
62. Yin, H.; Xu, L.; Porter, N.A. Free radical lipid peroxidation: Mechanisms and analysis. *Chem. Rev.* **2011**, *111*, 5944–5972. [CrossRef]
63. Liu, Y.; Zhang, D.; Hu, J.; Liu, G.; Chen, J.; Sun, L.; Jiang, Z.; Zhang, X.; Chen, Q.; Ji, B. Visible light-induced lipid peroxidation of unsaturated fatty acids in the retina and the inhibitory effects of blueberry polyphenols. *J. Agric. Food Chem.* **2015**, *63*, 9295–9305. [CrossRef]
64. Ayala, A.; Muñoz, M.F.; Argüelles, S. Lipid peroxidation: Production, metabolism, and signaling mechanisms of malondialdehyde and 4-hydroxy-2-nonenal. *Oxid. Med. Cell. Longev.* **2014**, *2014*, 360438. [CrossRef] [PubMed]
65. Micera, A.; Balzamino, B.O.; Di Zazzo, A.; Dinice, L.; Bonini, S.; Coassin, M. Biomarkers of neurodegeneration and precision therapy in retinal disease. *Front. Pharmacol.* **2021**, *11*, 601647. [CrossRef] [PubMed]
66. Gu, X.; Meer, S.G.; Miyagi, M.; Rayborn, M.E.; Hollyfield, J.G.; Crabb, J.W.; Salomon, R.G. Carboxyethylpyrrole protein adducts and autoantibodies, biomarkers for age-related macular degeneration. *J. Biol. Chem.* **2003**, *278*, 42027–42035. [CrossRef] [PubMed]
67. Kaemmerer, E.; Schutt, F.; Krohne, T.U.; Holz, F.G.; Kopitz, J. Effects of lipid peroxidation-related protein modifications on RPE lysosomal functions and POS phagocytosis. *Investig. Ophthalmol. Vis. Sci.* **2007**, *48*, 1342–1347. [CrossRef] [PubMed]
68. Ye, F.; Kaneko, H.; Hayashi, Y.; Takayama, K.; Hwang, S.J.; Nishizawa, Y.; Kimoto, R.; Nagasaka, Y.; Tsunekawa, T.; Matsuura, T.; et al. Malondialdehyde induces autophagy dysfunction and VEGF secretion in the retinal pigment epithelium in age-related macular degeneration. *Free. Radic. Biol. Med.* **2016**, *94*, 121–134. [CrossRef] [PubMed]
69. Yang, L.L.; Chen, H.; Wang, J.; Xia, T.; Sun, H.; Yuan, C.H.; Liu, S.L.; Chen, J.B. 4-HNE induces apoptosis of human retinal pigment epithelial cells by modifying HSP70. *Curr. Med. Sci.* **2019**, *39*, 442–448. [CrossRef] [PubMed]
70. Hollyfield, J.G.; Bonilha, V.L.; Rayborn, M.E.; Yang, X.; Shadrach, K.G.; Lu, L.; Ufret, R.L.; Salomon, R.G.; Perez, V.L. Oxidative damage-induced inflammation initiates age-related macular degeneration. *Nat. Med.* **2008**, *14*, 194–198. [CrossRef] [PubMed]
71. Subramaniam, M.D.; Iyer, M.; Nair, A.P.; Venkatesan, D.; Mathavan, S.; Eruppakotte, N.; Kizhakkillach, S.; kumar Chandran, M.; Roy, A.; Gopalakrishnan, A.V. Oxidative stress and mitochondrial transfer: A new dimension towards ocular diseases. *Genes Dis.* **2022**, *9*, 610–637. [CrossRef]
72. Fuhrmann, S.; Zou, C.; Levine, E.M. Retinal pigment epithelium development, plasticity, and tissue homeostasis. *Exp. Eye Res.* **2014**, *123*, 141–150. [CrossRef]
73. Lakkaraju, A.; Umapathy, A.; Tan, L.X.; Daniele, L.; Philp, N.J.; Boesze-Battaglia, K.; Williams, D.S. The cell biology of the retinal pigment epithelium. *Prog. Retin. Eye Res.* **2020**, *78*, 100846. [CrossRef]
74. Liang, F.-Q.; Godley, B.F. Oxidative stress-induced mitochondrial DNA damage in human retinal pigment epithelial cells: A possible mechanism for RPE aging and age-related macular degeneration. *Exp. Eye Res.* **2003**, *76*, 397–403. [CrossRef] [PubMed]
75. Booij, J.C.; Baas, D.C.; Beisekeeva, J.; Gorgels, T.G.; Bergen, A.A. The dynamic nature of Bruch's membrane. *Prog. Retin. Eye Res.* **2010**, *29*, 1–18. [CrossRef] [PubMed]
76. Bhutto, I.A.; McLeod, D.S.; Hasegawa, T.; Kim, S.Y.; Merges, C.; Tong, P.; Lutty, G.A. Pigment epithelium-derived factor (PEDF) and vascular endothelial growth factor (VEGF) in aged human choroid and eyes with age-related macular degeneration. *Exp. Eye Res.* **2006**, *82*, 99–110. [CrossRef] [PubMed]
77. Mazzoni, F.; Safa, H.; Finnemann, S.C. Understanding photoreceptor outer segment phagocytosis: Use and utility of RPE cells in culture. *Exp. Eye Res.* **2014**, *126*, 51–60. [CrossRef]
78. Sharma, R.; Bose, D.; Maminishkis, A.; Bharti, K. Retinal pigment epithelium replacement therapy for age-related macular degeneration: Are we there yet? *Annu. Rev. Pharmacol. Toxicol.* **2020**, *60*, 553–572. [CrossRef] [PubMed]
79. García-Onrubia, L.; Valentín-Bravo, F.J.; Coco-Martin, R.M.; González-Sarmiento, R.; Pastor, J.C.; Usategui-Martín, R.; Pastor-Idoate, S. Matrix metalloproteinases in age-related macular degeneration (AMD). *Int. J. Mol. Sci.* **2020**, *21*, 5934. [CrossRef]
80. Sadiq, I.Z. Free radicals and oxidative stress: Signaling mechanisms, redox basis for human diseases, and cell cycle regulation. *Curr. Mol. Med.* **2023**, *23*, 13–35. [CrossRef] [PubMed]
81. Wu, L.; Sedgwick, A.C.; Sun, X.; Bull, S.D.; He, X.-P.; James, T.D. Reaction-based fluorescent probes for the detection and imaging of reactive oxygen, nitrogen, and sulfur species. *Acc. Chem. Res.* **2019**, *52*, 2582–2597. [CrossRef] [PubMed]
82. Ifeanyi, O.E. A review on free radicals and antioxidants. *Int. J. Curr. Res. Med. Sci.* **2018**, *4*, 123–133.
83. Sauer, H.; Wartenberg, M.; Hescheler, J. Reactive oxygen species as intracellular messengers during cell growth and differentiation. *Cell. Physiol. Biochem.* **2001**, *11*, 173–186. [CrossRef]

84. Birben, E.; Sahiner, U.M.; Sackesen, C.; Erzurum, S.; Kalayci, O. Oxidative stress and antioxidant defense. *WAO J.* **2012**, *5*, 9–19. [CrossRef]
85. Su, L.J.; Zhang, J.H.; Gomez, H.; Murugan, R.; Hong, X.; Xu, D.; Jiang, F.; Peng, Z.Y. Reactive oxygen species-induced lipid peroxidation in apoptosis, autophagy, and ferroptosis. *Oxid. Med. Cell. Longev.* **2019**, *2019*, 5080843. [CrossRef]
86. Schieber, M.; Chandel, N.S. ROS function in redox signaling and oxidative stress. *Curr. Biol.* **2014**, *24*, R453–R462. [CrossRef] [PubMed]
87. Ray, P.D.; Huang, B.W.; Tsuji, Y. Reactive oxygen species (ROS) homeostasis and redox regulation in cellular signaling. *Cell. Signal.* **2012**, *24*, 981–990. [CrossRef]
88. Du, G.; Jiang, J.; Henning, N.J.; Safaee, N.; Koide, E.; Nowak, R.P.; Donovan, K.A.; Yoon, H.; You, I.; Yue, H.; et al. Exploring the target scope of KEAP1 E3 ligase-based PROTACs. *Cell. Chem. Biol.* **2022**, *29*, 1470–1481.e31. [CrossRef] [PubMed]
89. Cai, N.; Dai, S.D.; Liu, N.N.; Liu, L.M.; Zhao, N.; Chen, L. PI3K/AKT/mTOR signaling pathway inhibitors in proliferation of retinal pigment epithelial cells. *Int. J. Ophthalmol.* **2012**, *5*, 675–680. [PubMed]
90. Yu, H.; Lin, L.; Zhang, Z.; Zhang, H.; Hu, H. Targeting NF-κB pathway for the therapy of diseases: Mechanism and clinical study. *Signal Transduct. Target. Ther.* **2020**, *5*, 209. [CrossRef]
91. Abu Shelbayeh, O.; Arroum, T.; Morris, S.; Busch, K.B. PGC-1α Is a master regulator of mitochondrial lifecycle and ROS stress response. *Antioxidants* **2023**, *12*, 1075. [CrossRef] [PubMed]
92. Hughes, J.M.; Groot, A.J.; van der Groep, P.; Sersansie, R.; Vooijs, M.; van Diest, P.J.; Van Noorden, C.J.; Schlingemann, R.O.; Klaassen, I. Active HIF-1 in the normal human retina. *J. Histochem. Cytochem.* **2010**, *58*, 247–254. [CrossRef]
93. O'Shea, J.J.; Schwartz, D.M.; Villarino, A.V.; Gadina, M.; McInnes, I.B.; Laurence, A. The JAK-STAT pathway: Impact on human disease and therapeutic intervention. *Annu. Rev. Med.* **2015**, *66*, 311–328. [CrossRef]
94. Kong, F.; You, H.; Zheng, K.; Tang, R.; Zheng, C. The crosstalk between pattern-recognition receptor signaling and calcium signaling. *Int. J. Biol. Macromol.* **2021**, *192*, 745–756. [CrossRef] [PubMed]
95. Poljšak, B.; Dahmane, R. Free radicals and extrinsic skin aging. *Dermatol. Res. Pract.* **2012**, *2012*, 135206. [CrossRef]
96. Kim, G.H.; Kim, J.E.; Rhie, S.J.; Yoon, S. The role of oxidative stress in neurodegenerative diseases. *Exp. Neurobiol.* **2015**, *24*, 325. [CrossRef]
97. Ung, L.; Pattamatta, U.; Carnt, N.; Wilkinson-Berka, J.L.; Liew, G.; White, A.J. Oxidative stress and reactive oxygen species: A review of their role in ocular disease. *Clin. Sci.* **2017**, *131*, 2865–2883. [CrossRef] [PubMed]
98. Nebbioso, M.; Franzone, F.; Lambiase, A.; Bonfiglio, V.; Limoli, P.G.; Artico, M.; Taurone, S.; Vingolo, E.M.; Greco, A.; Polimeni, A. Oxidative stress implication in retinal diseases—A review. *Antioxidants* **2022**, *11*, 1790. [CrossRef] [PubMed]
99. Devasagayam, T.P.; Tilak, J.C.; Boloor, K.K.; Sane, K.S.; Ghaskadbi, S.S.; Lele, R.D. Free radicals and antioxidants in human health: Current status and future prospects. *J. Assoc. Physicians India* **2004**, *52*, 794–804. [PubMed]
100. Jomova, K.; Raptova, R.; Alomar, S.Y.; Alwasel, S.H.; Nepovimova, E.; Kuca, K.; Valko, M. Reactive oxygen species, toxicity, oxidative stress, and antioxidants: Chronic diseases and aging. *Arch. Toxicol.* **2023**, *97*, 2499–2574. [CrossRef]
101. Mirończuk-Chodakowska, I.; Witkowska, A.M.; Zujko, M.E. Endogenous non-enzymatic antioxidants in the human body. *Adv. Med. Sci.* **2018**, *63*, 68–78. [CrossRef] [PubMed]
102. Zafrilla, P.; Losada, M.; Perez, A.; Caravaca, G.; Mulero, J. Biomarkers of oxidative stress in patients with wet age related macular degeneration. *J. Nutr. Health Aging* **2013**, *17*, 219–222. [CrossRef]
103. Miao, L.; St Clair, D.K. Regulation of superoxide dismutase genes: Implications in disease. *Free. Radic. Biol. Med.* **2009**, *47*, 344–356. [CrossRef]
104. Imamura, Y.; Noda, S.; Hashizume, K.; Shinoda, K.; Yamaguchi, M.; Uchiyama, S.; Shimizu, T.; Mizushima, Y.; Shirasawa, T.; Tsubota, K. Drusen, choroidal neovascularization, and retinal pigment epithelium dysfunction in SOD1-deficient mice: A model of age-related macular degeneration. *Proc. Natl. Acad. Sci. USA* **2006**, *103*, 11282–11287. [CrossRef] [PubMed]
105. Kushwah, N.; Bora, K.; Maurya, M.; Pavlovich, M.C.; Chen, J. Oxidative stress and antioxidants in age-related macular degeneration. *Antioxidants* **2023**, *12*, 1379. [CrossRef] [PubMed]
106. Brown, E.E.; DeWeerd, A.J.; Ildefonso, C.J.; Lewin, A.S.; Ash, J.D. Mitochondrial oxidative stress in the retinal pigment epithelium (RPE) led to metabolic dysfunction in both the RPE and retinal photoreceptors. *Redox Biol.* **2019**, *24*, 101201. [CrossRef] [PubMed]
107. Anand, A.; Sharma, N.K.; Gupta, A.; Prabhakar, S.; Sharma, S.K.; Singh, R. Superoxide dismutase1 levels in North Indian population with age-related macular degeneration. *Oxid. Med. Cell. Longev.* **2013**, *2013*, 365046. [CrossRef] [PubMed]
108. Jia, L.; Dong, Y.; Yang, H.; Pan, X.; Fan, R.; Zhai, L. Serum superoxide dismutase and malondialdehyde levels in a group of Chinese patients with age-related macular degeneration. *Aging. Clin. Exp. Res.* **2011**, *23*, 264–267. [CrossRef] [PubMed]
109. Rex, T.S.; Tsui, I.; Hahn, P.; Maguire, A.M.; Duan, D.; Bennett, J.; Dunaief, J.L. Adenovirus-mediated delivery of catalase to retinal pigment epithelial cells protects neighboring photoreceptors from photo-oxidative stress. *Hum. Gene Ther.* **2004**, *15*, 960–967. [CrossRef]
110. Tokarz, P.; Kaarniranta, K.; Blasiak, J. Role of antioxidant enzymes and small molecular weight antioxidants in the pathogenesis of age-related macular degeneration (AMD). *Biogerontology* **2013**, *14*, 461–482. [CrossRef] [PubMed]
111. Wong-Riley, M. Energy metabolism of the visual system. *Eye Brain* **2010**, *2*, 99–116. [CrossRef] [PubMed]
112. Chakrabarty, R.P.; Chandel, N.S. Mitochondria as signaling organelles control mammalian stem cell fate. *Cell Stem Cell* **2021**, *28*, 394–408. [CrossRef]

113. Acuña-Castroviejo, D.; Martín, M.; Macías, M.; Escames, G.; León, J.; Khaldy, H.; Reiter, R.J. Melatonin, mitochondria, and cellular bioenergetics. *J. Pineal Res.* **2001**, *30*, 65–74. [CrossRef]
114. Garcia, I.; Jones, E.; Ramos, M.; Innis-Whitehouse, W.; Gilkerson, R. The little big genome: The organization of mitochondrial DNA. *Front. Biosci. (Landmark Ed.)* **2017**, *22*, 710.
115. Er, R.; Aydın, B.; Şekeroğlu, V.; Atlı Şekeroğlu, Z. Protective effect of Argan oil on mitochondrial function and oxidative stress against acrylamide-induced liver and kidney injury in rats. *Biomarkers* **2020**, *25*, 458–467. [CrossRef] [PubMed]
116. Zorov, D.B.; Juhaszova, M.; Sollott, S.J. Mitochondrial reactive oxygen species (ROS) and ROS-induced ROS release. *Physiol. Rev.* **2014**, *94*, 909–950. [CrossRef]
117. Guo, C.; Sun, L.; Chen, X.; Zhang, D. Oxidative stress, mitochondrial damage and neurodegenerative diseases. *Neural Regen. Res.* **2013**, *8*, 2003. [PubMed]
118. Lee, H.-C.; Wei, Y.-H. Oxidative stress, mitochondrial DNA mutation, and apoptosis in aging. *Exp. Biol. Med.* **2007**, *232*, 592–606.
119. Kong, M.; Guo, L.; Xu, W.; He, C.; Jia, X.; Zhao, Z.; Gu, Z. Aging-associated accumulation of mitochondrial DNA mutations in tumor origin. *J. Life. Med.* **2022**, *1*, 149–167. [CrossRef]
120. Rottenberg, H. The reduction in the mitochondrial membrane potential in aging: The role of the mitochondrial permeability transition Pore. *Int. J. Mol. Sci.* **2023**, *24*, 12295. [CrossRef]
121. Narendra, D.; Walker, J.E.; Youle, R. Mitochondrial quality control mediated by PINK1 and Parkin: Links to parkinsonism. *Cold Spring Harb. Perspect. Biol.* **2012**, *4*, a011338. [CrossRef]
122. Barodia, S.K.; Creed, R.B.; Goldberg, M.S. Parkin and PINK1 functions in oxidative stress and neurodegeneration. *Brain Res. Bull.* **2017**, *133*, 51–59. [CrossRef]
123. Tong, Y.; Zhang, Z.; Wang, S. Role of mitochondria in retinal pigment epithelial aging and degeneration. *Front. Aging* **2022**, *3*, 926627. [CrossRef]
124. Karimi, P.; Gheisari, A.; Gasparini, S.J.; Baharvand, H.; Shekari, F.; Satarian, L.; Ader, M. Crocetin prevents RPE cells from oxidative stress through protection of cellular metabolic function and activation of ERK1/2. *Int. J. Mol. Sci.* **2020**, *21*, 2949. [CrossRef]
125. Kaarniranta, K.; Uusitalo, H.; Blasiak, J.; Felszeghy, S.; Kannan, R.; Kauppinen, A.; Salminen, A.; Sinha, D.; Ferrington, D. Mechanisms of mitochondrial dysfunction and their impact on age-related macular degeneration. *Prog. Retin. Eye Res.* **2020**, *79*, 100858. [CrossRef]
126. Zhu, Y.; Liu, X.; Ding, X.; Wang, F.; Geng, X. Telomere and its role in the aging pathways: Telomere shortening, cell senescence and mitochondria dysfunction. *Biogerontology* **2019**, *20*, 1–16. [CrossRef]
127. Davalli, P.; Mitic, T.; Caporali, A.; Lauriola, A.; D'Arca, D. ROS, cell senescence, and novel molecular mechanisms in aging and age-related diseases. *Oxid. Med. Cell Longev.* **2016**, *2016*, 3565127. [CrossRef]
128. Almeida, C.; Amaral, M.D. A central role of the endoplasmic reticulum in the cell emerges from its functional contact sites with multiple organelles. *Cell Mol. Life. Sci.* **2020**, *77*, 4729–4745. [CrossRef]
129. Faitova, J.; Krekac, D.; Hrstka, R.; Vojtesek, B. Endoplasmic reticulum stress and apoptosis. *Cell Mol. Biol. Lett.* **2006**, *11*, 488–505. [CrossRef]
130. Almanza, A.; Carlesso, A.; Chintha, C.; Creedican, S.; Doultsinos, D.; Leuzzi, B.; Luís, A.; McCarthy, N.; Montibeller, L.; More, S.; et al. Endoplasmic reticulum stress signalling—From basic mechanisms to clinical applications. *FEBS J.* **2019**, *286*, 241–278. [CrossRef]
131. Malhotra, J.D.; Kaufman, R.J. Endoplasmic reticulum stress and oxidative stress: A vicious cycle or a double-edged sword? *Antioxid. Redox Signal.* **2007**, *9*, 2277–2293. [CrossRef]
132. Araki, K.; Nagata, K. Protein folding and quality control in the ER. *Cold Spring Harb. Perspect. Biol.* **2011**, *3*, a007526. [CrossRef]
133. Read, A.; Schröder, M. The unfolded protein response: An overview. *Biology* **2021**, *10*, 384. [CrossRef]
134. Chakrabarti, A.; Chen, A.W.; Varner, J.D. A review of the mammalian unfolded protein response. *Biotechnol. Bioeng.* **2011**, *108*, 2777–2793. [CrossRef]
135. Zeeshan, H.M.A.; Lee, G.H.; Kim, H.-R.; Chae, H.-J. Endoplasmic reticulum stress and associated ROS. *Int. J. Mol. Sci.* **2016**, *17*, 327. [CrossRef]
136. Ong, G.; Logue, S.E. Unfolding the Interactions between Endoplasmic Reticulum Stress and Oxidative Stress. *Antioxidants* **2023**, *12*, 981. [CrossRef]
137. Yang, X.; Zhuang, J.; Song, W.; Shen, W.; Wu, W.; Shen, H.; Han, S. Mitochondria-associated endoplasmic reticulum membrane: Overview and inextricable link with cancer. *J. Cel. Mol. Med.* **2023**, *27*, 906–919. [CrossRef]
138. Bertero, E.; Maack, C. Calcium signaling and reactive oxygen species in mitochondria. *Circ. Res.* **2018**, *122*, 1460–1478. [CrossRef]
139. Salminen, A.; Kauppinen, A.; Hyttinen, J.M.; Toropainen, E.; Kaarniranta, K. Endoplasmic reticulum stress in age-related macular degeneration: Trigger for neovascularization. *Mol. Med.* **2010**, *16*, 535–542. [CrossRef]
140. Kim, S.M.; Lee, H.M.; Hwang, K.A.; Choi, K.C. Benzo(a)pyrene induced cell cycle arrest and apoptosis in human choriocarcinoma cancer cells through reactive oxygen species-induced endoplasmic reticulum-stress pathway. *Food Chem. Toxicol.* **2017**, *107*, 339–348. [CrossRef]
141. Chan, C.M.; Huang, D.Y.; Huang, Y.P.; Hsu, S.H.; Kang, L.Y.; Shen, C.M.; Lin, W.W. Methylglyoxal induces cell death through endoplasmic reticulum stress-associated ROS production and mitochondrial dysfunction. *J. Cell. Mol. Med.* **2016**, *20*, 1749–1760. [CrossRef]

142. Bilbao-Malavé, V.; González-Zamora, J.; de la Puente, M.; Recalde, S.; Fernandez-Robredo, P.; Hernandez, M.; Layana, A.G.; Saenz de Viteri, M. Mitochondrial dysfunction and endoplasmic reticulum stress in age-related macular degeneration, role in pathophysiology, and possible new therapeutic strategies. *Antioxidants* **2021**, *10*, 1170. [CrossRef]
143. Petrukhin, K. New therapeutic targets in atrophic age-related macular degeneration. *Expert Opin. Ther. Targets* **2007**, *11*, 625–639. [CrossRef]
144. Sparrow, J.R.; Gregory-Roberts, E.; Yamamoto, K.; Blonska, A.; Ghosh, S.K.; Ueda, K.; Zhou, J. The bisretinoids of retinal pigment epithelium. *Prog. Retin. Eye Res.* **2012**, *31*, 121–135. [CrossRef]
145. Kim, H.J.; Montenegro, D.; Zhao, J.; Sparrow, J.R. Bisretinoids of the retina: Photo-oxidation, iron-catalyzed oxidation, and disease consequences. *Antioxidants* **2021**, *10*, 1382. [CrossRef]
146. Intartaglia, D.; Giamundo, G.; Conte, I. Autophagy in the retinal pigment epithelium: A new vision and future challenges. *FEBS J.* **2022**, *289*, 7199–7212. [CrossRef]
147. Kim, H.J.; Sparrow, J.R. Novel bisretinoids of human retina are lyso alkyl ether glycerophosphoethanolamine-bearing A2PE species. *J. Lipid. Res.* **2018**, *59*, 1620–1629. [CrossRef]
148. Tsin, A.; Betts-Obregon, B.; Grigsby, J. Visual cycle proteins: Structure, function, and roles in human retinal disease. *J. Biol. Chem.* **2018**, *293*, 13016–13021. [CrossRef]
149. Kim, H.J.; Sparrow, J.R. Bisretinoid phospholipid and vitamin A aldehyde: Shining a light. *J. Lipid. Res.* **2021**, *62*, 100042. [CrossRef]
150. Krohne, T.U.; Stratmann, N.K.; Kopitz, J.; Holz, F.G. Effects of lipid peroxidation products on lipofuscinogenesis and autophagy in human retinal pigment epithelial cells. *Exp. Eye Res.* **2010**, *90*, 465–471. [CrossRef]
151. Yakovleva, M.; Dontsov, A.; Trofimova, N.; Sakina, N.; Kononikhin, A.; Aybush, A.; Gulin, A.; Feldman, T.; Ostrovsky, M. Lipofuscin granule bisretinoid oxidation in the human retinal pigment epithelium forms cytotoxic carbonyls. *Int. J. Mol. Sci.* **2021**, *23*, 222. [CrossRef]
152. Garcia-Garcia, J.; Usategui-Martin, R.; Sanabria, M.R.; Fernandez-Perez, E.; Telleria, J.J.; Coco-Martin, R.M. Pathophysiology of age-related macular degeneration: Implications for treatment. *Ophthalmic Res.* **2022**, *65*, 615–636. [CrossRef]
153. Sparrow, J.R. Bisretinoids of RPE lipofuscin: Trigger for complement activation in age-related macular degeneration. *Adv. Exp. Med. Biol.* **2010**, *703*, 63–74. [CrossRef]
154. Zhou, J.; Kim, S.R.; Westlund, B.S.; Sparrow, J.R. Complement activation by bisretinoid constituents of RPE lipofuscin. *Investig. Ophthalmol. Vis. Sci.* **2009**, *50*, 1392–1399. [CrossRef] [PubMed]
155. Sparrow, J.R.; Duncker, T. Fundus autofluorescence and RPE lipofuscin in age-related macular degeneration. *J. Clin. Med.* **2014**, *3*, 1302–1321. [CrossRef] [PubMed]
156. Parmar, V.M.; Parmar, T.; Arai, E.; Perusek, L.; Maeda, A. A2E-associated cell death and inflammation in retinal pigmented epithelial cells from human induced pluripotent stem cells. *Stem Cell Res.* **2018**, *27*, 95–104. [CrossRef] [PubMed]
157. Wang, J.; Feng, Y.; Han, P.; Wang, F.; Luo, X.; Liang, J.; Sun, X.; Ye, J.; Lu, Y.; Sun, X. Photosensitization of A2E triggers telomere dysfunction and accelerates retinal pigment epithelium senescence. *Cell Death. Dis.* **2018**, *9*, 178. [CrossRef] [PubMed]
158. Sparrow, J.R.; Cai, B.; Jang, Y.P.; Zhou, J.; Nakanishi, K. A2E, a fluorophore of RPE lipofuscin, can destabilize membrane. In *Retinal Degenerative Diseases*; Springer: Berlin/Heidelberg, Germany, 2006; pp. 63–68.
159. Sparrow, J.R.; Cai, B. Blue light–induced apoptosis of A2E-containing RPE: Involvement of caspase-3 and protection by Bcl-2. *Investig. Ophthalmol. Vis. Sci.* **2001**, *42*, 1356–1362.
160. Kaur, G.; Tan, L.X.; Rathnasamy, G.; La Cunza, N.; Germer, C.J.; Toops, K.A.; Fernandes, M.; Blenkinsop, T.A.; Lakkaraju, A. Aberrant early endosome biogenesis mediates complement activation in the retinal pigment epithelium in models of macular degeneration. *Proc. Natl. Acad. Sci. USA* **2018**, *115*, 9014–9019. [CrossRef] [PubMed]
161. Cox, T.M.; Cachón-González, M.B. The cellular pathology of lysosomal diseases. *J. Pathol.* **2012**, *226*, 241–254. [CrossRef] [PubMed]
162. Song, Q.; Meng, B.; Xu, H.; Mao, Z. The emerging roles of vacuolar-type ATPase-dependent Lysosomal acidification in neurodegenerative diseases. *Transl. Neurodegener.* **2020**, *9*, 17. [CrossRef]
163. Appelqvist, H.; Wäster, P.; Kågedal, K.; Öllinger, K. The lysosome: From waste bag to potential therapeutic target. *J. Mol. Cell. Biol.* **2013**, *5*, 214–226. [CrossRef]
164. Keeling, E.; Lotery, A.J.; Tumbarello, D.A.; Ratnayaka, J.A. Impaired cargo clearance in the retinal pigment epithelium (RPE) underlies irreversible blinding diseases. *Cells* **2018**, *7*, 16. [CrossRef]
165. Sinha, D.; Valapala, M.; Shang, P.; Hose, S.; Grebe, R.; Lutty, G.A.; Zigler, J.S., Jr.; Kaarniranta, K.; Handa, J.T. Lysosomes: Regulators of autophagy in the retinal pigmented epithelium. *Exp. Eye Res.* **2016**, *144*, 46–53. [CrossRef] [PubMed]
166. Wiktor, A.; Sarna, M.; Wnuk, D.; Sarna, T. Lipofuscin-mediated photodynamic stress induces adverse changes in nanomechanical properties of retinal pigment epithelium cells. *Sci. Rep.* **2018**, *8*, 17929. [CrossRef]
167. Szweda, P.A.; Camouse, M.; Lundberg, K.C.; Oberley, T.D.; Szweda, L.I. Aging, lipofuscin formation, and free radical-mediated inhibition of cellular proteolytic systems. *Ageing Res. Rev.* **2003**, *2*, 383–405. [CrossRef]
168. Terman, A.; Kurz, T. Lysosomal iron, iron chelation, and cell death. *Antioxid. Redox Signal.* **2013**, *18*, 888–898. [CrossRef]
169. Ueda, K.; Kim, H.J.; Zhao, J.; Song, Y.; Dunaief, J.L.; Sparrow, J.R. Iron promotes oxidative cell death caused by bisretinoids of retina. *Proc. Natl. Acad. Sci. USA* **2018**, *115*, 4963–4968. [CrossRef]

170. Melidou, M.; Riganakos, K.; Galaris, D. Protection against nuclear DNA damage offered by flavonoids in cells exposed to hydrogen peroxide: The role of iron chelation. *Free Radic. Biol. Med.* **2005**, *39*, 1591–1600. [CrossRef]
171. Charkoudian, L.K.; Dentchev, T.; Lukinova, N.; Wolkow, N.; Dunaief, J.L.; Franz, K.J. Iron prochelator BSIH protects retinal pigment epithelial cells against cell death induced by hydrogen peroxide. *J. Inorg. Biochem.* **2008**, *102*, 2130–2135. [CrossRef] [PubMed]
172. Karlsson, M.; Kurz, T. Attenuation of iron-binding proteins in ARPE-19 cells reduces their resistance to oxidative stress. *Acta Ophthalmol.* **2016**, *94*, 556–564. [CrossRef] [PubMed]
173. Cheng, Y.; Ren, X.; Hait, W.N.; Yang, J.-M. Therapeutic targeting of autophagy in disease: Biology and pharmacology. *Pharmacol. Rev.* **2013**, *65*, 1162–1197. [CrossRef]
174. Wang, S.; Li, H.; Yuan, M.; Fan, H.; Cai, Z. Role of AMPK in autophagy. *Front. Physiol.* **2022**, *13*, 2479. [CrossRef]
175. Bednarczyk, M.; Zmarzły, N.; Grabarek, B.; Mazurek, U.; Muc-Wierzgoń, M. Genes involved in the regulation of different types of autophagy and their participation in cancer pathogenesis. *Oncotarget* **2018**, *9*, 34413–34428. [CrossRef] [PubMed]
176. Kumar, A.V.; Mills, J.; Lapierre, L.R. Selective autophagy receptor p62/SQSTM1, a pivotal player in stress and aging. *Front. Cell Dev. Biol.* **2022**, *10*, 793328. [CrossRef] [PubMed]
177. Golestaneh, N.; Chu, Y.; Xiao, Y.Y.; Stoleru, G.L.; Theos, A.C. Dysfunctional autophagy in RPE, a contributing factor in age-related macular degeneration. *Cell Death. Dis.* **2017**, *8*, e2537. [CrossRef] [PubMed]
178. Fisher, C.R.; Shaaeli, A.A.; Ebeling, M.C.; Montezuma, S.R.; Ferrington, D.A. Investigating mitochondrial fission, fusion, and autophagy in retinal pigment epithelium from donors with age-related macular degeneration. *Sci. Rep.* **2022**, *12*, 21725. [CrossRef]
179. Mitter, S.K.; Song, C.; Qi, X.; Mao, H.; Rao, H.; Akin, D.; Lewin, A.; Grant, M.; Dunn, W., Jr.; Ding, J.; et al. Dysregulated autophagy in the RPE is associated with increased susceptibility to oxidative stress and AMD. *Autophagy* **2014**, *10*, 1989–2005. [CrossRef] [PubMed]
180. Ferrington, D.A.; Sinha, D.; Kaarniranta, K. Defects in retinal pigment epithelial cell proteolysis and the pathology associated with age-related macular degeneration. *Prog. Retin. Eye Res.* **2016**, *51*, 69–89. [CrossRef] [PubMed]
181. Kaarniranta, K.; Sinha, D.; Blasiak, J.; Kauppinen, A.; Veréb, Z.; Salminen, A.; Boulton, M.E.; Petrovski, G. Autophagy and heterophagy dysregulation leads to retinal pigment epithelium dysfunction and development of age-related macular degeneration. *Autophagy* **2013**, *9*, 973–984. [CrossRef] [PubMed]
182. Radu, R.A.; Mata, N.L.; Bagla, A.; Travis, G.H. Light exposure stimulates formation of A2E oxiranes in a mouse model of Stargardt's macular degeneration. *Proc. Natl. Acad. Sci. USA* **2004**, *101*, 5928–5933. [CrossRef]
183. Kim, S.R.; Jang, Y.P.; Sparrow, J.R. Photooxidation of RPE lipofuscin bisretinoids enhances fluorescence intensity. *Vis. Res.* **2010**, *50*, 729–736. [CrossRef]
184. Thornalley, P.J. Protein and nucleotide damage by glyoxal and methylglyoxal in physiological systems-role in ageing and disease. *Drug. Metabol. Drug. Interact.* **2008**, *23*, 125–150. [CrossRef]
185. Ng, K.-P.; Gugiu, B.; Renganathan, K.; Davies, M.W.; Gu, X.; Crabb, J.S.; Kim, S.R.; Różanowska, M.B.; Bonilha, V.L.; Rayborn, M.E. Retinal pigment epithelium lipofuscin proteomics. *Mol. Cell Proteom.* **2008**, *7*, 1397–1405. [CrossRef]
186. Rowan, S.; Bejarano, E.; Taylor, A. Mechanistic targeting of advanced glycation end-products in age-related diseases. *Biochim. Biophys. Acta Mol. Basis. Dis.* **2018**, *1864*, 3631–3643. [CrossRef]
187. Sparvero, L.J.; Asafu-Adjei, D.; Kang, R.; Tang, D.; Amin, N.; Im, J.; Rutledge, R.; Lin, B.; Amoscato, A.A.; Zeh, H.J. RAGE (Receptor for Advanced Glycation Endproducts), RAGE ligands, and their role in cancer and inflammation. *J. Transl. Med.* **2009**, *7*, 17. [CrossRef] [PubMed]
188. Chaudhary, M.R.; Chaudhary, S.; Sharma, Y.; Singh, T.A.; Mishra, A.K.; Sharma, S.; Mehdi, M.M. Aging, oxidative stress and degenerative diseases: Mechanisms, complications and emerging therapeutic strategies. *Biogerontology* **2023**, *24*, 609–662. [CrossRef] [PubMed]
189. Xu, J.; Núñez, G. The NLRP3 inflammasome: Activation and regulation. *Trends Biochem. Sci.* **2023**, *48*, 331–344. [CrossRef]
190. Fernandes, A.F.; Zhou, J.; Zhang, X.; Bian, Q.; Sparrow, J.; Taylor, A.; Pereira, P.; Shang, F. Oxidative inactivation of the proteasome in retinal pigment epithelial cells. A potential link between oxidative stress and up-regulation of interleukin-8. *J. Biol. Chem.* **2008**, *283*, 20745–20753. [CrossRef]
191. Kaur, G.; Singh, N.K. The role of inflammation in retinal neurodegeneration and degenerative diseases. *Int. J. Mol. Sci.* **2021**, *23*, 386. [CrossRef]
192. Maran, J.J.; Mugisho, O.O. NLRP3 inflammasome plays a vital role in the pathogenesis of age-related diseases in the eye and brain. *Neural Regen. Res.* **2024**, *19*, 1425–1426. [CrossRef] [PubMed]
193. Mugisho, O.O.; Green, C.R.; Zhang, J.; Acosta, M.L.; Rupenthal, I.D. Connexin43 hemichannels: A potential drug target for the treatment of diabetic retinopathy. *Drug. Discov. Today* **2019**, *24*, 1627–1636. [CrossRef]
194. Celkova, L.; Doyle, S.L.; Campbell, M. NLRP3 inflammasome and pathobiology in AMD. *J. Clin. Med.* **2015**, *4*, 172–192. [CrossRef]
195. Chaudhary, P.; Janmeda, P.; Docea, A.O.; Yeskaliyeva, B.; Abdull Razis, A.F.; Modu, B.; Calina, D.; Sharifi-Rad, J. Oxidative stress, free radicals and antioxidants: Potential crosstalk in the pathophysiology of human diseases. *Front. Chem.* **2023**, *11*, 1158198. [CrossRef]
196. Riveros, M.E.; Ávila, A.; Schruers, K.; Ezquer, F. Antioxidant biomolecules and their potential for the treatment of difficult-to-treat depression and conventional treatment-resistant depression. *Antioxidants* **2022**, *11*, 540. [CrossRef]

197. Lü, J.M.; Lin, P.H.; Yao, Q.; Chen, C. Chemical and molecular mechanisms of antioxidants: Experimental approaches and model systems. *J. Cell. Mol. Med.* **2010**, *14*, 840–860. [CrossRef] [PubMed]
198. Gourgouli, D.M.; Gourgouli, I.; Spai, S.; Gourgouli, K.; Tzorovili, E.; Skouroliakou, M.; Papakonstantinou, D.; Moschos, M.M. Effect of the mediterranean diet on progression of dry form of age-related macular degeneration. *In Vivo* **2023**, *37*, 1809–1815. [CrossRef]
199. Girgis, S.; Lee, L.R. Treatment of dry age-related macular degeneration: A review. *Clin. Exp. Ophthalmol.* **2023**, *51*, 835–852. [CrossRef]
200. Lambros, M.L.; Plafker, S.M. Oxidative stress and the Nrf2 anti-oxidant transcription factor in age-related macular degeneration. *Adv. Exp. Med. Biol.* **2016**, *854*, 67–72. [CrossRef]
201. Veleri, S.; Lazar, C.H.; Chang, B.; Sieving, P.A.; Banin, E.; Swaroop, A. Biology and therapy of inherited retinal degenerative disease: Insights from mouse models. *Dis. Models Mech.* **2015**, *8*, 109–129. [CrossRef] [PubMed]
202. Huang, S.; Liu, C.H.; Wang, Z.; Fu, Z.; Britton, W.R.; Blomfield, A.K.; Kamenecka, T.M.; Dunaief, J.L.; Solt, L.A.; Chen, J. REV-ERBα regulates age-related and oxidative stress-induced degeneration in retinal pigment epithelium via NRF2. *Redox Biol.* **2022**, *51*, 102261. [CrossRef]
203. Li, W.; Khor, T.O.; Xu, C.; Shen, G.; Jeong, W.S.; Yu, S.; Kong, A.N. Activation of Nrf2-antioxidant signaling attenuates NFkappaB-inflammatory response and elicits apoptosis. *Biochem. Pharmacol.* **2008**, *76*, 1485–1489. [CrossRef] [PubMed]
204. Bellezza, I.; Giambanco, I.; Minelli, A.; Donato, R. Nrf2-Keap1 signaling in oxidative and reductive stress. *Biochim. Biophys. Acta Mol. Cell Res.* **2018**, *1865*, 721–733. [CrossRef]
205. Nakagami, Y. Nrf2 Is an attractive therapeutic target for retinal diseases. *Oxid. Med. Cell Longev.* **2016**, *2016*, 7469326. [CrossRef] [PubMed]
206. Sotler, R.; Poljšak, B.; Dahmane, R.; Jukić, T.; Pavan Jukić, D.; Rotim, C.; Trebše, P.; Starc, A. Prooxidant activities of antioxidants and their impact on health. *Acta Clin. Croat.* **2019**, *58*, 726–736. [CrossRef] [PubMed]
207. Zhang, Y.; Yang, J.; Na, X.; Zhao, A. Association between β-carotene supplementation and risk of cancer: A meta-analysis of randomized controlled trials. *Nutr. Rev.* **2023**, *81*, 1118–1130. [CrossRef] [PubMed]
208. Yang, J.; Zhang, Y.; Na, X.; Zhao, A. β-Carotene supplementation and risk of cardiovascular disease: A systematic review and meta-analysis of randomized controlled trials. *Nutrients* **2022**, *14*, 1284. [CrossRef] [PubMed]
209. Sackett, C.S.; Schenning, S. The age-related eye disease study: The results of the clinical trial. *Insight* **2002**, *27*, 5–7. [PubMed]
210. Chew, E.Y.; Clemons, T.E.; Agrón, E.; Domalpally, A.; Keenan, T.D.L.; Vitale, S.; Weber, C.; Smith, D.C.; Christen, W. Long-term outcomes of adding lutein/zeaxanthin and ω-3 fatty acids to the AREDS supplements on age-related macular degeneration progression: AREDS2 report 28. *JAMA Ophthalmol.* **2022**, *140*, 692–698. [CrossRef] [PubMed]
211. Arnold, C.; Winter, L.; Fröhlich, K.; Jentsch, S.; Dawczynski, J.; Jahreis, G.; Böhm, V. Macular xanthophylls and ω-3 long-chain polyunsaturated fatty acids in age-related macular degeneration: A randomized trial. *JAMA Ophthalmol.* **2013**, *131*, 564–572. [CrossRef] [PubMed]
212. Chua, B.; Flood, V.; Rochtchina, E.; Wang, J.J.; Smith, W.; Mitchell, P. Dietary fatty acids and the 5-year incidence of age-related maculopathy. *Arch. Ophthalmol.* **2006**, *124*, 981–986. [CrossRef] [PubMed]
213. Seddon, J.M.; George, S.; Rosner, B. Cigarette smoking, fish consumption, omega-3 fatty acid intake, and associations with age-related macular degeneration: The US Twin Study of Age-Related Macular Degeneration. *Arch. Ophthalmol.* **2006**, *124*, 995–1001. [CrossRef]
214. Ho, L.; van Leeuwen, R.; Witteman, J.C.; van Duijn, C.M.; Uitterlinden, A.G.; Hofman, A.; de Jong, P.T.; Vingerling, J.R.; Klaver, C.C. Reducing the genetic risk of age-related macular degeneration with dietary antioxidants, zinc, and ω-3 fatty acids: The Rotterdam study. *Arch. Ophthalmol.* **2011**, *129*, 758–766. [CrossRef]
215. Rexrode, K.M.; Lee, I.M.; Cook, N.R.; Hennekens, C.H.; Buring, J.E. Baseline characteristics of participants in the Women's Health Study. *J. Women's Health Gend. Based Med.* **2000**, *9*, 19–27. [CrossRef] [PubMed]
216. Schnebelen-Berthier, C.; Acar, N.; Simon, E.; Thabuis, C.; Bourdillon, A.; Mathiaud, A.; Dauchet, L.; Delcourt, C.; Benlian, P.; Crochet, M.; et al. The ALGOVUE clinical trial: Effects of the daily consumption of eggs enriched with lutein and docosahexaenoic acid on plasma composition and macular pigment optical density. *Nutrients* **2021**, *13*, 3347. [CrossRef] [PubMed]
217. Zanón-Moreno, V.; Domingo Pedrol, J.C.; Sanz-González, S.M.; Raga-Cervera, J.; Salazar-Corral, J.; Pinazo-Durán, M.D. Feasibility study of a docosahexaenoic acid-optimized nutraceutical formulation on the macular levels of lutein in a healthy mediterranean population. *Ophthalmic Res.* **2021**, *64*, 1068–1076. [CrossRef] [PubMed]
218. Feher, J.; Kovacs, B.; Kovacs, I.; Schveoller, M.; Papale, A.; Balacco Gabrieli, C. Improvement of visual functions and fundus alterations in early age-related macular degeneration treated with a combination of acetyl-L-carnitine, n-3 fatty acids, and coenzyme Q10. *Ophthalmologica* **2005**, *219*, 154–166. [CrossRef] [PubMed]
219. Piccardi, M.; Marangoni, D.; Minnella, A.M.; Savastano, M.C.; Valentini, P.; Ambrosio, L.; Capoluongo, E.; Maccarone, R.; Bisti, S.; Falsini, B. A longitudinal follow-up study of saffron supplementation in early age-related macular degeneration: Sustained benefits to central retinal function. *Evid. Based Complement. Altern. Med.* **2012**, *2012*, 429124. [CrossRef]
220. Broadhead, G.K.; Grigg, J.R.; McCluskey, P.; Hong, T.; Schlub, T.E.; Chang, A.A. Saffron therapy for the treatment of mild/moderate age-related macular degeneration: A randomised clinical trial. *Graefes. Arch. Clin. Exp. Ophthalmol.* **2019**, *257*, 31–40. [CrossRef] [PubMed]

221. Erie, J.C.; Good, J.A.; Butz, J.A.; Pulido, J.S. Reduced zinc and copper in the retinal pigment epithelium and choroid in age-related macular degeneration. *Am. J. Ophthalmol.* **2009**, *147*, 276–282.e1. [CrossRef] [PubMed]
222. Newsome, D.A. A randomized, prospective, placebo-controlled clinical trial of a novel zinc-monocysteine compound in age-related macular degeneration. *Curr. Eye Res.* **2008**, *33*, 591–598. [CrossRef] [PubMed]
223. Chew, E.Y.; Clemons, T.E.; Agrón, E.; Sperduto, R.D.; Sangiovanni, J.P.; Kurinij, N.; Davis, M.D. Long-term effects of vitamins C and E, β-carotene, and zinc on age-related macular degeneration: AREDS report no. 35. *Ophthalmology* **2013**, *120*, 1604–1611.e4. [CrossRef]
224. Ma, L.; Yan, S.F.; Huang, Y.M.; Lu, X.R.; Qian, F.; Pang, H.L.; Xu, X.R.; Zou, Z.Y.; Dong, P.C.; Xiao, X.; et al. Effect of lutein and zeaxanthin on macular pigment and visual function in patients with early age-related macular degeneration. *Ophthalmology* **2012**, *119*, 2290–2297. [CrossRef]
225. Bartlett, H.E.; Eperjesi, F. Effect of lutein and antioxidant dietary supplementation on contrast sensitivity in age-related macular disease: A randomized controlled trial. *Eur. J. Clin. Nutr.* **2007**, *61*, 1121–1127. [CrossRef] [PubMed]
226. Richer, S.; Stiles, W.; Statkute, L.; Pulido, J.; Frankowski, J.; Rudy, D.; Pei, K.; Tsipursky, M.; Nyland, J. Double-masked, placebo-controlled, randomized trial of lutein and antioxidant supplementation in the intervention of atrophic age-related macular degeneration: The Veterans LAST study (Lutein Antioxidant Supplementation Trial). *Optometry* **2004**, *75*, 216–230. [CrossRef] [PubMed]
227. Weigert, G.; Kaya, S.; Pemp, B.; Sacu, S.; Lasta, M.; Werkmeister, R.M.; Dragostinoff, N.; Simader, C.; Garhöfer, G.; Schmidt-Erfurth, U.; et al. Effects of lutein supplementation on macular pigment optical density and visual acuity in patients with age-related macular degeneration. *Investig. Ophthalmol. Vis. Sci.* **2011**, *52*, 8174–8178. [CrossRef] [PubMed]
228. Souied, E.H.; Delcourt, C.; Querques, G.; Bassols, A.; Merle, B.; Zourdani, A.; Smith, T.; Benlian, P. Oral docosahexaenoic acid in the prevention of exudative age-related macular degeneration: The Nutritional AMD Treatment 2 study. *Ophthalmology* **2013**, *120*, 1619–1631. [CrossRef] [PubMed]
229. Wenzel, A.J.; Gerweck, C.; Barbato, D.; Nicolosi, R.J.; Handelman, G.J.; Curran-Celentano, J. A 12-wk egg intervention increases serum zeaxanthin and macular pigment optical density in women. *J. Nutr. Biochem.* **2006**, *136*, 2568–2573. [CrossRef]
230. Kelly, E.R.; Plat, J.; Haenen, G.R.; Kijlstra, A.; Berendschot, T.T. The effect of modified eggs and an egg-yolk based beverage on serum lutein and zeaxanthin concentrations and macular pigment optical density: Results from a randomized trial. *PLoS ONE* **2014**, *9*, e92659. [CrossRef] [PubMed]
231. Merle, B.M.J.; Buaud, B.; Korobelnik, J.F.; Bron, A.; Delyfer, M.N.; Rougier, M.B.; Savel, H.; Vaysse, C.; Creuzot-Garcher, C.; Delcourt, C. Plasma long-chain omega-3 polyunsaturated fatty acids and macular pigment in subjects with family history of age-related macular degeneration: The Limpia Study. *Acta Ophthalmol.* **2017**, *95*, e763–e769. [CrossRef]
232. Christen, W.G.; Cook, N.R.; Manson, J.E.; Buring, J.E.; Chasman, D.I.; Lee, I.M.; Bubes, V.; Li, C.; Haubourg, M.; Schaumberg, D.A. Effect of vitamin D and ω-3 fatty acid supplementation on risk of age-related macular degeneration: An ancillary study of the VITAL randomized clinical trial. *JAMA Ophthalmol.* **2020**, *138*, 1280–1289. [CrossRef]
233. Piatti, A.; Croce, A.; Mazzacane, D.; Traina, G.; Ambrosino, L.; Boni, L.; Lisi, L.; Cascella, M.C.; Grunberger, A. Effect of 2-year nutritional supplementation on progression of age-related macular degeneration. *Eur. J. Ophthalmol.* **2020**, *30*, 376–381. [CrossRef]
234. Taylor, H.R.; Tikellis, G.; Robman, L.D.; McCarty, C.A.; McNeil, J.J. Vitamin E supplementation and macular degeneration: Randomised controlled trial. *BMJ* **2002**, *325*, 11. [CrossRef]
235. Richer, S. Multicenter ophthalmic and nutritional age-related macular degeneration study—Part 2: Antioxidant intervention and conclusions. *J. Am. Optom. Assoc.* **1996**, *67*, 30–49.
236. ReNEW: Phase 3 Study of Efficacy of Subcutaneous Elamipretide in Subjects with Dry Age-Related Macular Degeneration (Dry AMD) (ReNEW). Identifier: NCT06373731. Available online: https://clinicaltrials.gov/study/NCT06373731?term=NCT06373731&rank=1 (accessed on 22 April 2024).
237. Study to Evaluate the Efficacy and Safety of Oral CT1812 in Participants with Geographic Atrophy (GA) Secondary to Dry Age-Related Macular Degeneration (AMD). Identifier: NCT05893537. Available online: https://clinicaltrials.gov/study/NCT05893537?term=NCT05893537&rank=1 (accessed on 22 April 2024).
238. A Masked, Placebo-Controlled Study to Assess Iptacopan in Age-Related Macular Degeneration. Identifier: NCT05230537. Available online: https://clinicaltrials.gov/study/NCT05230537?term=NCT05230537&rank=1 (accessed on 22 April 2024).
239. Zimura in Participants with GEOGRAPHIC Atrophy Secondary to Dry Age-Related Macular Degeneration. Identifier: NCT02686658. Available online: https://clinicaltrials.gov/study/NCT02686658?term=NCT02686658&rank=1 (accessed on 22 April 2024).
240. A Clinical Trial Designed to Evaluate The Safety and Exploratory Efficacy of 1.0 Mg Luminate® (Alg-1001) as a Treatment for Non-Exudative Macular Degeneration. Identifier: NCT03626636. Available online: https://clinicaltrials.gov/study/NCT03626636?term=NCT03626636&rank=1 (accessed on 22 April 2024).
241. Effects of Antiplatelet and Antioxidant Agents on Drusen Progression: A Pilot, Prospective Cohort Study. Identifier: NCT06165068. Available online: https://clinicaltrials.gov/study/NCT06165068?term=NCT06165068&rank=1 (accessed on 22 April 2024).
242. Study to Evaluate Safety and Efficacy of EG-301 in Patients with Nonfocal Geographic Atrophy Secondary to dAMD. Identifier: NCT05170048. Available online: https://clinicaltrials.gov/study/NCT05170048?term=NCT05170048&rank=1 (accessed on 22 April 2024).

243. Jaffe, G.J.; Schmitz-Valckenberg, S.; Boyer, D.; Heier, J.; Wolf-Schnurrbusch, U.; Staurenghi, G.; Schmidt-Erfurth, U.; Holz, F.G. Randomized trial to evaluate tandospirone in geographic atrophy secondary to age-related macular degeneration: The GATE study. *Am. J. Ophthalmol.* **2015**, *160*, 1226–1234. [CrossRef]
244. A Study of Danicopan in Participants with Geographic Atrophy Secondary to Age-Related Macular Degeneration. Identifier: NCT05019521. Available online: https://clinicaltrials.gov/study/NCT05019521?term=NCT05019521&rank=1 (accessed on 22 April 2024).
245. Kim, B.J.; Hunter, A.; Brucker, A.J.; Hahn, P.; Gehrs, K.; Patel, A.; Edwards, A.O.; Li, Y.; Khurana, R.N.; Nissim, I.; et al. Orally administered alpha lipoic acid as a treatment for geographic atrophy: A Randomized clinical trial. *Ophthalmol. Retin.* **2020**, *4*, 889–898. [CrossRef]
246. Zaynab, M.; Fatima, M.; Abbas, S.; Sharif, Y.; Umair, M.; Zafar, M.H.; Bahadar, K. Role of secondary metabolites in plant defense against pathogens. *Microb. Pathog.* **2018**, *124*, 198–202. [CrossRef] [PubMed]
247. Lund, M.N. Reactions of plant polyphenols in foods: Impact of molecular structure. *Trends. Food Sci. Technol.* **2021**, *112*, 241–251. [CrossRef]
248. Shao, Y.; Yu, H.; Yang, Y.; Li, M.; Hang, L.; Xu, X. A solid dispersion of quercetin shows enhanced Nrf2 activation and protective effects against oxidative injury in a mouse model of dry age-related macular degeneration. *Oxid. Med. Cell. Longev.* **2019**, *2019*, 1479571. [CrossRef]
249. Salimiagdam, N.; Chwa, M.; Nesburn, A.; Kenney, M.C. Effects of quercetin in AMD cybrid Cell lines: Implications for a therapeutic role in AMD. *Investig. Ophthalmol. Vis. Sci.* **2022**, *63*, 467-A0004.
250. Cao, X.; Liu, M.; Tuo, J.; Shen, D.; Chan, C.-C. The effects of quercetin in cultured human RPE cells under oxidative stress and in Ccl2/Cx3cr1 double deficient mice. *Exp. Eye Res.* **2010**, *91*, 15–25. [CrossRef]
251. Kook, D.; Wolf, A.H.; Alice, L.Y.; Neubauer, A.S.; Priglinger, S.G.; Kampik, A.; Welge-Lüssen, U.C. The protective effect of quercetin against oxidative stress in the human RPE in vitro. *Investig. Ophthalmol. Vis. Sci.* **2008**, *49*, 1712–1720. [CrossRef] [PubMed]
252. Hytti, M.; Piippo, N.; Salminen, A.; Honkakoski, P.; Kaarniranta, K.; Kauppinen, A. Quercetin alleviates 4-hydroxynonenal-induced cytotoxicity and inflammation in ARPE-19 cells. *Exp. Eye Res.* **2015**, *132*, 208–215. [CrossRef]
253. Cheng, S.C.; Huang, W.C.; JH, S.P.; Wu, Y.H.; Cheng, C.Y. Quercetin inhibits the production of IL-1β-induced inflammatory cytokines and chemokines in ARPE-19 cells via the MAPK and NF-κB signaling pathways. *Int. J. Mol. Sci.* **2019**, *20*, 2957. [CrossRef] [PubMed]
254. Kim, J.; Jin, H.L.; Jang, D.S.; Jeong, K.W.; Choung, S.Y. Quercetin-3-O-α-l-arabinopyranoside protects against retinal cell death via blue light-induced damage in human RPE cells and Balb-c mice. *Food Funct.* **2018**, *9*, 2171–2183. [CrossRef] [PubMed]
255. Wang, Y.; Kim, H.J.; Sparrow, J.R. Quercetin and cyanidin-3-glucoside protect against photooxidation and photodegradation of A2E in retinal pigment epithelial cells. *Exp. Eye Res.* **2017**, *160*, 45–55. [CrossRef] [PubMed]
256. Zhang, Y.; Yang, Y.; Yu, H.; Li, M.; Hang, L.; Xu, X. Apigenin protects mouse retina against oxidative damage by regulating the Nrf2 pathway and autophagy. *Oxid. Med. Cell. Longev.* **2020**, *2020*, 9420704. [CrossRef] [PubMed]
257. Feng, J.H.; Dong, X.W.; Yu, H.L.; Shen, W.; Lv, X.Y.; Wang, R.; Cheng, X.X.; Xiong, F.; Hu, X.L.; Wang, H. Cynaroside protects the blue light-induced retinal degeneration through alleviating apoptosis and inducing autophagy in vitro and in vivo. *Phytomedicine* **2021**, *88*, 153604. [CrossRef] [PubMed]
258. Kim, S.R.; Nakanishi, K.; Itagaki, Y.; Sparrow, J.R. Photooxidation of A2-PE, a photoreceptor outer segment fluorophore, and protection by lutein and zeaxanthin. *Exp. Eye Res.* **2006**, *82*, 828–839. [CrossRef] [PubMed]
259. Sasaki, M.; Yuki, K.; Kurihara, T.; Miyake, S.; Noda, K.; Kobayashi, S.; Ishida, S.; Tsubota, K.; Ozawa, Y. Biological role of lutein in the light-induced retinal degeneration. *J. Nutr. Biochem.* **2012**, *23*, 423–429. [CrossRef] [PubMed]
260. Yang, J.; Li, D.; Zhang, Y.; Zhang, L.; Liao, Z.; Aihemaitijiang, S.; Hou, Y.; Zhan, Z.; Xie, K.; Zhang, Z. Lutein protected the retina from light induced retinal damage by inhibiting increasing oxidative stress and inflammation. *J. Funct. Foods* **2020**, *73*, 104107. [CrossRef]
261. Arunkumar, R.; Gorusupudi, A.; Li, B.; Blount, J.D.; Nwagbo, U.; Kim, H.J.; Sparrow, J.R.; Bernstein, P.S. Lutein and zeaxanthin reduce A2E and iso-A2E levels and improve visual performance in Abca4(−/−)/Bco2(−/−) double knockout mice. *Exp. Eye Res.* **2021**, *209*, 108680. [CrossRef] [PubMed]
262. Bian, Q.; Gao, S.; Zhou, J.; Qin, J.; Taylor, A.; Johnson, E.J.; Tang, G.; Sparrow, J.R.; Gierhart, D.; Shang, F. Lutein and zeaxanthin supplementation reduces photooxidative damage and modulates the expression of inflammation-related genes in retinal pigment epithelial cells. *Free Radic. Biol. Med.* **2012**, *53*, 1298–1307. [CrossRef]
263. Sahin, K.; Gencoglu, H.; Akdemir, F.; Orhan, C.; Tuzcu, M.; Sahin, N.; Yilmaz, I.; Juturu, V. Lutein and zeaxanthin isomers may attenuate photo-oxidative retinal damage via modulation of G protein-coupled receptors and growth factors in rats. *Biochem. Biophys. Res. Commun.* **2019**, *516*, 163–170. [CrossRef] [PubMed]
264. Sahin, K.; Akdemir, F.; Orhan, C.; Tuzcu, M.; Gencoglu, H.; Sahin, N.; Ozercan, I.H.; Ali, S.; Yilmaz, I.; Juturu, V. (3R, 3'R)-zeaxanthin protects the retina from photo-oxidative damage via modulating the inflammation and visual health molecular markers. *Cutan. Ocul. Toxicol.* **2019**, *38*, 161–168. [CrossRef] [PubMed]
265. Lin, C.W.; Yang, C.M.; Yang, C.H. Protective effect of astaxanthin on blue light-emitting diode-induced retinal cell damage via free radical scavenging and activation of PI3K/Akt/Nrf2 pathway in 661W cell model. *Mar. Drugs* **2020**, *18*, 387. [CrossRef] [PubMed]

266. Liu, Y.; Guo, Z.; Wang, S.; Liu, Y.; Wei, Y. Fucoxanthin pretreatment ameliorates visible light-induced phagocytosis disruption of RPE cells under a lipid-rich environment via the Nrf2 pathway. *Mar. Drugs* **2021**, *20*, 15. [CrossRef] [PubMed]
267. Laabich, A.; Vissvesvaran, G.P.; Lieu, K.L.; Murata, K.; McGinn, T.E.; Manmoto, C.C.; Sinclair, J.R.; Karliga, I.; Leung, D.W.; Fawzi, A.; et al. Protective effect of crocin against blue light- and white light-mediated photoreceptor cell death in bovine and primate retinal primary cell culture. *Investig. Ophthalmol. Vis. Sci.* **2006**, *47*, 3156–3163. [CrossRef] [PubMed]
268. Lin, Y.H.; Sheu, S.J.; Liu, W.; Hsu, Y.T.; He, C.X.; Wu, C.Y.; Chen, K.J.; Lee, P.Y.; Chiu, C.C.; Cheng, K.C. Retinal protective effect of curcumin metabolite hexahydrocurcumin against blue light-induced RPE damage. *Phytomedicine* **2023**, *110*, 154606. [CrossRef] [PubMed]
269. Kim, J.; Kim, C.S.; Moon, M.K.; Kim, J.S. Epicatechin breaks preformed glycated serum albumin and reverses the retinal accumulation of advanced glycation end products. *Eur. J. Pharmacol.* **2015**, *748*, 108–114. [CrossRef]
270. Thichanpiang, P.; Wongprasert, K. Green tea polyphenol epigallocatechin-3-gallate attenuates TNF-α-induced intercellular adhesion molecule-1 expression and monocyte adhesion to retinal pigment epithelial cells. *Am. J. Chin. Med.* **2015**, *43*, 103–119. [CrossRef] [PubMed]
271. Qi, S.; Wang, C.; Song, D.; Song, Y.; Dunaief, J.L. Intraperitoneal injection of (-)-Epigallocatechin-3-gallate protects against light-induced photoreceptor degeneration in the mouse retina. *Mol. Vis.* **2017**, *23*, 171–178.
272. Alaimo, A.; Di Santo, M.C.; Domínguez Rubio, A.P.; Chaufan, G.; García Liñares, G.; Pérez, O.E. Toxic effects of A2E in human ARPE-19 cells were prevented by resveratrol: A potential nutritional bioactive for age-related macular degeneration treatment. *Arch. Toxicol.* **2020**, *94*, 553–572. [CrossRef]
273. Moshtaghion, S.M.; Caballano-Infantes, E.; Plaza Reyes, Á.; Valdés-Sánchez, L.; Fernández, P.G.; de la Cerda, B.; Riga, M.S.; Álvarez-Dolado, M.; Peñalver, P.; Morales, J.C.; et al. Piceid octanoate protects retinal cells against oxidative damage by regulating the Sirtuin 1/Poly-ADP-ribose polymerase 1 axis in vitro and in rd10 mice. *Antioxidants* **2024**, *13*, 201. [CrossRef] [PubMed]
274. Cia, D.; Cubizolle, A.; Crauste, C.; Jacquemot, N.; Guillou, L.; Vigor, C.; Angebault, C.; Hamel, C.P.; Vercauteren, J.; Brabet, P. Phloroglucinol protects retinal pigment epithelium and photoreceptor against all-trans-retinal-induced toxicity and inhibits A2E formation. *J. Cell. Mol. Med.* **2016**, *20*, 1651–1663. [CrossRef]
275. Zhu, X.; Wang, K.; Zhou, F.; Zhu, L. Paeoniflorin attenuates atRAL-induced oxidative stress, mitochondrial dysfunction and endoplasmic reticulum stress in retinal pigment epithelial cells via triggering Ca(2+)/CaMKII-dependent activation of AMPK. *Arch. Pharm. Res.* **2018**, *41*, 1009–1018. [CrossRef] [PubMed]
276. Hsu, M.L.; Huang, W.C.; Zhou, Y.R.; Hu, S.; Huang, C.H.; Wu, S.J. Oleuropein protects human retinal pigment epithelium cells from IL-1β-induced inflammation by blocking MAPK/NF-κB signaling pathways. *Inflammation* **2022**, *45*, 297–307. [CrossRef] [PubMed]
277. Song, D.; Song, J.; Wang, C.; Li, Y.; Dunaief, J.L. Berberine protects against light-induced photoreceptor degeneration in the mouse retina. *Exp. Eye Res.* **2016**, *145*, 1–9. [CrossRef]
278. Kim, J.; Kim, K.M.; Kim, C.-S.; Sohn, E.; Lee, Y.M.; Jo, K.; Kim, J.S. Puerarin inhibits the retinal pericyte apoptosis induced by advanced glycation end products in vitro and in vivo by inhibiting NADPH oxidase-related oxidative stress. *Free Radic. Biol. Med.* **2012**, *53*, 357–365. [CrossRef] [PubMed]
279. Chen, X.; Han, R.; Hao, P.; Wang, L.; Liu, M.; Jin, M.; Kong, D.; Li, X. Nepetin inhibits IL-1β induced inflammation via NF-κB and MAPKs signaling pathways in ARPE-19 cells. *Biomed Pharmacother.* **2018**, *101*, 87–93. [CrossRef]
280. Kim, J.; Cho, K.; Choung, S.Y. Protective effect of Prunella vulgaris var. L extract against blue light induced damages in ARPE-19 cells and mouse retina. *Free Radic. Biol. Med.* **2020**, *152*, 622–631. [CrossRef]
281. Li, L.; Chen, W.; Ji, X.; Li, L.; Wang, H.; Wang, J.; Qiao, C.; Zhang, N.; Guo, Y.; Wang, H. Wolfberry water extract attenuates blue light-emitting diode damage to ARPE-19 cells and mouse retina by activating the NRF2 signaling pathway. *J. Food Sci.* **2023**, *88*, 2229–2245. [CrossRef]
282. Lee, S.J.; Roh, Y.J.; Kim, J.E.; Jin, Y.J.; Song, H.J.; Seol, A.; Park, S.H.; Douangdeuane, B.; Souliya, O.; Choi, S.I.; et al. Protective effects of Dipterocarpus tuberculatus in blue light-induced macular degeneration in A2E-laden ARPE19 cells and retina of Balb/c mice. *Antioxidants* **2023**, *12*, 329. [CrossRef]
283. Koraneeyakijkulchai, I.; Phumsuay, R.; Thiyajai, P.; Tuntipopipat, S.; Muangnoi, C. Anti-inflammatory activity and mechanism of sweet corn extract on IL-1β-induced inflammation in a human retinal pigment epithelial cell line (ARPE-19). *Int. J. Mol. Sci.* **2023**, *24*, 2462. [CrossRef] [PubMed]
284. Xie, Z.; Wu, X.; Gong, Y.; Song, Y.; Qiu, Q.; Li, C. Intraperitoneal injection of Ginkgo biloba extract enhances antioxidation ability of retina and protects photoreceptors after light-induced retinal damage in rats. *Curr. Eye Res.* **2007**, *32*, 471–479. [CrossRef] [PubMed]
285. Cho, H.M.; Lee, S.J.; Choung, S.Y. Protective effects of Panax ginseng berry extract on blue light-induced retinal damage in ARPE-19 cells and mouse retina. *J. Ginseng. Res.* **2023**, *47*, 65–73. [CrossRef] [PubMed]
286. Kim, D.H.; Choi, Y.R.; Shim, J.; Choi, Y.S.; Kim, Y.T.; Kim, M.K.; Kim, M.J. Suppressive effect of Arctium Lappa L. leaves on retinal damage against A2E-induced ARPE-19 cells and mice. *Molecules* **2020**, *25*, 1737. [CrossRef]
287. Yoon, S.M.; Lee, B.L.; Guo, Y.R.; Choung, S.Y. Preventive effect of Vaccinium uliginosum L. extract and its fractions on age-related macular degeneration and its action mechanisms. *Arch. Pharm. Res.* **2016**, *39*, 21–32. [CrossRef] [PubMed]

288. Pham, T.N.M.; Shin, C.Y.; Park, S.H.; Lee, T.H.; Ryu, H.Y.; Kim, S.B.; Auh, K.; Jeong, K.W. Solanum melongena L. extract protects retinal pigment epithelial cells from blue light-induced phototoxicity in in vitro and in vivo models. *Nutrients* **2021**, *13*, 359. [CrossRef] [PubMed]
289. Shin, C.Y.; Lee, M.H.; Kim, H.M.; Chung, H.C.; Kim, D.U.; Lee, J.H.; Jeong, K.W. Protective effect of Ribes nigrum extract against blue light-induced retinal degeneration in vitro and in vivo. *Antioxidants* **2022**, *11*, 832. [CrossRef] [PubMed]
290. Kim, M.J.; Kim, D.H.; Kwak, H.S.; Yu, I.S.; Um, M.Y. Protective effect of Chrysanthemum boreale flower extracts against A2E-induced retinal damage in ARPE-19 cell. *Antioxidants* **2022**, *11*, 669. [CrossRef] [PubMed]
291. Park, S.I.; Lee, E.H.; Kim, S.R.; Jang, Y.P. Anti-apoptotic effects of Curcuma longa L. extract and its curcuminoids against blue light-induced cytotoxicity in A2E-laden human retinal pigment epithelial cells. *J. Pharm. Pharmacol.* **2017**, *69*, 334–340. [CrossRef]
292. Maccarone, R.; Di Marco, S.; Bisti, S. Saffron supplement maintains morphology and function after exposure to damaging light in mammalian retina. *Investig. Ophthalmol. Vis. Sci.* **2008**, *49*, 1254–1261. [CrossRef]
293. Cho, H.M.; Jo, Y.D.; Choung, S.Y. Protective effects of Spirulina maxima against blue light-induced retinal damages in A2E-laden ARPE-19 cells and Balb/c mice. *Nutrients* **2022**, *14*, 401. [CrossRef]
294. Organisciak, D.T.; Darrow, R.M.; Rapp, C.M.; Smuts, J.P.; Armstrong, D.W.; Lang, J.C. Prevention of retinal light damage by zinc oxide combined with rosemary extract. *Mol. Vis.* **2013**, *19*, 1433–1445.
295. Liu, Y.; Liu, M.; Chen, Q.; Liu, G.M.; Cao, M.J.; Sun, L.; Lu, Z.; Guo, C. Blueberry polyphenols ameliorate visible light and lipid-induced injury of retinal pigment epithelial cells. *J. Agric. Food Chem.* **2018**, *66*, 12730–12740. [CrossRef] [PubMed]
296. Liu, Y.; Song, X.; Zhang, D.; Zhou, F.; Wang, D.; Wei, Y.; Gao, F.; Xie, L.; Jia, G.; Wu, W.; et al. Blueberry anthocyanins: Protection against ageing and light-induced damage in retinal pigment epithelial cells. *Br. J. Nutr.* **2012**, *108*, 16–27. [CrossRef]
297. Tülüce, Y.; Ozkol, H.; Koyuncu, I. Photoprotective effect of flax seed oil (*Linum usitatissimum* L.) against ultraviolet C-induced apoptosis and oxidative stress in rats. *Toxicol. Ind. Health* **2012**, *28*, 99–107. [CrossRef] [PubMed]
298. Chang, C.H.; Chiu, H.F.; Han, Y.C.; Chen, I.H.; Shen, Y.C.; Venkatakrishnan, K.; Wang, C.K. Photoprotective effects of cranberry juice and its various fractions against blue light-induced impairment in human retinal pigment epithelial cells. *Pharm. Biol.* **2017**, *55*, 571–580. [CrossRef]
299. Tanaka, J.; Nakanishi, T.; Ogawa, K.; Tsuruma, K.; Shimazawa, M.; Shimoda, H.; Hara, H. Purple rice extract and anthocyanidins of the constituents protect against light-induced retinal damage in vitro and in vivo. *J. Agric. Food Chem.* **2011**, *59*, 528–536. [CrossRef]
300. Owoyele, B.V.; Ayilara, O.G. Coconut oil protects against light-induced retina degeneration in male Wistar rats. *Pathophysiology* **2019**, *26*, 89–95. [CrossRef] [PubMed]
301. Ogawa, K.; Kuse, Y.; Tsuruma, K.; Kobayashi, S.; Shimazawa, M.; Hara, H. Protective effects of bilberry and lingonberry extracts against blue light-emitting diode light-induced retinal photoreceptor cell damage in vitro. *BMC Complement. Altern. Med.* **2014**, *14*, 120. [CrossRef]
302. Zhao, Z.; Sun, T.; Jiang, Y.; Wu, L.; Cai, X.; Sun, X.; Sun, X. Photooxidative damage in retinal pigment epithelial cells via GRP78 and the protective role of grape skin polyphenols. *Food Chem. Toxicol.* **2014**, *74*, 216–224. [CrossRef]
303. Wu, M.R.; Lin, C.H.; Ho, J.D.; Hsiao, G.; Cheng, Y.W. Novel protective effects of *Cistanche tubulosa* extract against low-luminance blue light-induced degenerative retinopathy. *Cell. Physiol. Biochem.* **2018**, *51*, 63–79. [CrossRef] [PubMed]
304. Perretti, M.; Dalli, J. Resolution pharmacology: Focus on pro-resolving annexin A1 and lipid mediators for therapeutic innovation in inflammation. *Annu. Rev. Pharmacol. Toxicol.* **2023**, *63*, 449–469. [CrossRef]
305. Yu, X.; Chen, K.; Wei, N.; Zhang, Q.; Liu, J.; Mi, M. Dietary taurine reduces retinal damage produced by photochemical stress via antioxidant and anti-apoptotic mechanisms in Sprague-Dawley rats. *Br. J. Nutr.* **2007**, *98*, 711–719. [CrossRef]
306. Tanito, M.; Masutani, H.; Nakamura, H.; Ohira, A.; Yodoi, J. Cytoprotective effect of thioredoxin against retinal photic injury in mice. *Investig. Ophthalmol. Vis. Sci.* **2002**, *43*, 1162–1167.
307. Xie, T.; Cai, J.; Yao, Y.; Sun, C.; Yang, Q.; Wu, M.; Xu, Z.; Sun, X.; Wang, X. LXA4 protects against blue-light induced retinal degeneration in human A2E-laden RPE cells and Balb-c mice. *Ann. Transl. Med.* **2021**, *9*, 1249. [CrossRef]
308. Shaban, H.; Borrás, C.; Viña, J.; Richter, C. Phosphatidylglycerol potently protects human retinal pigment epithelial cells against apoptosis induced by A2E, a compound suspected to cause age-related macula degeneration. *Exp. Eye Res.* **2002**, *75*, 99–108. [CrossRef]
309. Orhan, C.; Tuzcu, M.; Gencoglu, H.; Sahin, E.; Sahin, N.; Ozercan, I.H.; Namjoshi, T.; Srivastava, V.; Morde, A.; Rai, D.; et al. Different doses of β-cryptoxanthin may secure the retina from photooxidative injury resulted from common LED sources. *Oxid. Med. Cell. Longev.* **2021**, *2021*, 6672525. [CrossRef] [PubMed]
310. Kim, O.S.; Kim, J.; Kim, C.S.; Kim, N.H.; Kim, J.S. KIOM-79 prevents methyglyoxal-induced retinal pericyte apoptosis in vitro and in vivo. *J. Ethnopharmacol.* **2010**, *129*, 285–292. [CrossRef] [PubMed]
311. Vincent, M.; Simon, L.; Brabet, P.; Legrand, P.; Dorandeu, C.; Him, J.L.K.; Durand, T.; Crauste, C.; Begu, S. Formulation and evaluation of SNEDDS loaded with original lipophenol for the oral route to prevent dry AMD and Stargardt's disease. *Pharmaceutics* **2022**, *14*, 1029. [CrossRef]
312. Kim, J.; Kim, C.S.; Sohn, E.; Lee, Y.M.; Jo, K.; Kim, J.S. KIOM-79 protects AGE-induced retinal pericyte apoptosis via inhibition of NF-kappaB activation in vitro and in vivo. *PLoS ONE* **2012**, *7*, e43591. [CrossRef]

313. Ni, Y.Q.; Xu, G.Z.; Hu, W.Z.; Shi, L.; Qin, Y.W.; Da, C.D. Neuroprotective effects of naloxone against light-induced photoreceptor degeneration through inhibiting retinal microglial activation. *Investig. Ophthalmol. Vis. Sci.* **2008**, *49*, 2589–2598. [CrossRef] [PubMed]
314. Zhang, C.; Lei, B.; Lam, T.T.; Yang, F.; Sinha, D.; Tso, M.O. Neuroprotection of photoreceptors by minocycline in light-induced retinal degeneration. *Investig. Ophthalmol. Vis. Sci.* **2004**, *45*, 2753–2759. [CrossRef] [PubMed]
315. Kraus, R.L.; Pasieczny, R.; Lariosa-Willingham, K.; Turner, M.S.; Jiang, A.; Trauger, J.W. Antioxidant properties of minocycline: Neuroprotection in an oxidative stress assay and direct radical-scavenging activity. *J. Neurochem.* **2005**, *94*, 819–827. [CrossRef] [PubMed]
316. Mandala, A.; Armstrong, A.; Girresch, B.; Zhu, J.; Chilakala, A.; Chavalmane, S.; Chaudhary, K.; Biswas, P.; Ogilvie, J.; Gnana-Prakasam, J.P. Fenofibrate prevents iron induced activation of canonical Wnt/β-catenin and oxidative stress signaling in the retina. *NPJ Aging Mech. Dis.* **2020**, *6*, 12. [CrossRef] [PubMed]
317. Zhou, J.; Jang, Y.P.; Chang, S.; Sparrow, J.R. OT-674 suppresses photooxidative processes initiated by an RPE lipofuscin fluorophore. *Photochem. Photobiol.* **2008**, *84*, 75–80. [CrossRef] [PubMed]
318. Biswal, M.R.; Han, P.; Zhu, P.; Wang, Z.; Li, H.; Ildefonso, C.J.; Lewin, A.S. Timing of Antioxidant Gene Therapy: Implications for Treating Dry AMD. *Investig. Ophthalmol. Vis. Sci.* **2017**, *58*, 1237–1245. [CrossRef]
319. Askou, A.L. Development of gene therapy for treatment of age-related macular degeneration. *Acta Ophthalmol.* **2014**, *92*, 1–38. [CrossRef] [PubMed]
320. Berkowitz, S.T.; Finn, A.P. Gene therapy for age-related macular degeneration: Potential, feasibility, and pitfalls. *Curr. Opin. Ophthalmol.* **2024**, *35*, 170–177. [CrossRef]
321. Khanani, A.M.; Thomas, M.J.; Aziz, A.A.; Weng, C.Y.; Danzig, C.J.; Yiu, G.; Kiss, S.; Waheed, N.K.; Kaiser, P.K. Review of gene therapies for age-related macular degeneration. *Eye* **2022**, *36*, 303–311. [CrossRef]

antioxidants

MDPI

Article

The microRNA Let-7f Induces Senescence and Exacerbates Oxidative Stress in Retinal Pigment Epithelial Cells

Christina Ortiz [1], Houda Tahiri [2], Chun Yang [2], Claudia Gilbert [2], Carl Fortin [2] and Pierre Hardy [1,2,3,*]

[1] Departments of Pharmacology and Physiology, Faculty of Medicine, Université de Montréal, Montréal, QC H3T 1J4, Canada; christina.ortiz@cnrc-nrc.gc.ca
[2] CHU Sainte-Justine Research Center, Université de Montréal, Montréal, QC H3T 1C5, Canada; houda.tahiri.hsj@ssss.gouv.qc.ca (H.T.); cyang_09@yahoo.com (C.Y.); claudia.gilbert2.hsj@ssss.gouv.qc.ca (C.G.); carl.fortin.hsj@ssss.gouv.qc.ca (C.F.)
[3] Department of Pediatrics, Faculty of Medicine, Université de Montréal, Montréal, QC H3T 1J4, Canada
* Correspondence: pierre.hardy.med@ssss.gouv.qc.ca; Tel.: +1-514-345-4931 (ext. 3656)

Abstract: This study aims to investigate the role of microRNA let-7f in the dysfunction and degeneration of retinal pigment epithelium (RPE) cells through the induction of senescence and oxidative stress. Furthermore, we explore whether let-7f inhibition can protect these cells against sodium iodate (SI)-induced oxidative stress. Oxidative stress and let-7f expression are reciprocally regulated in retinal pigment epithelial cells. Overexpression of let-7f in ARPE-19 cells induced oxidative stress as demonstrated by increased reactive oxygen species (ROS) production as well as senescence. Inhibition of let-7f successfully protected RPE cells from the detrimental effects induced by SI. In addition, let-7f overexpression induced RPE cellular dysfunction by diminishing their migratory capabilities and reducing the phagocytosis of porcine photoreceptor outer segments (POS). Results were further confirmed in vivo by intravitreal injections of SI and let-7f antagomir in C57BL/6 mice. Our results provide strong evidence that let-7f is implicated in the dysfunction of RPE cells through the induction of senescence and oxidative injury. These findings may help to uncover novel and relevant processes in the pathogenesis of dry AMD.

Keywords: dry age-related macular degeneration; microRNA let-7f; oxidative stress; senescence

1. Introduction

The retinal pigment epithelium (RPE) is a specialized monolayer of cells located at the outermost layer of the retina [1,2]. RPE cells are multifunctional and essential for maintaining proper vision. In addition to forming the blood–retinal barrier, playing a role in the visual cycle and absorbing excess scattered light, RPE cells are the caretakers of photoreceptor cells. RPE cells are responsible for the phagocytosis and clearance of shed photoreceptor tips and are thus fundamental in maintaining photoreceptor survival and functioning [3,4]. RPE cells must meet high energy demands to perform their many functions, rendering them particularly susceptible to oxidative injury. The excessive production of reactive oxygen species (ROS) in the RPE is usually counterbalanced by an efficient endogenous antioxidant defense mechanism. However, with aging, the strength of this defense system declines, leading to progressive dysfunction and the eventual degeneration or death of RPE cells. When coupled with additional oxidant-promoting stressors, such as smoking, obesity and genetics, age-associated damage to the RPE may lead to the development of various ocular diseases such as age-related macular degeneration (AMD) [5,6].

In developed countries, AMD is the primary cause of blindness and visual impairment amongst older people. There exist two forms of this disease: dry AMD and wet AMD. Wet AMD, also known as neovascular AMD, can progress rapidly causing vision loss within days or weeks due to the growth of abnormal blood vessels underneath the retina which damage the RPE monolayer. Although it is the less severe form of the disorder, approximately 90% of

all people with AMD suffer from the dry form, which is characterized by the accumulation of sub-RPE lipid waste deposits, also known as drusen, which induce atrophy of the RPE monolayer. To date, there exist no approved treatments capable of going beyond merely slowing the progression of this disease [7,8]. Decades of research have indicated that chronic oxidative stress at the RPE is a major contributing factor to the pathogenesis of dry AMD [6,7,9]. Another key player in the development and progression of dry AMD is senescence. Senescent RPE cells were first identified in older primates by Mishima et al. in 1999 [10]. More recent studies have revealed that oxidative stress induces premature senescence in RPE cells, thereby further exacerbating cellular dysfunction [11–13].

MicroRNAs are small non-coding RNAs that can silence gene expression by interacting with the 3′-UTR of target mRNAs, making them master regulators of post-transcriptional gene expression in various cellular pathways [14]. The first discovered miRNAs, the let-7 family, are comprised of 12 members (let-7a-1, 7a-2, 7a-3, 7b, 7c, 7d, 7e, 7f-1, 7f-2, 7g, 7i and mir-98) and are highly conserved across species. In humans, this family of miRNAs has well-established functions in cellular differentiation, cell cycle regulation and tumor suppression [15,16]. Additionally, they have been associated with the regulation of aging, oxidative stress and senescence in various cell types, including many related to ocular tissues [17–22]. A recent study by Wooff et al. has identified four members of the let-7 family, including let-7f, amongst the top ten most abundant miRNAs in extracellular vesicles released by photo-oxidative damaged retinas [23]. Despite substantial evidence linking let-7 miRNAs to age-related retinal disorders, their functional roles in the RPE remain essentially unexplored. In the present study, we examined the in vitro and in vivo expression of let-7f in RPE cells under sodium iodate (SI)-induced oxidative stress. Our findings provide novel evidence for the implication of let-7f in the dysfunction and the induction of senescence in RPE cells.

2. Materials and Methods

2.1. Animals

The animal protocol (#2021-3125) was approved by the CHU Sainte-Justine Research Center Animal Welfare Committee CIBPAR and followed the guidelines of the Canadian Council on Animal Care and the Guide for the Care and Use of Laboratory Animals published by the US National Institutes of Health. Six eight-week-old female C57BL/6J mice were purchased from Charles River (St. Constant, QC, Canada) and housed in a pathogen-free environment with a 12:12 h light/dark cycle with free access to chow and water.

2.2. In Vivo Retinal Degeneration Mouse Model

The mouse model of sodium iodate (SI)-induced retinal degeneration is a well-established, widely used model for pro-oxidant-induced RPE degeneration [24,25]. Before injection, SI was dissolved in saline and sterilized. Mice received a single systemic tail-vein injection of 50 mg/kg. One group of mice was injected intravitreously with 1 µg let-7f antagomir (hsa-let-7f-5p miRNA antagomir, Applied Biological Materials, Richmond, BC, Canada) using Invivofectamine® 3.0 (Thermo Scientific, Rockford, IL, USA), 24 h prior to SI injection. As an internal control, the contralateral eye was injected with 1 µg scrambled miRNA. The mice were sacrificed and their eyes were collected on days 0, 3, 5, 7 and 10. A minimum of three mice was used for each treatment group.

2.3. Retinal Histology

After sacrifice, mice were enucleated and whole eyes were fixed in 4% PFA for 1 h at room temperature, washed in PBS and cryoprotected overnight at 4 °C in a 30% sucrose solution. Eyes were then embedded and snap frozen in O.C.T (Sakura Finetek, Torrance, California, USA). Sagittal 10 µm retinal cryosections were prepared with a Cryostat Epredia (CryoStar NX50, Thermo Scientific, Rockford, IL, USA) microtome. Sections were stained with hematoxylin and eosin (H&E) following standard protocols. Images were obtained

using a brightfield Leica DMi8 inverted microscope (Leica Microsystems, Mannheim, Germany) at 20×.

2.4. RPE/Eyecup Wholemount Preparation and Labeling

After sacrifice, mice were enucleated and whole eyes were fixed in 4% PFA for 1 h at room temperature. Under a dissecting microscope, eyes were cleaned of extraocular tissue and carefully dissected to remove the anterior segment (i.e., cornea, iris, ciliary body and lens). Four radial cuts were made toward the optic nerve to facilitate flattening of the posterior eyecup, resulting in a petal-shaped structure, and then the neural retina was gently peeled away, exposing the intact RPE monolayer. RPE/eyecups were then carefully deposited into 96-well plates, permeabilized with 0.1% Triton X-100 at room temperature for 1 h and incubated at 4 °C overnight with Phalloidin-iFluor-488 (1:100, Abcam) in 1% bovine serum albumin (BSA). RPE/eyecups were transferred onto slides with the RPE layer facing up using a plastic transfer pipette. Excess liquid on the slide, around the tissue was absorbed using a kimwipe and the ends of the wholemount were gently extended to prevent folding of the petals prior to addition of mounting liquid (ProLong Diamond Antifade, Thermo Scientific, Rockford, IL, USA) and coverslip. Wholemount images were generated using a laser scanning confocal microscope (Leica TCS SP8-STED, Leica Microsystems, Mannheim, Germany) and Z-stacking. For each wholemount, four images (one image per petal, ~300 μm × 300 μm) were used for analysis. Damaged area was measured using Fiji/ImageJ software v1.54h.

2.5. Cell Culture

Human RPE cells (ARPE-19) were purchased from American Type Culture Collection (ATCC, CRL-2302) and cultured in Dulbecco's modified Eagle's medium (DMEM)/F12 (Gibco, Thermo Scientific, Rockford, IL, USA) supplemented with 10% fetal bovine serum, 100 U/mL penicillin and 100 μg/mL streptomycin and maintained at 37 °C in a humidified 5% CO_2 atmosphere. Only cell passages 6 through 13 were used for the following experiments unless otherwise indicated.

2.6. Cell Transfection and Treatments

With a TransIT-X2® Dynamic Delivery System (Mirus Bio LLC, Madison, WI, USA), ARPE-19 cells (80% confluency) were transfected with 50 nM hsa-let-7f-5p mirVana miRNA mimic (Ambion, Thermo Scientific, Rockford, IL, USA) for 48 h to induce the overpression of let-7f. To inhibit let-7f expression, cells were transfected with 20 nM hsa-let-7f-5p miRNA antagomir (Applied Biological Materials, Solana Beach, CA, USA) for 48 h. For each experiment, control cells were transfected with their respective scrambled miRNA (Sc). Another group of cells was treated with 5 mM SI (Sigma-Aldrich, Oakville, ON, Canada) 1 h after transfection with let-7f antagomir. A 50 mM working solution of SI was freshly prepared by dissolving in DMEM/F12 media and sterilized through a 0.22 μm syringe filter. SI added to the cells every 24 h to ensure stability.

2.7. Cell Viability Assays

ARPE-19 cells were plated (1×10^4 cells/well) onto 96-well black plates and treated according to the procedure described above. Cell viability was quantified using PrestoBlue® assay (Invitrogen, Waltham, MA, USA, Thermo Fisher Scientific, Fresno, CA, USA) by adding 10 μL/well of the reagent and incubating in the dark at 37 °C for 30 min. Fluorescence was read using a microplate reader (CLARIOstar, BMG Labtech; excitation 535 nm, emission 615 nm).

2.8. [^{3}H]-Thymidine Incorporation Proliferation Assays

ARPE-19 cells were plated (5×10^4 cells/well) onto 24-well plates and the incorporation of radioactive thymidine into DNA was used to quantify the rate of DNA synthesis. Briefly, 10 μCi [^{3}H]-thymidine was added per well, and cells were treated as described

above. Thymidine incorporation was measured 48 h after cell transfections and treatments using a liquid scintillation counter (PerkinElmer, Waltham, MA, USA).

2.9. Scratch Wound Migration Assays

Cell migration was evaluated by plating ARPE-19 cells (5×10^4 cells/well) onto 24-well plates and immediately prior to transfection, the narrow end of a p1000 tip was used to scratch a straight line diagonally through the cells across the center of the whole well. Cells were washed with PBS and fresh media was added to remove cellular debris. Images of the center of the well, where scratch was more linear, were taken at time points 0 (immediately after the scratch wound), 24, 48 and 72 h at 4X using live-cell imaging IncuCyte™ system (Essen Bioscience, Ann Arbor, MI, USA). Scratch wound area, represented by the total area of blue-outlined sections, was calculated using Fiji/ImageJ software v1.54h. The percent of healed gap wound area was calculated by the reduction in wound area at 72 h compared to wound area at time 0.

2.10. Isolation and Fluorescence Labeling of Photoreceptor Outer Segments

Photoreceptor outer segments (POS) were isolated and purified from 20 fresh adult porcine eyes purchased from Abattoir Campbell (Saint-Sébastien, QC, Canada), according to a modified method [26]. Briefly, eyes were dissected, and retinas were homogenized in a solution containing 20% sucrose, 20 mM Tris/Acetate pH 7.2, 2 mM $MgCl_2$, 10 mM glucose and 5 mM taurine. Homogenized solution was filtered 3 times through gauze to remove large debris. Crude isolate was carefully overlaid over a linear gradient of 25–60% sucrose and ultra-centrifuged at 25,000 rpm (CP90NX, Hitachi, Tokyo, Japan) for 48 min at 4 °C. POS fraction was identified as a sharp single pink band in the upper part of the gradient. POS were collected, washed and resuspended in 2.5% sucrose in DMEM. POS were counted with a hemocytometer. POS resuspension was diluted to 1×10^8 POS/mL in 2.5% sucrose in DMEM, aliquoted and stored at −80 °C. A portion of collected POS was labeled with fluorescein-5-isothiocyanate (FITC) by incubating in a 2 mg/mL FITC solution for 1 h at room temperature in the dark with rotation to ensure labeling of all POS. Labeled-POS were washed twice by extensive resuspension in a solution of 10% sucrose, 20 mM phosphate buffer pH 7.2 and 5 mM taurine to remove unbound FITC. Labeled-POS were counted, resuspended and aliquoted as described for unlabelled-POS.

2.11. Phagocytosis Assays

For phagocytic activity assays, ARPE-19 cells were plated (1×10^4 cells/well) onto 96-well black plates in complete medium until 100% confluence was achieved, followed by two weeks of sub-culturing in complete media reduced to 1% FBS to achieve mature cell polarization and tight-junction formation, indicated by cells forming a highly dense hexagonal shaped monolayer and displaying increased pigmentation. After transfection, mature and polarized cells were fed with FITC-POS (10 POS/cell) and incubated for 6 h at 37 °C. Unbound POS were removed by extensive washing with PBS. The fluorescence of phagocytosed FITC-POS was recorded with a fluorescent microplate reader (CLARIOstar, BMG Labtech; excitation 483 nm, emission 530 nm).

2.12. Immunofluorescence Staining

ARPE-19 cells (5×10^4 cells/well) were grown on coverslips inserted into 24-well plates. After treatment, cells were fixed in 4% PFA for 15 min followed by permeabilization and blocking in 0.1% Triton X-100, 2% normal goat serum and 1% BSA in PBS for 1 h at room temperature. Cells were then incubated overnight at 4 °C with rabbit anti-human Ki67 (1:500, Abcam, Cambridge, UK) in 1% BSA, washed three times in PBS, incubated with secondary antibody AlexaFluor-594 (1:500, Molecular Probes, Eugene, OR, USA) for 1 h at room temperature and then mounted onto slides with mounting liquid containing DAPI (ProLong Diamond Antifade, Thermo Scientific, Rockford, IL, USA). Images of 3 random frames were captured at 10× using a Leica DMi8 (Leica Microsystems, Mannheim, Ger-

many) inverted wide-field fluorescence microscope and analyzed with Fiji/ImageJ software v1.54h. The percent of Ki67 positive cells was calculated based on the number of Ki67 positive cells divided by the number of DAPI positive cells.

2.13. Senescence-Associated β-Galactosidase Assays

ARPE-19 cells were plated (5×10^4 cells/well) onto 24-well plates, transfected and stained with Senescence-Associated β-Galactosidase (SA-β-gal) Staining Kit (Cell Signaling, #9860) in which the activity of lysosomal β-galactosidase enzyme at pH 6, cleaves and converts substrate X-gal into a visually detectable oxidized blue product [27]. Briefly, cells were fixed in provided 1X fixative solution for 15 min at room temperature. After washing three times with PBS, cells were incubated in freshly prepared β-gal staining solution (1 mg/mL X-gal, pH 6) overnight at 37 °C in a dry incubator (no CO_2). Ensuring a final pH of 6.0 for the β-gal staining solution was crucial in preventing false positives or false negatives. Cells were washed, rinsed in methanol and air-dried before microscopic examination. Brightfield images of at least 100 cells per frame (10×), were taken with a Leica DMi8-inverted microscope (Leica Microsystems, Mannheim, Germany). Senescent cells were identified by the development of blue coloration as well as an enlarged, flattened cell morphology.

2.14. Measurement of Intracellular Reactive Oxygen Species Production

Intracellular production of ROS was measured with a 5-(and-6)-chloromethyl-2′,7′-dichlorodihydrofluorescein diacetate fluorescent probe (CM-H_2DCFDA, Thermo Scientific, Rockford, IL, USA). ARPE-19 cells were plated (1×10^4 cells/well) onto 96-well black plates, transfected as described above and incubated with 5 μM CM-H_2DCFDA for 30 min at 37 °C. Fluorescence intensity was measured with a microplate reader (CLARIOstar, BMG Labtech; excitation 493 nm, emission 516 nm).

2.15. MitoSOX Assays

The production of mitochondrial superoxide was detected in live cells with MitoSOX Red dye (Thermo Scientific, Rockford, IL, USA). Cells were plated (1×10^4 cells/dish) onto 35-mm glass bottom dishes (MatTek, Ashland, MA, USA), transfected and incubated with 2.5 μM MitoSOX for 10 min at 37 °C. After washing 3 times in PBS, cells were incubated with a 1 μg/mL Hoechst staining solution (Thermo Scientific, Rockford, IL, USA) for 5 min at 37 °C. At least 3 images (20×) were taken per dish using a laser scanning confocal microscope (Leica TCS SP8-STED, Leica Microsystems, Mannheim, Germany) and Z-stacking. MitoSOX red fluorescence intensity was measured using Fiji/ImageJ software v1.54h.

2.16. Western Blotting

ARPE-19 cells were plated (2×10^6 cells/dish) onto 10-cm dishes and collected 48 h post-transfection. Proteins were extracted from cells by lysis in a lysis buffer solution containing M-PER, 1X protease inhibitor and 1X phosphatase inhibitor (Thermo Scientific, Rockford, IL, USA) for 1 h at 4 °C with inversion. Lysates were centrifuged at 13,000 rpm for 10 min at 4 °C. The aqueous protein solution was collected and concentrated using Amicon Ultra 10 k filters (Millipore, Sigma-Aldrich, Oakville, ON, Canada). Protein concentration was measured using Bradford assay (Sigma-Aldrich, Sigma-Aldrich, Oakville, ON, Canada) and 40 μg protein sample was loaded per well into 12% polyacrylamide gels, separated via electrophoresis and transferred at 4 °C overnight onto polyvinylidene difluoride (PVDF) membranes (Millipore, Bedford, MA, USA). Membranes were blocked in 5% BSA for 2 h and incubated with mouse anti-human $p16^{INK4a}$ (1:500, Lifespan Biosciences, Shirley, MA, USA), mouse anti-human $p21^{Waf/Cip1}$ (1:500, Lifespan Biosciences) or rabbit anti-human β-actin (1:5000, Novus Biologicals, Centennial, CO, USA) at 4 °C overnight. Next, membranes were incubated with HRP-conjugated anti-mouse or anti-rabbit (1:2500, Santa Cruz Biotechnology, Dallas, TX, USA) secondary antibodies for 1 h at room temperature.

Protein bands were detected with an enhanced chemiluminescence (ECL) kit (Bio-Rad Laboratories, Hercules, CA, USA) using an ECL detection system (ImageQuant LAS 500, GE Healthcare Systems, Chicago, IL, USA). Blots were quantified via densitometry using ImageLab Software (V6.0.1 Bio-Rad Laboratories, Hercules, CA, USA) and normalized to β-actin.

2.17. Quantitative Real-Time PCR

Total miRNA was isolated from RPE/eyecups of mice or ARPE-19 cells using miRNAeasy kit (Qiagen, Toronto, ON, Canada). cDNA was prepared from total miRNA using the miRCURY LNA RT cDNA synthesis kit (Qiagen, Toronto, ON, Canada) as directed by the manufacturer. miRNA qPCR assays were performed in 96-well PCR plates (Bio-Rad Laboratories, Hercules, CA, USA). Total reaction volume of 10 µL per well contained 5 µL 2X miRCURY SYBR Green Master Mix, 3 µL 1 ng/µL cDNA (diluted 1:60), 1 µL specific primer mix (10µM) and 1 µL RNAse-free water. The reactions were performed on a LightCycler 96 Roche platform (Roche, IN, USA). Primers for let-7f and 103a-3p were obtained by Qiagen, Toronto, ON, Canada; primers are considered proprietary to the suppliers, not available to the public. miRNA expression was calculated by the $2^{-\Delta\Delta Ct}$ method and normalized to reference gene 103a-3p.

2.18. Statistical Analysis

Results are presented as means ± SD from at least three independent experiments performed with a minimum of 3 replicates per conditions. Two-tailed Student's *t*-test was used to determine significant differences between two groups. One-way ANOVA followed by post-hoc Bonferroni test was used for the comparison of means from three or more groups. The threshold for statistical significance was set at $p < 0.05$.

3. Results

3.1. Let-7f Is Upregulated and Induces Oxidative Stress in RPE Cells

Let-7f expression has been shown to be upregulated in various age-related ocular disorders and to be modulated by oxidative stress [20,21,28,29]. We first investigated the expression of let-7f in RPE cells exposed to SI-induced oxidative stress. We demonstrated that let-7f expression increased dose-dependently in ARPE-19 cells treated with SI (Figure 1A). Additionally, we verified that the upregulation of let-7f was not limited to SI-induced oxidative stress: a similar dose-dependent increase in let-7f expression was observed in ARPE-19 cells treated with hydrogen peroxide (H_2O_2), another common inducer of oxidative stress (Figure S1A). To confirm our in vitro findings, we examined the expression of let-7f using the in vivo SI mouse model of oxidant-induced RPE damage. With H&E staining, we validated the model by demonstrating an overall thinning of the retinal layers along with the degeneration and formation of large drusen-like deposits at the RPE in mice injected with 50 mg/kg SI (Figure S2). Interestingly, the expression of let-7f in RPE/eyecups increased significantly at days 3 and 5 after SI injection, then returned to baseline levels at days 7 and 10 (Figure 1B). No significant change in let-7f expression was observed in the neural retina (Figure S1B), further suggesting that the relationship between let-7f and oxidative stress is localized to the RPE. Based on these results, we sought to determine whether the overexpression of let-7f could induce oxidative injury in healthy RPE cells. Oxidative stress was assessed at the intracellular and mitochondrial levels. ARPE-19 cells transfected with 50 nM let-7f miRNA showed approximately a 1.5-fold increase in the production of intracellular ROS than that observed in scramble (Sc) control transfected cells (Figure 1C). Similarly, the production of mtROS increased in let-7f overexpressing cells as revealed via MitoSOX red fluorescence intensity (Figure 1D,E). Overall, our findings suggest that let-7f plays a role in the regulation and induction of oxidative stress in RPE cells.

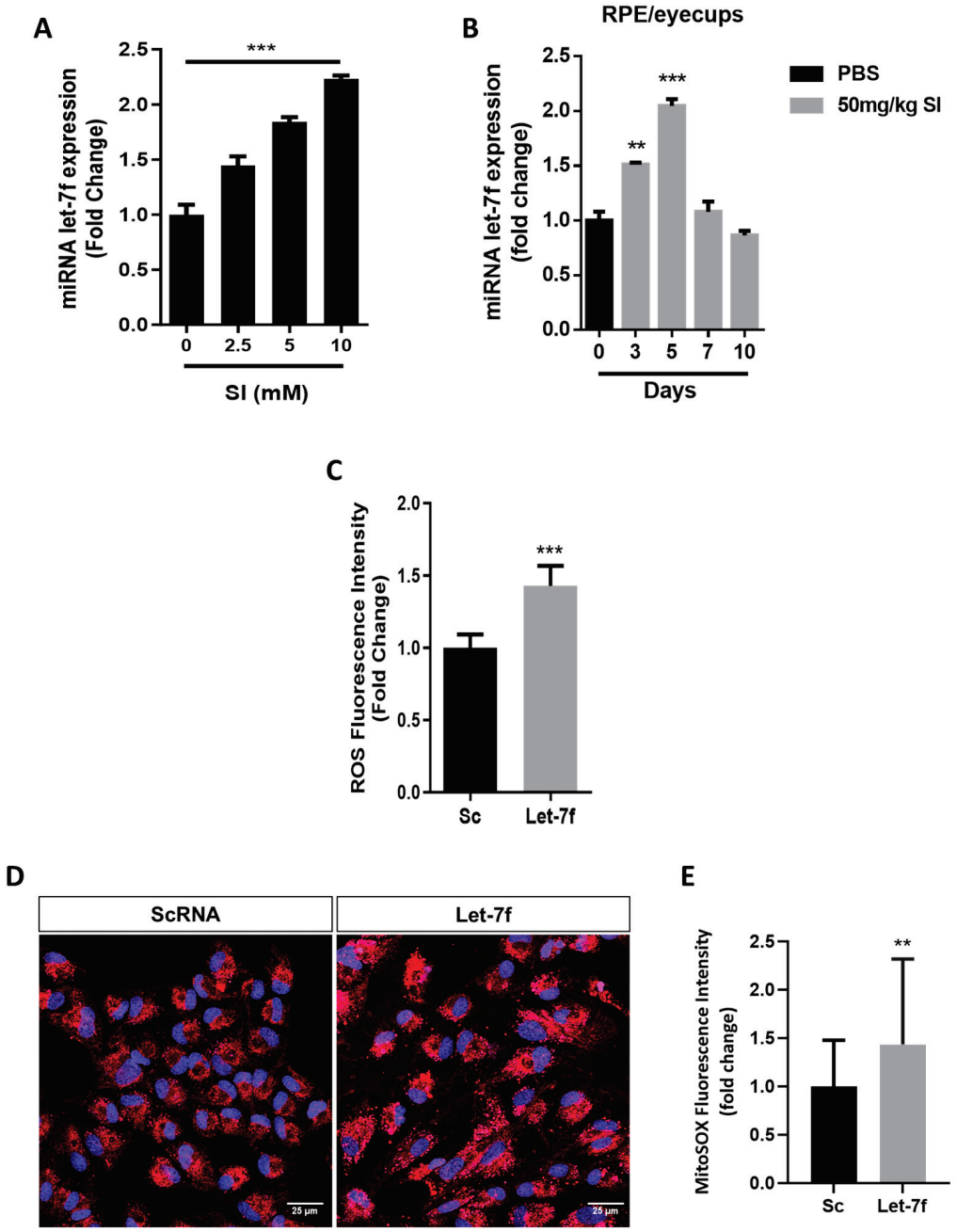

Figure 1. Oxidative stress is regulated by let-7f in RPE cells. (**A**) ARPE-19 cells were treated with increasing doses of SI (0, 2.5, 5 and 10 mM) for 48 h. The expression of let-7f miRNA was evaluated via RT-qPCR and expressed as a fold change versus untreated cells (0 mM). *** $p < 0.001$ vs. Untr. (**B**) Six eight-week-old female C57BL/6J mice were injected via the tail vein with 50 mg/kg SI or with vehicle (PBS) and sacrificed on days 0, 3, 5, 7 and 10. Total miRNA was isolated from RPE/eyecups and let-7f expression was quantified via RT-qPCR and expressed as fold change versus control retina (day 0, PBS). ** $p < 0.01$, *** $p < 0.001$ vs. CTL. (**C**) Let-7f overexpression was achieved by transfecting ARPE-19 cells with 50 nM let-7f mimic for 48 h and oxidative stress was then evaluated using CM-H_2DCFDA assay to quantify the production of intracellular ROS. ROS fluorescence intensity was measured and presented as a fold change versus scramble control (Sc). *** $p < 0.001$ vs. Sc. (**D**) MitoSOX superoxide assay was used to detect mitochondrial ROS. Representative confocal images of live cells stained with MitoSOX (red) and Hoechst (nuclear DNA, blue). Scale bar = 25 µm. (**E**) Quantification of MitoSOX fluorescence intensity expressed as a fold change versus scramble control (Sc). ** $p < 0.01$ vs. Sc. All data are expressed as the mean ± SD ($n = 3$).

3.2. Let-7f Overexpression Promotes RPE Cellular Dysfunction

Having shown that the overexpression of let-7f induces oxidative stress in RPE cells (Figure 1), we hypothesized that its upregulation could also promote cellular dysfunction. A major role of the RPE is the efficient phagocytosis of shed photoreceptor outer segments (POS), a mechanism shown to be impaired by oxidative injury [30]. To explore the effects of let-7f on RPE phagocytic activity, we fed FITC-labeled POS (FITC-POS) to mature polarized ARPE-19 cells for a period of 6 h. The optimal POS incubation period was determined in preliminary testing (Figure S3). Although a 24 h incubation yielded a higher rate of phagocytosis, we opted for the 6 h incubation period due to evidence indicating that the inhibition of phagocytosis by oxidative stress is transient and can be restored after 24 h, giving rise to false negatives [31]. The fluorescence intensity of engulfed POS was measured and a reduction of approximately 10% in phagocytic activity was observed in ARPE-19 cells transfected with let-7f (Figure 2A). In addition, we examined the functional effects of let-7f on RPE cellular migration and proliferation—two important mechanisms that can be activated by the in vivo human RPE upon injury or cell death at the macula, as seen in geographic atrophy [32,33]. We observed that the overexpression of let-7f resulted in a significant decrease of both ARPE-19 cellular migration and proliferation, as revealed by scratch wound and ^{3}H-thymidine incorporation assays, respectively (Figure 2B–D). Likewise, cellular viability was significantly reduced in cells overexpressing let-7f (Figure 2E). Comparably, preliminary tests using primary mouse RPE cells, which were characterized via RPE65 staining and successfully transfected with let-7f, revealed a dramatic decreased in cellular viability upon let-7f overexpression (Figure S4A–C). Our findings along with the detailed literature that has classified the let-7 family of miRNAs as major cell cycle regulators, shifted our interest towards investigating the possibility of let-7f-induced cell cycle arrest and senescence in RPE cells [15].

3.3. Overexpression of Let-7f Induces Senescence in RPE Cells

Oxidative stress-induced senescence has been extensively associated with the development and progression of dry AMD [12]. To initiate our investigation, we examined the cellular expression of Ki67 nuclear protein marker, whose absence is indicative of cell cycle arrest at the G_0 phase. Immunofluorescence staining revealed a substantial decrease in the number of Ki67 positive ARPE-19 cells when transfected with let-7f, suggesting an increase in cells arrested at G_0 phase (Figure 3A,B). In addition to cell cycle arrest, a classic marker of cellular senescence is high activity of lysosomal β-galactosidase (β-gal) enzyme, referred to as senescence-associated β-gal (SA-β-gal), which can be detected and observed through SA-β-gal staining at pH 6 [27,34]. Consistently, overexpression of let-7f led to a dramatic increase in the number of senescent ARPE-19 cells, confirmed by the development of blue coloration upon SA-β-gal staining (Figure 3C,D). To further support our findings, we evaluated the protein expression levels of $p16^{INK4a}$ and $p21^{Waf/Cip1}$, two cyclin-dependent kinase inhibitors whose upregulations are established markers of senescence. Transfection of let-7f in ARPE-19 cells significantly increased the protein expression of $p16^{INK4a}$ by approximately twofold, though no significant change in $p21^{Waf/Cip1}$ protein expression was detected (Figure 3E). Interestingly, overexpression of let-7f in primary RPE cells led to the upregulation of $p16^{INK4a}$ and $p21^{Waf/Cip1}$ mRNA expression levels (Figure S4D). Collectively, our results strongly suggest that let-7f is involved in the induction of senescence in RPE cells.

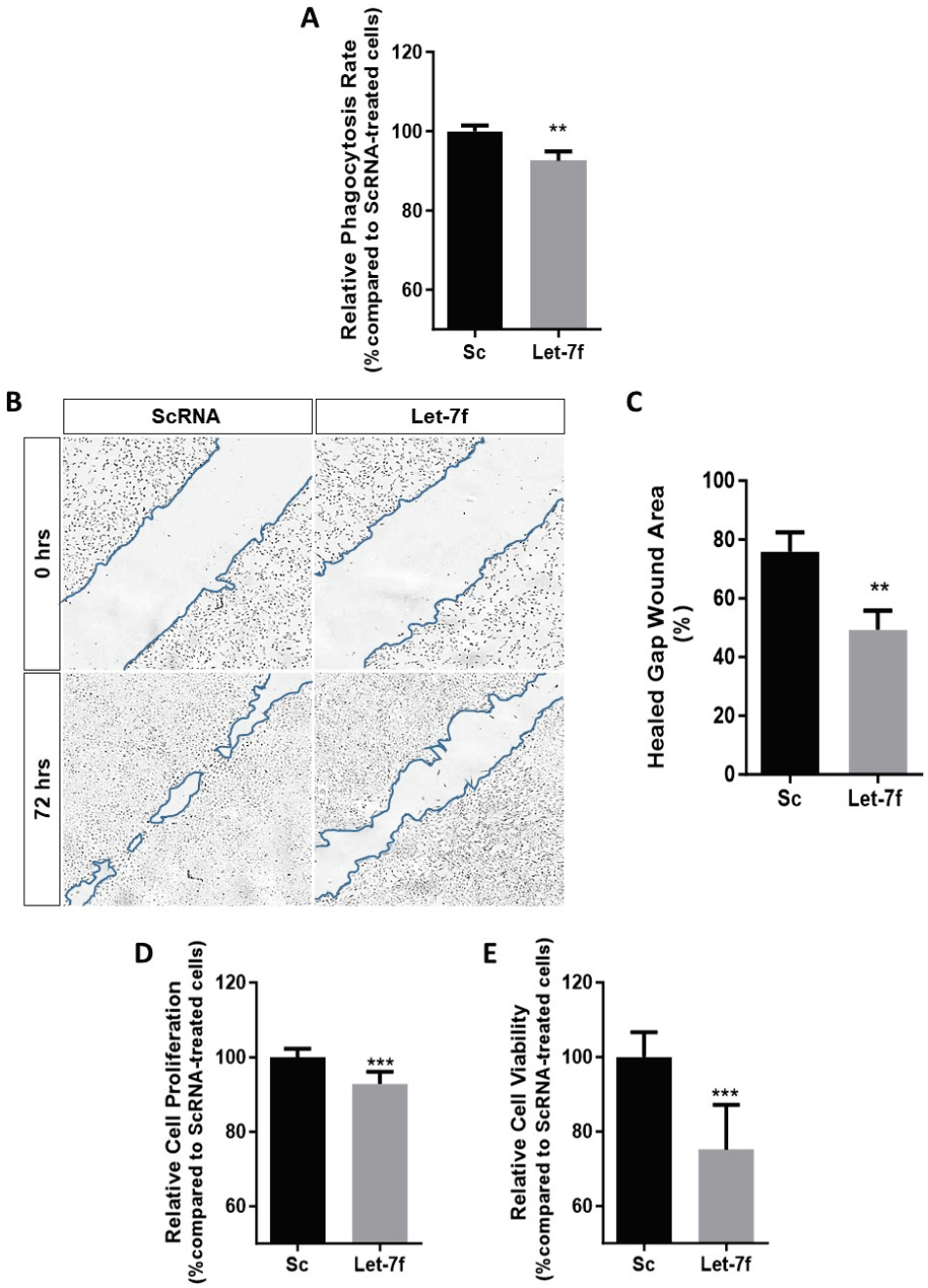

Figure 2. Let-7f induces cellular dysfunction in human retinal pigment epithelial cells. ARPE-19 cells were transfected with 50 nM let-7f mimic for 48 h and cellular functionality was examined. (**A**) Fluorescence intensity of engulfed POS-FITC was quantified over 6 h and expressed as a percentage compared to scramble control (Sc). (**B**) Representative images of scratch wound healing assay used to evaluate migration (4X). A scratch was made across confluent ARPE-19 cells and wound-healing was observed for 72 h. (**C**) Wound gap area was measured with ImageJ software v1.54h and the percent of healed gap wound area was calculated by the area reduction compared to time 0 and presented relative to scramble control (Sc). (**D**) Cellular proliferation was determined via [3H]-thymine incorporation assay and presented as percentage versus scramble control cells (Sc). (**E**) Cellular viability was analyzed using PrestoBlue® assay and fluorescence intensity was measured and expressed as a percentage compared to scramble control cells (Sc). ** $p < 0.01$, *** $p < 0.001$ vs. Sc. All data are expressed as the mean ± SD ($n = 3$).

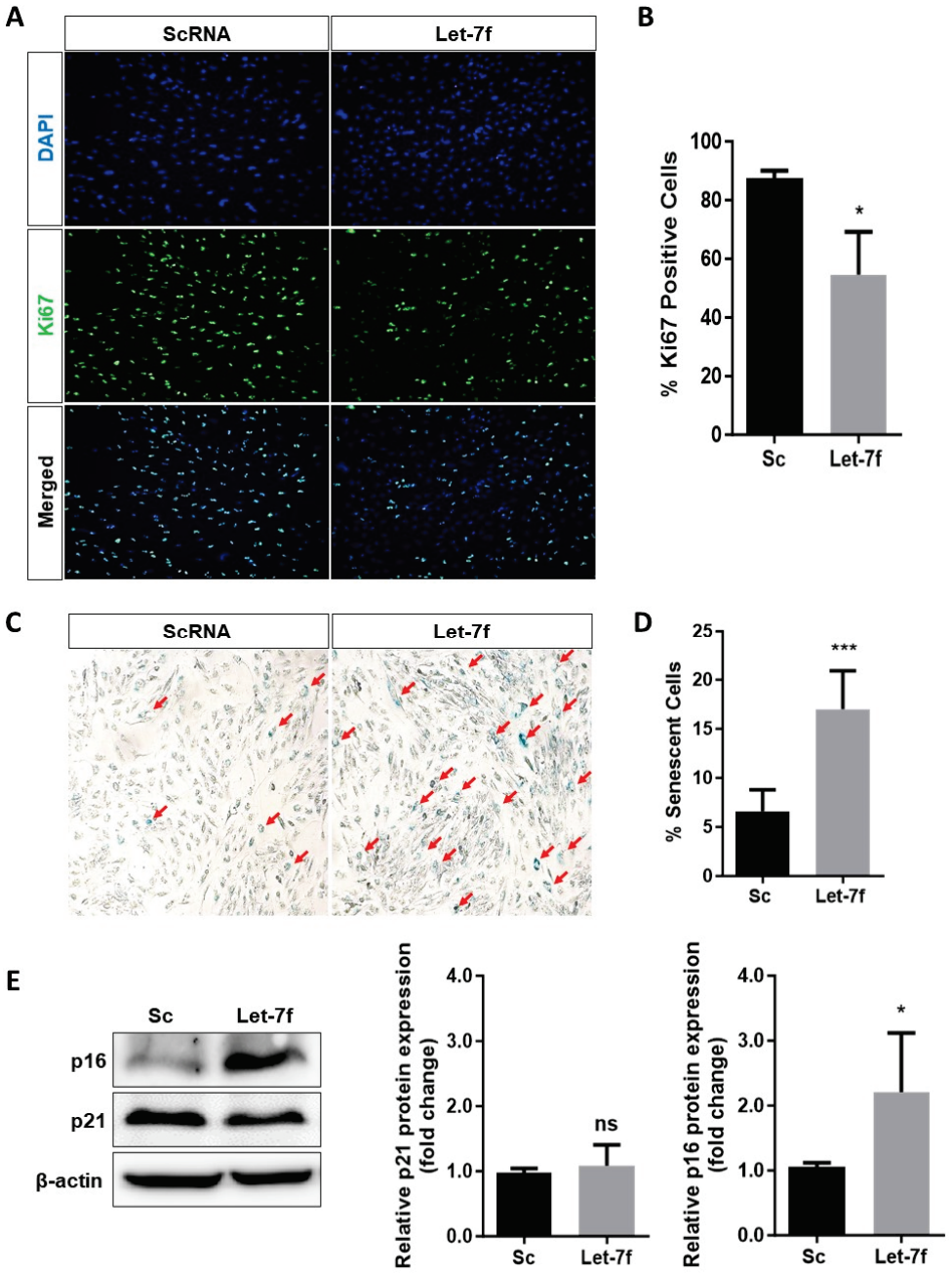

Figure 3. Let-7f induces a senescence phenotype in human retinal pigment epithelial cells. ARPE-19 cells were transfected with 50 nM let-7f mimic for 48 h and senescence was examined through various assays. (**A**) Proliferating cells were identified via immunofluorescent staining of Ki67 (green) positive cells and nuclei (DAPI, blue) (10×). (**B**) The percent of Ki67 positive cells was calculated based on the number of Ki67 positive cells divided by the total number of cells (DAPI positive) and expressed versus scramble control (Sc). (**C**) Representative images of senescence-associated β-galactosidase (SA-β-gal) staining used to detect senescent ARPE-19 cells. Senescent cells were identified by the development of blue coloration and an enlarged, flattened morphology as indicated by the red arrows (10×). (**D**) Percentage of senescent ARPE-19 cells was compared to scramble control (Sc). (**E**) The protein expression levels of cyclin-dependent kinase inhibitors $p16^{INK4a}$ and $p21^{Waf/Cip1}$ were detected via western blotting. Band densitometry was calculated using ImageLab Software and normalized to β-actin. Results were presented as a fold change compared to scramble control cells (Sc). * $p < 0.05$, *** $p < 0.001$ vs. Sc. ns: not significant. All data are expressed as the mean ± SD ($n = 3$).

3.4. Let-7f Inhibition Protects RPE Cells against SI-Induced Oxidative Injury

We next investigated the protective potential of let-7f inhibition against the deleterious effects of oxidative injury on RPE cells. To this end, ARPE-19 cells were transfected with 20 nM let-7f antagomir (anti-let-7f), and subsequently treated with 5 mM SI. The concentration and duration of SI treatment were optimized to generate sub-lethal cytotoxic effects still capable of inducing oxidative injury, a model better representative of the chronic stress occurring in the in vivo RPE during the progression of dry AMD [35]. Previous studies have identified the EC50 of SI in ARPE-19 cells to be approximately 10 mM when exposed for 24 h and that an acute non-lethal dose at concentrations of 10 mM or lower allows the investigation of the early effects of oxidative injury in RPE cells [36,37]. The concentration of 5 mM (double-dose) was selected for reason that this dose displayed sub-lethal effects (Figure S5) yet was sufficient in inducing oxidative stress (Figure S6) and upregulating the expression of let-7f miRNA in ARPE-19 cells (Figure 1A). As expected, treatment with SI increased intracellular ROS production by almost twofold in ARPE-19 cells. Notably, let-7f inhibition significantly protected cells from this increase (Figure 4A). Additionally, the inhibition of let-7f in ARPE-19 cells helped to prevent the loss in viability and proliferation induced by pro-oxidant SI (Figure 4B,C). Furthermore, SA-β-gal staining revealed that let-7f inhibition impressively suppressed ARPE-19 cellular senescence brought on by SI (Figure 4D,E). To verify whether the protective potential of let-7f inhibition in vitro could be translated to the in vivo RPE, we used the well-established mouse model of SI-induced retinal degeneration which we described and validated (Figure S2). Mice received an intravitreal injection of a let-7f antagomir (anti-let7f) or a scrambled control mimic (Sc) 24 h prior to a systemic injection with 50 mg/kg SI. Seven days later, animals were sacrificed and RPE/eyecup wholemounts were prepared from dissected retina for immunofluorescent evaluation. Phalloidin staining showed no evident disruptions in the overall morphology and organization of the RPE monolayer in mice injected only with scrambled control. In contrast, treatment with SI completely disrupted the morphology of the RPE monolayer, causing degeneration and substantial areas of cell loss. Pre-treatment with let-7f antagomir (anti-let7f + SI) resulted in a significant reduction of damaged area though not a complete rescue of the RPE (Figure 4F,G). Together, our results have demonstrated the protective potential of let-7f inhibition against oxidative injury in RPE cells.

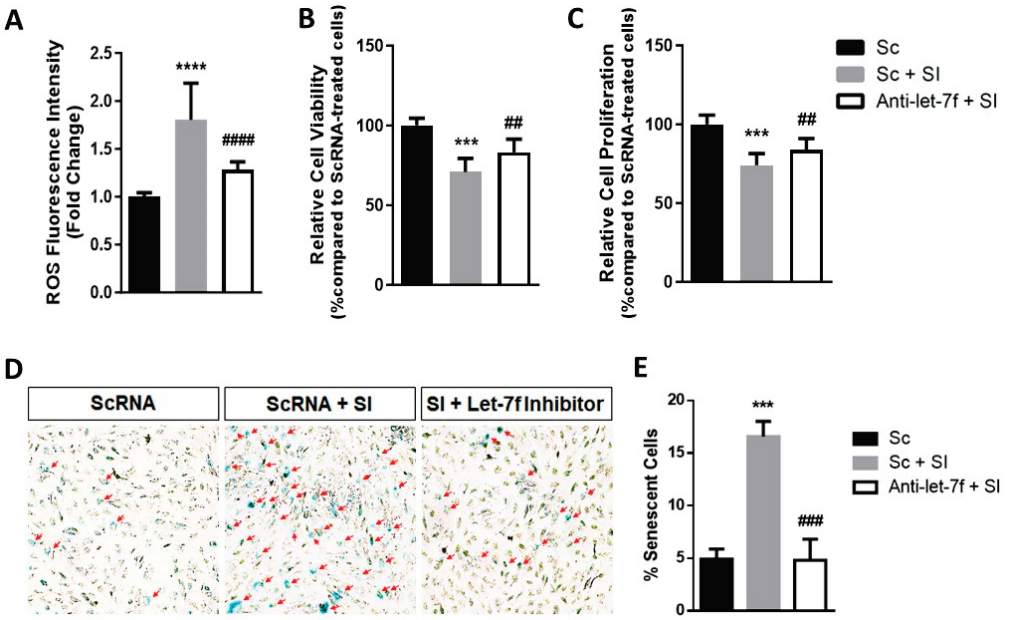

Figure 4. *Cont.*

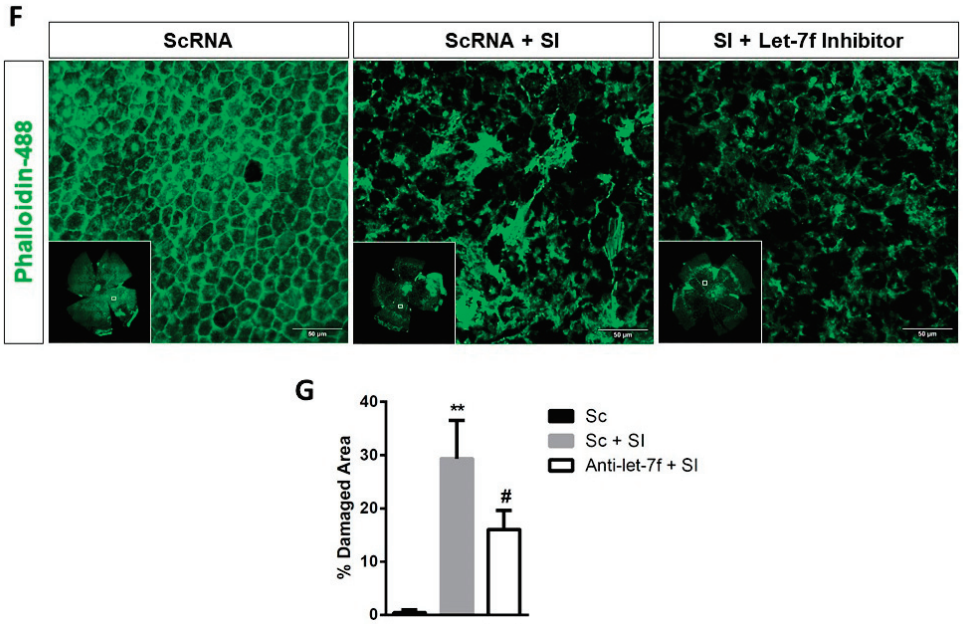

Figure 4. Inhibition of let-7f protects retinal pigment epithelial cells from sodium iodate-induced oxidative injury in vitro and in vivo. ARPE-19 cells were transfected with 20 nM let-7f antagomir (anti-let-7f) or with a scramble miRNA (Sc) and treated with 5 mM of SI for an additional 48 h. (**A**) The intracellular production of ROS was measured using CM-H_2DCFDA assay and ROS fluorescence intensity was presented as a fold change versus scramble control (Sc). (**B**) Cellular viability was analyzed using PrestoBlue® assay and fluorescence intensity was expressed as a percentage compared to scramble control cells (Sc). (**C**) Cellular proliferation was determined via [^{3}H]-thymine incorporation assay and presented as a percentage versus scramble control cells (Sc). (**D**) Representative images of senescent cells detected via senescence-associated β-galactosidase (SA-β-gal) staining. Senescent cells were identified by the development of blue coloration and an enlarged and flattened shape morphology as indicated by the red arrows (10×). (**E**) Percentage of senescent ARPE-19 cells was compared to scramble control (Sc). (**F**) Six eight-week-old female C57BL/6J mice received an intravitreal injection of 1μg let-7f antagomir (anti-let-7f) or scramble miRNA (Sc) 24 h prior to tail-vein injection with 50 mg/kg SI. Mice were sacrificed a week later and RPE/eyecup wholemounts were prepared from dissected retina. Shown are fluorescent confocal images of RPE/eyecups stained with phalloidin-488 to visualize RPE monolayer morphology and damaged areas. Scale bar = 50 μm. (**G**) Percent damaged area was calculated using ImageJ software v1.54h and compared to scramble control (Sc) RPE/eyecups. ** $p < 0.01$, *** $p < 0.001$, **** $p < 0.0001$ vs. Sc. # $p < 0.05$, ## $p < 0.01$, ### $p < 0.001$, #### $p < 0.0001$ vs. Sc + SI. All data are expressed as the mean ± SD ($n = 3$).

4. Discussion

Recently, miRNAs have become attractive therapeutic targets for AMD as they regulate multiple pathways in RPE cells and have been shown to play a role in the development and progression of this disorder [14,38–40]. Various studies have linked let-7f and its family to age-related ocular disorders as they are found to be highly expressed in aged lens, vitreous and retina and can also modulate oxidative stress and senescence in numerous cell types [20–22,28,29,41–43]. Despite the evidence, the functional effects of these miRNAs on RPE cells have remained largely uninvestigated. Thus, the present study examines the relationship between let-7f and oxidative stress in RPE cells, as well as its implication in cellular dysfunction.

Our initial in vitro results demonstrated that the expression of let-7f increased dose-dependently in ARPE-19 cells treated with the pro-oxidant sodium iodate (SI). We confirmed that this upregulation was a consequence of oxidative stress that was not limited to SI by demonstrating a similar response in cells treated with H_2O_2. These results are

consistent with those reported by Li et al., demonstrating increased expression of let-7f in H_2O_2-treated human neuroblastoma cells associated with Alzheimer's disease [44]. These findings are particularly noteworthy due to the many pathological features shared between AMD and Alzheimer's disease [45,46].

Using an in vivo mouse model of SI-induced RPE degeneration, we observed an initial upregulation in let-7f expression, similar to the upregulation of miR-144 reported by Jadeja et al. using the same model [47]. Another such study demonstrated that following SI administration, rat plasma miR-124 expression levels increased significantly at days 3 and 4, and returned to baseline on day 8 [48]. Combined, the data suggests the existence of an initial miRNA response triggered by early oxidative injury in RPE cells, which could serve as useful targets in the search for predictive biomarkers and in the development of treatments for the early onset of AMD. Moreover, let-7f expression was found to be upregulated in photo-oxidative damaged rat retinas and in the plasma of monkeys exposed to cigarette smoke, two well-known risk factors associated with the development of AMD [22,49]. In line with these observations, we demonstrated that overexpression of let-7f in ARPE-19 cells promoted the production of intracellular and mitochondrial ROS. Oxidative stress has been reported to induce RPE cellular damage and dysfunction [6,7,9]. Indeed, we observed that cells transfected with let-7f exhibited decreased phagocytic activity, cellular migration, proliferation and viability. Interestingly, a recent study by Yang et al. has demonstrated that SI induces oxidative stress and promotes wound healing of ARPE-19 cells [50]. On the other hand, our results show that overexpression of let-7f induces oxidative stress but instead inhibits wound healing of ARPE-19 cells. After careful evaluation of both studies, many factors can be identified as contributors to this discrepancy. A major difference is the exposure of SI to ARPE-19 cells. Yang et al.'s team reports increased cellular migration after treatment with 2 mM SI for 24 h. According to our findings, treatment with 2 mM SI did not lead to the significant overexpression of let-7f that was achieved using a dose of 5 mM, and may be the reason for the contrasting results. Additionally, Yang et al. examined the protein expression of several EMT markers as well as signaling factors of the antioxidant response element, and reported increased expression upon SI treatment. However, the majority of their findings also revealed that maximum protein expression was achieved at 1.5 mM SI and decreased at 2 mM, which suggest the possibility that at higher doses, such as the 5 mM used in our study, migration may be inhibited. Overall, our findings provide strong evidence for a relationship between let-7f and oxidative stress in the RPE.

Cellular senescence, both stress- and age-induced, has emerged as a key player in the development and progression of age-associated disorders, such as AMD [12,51]. Numerous studies have shown that oxidative stress at the RPE can induce cellular senescence, further exacerbating the effects of the injury [11,52,53]. Through the increase in Ki67-negative and SA-β-gal-stained cells, along with the upregulation of senescent protein marker $p16^{INK4a}$, our data demonstrates that overexpression of let-7f induces RPE cellular senescence. Surprisingly, the expression level of senescent protein marker $p21^{Waf/Cip1}$ remained essentially unchanged. Such an observation could be attributed to the fact that activation of $p21^{Waf/Cip1}$ in senescent cells is transient, whilst $p16^{INK4a}$ remains constitutively expressed to maintain the senescent state [54]. Our findings are consistent with those of previous works demonstrating that let-7f and other members of its family can induce cell cycle arrest at the G_0/G_1 phase [16,55,56]. Specifically, let-7f is found to be upregulated in both oxidative stress and age-induced senescent cells [18,42,57,58]. Together, our findings strongly suggest that let-7f may play an important role in both age-associated and stress-induced senescence of the RPE.

We next examined the protective potential of let-7f inhibition against SI-induced oxidative injury in RPE cells. Our in vitro findings demonstrated that the inhibition of let-7f proved capable of protecting ARPE-19 cells against ROS overproduction, cellular dysfunction and the induction of senescence generated by exposure to SI. Furthermore, our in vivo observations are consistent with that of the literature in revealing RPE monolayer degeneration and severe morphological disruption following systemic injection of

SI [24,25,59,60]. Pre-treatment with a let7f inhibitor significantly decreased the areas of damaged or lost RPE cells but failed to preserve the overall structure of the RPE monolayer. The resultant incomplete protection could be due in part to other members of the let-7 family compensating for the suppression of let-7f. More importantly, miRNA networks are highly complex and involve multiple players that can act simultaneously on various cellular pathways, emphasizing both the difficulty and the importance of understanding the role of every piece of the miRNA puzzle.

Our study is the first to report a protective effect against oxidative injury in RPE cells through the inhibition of let-7f. Interestingly, this finding is contradictory to that of another in which let-7f protected against H_2O_2-induced oxidative damage in neuroblastoma cells, despite an initial upregulation in let-7f expression following oxidative injury as was observed in our study [44]. This discrepancy may be attributed to differences in cell type and chemical stressor as well as their model's focus on inducing apoptotic damage by oxidative stress rather than the sub-lethal stress we chose to examine, likely activating different response pathways in RPE cells. Hence, a deeper understanding of the functional and regulatory roles played by this miRNA in the RPE is crucial.

5. Conclusions

Our findings successfully demonstrate the implication of let-7f in the degeneration and dysfunction of RPE cells through the regulation of oxidative stress and senescence. Further mechanistic studies and investigation towards this relationship could provide novel insights into the pathogenesis, diagnosis and future treatments of dry AMD.

Supplementary Materials: The following supporting information can be downloaded at: https://www.mdpi.com/article/10.3390/antiox13060646/s1, Figure S1. Oxidative stress upregulates let-7f expression in RPE cells. Figure S2. Hematoxylin & eosin (H&E) stained retinal sections demonstrate time-dependent retinal injury in the sodium iodate-induced mouse model of dry AMD. Figure S3. ARPE-19 time-dependent phagocytosis of photoreceptor outer segments (POS). Figure S4. Overexpression of let-7f induces cellular dysfunction in primary RPE cells. Figure S5. Sodium iodate (SI) decreases RPE cellular viability in a time and dose-dependent manner. Figure S6. Sodium iodate (SI) increases ROS production in RPE cells in a time and dose-dependent manner. Table S1: Sequences of quantitative RT-PCR primers.

Author Contributions: Conceptualization C.O., H.T., C.Y. and P.H.; methodology, C.O., H.T., C.Y., C.G. and C.F.; investigation C.O., H.T., C.G. and C.F.; Validation C.O., H.T. and P.H.; Visualization C.O.; writing—original draft preparation C.O.; writing—review and editing C.O., H.T. and P.H.; Project administration P.H.; Funding Acquisition P.H.; Supervision H.T. and P.H. All authors have read and agreed to the published version of the manuscript.

Funding: This research was funded by the Dr. Christine Corriveau Ocular Oncology Research Fund, Université de Montréal.

Institutional Review Board Statement: The animal protocol was approved by the CHU Sainte-Justine Research Center Animal Welfare Committee CIBPAR and followed the guidelines of the Canadian Council on Animal Care and the Guide for the Care and Use of Laboratory Animals published by the US National Institutes of Health.

Informed Consent Statement: Not applicable.

Data Availability Statement: The data are contained within this article.

Conflicts of Interest: The authors declare no conflicts of interest.

References

1. Simó, R.; Villarroel, M.; Corraliza, L.; Hernández, C.; Garcia-Ramírez, M. The Retinal Pigment Epithelium: Something More than a Constituent of the Blood-Retinal Barrier—Implications for the Pathogenesis of Diabetic Retinopathy. *J. Biomed. Biotechnol.* **2010**, *2010*, 190724. [CrossRef]
2. Yang, S.; Zhou, J.; Li, D. Functions and Diseases of the Retinal Pigment Epithelium. *Front. Pharmacol.* **2021**, *12*, 727870. [CrossRef]

3. Kwon, W.; Freeman, S.A. Phagocytosis by the Retinal Pigment Epithelium: Recognition, Resolution, Recycling. *Front. Immunol.* **2020**, *11*, 604205. [CrossRef]
4. Strauss, O. The Retinal Pigment Epithelium in Visual Function. *Physiol. Rev.* **2005**, *85*, 845–881. [CrossRef]
5. Plafker, S.M.; O'Mealey, G.B.; Szweda, L.I. Mechanisms for countering oxidative stress and damage in retinal pigment epithelium. *Int. Rev. Cell Mol. Biol.* **2012**, *298*, 135–177.
6. Datta, S.; Cano, M.; Ebrahimi, K.; Wang, L.; Handa, J.T. The impact of oxidative stress and inflammation on RPE degeneration in non-neovascular AMD. *Prog. Retin. Eye Res.* **2017**, *60*, 201–218. [CrossRef]
7. Jarrett, S.G.; Boulton, M.E. Consequences of oxidative stress in age-related macular degeneration. *Mol. Asp. Med.* **2012**, *33*, 399–417. [CrossRef]
8. Coleman, H.R.; Chan, C.C.; Ferris, F.L., 3rd; Chew, E.Y. Age-related macular degeneration. *Lancet* **2008**, *372*, 1835–1845. [CrossRef]
9. Beatty, S.; Koh, H.-H.; Phil, M.; Henson, D.; Boulton, M. The role of oxidative stress in the pathogenesis of age-related macular degeneration. *Surv. Ophthalmol.* **2000**, *45*, 115–134. [CrossRef]
10. Mishima, K.; Handa, J.T.; Aotaki-Keen, A.; Lutty, G.A.; Morse, L.S.; Hjelmeland, L.M. Senescence-associated beta-galactosidase histochemistry for the primate eye. *Investig. Ophthalmol. Vis. Sci.* **1999**, *40*, 1590–1593.
11. Aryan, N.; Betts-Obregon, B.S.; Perry, G.; Tsin, A.T. Oxidative Stress Induces Senescence in Cultured RPE Cells. *Open Neurol. J.* **2016**, *10*, 83–87. [CrossRef]
12. Kozlowski, M.R. RPE cell senescence: A key contributor to age-related macular degeneration. *Med. Hypotheses* **2012**, *78*, 505–510. [CrossRef]
13. Tong, Y.; Wang, S. Not All Stressors Are Equal: Mechanism of Stressors on RPE Cell Degeneration. *Front. Cell Dev. Biol.* **2020**, *8*, 591067. [CrossRef]
14. Du, S.W.; Palczewski, K. MicroRNA regulation of critical retinal pigment epithelial functions. *Trends Neurosci.* **2022**, *45*, 78–90. [CrossRef]
15. Roush, S.; Slack, F.J. The let-7 family of microRNAs. *Trends Cell Biol.* **2008**, *18*, 505–516. [CrossRef]
16. Johnson, C.D.; Esquela-Kerscher, A.; Stefani, G.; Byrom, M.; Kelnar, K.; Ovcharenko, D.; Wilson, M.; Wang, X.; Shelton, J.; Shingara, J.; et al. The let-7 MicroRNA Represses Cell Proliferation Pathways in Human Cells. *Cancer Res.* **2007**, *67*, 7713. [CrossRef]
17. Engedal, N.; Žerovnik, E.; Rudov, A.; Galli, F.; Olivieri, F.; Procopio, A.D.; Rippo, M.R.; Monsurrò, V.; Betti, M.; Albertini, M.C. From Oxidative Stress Damage to Pathways, Networks, and Autophagy via MicroRNAs. *Oxidative Med. Cell. Longev.* **2018**, *2018*, 4968321. [CrossRef]
18. Wagner, W.; Horn, P.; Castoldi, M.; Diehlmann, A.; Bork, S.; Saffrich, R.; Benes, V.; Blake, J.; Pfister, S.; Eckstein, V. Replicative senescence of mesenchymal stem cells: A continuous and organized process. *PLoS ONE* **2008**, *3*, e2213. [CrossRef]
19. Inukai, S.; de Lencastre, A.; Turner, M.; Slack, F. Novel microRNAs differentially expressed during aging in the mouse brain. *PLoS ONE* **2012**, *7*, e40028. [CrossRef]
20. Peng, C.-H.; Liu, J.-H.; Woung, L.-C.; Lin, T.-J.; Chiou, S.-H.; Tseng, P.-C.; Du, W.-Y.; Cheng, C.-K.; Hu, C.-C.; Chien, K.-H. MicroRNAs and cataracts: Correlation among let-7 expression, age and the severity of lens opacity. *Br. J. Ophthalmol.* **2012**, *96*, 747–751. [CrossRef]
21. Akamine, P.S.; Lima, C.R.; Lustoza-Costa, G.J.; Fuziwara, C.S.; Del Debbio, C.B.; Kimura, E.T.; Santos, M.F.; Hamassaki, D.E. Age-related increase of let-7 family microRNA in rat retina and vitreous. *Exp. Eye Res.* **2021**, *204*, 108434. [CrossRef]
22. Smit-McBride, Z.; Nguyen, J.; Elliott, G.W.; Wang, Z.; McBride, R.A.; Nguyen, A.T.; Oltjen, S.L.; Yiu, G.; Thomasy, S.M.; Pinkerton, K.E.; et al. Effects of aging and environmental tobacco smoke exposure on ocular and plasma circulatory microRNAs in the Rhesus macaque. *Mol. Vis.* **2018**, *24*, 633–646.
23. Wooff, Y.; Cioanca, A.V.; Chu-Tan, J.A.; Aggio-Bruce, R.; Schumann, U.; Natoli, R. Small-Medium Extracellular Vesicles and Their miRNA Cargo in Retinal Health and Degeneration: Mediators of Homeostasis, and Vehicles for Targeted Gene Therapy. *Front. Cell. Neurosci.* **2020**, *14*, 160. [CrossRef]
24. Chowers, G.; Cohen, M.; Marks-Ohana, D.; Stika, S.; Eijzenberg, A.; Banin, E.; Obolensky, A. Course of Sodium Iodate–Induced Retinal Degeneration in Albino and Pigmented Mice. *Investig. Ophthalmol. Vis. Sci.* **2017**, *58*, 2239–2249. [CrossRef]
25. Kannan, R.; Hinton, D.R. Sodium iodate induced retinal degeneration: New insights from an old model. *Neural Regen. Res.* **2014**, *9*, 2044–2045.
26. Mazzoni, F.; Mao, Y.; Finnemann, S.C. Advanced Analysis of Photoreceptor Outer Segment Phagocytosis by RPE Cells in Culture. *Methods Mol. Biol.* **2019**, *1834*, 95–108.
27. Valieva, Y.; Ivanova, E.; Fayzullin, A.; Kurkov, A.; Igrunkova, A. Senescence-Associated β-Galactosidase Detection in Pathology. *Diagnostics* **2022**, *12*, 2309. [CrossRef]
28. Elmasry, K.; Mohamed, R.; Sharma, I.; Elsherbiny, N.M.; Liu, Y.; Al-Shabrawey, M.; Tawfik, A. Epigenetic modifications in hyperhomocysteinemia: Potential role in diabetic retinopathy and age-related macular degeneration. *Oncotarget* **2018**, *9*, 12562–12590. [CrossRef]
29. Seong, H.; Cho, H.K.; Kee, C.; Song, D.H.; Cho, M.C.; Kang, S.S. Profiles of microRNA in aqueous humor of normal tension glaucoma patients using RNA sequencing. *Sci. Rep.* **2021**, *11*, 19024. [CrossRef]
30. Olchawa, M.M.; Pilat, A.K.; Szewczyk, G.M.; Sarna, T.J. Inhibition of phagocytic activity of ARPE-19 cells by free radical mediated oxidative stress. *Free Radic. Res.* **2016**, *50*, 887–897. [CrossRef]

31. Olchawa, M.M.; Herrnreiter, A.M.; Skumatz, C.M.; Zareba, M.; Sarna, T.J.; Burke, J.M. Photosensitized oxidative stress to ARPE-19 cells decreases protein receptors that mediate photoreceptor outer segment phagocytosis. *Investig. Ophthalmol. Vis. Sci.* **2013**, *54*, 2276–2287. [CrossRef]
32. Al-Hussaini, H.; Kam, J.H.; Vugler, A.; Semo, M.; Jeffery, G. Mature retinal pigment epithelium cells are retained in the cell cycle and proliferate in vivo. *Mol. Vis.* **2008**, *14*, 1784–1791.
33. Oganesian, A.; Bueno, E.; Yan, Q.; Spee, C.; Black, J.; Rao, N.A.; Lopez, P.F. Scanning and transmission electron microscopic findings during RPE wound healing in vivo. *Int. Ophthalmol.* **1997**, *21*, 165–175. [CrossRef]
34. Debacq-Chainiaux, F.; Erusalimsky, J.D.; Campisi, J.; Toussaint, O. Protocols to detect senescence-associated beta-galactosidase (SA-βgal) activity, a biomarker of senescent cells in culture and in vivo. *Nat. Protoc.* **2009**, *4*, 1798–1806. [CrossRef]
35. Zhang, X.Y.; Ng, T.K.; Brelén, M.E.; Wu, D.; Wang, J.X.; Chan, K.P.; Yung, J.S.Y.; Cao, D.; Wang, Y.; Zhang, S.; et al. Continuous exposure to non-lethal doses of sodium iodate induces retinal pigment epithelial cell dysfunction. *Sci. Rep.* **2016**, *6*, 37279. [CrossRef]
36. Hanus, J.; Anderson, C.; Sarraf, D.; Ma, J.; Wang, S. Retinal pigment epithelial cell necroptosis in response to sodium iodate. *Cell Death Discov.* **2016**, *2*, 16054. [CrossRef]
37. Pan, F.; Shu, Q.; Xie, H.; Zhao, L.; Wu, P.; Du, Y.; Lu, J.; He, Y.; Wang, X.; Peng, H. Protective effects of triptolide against oxidative stress in retinal pigment epithelium cells via the PI3K/AKT/Nrf2 pathway: A network pharmacological method and experimental validation. *Aging* **2024**, *16*, 3955–3972. [CrossRef]
38. ElShelmani, H.; Brennan, I.; Kelly, D.J.; Keegan, D. Differential Circulating MicroRNA Expression in Age-Related Macular Degeneration. *Int. J. Mol. Sci.* **2021**, *22*, 12321. [CrossRef]
39. Szemraj, M.; Bielecka-Kowalska, A.; Oszajca, K.; Krajewska, M.; Goś, R.; Jurowski, P.; Kowalski, M.; Szemraj, J. Serum microRNAs as potential biomarkers of AMD. *Med. Sci. Monit. Int. Med. J. Exp. Clin. Res.* **2015**, *21*, 2734. [CrossRef]
40. Mao, K.; Wu, X. Microarray Analysis of Small Extracellular Vesicle-Derived miRNAs Involved in Oxidative Stress of RPE Cells. *Oxidative Med. Cell. Longev.* **2020**, *2020*, 7658921. [CrossRef]
41. Zhou, Q.; Frost Robert, J.A.; Anderson, C.; Zhao, F.; Ma, J.; Yu, B.; Wang, S. let-7 Contributes to Diabetic Retinopathy but Represses Pathological Ocular Angiogenesis. *Mol. Cell. Biol.* **2017**, *37*, e00001-17. [CrossRef]
42. Maes, O.C.; Sarojini, H.; Wang, E. Stepwise up-regulation of MicroRNA expression levels from replicating to reversible and irreversible growth arrest states in WI-38 human fibroblasts. *J. Cell. Physiol.* **2009**, *221*, 109–119. [CrossRef]
43. Keyes, W.M.; Mills, A.A. p63: A new link between senescence and aging. *Cell Cycle* **2006**, *5*, 260–265. [CrossRef]
44. Li, K.; Wang, Z.-Q.; Zhang, J.-L.; Lv, P.-Y. MicroRNA let-7f protects against H2O2-induced oxidative damage in neuroblastoma cells by targeting AKT-2. *Arch. Med. Sci.* **2020**, *16*. [CrossRef]
45. Wen, L.-Y.; Wan, L.; Lai, J.-N.; Chen, C.S.; Chen, J.J.-Y.; Wu, M.-Y.; Hu, K.-C.; Chiu, L.-T.; Tien, P.-T.; Lin, H.-J. Increased risk of Alzheimer's disease among patients with age-related macular degeneration: A nationwide population-based study. *PLoS ONE* **2021**, *16*, e0250440. [CrossRef]
46. Pogue, A.I.; Lukiw, W.J. Up-regulated Pro-inflammatory MicroRNAs (miRNAs) in Alzheimer's disease (AD) and Age-Related Macular Degeneration (AMD). *Cell. Mol. Neurobiol.* **2018**, *38*, 1021–1031. [CrossRef]
47. Jadeja, R.N.; Jones, M.A.; Abdelrahman, A.A.; Powell, F.L.; Thounaojam, M.C.; Gutsaeva, D.; Bartoli, M.; Martin, P.M. Inhibiting microRNA-144 potentiates Nrf2-dependent antioxidant signaling in RPE and protects against oxidative stress-induced outer retinal degeneration. *Redox Biol.* **2020**, *28*, 101336. [CrossRef]
48. Peng, Q.; Collette, W., III; Giddabasappa, A.; David, J.; Twamley, M.; Kalabat, D.; Aguirre, S.A.; Huang, W. Editor's Highlight: Plasma miR-183/96/182 Cluster and miR-124 are Promising Biomarkers of Rat Retinal Toxicity. *Toxicol. Sci.* **2016**, *152*, 273–283. [CrossRef]
49. Chu-Tan, J.A.; Cioanca, A.V.; Feng, Z.P.; Wooff, Y.; Schumann, U.; Aggio-Bruce, R.; Patel, H.; Rutar, M.; Hannan, K.; Panov, K.; et al. Functional microRNA targetome undergoes degeneration-induced shift in the retina. *Mol. Neurodegener.* **2021**, *16*, 60. [CrossRef]
50. Yang, Y.C.; Chien, Y.; Yarmishyn, A.A.; Lim, L.Y.; Tsai, H.Y.; Kuo, W.C.; Tsai, P.H.; Yang, S.H.; Hong, S.I.; Chen, S.J.; et al. Inhibition of oxidative stress-induced epithelial-mesenchymal transition in retinal pigment epithelial cells of age-related macular degeneration model by suppressing ERK activation. *J. Adv. Res.* **2024**, *60*, 141–157. [CrossRef]
51. Davalli, P.; Mitic, T.; Caporali, A.; Lauriola, A.; D'Arca, D. ROS, Cell Senescence, and Novel Molecular Mechanisms in Aging and Age-Related Diseases. *Oxidative Med. Cell. Longev.* **2016**, *2016*, 3565127. [CrossRef]
52. Blasiak, J.; Piechota, M.; Pawlowska, E.; Szatkowska, M.; Sikora, E.; Kaarniranta, K. Cellular Senescence in Age-Related Macular Degeneration: Can Autophagy and DNA Damage Response Play a Role? *Oxidative Med. Cell. Longev.* **2017**, *2017*, 5293258. [CrossRef]
53. Yang, C.; Shani, S.; Tahiri, H.; Ortiz, C.; Gu, M.; Lavoie, J.-C.; Croteau, S.; Hardy, P. Extracellular microparticles exacerbate oxidative damage to retinal pigment epithelial cells. *Exp. Cell Res.* **2020**, *390*, 111957. [CrossRef]
54. Stein, G.H.; Drullinger, L.F.; Soulard, A.; Dulić, V. Differential roles for cyclin-dependent kinase inhibitors p21 and p16 in the mechanisms of senescence and differentiation in human fibroblasts. *Mol. Cell. Biol.* **1999**, *19*, 2109–2117. [CrossRef]
55. Yan, S.; Han, X.; Xue, H.; Zhang, P.; Guo, X.; Li, T.; Guo, X.; Yuan, G.; Deng, L.; Li, G. Let-7f Inhibits Glioma Cell Proliferation, Migration, and Invasion by Targeting Periostin. *J. Cell Biochem.* **2015**, *116*, 1680–1692.
56. Zhang, W.-F.; Xiong, Y.-W.; Zhu, T.-T.; Xiong, A.-Z.; Bao, H.-h.; Cheng, X.-S. MicroRNA let-7g inhibited hypoxia-induced proliferation of PASMCs via G0/G1 cell cycle arrest by targeting c-myc. *Life Sci.* **2017**, *170*, 9–15.

57. Lee, S.; Jung, J.W.; Park, S.B.; Roh, K.; Lee, S.Y.; Kim, J.H.; Kang, S.K.; Kang, K.S. Histone deacetylase regulates high mobility group A2-targeting microRNAs in human cord blood-derived multipotent stem cell aging. *Cell Mol. Life Sci.* **2011**, *68*, 325–336.
58. Pienimaeki-Roemer, A.; Konovalova, T.; Musri, M.M.; Sigruener, A.; Boettcher, A.; Meister, G.; Schmitz, G. Transcriptomic profiling of platelet senescence and platelet extracellular vesicles. *Transfusion* **2017**, *57*, 144–156. [CrossRef]
59. Machalińska, A.; Lubiński, W.; Kłos, P.; Kawa, M.; Baumert, B.; Penkala, K.; Grzegrzółka, R.; Karczewicz, D.; Wiszniewska, B.; Machaliński, B. Sodium iodate selectively injuries the posterior pole of the retina in a dose-dependent manner: Morphological and electrophysiological study. *Neurochem. Res.* **2010**, *35*, 1819–1827.
60. Moriguchi, M.; Nakamura, S.; Inoue, Y.; Nishinaka, A.; Nakamura, M.; Shimazawa, M.; Hara, H. Irreversible Photoreceptors and RPE Cells Damage by Intravenous Sodium Iodate in Mice Is Related to Macrophage Accumulation. *Investig. Ophthalmol. Vis. Sci.* **2018**, *59*, 3476–3487. [CrossRef]

antioxidants

MDPI

Article

Protective Effects of 7S,15R-Dihydroxy-16S,17S-Epoxy-Docosapentaenoic Acid (diHEP-DPA) against Blue Light-Induced Retinal Damages in A2E-Laden ARPE-19 Cells

Seung-Yub Song [1,2,†], Dae-Hun Park [3,†], Sung-Ho Lee [1,2], Han-Kyu Lim [2,4], Jin-Woo Park [1,2], Jeong-Woo Seo [5] and Seung-Sik Cho [1,2,*]

[1] Department of Pharmacy, College of Pharmacy, Mokpo National University, Muan 58554, Jeonnam, Republic of Korea; tgb1007@naver.com (S.-Y.S.); tjdgh0730@naver.com (S.-H.L.); jwpark@mnu.ac.kr (J.-W.P.)
[2] Biomedicine, Health & Life Convergence Sciences, BK21 Four, College of Pharmacy, Mokpo National University, Muan 58554, Jeonnam, Republic of Korea; limhk@mokpo.ac.kr
[3] College of Oriental Medicine, Dongshin University, Naju-si 58245, Jeonnam, Republic of Korea; dhj1221@hanmail.net
[4] Department of Marine and Fisheries Resources, Mokpo National University, Muan 58554, Jeonnam, Republic of Korea
[5] Microbial Biotechnology Research Center, Korea Research Institute of Bioscience and Biotechnology (KRIBB), Jeongeup-si 56212, Jeollabuk-do, Republic of Korea; jwseo@kribb.re.kr
* Correspondence: sjason1@naver.com; Tel.: +82-61-450-2687
† These authors contributed equally to this work.

Abstract: The purpose of this study was to investigate the protective effects of 7S,15R-dihydroxy-16S,17S-epoxy-docosapentaenoic acid (diHEP-DPA) in retinal pigment epithelial (RPE) cell damage. ARPE-19 cells, a human RPE cell line, were cultured with diHEP-DPA and Bis-retinoid N-retinyl-N-retinylidene ethanolamine (A2E), followed by exposure to BL. Cell viability and cell death rates were determined. Western blotting was performed to determine changes in apoptotic factors, mitogen-activated protein kinase (MAPK) family proteins, inflammatory proteins, and oxidative and carbonyl stresses. The levels of pro-inflammatory cytokines in the culture medium supernatants were also measured. Exposure to A2E and BL increased the ARPE-19 cell death rate, which was alleviated by diHEP-DPA in a concentration-dependent manner. A2E and BL treatments induced apoptosis in ARPE-19 cells, which was also alleviated by diHEP-DPA. Analysis of the relationship with MAPK proteins revealed that the expression of p-JNK and p-P38 increased after A2E and BL treatments and decreased with exposure to diHEP-DPA in a concentration-dependent manner. DiHEP-DPA also affected the inflammatory response by suppressing the expression of inflammatory proteins and the production of pro-inflammatory cytokines. Furthermore, it was shown that diHEP-DPA regulated the proteins related to oxidative and carbonyl stresses. Taken together, our results provide evidence that diHEP-DPA can inhibit cell damage caused by A2E and BL exposure at the cellular level by controlling various pathways involved in apoptosis and inflammatory responses.

Keywords: docosahexaenoic acid; diHEP-DPA; blue light; eye health; ARPE-19

1. Introduction

Docosahexaenoic acid (DHA) is the major omega-3 long-chain polyunsaturated fatty acid (n-3 PUFA) found in the human brain and retina in eyes [1]. In response to pathogen invasion or tissue injury, polyunsaturated fatty acids such as DHA are released locally from membrane phospholipids or delivered to sites of inflammation by tissue oedema for subsequent conversion to specialized mediators by cells in the exudates [2]. DHA is closely related to fetal development [3], prevents preterm birth and cardiovascular disease [4], and improves cognitive function and eye health in adults and older adults [5].

In particular, DHA is an important factor in the development of fetuses and infants, but it has recently been reported that consuming n-3 PUFA or fish improves eye health in the elderly [5]. In particular, with regard to AMD, Christen et al. and Seddon et al. reported that high intake of n-3 PUFA as well as fish intake are effective for early and late AMD [6,7].

DHA is known to be most abundant in fish oil, with a DHA content of approximately 12% [1]. Highly concentrated oil produced from fish oil is sold as a medicinal or functional food. Recently, research on the synthesis of DHA derivatives through enzymatic reactions has been conducted, with a focus on lipid autacoids such as specialized pro-resolving mediators (SPM). SPMs are composed of lipoxins, E-series, and D-series resolvins, protectins, and maresins. Individual members of the SPM family serve as agonists at cognate receptors to induce cell-type specific responses. E-type resolvin can be synthesized from eicosapentanoic acid, and the representative substances are RvE1 and RvE2. In docosahexanoic acid, D-type resolvin, protectin, and maresin are derived. RvD1 is the most common substance in D-type resolvin. Protectin D1 and NPD1 are representative protectins. Mar1 is a typical SPM for Maresins [8].

SPMs are enzymatically extracted from essential fatty acids and play important roles in tissue inflammation. In addition, lipid mediators are part of a large family of pro-catalytic molecules, including proteins and gases that suppress inflammation.

Inflammatory responses are regulated in vivo by several pro-inflammatory mediators, including various lipid mediators (e.g., prostaglandins and leukotrienes), cytokines, and chemokines. These events have overlapping and distinct functions, ultimately leading to increased vascular permeability and the regulation of leukocyte migration. This leads to various dysfunctions, including inflammation, erythema, and tumors, which are the main signs of tissue inflammation [9].

Recently, SPMs have received sustained attention as anti-inflammatory factors that are produced during acute inflammatory responses. Many researchers have attempted to synthesize new SPMs [9–11]. intracellular inflammatory responses, granulocytes cause apoptosis in tissues. Subsequently, apoptotic neutrophils induce the conversion of macrophages into anti-inflammatory macrophages [12]. then produced by efferocytosis, contributing to fever, inflammation, and pain relief [13].

In response to pathogen invasion or tissue damage, polyunsaturated fatty acids are released locally from membrane phospholipids or delivered to the site of inflammation by tissue edema and are converted into special mediators by cells in the exudate [2]. Arachidonic acid (C20:4n-6) produces eicosanoids (prostaglandins and cysteinyl leukotrienes) that are involved in metabolism and can direct peripheral blood neutrophils to infected areas. Prostaglandin E2 (PGE2) and PGI2 regulate blood flow, while leukotriene C4 (LTC4) and LTD4 regulate vascular permeability. Neutrophils can move to the site of inflammation via the chemotaxis of LTB4 [14,15]. Early in the acute inflammatory response, pro-resolving mediator biosynthesis is initiated through a lipid mediator class switch, in which arachidonic acid metabolism switches from leukotriene production to lipoxin production [16].

SPMs can be extracted from essential fatty acids, including arachidonic acid, eicosapentaenoic acid (EPA; C20:5n-3), and docosahexaenoic acid (DHA; C22:6n-3), using lipoxygenase (LOX). SPMs are stereoselective, and the structural analysis of most SPMs is known [17].

Lipoxins are well studied SPMs. Lipoxins can be produced by intercellular biosynthesis via various pathways [18]. The first pathway is synthesized by 5-LOX from leukocytes and 12-LOX from platelets in the vascular system, whereas the second pathway involves epithelial cells, eosinophils, and monocytes. One example is the pathway through which SPMs are produced from arachidonic acid by 15-LOX or 5-LOX produced by leukocytes [19,20]. In addition to lipoxins, SPMs are converted from omega-3 fatty acids in resolving exudates; representative SPMs include resolvin, protectin, and maresin [10].

The two major resolvins derived from DHA are the D family (RvD1–RvD6) and AT isomers (AT-RvD1–RvD6) [21]. D-series resolvins are produced enzymatically by 15-LOX-

mediated conversion of DHA to 17(S)-hydroperoxyDHA (17(S)-HpDHA) and subsequent conversion by 5-LOX [22].

Recent studies have reported that SPMs such as 17(S)-hydroxy-DHA and protectin D1 are produced in the human respiratory tract because DHA is abundant in the respiratory mucosa of healthy individuals [23,24].

SPMs have been reported to control tissue damage by controlling inflammation at extremely low concentrations in the picogram-to-nanogram range. In particular, fatty acid-derived substances such as SPMs are known to be involved in resolution responses along with annexin A1 [25], TGFβ, interleukin-10 [26], microRNA [27], and carbon monoxide [28].

Based on the role of these in vivo SPMs in restoring normal cell damage through strong autacoid behavior at low concentrations, this study aimed to develop SPM derivatives that could be administered orally and externally.

SPMs exert immunomodulatory effects on various cells at the pico/nanogram level. The main cell types of SPMs include neutrophils [9], monocytes, macrophages [11], natural killer cells [29], Tregs [30], and bronchial epithelial cells [31].

To date, research has mainly been performed on SPMs in inflammation and immune-related cells, but there has been no research on new SPMs in eye-related cells (retinal pigment epithelial [RPE] cells), which our research team targeted in this study.

Recently, it has been reported that excessive viewing of video devices such as smartphones increases the risk of myopia, strabismus, dry eye syndrome, and macular degeneration [32]. In particular, there is a risk of continuous exposure to blue light (BL), which is known to be one of the causes of age-related macular degeneration [33]. This is being emphasized. emitted from imaging devices is a type of visible light with a short wavelength of 380–500 nm (nanometers). The shorter the wavelength, the greater the energy, and when accumulated, it causes substantial damage to retinal cells [34]. Due to their high energy, short wavelengths can increase free radicals in the body, damaging the DNA of cells and are known to be one of the risk factors for uveal melanoma.

Recently, long-term exposure to BL was shown to cause excessive oxidative stress in dry age-related macular degeneration (AMD). In a mouse in vivo long-term exposure model, BL weakened the retinal layer, caused apoptosis of retinal cells, and intensified damage to the mitochondria. Particularly, mitochondrial function has been reported to deteriorate [35].

Previously, we obtained a new SPM derivative, 7S,15R-Dihydroxy-16S,17S-epoxy-docosapentaenoic acid (diHEP-DPA), through enzyme synthesis and reported that it showed anti-cancer [36], anti-ulcerative [37], and anti-inflammatory [38] effects via oral administration in vivo.

While previous studies examined the possibility of developing diHEP-DPA as an oral preparation, in the present study, considering the hydrophobicity of diHEP-DPA and its high activity at concentrations below micromolar levels, basic experiments were conducted to develop an ophthalmic drug.

In the present study, we analyze the mechanism of action of diHEP-DPA at the cellular level. The results of our study provide evidence for the development of diHEP-DPA as an effective ocular drug for the treatment of macular degeneration. Our findings provide guidance for future in vivo tests, administration routes, and mechanism studies in tissue.

2. Materials and Methods

2.1. Cell Culture

Human RPE cells (ARPE-19 cells) were purchased from the American Type Culture Collection (ATCC, Manassas, VA, USA). The ARPE-19 cells were maintained in Dulbecco's Modified Eagle's Medium (DMEM, Gibco, Paisley, UK). The medium was supplemented with 10% fetal bovine serum (FBS, Gibco) and 1% penicillin/streptomycin (Gibco) at 37 °C and kept in an atmosphere containing 5% CO_2.

2.2. Cell Viability Assay

Cell viability was measured by the 3-(4,5-dimethylthiazol-2-yl)-2,5-diphenyltetrazolium bromide (MTT, Sigma-Aldrich, Saint Louis, MO, USA) method. diHEP-DPA was obtained from DHA through an enzymatic reaction using cyanobacterial lipoxygenase and purified (purity > 98%) as previously described [39]. ARPE-19 cells were seeded in a 96 well-plate density of 5×10^3 cells/well containing 100 μL of the culture medium. After 24-h incubation, the cells were continuously treated with lutein (Sigma-Aldrich, 10 μM), diHEP-DPA (1, 5, or 10 μM) for 24 h. After 10 μL of MTT solution (5 mg/mL) were added to each well, the plates were further incubated for 2 h. After the medium was removed, formazan crystals were dissolved with 100 μL of dimethyl sulfoxide (DMSO). Absorbance was then measured at a wavelength of 570 nm using a Multiskan SkyHigh Microplate Spectrophotometer (Thermo Fisher Scientific, Waltham, MA, USA). Afterwards, ARPE-19 cells (2×10^3 cells/well) were treated with lutein (Sigma-Aldrich, 10 μM) and diHEP-DPA (1, 5, or 10 μM) for 24 h. After A2E (10 μM) treatment, the cells were exposed to BL (20 mW/cm^2) for 15 min. After 24 h, an MTT assay was then conducted to evaluate the inhibition of A2E- and BL-induced ARPE-19 cells.

2.3. Fluorescence Activated Cell Sorting (FACS) Assay

ARPE-19 cells were seeded in a 6-well plate (2×10^5 cells/well) for 24 h. Thereafter, different concentrations of diHEP-DPA (1, 5, or 10 μM) and lutein (Sigma-Aldrich, 10 μM) were added for 24 h. After A2E (10 μM) treatment, exposure to BL (20 mW/cm^2) for 15 min was performed. After 24 h, the cells were washed with PBS (Lonza, Walkersville, MD, USA), harvested using trypsin, and centrifuged. The cells were then resuspended in binding buffer (400 μL) and incubated in Alexa Fluor 488 annexin V (5 μL) and PI (1 mg/mL, 1 μL) for 15 min under room temperature and darkness. Cell sorting analysis of the collected cells was performed using the Guava Easycyte reagent (Millipore, Burlington, MA, USA).

2.4. TUNEL Assay

A Click-iT^{TM} Plus TUNEL assay kit (Invitrogen, Carlsbad, CA, USA) was used, and all assays were conducted according to the manufacturer's guidelines. ARPE-19 cells were seeded in a 4-chamber with 1×10^4 cells/well. After 24 h, the medium was removed and treated with diHEP-DPA (1, 5, or 10 μM) and lutein (10 μM, Sigma-Aldrich, Saint Louis, MO, USA). After 24 h and A2E (10 μM) treatment, the cells were exposed to BL (20 mW/cm^2) for 15 min. The medium was then removed, and the cells were washed with PBS (Lonza, Walkersville, MD, USA) and fixed with 4% formaldehyde (Daejung, Siheung-si, Gyeonggi-do, Republic of Korea) in PBS for 15 min. Thereafter, 0.25% Triton X-100 (Sigma-Aldrich, Saint Louis, MO, USA) was added to fixed cells in PBS for 10 min. The cells were then incubated in 50 liters of TdT reaction solution for 60 min at 37 °C. The nucleus was then stained with DAPI (Thermo Fisher, Waltham, MA, USA), and images were acquired using a K1-Fluo confocal microscope (excitation and emission 495/519 nm Nanoscope Systems, Daejeon, Republic of Korea).

2.5. Western Blot

ARPE-19 cells were seeded in 100 a ϕ dish with 4×10^5 cells/well. After 24 h, the medium was removed and treated with diHEP-DPA (1, 5, or 10 μM) and lutein (Sigma-Aldrich, 10 μM). After 24 h, the supernatants were aspirated and treated with A2E (10 μM) and BL (20 mW/cm^2) for 15 min. The cells were collected using a protease inhibitor cocktail (Thermo Fisher Scientific) and RIPA-based lysis buffer (Thermo Fisher Scientific) and centrifuged for 20 min. Protein concentrations were determined using a bicinchoninic acid protein assay kit (Thermo Fisher Scientific). The proteins were separated by SDS-PAGE, and electric transfer was conducted with a PVDF membrane for 3 h at 100 V. The membrane was incubated in 5% skin milk blocking for 2 h at 4 °C. Primary antibodies were incubated overnight at 4 °C. Primary antibodies were used for Bcl-xL (Invitrogen, Carlsbad, CA, USA), Bcl-2 (Invitrogen), Bad (Santa crusz biotechnology, Dallas, TX, USA), Bim

(Santa crusz biotechnology), *p*-JNK (Cell signaling technology, 9102, Danvers, MA, USA), JNK (Cell signaling technology), P38 (Cell signaling technology), *p*-NF-κB (Thermo Fisher Scientific Inc.), NF-κB (Invitrogen), COX-2 (Abcam, Cambridge, UK), PGE_2 (Bioss, Woburn, MA, USA), Keap1 (Invitrogen), Nrf2 (Invitrogen), SOD1 (Invitrogen), iNOS (Invitrogen), 4-HNE (Abcam), and GADPH (Invitrogen). Primary antibodies were used at 100-fold (Bad, Bim), 1000-fold (Bcl-xL, Bcl-2, p-JNK, JNK, p-P38, P38, p-NF-κB, NF-κB, COX-2, PGE2, Keap1, Nrf2, SOD1, iNOS, and 4-HNE), and 5000-fold (GAPDH) dilutions. All secondary antibodies were used at 5000-fold dilutions. The membrane was washed three times with Tris-buffered saline containing Tween (TBST) for 15 min. The membranes were incubated with secondary antibodies for 2 h at 4 °C. The secondary antibodies used were goat anti-rabbit IgG (Jackson ImmunoResearch, 111-035-003, West Grove, PA, USA) and goat anti-mouse IgG (Jackson ImmunoResearch, 115-035-003). The protein bands were detected using an enhanced chemiluminescence kit (Thermo Fisher Scientific and Davinch-Western™, Davinch-K, Seoul, Republic of Korea).

2.6. ELISA Analysis

Tumor necrosis factor alpha (TNF-α), interleukin 1-beta (IL-1β), and interleukin-6 (IL-6) concentrations were measured using the Human ELISA kit (Invitrogen, BD Biosciences, Franklin Lakes, NJ, USA). Capture antibodies were incubated overnight at 4 °C. After The plate was washed three times with 0.05% Tween-20 in PBS, and standards and samples (100 μL) were incubated for 2 h at 4 °C. Thereafter, the plate was removed, and the standard and sample solutions were incubated (100 μL/well) for 1 h at room temperature for the detection of antibodies. After the plate was added, stop solution (50 μL/well) was measured at 450 nm with a microplate reader (Perkin Elmer, Waltham, MA, USA).

2.7. Immunofluorescence (IF) Analysis

p-NF-κB and COX-2, Nrf2, and Keap1 expression levels were measured using immunofluorescence. ARPE-19 cells were seeded in 4-chamber with 1 x 10^4 cells/well. After 24 h, the medium was removed and treated with diHEP-DPA (1, 5, or 10 μM) and lutein (Sigma-Aldrich, 10 μM). After 24 h, the cells were treated with A2E (10 μM) and exposed to BL (20 mW/cm^2) for 15 min. The medium was then removed, and the cells were washed with PBS (Lonza, Walkersville, MD, USA) and fixed with 4% formaldehyde (Daejung, Siheung-si, Gyeonggi-do, Republic of Korea) in PBS for 15 min. Then, 0.25% Triton X-100 (Sigma-Aldrich, Saint Louis, MO, USA) was added to the fixed cells in PBS for 5 min. The cells were then blocked with 1% Bovine Serum Albumin (BSA) for 1 h, and primary antibodies were incubated overnight at 4 °C. Thereafter, the cells were washed thrice with PBS (Lonza) for 5 min. Cells were incubated with secondary antibodies for 2 h under 4 °C and darkness. The nucleus was then stained with DAPI (Thermo Fisher). *p*-NF-κB (Thermo Fisher Scientific Inc.), COX-2 (Abcam), Nrf2 (Invitrogen), Keap1 (Invitrogen), Alexa Fluor 488-conjugated anti-rabbit IgG (493/518mm, A3273, Invitrogen), and Alexa Fluor 555-conjugated anti-goat IgG (553/568nm, A32816, Invitrogen) were used. A K1-Fluo confocal microscope (Nanoscope Systems) was used for image acquisition and fluorescence intensity analysis.

2.8. Statistical Analysis

The results are expressed as mean ± standard deviation (SD). Group differences were evaluated using one-way analysis of variance (ANOVA), followed by Dunnett's multiple comparison test. Statistical significance was set at $p < 0.05$.

3. Results and Discussion

3.1. diHEP-DP- Inhibited Cell Death Caused by A2E Treatment and BL Exposure

As shown in Figure 1A, lutein and diHEP-DPA are considered safe at concentrations within 10 μM, so future experiments were performed within the concentration range of 10 μM. A2E and BL-induced cytotoxicity was reduced in a concentration-dependent manner.

When treated with A2E and BL, the cell survival rate was about 70%; Lutein showed a survival rate of 89% at a concentration of 10 μM, and diHEP-DPA showed a survival rate of 83% at a concentration of 10 μM (Figure 1B).

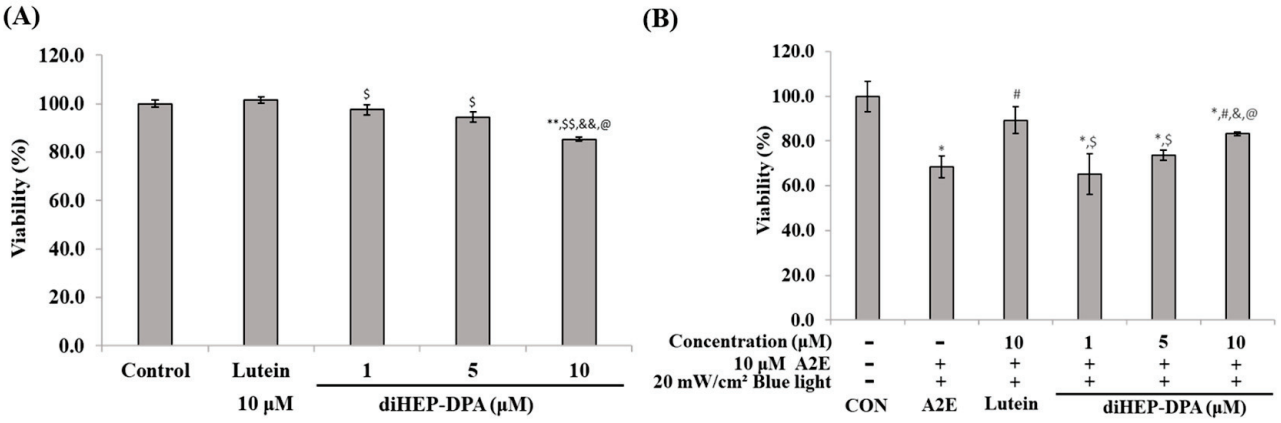

Figure 1. Effects of diHEP-DPA on cell viability. (**A**) Viability of ARPE-19 cells treated with lutein (10 μM) and diHEP-DPA (1 to 10 μM) for 24 h; (**B**) diHEP-DPA prevented A2E and blue light-induced cell death. The values are expressed as the mean ± S.D. (n = 3) of three individual experiments. "*" $p < 0.05$ vs. CON; "**" $p < 0.001$ vs. CON; "#" $p < 0.05$ vs. A2E; "$" $p < 0.05$ vs. Lutein; "$$" $p < 0.001$ vs. Lutein; "&" $p < 0.05$ vs. 1 μM; "&&" $p < 0.001$ vs. 1 μM; "@" $p < 0.05$ vs. 5 μM.

3.2. diHEP-DPA Regulated the Apoptosis Caused by BL in A2E-Laden ARPE-19 Cells

As shown in Figure 2, when cells were treated with A2E and BL simultaneously, apoptotic cells increased to 13%, but the lutein (10 μM) treatment group showed a 10% reduction effect. diHEP-DPA reduced apoptotic cells in a concentration-dependent manner to 8% at a concentration of 10 μM. Figure 2B shows that diHEP-DPA reduced A2E- and BL-induced apoptosis in a concentration-dependent manner.

Figure 3 shows the expression regulation pattern for apoptosis-related biomarkers. When A2E and BL were treated simultaneously, the expression of Bcl-xL and BCl-2 decreased, but the lutein 10 μM treatment group and the diHEP-DPA 5 μM treatment group were found to be restored to almost the same level as the control. In the case of Bad and Bim, lutein could not reduce the increased expression by A2E and BL, but diHEP-DPA decreased the expression level in a concentration-dependent manner.

3.3. diHEP-DPA Regulated the JNK and p38 in A2E and BL-Induced Apoptosis

As shown in Figure 4, by examining the expression of MAPK-related proteins related to apoptosis, we found that the phosphorylation of p38 and JNK increased when A2E and BL were simultaneously administered (Figure 4A), and diHEP-DPA reduced the expression of *p*-p38 and *p*-JNK in a concentration-dependent manner. When compared to the control group (lutein, 10 μM) at the same concentration, diHEP-DPA strongly inhibited the expression of *p*-p38 and *p*-JNK (Figure 4B).

3.4. diHEP-DPA Regulated the Inflammatory Response Caused by BL in A2E-Laden ARPE-19 Cells

diHEP-DPA was confirmed to be effective in regulating the inflammatory factors that were increased by A2E and BL. As shown in Figure 5A,B, diHEP-DPA reduced the expression of p-NF-kB, iNOS, COX-2, and PGE2, which was increased by A2E and BL, in a concentration-dependent manner. In addition, diHEP-DPA decreased the production of proinflammatory cytokines such as TNF-α, IL-6, and IL1-1β in a concentration-dependent manner.

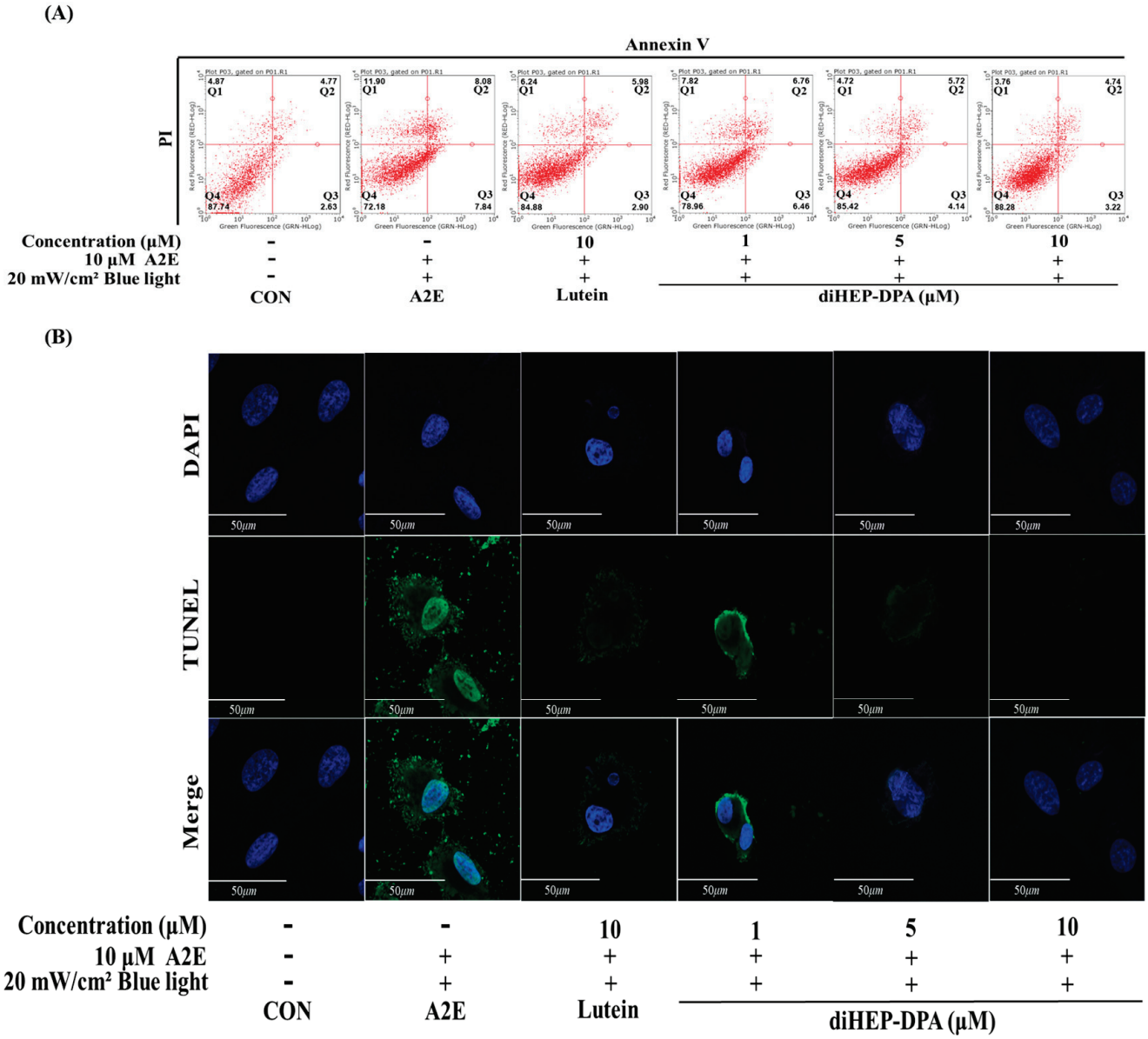

Figure 2. diHEP-DPA decreases apoptosis and necroptosis induced by blue light in A2E-laden retinal pigment epithelium (ARPE-19) cells. (**A**) Representative dot-plots showing the dual parameters used for Annexin V/PI staining and flow cytometry. Q1: Necroptosis cells; Q2: Late apoptosis cells; Q3: Early apoptosis; Q4: Live cells; (**B**) TUNEL results showed that the apoptosis decreased with the increase in DIHEP-DPA concentration. ARPE-19 cells were fixed and probed against α-tubulin (green). The cells were counterstained with DAPI (blue) and visualized by confocal microscopy. Scale bor, 50 μm. Magnifiaction ×400.

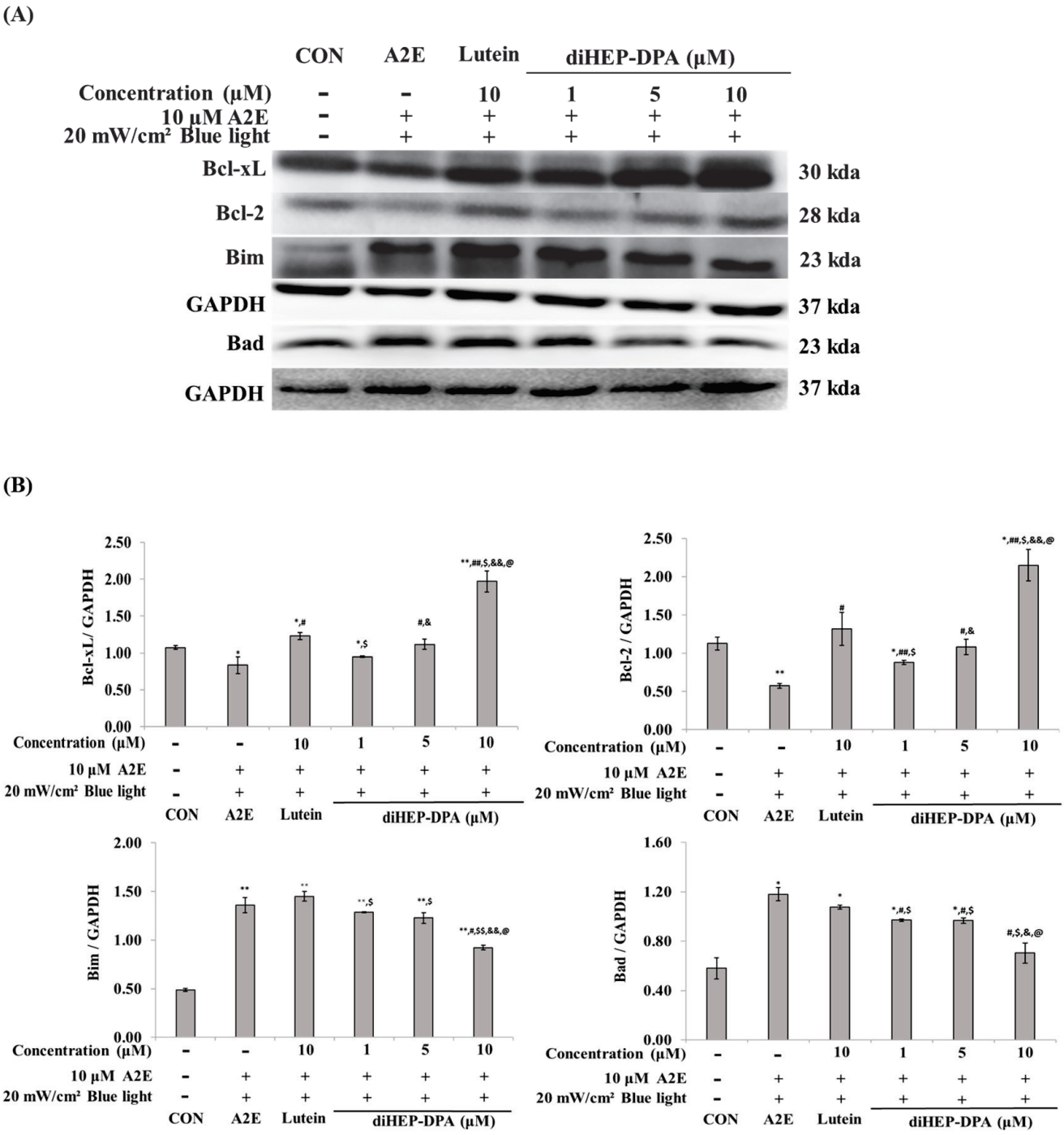

Figure 3. Western blot analysis of Bcl-family proteins induced by blue light in A2E-laden retinal pigment epithelium (ARPE-19) cells. (**A**) Western blot analysis indicating the expression of Bcl-xL, Bcl-2, Bax, Bad, Bim, and GAPDH. (**B**) Quantifications were approximated using densitometry (Image J software version 1.8.0), and results were normalized to GAPDH. The values are expressed as the mean ± S.D. (n = 3) of three individual experiments. "*" $p < 0.05$ vs. CON; "**" $p < 0.001$ vs. CON; "#" $p < 0.05$ vs. A2E; "##" $p < 0.001$ vs. A2E; "$" $p < 0.05$ vs. Lutein; "$$" $p < 0.001$ vs. Lutein; "&" $p < 0.05$ vs. 1 μM; "&&" $p < 0.001$ vs. 1 μM; "@" $p < 0.05$ vs. 5 μM.

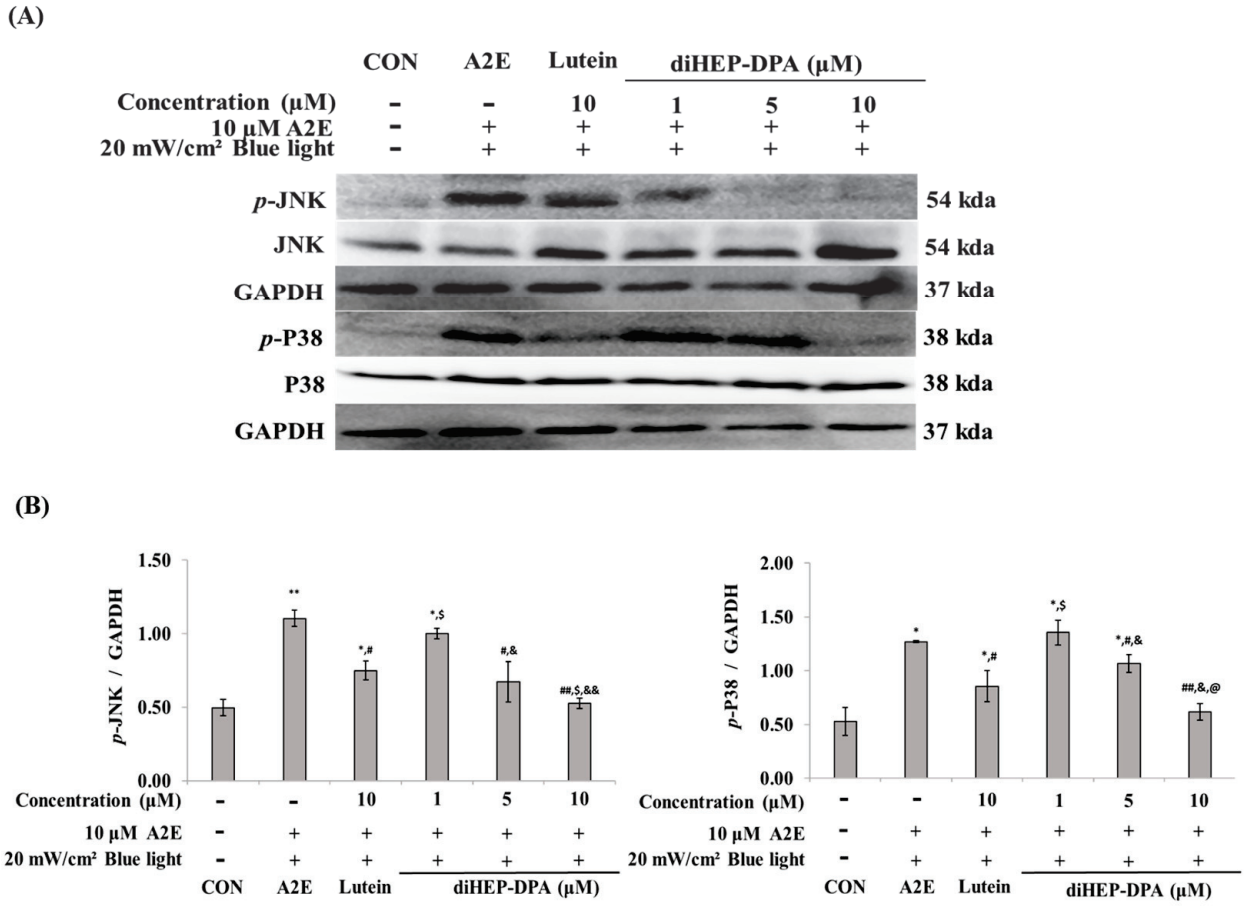

Figure 4. Western blot analysis of mitogen-activated protein kinase (MAPK) family proteins induced by blue light in A2E-laden retinal pigment epithelium (ARPE-19) cells. (**A**) Western blot analysis indicating the expression of *p*-JNK, JNK, *p*-P38, P38, and GAPDH. (**B**) Quantifications were approximated using densitometry (Image J software version 1.8.0), and results were normalized to GAPDH. The values are expressed as the mean ± S.D. (n = 3) of three individual experiments. "*" $p < 0.05$ vs. CON; "**" $p < 0.001$ vs. CON; "#" $p < 0.05$ vs. A2E; "##" $p < 0.001$ vs. A2E; "$" $p < 0.05$ vs. Lutein; "&" $p < 0.05$ vs. 1 μM; "&&" $p < 0.001$ vs. 1 μM; "@" $p < 0.05$ vs. 5 μM.

3.5. diHEP-DPA Regulated the Oxidative Stress and Carbonyl Stress Induced by A2E and BL Exposure in ARPE-19 Cells

To further confirm that apoptosis and inflammatory responses caused by exposure to A2E and BL are related to oxidative/carbonyl stress, proteins typically expressed during oxidative/carbonyl stress were selected and their expression patterns were confirmed. diHEP-DPA increased the expression levels of Keap-1, NRF-2, and SOD1, which were reduced by A2E and BL, in a concentration-dependent manner, and the efficacy of the control group treated with 10 μM lutein and the group treated with 5 μM diHEP-DPA were similar. In the case of 4-HNE, the expression was increased by A2E and BL treatment, and diHEP-DPA showed a concentration-dependent expression pattern at concentrations up to 10 μM (Figure 6A,B). As shown in Figure 6C, the immunofluorescence assay confirmed that diHEP-DPA induced the expression of Kaep-1 and NRF-2 in a concentration-dependent manner.

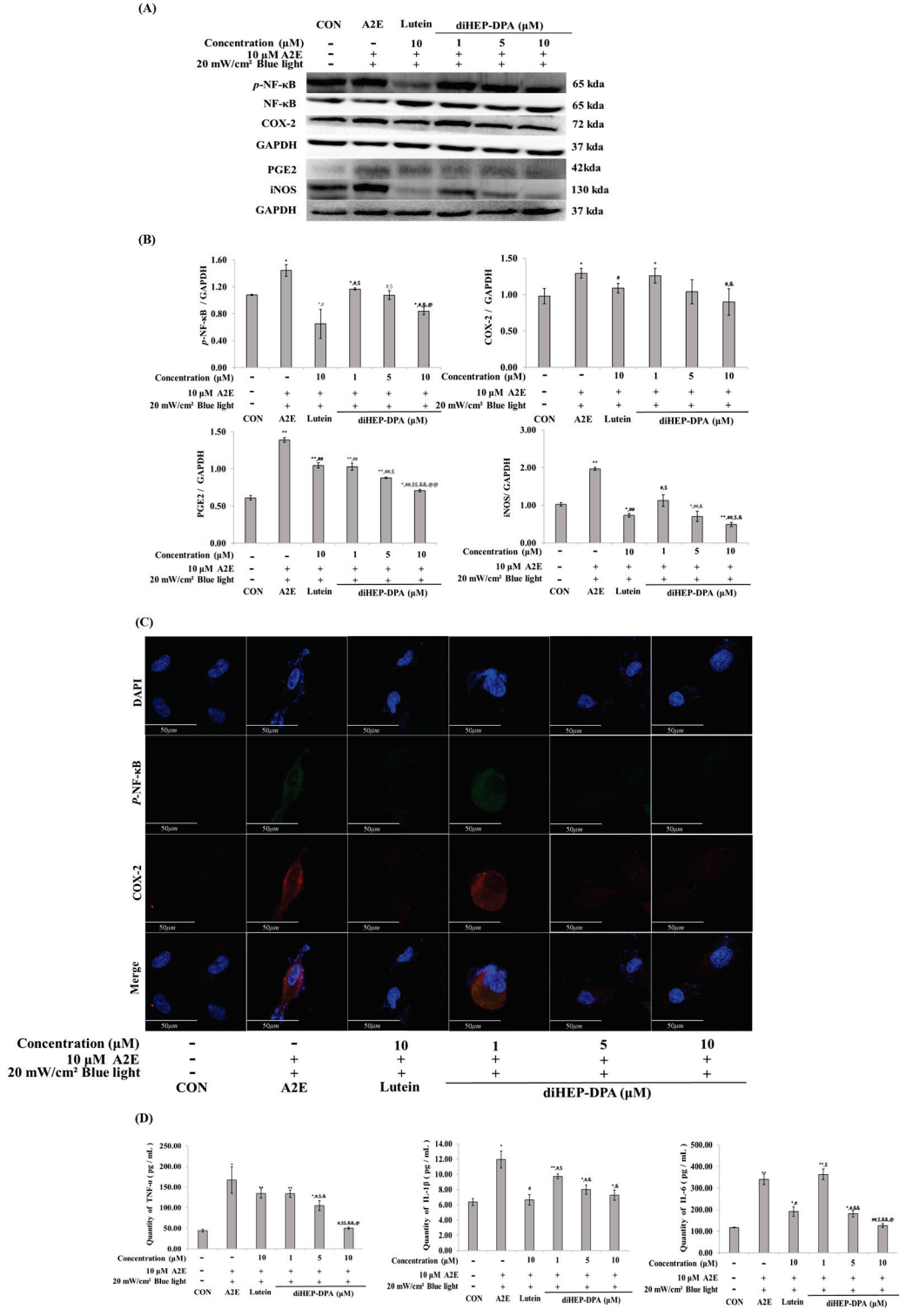

Figure 5. diHEP-DPA decreases inflammatory and pro-inflammatory cytokines induced by blue light in A2E-laden retinal pigment epithelium (ARPE-19) cells. (**A**) Western blot analysis indicating the expression of *p*-NF-κB, NF-κB, COX-2, PGE2, iNOS, and GAPDH. (**B**) Quantifications were approximated using densitometry (Image J software version 1.8.0), and results were normalized to GAPDH. (**C**) Immunofluorescence images showing qualitative expression of P-NF-κB (green), COX-2 (red). Cells were counterstained with DAPI (blue) and visualized by confocal microscopy. Scale bor,

50 μm. Magnifiaction ×400. (**D**) Quantitative analysis of TNF-α, IL-1β, and IL-6 cytokines with an ELISA kit. The values are expressed as the mean ± S.D. (n = 3) of three individual experiments. "*" $p < 0.05$ vs. CON; "**" $p < 0.001$ vs. CON; "#" $p < 0.05$ vs. A2E; "##" $p < 0.001$ vs. A2E; "$" $p < 0.05$ vs. Lutein; "$$" $p < 0.001$ vs. Lutein; "&" $p < 0.05$ vs. 1 μm; "&&" $p < 0.001$ vs. 1 μm; "@" $p < 0.05$ vs. 5 μM; "@@" $p < 0.001$ vs. 5 μM.

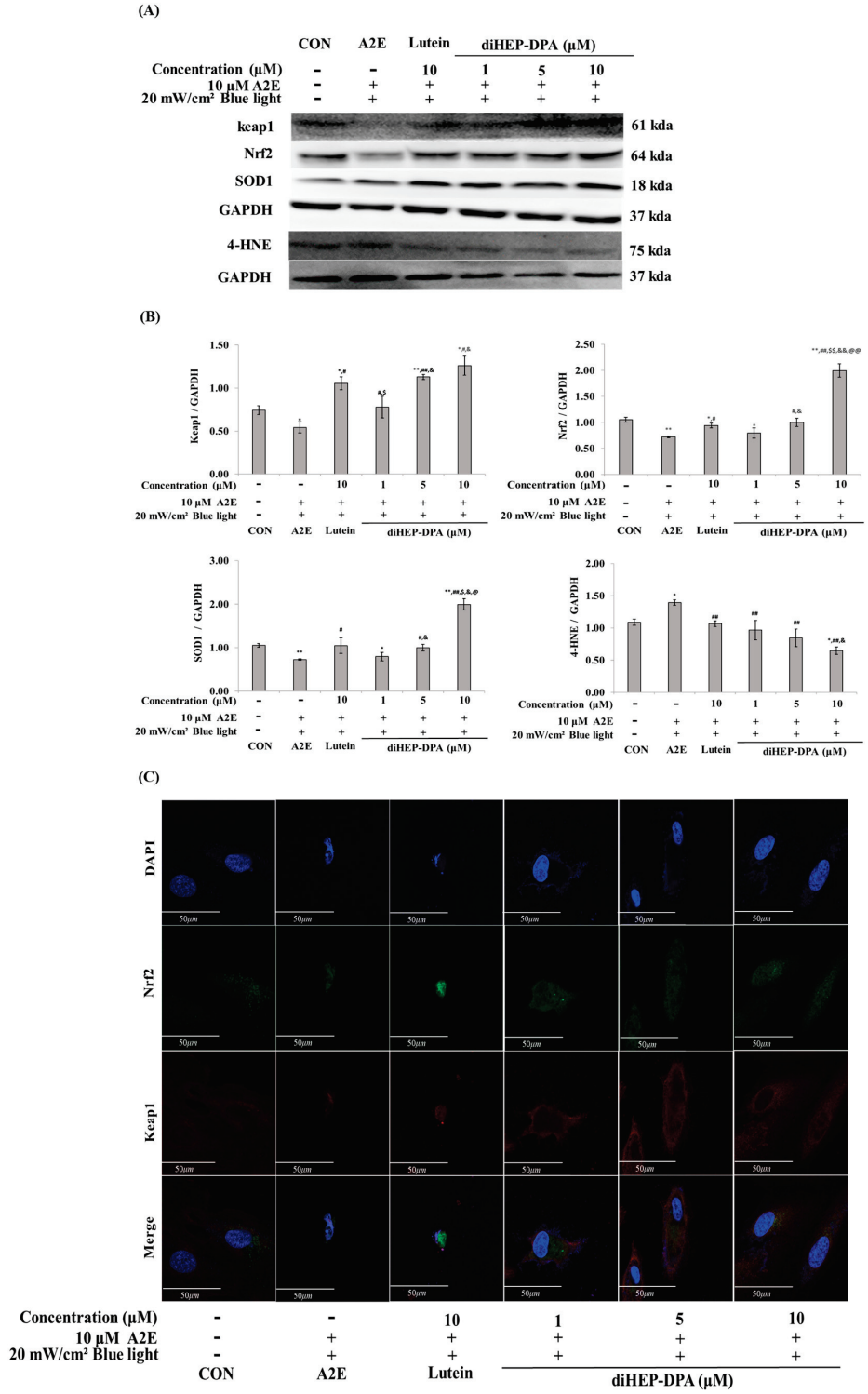

Figure 6. diHEP-DPA decreases oxidative stress and carbonyl stress induced by blue light in A2E-laden retinal pigment epithelium (ARPE-19) cells. (**A**) Western blot analysis indicating the expression

of Keap1, Nrf2, SOD1, 4-HNE, and GAPDH. (**B**) Quantifications were approximated using densitometry (Image J software version 1.8.0), and results were normalized to GAPDH. (**C**) Immunofluorescence images showing qualitative expression of Nrf2 (green) and Keap1 (red). Cells were counterstained with DAPI (blue) and visualized by confocal microscopy. Scale bor, 50 μm. Magnifiaction ×400. The values are expressed as the mean ± S.D. (n = 3) of three individual experiments. "*" $p < 0.05$ vs. CON; "**" $p < 0.001$ vs. CON; "#" $p < 0.05$ vs. A2E; "##" $p < 0.001$ vs. A2E; "$" $p < 0.05$ vs. Lutein; "$$" $p < 0.001$ vs. Lutein; "&" $p < 0.05$ vs. 1 μm; "&&" $p < 0.001$ vs. 1 μm; "@" $p < 0.05$ vs. 5 μM; "@@" $p < 0.001$ vs. 5 μM.

4. Discussion

In the present study, we showed that the treatment of retinal oxide (A2E) with BL caused cytotoxicity in RPE cells. Lutein and diHEP-DPA regulated the apoptosis and inflammatory responses induced by A2E and BL. BL has been reported to cause macular degeneration and cataracts by damaging the eye cells [40]. In previous studies, cell damage has been induced by A2E with BL treatments. Recently, long-term exposure to BL has been reported to cause excessive oxidative stress in dry age-related macular degeneration (AMD); in a mouse in vivo long-term exposure model, BL weakened the retinal layer, caused apoptosis in retinal cells, and intensified the damage to mitochondria. In particular, mitochondrial function has been reported to deteriorate [40].

It was reported that in a rat model of macular degeneration, a diet rich in DHA and EPA reduced the development of retinal lesions. Furthermore, in a rat model of oxygen-induced retinopathy, increasing tissue levels of ω-3 by diet or genetic manipulation reduced pathological retinal neovascularization. In addition to resolvin, another DHA-derived lipid mediator, 10,17(S)-docosatriene, has been identified in both humans and rodents. DHA is generally present in the eye and respiratory mucosa, and SPMs such as protectin D1 have been reported to be produced in the human respiratory tract as well. Therefore, it can be seen that not only DHA but also DHA derivatives act as autacoids in vivo and have strong anti-inflammatory and immunomodulatory properties.

Thus, we reported that diHEP-DPA, a DHA derivative capable of enzymatic mass production, has anti-apoptotic and anti-inflammatory effects on ARPE-19 cells damaged by A2E and BL at a low concentrations of 10 μM or less.

Lutein is a representative eye health medicine widely sold as an ingredient in medicines and health foods. Lutein, one of the carotenoid pigments in the retina, is widely used clinically worldwide as a substance to prevent retinal degeneration [41], and protective and antioxidant effects have been reported in ARPE-19 cell and mouse models [42].

Therefore, we used lutein as a control and determined that it alleviates ARPE-19 cell damage at a concentration of 10 μM.

Studies on diHEP-DPA's anticancer and ulcerative colitis effects have been previously reported [36,37]. This is the first study to report the eye protective effect of diHEP-DPA. When RPE cells are treated with A2E at an appropriate concentration and irradiated with BL for a certain period, A2E is oxidized to oxi-A2E, which accumulates within the cells, causing cytotoxicity and apoptosis. Retinal epithelial cells are usually damaged by fluorescent dyes such as lipofuscin. The photoreceptor cells die sequentially after cell death [43]. Therefore, we attempted to explain how new lipid autacoids, such as SPMs, protect RPE cells against apoptosis caused by BL. As shown in Figure 1, lutein and diHEP-DPA were shown to alleviate cytotoxicity caused by A2E and BL at the 10 μM level; hence, experiments were conducted at concentrations below 10 μM (Figure 1).

Janet et al. reported that BL exposure causes A2E oxidation and generates reactive oxygen species (ROS), including hydrogen peroxide and superoxide anion [44]. ROS are known to cause oxidative stress and apoptosis [45], and oxidative stress and inflammatory responses are associated with the apoptosis of RPE cells [46].

MAPKs have been implicated in many human pathologies, including neurodegenerative diseases (e.g., Alzheimer's disease, Parkinson's disease, and amyotrophic lateral sclerosis), diabetes, obesity, and various cancers [47]. Considering that MAPKs play a cen-

tral role in most cell signaling systems, changes in the expression and function of various MAPK signaling intermediates have also been reported in RPE cells. It is well known that MAPKs have various effects on cell differentiation. ERK1/2 is associated with cell proliferation and differentiation, and p38 is known to be closely related to inflammation, apotosis, and stress responses in addition to cell proliferation and differentiation. JNK is also associated with apoptosis, cell proliferation, and cell differentiation [48].

In the present study, we confirmed that A2E and BL activate p38 and JNK and are consequently related to apoptotic/inflammatory responses.

Ultraviolet rays are a representative factor affecting eye diseases, and in relation to MAPKs, it has been reported to increase the expression of ERK1/2, JNK, and p38 in RPE cells [49]. Representative substances that regulate MAPKs activity have been reported, including resveratrol derived from grapes [50]. Numerous studies have reported that bioactive substances other than resveratrol regulate MAPK signaling. However, we are the first to report a study on MAPK-mediated apoptosis and inflammation of SPMs, such as diHEP-DPA, by A2E and BL in ARPE-19 cells.

Cigarette smoke and Cd have also been reported to affect RPE cells, and autophagic cell death has been reported to be induced by the activation of ERK, JNK, and p38 [51]. Tsao et al. reported that when RPE cells were treated with hydrogen peroxide, ERK1/2 was not involved in cell death; however, cell death was affected by JNK and p38 activation [52]. Ryter et al. reported that apoptosis occurs through continuous activation of ERK1/2 [53]. In our study, treatment with A2E and BL induced JNK and p38 activation, similar to the results of Tsao et al., in which diHEP-DPA downregulated JNK and p38 activation induced by A2E and BL (Figure 4).

Bcl-xL and BCL-2 contribute to the inhibition and regulation of mitochondrial apoptosis. In particular, overexpression of BcL regulates cytochrome c release from mitochondria and caspase activity [54], and diHEP-DPA increases the expression of Bcl-xL and Bcl-2 by approximately a factor of 1.5 times more than lutein. Additionally, the expression of Bad and Bim, pro-apoptotic factors, was increased by A2E and BL treatment, respectively, and was suppressed by lutein and diHEP-DPA, which is consistent with the report that factors such as Bad form a dimer with Bcl-xL. These results indicate that diHEP-DPA inhibited RPE cell death by regulating the apoptotic pathway (Figure 3).

Retinal cell damage due to visible light exposure occurs via type I (free radical) and type II (oxygen-dependent) mechanisms. Apoptosis is induced by a type II mechanism [55]. Exposure of cells to BL generates ROS, which damage mitochondrial DNA and cell structure and cause RPE cell death [56,57].

In the present study, we found that A2E and BL exposure induces oxidative stress in ARPE-19 cells, affecting the Keap1/NRF2 pathway, and diHEP-DPA regulates Keap1/NRF2 and SOD1 to alleviate apoptosis and inflammation caused by oxidative stress (Figure 6).

Under oxidative stress, cholesterol is converted to oxysterol, another lipid compound vulnerable to ROS attack. Representative substances include 7-keto-cholesterol, 7β-hydroxy-cholesterol, 5α,6α- and 5β,6β-epoxy- cholesterol, and cholestan-3β,5α,6β-triol. These oxysterols have been reported to cause eye diseases (e.g., macular degeneration [58] and dry eye [59]).

Continuous exposure to oxidative stress in RPE cells can damage cellular organelles, such as mitochondria [60], which ultimately causes the worsening of eye diseases, such as macular degeneration. Therefore, oxidative stress-induced RPE damage is considered a key pathological factor.

Microglial activation induced by light exposure causes an inflammatory response, which has been reported to be related to the development of macular degeneration [61]. In particular, it has been reported that reactive microglia accumulate in the subretinal space and release pro-inflammatory cytokines such as TNF-α, IL-1β, and IL-6 [62].

Many reports on the molecular mechanisms underlying the link between oxidative stress and inflammation in RPE cells have not been confirmed. However, Yang et al. reported that 4-HNE induces the production of IL-6, IL-1, and TNF-α through HSP70

outflow from RPE cells [63]. In our study, we confirmed that when RPE cells were treated with A2E and BL, 4-HNE expression was induced by oxidative stress, and diHEP-DPA alleviated this effect (Figure 6). This result is related to the data in Figure 5, in which the cytokines (TNF-α, IL-1β, and IL-6) increased by A2E and BL treatment were downregulated by diHEP-DPA.

Taken together, diHEP-DPA treatment alleviated the apoptosis and inflammatory responses due to oxidative and carbonyl stresses induced by A2E and BL treatment in ARPE-19 cells in a concentration-dependent manner at concentrations below 10 μM.

5. Conclusions

We demonstrated that diHEP-DPA, obtained by the enzymatic reaction of DHA, can regulate apoptosis and inflammatory responses induced by A2E and BL. It was confirmed that diHEP-DPA regulates the expression of MAPK-related proteins related to apoptosis in RPE cells and is involved in apoptosis and inflammatory responses caused by oxidative and carbonyl stresses. For the development of diHEP-DPA as a treatment material for macular degeneration in the future, in vivo and pathological analyses are necessary to apply diHEP-DPA as an eye drop preparation.

In this study, we showed that SPMs produced in human cells have limitations in treating diseases caused by exposure to A2E and BL, and that substances such as diHEP-DPA are sufficient as potential treatments for eye diseases.

Author Contributions: Conceptualization, S.-S.C., J.-W.S. and H.-K.L.; investigation, S.-Y.S., D.-H.P. and S.-H.L.; data curation, S.-Y.S., J.-W.P. and D.-H.P.; writing—original draft preparation, S.-S.C. All authors have read and agreed to the published version of the manuscript.

Funding: This work was supported by the National Research Foundation of Korea (NRF) grant funded by the Korea government (MSIT) (No. 2022R1A5A8033794) and was supported by the Korea Institute of Marine Science and Technology Promotion (KIMST), funded by the Ministry of Oceans and Fisheries (20220572).

Informed Consent Statement: Not applicable.

Data Availability Statement: Should any raw data files be needed; they are available from the corresponding author upon reasonable request.

Conflicts of Interest: The authors declare no conflicts of interest.

References

1. Li, J.; Pora, B.L.R.; Dong, K.; Hasjim, J. Health benefits of docosahexaenoic acid and its bioavailability: A review. *Food Sci. Nutr.* **2021**, *9*, 5229–5243. [CrossRef] [PubMed]
2. Kasuga, K.; Yang, R.; Porter, T.F.; Agrawal, N.; Petasis, N.A.; Irimia, D.; Toner, M.; Serhan, C.N. Rapid appearance of resolvin precursors in inflammatory exudates: Novel mechanisms in resolution. *J. Immunol.* **2008**, *181*, 8677–8687. [CrossRef] [PubMed]
3. Rahimi, V.; Tavanai, E.; Falahzadeh, S.; Ranjbar, A.R.; Farahani, S. Omega-3 fatty acids and health of auditory and vestibular systems: A comprehensive review. *Eur. J. Nutr.* **2024**. [CrossRef]
4. Dinu, M.; Sofi, F.; Lotti, S.; Colombini, B.; Mattioli, A.V.; Catapano, A.L.; Casula, M.; Baragetti, A.; Wong, N.D.; Steg, P.G.; et al. Effects of omega-3 fatty acids on coronary revascularization and cardiovascular events: A meta-analysis. *Eur. J. Prev. Cardiol.* **2024**. [CrossRef] [PubMed]
5. Mun, J.G.; Legette, L.L.; Ikonte, C.J.; Mitmesser, S.H. Choline and DHA in Maternal and Infant Nutrition: Synergistic Implications in Brain and Eye Health. *Nutrients* **2019**, *11*, 1125. [CrossRef]
6. Christen, W.G.; Schaumberg, D.A.; Glynn, R.J.; Buring, J.E. Dietary ω-3 Fatty Acid and Fish Intake and Incident Age-Related Macular Degeneration in Women. *Arch. Ophthalmol.* **2011**, *129*, 921–929. [CrossRef]
7. Seddon, J.M.; George, S.; Rosner, B. Cigarette smoking, fish consumption, omega-3 fatty acid intake, and associations with age-related macular degeneration: The US Twin Study of Age-Related Macular Degeneration. *Arch. Ophthalmol.* **2006**, *124*, 995–1001. [CrossRef]
8. Basil, M.C.; Levy, B.D. Specialized pro-resolving mediators: Endogenous regulators of infection and inflammation. *Nat. Rev. Immunol.* **2016**, *16*, 51–67. [CrossRef]
9. Serhan, C.N. Pro-resolving lipid mediators are leads for resolution physiology. *Nature* **2014**, *510*, 92–101. [CrossRef]
10. Serhan, C.N.; Dalli, J.; Colas, R.A.; Winkler, J.W.; Chiang, N. Protectins and maresins: New pro-resolving families of mediators in acute inflammation and resolution bioactive metabolome. *Biochim. Biophys. Acta* **2015**, *1851*, 397–413. [CrossRef]

11. Serhan, C.N.; Savill, J. Resolution of inflammation: The beginning programs the end. *Nat. Immunol.* **2005**, *6*, 1191–1197. [CrossRef] [PubMed]
12. Dalli, J.; Serhan, C.N. Specific lipid mediator signatures of human phagocytes: Microparticles stimulate macrophage efferocytosis and pro-resolving mediators. *Blood* **2012**, *120*, e60–e72. [CrossRef] [PubMed]
13. Freire-de-Lima, C.G.; Xiao, Y.Q.; Gardai, S.J.; Bratton, D.L.; Schiemann, W.P.; Henson, P.M. Apoptotic cells, through transforming growth factor-beta, coordinately induce anti-inflammatory and suppress pro-inflammatory eicosanoid and NO synthesis in murine macrophages. *J. Biol. Chem.* **2006**, *281*, 38376–38384. [CrossRef]
14. Nathan, C. Points of control in inflammation. *Nature* **2002**, *420*, 846–852. [CrossRef] [PubMed]
15. Badr, K.F.; DeBoer, D.K.; Schwartzberg, M.; Serhan, C.N. Lipoxin A4 antagonizes cellular and in vivo actions of leukotriene D4 in rat glomerular mesangial cells: Evidence for competition at a common receptor. *Proc. Natl. Acad. Sci. USA* **1989**, *86*, 3438–3442. [CrossRef]
16. Levy, B.D.; Clish, C.B.; Schmidt, B.; Gronert, K.; Serhan, C.N. Lipid mediator class switching during acute inflammation: Signals in resolution. *Nat. Immunol.* **2001**, *2*, 612–619. [CrossRef] [PubMed]
17. Serhan, C.N.; Petasis, N.A. Resolvins and protectins in inflammation resolution. *Chem. Rev.* **2011**, *111*, 5922–5943. [CrossRef]
18. Serhan, C.N.; Sheppard, K.A. Lipoxin formation during human neutrophil-platelet interactions. Evidence for the transformation of leukotriene A4 by platelet 12-lipoxygenase in vitro. *J. Clin. Investig.* **1990**, *85*, 772–780. [CrossRef] [PubMed]
19. Levy, B.D.; Romano, M.; Chapman, H.A.; Reilly, J.J.; Drazen, J.; Serhan, C.N. Human alveolar macrophages have 15-lipoxygenase and generate 15(S)-hydroxy-5,8,11-cis-13-trans-eicosatetraenoic acid and lipoxins. *J. Clin. Investig.* **1993**, *92*, 1572–1579. [CrossRef]
20. Serhan, C.N.; Hamberg, M.; Samuelsson, B. Lipoxins: Novel series of biologically active compounds formed from arachidonic acid in human leukocytes. *Proc. Natl. Acad. Sci. USA* **1984**, *81*, 5335–5339. [CrossRef]
21. Serhan, C.N.; Arita, M.; Hong, S.; Gotlinger, K. Resolvins, docosatrienes, and neuroprotectins, novel omega-3-derived mediators, and their endogenous aspirin-triggered epimers. *Lipids* **2004**, *39*, 1125–1132. [CrossRef] [PubMed]
22. Hong, S.; Gronert, K.; Devchand, P.R.; Moussignac, R.L.; Serhan, C.N. Novel docosatrienes and 17S-resolvins generated from docosahexaenoic acid in murine brain, human blood, and glial cells. Autacoids in anti-inflammation. *J. Biol. Chem.* **2003**, *278*, 14677–14687. [CrossRef] [PubMed]
23. Freedman, S.D.; Blanco, P.G.; Zaman, M.M.; Shea, J.C.; Ollero, M.; Hopper, I.K.; Weed, D.A.; Gelrud, A.; Regan, M.M.; Laposata, M.; et al. Association of cystic fibrosis with abnormalities in fatty acid metabolism. *New Engl. J. Med.* **2004**, *350*, 560–569. [CrossRef]
24. Levy, B.D.; Kohli, P.; Gotlinger, K.; Haworth, O.; Hong, S.; Kazani, S.; Israel, E.; Haley, K.J.; Serhan, C.N. Protectin D1 is generated in asthma and dampens airway inflammation and hyperresponsiveness. *J. Immunol.* **2007**, *178*, 496–502. [CrossRef] [PubMed]
25. Perretti, M.; D'Acquisto, F. Annexin A1 and glucocorticoids as effectors of the resolution of inflammation. *Nat. Rev. Immunol.* **2009**, *9*, 62–70. [CrossRef] [PubMed]
26. Bannenberg, G.L.; Chiang, N.; Ariel, A.; Arita, M.; Tjonahen, E.; Gotlinger, K.H.; Hong, S.; Serhan, C.N. Molecular circuits of resolution: Formation and actions of resolvins and protectins. *J. Immunol.* **2005**, *174*, 4345–4355. [CrossRef] [PubMed]
27. Recchiuti, A.; Krishnamoorthy, S.; Fredman, G.; Chiang, N.; Serhan, C.N. MicroRNAs in resolution of acute inflammation: Identification of novel resolvin D1-miRNA circuits. *FASEB J. Off. Publ. Fed. Am. Soc. Exp. Biol.* **2011**, *25*, 544–560. [CrossRef] [PubMed]
28. Shinohara, M.; Kibi, M.; Riley, I.R.; Chiang, N.; Dalli, J.; Kraft, B.D.; Piantadosi, C.A.; Choi, A.M.; Serhan, C.N. Cell-cell interactions and bronchoconstrictor eicosanoid reduction with inhaled carbon monoxide and resolvin D1. *Am. J. Physiol. Lung Cell. Mol. Physiol.* **2014**, *307*, L746–L757. [CrossRef]
29. Thorén, F.B.; Riise, R.E.; Ousbäck, J.; Della Chiesa, M.; Alsterholm, M.; Marcenaro, E.; Pesce, S.; Prato, C.; Cantoni, C.; Bylund, J.; et al. Human NK Cells induce neutrophil apoptosis via an NKp46- and Fas-dependent mechanism. *J. Immunol.* **2012**, *188*, 1668–1674. [CrossRef]
30. Krishnamoorthy, N.; Burkett, P.R.; Dalli, J.; Abdulnour, R.E.; Colas, R.; Ramon, S.; Phipps, R.P.; Petasis, N.A.; Kuchroo, V.K.; Serhan, C.N.; et al. Cutting edge: Maresin-1 engages regulatory T cells to limit type 2 innate lymphoid cell activation and promote resolution of lung inflammation. *J. Immunol.* **2015**, *194*, 863–867. [CrossRef]
31. Nordgren, T.M.; Heires, A.J.; Wyatt, T.A.; Poole, J.A.; LeVan, T.D.; Cerutis, D.R.; Romberger, D.J. Maresin-1 reduces the pro-inflammatory response of bronchial epithelial cells to organic dust. *Respir. Res.* **2013**, *14*, 51. [CrossRef] [PubMed]
32. Chidi-Egboka, N.C.; Jalbert, I.; Golebiowski, B. Smartphone gaming induces dry eye symptoms and reduces blinking in school-aged children. *Eye* **2023**, *37*, 1342–1349. [CrossRef] [PubMed]
33. Zhao, Z.C.; Zhou, Y.; Tan, G.; Li, J. Research progress about the effect and prevention of blue light on eyes. *Int. J. Ophthalmol.* **2018**, *11*, 1999–2003. [CrossRef]
34. Theruveethi, N.; Bui, B.V.; Joshi, M.B.; Valiathan, M.; Ganeshrao, S.B.; Gopalakrishnan, S.; Kabekkodu, S.P.; Bhat, S.S.; Surendran, S. Blue Light-Induced Retinal Neuronal Injury and Amelioration by Commercially Available Blue Light-Blocking Lenses. *Life* **2022**, *12*, 243. [CrossRef]
35. Wang, L.; Yu, X.; Zhang, D.; Wen, Y.; Zhang, L.; Xia, Y.; Chen, J.; Xie, C.; Zhu, H.; Tong, J.; et al. Long-term blue light exposure impairs mitochondrial dynamics in the retina in light-induced retinal degeneration in vivo and in vitro. *J. Photochem. Photobiol. B Biol.* **2023**, *240*, 112654. [CrossRef]

36. Su, Y.; Choi, H.S.; Choi, J.H.; Kim, H.S.; Jang, Y.S.; Seo, J.W. 7S,15R-Dihydroxy-16S,17S-epoxy-docosapentaenoic Acid Overcomes Chemoresistance of 5-Fluorouracil by Suppressing the Infiltration of Tumor-Associated Macrophages and Inhibiting the Activation of Cancer Stem Cells in a Colorectal Cancer Xenograft Model. *Mar. Drugs* **2023**, *21*, 80. [CrossRef]
37. Wang, L.; Choi, H.S.; Su, Y.; Lee, B.; Choi, J.H.; Jang, S.H.; Jang, Y.S.; Seo, J.W. Protective effect of 17S-epoxy-docosapentaenoic acid against dextran sulfate sodium induced ulcerative colitis in BALB/c mice. *Mol. Med. Rep.* **2022**, *26*, 278. [CrossRef] [PubMed]
38. Wang, L.; Choi, H.S.; Su, Y.; Ju, J.H.; Heo, S.Y.; Yi, J.J.; Oh, B.R.; Jang, Y.S.; Seo, J.W. The docosahexaenoic acid derivatives, diHEP-DPA and TH-DPA, synthesized via recombinant lipoxygenase, ameliorate disturbances in lipid metabolism and liver inflammation in high fat diet-fed mice. *Life Sci.* **2022**, *291*, 120219. [CrossRef]
39. Yi, J.-J.; Heo, S.-Y.; Ju, J.-H.; Oh, B.-R.; Son, W.S.; Seo, J.-W. Synthesis of two new lipid mediators from docosahexaenoic acid by combinatorial catalysis involving enzymatic and chemical reaction. *Sci. Rep.* **2020**, *10*, 18849. [CrossRef]
40. Wu, J.; Seregard, S.; Algvere, P.V. Photochemical damage of the retina. *Surv. Ophthalmol.* **2006**, *51*, 461–481. [CrossRef]
41. Agrón, E.; Mares, J.; Clemons, T.E.; Swaroop, A.; Chew, E.Y.; Keenan, T.D.L. Dietary Nutrient Intake and Progression to Late Age-Related Macular Degeneration in the Age-Related Eye Disease Studies 1 and 2. *Ophthalmology* **2021**, *128*, 425–442. [CrossRef] [PubMed]
42. Jo, Y.-D.; Kim, J.; Choung, S.-Y. Protective effects of quercetin-3-O-α-l-arabinopyranoside against UVA induced apoptosis via regulating inflammatory pathways in ARPE-19 cells and Balb/c mice. *J. Funct. Foods* **2019**, *62*, 103541. [CrossRef]
43. Marie, M.; Gondouin, P.; Pagan, D.; Barrau, C.; Villette, T.; Sahel, J.; Picaud, S. Blue-violet light decreases VEGFa production in an in vitro model of AMD. *PLoS ONE* **2019**, *14*, e0223839. [CrossRef]
44. Sparrow, J.R.; Zhou, J.; Ben-Shabat, S.; Vollmer, H.; Itagaki, Y.; Nakanishi, K. Involvement of oxidative mechanisms in blue-light-induced damage to A2E-laden RPE. *Investig. Ophthalmol. Vis. Sci.* **2002**, *43*, 1222–1227.
45. Fang, Y.; Su, T.; Qiu, X.; Mao, P.; Xu, Y.; Hu, Z.; Zhang, Y.; Zheng, X.; Xie, P.; Liu, Q. Protective effect of alpha-mangostin against oxidative stress induced-retinal cell death. *Sci Rep* **2016**, *6*, 21018. [CrossRef]
46. Wang, Y.; Shen, D.; Wang, V.M.; Yu, C.R.; Wang, R.X.; Tuo, J.; Chan, C.C. Enhanced apoptosis in retinal pigment epithelium under inflammatory stimuli and oxidative stress. *Apoptosis Int. J. Program. Cell Death* **2012**, *17*, 1144–1155. [CrossRef]
47. Kyosseva, S.V. Targeting MAPK Signaling in Age-Related Macular Degeneration. *Ophthalmol. Eye Dis.* **2016**, *8*, 23–30. [CrossRef]
48. Zhang, W.; Liu, H.T. MAPK signal pathways in the regulation of cell proliferation in mammalian cells. *Cell Res.* **2002**, *12*, 9–18. [CrossRef]
49. Roduit, R.; Schorderet, D.F. MAP kinase pathways in UV-induced apoptosis of retinal pigment epithelium ARPE19 cells. *Apoptosis Int. J. Program. Cell Death* **2008**, *13*, 343–353. [CrossRef]
50. Chan, C.M.; Huang, C.H.; Li, H.J.; Hsiao, C.Y.; Su, C.C.; Lee, P.L.; Hung, C.F. Protective effects of resveratrol against UVA-induced damage in ARPE19 cells. *Int. J. Mol. Sci.* **2015**, *16*, 5789–5802. [CrossRef]
51. Cagnol, S.; Chambard, J.C. ERK and cell death: Mechanisms of ERK-induced cell death--apoptosis, autophagy and senescence. *FEBS J.* **2010**, *277*, 2–21. [CrossRef] [PubMed]
52. Tsao, Y.P.; Ho, T.C.; Chen, S.L.; Cheng, H.C. Pigment epithelium-derived factor inhibits oxidative stress-induced cell death by activation of extracellular signal-regulated kinases in cultured retinal pigment epithelial cells. *Life Sci.* **2006**, *79*, 545–550. [CrossRef] [PubMed]
53. Ho, T.C.; Yang, Y.C.; Cheng, H.C.; Wu, A.C.; Chen, S.L.; Chen, H.K.; Tsao, Y.P. Activation of mitogen-activated protein kinases is essential for hydrogen peroxide -induced apoptosis in retinal pigment epithelial cells. *Apoptosis Int. J. Program. Cell Death* **2006**, *11*, 1899–1908. [CrossRef] [PubMed]
54. Jürgensmeier, J.M.; Xie, Z.; Deveraux, Q.; Ellerby, L.; Bredesen, D.; Reed, J.C. Bax directly induces release of cytochrome c from isolated mitochondria. *Proc. Natl. Acad. Sci. USA* **1998**, *95*, 4997–5002. [CrossRef] [PubMed]
55. Glickman, R.D. Phototoxicity to the retina: Mechanisms of damage. *Int. J. Toxicol.* **2002**, *21*, 473–490. [CrossRef]
56. Kernt, M.; Walch, A.; Neubauer, A.S.; Hirneiss, C.; Haritoglou, C.; Ulbig, M.W.; Kampik, A. Filtering blue light reduces light-induced oxidative stress, senescence and accumulation of extracellular matrix proteins in human retinal pigment epithelium cells. *Clin. Exp. Ophthalmol.* **2012**, *40*, e87–e97. [CrossRef] [PubMed]
57. King, A.; Gottlieb, E.; Brooks, D.G.; Murphy, M.P.; Dunaief, J.L. Mitochondria-derived reactive oxygen species mediate blue light-induced death of retinal pigment epithelial cells. *Photochem. Photobiol.* **2004**, *79*, 470–475. [CrossRef]
58. Chen, S.J.; Lin, T.B.; Peng, H.Y.; Liu, H.J.; Lee, A.S.; Lin, C.H.; Tseng, K.W. Cytoprotective Potential of Fucoxanthin in Oxidative Stress-Induced Age-Related Macular Degeneration and Retinal Pigment Epithelial Cell Senescence In Vivo and In Vitro. *Mar. Drugs* **2021**, *19*, 114. [CrossRef]
59. de Souza, R.G.; Yu, Z.; Hernandez, H.; Trujillo-Vargas, C.M.; Lee, A.; Mauk, K.E.; Cai, J.; Alves, M.R.; de Paiva, C.S. Modulation of Oxidative Stress and Inflammation in the Aged Lacrimal Gland. *Am. J. Pathol.* **2021**, *191*, 294–308. [CrossRef]
60. Kaarniranta, K.; Uusitalo, H.; Blasiak, J.; Felszeghy, S.; Kannan, R.; Kauppinen, A.; Salminen, A.; Sinha, D.; Ferrington, D. Mechanisms of mitochondrial dysfunction and their impact on age-related macular degeneration. *Prog. Retin. Eye Res.* **2020**, *79*, 100858. [CrossRef]
61. Fiorani, L.; Passacantando, M.; Santucci, S.; Di Marco, S.; Bisti, S.; Maccarone, R. Cerium Oxide Nanoparticles Reduce Microglial Activation and Neurodegenerative Events in Light Damaged Retina. *PLoS ONE* **2015**, *10*, e0140387. [CrossRef] [PubMed]

62. Guillonneau, X.; Eandi, C.M.; Paques, M.; Sahel, J.A.; Sapieha, P.; Sennlaub, F. On phagocytes and macular degeneration. *Prog. Retin. Eye Res.* **2017**, *61*, 98–128. [CrossRef] [PubMed]
63. Yang, H.J.; Hu, R.; Sun, H.; Bo, C.; Li, X.; Chen, J.B. 4-HNE induces proinflammatory cytokines of human retinal pigment epithelial cells by promoting extracellular efflux of HSP70. *Exp. Eye Res.* **2019**, *188*, 107792. [CrossRef] [PubMed]

antioxidants

MDPI

Article

AIBP Protects Müller Glial Cells Against Oxidative Stress-Induced Mitochondrial Dysfunction and Reduces Retinal Neuroinflammation

Seunghwan Choi [1], Soo-Ho Choi [2], Tonking Bastola [1], Keun-Young Kim [3], Sungsik Park [1], Robert N. Weinreb [1], Yury I. Miller [2] and Won-Kyu Ju [1,*]

[1] Hamilton Glaucoma Center, Shiley Eye Institute, Viterbi Family Department of Ophthalmology, University of California San Diego, La Jolla, CA 92039, USA; seunghwan.choi@prazertx.com (S.C.); tbastola@health.ucsd.edu (T.B.); sup012@ucsd.edu (S.P.); rweinreb@health.ucsd.edu (R.N.W.)
[2] Department of Medicine, University of California San Diego, La Jolla, CA 92039, USA; soc002@health.ucsd.edu (S.-H.C.); yumiller@health.ucsd.edu (Y.I.M.)
[3] National Center for Microscopy and Imaging Research, Department of Neurosciences, University of California San Diego, La Jolla, CA 92039, USA; kkim@health.ucsd.edu
* Correspondence: wju@health.ucsd.edu

Abstract: Glaucoma, an optic neuropathy with the loss of retinal ganglion cells (RGCs), is a leading cause of irreversible vision loss. Oxidative stress and mitochondrial dysfunction have a significant role in triggering glia-driven neuroinflammation and subsequent glaucomatous RGC degeneration in the context of glaucoma. It has previously been shown that apolipoprotein A-I binding protein (APOA1BP or AIBP) has an anti-inflammatory function. Moreover, *Apoa1bp*$^{-/-}$ mice are characterized by retinal neuroinflammation and RGC loss. In this study, we found that AIBP deficiency exacerbated the oxidative stress-induced disruption of mitochondrial dynamics and function in the retina, leading to a further decline in visual function. Mechanistically, AIBP deficiency-induced oxidative stress triggered a reduction in glycogen synthase kinase 3β and dynamin-related protein 1 phosphorylation, optic atrophy type 1 and mitofusin 1 and 2 expression, and oxidative phosphorylation, as well as the activation of mitogen-activated protein kinase (MAPK) in Müller glia dysfunction, leading to cell death and inflammatory responses. In vivo, the administration of recombinant AIBP (rAIBP) effectively protected the structural and functional integrity of retinal mitochondria under oxidative stress conditions and prevented vision loss. In vitro, incubation with rAIBP safeguarded the structural integrity and bioenergetic performance of mitochondria and concurrently suppressed MAPK activation, apoptotic cell death, and inflammatory response in Müller glia. These findings support the possibility that AIBP promotes RGC survival and restores visual function in glaucomatous mice by ameliorating glia-driven mitochondrial dysfunction and neuroinflammation.

Keywords: glaucoma; neuroinflammation; retinal ganglion cells; oxidative stress; AIBP; mitochondria; Müller glia

1. Introduction

Glaucoma, an optic neuropathy with the loss of retinal ganglion cells (RGCs), is a leading global cause of irreversible vision loss and blindness [1]. The common critical pathological phenotypes of this optic neuropathy include progressive optic nerve axon degeneration and RGC death, ultimately with some efficacy, but they are often inadequate to stop disease progression [1,2]. Hence, investigating the underlying pathophysiological mechanisms of glaucoma is crucial. Understanding these mechanisms could supplement IOP-lowering strategies or offer independent approaches to improve treatment efficacy.

Vision impairment in common glaucomatous retinal degenerative conditions is significantly influenced by oxidative stress, a recognized risk factor in glaucoma [3–7]. Therapeutic strategies targeting oxidative stress and mitochondrial dysfunction are of interest

for potential glaucoma treatments. Importantly, clinical studies have linked primary open-angle glaucoma to specific mitochondrial cytochrome c oxidase subunit I of the oxidative phosphorylation (OXPHOS) complex IV [8] and single-nucleotide polymorphisms of toll-like receptor 4 (TLR4) [9]; this suggests a connection between OXPHOS stress-induced mitochondrial dysfunction and TLR4-mediated neuroinflammation in glaucoma neurodegeneration. However, the precise mechanisms linking oxidative stress, mitochondrial dysfunction, and neuroinflammation in glaucoma remain poorly understood.

Apolipoprotein A-I binding protein (AIBP; gene name APOA1BP alias also known as NAXE) is a secreted protein that regulates cholesterol removal from the plasma membrane [10–12]. Extracellular AIBP binds to TLR4, thereby directing cholesterol depletion to inflammatory cells with high levels of TLR4 expression [13,14]. Intracellular AIBP is localized in mitochondria and modulates mitophagy by regulating Parkin and mitofusin (MFN) 1 and MFN2. Under oxidative stress conditions, this regulatory mechanism helps eliminate damaged mitochondria in macrophages [13–15]. We have demonstrated that AIBP expression is significantly downregulated in mouse and human glaucomatous retina [14,15] and that AIBP deficiency induces mitochondrial dysfunction in Müller glial cells [14–16]. Since Müller glial cells regulate retinal neuroinflammation [14–16], we hypothesized that AIBP deficiency is associated with RGC damage and visual dysfunction under oxidative stress conditions.

In the present study, we found that AIBP deficiency exacerbated the oxidative stress-induced impairment of mitochondrial dynamics, biogenesis, and function in Müller glia, leading to impaired visual function. Conversely, the administration of recombinant AIBP (rAIBP) restored mitochondrial dynamics and function in the retina and improved visual function under oxidative stress. rAIBP administration reduced TLR4-associated lipid rafts, restored mitochondrial dynamics and function, decreased inflammasome activation and inflammatory response, and reduced Müller glial cell death. This protection may promote RGC survival and restore visual function by ameliorating glia-driven mitochondrial dysfunction and neuroinflammation in glaucoma.

2. Materials and Methods

2.1. Animals

C57BL/6J (The Jackson Laboratory, Bar Harbor, ME, USA) and AIBP knock-out (*Apoa1bp*$^{-/-}$) mice were housed in covered cages, fed with a standard rodent diet ad libitum, and kept on a 12 h light/12 h dark cycle. C57BL/6J mice were bred in-house for experiments and used as wild-type (WT) mice. *Apoa1bp*$^{-/-}$ mice on a C57BL/6J background were generated in our laboratory, as previously reported [15]. Animals were assigned randomly to experimental and control groups. Visual function tests were studied with 10-month-old male and female mice. Research in ophthalmic vision involving animals was conducted in accordance with the Association for Research in Vision and Ophthalmology Statement for the Use of Animals in Ophthalmic Vision Research and under protocols approved by the Institutional Animal Care and Use Committee at the University of California, San Diego (CA, USA). (IACUC S12063 for mouse).

2.2. Recombinant AIBP

N-terminal His-tagged AIBP was produced in a baculovirus/insect cell expression system to allow for post-translational modification and to ensure endotoxin-free preparation as previously described [17,18]. A bulk production of recombinant AIBP was ordered from Selvita Inc. (Kraków, Poland) and was stored at −80 °C.

2.3. Induction of Retinal Oxidative Stress

To induce oxidative stress, mice received intraperitoneal (IP) injections of paraquat (PQ) (15 mg/kg, Sigma-Aldrich, St. Louis, MO, USA) in saline solution three times for 1 week as previously described [19]. Measurements for visual function tests (n = 6 to 8

mice per group) such as pattern electroretinogram (pERG), pattern visual evoked potential (pVEP), and virtual optomotor response were assessed 1 week after PQ treatment.

2.4. Tissue Preparation

Mice were anesthetized by an IP injection of a mixture of ketamine (100 mg/kg, Ketaset; Fort Dodge Animal Health, Fort Dodge, IA, USA) and xylazine (9 mg/kg, TranquiVed; Vedeco, Inc., St. Joseph, MO, USA) before cervical dislocation. For immunohistochemistry (n = 3 mice per group), the retinas were dissected from the choroids and fixed with 4% paraformaldehyde (Sigma-Aldrich) in PBS (pH 7.4) for a duration of 2 h at 4 °C. Retinas were washed several times with PBS then dehydrated through graded levels of ethanol and embedded in polyester wax. For Western blot and PCR analysis, extracted retinas were immediately used.

2.5. Immunohistochemistry

The immunohistochemical staining of 7 μm wax sections of full-thickness retinas was performed. Sections from wax blocks from each group (n = 4 retinas/group) were used for immunohistochemical analysis. To prevent non-specific background, tissues were incubated in 1% bovine serum albumin (BSA, Sigma-Aldrich)/PBS for 1 h at room temperature before incubation with the primary antibodies for 16 h at 4 °C. After several wash steps, the tissues were incubated with the secondary antibodies for 4 h at 4 °C and subsequently washed with PBS. The sections were counterstained with the nucleic acid stain Hoechst 33342 (1 μg/mL; Invitrogen, Carlsbad, CA, USA) in PBS. Images were acquired using Keyence All-in-One Fluorescence microscopy (BZ-X810, Keyence Corp. of America, Itasca, IL, USA). Each target protein fluorescent integrated intensity in pixel per area was measured using the ImageJ software version 1.54i [National Institutes of Health (NIH), Bethesda, MD, USA]. All imaging parameters remained the same and were corrected with background subtraction. The primary and secondary antibodies used in this study are presented in Supplementary Table S1.

2.6. pERG and pVEP Analysis

pERG and pVEP were measured with a Celeris apparatus (Diagnosys, Lowell, MA, USA) as previously reported [14,15]. After dark adaptation overnight, the mice were anesthetized with intraperitoneal injections of a cocktail of ketamine/xylazine under red light, and a mixture of 0.5% tropicamide and 2.5% phenylephrine was applied directly to the eye to dilate pupils. Eyes were also treated with 1% proparacaine drops and 0.3% hypromellose gel to prevent corneal drying and cataracts. pERG responses were recorded using alternating, reversing, black and white vertical stimuli at 1 Hz (2 reversals per second) and 50 candela/m^2 delivered by the pattern stimulator. Then, 200 traces were recorded per eye, and averaged waveforms were calculated in which amplitudes (μV) were measured from the P1 peak to the N2 trough. At the same time, pVEP responses were recorded. For all the recordings, ground and reference needle electrodes were placed subcutaneously in the tail and snout, and the active electrode was placed subdermally in the midline of the head at the location of the visual cortex. Each eye was separately exposed to 100 flashes of 1 Hz, 0.05 cd s/m^2 white light through the corneal stimulators and recorded for 300 ms with a sample frequency of 2000 Hz. Then, 200 traces were recorded per eye, and averaged waveforms were calculated in which amplitudes (μV) were measured from the P1 peak to the N1 trough. For each mouse, we performed five trials and swept 100 times per trial. The low- and high-filter frequency cutoffs for pVEP were set to 1.25 Hz and 100 Hz. All data measurements were recorded while maintaining a constant body temperature between 37 °C and 38 °C using the system's heat pads. The data were analyzed by the software Espion V6 (Diagnosys) [20,21].

2.7. Virtual Optomotor Response Analysis

Spatial frequency was analyzed on a virtual optomotor system (OptoMotry; Cerebral Mechanics Inc., Lethbridge, AB, Canada) as previously reported [15,19,22]. Unanesthetized mice were placed on an unrestricted platform in the center of a virtual cylinder comprising four monitors arranged in a square (arena) that project a sinusoidal grating (i.e., white versus black vertical bars) rotating at 12 deg/s. Mice were monitored by a camera mounted at the top of the arena, while a cursor placed on the forehead centered the rotation of the cylinder at the animal's viewing position. To assess visual acuity, tracking was determined when the mouse stopped moving its body and only head-tracking movement was observed. The spatial frequency threshold, a measure of visual acuity, was determined automatically using the accompanying OptoMotry software (Version 2.1.0), which uses a step-wise paradigm based upon head-tracking movements at 100% contrast. Spatial frequency began at 0.042 cyc/deg, which gradually increased until head movement was no longer observed.

2.8. Cell Culture and rAIBP Administration

rMC-1 cells, immortalized rat retinal Müller glial cell line (Kerafast, Boston, MA, USA), were grown in Dulbecco's Modified Eagle Medium (DMEM, Corning Inc, New York, NY, USA) supplemented with 5% fetal bovine serum and 1% penicillin/streptomycin solution at 37 °C in a humidified CO_2 incubator. The cells were seeded into six-well plates at a density of 2×10^5 cells/well and maintained for 24 h. Subsequently, the cells were pretreated with 0.2 μg/mL rAIBP or BSA as a control for 2 h, followed by stimulation with PQ (500 μM) for 24 h. A cell culture experiment was performed with 3 independent experiments.

2.9. siRNA Transfection

rMC-1 cells were transfected with scramble siRNA or AIBP siRNA purchased from Origene (Rockville, MD, USA) using the Amaxa Nucleofector (Lonza Group, Basel, Switzerland). Briefly, the cells (3×10^6) were resuspended in 100 μL of nucleofector solution mix followed by the addition of 20 nM of scramble siRNA or AIBP siRNA and transfected according to the manufacturer's instructions. The cells were seeded into six-well plates at a density of 5×10^5 cells/well and maintained for 24 h.

2.10. Mitochondrial Membrane Potential (MMP) and Mitochondrial Reactive Oxygen Species (mtROS) Measurement

rMC-1 cells were seeded into 6-well plates at a density of 2×10^5 cells/well, maintained for 24 h, and treated with the indicated materials for 24 h. MMP was determined by flow cytometry. The cells were incubated with TMRE solution (200 nM, Invitrogen) for 30 min at 37 °C. The intracellular mtROS level in rMC-1 cells was measured by flow cytometry. After treatment, the cells were incubated with mitoSOX solution (500 nM, Invitrogen) at 37 °C for 30 min.

2.11. Western Blot Analyses

Retina tissues and rMC-1 cells were homogenized on ice for 1 min using a modified RIPA lysis buffer [50 mM Tris-HCl, pH 8.0, 150 mM NaCl, 1% Nonidet P-40, 0.5% deoxycholic acid, 0.1% sodium dodecyl sulfate (SDS)], containing protease and phosphatase inhibitor cocktail (ThermoFisher Scientific, San Diego, CA, USA), and incubated on ice for 30 min for complete cell lysis. Harvested retinas were homogenized in RIPA buffer using a motorized tissue grinder (ThermoFisher Scientific). Cell and tissue debris was removed by centrifugation at 12,000× *g* for 15 min. Lysates (10 μg of protein) were separated by 4–20% Mini-PROTEAN TGX-precast protein gel electrophoresis (Bio-Rad, Hercules, CA, USA), and target protein levels were determined by Western blot analysis [19]. The membranes were blocked with 5% non-fat dry milk in PBS/0.1% Tween-20 (PBS-T) for 1 h at room temperature, then incubated with primary antibodies overnight at 4 °C. After washing several times with PBS-T, the membranes were incubated with horseradish peroxidase-conjugated goat anti-mouse or rabbit IgG (1:1000–7000; Bio-Rad; Cat# 1721011 or 1706515) for 1 h at

room temperature and developed using an enhanced chemiluminescence substrate system. The images were captured and quantified using the ImageQuant™ LAS 4000 system (GE Healthcare Bio-Science, Piscataway, NJ, USA) and ImageJ software (NIH). For each experiment, we conducted multiple biological replicates (at least 3 replicates), quantified the results, calculated averages, and presented the data as bar graphs. The blots shown were carefully selected based on these quantitative data to ensure clarity and consistency.

2.12. Immunocytochemistry

rMC-1 cells were fixed in 4% paraformaldehyde for 15 min at room temperature. After gently washing, the cells were permeabilized with 0.1% triton X-100 and incubated with a cleaved caspase-3 antibody for 16 h at 4 °C. After three wash steps, the cells were incubated with Alexa Fluor-568 conjugated donkey anti-rabbit IgG antibody for 2 h. For nuclear staining, the cells were further incubated with Hoechst 33342 (1 μg/mL, Invitrogen) for 5 min. Images were acquired using Keyence All-in-One Fluorescence microscopy (BZ-X810, Keyence). Each target protein fluorescent integrated intensity in pixel per area was measured using the ImageJ software (NIH) as described above.

2.13. Quantitative Real-Time PCR (qRT-PCR) Analysis

Total mRNAs were isolated from rMC-1 using a Trizol reagent. cDNAs were prepared from 1 μg of RNA using a SuperScript III First-strand synthesis system (Invitrogen). qRT-PCR was performed with the PowerUp SYBR master mix (Applied Biosystems, Forster City, MA, USA) according to the manufacturer's instructions. The mRNA levels of target genes were determined and quantitated using their specific primers and normalized to glyceraldehyde-3-phosphate dehydrogenase (GAPDH) [23]. The primers used in this study are presented in Supplementary Table S2.

2.14. Oxygen Consumption Rate (OCR) and Extracellular Acidification Rate (ECAR) Analyses

rMC-1 cells (5×10^4 per well) were seeded into Seahorse XF24-well plates. At 24 h, cells were pretreated with either BSA or rAIBP (0.2 μg/mL) for 2 h, followed by exposure to PQ (50 μM). OCR and ECAR were measured using an XF24 Extracellular Flux analyzer (Agilent, La Jolla, CA, USA). For OCR analysis, we used a Seahorse XF cell mito stress test kit (Agilent) as previously reported [5,24,25]. After measuring basal respiration, oligomycin (2 μg/mL, Sigma-Aldrich), an inhibitor of ATP synthesis; carbonyl cyanide 4-(trifluoromethoxy) phenylhydrazone (FCCP; 1 μM, Sigma-Aldrich), the uncoupler; and rotenone (2 μM, Sigma-Aldrich), an inhibitor of mitochondrial complex I, were sequentially added to measure maximal respiration, ATP-linked respiration, and spare respiratory capacity. For ECAR analysis, we used a Seahorse XF cell glycolysis stress test kit (Agilent). Glucose (10 mM, Sigma-Aldrich), oligomycin (1 μM, Sigma-Aldrich), and 2-deoxyglucose (2-DG, 50 mM, Sigma-Aldrich) were sequentially added to measure glycolysis, glycolytic capacity, and glycolytic reserve.

2.15. Immunofluorescence Staining of TLR4-Associated Lipid Rafts

After exposure to oxidative stress, rMC-1 cells were immediately put on ice, washed once with cold PBS, and fixed with 4% PFA for 10 min. Cells were washed twice with cold PBS and incubated with blocking buffer containing 5% FBS for 30 min without permeabilization, followed by staining with Cholera Toxin B (CTxB)-Alexa Fluor 594 (Invitrogen) to stain lipid rafts and rabbit anti-TLR4 antibody (Proteintech, Rosemont, IL, USA) for 2 h at room temperature, washed and incubated with anti-rabbit Alexa Fluor 647 conjugated secondary antibody (Invitrogen) for 1 h at room temperature. Cells were washed five times, and coverslips were mounted with Prolong Gold with DAPI (Invitrogen) into slides. Image acquisition was conducted using Keyence All-in-One Fluorescence microscopy (BZ-X810, Keyence), and image analysis was performed using ImageJ software (NIH). A colocalization assessment was executed using the colocalization finder plugin, facilitating the calculation of Pearson's coefficients.

2.16. Statistical Analysis

For comparison between two groups that have a small number of samples related to a fixed control, statistical analysis was conducted utilizing nonparametric analysis and a one-sample *t*-test. For comparison between two independent groups, a two-tailed Student's *t*-test was performed. For multiple group comparisons, we used either a one-way ANOVA or two-way ANOVA, using GraphPad Prism (Version 10, GraphPad, San Diego, CA, USA). Statistically, significance was defined as a p value below 0.05.

3. Results

3.1. AIBP Deficiency Exacerbates Visual Dysfunction Induced by Oxidative Stress

AIBP expression is diminished in RGCs affected by glaucomatous damage in both human and mouse retinas [14,15]. Moreover, AIBP deficiency enhances the susceptibility of RGCs to elevated IOP, leading to impaired visual function [14,15]. Given that oxidative stress is a critical causative factor of glaucomatous retinal degeneration [3–7] and AIBP deficiency is linked to oxidative stress in the retina of *Apoa1bp*$^{-/-}$ mice [15], we tested whether AIBP deficiency intensifies the impairment of visual function induced by oxidative stress. To induce oxidative stress in vivo, 10-month-old WT or *Apoa1bp*$^{-/-}$ mice received three intraperitoneal injections of PQ within 1 week [19]. PQ is known as a ROS inducer and triggers mitochondrial superoxide production in OXPHOS complex I, resulting in oxidative stress [26]. First, we assessed RGC function through pERG analyses and observed a significant decrease in pERG amplitude in WT mice under oxidative stress (Figure 1a,b). Interestingly, our results revealed that oxidative stress further exacerbated the reduction in pERG amplitude in *Apoa1bp*$^{-/-}$ mice compared with WT mice (Figure 1a,b). In agreement with earlier studies [15], we found that AIBP deficiency also led to a significant decrease in pERG amplitude in naïve *Apoa1bp*$^{-/-}$ compared to WT mice (Supplementary Figure S1a,b). Next, we assessed spatial frequency using a virtual-reality optomotor system [15,19]. Consistent with pERG data, we found that AIBP deficiency intensified the reduction in spatial frequency induced by oxidative stress (Figure 1c). In addition, we assessed central vision function using a VEP analysis [15,19]. There was no statistically significant difference in pVEP latency, an indicator of disruptions or delays along visual pathways, or amplitude, an indicator of the reflection of the number of functional optic nerve fibers, among the experimental groups (Figure 1d). AIBP deficiency did not change pVEP latency or amplitude naïve *Apoa1bp*$^{-/-}$ mice compared with WT mice (Supplementary Figure S1c). Our results suggest that, under oxidative stress conditions, AIBP deficiency exacerbates impaired visual function, likely due to the functional loss of RGCs, but causes no significant damage to the optic nerve or the conduction and processing of visual information.

Given that *Apoa1bp*$^{-/-}$ mouse and glaucomatous human and mouse Müller glial cells showed significant increases in TLR4 and interleukin 1β (IL-1β) protein expression in human and mouse retinas [15], we tested whether AIBP deficiency enhanced oxidative stress-induced TLR4 and IL-1β protein expression in the retina. TLR4 immunoreactivity showed a remarkable increase in the WT retina under the conditions of oxidative stress alone and oxidative stress with AIBP deficiency. However, there was no statistically significant difference in TLR4 immunoreactivity between WT and *Apoa1bp*$^{-/-}$ retinas subjected to oxidative stress alone and those with AIBP deficiency during oxidative stress (Figure 1e). On the other hand, the retina exposed to oxidative stress alone showed a notable increase in IL-1β immunoreactivity. Furthermore, AIBP deficiency showed a remarkable increase in IL-1β immunoreactivity in the retina compared with the WT retina exposed to oxidative stress (Figure 1e). In addition, both TLR4 and IL-1β immunoreactivities were increased in the processes and endfeet of glutamine synthase (GS)-positive Müller glial cells in the inner retina under the conditions of both oxidative stress in WT and oxidative stress with AIBP deficiency (Figure 1e).

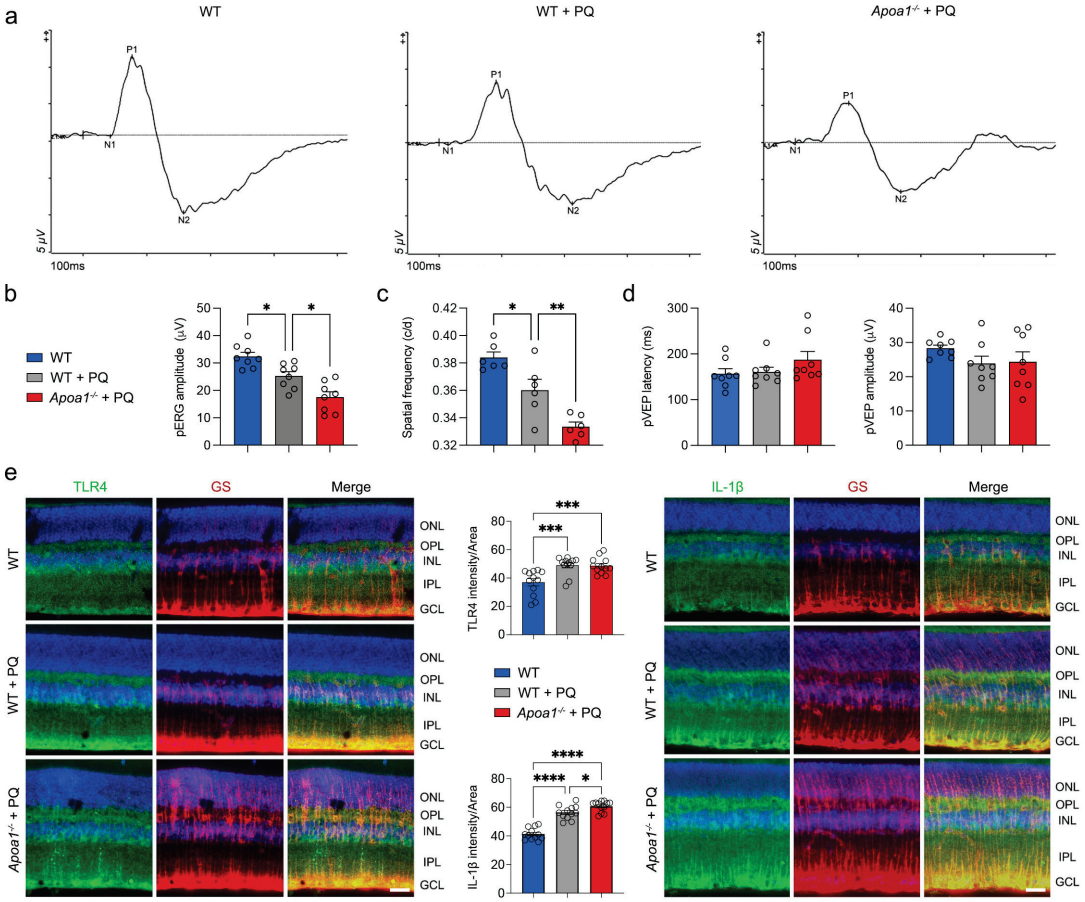

Figure 1. AIBP deficiency exacerbates visual dysfunction induced by oxidative stress. (**a**) Representative graphs of total recordings of pERG analysis among groups. (**b**) Quantification analysis of pERG test among groups. $N = 8$ mice. (**c**) Quantification analysis of optomotor response among groups. $N = 8$ mice. (**d**) Quantification analysis of pVEP tests among groups. $N = 8$ mice. (**e**) TLR4 and IL-1β immunohistochemistry in retina. Representative images show TLR4- and IL-1β-positive Müller glial cells in retina. Note that quantification analysis showed significant increase in IL-1β immunoreactive intensity under oxidative stress with AIBP deficiency compared with oxidative stress alone. $N = 10$ sections from middle area of retina from 3 mice. Images were taken with 20X magnification. Scale bar: 20 μm. Error bars represent SEM. Statistical significance was determined using one-way ANOVA test. * $p < 0.05$; ** $p < 0.01$; *** $p < 0.001$; **** $p < 0.0001$. pERG, pattern electroretinogram; PQ, paraquat; pVEP, pattern visual evoked potential; WT, wild-type.

3.2. AIBP Deficiency Intensifies Impairment of Retinal Mitochondrial Dynamics, OXPHOS Activity, and Mitochondrial Biogenesis Induced by Oxidative Stress

AIBP deficiency compromised mitochondrial structure and function in Müller glia and RGCs in *Apoa1bp*$^{-/-}$ mice [15]. Given that AIBP deficiency triggered dynamin-related protein 1 (DRP1) dephosphorylation at serine 637 (pDRP1 S637), an indicator of mitochondrial fragmentation, in the *Apoa1bp*$^{-/-}$ retina [15], we investigated whether oxidative stress intensifies excessive mitochondrial fragmentation-mediated mitochondrial impairment in 10-month-old WT and *Apoa1bp*$^{-/-}$ retinas by measuring the phosphorylation of glycogen synthase kinase 3β (GSK3β), DRP1 at serine 616 (S616), and DRP1 S637. GSK3β is a protein kinase that directly or indirectly regulates the phosphorylation of DRP1 S616 and S637 [27,28]. We observed a significant increase in pDRP1 S616 but a significant decrease in pDRP1 S637 in the *Apoa1bp*$^{-/-}$ retina compared with the WT retina under the conditions of oxidative stress (Figure 2a; Supplementary Figure S2a). In the presence of oxidative stress, GSK3β activation was significantly enhanced in the WT retina due to GSK3β dephosphorylation (Supplementary Figure S2b). Furthermore, oxidative stress

further intensified GSK3β dephosphorylation in the *Apoa1bp*$^{-/-}$ retina (Supplementary Figure S2b). Based on our findings of the reduced protein expression of optic atrophy type 1 (OPA1) and MFN2, mitochondrial fusion proteins, in the *Apoa1bp*$^{-/-}$ retina [15], we tested whether oxidative stress exacerbated the impairment of mitochondrial fusion activity in the *Apoa1bp*$^{-/-}$ retina by measuring OPA1, MFN1, and MFN2 protein expression. Under the conditions of oxidative stress, OPA1, MFN1, and MFN2 protein expressions were significantly decreased in the WT retina. AIBP deficiency further exacerbated the loss of OPA1, MFN1, and 2 protein expression in the *Apoa1bp*$^{-/-}$ retina compared with WT treated with PQ (Figure 2b). Under oxidative stress conditions, the expression of OPA1, MFN1, and MFN2 proteins was significantly reduced in the WT retina. In *Apoa1bp*$^{-/-}$ mice, this loss of OPA1, MFN1, and MFN2 expression in the retina was further aggravated compared to the PQ-treated WT retina (Figure 2b). Additionally, we observed a significant decrease in the long isoform of OPA1 (L-OPA1), which is mainly responsible for mitochondrial fusion, following a similar trend to total OPA1. In contrast, the short isoform of OPA1 (S-OPA1), associated with mitochondrial fission, remained unchanged. Based on our observation of a deteriorating mitochondrial network under the conditions of oxidative stress combined with AIBP deficiency, we further assessed whether OXPHOS function and mitochondrial biogenesis are compromised in the context of oxidative stress and AIBP deficiency. In PQ-treated WT mice, there was a significant decrease in the OXPHOS complex, as well as peroxisome proliferator-activated receptor-gamma coactivator 1α (PGC-1α) and mitochondrial transcription factor A (TFAM) protein expression in the retina, which were all further significantly reduced in PQ-treated *Apoa1bp*$^{-/-}$ mice (Figure 2c,d).

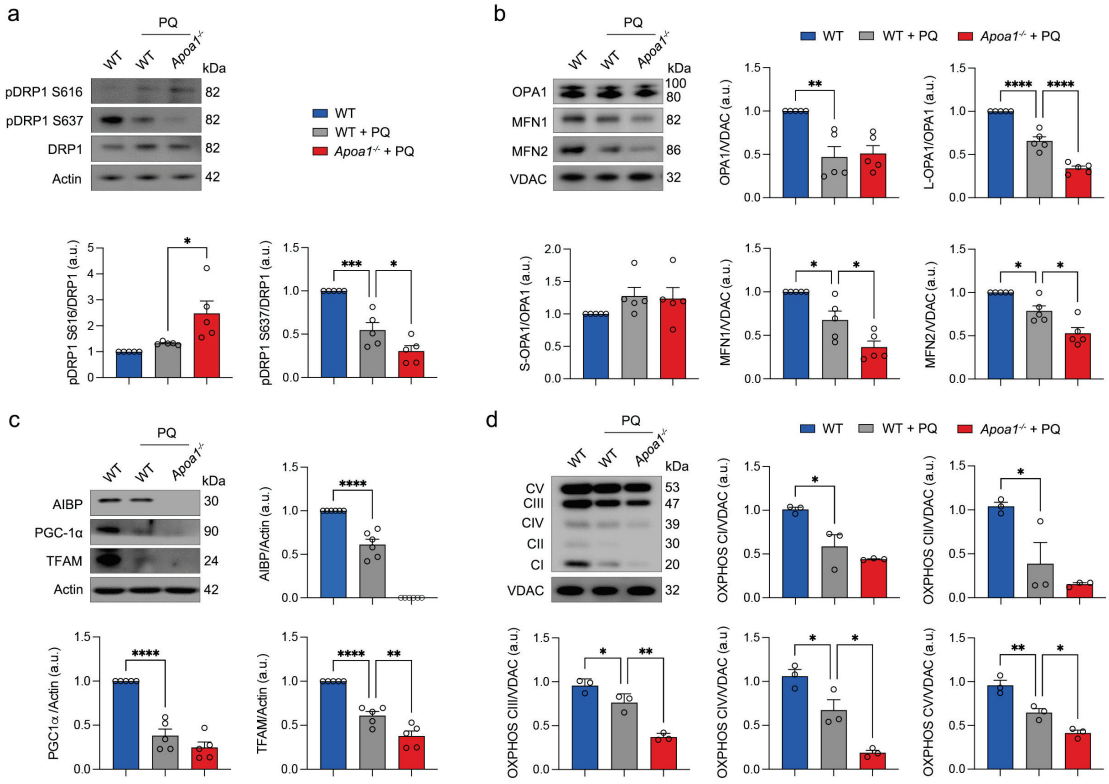

Figure 2. AIBP deficiency intensifies impairment of retinal mitochondrial dynamics, OXPHOS activity, and mitochondrial biogenesis induced by oxidative stress. (**a**) Total DRP1, phospho-DRP S616, and phospho-DRP1 S637 expression in retina. *N* = 3 mice. (**b**) OPA1, MFN1, and MFN2 expression in retina. *N* = 3 to 6 retinas from 3 mice. (**c**) AIBP, PGC-1α, and TFAM expression in retina. *N* = 3 mice. (**d**) OXPHOS complex expression in retina. *N* = 3 retinas from mice. Error bars represent SEM. Statistical significance was determined using one-way ANOVA test. * $p < 0.05$; ** $p < 0.01$; *** $p < 0.001$; **** $p < 0.0001$. PQ, paraquat; WT, wild-type.

3.3. Oxidative Stress Worsens Structural and Functional Impairment of Mitochondria in Müller Glial Cells Lacking AIBP

Oxidative stress induced by PQ is involved in inflammation and neuronal injury through the disruption of glial cell function [29,30]. Since glaucomatous retinal injury triggers mitochondrial dysfunction in impaired Müller glial cells linked to AIBP deficiency, oxidative stress, and inflammatory response, we tested whether oxidative stress exacerbates the structural and functional impairment of mitochondria in Müller glial cells lacking AIBP. To induce oxidative stress conditions in vitro, we employed PQ and used rMC-1 cells. The cells were treated with various concentrations of PQ (25, 50, 100, 200, 500, 1000, or 2000 μM) for 24 h (Supplementary Figure S3). We observed a PQ dose-dependent decrease in cell viability and an increase in cell death (Supplementary Figure S3a,b). Using an MTT assay to assess mitochondrial activity, we established the PQ concentration to be 500 μM which alters mitochondrial activity but does not induce cell death, as indicated by LDH release (Supplementary Figure S3b). To further assess mitochondrial dysfunction along with AIBP expression under these oxidative conditions, we also quantified MMP and measured mtROS generation at 24 h after exposure to oxidative stress. We observed that PQ-induced oxidative stress significantly induced the loss of MMP, resulting in increased mtROS generation (Supplementary Figure S3c,d). Notably, the expression level of AIBP was significantly reduced by 500 μM PQ (Supplementary Figure S3e).

We then examined whether AIBP knockdown compromises mitochondrial respiratory function in rMC-1 cells by AIBP knockdown and Seahorse analysis. We observed a significant reduction in basal and maximal respiration, along with decreases in ATP-linked production and spare respiratory capacity in rMC-1 cells with AIBP knockdown (Figure 3a,b; Supplementary Figure S4). Subsequently, we determined the impact of oxidative stress on the impairment of MMP, a crucial factor for energy production in mitochondria, and an increase in ROS production in rMC-1 cells with AIBP deficiency. Remarkably, oxidative stress further exacerbated the reduction in MMP and the generation of ROS in rMC-1 cells with AIBP knockdown (Figure 3c; Supplementary Figure S4). Given that oxidative stress, in conjunction with AIBP knockdown, exacerbated impaired mitochondrial dynamics by increasing pDRP1 S616 and decreasing pDRP1 S637 in the retina, we then determined how oxidative stress intensifies the deregulation of mitochondrial dynamics in rMC-1 cells with AIBP knockdown. Notably, rMC-1 cells with AIBP knockdown showed a significant increase in pDRP1 S616 but a decrease in pDRP1 S637 in response to oxidative stress (Figure 3d; Supplementary Figure S4), indicating the induction of extensive mitochondrial fragmentation. Lastly, we explored the impact of oxidative stress with AIBP knockdown on mitochondrial respiratory function in rMC-1 cells. Importantly, oxidative stress triggered a significant reduction in all respiratory activities, including basal and maximal respiration, ATP-linked production, and spare respiratory capacity, in rMC-1 cells with AIBP knockdown compared with control rMC-1 cells treated with PQ (Figure 3e,f).

3.4. Oxidative Stress Exacerbates MAPK Activation and Apoptotic Cell Death and Inflammatory Response in Müller Glial Cells Lacking AIBP

Given that mitogen-activated protein kinase (MAPK)-associated signaling pathways are linked to oxidative stress in Müller glial cells from glaucomatous human and mouse retinas [14,15], we tested the impact of oxidative stress on MAPK (p38 and ERK1/2) activation and apoptotic cell death in rMC-1 cells lacking AIBP. Oxidative stress significantly intensified the activation of p38 and ERK1/2 by increasing the phosphorylation of p38 (pp38) and ERK1/2 (pERK1/2) in rMC-1cells with AIBP knockdown (Figure 4a). We then examined whether oxidative stress exacerbates caspase-mediated apoptotic cell death in rMC-1 cells lacking AIBP. We observed that oxidative stress intensified the activation of caspase-1 and -3, along with increasing caspase-3 immunoreactivity, in rMC-1 cells with AIBP knockdown (Figure 4b–d), indicating an increased activation of caspase-3-mediated apoptotic cell death. The inflammasome is activated by various stimuli, including oxidative stress, leading to the activation of caspase-3 and the regulation of inflammatory responses [31]. In parallel,

we found that oxidative stress exacerbated NLRP3-mediated inflammasome activation and increased the mRNA expression of the inflammatory cytokines IL-1β, IL-6, and TNF-α (Figure 4e).

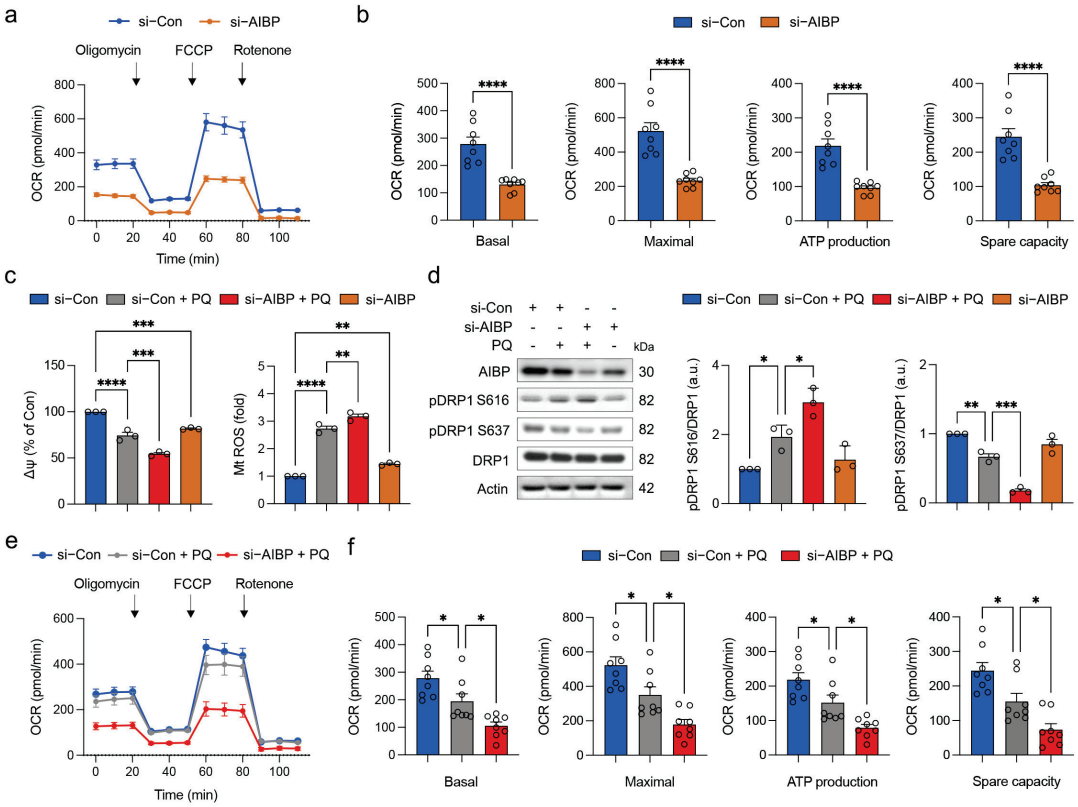

Figure 3. Oxidative stress worsens structural and functional impairment of mitochondria in Müller glia cells lacking AIBP. (**a**) Oligomycin A, FCCP and rotenone were sequentially added at indicated time point. Basal respiration indicates starting basal OCR and value which was set to 100%. Maximum respiration represents ratio between FCCP uncoupled OCR and basal OCR. (**b**) Quantitative analyses of basal, maximal, and ATP-linked respiration and spare respiratory capacity in rMC-1 cells. $N = 8$ replicated wells. (**c**) Quantitative analysis of MMP and mitochondrial ROS. $N = 3$ independent experiments in rMC-1 cells. (**d**) AIBP, total DRP1, phospho-DRP S616, and phospho-DRP1 S637 expression in rMC-1 cells. $N = 3$ independent experiments. (**e**) Oligomycin A, FCCP and rotenone were sequentially added at indicated time point. Basal respiration indicates starting basal OCR and value which was set to 100%. Maximum respiration represents ratio between FCCP uncoupled OCR and basal OCR. (**f**) Quantitative analyses of basal, maximal, and ATP-linked respiration and spare respiratory capacity in rMC-1 cells. $N = 8$ replicated wells. Error bars represent SEM. Statistical significance was determined using one-way ANOVA test. * $p < 0.05$; ** $p < 0.01$; *** $p < 0.001$; **** $p < 0.0001$. PQ, paraquat; FCCP, carbonyl cyanide p-trifluoromethoxyphenylhydrazone; OCR, oxygen consumption rate.

3.5. The Administration of rAIBP Prevents Visual Dysfunction, Restores Mitochondrial Dynamics, and Enhances OXPHOS Activity in the Retina

Based on our observations of intensified visual dysfunction under the combined conditions of oxidative stress and AIBP deficiency (Figure 1), we hypothesized that the administration of rAIBP could potentially protect visual function in mice exposed to oxidative stress in vivo. To test the effect of rAIBP on visual function, we intravitreally injected rAIBP (1 μL, 0.5 mg/mL) or BSA (1 μL, 0.5 mg/mL) into the eyes of 10 mo old C57BL/6J mice at 2 days before the induction of oxidative stress by three IP injections for 1 week as described in the Methods Section. Similar to the experiments shown in Figure 1, we performed three different visual function tests, including pERG, pVEP, and

optomotor response. Compared to oxidative stress-exposed mice treated with BSA (control), we observed that the administration of rAIBP protected RGC function as measured by pERG amplitude in mice exposed to oxidative stress (Figure 5a,b). In addition, we found a significant protection of optomotor responses through the administration of rAIBP, as evidenced by the preserved spatial frequency, in comparison to oxidative stress-exposed mice treated with BSA (Figure 5c). However, there was no statistically significant difference in pVEP amplitude and latency among the groups (Figure 5d). Because our results showed compromised mitochondrial dynamics and decreased OXPHOS activity (Figure 2), we tested whether the administration of rAIBP ameliorates the impairment of mitochondrial dynamics and OXPHOS in the retina subjected to oxidative stress. The administration of rAIBP significantly restored the expression level of the OPA1 protein and decreased pDRP1 S616 and increased pDRP1 S637 in the retina subjected to oxidative stress (Figure 5e). Moreover, we observed a substantial recovery in OXPHOS complexes I-III; however, there was no statistically significant difference in OXPHOS complexes IV and V among the experimental groups (Figure 5f).

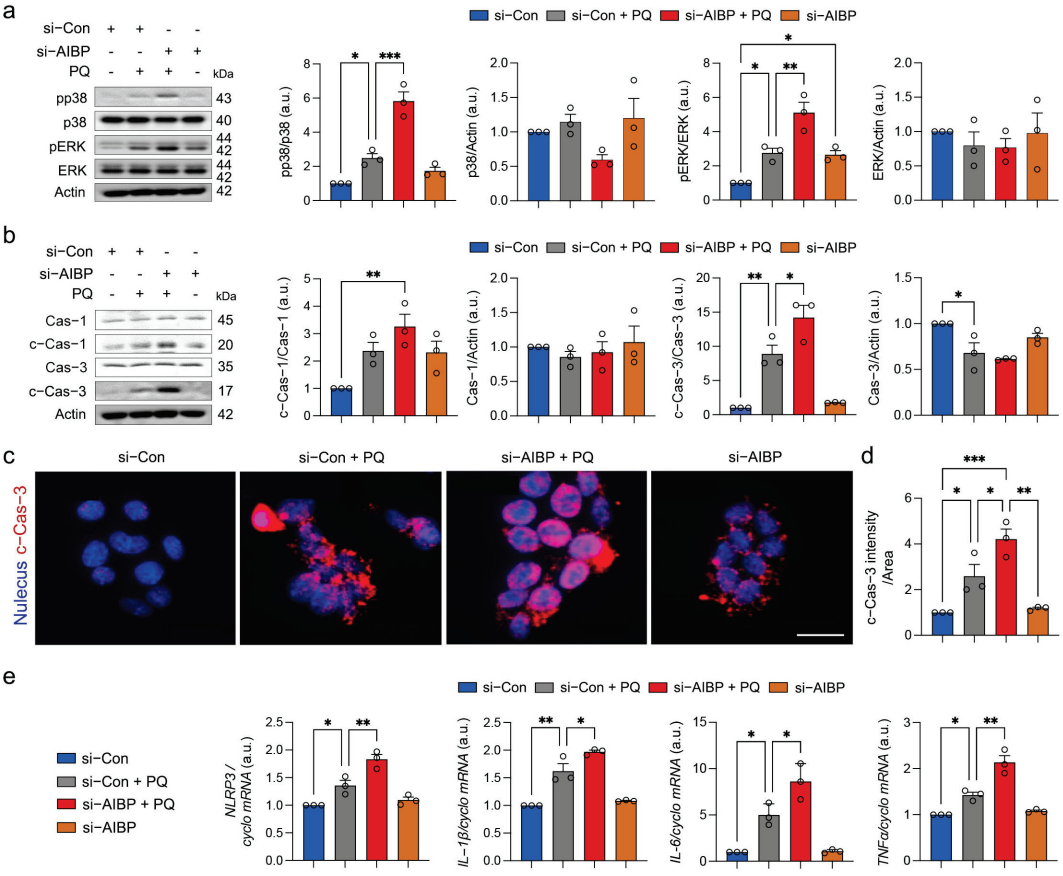

Figure 4. Oxidative stress exacerbates MAPK activation and apoptotic cell death and inflammatory response in Müller glia cells lacking AIBP. (**a**) p38, phospho-p38 (pp38), ERK1/2, phospho-ERK1/2 (pERK1/2) expression in rMC-1 cells. $N = 3$ independent experiments. (**b**) caspase-1, cleaved caspase-1, caspase-3, and cleaved caspase-3 expression in rMC-1 cells. $N = 3$ independent experiments. (**c**,**d**) Representative images show cleaved caspase-3-positive rMC-1 cells in the retina. Note that quantification analysis showed a significant increase in cleaved caspase-3 immunoreactive intensity in rMC-1 cells under oxidative stress with AIBP knockdown compared with control rMC-1 cells. $N = 3$ independent experiments. (**e**) Quantitative real-time PCR analysis of *Nlrp3*, *Il-1β*, *Il-6*, and *Tnfα* mRNA expression in rMC-1 cells. Error bars represent SEM. Statistical significance was determined using one-way ANOVA test. * $p < 0.05$; ** $p < 0.01$; *** $p < 0.001$. PQ, paraquat.

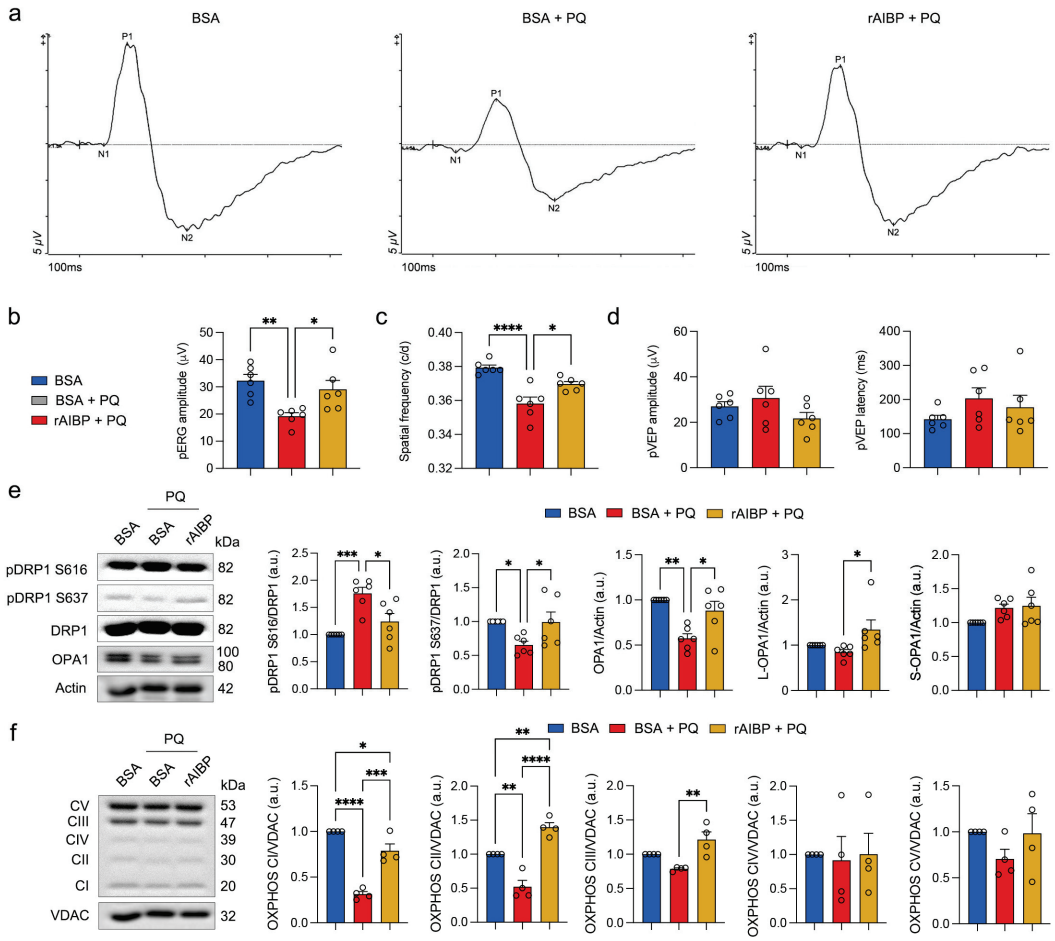

Figure 5. Administration of rAIBP prevents visual dysfunction, restores mitochondrial dynamics, and enhances OXPHOS activity in retina. (**a**) Representative graphs of total recordings of pERG analysis among groups. (**b**) Quantification analysis of pERG test among groups. $N = 6$ mice. (**c**) Quantification analysis of optomotor response among groups. $N = 6$ mice. (**d**) Quantification analysis of pVEP tests among groups. $N = 6$ mice. (**e**) OPA1, total DRP1, phospho-DRP S616, and phospho-DRP1 S637 expression in retina. $N = 3$ mice. (**f**) OXPHOS complex expression in retina. $N = 3$ mice. Error bars represent SEM. Statistical significance was determined using one-way ANOVA test. * $p < 0.05$; ** $p < 0.01$; *** $p < 0.001$; **** $p < 0.0001$. BSA, bovine serum albumin; PQ, paraquat; pERG, pattern electroretinogram; pVEP, pattern visual evoked potential.

3.6. Administration of rAIBP Reduced TLR4-Associated Lipid Rafts in Müller Glial Cells Exposed to Oxidative Stress

Given our observation of a substantial elevation in TLR4 expression and TLR4-associated lipid rafts in glaucomatous retinas [14], we tested whether rAIBP administration could decrease TLR4 activation and TLR4 lipid raft formation in rMC-1 cells against oxidative stress. Employing an immunofluorescence staining of TLR4-associated lipid rafts [14], we measured TLR4 expression and TLR4-associated lipid raft formation in rMC-1 cells. Under oxidative stress alone, there was a significant increase in TLR4 surface expression and TLR4-associated lipid rafts in BSA-treated rMC-1 cells (Figure 6a,b). The administration of rAIBP significantly reduced TLR4 surface expression and TLR4-associated lipid rafts in rMC-1 cells compared to BSA-treated rMC-1 cells under oxidative stress conditions (Figure 6a,b).

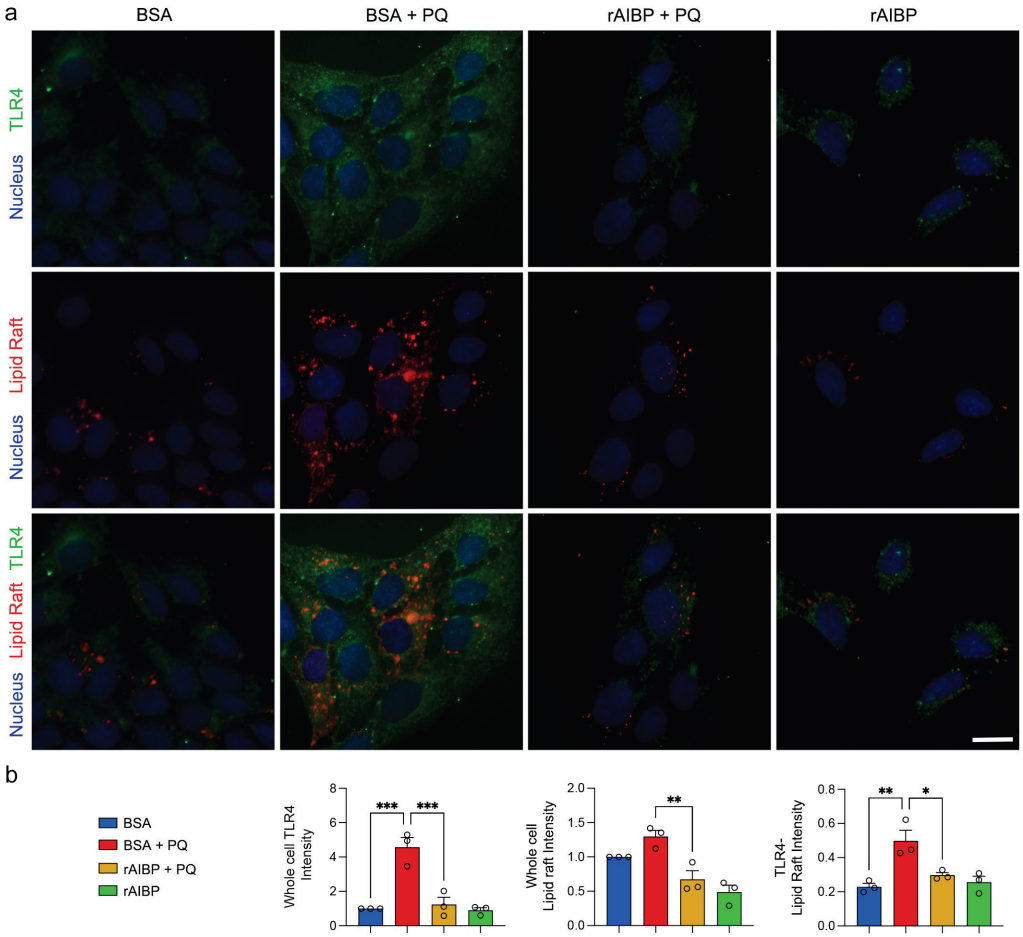

Figure 6. Administration of rAIBP reduced TLR4-associated lipid rafts in Müller glia exposed to oxidative stress. (**a**) Representative images of TLR4 (green)-LR (red) immunoreactivity (red). Scale bar: 10 μm. (**b**) Quantitative fluorescent intensity of TLR4-LR immunoreactivity in rMC-1 cells. $N = 3$ independent experiments. Scale bar: 10 μm. Error bars represent SEM. Statistical significance was determined using one-way ANOVA test. * $p < 0.05$; ** $p < 0.01$; *** $p < 0.001$. LR, lipid raft; PQ, paraquat; BSA, bovine serum albumin.

3.7. Administration of rAIBP Preserves Mitochondrial Function and Dynamics in Müller Glial Cells Exposed to Oxidative Stress

To investigate the protective role of rAIBP administration in mitochondrial function and dynamics in Müller glial cells, we incubated cultured rMC-1 cells with rAIBP before inducing oxidative stress with PQ. Our findings revealed that the administration of rAIBP effectively preserved MMP and suppressed ROS generation in rMC-1 cells exposed to oxidative stress (Figure 7a). We then examined mitochondrial dynamics and found that the administration of rAIBP prevented changes in the levels of pDRP1 S616 and pDRP1 S637 in rMC-1 cells under oxidative stress conditions (Figure 7b; Supplementary Figure S5). To test mitochondrial respiratory and glycolytic function, we measured OCR and ECAR in rMC-1 cells treated with rAIBP under oxidative stress conditions. The administration of rAIBP showed a significant preservation of respiratory activities, including basal and maximal respiration, and ATP-linked production in rMC-1 cells subjected to oxidative stress (Figure 7c,d). However, there was no statistically significant difference in spare respiratory capacity in rMC-1 cells between BSA- and rAIBP-treated rMC-1 cells under oxidative stress conditions (Figure 7c,d). In addition, we found that oxidative stress triggered increases in glycolysis and glycolytic capacity (Figure 7e,f). Still, there was no statistically significant difference in glycolytic reserve in rMC-1 cells (Figure 7e,f). The administration of rAIBP did not result in a statistically significant difference in glycolysis, glycolytic capacity, or

glycolytic reserve compared with BSA-treated rMC-1 cells under oxidative stress conditions (Figure 7e,f).

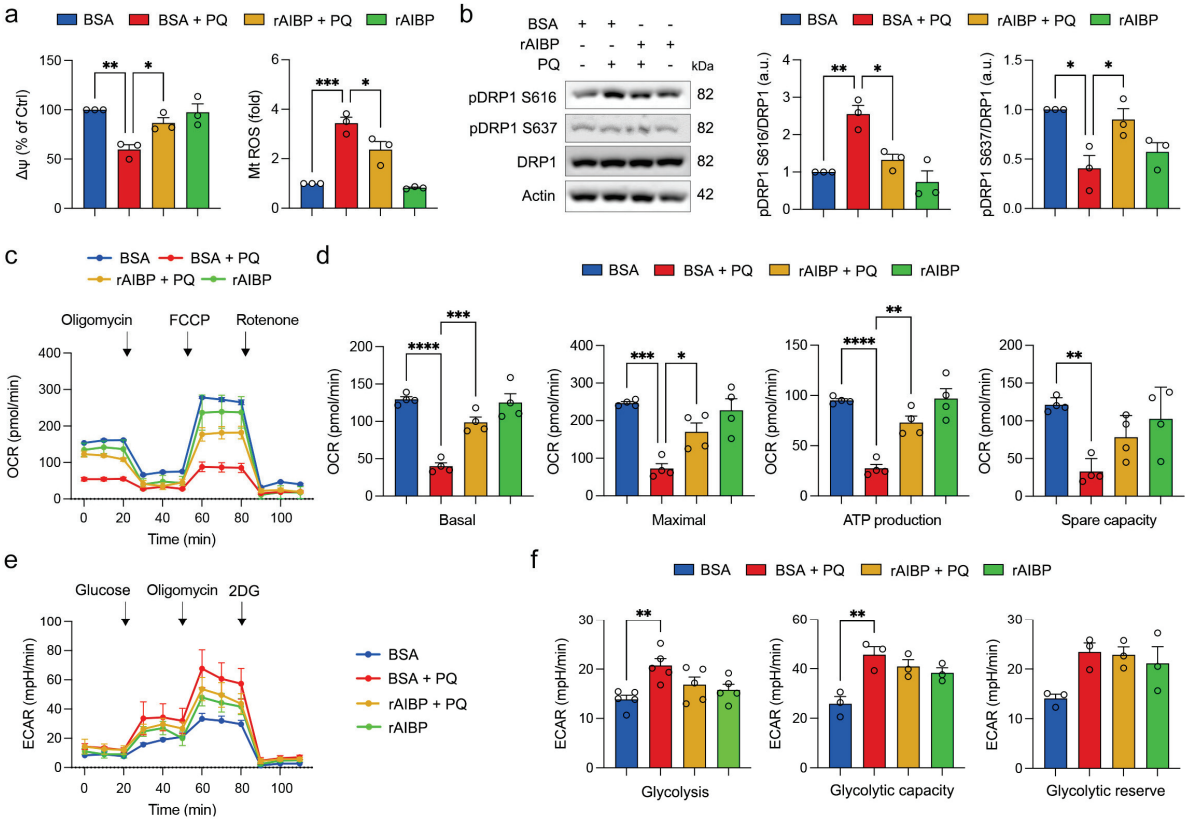

Figure 7. Administration of rAIBP preserves mitochondrial function and dynamics in Müller glia exposed to oxidative stress. (**a**) Quantitative analysis of MMP and mitochondrial ROS in rMC-1 cells. N = 3 independent experiments. (**b**) Total DRP1, phospho-DRP S616, and phospho-DRP1 S637 expression in rMC-1 cells. N = 3 independent experiments. (**c**) Oligomycin A, FCCP and rotenone were sequentially added at indicated time point. Basal respiration indicates starting basal OCR and value which was set to 100%. Maximum respiration represents ratio between FCCP uncoupled OCR and basal OCR. (**d**) Quantitative analyses of basal, maximal, and ATP-linked respiration and spare respiratory capacity in rMC-1 cells. N = 4 replicated wells. (**e**) Glucose, oligomycin A and 2DG were sequentially added at indicated time point. (**f**) Quantitative analyses of glycolysis, glycolytic capacity, and glycolytic reserve in rMC-1 cells. N = 5 replicated wells. Error bars represent SEM. Statistical significance was determined using one-way ANOVA test. * $p < 0.05$; ** $p < 0.01$; *** $p < 0.001$; **** $p < 0.0001$. BSA, bovine serum albumin; PQ, paraquat; FCCP, carbonyl cyanide p-trifluoromethoxyphenylhydrazone; OCR, oxygen consumption rate; ECAR, extracellular acidification rate.

3.8. Administration of rAIBP Inhibits MAPK Activation, Apoptotic Cell Death, and Inflammatory Response in Müller Glial Cells Exposed to Oxidative Stress

After observing MAPK activation, caspase-1 and -3 activation, and inflammatory response in Müller glial cells lacking AIBP under oxidative stress conditions, we examined whether rAIBP administration could protect against these adverse effects in rMC-1 cells induced by oxidative stress. We found that the administration of rAIBP significantly inhibited the activation of p38 and ERK1/2, evidenced by the decreased levels of pp38 and pERK1/2 in rMC-1 cells compared with BSA-treated rMC-1 cells under oxidative stress conditions (Figure 8a). Additionally, we observed that the administration of rAIBP had a significant inhibitory effect on the activation of caspase-1 and -3, accompanied by reduced caspase-3 immunoreactivity in rMC-1 cells compared with BSA-treated rMC-1

cells under oxidative stress conditions (Figure 8b–d). This suggests an inhibition of caspase-mediated apoptotic cell death by rAIBP administration. Notably, our results also revealed that the administration of rAIBP significantly inhibited inflammasome activation and the inflammatory response, as evidenced by the decreased expression levels of the *Nlrp3*, *Il-1β*, *Il-6*, and *Tnf-α* genes in rMC-1 cells compared with BSA-treated rMC-1 cells under oxidative stress conditions (Figure 8e).

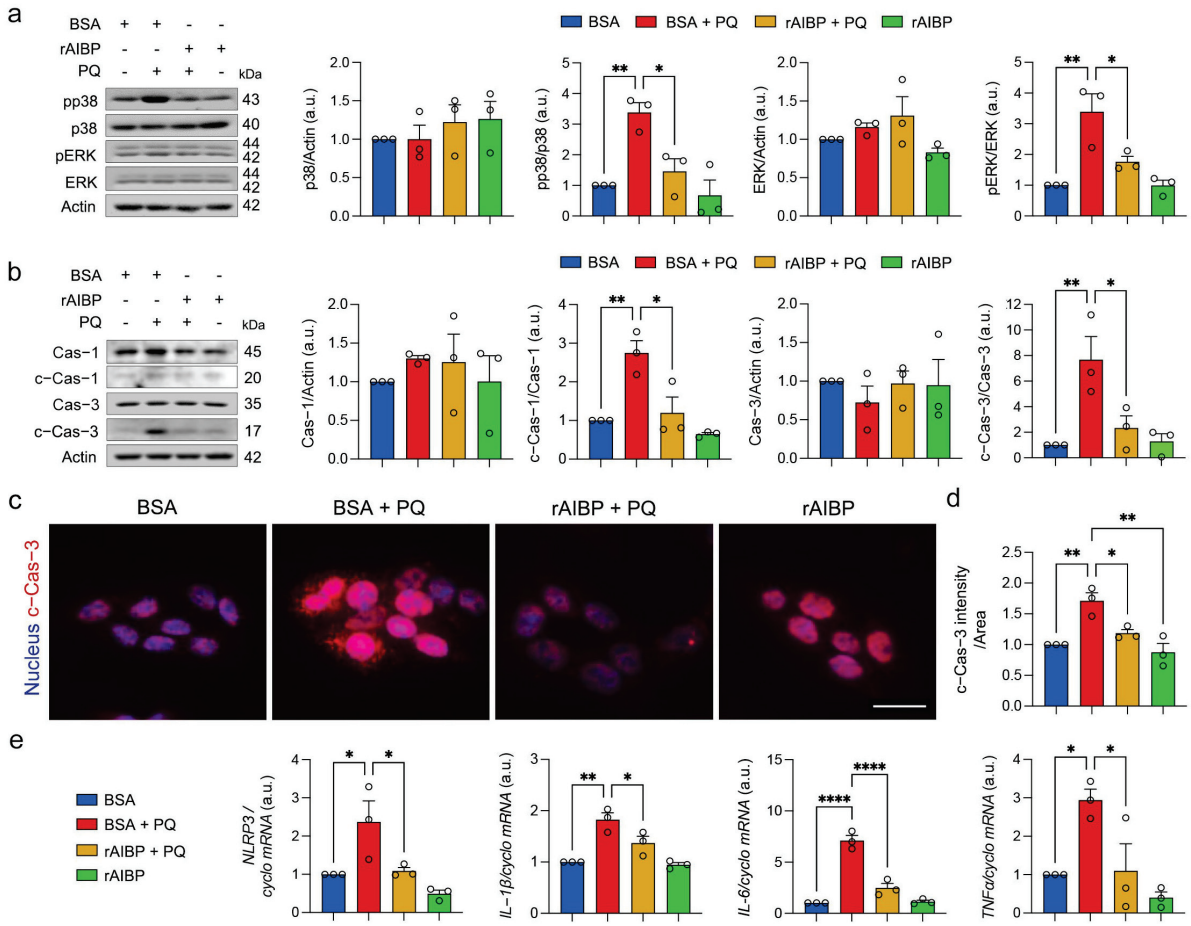

Figure 8. Administration of rAIBP inhibits MAPK activation, apoptotic cell death, and inflammatory response in Müller glia exposed to oxidative stress. (**a**) p38, phospho-p38 9 (pp38), ERK1/2, phospho-ERK1/2 (pERK1/2) expression in rMC-1 cells. *N* = 3 independent experiments. (**b**) caspase-1, cleaved caspase-1, caspase-3, and cleaved caspase-3 expression in rMC-1 cells. *N* = 3 independent experiments. (**c**) Representative images show cleaved caspase-3-positive rMC-1 cells. (**d**) Note that quantification analysis showed significant decrease in cleaved caspase-3 immunoreactive intensity in rMC-1 cells with rAIBP treatment compared with BSA-treated cells under oxidative stress. *N* = 3 independent experiments. (**e**) Quantitative real-time PCR analysis of *Nlrp3*, *Il-1β*, *Il-6*, and *Tnfα* mRNA expression in rMC-1 cells. Error bars represent SEM. Statistical significance was determined using one-way ANOVA test. * $p < 0.05$; ** $p < 0.01$; **** $p < 0.0001$. PQ, paraquat; BSA, bovine serum albumin.

4. Discussion

Our recent study showed a crucial link between Müller glial cells and the increased expression of TLR4 and IL-1β in glaucomatous retinas [14–16]. In addition, we found that administering rAIBP protects RGCs against acute IOP elevation by suppressing cytokine production and inflammatory response [15]. Nevertheless, the precise mechanisms through which AIBP confers protection in Müller glial cells and their mitochondria have yet to be fully elucidated. This study unveils significant new findings suggesting that AIBP protects Müller glial cells against oxidative stress. In AIBP-deficient mice, the detrimental effects

of oxidative stress on mitochondrial function and inflammatory reactions are exacerbated, leading to worsening vision impairment. Notably, the administration of rAIBP mitigates these consequences by reducing TLR4-associated lipid rafts. This action preserves mitochondrial dynamics and function while dampening inflammatory responses in Müller glial cells under oxidative stress, ultimately improving RGC and visual function.

Müller glial cells, the most abundant glial cells in the retina, exhibit a radial arrangement that spans the entire retinal thickness. Müller glial cells play crucial roles in the retina by establishing vital connections with retinal neurons. These functions encompass maintaining cholesterol balance, clearing waste products through phagocytosis, shielding neurons from excessive exposure to neurotransmitters like glutamate, and supplying end products from anaerobic metabolism [32–35]. Reactive glial cells, such as astrocytes and microglial cells, are closely associated with glaucomatous neuroinflammation [36]. In contrast, the involvement of reactive Müller glial cells and their mitochondrial dysfunction remains to be elucidated in glaucomatous neuroinflammation. Oxidative stress, mitochondrial dysfunction, and inflammation associated with glial activation are crucial pathogenic mechanisms in the glaucomatous retina [5,15,36,37]. Our recent findings indicated that Müller glial cells lacking AIBP display extensive mitochondrial fragmentation and reduced ATP production, resulting in Müller glial cell dysfunction linked to oxidative stress and inflammatory response [15]. Furthermore, our recent findings revealed a notable decrease in AIBP levels within glaucomatous human RGCs and Müller glial cells [14,15]. This is accompanied by increased cholesterol accumulation and TLR4-associated lipid raft formation, as well as MAPK activation, metabolic energy stress, and inflammatory responses in Müller glial cells [14,16]. Hence, these findings strongly suggested that oxidative stress could be a critical process regulated by AIBP in the context of retinal inflammation and associated with mitochondrial stress in Müller glial cells in glaucomatous neuroinflammation.

In this study, we observed a deterioration in visual function in *Apoa1bp*$^{-/-}$ mice when exposed to oxidative stress, correlating with exacerbated impairments in mitochondrial dynamics, OXPHOS activity, and mitochondrial biogenesis in the *Apoa1bp*$^{-/-}$ retina. Notably, these effects were associated with the activation of Müller glial cells, culminating in heightened inflammatory responses. Significantly, Müller glial cells lacking AIBP demonstrated increased vulnerability to degeneration, characterized by MMP loss, elevated mtROS production, excessive mitochondrial fragmentation, and compromised mitochondrial respiration, particularly under oxidative stress conditions. Oxidative stress is linked to the activation of multiple signaling pathways of MAPKs, such as p38 and ERK1/2 [38,39]. Since AIBP deficiency and glaucomatous damage activated p38 and ERK1/2 by increasing the phosphorylation of p38 and ERK1/2 in the retina [14,15], we observed that oxidative stress worsened the increase in the phosphorylation of p38 and ERK1/2 in Müller glial cells lacking AIBP. Thus, these findings strongly suggest a vicious cycle where oxidative stress initiates AIBP deficiency, leading to a cascade involving oxidative stress, AIBP deficiency, mitochondrial dysfunction, and MAPK activation in Müller glial cells. Ultimately, this cascade may trigger inflammasome activation, apoptotic cell death, and inflammatory response in oxidative stress-mediated glaucomatous neuroinflammation.

Both the restoration of AIBP expression and the administration of rAIBP significantly reduced neuroinflammation and protected RGCs in acute or chronic experimental animal models of glaucoma [14,15]. Recent evidence indicates that AIBP plays a multifaceted role, involving extracellular cholesterol efflux from the cell membrane and various intracellular functions within the mitochondria [5,11,13,15,16,40]. Specifically, intracellular AIBP has been shown to regulate autophagy/mitophagy in macrophages [13]. This study suggested that mitochondria-associated AIBP enhances mitophagy, thereby contributing to mitochondrial quality control and preventing macrophage death in atherosclerosis [13]. In this study, our findings indicated that administering rAIBP improved visual function in mice and maintained mitochondrial dynamics and function in retinal cells, including Müller glial cells, under oxidative stress conditions. These effects were supported by preventing mitochondrial fragmentation and restoring mitochondrial fusion activity and OXPHOS activity.

Thus, our findings suggest that AIBP would be critical in protecting retinal mitochondria against oxidative stress. Further studies will delve into how administering rAIBP regulates mitophagy, thereby preserving mitochondrial quality control and safeguarding Müller glial cells.

Glia-driven neuroinflammation is evident in both glaucomatous human and mouse retinas, characterized by an increased expression of TLR4 and IL-1β within activated Müller glial cells [14,15]. Our observations are particularly noteworthy given that TLR4 activation typically triggers the MAPK/NFκB pathway and NLRP3 inflammasomes, resulting in an increased production of proinflammatory cytokines [41–43]. We found that the administration of rAIBP notably diminished TLR4-associated lipid rafts in Müller glial cells subjected to oxidative stress. Furthermore, this effect was strongly correlated with reduced MAPK activation, a suppressed NLRP3-associated inflammasome pathway, and mitigated inflammatory responses in Müller glial cells under oxidative stress conditions. Importantly, considering the established role of AIBP in reducing cholesterol deposition in glaucomatous retinas [14], our findings collectively suggest that extracellular rAIBP administration may potentially contribute to the prevention of neuroinflammation and cell death in Müller glial cells. This could be achieved through the inhibition of cholesterol deposition, reducing TLR4 inflammaraft formation, and the mitigation of mitochondrial dysfunction during oxidative stress-induced glaucomatous neuroinflammation and neurodegeneration.

Our study proposes a novel concept that oxidative stress triggers AIBP deficiency in Müller glial cells, which consequently increases the activation of TLR4 lipid rafts. This then leads to mitochondrial dysfunction, inflammasome activation, neuroinflammation, cell death, and, ultimately, vision impairment (Supplementary Figure S6). Notably, our findings support the notion that administering rAIBP counteracts these dysfunctional outcomes, safeguarding Müller glial cells. Hence, this protection may promote RGC survival and restore visual function by ameliorating glia-driven mitochondrial dysfunction and neuroinflammation in glaucoma.

Supplementary Materials: The following supporting information can be downloaded at: https://www.mdpi.com/article/10.3390/antiox13101252/s1, Table S1: Lists of antibodies; Table S2: Lists of PCR primers; Figure S1: AIBP deficiency exacerbates visual dysfunction induced by oxidative stress. (a) Representative graphs of total recordings of pERG analysis. (b) Quantification analysis of pERG and pVEP tests. N = 8 mice. Error bars represent SEM. Statistical significance determined using a two-tailed Student's t-test. * $p < 0.05$. See Figure 1a,b; Figure S2: AIBP deficiency intensifies impairment of retinal mitochondrial dynamics, OXPHOS activity, and mitochondrial biogenesis induced by oxidative stress. (a) Quantification of total DRP1 expression in the retina. N = 3 mice. (b) Total GSK3b and phospho-GSK3b expression in the retina. N = 3 mice. Error bars represent SEM. Statistical significance determined using a one-way ANOVA test. * $p < 0.05$; ** $p < 0.01$. See Figure 2a; Figure S3: Oxidative stress worsens structural and functional impairment of mitochondria in Müller glial cells lacking AIBP. The rMC1 cells were treated with various concentrations of PQ (25, 50, 100, 200, 500, 1000, or 2000 μM) for 24 h. (a) Quantitative analysis of cell viability in rMC1 cells using an MTT assay. (b) Quantitative analysis of cell death in rMC1 cells using an LDH assay. (c) Quantitative analysis of MMP in rMC1 cells. (d) Quantitative analysis of mitochondrial ROS in rMC1 cells. (e) Quantitative analysis of AIBP expression in rMC1 cells. N = 3 independent experiments in rMC1 cells. Error bars represent SEM. Statistical significance determined using a one-way ANOVA test. * $p < 0.05$; ** $p < 0.01$; *** $p < 0.001$; **** $p < 0.0001$. See Figure 3; Figure S4: Oxidative stress worsens structural and functional impairment of mitochondria in Müller glial cells lacking AIBP. Quantification of AIBP and total DRP1 expression in the retina. N = 3 mice. Error bars represent SEM. Statistical significance determined using a one-way ANOVA test. * $p < 0.05$; ** $p < 0.01$. See Figure 3d; Figure S5: Administration of rAIBP preserves mitochondrial function and dynamics in Müller glial cells exposed to oxidative stress. Quantification of total DRP1 expression in the retina. N = 3 mice. Error bars represent SEM. See Figure 7b; Figure S6: Schematic overview of AIBP-mediated protective effect on glia-driven neuroinflammation and vision impairment. Our study proposes a novel concept that oxidative stress triggers AIBP deficiency in Müller glial cells, which consequently increases activation of TLR4-lipid raft. This then leads to mitochondrial dysfunction, inflammasome activation, neuroinflammation, cell death, and ultimately vision impairment.

Author Contributions: Conceptualization, W.-K.J.; methodology S.C., S.-H.C., T.B., K.-Y.K., S.P. and W.-K.J.; resources, W.-K.J.; writing—original draft preparation, S.C. and W.-K.J.; writing—review and editing, S.C., S.-H.C., K.-Y.K., R.N.W., Y.I.M. and W.-K.J.; supervision, W.-K.J.; funding acquisition, S.-H.C., K.-Y.K., Y.I.M. and W.-K.J. All authors have read and agreed to the published version of the manuscript.

Funding: This work was supported in part by NIH grants EY031697 (W.-K.J.), EY034116 (W.-K.J., S.-H.C. and K.-Y.K.), NS129684 (W.-K.J.), AG081004 (W.-K.J.), P30EY022589 (Vision Core Grant), HL136275 (Y.I.M.), HL171505 (Y.I.M.), and AG081037 (Y.I.M. and W.-K.J.), as well as an unrestricted grant from Research to Prevent Blindness (New York, NY).

Institutional Review Board Statement: The animal study protocol was approved by the IACUC of University of California, San Diego (protocol code S12063, 31 July 2023).

Informed Consent Statement: Not applicable.

Data Availability Statement: The original contributions presented in the study are included in the article/Supplementary Material, further inquiries can be directed to the corresponding author.

Acknowledgments: We would like to acknowledge the kind gift of a rabbit polyclonal anti-AIBP antibody from Longhou Fang (Houston Methodist Research Institute.

Conflicts of Interest: W.-K.J., S.-H.C. and Y.I.M. are co-inventors named on patents and patent applications by the University of California, San Diego. YIM is a scientific co-founder of Raft Pharmaceuticals LLC. The terms of this arrangement were reviewed and approved by the University of California, San Diego, in accordance with its conflict-of-interest policies. The other authors declare no conflicts of interest.

References

1. Weinreb, R.N.; Khaw, P.T. Primary open-angle glaucoma. *Lancet* **2004**, *363*, 1711–1720. [CrossRef]
2. Weinreb, R.N.; Leung, C.K.; Crowston, J.G.; Medeiros, F.A.; Friedman, D.S.; Wiggs, J.L.; Martin, K.R. Primary open-angle glaucoma. *Nat. Rev. Dis. Primers* **2016**, *2*, 16067. [CrossRef]
3. Tezel, G. Oxidative stress in glaucomatous neurodegeneration: Mechanisms and consequences. *Prog. Retin. Eye Res.* **2006**, *25*, 490–513. [CrossRef]
4. Lee, D.; Shim, M.S.; Kim, K.Y.; Noh, Y.H.; Kim, H.; Kim, S.Y.; Weinreb, R.N.; Ju, W.K. Coenzyme Q10 inhibits glutamate excitotoxicity and oxidative stress-mediated mitochondrial alteration in a mouse model of glaucoma. *Invest. Ophthalmol. Vis. Sci.* **2014**, *55*, 993–1005. [CrossRef]
5. Ju, W.K.; Perkins, G.A.; Kim, K.Y.; Bastola, T.; Choi, W.Y.; Choi, S.H. Glaucomatous optic neuropathy: Mitochondrial dynamics, dysfunction and protection in retinal ganglion cells. *Prog. Retin. Eye Res.* **2023**, *95*, 101136. [CrossRef]
6. Mathew, D.J.; Sivak, J.M. Lipid mediators in glaucoma: Unraveling their diverse roles and untapped therapeutic potential. *Prostaglandins Other Lipid Mediat.* **2024**, *171*, 106815. [CrossRef]
7. Sanz-Morello, B.; Ahmadi, H.; Vohra, R.; Saruhanian, S.; Freude, K.K.; Hamann, S.; Kolko, M. Oxidative Stress in Optic Neuropathies. *Antioxidants* **2021**, *10*, 1538. [CrossRef]
8. Collins, D.W.; Gudiseva, H.V.; Chavali, V.R.M.; Trachtman, B.; Ramakrishnan, M.; Merritt, W.T., III.; Pistilli, M.; Rossi, R.A.; Blachon, S.; Sankar, P.S.; et al. The MT-CO1 V83I Polymorphism is a Risk Factor for Primary Open-Angle Glaucoma in African American Men. *Invest. Ophthalmol. Vis. Sci.* **2018**, *59*, 1751–1759. [CrossRef]
9. Navarro-Partida, J.; Martinez-Rizo, A.B.; Ramirez-Barrera, P.; Velazquez-Fernandez, J.B.; Mondragon-Jaimes, V.A.; Santos-Garcia, A.; Benites-Godinez, V. Association of Toll-like receptor 4 single-nucleotide polymorphisms Asp299Gly and Thr399Ile with the risk of primary open angle glaucoma. *Graefe's Arch. Clin. Exp. Ophthalmol.* **2017**, *255*, 995–1001. [CrossRef]
10. Ritter, M.; Buechler, C.; Boettcher, A.; Barlage, S.; Schmitz-Madry, A.; Orso, E.; Bared, S.M.; Schmiedeknecht, G.; Baehr, C.H.; Fricker, G.; et al. Cloning and characterization of a novel apolipoprotein A-I binding protein, AI-BP, secreted by cells of the kidney proximal tubules in response to HDL or ApoA-I. *Genomics* **2002**, *79*, 693–702. [CrossRef]
11. Fang, L.; Choi, S.H.; Baek, J.S.; Liu, C.; Almazan, F.; Ulrich, F.; Wiesner, P.; Taleb, A.; Deer, E.; Pattison, J.; et al. Control of angiogenesis by AIBP-mediated cholesterol efflux. *Nature* **2013**, *498*, 118–122. [CrossRef]
12. Zhang, M.; Li, L.; Xie, W.; Wu, J.F.; Yao, F.; Tan, Y.L.; Xia, X.D.; Liu, X.Y.; Liu, D.; Lan, G.; et al. Apolipoprotein A-1 binding protein promotes macrophage cholesterol efflux by facilitating apolipoprotein A-1 binding to ABCA1 and preventing ABCA1 degradation. *Atherosclerosis* **2016**, *248*, 149–159. [CrossRef]
13. Choi, S.H.; Agatisa-Boyle, C.; Gonen, A.; Kim, A.; Kim, J.; Alekseeva, E.; Tsimikas, S.; Miller, Y.I. Intracellular AIBP (Apolipoprotein A-I Binding Protein) Regulates Oxidized LDL (Low-Density Lipoprotein)-Induced Mitophagy in Macrophages. *Arterioscler. Thromb. Vasc. Biol.* **2021**, *41*, e82–e96. [CrossRef]
14. Ju, W.K.; Ha, Y.; Choi, S.; Kim, K.Y.; Bastola, T.; Kim, J.; Weinreb, R.N.; Zhang, W.; Miller, Y.I.; Choi, S.H. Restoring AIBP expression in the retina provides neuroprotection in glaucoma. *bioRxiv* **2023**. [CrossRef]

15. Choi, S.H.; Kim, K.Y.; Perkins, G.A.; Phan, S.; Edwards, G.; Xia, Y.; Kim, J.; Skowronska-Krawczyk, D.; Weinreb, R.N.; Ellisman, M.H.; et al. AIBP protects retinal ganglion cells against neuroinflammation and mitochondrial dysfunction in glaucomatous neurodegeneration. *Redox Biol.* **2020**, *37*, 101703. [CrossRef]
16. Choi, S.; Choi, S.H.; Bastola, T.; Park, Y.; Oh, J.; Kim, K.Y.; Hwang, S.; Miller, Y.I.; Ju, W.K. AIBP: A New Safeguard against Glaucomatous Neuroinflammation. *Cells* **2024**, *13*, 198. [CrossRef]
17. Woller, S.A.; Choi, S.H.; An, E.J.; Low, H.; Schneider, D.A.; Ramachandran, R.; Kim, J.; Bae, Y.S.; Sviridov, D.; Corr, M.; et al. Inhibition of Neuroinflammation by AIBP: Spinal Effects upon Facilitated Pain States. *Cell Rep.* **2018**, *23*, 2667–2677. [CrossRef]
18. Choi, S.H.; Wallace, A.M.; Schneider, D.A.; Burg, E.; Kim, J.; Alekseeva, E.; Ubags, N.D.; Cool, C.D.; Fang, L.; Suratt, B.T.; et al. AIBP augments cholesterol efflux from alveolar macrophages to surfactant and reduces acute lung inflammation. *JCI Insight* **2018**, *3*, e120519. [CrossRef]
19. Edwards, G.; Lee, Y.; Kim, M.; Bhanvadia, S.; Kim, K.Y.; Ju, W.K. Effect of Ubiquinol on Glaucomatous Neurodegeneration and Oxidative Stress: Studies for Retinal Ganglion Cell Survival and/or Visual Function. *Antioxidants* **2020**, *9*, 952. [CrossRef]
20. Queirós, A.; Pereira-da-Mota, A.F.; Costa, J.; Amorim-de-Sousa, A.; Fernandes, P.R.; González-Méijome, J.M. Retinal response of low myopes during orthokeratology treatment. *J. Clin. Med.* **2020**, *9*, 2649. [CrossRef]
21. Gramlich, O.W.; Godwin, C.R.; Wadkins, D.; Elwood, B.W.; Kuehn, M.H. Early functional impairment in experimental glaucoma is accompanied by disruption of the GABAergic system and inceptive neuroinflammation. *Int. J. Mol. Sci.* **2021**, *22*, 7581. [CrossRef]
22. Prusky, G.T.; Alam, N.M.; Beekman, S.; Douglas, R.M. Rapid quantification of adult and developing mouse spatial vision using a virtual optomotor system. *Investig. Ophthalmol. Vis. Sci.* **2004**, *45*, 4611–4616. [CrossRef]
23. Choi, S.; Park, M.; Kim, J.; Park, W.; Kim, S.; Lee, D.-K.; Hwang, J.Y.; Choe, J.; Won, M.-H.; Ryoo, S. TNF-α elicits phenotypic and functional alterations of vascular smooth muscle cells by miR-155-5p–dependent down-regulation of cGMP-dependent kinase 1. *J. Biol. Chem.* **2018**, *293*, 14812–14822. [CrossRef]
24. Bastola, T.; Perkins, G.A.; Huu, V.A.N.; Ju, S.; Kim, K.Y.; Shen, Z.; Skowronska-Krawczyk, D.; Weinreb, R.N.; Ju, W.K. Activating soluble adenylyl cyclase protects mitochondria, rescues retinal ganglion cells, and ameliorates visual dysfunction caused by oxidative stress. *bioRxiv* **2024**. [CrossRef]
25. Ju, W.K.; Shim, M.S.; Kim, K.Y.; Park, T.L.; Ahn, S.; Edwards, G.; Weinreb, R.N. Inhibition of cAMP/PKA Pathway Protects Optic Nerve Head Astrocytes against Oxidative Stress by Akt/Bax Phosphorylation-Mediated Mfn1/2 Oligomerization. *Oxid. Med. Cell. Longev.* **2019**, *2019*, 8060962. [CrossRef]
26. Cocheme, H.M.; Murphy, M. P: Complex I is the major site of mitochondrial superoxide production by paraquat. *J. Biol. Chem.* **2008**, *283*, 1786–1798. [CrossRef]
27. Chou, C.-H.; Lin, C.-C.; Yang, M.-C.; Wei, C.-C.; Liao, H.-D.; Lin, R.-C.; Tu, W.-Y.; Kao, T.-C.; Hsu, C.-M.; Cheng, J.-T. GSK3beta-mediated Drp1 phosphorylation induced elongated mitochondrial morphology against oxidative stress. *PLoS ONE* **2012**, *7*, e49112. [CrossRef]
28. Yan, J.; Liu, X.-H.; Han, M.-Z.; Wang, Y.-M.; Sun, X.-L.; Yu, N.; Li, T.; Su, B.; Chen, Z.-Y. Blockage of GSK3β-mediated Drp1 phosphorylation provides neuroprotection in neuronal and mouse models of Alzheimer's disease. *Neurobiol. Aging* **2015**, *36*, 211–227. [CrossRef]
29. Blanco-Ayala, T.; Andérica-Romero, A.C.; Pedraza-Chaverri, J. New insights into antioxidant strategies against paraquat toxicity. *Free. Radic. Res.* **2014**, *48*, 623–640. [CrossRef]
30. Kim, S.; Pajarillo, E.; Nyarko-Danquah, I.; Aschner, M.; Lee, E. Role of Astrocytes in Parkinson's Disease Associated with Genetic Mutations and Neurotoxicants. *Cells* **2023**, *12*, 622. [CrossRef]
31. Shi, S.; Chen, Y.; Luo, Z.; Nie, G.; Dai, Y. Role of oxidative stress and inflammation-related signaling pathways in doxorubicin-induced cardiomyopathy. *Cell. Commun. Signal* **2023**, *21*, 61. [CrossRef]
32. Kobat, S.G.; Turgut, B. Importance of Müller Cells. *Beyoglu Eye J.* **2020**, *5*, 59.
33. Reichenbach, A.; Bringmann, A. New functions of Müller cells. *Glia* **2013**, *61*, 651–678. [CrossRef]
34. Leger-Charnay, E.; Masson, E.A.Y.; Morala, T.; Martine, L.; Buteau, B.; Leclere, L.; Bretillon, L.; Gambert, S. Is 24(S)-hydroxycholesterol a potent modulator of cholesterol metabolism in Muller cells? An in vitro study about neuron to glia communication in the retina. *Exp. Eye Res.* **2019**, *189*, 107857. [CrossRef]
35. Gambert, S.; Gabrielle, P.H.; Masson, E.; Leger-Charnay, E.; Ferrerro, A.; Vannier, A.; Gendrault, C.; Lachot, M.; Creuzot-Garcher, C.; Bron, A.; et al. Cholesterol metabolism and glaucoma: Modulation of Muller cell membrane organization by 24S-hydroxycholesterol. *Chem. Phys. Lipids* **2017**, *207*, 179–191. [CrossRef]
36. Tezel, G. Molecular regulation of neuroinflammation in glaucoma: Current knowledge and the ongoing search for new treatment targets. *Prog. Retin. Eye Res.* **2022**, *87*, 100998. [CrossRef]
37. Baudouin C, Kolko M, Melik-Parsadaniantz S, Messmer EM: Inflammation in Glaucoma: From the back to the front of the eye, and beyond. *Prog. Retin. Eye Res.* **2021**, *83*, 100916. [CrossRef]
38. Harada, C.; Namekata, K.; Guo, X.; Yoshida, H.; Mitamura, Y.; Matsumoto, Y.; Tanaka, K.; Ichijo, H.; Harada, T. Differentiation: ASK1 deficiency attenuates neural cell death in GLAST-deficient mice, a model of normal tension glaucoma. *Cell Death Differ.* **2010**, *17*, 1751–1759. [CrossRef]
39. Wang, C.; Ren, Y.L.; Zhai, J.; Zhou, X.Y.; Wu, J. Down-regulated LAMA4 inhibits oxidative stress-induced apoptosis of retinal ganglion cells through the MAPK signaling pathway in rats with glaucoma. *Cell Cycle* **2019**, *18*, 932–948. [CrossRef]

40. Schneider, D.A.; Choi, S.H.; Agatisa-Boyle, C.; Zhu, L.; Kim, J.; Pattison, J.; Sears, D.D.; Gordts, P.; Fang, L.; Miller, Y.I. AIBP protects against metabolic abnormalities and atherosclerosis. *J. Lipid Res.* **2018**, *59*, 854–863. [CrossRef]
41. Qi, Y.; Zhao, M.; Bai, Y.; Huang, L.; Yu, W.; Bian, Z.; Zhao, M.; Li, X. Retinal ischemia/reperfusion injury is mediated by Toll-like receptor 4 activation of NLRP3 inflammasomes. *Invest. Ophthalmol. Vis. Sci.* **2014**, *55*, 5466–5475. [CrossRef]
42. Chi, W.; Li, F.; Chen, H.; Wang, Y.; Zhu, Y.; Yang, X.; Zhu, J.; Wu, F.; Ouyang, H.; Ge, J.; et al. Caspase-8 promotes NLRP1/NLRP3 inflammasome activation and IL-1beta production in acute glaucoma. *Proc. Natl. Acad. Sci. USA* **2014**, *111*, 11181–11186. [CrossRef]
43. Kim, S.Y.; Jin, C.Y.; Kim, C.H.; Yoo, Y.H.; Choi, S.H.; Kim, G.Y.; Yoon, H.M.; Park, H.T.; Choi, Y.H. Isorhamnetin alleviates lipopolysaccharide-induced inflammatory responses in BV2 microglia by inactivating NF-kappaB, blocking the TLR4 pathway and reducing ROS generation. *Int. J. Mol. Med.* **2019**, *43*, 682–692.

MDPI AG
Grosspeteranlage 5
4052 Basel
Switzerland
Tel.: +41 61 683 77 34

Antioxidants Editorial Office
E-mail: antioxidants@mdpi.com
www.mdpi.com/journal/antioxidants

Academic Open
Access Publishing

mdpi.com

ISBN 978-3-7258-4528-6